Effects of Vascular Nitric Oxide Bioactivity and Vascular Ageing on Arterial Blood Pressure and Flow Waveforms

By

Anthony A.E. Hunt

Department of Bioengineering

Imperial College London

This thesis is submitted for

The Degree of Doctor of Philosophy

Of

Imperial College London

2011

Declaration of Originality

The experiments and resulting data described in this thesis are the original work of Anthony Hunt; collaborators have been named in the relevant text of the thesis. Sources of work of others included in this thesis are referenced.

ABSTRACT

Analysis of blood pressure and flow waveforms may lead to improved diagnosis of arterial dysfunction and disease. This thesis describes experiments to investigate the characteristic alteration of peripheral waveforms produced by stimulated release of vascular nitric oxide (an effect that is attenuated by endothelial dysfunction) and the changes that occur with age.

In vivo experiments were conducted in anaesthetised rabbits and *in vitro* experiments employed a polyurethane model of the human aorta and its principal branches. Blood pressure, blood flow, pulse wave velocities and vessel diameter were recorded in the rabbit abdominal aorta. Equivalent recordings were obtained from the model aorta. Data were analysed in the time domain using wave intensity analysis after separation of reservoir (Windkessel) pressure and wave pressure.

Effects of acetylcholine (Ach) and N^G-nitro-L-arginine methyl ester (L-NAME) were investigated *in vivo*. Ach (which promotes endothelial production of nitric oxide) increased wave reflection, whilst L-NAME (which inhibits nitric oxide production) decreased it. These trends were opposite to the expected ones, and do not account for the established effects of nitric oxide on peripheral arterial waveforms. Further work is required to investigate these contradictions.

Arterial stiffening in immature and mature rabbits was attempted by supplementing their diet with fructose. Fructose is known to form advanced glycation end-products in arterial walls and hence to stiffen arteries. Unexpectedly, fructose did not affect haemodynamic function. However, immature control rabbits had markedly reduced aortic wave reflection compared to mature control rabbits, indicating that the former have arterial impedances that are better matched for incident wave propagation.

Wrapping the model aorta in Clingfilm was used to simulate age- or drug-induced stiffening of the aorta *in vivo*. Increased pulse pressure was observed, resembling the isolated systolic hypertension prevalent in aged populations. The model has potential for modelling haemodynamic function in health and disease.

To

Christine

My family

****

In Memory of

My Mother

My Father

and

Nicola

ACKNOWLEDGEMENTS

There are two to whom I owe equal thanks but in different ways. I thank Christine deeply for her love and support throughout the years of my postgraduate work. She has been of great strength to me, encouraging me through episodes of crises of confidence, always interested in my work and of great practical help too; I am indebted to her. I thank most sincerely my supervisor Prof. Peter Weinberg who gave me the wonderful opportunity of my postgraduate work. I thank him for his kindness, endless great patience and encouragement. I add my gratitude for his help and advice given to me during the preparation and writing of my thesis. His skilful eloquence with words is enviable!

I am grateful to Dr. Rob Fenton (Institute of Biomedical Engineering) for the introductions to Imperial College London and to Prof. Peter Weinberg. I thank Prof. Kim Parker (Emeritus Professor, Department of Bioengineering) for many interesting discussions on haemodynamics, for his patience in explaining analysis of haemodynamic data in the time domain, and for the use of MATLAB algorithms he has written; in this context, I add much thanks to Nur Abd Razak (3rd year undergraduate, 2009) for her help in applying the algorithms to data of my work. I add my thanks to Dr. Jordi Alastruey Arimon (Fellow of Department of Bioengineering and Aeronautics) for many interesting discussions on pulse wave propagation and, in the early years of my work, for his patiently given explanations on the workings of the 1-D numerical computation of arterial pulse wave propagation. I thank Dr. Lindsey Clarke (Postdoctoral Researcher, Department of Bioengineering) for her great help, from time-to-time when she could spare her time, with setting up my *in vivo* experiments and advice on the organising of rabbits within the CBS, in this respect also I thank Dr. Zahra Mohri (Postdoctoral Researcher, Department of Bioengineering). Another to whom I am very grateful is Dr. Jean Martial Mari (Ultrasonics, Physiological Fluids Flow, Department of Bioengineering, 2010), I thank him for his collaboration in operating the Ultrasonix to measure aortic diameter required in some *in vivo* experiments. I thank sincerely the staff of the CBS for their help in the daily preparation of fructose drink for rabbits during those experiments. I thank friends and former colleagues at GlaxoSmithKline for donating some Millar Mikro-tip catheters earlier in my studentship, and much included in my thanks are Dr. Jim Louttit, Dr. Miles Maxwell, Dr. Jill Coates and Dr. Mike Drew for their continued encouragement and frequent enquiries into my progress! Also, and all important, I thank many friends and all my family for the encouragement they have given me.

I most gratefully acknowledge the financial support I received as a bursary from the BBSRC Doctoral Training Grant.

CONTENTS

LIST of TABLES

CHAPTER 1

INTRODUCTION

This chapter introduces the general area and topics of interest of this thesis; topics specific to individual investigations are covered in the Introductions to the relevant chapters. Hypotheses to be tested are stated at the end of the introduction of Chapters 4, 5, 7.

Wave phenomena in the cardiovascular system have been of interest to physiologists and physicians for many years; the history of this is fully reviewed in such publications as *Blood Flow in Arteries* (McDonald 1960, 1974), or latterly in *McDonald's Blood Flow in Arteries* (Nichols and O'Rourke 1990, 1998, 2005), *Hemodynamics* (Milnor 1982, 1989), *The Mechanics of the Circulation* (Caro, Pedley, Schroter and Seed 1978, 2011). The fact that there are several editions to some of these well known publications is testament to the increase of interest in this important area of cardiovascular research.

Measurement of velocity of the pulse wave (pulse wave velocity, or PWV) along arteries (e.g. aorta, proximal aorta-femoral, brachial-radial) is a frequently used and well evaluated technique for assessing arterial health (Nichols and O'Rourke, 2005); higher than normal aortic PWV indicates risk of cardiovascular morbidity or mortality. PWV is measured by using either the blood pressure pulse (Avolio *et al*., 1983, 1985; Asmar *et al*., 1995; Blacher *et al*., 1999; Meaume *et al*., 2001), or the blood flow pulse (Laogun and Gosling, 1982; Kontis and Gosling, 1989; Lehmann *et al*., 1993, 1994; Cruickshank *et al*., 2002). Measurement of PWV, or wave speed, is an important part of the methodology reported in this thesis and is discussed in detail in Chapters 2 and 3. Measurement of PWV does not give information on the pressure pulse *waveform*, which reveals additional useful diagnostic features.

Endeavours to understand the nature of pulsatile blood pressure and flow waveforms in the arterial system will hopefully lead to improved methods of diagnosing and treating disorders of the arterial system. Such endeavours have led to technologies for non-invasive registration of arterial blood pressure waveforms, exemplified by the SphygmoCor system (sphygmogram; O'Rourke and Gallagher, 1996; Nichols and O'Rourke, 2005), HDI PulseWave system (Cohn *et al*., 1995), PulseTrace system (Chowienczyk *et al*., 1999;

Millasseau *et al*., 2000). (See also reviews by Raitakari and Celermajer (2000) and Oliver and Webb (2003) of techniques for non-invasive assessment of arterial health).

The SphygmoCor system works on the basis of recording a pressure pulse from a peripheral artery and using that recording to derive by transfer function the central aortic pressure waveform. The peripheral waveform is usually recorded from a radial or carotid artery by a non-invasive technique known as *applanation tonometry*. This technique is fully explained by Mackay *et al*. (1960), Pressman and Newgard (1963), Drzewiecki *et al*. (1983), Kelly *et al*. (1989a, b); briefly a transducer (Millar SPT-301 NI Pulse Transducer Pen) is pressed against the artery to flatten it partially (applanate), allowing the pulse to be sensed. The details of the peripheral pulse waveform are registered in the SphygmoCor device which has software algorithms designed to effect a transfer function that converts (transforms) the peripheral pressure waveform back into the original waveform that propagated in the central aorta. O'Rourke (1982) and Nichols and O'Rourke (2005) argue that measurement of just systolic and diastolic pressures by sphygmomanometry is not sufficient for diagnosis of cardiovascular disease or risk of it; it does not give clinicians any information on the pressure waveform itself. Furthermore, measurement of systolic and diastolic blood pressure taken from a *peripheral* artery (e.g. the brachial artery) is not directly relevant to the health needs of the heart, which is much more sensitive to the central aortic pressure. Indeed, the CAFE wing of the ASCOT trial (Williams *et al*. 2006) points out that the central aortic and peripheral arterial systolic pressures differ in their responses to β-adrenoceptor blocking (atenolol) and calcium channel blocking (amlodipine) antihypertensive drugs; both types of antihypertensive drug appear to reduce systolic blood pressure in the peripheral artery but only the calcium channel blocker, amlodipine, reduces systolic pressure in the aorta. This, it is argued, explains why amlodipine is more effective than atenolol in reducing cardiac events, despite their apparently similar antihypertensive efficacy as assessed from pressure measurements at the brachial (peripheral) artery. Nichols and O'Rourke (2005) emphasize that knowledge of the difference between central and peripheral arterial pressure waveforms aids diagnosis in vascular ageing. The diastolic pressure is not greatly different between the central aorta and large peripheral arteries (e.g. brachial, radial); diastolic pressure decreases slightly as the pressure wave propagates from central to peripheral arteries. However, the systolic pressure increases markedly as the waveform travels to the periphery. This amplification phenomenon is due to at least two factors: i) the forward incident waves summating with reflected waves from the peripheral small arteries and arterioles, ii) the gradual increase in elastic modulus (stiffening) of arteries progressing peripherally from the ascending aorta, which is very distensible and has low elastic modulus. This difference is marked in young humans, where pressure pulse amplification is obvious (Wilkinson *et al*.,

2001). However, the amplification gradually becomes less with the ageing arterial system, when the aorta becomes stiffer so its elastic modulus increases to values equivalent to that of peripheral arteries.

The HDI PulseWave system analyses recordings of peripheral arterial pressure waveforms obtained non-invasively by tonometry or by a finger pulse monitor. The software of the HDI PulseWave system has an algorithm that analyses the diastolic decay of peripheral arterial pressure waveforms (as per Goldwyn and Watt, 1976; Watt and Burrus, 1976) and calculates compliance of large capacitance arteries (assigned C1) and oscillatory compliance of small peripheral arteries (assigned C2). C1 and more so C2 are decreased by hypertension and heart failure (Finkelstein et al., 1985; McVeigh *et al*., 1991; Cohn *et al*., 1995). The reliability of the HDI PulseWave system in terms of haemodynamic data obtained is debated (Segers *et al*., 1997, 2001; Resnick *et al*., 2001; Rietzschel *et al*., 2001; Manning *et al*., 2002). The clinical application of the HDI PulseWave system remains to be established (Oliver and Webb, 2003).

The PulseTrace system analyses the pressure pulse waveform of a digital artery – the pulse is detected by a finger monitor. The software algorithm derives values from the shape of the pulse waveform, namely the dicrotic notch (Figure 1.1), and is used to assess vascular endothelial function and, more specifically, nitric oxide function (Chowienczyk *et al*., 1999; Millasseau *et al*., 2000). This aspect is particularly relevant to the discussion in the following paragraphs.

New technology is important but so also are simple diagnostic procedures. A device for *non-invasive* recording of arterial pulse waveforms along with a *non-invasive* diagnostic procedure would be ideal. Together these could be employed in GP clinics as an "early-warning" defence against vascular diseases such as atherosclerosis (discussed below); this would help to avoid delays in treatment. An important example of an unmet clinical need of this type is the assessment of vascular nitric oxide bioactivity, which is dependent on vascular endothelial function. Basal vascular nitric oxide bioactivity does not vary much between patient groups and controls but decreased *stimulated* release of nitric oxide does occur in patients with vascular disease. Thus, Chowienczyk *et al*. (1999) used albuterol as a stimulus for nitric oxide release from the vascular endothelium; albuterol (given by inhalation) lowered the dicrotic notch (see below) of the pulse waveform as recorded from the digital artery using photoplethysmography, but this effect of albuterol was impaired in type II diabetics, indicating vascular endothelial dysfunction in these patients. We speculate that it may also be possible to use insulin or sugar in this way. Insulin is known to cause release of nitric oxide from healthy vascular endothelium (Steinberg *et al*., 1994; Baron, 1996, 1999,

2002); raised serum insulin (hence raised nitric oxide) alters the arterial pulse waveform (Westerbacka *et al*., 1999). This alteration also results from acute hyperglycaemia induced easily by ingestion of glucose solution, which raises serum insulin levels (Wilkinson *et al*., 1998) – waveforms, recorded in these two studies with the SphygmoCor system, could be assessed for indications of vascular endothelial dysfunction.

Development of techniques and procedures for assessing vascular nitric oxide bioactivity, dependent on vascular endothelial function, is particularly important because of the key roles played by nitric oxide in vascular physiology and pathology. Nitric oxide is produced from the endothelial cell layer that lines the lumen of blood vessels (Shimokawa and Vanhoutte, 1997; Fleming and Busse, 1999; Mombouli and Vanhoutte, 1999). Nitric oxide is, to list a few, anti-atherogenic, anti-proliferative, it inhibits adhesion of platelets and leukocytes to the vessel wall, relaxes smooth muscle, maintains vascular function and vessel distensibility (Shimokawa, 1999; Drexler and Hornig, 1999; John and Schmeider, 2000). Some common conditions which greatly increase the risk of endothelial dysfunction, hence impair vascular nitric oxide production and bioactivity, are tobacco smoking, hypertension, diabetes types I & II, obesity, diet rich in fats (Widlansky *et al*., 2003; Endemann and Schiffrin, 2004; Unal *et al*., 2004); smoking is one of the worst risk factors (Unal *et al*., 2004).

If the vascular endothelium of elastic arteries is damaged or becomes dysfunctional and nitric oxide production is impaired, atherosclerosis ensues (Celermajer, 1997; Shimokawa, 1999). Atherosclerosis is a major cause of disability (peripheral vascular disease, stroke, congestive heart failure) and death (cardiac arrest) in the Western population (Ross, 1993; Glass and Witztum, 2001; Lusis, 2000). Atherosclerosis is not an age dependent disease as it can affect arteries of both young and elderly people, and it does increase with age (Ross, 1993; Sloop *et al*. 1998; Lusis, 2000). It is an inflammatory disease occurring under the vascular endothelial lining of the lumen of large and medium sized arteries (Ross, 1999; Lusis, 2000; Glass, 2001; Libby, 2001; Libby *et al*., 2002). The disease progresses to form plaques which increase in size and so encroach into the lumen of the artery. In response to plaque development, the affected part of the artery can remodel to maintain its lumen diameter to allow un-restricted passage of blood; eventually this remodelling process halts, the plaque continues to increase, resulting in a stenosis which compromises blood flow, so downstream organs become starved of blood, become ischaemic and eventually necrotic when the supply of blood is decreased to insufficiency. Stenotic arteries are certainly a health problem but by far the greatest number of atherosclerotic vascular accidents are due to plaque rupture. Depending on the plaque structure, plaque exists as either stable or unstable plaque; the latter tend to rupture, exposing their highly thrombogenic contents to the blood – thrombogenesis is rapid and either swiftly blocks the affected artery or embolises

to cause more wide spread blockage downstream (Falk, 1992; Falk *et al*., 1995; Davies, 1996; Libby, 2001; Naghavi *et al*, 2003).

Since a dysfunctional vascular endothelium greatly increases the risk of atherosclerosis, and many of the population succumb to atherosclerosis with its attendant morbid catastrophic events, an “early-warning system” (mentioned above) for the early detection and diagnosis of vascular endothelial dysfunction and reduced bioactivity of vascular nitric oxide would be of great clinical value. A number of investigators have suggested using the height of the dicrotic notch as an indicator. The pressure pulse of a peripheral artery (human digital artery; rabbit central ear artery) has a waveform that is characterised by a distinct dicrotic notch (see also Chowienczyk *et al*., 1999). From experiments using rabbits, Weinberg *et al*. (2001), extending earlier results of Klemsdal *et al*. (1994), observed that intravenous doses of acetylcholine, which stimulates endothelial cell release of nitric oxide (increasing vascular nitric oxide bioactivity), caused the dicrotic notch to fall in relation to the overall pulse amplitude (Figure 1.1). Conversely, intravenous doses of L-NAME which reduces endothelial cell production of nitric oxide (decreasing vascular nitric oxide bioactivity) caused the dicrotic notch to rise in relation to the overall pulse amplitude (Figure 1.1). These effects on the level of dicrotic notch in relation to the overall pulse amplitude seemed to be specific to vascular nitric oxide bioactivity since other drugs which affected arterial function independently of vascular nitric oxide bioactivity did not affect the dicrotic notch (Nier *et al*., 2008).

Nier, (2007) and Nier and Weinberg, (2007) also investigated *in vivo* the effect of raised serum insulin and glucose levels on the arterial pulse waveform of the central ear artery of rabbits; they observed that insulin or glucose lowered the dicrotic notch of the waveform, an effect they suggested was due to released vascular nitric oxide. Chapter 4 of this thesis describes experiments to determine what haemodynamic changes occur in response to changes in nitric oxide bioactivity to cause these characteristic changes in the peripheral arterial pulse waveform.

FIGURE 1.1: Peripheral Arterial Pulse Waveform of the Rabbit Central Ear Artery showing the Effects of L-NAME and Acetylcholine on the Height of the Dicrotic Notch Relative to the Pulse Amplitude.

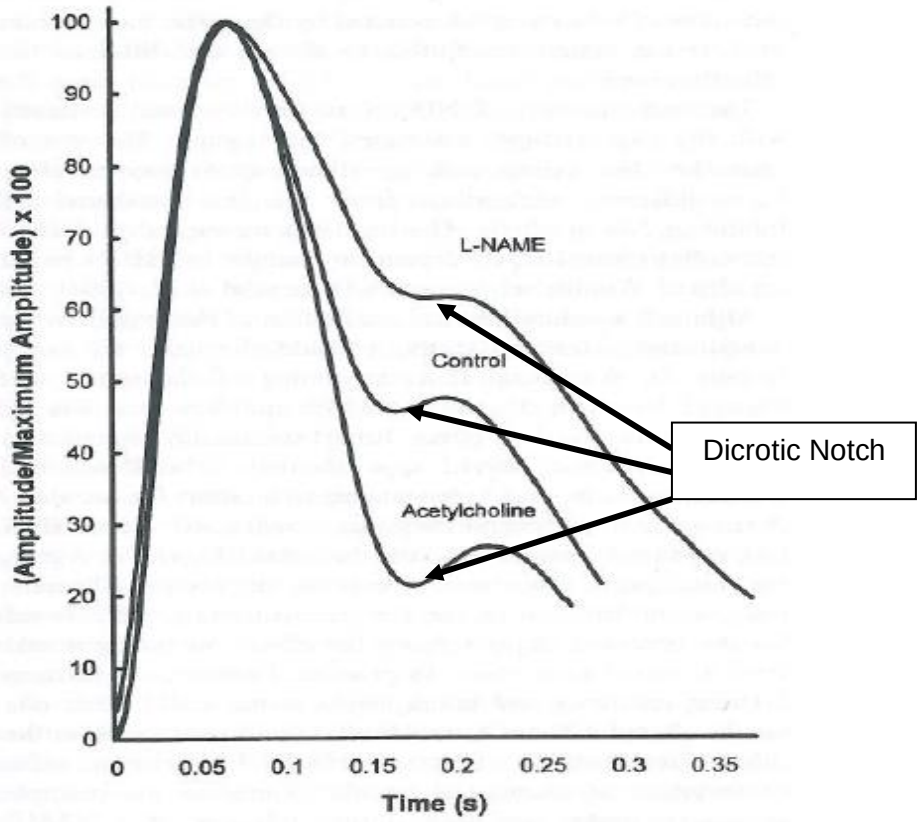

Modified from Weinberg *et al*., 2001

Effects of age on the arterial system are also the subject of a later chapter of this thesis. With increasing age, nitric oxide bioactivity tends to decrease, PWV tends to increase (at least after childhood), and the risk of cardiovascular disease increases. Vascular ageing is a general term for the deterioration of health and function of the vascular system over time. This deterioration can occur sooner (premature ageing) or later in life. When considering the effects of age, different types of cardiovascular disease have to be distinguished. The terms *athero*sclerosis and *arterio*sclerosis are often used synonymously. Nichols and O'Rourke (1990, 1998, and 2005) comment on the two terms and recommend that *athero*sclerosis be used to refer to the disease described above and that *arterio*sclerosis be the term to refer to the process of vascular ageing, though, quote: "*recognising of course that all conditions may be seen together*". Robert (1999) advocates classifying the major vascular diseases into two classes, namely *atheromatosis* and *arteriosclerosis*; with details from Robert (1999) these definitions may be construed:

> *Atheromatosis* is the process of lipid lesion development and then lipidic plaque formation at the intima of the arterial wall. This process can and does start early in life, being frequently observed in children who consume inadequate diets rich in saturated fat and cholesterol.
>
> *Arteriosclerosis* is the process of arterial wall thickening and increased stiffening characterised by increased collagen-elastin ratio and diffuse deposition of calcium and lipids (the latter by a process different to that of atheromatosis). It does appear to be mainly a vascular condition of the elderly.
>
> *(Athero-* means *fat* or *gruel*, describing the substance within plaque; *-sclerosis* means hardening).

However, Robert (1999) pointed out that the separation of these two processes is artificial for human pathology since most autopsies report atheromatous plaques and arteriosclerotic modifications existing together in the vascular wall. Thus, according to Robert (1999), Marchand proposed to designate the human lesion by the combined term of *atheroarteriosclerosis*. For the purpose of this thesis the term atherosclerosis rather than atheromatosis is used for the intimal process of lipid lesion and plaque development; the term arteriosclerosis is used for the diffuse ageing process of the vascular wall.

As noted, atherosclerosis can affect arteries of young and elderly people, but its prevalence generally increases with age (Ross, 1993; Sloop *et al*. 1998; Lusis, 2000). The prevalence also depends on lifestyle (e.g. smoking, diet) and pre-disposing risk factors (e.g. diabetes, genetic factors). Sloop *et al*. (1998) observed that the distribution of atherosclerotic lesions

around the ostia of arteries branching off the aorta is also age-dependent. Weinberg and co-workers have observed similarly in experiments with rabbits (Barnes and Weinberg, 1998; Staughton *et al*., 2001; Weinberg, 2002, 2004). Thus atherosclerosis might have features in its development that respond to vascular ageing. Sloop *et al*. (1998) hypothesised that age-related patterns of atherosclerotic lesions in the aortic luminal wall about the intercostal ostia relate to age-related changes in aortic blood flow characteristics, namely the magnitudes and interactions of retrograde (late systole to early diastole) and antegrade (late diastole) blood flow in the aorta and at the intercostal ostia; retrograde and antegrade interaction was postulated to be modulated by arterial elasticity, which decreases with increasing age – retrograde flow decreases with increased arterial stiffness. Thus, physical properties of the aorta appear to influence atherogenesis.

A study by Hunt *et al*. (2001) comparing the physical properties of aortas of hyperlipidaemic and normal rabbits found that, even *before* development of atherosclerotic plaque, the hyperlipidaemic rabbits had much reduced aortic distensibility, increased aortic β-stiffness index (defined by Hayashi *et al*., 1974, 1980; Kawasaki *et al*., 1987) and increased aortic wall residual stress-strain (Fung and Liu, 1989; Humphrey, 1995), thus indicating that hyperlipidaemia, as well as age, can affect the physical make-up of aortas of rabbits.

One of the pathologies of ageing is the process of non-enzymatic glycosylation (glycation) of proteins (Figure 1.2) (Bierhaus *et al*., 1998; Ulrich and Cerami, 2001). The process in artery walls, especially of the elastic conduit arteries, involves reducing sugars (e.g. glucose) reacting with the protein chains of collagen (a major structural element of artery walls) and elastin (a major structural element for Windkessel function of aorta and conduit arteries) to form protein-protein cross-links; these cross-links “stiffen” the collagen and elastin structures (Brownlee *et al*., 1988; Reddy, 2004; Brüel and Oxland, 1996). The cross-linked proteins are irreversible adducts of the Maillard reaction and referred to as Advanced Glycation End products (AGEs) (Figure 1.2). MacDonald *et al*. (1992) were first to demonstrate a relationship between AGEs and age (29-82 years) using human mesenteric arteries and collagen-linked fluorescence which reflects AGE accumulation. Chapter 5 has more details on AGEs with the view of experimental application. Briefly, experiments were designed to mimic vascular ageing in rabbits by supplementing their diet with 10% fructose drink for 2 weeks (fructose is potent in forming AGEs – Schalkwijk *et al*., 2004), then to compare haemodynamic data from fructose treated rabbits with controls.

AGEs certainly exacerbate, if not contribute to initiating, atherogenesis. Since AGEs are associated with vascular ageing, then perhaps AGEs have a contributory role in age-dependent worsening of atherosclerosis. One could even hypothesise that AGEs distribute

in the aorta in an age dependent manner and mediate age-dependent patterns of atheromatous fatty streaks and plaque. AGEs chemically react with endothelium-derived nitric oxide thereby decreasing its bioactivity and thus reducing its vasodilatory, vascular protective and anti-proliferative functions (Bucala *et al*., 1991; Vlassara *et al*., 1994; Stitt *et al*., 1997). AGEs can also induce expression of the vasoconstrictor endothelin-1 (Bierhaus *et al*., 1998). Furthermore, glycation of LDL results in AGEs of LDL; LDL-AGEs are atherogenic and like oxidised-LDL are not recognised by the LDL clearance receptors of the hepatic system (Stitt *et al*., 1997; Tabas, 1999; Bierhaus *et al*., 1998). Thus, AGEs are toxic so their elimination is important. Excretion in urine is one route of elimination, while another is by endocytosis via cell surface AGE-receptors. Endocytosis enables degradation and turnover of AGEs; however, the same cell surface AGE-receptors, on binding with AGEs, stimulate production of reactive oxygen species, release of cytokines and growth factors. Thus, AGE receptors have a 'double-edge sword' reputation, on the one hand they eliminate toxic AGEs but on the other hand they are stimulated by AGEs to promote overt growth of tissues and inflammatory processes (Bierhaus *et al*., 1998; Schmidt *et al*., 1999; Ulrich and Cerami, 2001; Vlassara, 2001).

FIGURE 1.2: Non-enzymatic Glycosylation (Glycation) of Proteins and Formation of AGEs by the Maillard Reaction.

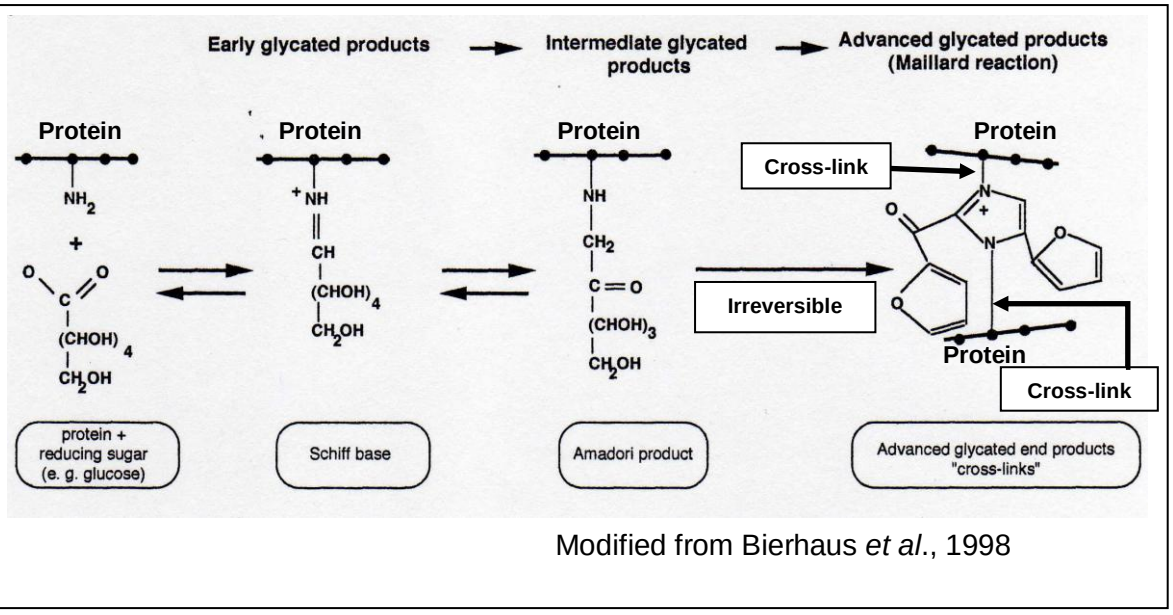

Modified from Bierhaus *et al*., 1998

Brownlee *et al*. (1986) were the first to demonstrate *in vitro* and *in vivo* that aminoguanidine (a small nucleophilic hydrazine compound) could inhibit formation of glycosylated protein-protein cross-links. Aminoguanidine reacts with the Amadori product (Figure 1.2) to form a substituted Amadori product that is not reactive (Brownlee *et al*., 1988; Stitt *et al*., 1997), thereby inhibiting the reaction from proceeding to the irreversible Maillard reaction which forms AGEs (Figure 1.2). Aminoguanidine is classed as an *inhibitor* of AGE formation and is potent and specific in this action (Stitt *et al*., 1997). This finding opened the way for potential therapies to treat complications due to AGE formation in diabetics.

Huijberts *et al.* (1993) observed that diabetic rats treated with aminoguanidine, compared to control rats, had increased carotid arterial compliance, decreased aortic characteristic impedance, decreased ratio of left ventricular oscillatory power output / total power output and decreased arterial pulse pressure. Thus aminoguanidine increased vascular compliance and improved left ventricular-arterial coupling, indicating attenuation of AGE formation; this was similarly found in an ageing study with normotensive non-diabetic rats (Corman *et al*., 1998). Lin *et al*., (2004) observed that aminoguanidine prevented fructose-induced arterial stiffening as indicated by decreases in aortic characteristic impedance and aortic pulse wave speed. (An attempt to accelerate vascular ageing with fructose feeding is described in Chapter 5). With regard to atherosclerosis in humans exhibiting diabetic nephropathy, aminoguanidine decreased LDL-cholesterol (-28%), total cholesterol (-19%) and triglycerides (-19) (Stitt *et al*., 1997). Bierhaus *et al*. (1998) reviewed ameliorative effects of aminoguanidine on experimental diabetic pathologies of: glomerular basement membrane; retina; peripheral nerve. In non-diabetic rats aminoguanidine ameliorated the age-associated increase in serum and tissue AGEs and age-dependent decline in cardiovascular and renal function.

Aminoguanidine prevents ongoing formation of AGEs but it does not destroy AGEs once they exist, (Bierhaus *et al*., 1998). The clinical requirement to clear tissues and matrix structures of irreversibly bound AGEs has initiated research to obtain compounds that will cleave the cross-links of AGEs to structural proteins (cross-linking AGE is shown diagrammatically in Figure 1.2). The first such compound, a *breaker* of AGE cross-links, was N-phenacylthiazolium bromide (PTB) which reacts with and cleaves covalent AGE-protein cross-links *in vitro* and *in vivo* (Vasan *et al*., 1996). PTB was the prototype of cross-link, or AGE, breakers; ALT-711 (phenyl-4,5-dimethylthazolium chloride) was synthesised and is a stable derivative of PTB (Doggrell, 2001). ALT-711 has the generic name Alagebrium chloride.

ALT-711 (Alagebrium) administered to diabetic rats decreased their elevated arterial stiffness as measured by systemic arterial compliance, aortic characteristic impedance and carotid arterial distensibility and compliance (Wolffenbuttel *et al*., 1998). ALT-711 improved cardiac performance in aged dogs (Asif *et al*., 2000), aged primates (Vaitkevicius *et al*., 2001) and aged spontaneously hypertensive rats and aortic distensibility of the latter (Susic *et al*., 2004a & b). All these ameliorating effects of ALT-711 on arterial and cardiac performance were stated as due to breaking of AGE cross-links (Susic *et al*., 2004). Clinical trials were carried out with ALT-711, these were: DIAMOND; SAPPHIRE; SILVER; SPECTRA; PEDESTAL. The first trial, DIAMOND, included a section for evaluation of the effect of ALT-711 on total arterial compliance in elderly patients with indications of stiffened vasculature (arterial pulse pressures ≥60mmHg; systolic pressures ≥140mmHg) – it was found that ALT-711 increased arterial compliance (Kass *et al*., 2001; Bakris *et al*., 2004). This finding indicated that ALT-711 could have efficacy for treatment of systolic hypertension and so the three clinical trials SAPPHIRE, SILVER, and SPECTRA were set up to establish its effects on systolic hypertension. Findings were equivocal in one study where results were confounded by systolic blood pressure decreasing across all dose groups including the placebo group; however, in the study for ambulatory blood pressure measurements ALT-711 showed significant efficacy in decreasing systolic blood pressure (Bakris *et al*., 2004).

Let us now consider systolic hypertension, which is also referred to as isolated systolic hypertension (ISH). ISH is a condition of reduced large artery distensibility, i.e. stiffening of the large elastic arteries, especially the aorta. ISH is defined as systolic blood pressure (SBP) over diastolic blood pressure (DBP) of these values:

SBP/DBP	
≥140/<90 mmHg	(Guidelines for the Management of Hypertension)
≥160/<90 mmHg	(Framingham & SHEP trials)
≥180/<90 mmHg	(STOP-HT trial)

ISH is a condition that commonly afflicts the elderly, is poorly controlled with current anti-hypertensive treatments (Lloyd-Jones *et al*., 2000; Alam *et al*., 2003; Salvetti and Versari, 2003), is a risk factor for stroke, congestive heart failure, and end-organ damage (e.g. retina, kidneys). Because ISH is associated with amplified systolic pressures (Hansson, 1987; Lever, 1987; Borhani *et al*., 1991; Kaplan *et al*., 1992; Waeber, 2003; Chaudhry et al., 2004) and wide pulse pressure (Domanski *et al*., 1999, 2002; ; Benetos *et al*., 1997; Franklin *et al*., 1999; Asmar *et al*., 2001; Laurent *et al*., 2001; Vaccarino *et al*., 2001; Wilkinson and Cockcroft, 2000), it has a deleterious impact on cardiac left ventricular function by raising cardiac afterload hence a risk factor for congestive heart failure. Such ailments burden

medical resources, thus, prevention or amelioration of ISH would help to maintain a healthy elderly population, a population that is continuing to increase.

ISH results from a pathological process that Nichols and O'Rourke (2005) refer to as *arterio*sclerosis, rather than *athero*sclerosis (see above and also Robert, 1999), and is an abnormally enhanced ageing process of elastic arteries. Greenwald (2007) gives a clear review on factors that are involved in arteriosclerosis. Certainly arteriosclerosis is a result of fragmentation of elastic laminae and elastic fibres with diffuse deposition of calcium and lipid *within* the artery wall (Robert 1999). Another cause of arteriosclerosis is time-dependent, non-enzymatic, protein glycosylation of collagen and elastin. This has already been discussed above, but further consequences of it for elastin are added here. Elastin is not as long-lived as collagen and when its normal nature is changed it becomes susceptible to degradation by elastases to produce elastin peptides. Levels of elastases progressively increase in the ageing vasculature, particularly in the ageing human aorta. Concomitant increased breakdown of elastin occurs with resultant increase of soluble elastin peptides released into the plasma (Robert, 1996, 1999). Elastin peptides are pharmacologically active. Elastin and its peptides bind to a receptor comprising a protein complex that forms a trans-membrane link between the extracellular matrix and intracellular compartment (Mecham *et al*., 1989); the extra-cellular (membrane surface) subunit is that part to which elastin and its peptides bind, as does laminin, lactose and the synthetic elastin peptide VGVAPG (Mecham *et al*., 1989). Robert (1996; 1999) refers to this receptor as the elastin-laminin receptor. Such receptors exist on vascular smooth muscle cells and endothelial cells; when those on endothelial cells are stimulated by elastin or elastin peptides they mediate nitric oxide dependent vasorelaxation (Faury *et al*., 1995). This vasorelaxing effect exhibits age-dependency; it is weak in aortas of young rats (≤2 months), marked in those of 4 months and wanes progressively with age in those of old rats (≥12 months) (Robert, 1999). The elastin-laminin receptor on endothelial cells can also mediate production of superoxide (Robert 1996; 1999), it is suggested that this takes place when the receptor is excessively stimulated by elastin peptides. As stated above, elastin peptides increase in the plasma as ageing proceeds, this provides the potential for excessive and maintained stimulation of the receptor and such stimulation is thought to cause concomitant release of both nitric oxide and superoxide, which then combine to produce the toxic peroxynitrite anion ($ONOO^-$). Normally, $ONOO^-$ is neutralised by reduced glutathione, the production of which declines with age (Robert, 1996). Thus, excessive stimulation of the elastin-laminin receptor in old-age effectively causes endothelial dysfunction, so damaging the vascular structures as to lead to arteriosclerosis and associated vascular diseases, e.g. ISH. Maguire *et al*. (2003)

observed vasoconstrictor responses to elastin peptide VGVAPG in arteries sampled from elderly patients. Simulation of stiffened aorta and iliac arteries is the topic of Chapter 7.

So far, consideration has been given to the aorta and large elastic conduit arteries. However, the distal muscular arteries are not affected by ageing and perhaps might have some compensatory functions to overall systemic arterial compliance as the elastic arteries stiffen with age (Boutouyrie *et al*., 1992; Bortolotto *et al*., 1999; van der Heijden-Spek *et al*., 2000).

Wave reflections and their role in determining arterial blood pressure and flow waveforms are a major part of this thesis. Are reflected waves a principal component of the raised systolic pressure in ISH? Or is the raised systolic pressure a direct result of reduced ("stiffened") Windkessel function of the aorta and/or large elastic conduit arteries? This is a debated topic. The vasculature, certainly the healthy vasculature, is "designed" in a manner that would be expected to absorb reflections (McDonald, 1974 – Chap.12, an opinion expressed by Womersley). The concept of "wave trapping" has been proposed by Parker (2009). Baksi *et al*. (2009) have proposed from meta-analysis of past published data for arterial pulse waveforms of 13,770 subjects that evidence is weak for any significant shift in timing of reflections arriving in diastole to arriving in systole with progression of age. If timing of reflections in the aorta do not change significantly with age then this brings into question the interpretation of data of Murgo *et al*. (1980) for pressure waveforms categorised as Types A, B, C (also latterly Type D – Nichols and O'Rourke 2005) on which the interpretation of SphygmoCor data is dependent. Mitchell *et al*. (2004) and Mitchell (2009) propose that increase in central aortic stiffness, change in aortic geometry and increased forward wave amplitude, rather than wave reflection, are responsible for most of the increase in pulse pressure in the elderly. Consistent with this are the findings of Davies *et al*. (2009) that arterial reservoir (Windkessel) function rather than wave reflection changes markedly with ageing, and that arterial reservoir function mainly determines the augmentation index.

Blood pressure and flow waveforms are much studied in the ascending aorta, however for this thesis blood pressure and flow waveforms were studied in the abdominal aorta of rabbits (Chapters 4 & 5) and in the abdominal aorta section of a polyurethane model of a human aorta (Chapter 7). The aim of this thesis was to determine what relationship, if any, abdominal aortic blood pressure and flow wave phenomena might have with blood pressure and flow waveforms in distal arteries, e.g. in the central ear, or auricular, artery of rabbits. Such studies might contribute to further our understanding of the pulse waveform in the human digital artery for assessment of cardiovascular health.

The chapters of the thesis are as follows. Chapter 2 gives a brief account of the theory and mathematics pertaining to separation of the measured pressure pulse into reservoir (Windkessel) pressure and wave pressure along with wave intensity analysis in the time domain; wave speed is also considered. Chapter 3 gives an account on the general methodology for all the *in vivo* experiments with rabbits. Chapter 4 discusses experiments designed to alter vascular nitric oxide bioactivity and the effect of this on pressure pulse waveforms. Chapter 5 looks into the effects of fructose diet on haemodynamics in immature and mature rabbits; also comparison is made between haemodynamics of immature and mature rabbits. Chapter 6 describes the assessment of polyurethane material for manufacture of the model aorta, and chapter 7 describes experiments with the model aorta simulating disease of stiffening the aorta. Chapter 8 gives a final discussion on the work with retrospective comment on limitations of experiments and prospective comment on technical improvements for future experiments; finally conclusions are stated.

CHAPTER 2

THEORETICAL AND MATHEMATICAL ASPECTS

Since arterial waveforms are the subject of this thesis, it is appropriate to define the term 'wave'. Arterial waves propagate, some text-book definitions for propagated waves are:

A disturbance travelling through a medium by means of the periodic motion of its particles is a wave motion (Verwiebe *et al*., 1962).

Wave motion is often defined as the propagation of a disturbance through a medium without the translation of the medium (McKenzie, 1965).

A progressive or travelling wave consists of a disturbance moving from a source to surrounding places as a result of which energy is transferred from one point to another (Duncan, 1978).

In short, a wave is a propagating disturbance.

In the vascular system, ejection of a volume (the stroke volume) of blood from the heart during systole into the ascending aorta expands the walls of the ascending aorta, i.e. radial or circumferential distension, simultaneously initiating a pressure pulse. The pressure and distension decay quasi-exponentially during diastole. This pressure pulse and accompanying wall distension propagate as an incident wave along the aorta and from the aorta along the large, medium, small conduit arteries and peripheral arteries. The wave encounters discontinuities, e.g. tapering of the aorta, bifurcations and branching, and finally the arterioles; discontinuities reflect some of the wave energy and these reflections interact with later parts or instances of the incident wave so changing its shape as it propagates away from the heart (*Blood Flow in Arteries* - McDonald 1960, 1974; *McDonald's Blood Flow in Arteries* - Nichols and O'Rourke 1990, 1998, 2005; *Hemodynamics* - Milnor 1982, 1989; *The Mechanics of the Circulation* - Caro, Pedley, Schroter and Seed 1978, 2011). Thus propagating waves have velocity and some of their energy is reflected. Pulse wave velocity, or wave speed, and wave reflection are important aspects of wave phenomena in the cardiovascular system and are discussed further. Note, however, that this chapter is not intended as an in depth treatise on the theory and mathematics applied to the study of

cardiovascular waveforms since this thesis does not explore these principles but, instead, uses them as tools to generate and analyse haemodynamic data.

Pulse wave velocity (PWV) is the *regional* wave speed over a measured length of artery and was measured by the foot-to-foot method; the practical aspects of this measurement are discussed in Chapter 3. Furthermore, the *local* wave speed at a position in an artery was also measured; this measurement was made by use of the PU-loop method which is discussed below.

Any given phase of the arterial pulse wave (the systolic foot in this case) travels at the phase velocity. Phase velocity, c_{ph}, is given by:

$$c_{ph} = \frac{2\pi f \Delta x}{\Delta\varphi} \quad \text{(stated in Milner, 1989)} \ldots\ldots\ldots\ldots\ldots\ldots\ldots\ldots\ldots\ldots \text{(Eq. 2.1)}$$

where:
$f =$ harmonic frequency
$\Delta x =$ distance between measurement locations
$\Delta\varphi =$ phase difference between measurement locations

Phase velocity may depend on frequency, a property known as wave dispersion. Hence PWV can be expressed as the phase velocity at different harmonic frequencies (the fundamental being that of heart rate). Measured phase velocity may also be affected by reflections

'*True* phase velocity' is that measured when no reflections exist (Milnor, 1989). When phase velocity is measured *in vivo* or in model circulations where reflected waves abound, it is referred to as the '*apparent* phase velocity' (Malindzak and Meredith, 1970; Segers *et al.*, 1998; Segers *et al.*, 2000) and is ascribed c_{app}. The true phase velocity is close to the average of apparent phase velocities at harmonic frequencies greater than 2Hz – the significance of these higher frequency harmonics is that they are free of reflections. (This is also the frequency range of the input impedances whose average is the characteristic impedance; in the absence of wave reflections, characteristic impedance is equal to PWV multiplied by the density of blood). Average apparent phase velocity is close to the foot-to-foot PWV if the latter is measured at locations distant from sites of wave reflections, so that the measurements are not contaminated by reflections occurring early in the cardiac cycle. (Reflections from the previous beat are assumed to have died away by late diastole/early systole).

Foot-to-foot PWV is affected by the structural composition and geometry of the artery or arteries encountered during its travel. That of course underlies its clinical and experimental

utility, in particular for assessing arterial stiffness. The Moens-Kortweg equation shows that PWV depends on incremental Young's modulus E_{inc}, wall thickness h, vessel radius r and the density of blood ρ, as follows:

$$PWV = \sqrt{\frac{E_{inc} \cdot h}{2r\rho}} \quad \text{(Eq. 2.2)}$$

The PWV so measured might represent that for a given artery if over a short length of the artery or an average for several arteries if travelled over a series of arteries. However, average PWV is not a simple arithmetic average but is an average weighted to those arteries in the series with the slowest PWV. With this in mind, for the work of this thesis, PWV was measured only over a regional distance of 50mm (Chapter 3).

In addition to measurement of foot-to-foot PWV (i.e. *regional* wave speed), another measure, namely for *local* wave speed, at a position in an artery was obtained from the ratio of pressure gradient, *dP*, to the flow velocity gradient, *dU*, of the pressure and velocity pulse (Khir *et al*., 2001; Khir and Parker, 2002; Khir *et al*., 2004; Khir and Parker, 2005). This relation for local wave speed (c) in an artery is derived from the water-hammer equation:

$$\rho c_{\pm} = \pm \frac{dP_{\pm}}{dU_{\pm}} \ (\text{water hammer equation}) \quad \text{(Eq. 2.3)}$$

thus:

$$c_{\pm} = \pm \frac{dP_{\pm}}{dU_{\pm}} . \frac{1}{\rho} \quad \text{(Eq. 2.4)}$$

$\rho = \text{density of blood } 1050 \text{ kg. m}^{-3}$
$\pm$ subscript denotes $+$ for incident (forward)going and $-$ for reflected (backward)going.

This equation applies when no reflections exist, hence $\frac{dP}{dU}$ is usually measured during early systole since that is when pressure and flow pulses are most likely to be reflection-free. Values for $\frac{dP}{dU}$ are obtained by plotting pulse pressure against the associated flow velocity to obtain pressure-velocity loops (Figure 2.2) (Khir *et al*., 2001; Khir and Parker, 2002; Khir *et al*., 2004; Khir and Parker, 2005); the loop shows linearity in early systole, and it is the slope of this linear portion that gives c. Furthermore, the water hammer equation applies in a frictionless system which is assumed in large arteries such as the aorta.

There are other measures of local wave speed which have not been applied in the work of this thesis; they are: 'sum of squares', lnDU-loop and D^2P-loop (D = vessel diameter; U =

blood flow velocity; *P* = blood pressure). The 'sum of squares' has been applied clinically (Davies *et al*., 2006) and lnDU-loop was proposed by Feng and Khir (2010). All measures have recently been compared using 1-D numerical modelling (Alastruey, 2011).

As already noted, local wave speed, *c*, relates closely to characteristic impedance which, derived in the time domain, is the ratio of the gradients *dP* to *dQ*, where *Q* is volume flow (Dujardin and Stone, 1981; Li, 1986; Mitchell *et al*., 1997 and 2001).

Wave reflections and wave travel in general are further analysed using methods developed by Parker and co-workers (Parker, 2009). A wave can be repeated many times uninterrupted and evenly, as in a sinusoidal wave train, or can occur as a single event (pulse). Parker (2009) noted that waves can be analysed in *two* ways, either as a summation of sinusoidal wavetrains each as a harmonic component (the Fourier concept – analysis in the frequency domain) or as a summation of a sequence of small wavelets or wavefronts (analysis in the time domain); either way the component parts combine to give the observed wave. Arterial pressure pulses occur repetitively but if the heart misses a beat then little or no pulse results; thus although a pressure recording over many heartbeats gives the impression of a regularly repeating wave train, it is in fact composed of individual beats with little beat-to-beat interaction. Wave analysis is spoken of in terms of either frequency domain or time domain, however they are equivalent when used to separate forward-going and backward going waves (Hughes and Parker, 2009) because the two approaches both depend on a value for wave speed which, as stated above, relates directly to characteristic impedance (frequency domain) and the water hammer equation (time domain) (Hughes and Parker, 2009).

Fourier analysis is not used in this thesis; instead the approach is that of considering pressure and flow waves as individual events made up of wavelets. Thus following Parker and co-workers (Parker, 2009), data are analysed in the time domain rather than in the frequency domain. These methods of pulse wave analysis, termed Wave Intensity Analysis (WIA), used for physiological purposes in this thesis are also being explored and developed for clinical use (Koh *et al*., 1998; Jones *et al*., 2002; Zambanini *et al*., 2005; Curtis *et al*., 2007; Sugawara *et al*., 2009).

Wave theory applied to wave phenomena in the arterial system is built on three fundamental laws (Sherwin *et al*., 2003; Parker, 2009; Alastruey *et al*., 2009):

- Conservation of mass:

$$\frac{\partial A}{\partial t} + \frac{\partial (AU)}{\partial x} = 0 \quad \text{(Eq. 2.5)}$$

- Conservation of momentum:

$$\frac{\partial U}{\partial t} + U\frac{\partial U}{\partial x} + \frac{1}{\rho}\frac{\partial P}{\partial x} = \frac{f}{\rho A} \quad \text{(Eq. 2.6)}$$

- Tube law:

$$P = \frac{\beta}{A_0}\left(\sqrt{A} - \sqrt{A_0}\right); \qquad \beta(x) = \frac{4}{3}\sqrt{\pi}.hE \quad \text{(Eq. 2.7)}$$

Where:
A = cross-sectional area of the vessel lumen
A_0 = cross-sectional area of the vessel lumen at zero pressure
U = average axial velocity
P = average internal pressure over the cross-section
ρ = density of blood: 1050 Kg.m^{-3}
f = frictional force per unit length = -8μπU assuming Poiseuille's flow; μ is viscosity of blood 4 mPa s
β = elastic properties of the artery wall
h = vessel wall thickness
E = Young's modulus of vessel wall

Equations 2.5 – 2.7 form a system of hyperbolic partial differential equations; the solution to such a system can be obtained by the method of characteristics first proposed by Riemann (1859 & 1860 – as referenced in Parker, 2009 b & a respectively). Thus, the method of characteristics was utilised by Parker and Jones (1990) and Parker (2009) for WIA of arterial blood pressure and flow waves. Use of the method of characteristics has been reviewed by Bergel and Schultz (1972); it has been used for modelling fluid dynamics (Barnard *et al*., 1966 a, b) and haemodynamic analysis and modelling (Skalak 1972; Pythoud *et al*., 1996; Alastruey, 2006; Matthys *et al*., 2007). Although McDonald (1974) was one to popularise the use of Fourier analysis for haemodynamic data, he did so from choice, rather than preference, and did not consider it as superior to other methods; indeed, he acknowledged the method of characteristics as an alternative.

The water hammer equation (Eq. 2.3) follows from the algebraic process of method of characteristics and is fundamental to the relationship between changes in pressure and velocity in any wavefront (Parker, 2009):

With Eq. 2.3 in mind, the following algebra is taken from Parker, 2009.

Wave intensity, *dI*, is defined as:

$$dI = dPdU \quad \text{(Eq. 2.8)}$$

The SI units for wave intensity are $W.m^{-2}$, i.e. dimensions of [power][area]$^{-1}$; this is the energy flux per unit area of the propagating wave. For this thesis, wave intensity was considered in terms of wave energy, which is the integral of intensity:

$$wave\ energy = \int_{t_{start}}^{t_{end}} dIdt \quad \text{(Eq. 2.9)}$$

Where t_{start} is the initiation of the intensity curve from zero intensity, and t_{end} is the end of the intensity curve when it returns to zero intensity. For analysis of data, those points of initiation and end of intensity were selected subjectively from WIA plots (Figure 2.4) and mouse-clicked; a MATLAB routine was used for calculations (see Appendix: Extra Data). The SI units for wave energy are $J.m^{-2}$.

Wave intensity analysis (WIA) reveals two components of waves, namely compression and expansion waves (incident and reflected) (Figure 2.4).

However, Eq. 2.8 is the total wave intensity. For comprehensive WIA, wave separation is required to reveal incident (+) and reflected (-) wave components; thus:

$$dP = dP_+ + dP_- \quad \text{(Eq. 2.10)}$$
$$dU = dU_+ + dU_- \quad \text{(Eq. 2.11)}$$
$$dI = dI_+ + dI_- \quad \text{(Eq. 2.12)}$$

It follows, with the water hammer equation (Eq. 2.3):

$$dP_+ = \rho c dU_+ \quad for\ forward, incident, wavefronts\ (+) \quad \text{(Eq. 2.13)}$$
$$dP_- = -\rho c dU_- \quad for\ backward, reflected, wavefronts\ (-) \quad \text{(Eq. 2.14)}$$

that

$$dP_\pm = \frac{1}{2}(dP \pm \rho c dU) \quad \text{(Eq. 2.15)}$$

or equivalently

$$dU_\pm = \frac{1}{2}\left(dU \pm \frac{dP}{\rho c}\right) \quad \text{(Eq. 2.16)}$$

and

$$dI_{\pm} \equiv dP_{\pm} dU_{\pm} = \frac{\pm 1}{4\rho c}(dP \pm \rho c dU)^2 \quad \text{(Eq. 2.17)}$$

Another step in the analysis of data in this thesis is application of 'the reservoir-wave hypothesis' (Wang *et al*., 2003; Parker, 2009; Tyberg *et al*., 2009). This hypothesis proposes that arterial pressure comprises two components:

- *The reservoir pressure* which is the space-independent pressure during systole that distends the elastic conduit arteries followed by their return to decreased distension during diastole – this is the Windkessel function. In this thesis, the 'reservoir pressure' is stated as 'reservoir (Windkessel) pressure'.
- *The wave pressure* which propagates the incident arterial pressure pulse and interacts with reflected waves to shape the pulse waveform.

Thus, the 'measured (total) arterial pressure' pulse is the sum of the two component pressures: the 'reservoir (Windkessel) pressure' and the 'wave pressure'; the latter is derived by subtraction of reservoir (Windkessel) pressure from the measured (total) pressure (Figure 2.1). The reservoir-wave hypothesis sets out a mathematical model for calculation of reservoir (Windkessel) pressure and this is outline below.

The importance of the reservoir-wave hypothesis is that it describes the difference in the waveforms of arterial pressure and flow. The measured (total) pressure pulse waveform has a very different shape to that of the associated flow waveform. During diastole the pressure is decaying while there is little or no flow, certainly no flow decay curve, which could be associated with that of the pressure decay – this is clearly observed for pressure and flow in the ascending aorta. Subtraction of the reservoir pressure from the measured (total) pressure at the ascending aorta gives wave pressure whose waveform is almost exactly that of the associated flow waveform – zero pressure associated with zero flow during diastole (Wang *et al*., 2003). Thus, the reservoir-wave hypothesis challenges the validity of previous concepts of a large reflected wave during diastole that obliterates flow but yet supports the diastolic pressure decay. The reservoir-wave hypothesis unifies the time domain Windkessel theories with the frequency domain transmission-line theories of arterial haemodynamics.

Wang *et al*. (2003) and Tyberg *et al*. (2009) developed the reservoir-wave hypothesis for calculation of reservoir and wave pressures in the ascending aorta; their calculations used measured ascending aortic blood pressure and associated measured ascending aortic blood flow – the general solution is:

(from Wang *et al.*, 2003; Tyberg *et al.*, 2009):

$$P_{Wk}(t) - P_{\infty} = (P_0 - P_{\infty})e^{\frac{-t}{RC}} + e^{\frac{-t}{RC}} \int_{t_0}^{t} \frac{Q_{in}(t')}{C} e^{\frac{t'}{RC}} dt' \quad \text{(Eq. 2.18)}$$

Where:

P_{Wk} = reservoir or Windkessel pressure
P_{∞} = the asymptotic pressure of the diastolic exponential decay
P_0 = pressure at the onset of cardiac ejection, or end diastolic pressure at t_0
R = resistance of the peripheral systemic circulation, determined from experimental data

C = total systemic arterial compliance determined from experimental data
Q_{in} = stroke cardiac output which is 0 during diastole

During diastole when $Q_{in} = 0$, pressure is an exponential decay with time constant $\tau = RC$

Thus, once reservoir (Windkessel) pressure (P_{Wk}) is solved then wave pressure (P_W) can be obtained from measured (total) pressure (P_T):

$$P_W = P_T - P_{Wk} \quad \text{(Eq. 2.19)}$$

Davies *et al*. (2007), Aguado-Sierra *et al*. (2008) and Parker *et al*. (2011) proposed calculation of the reservoir pressure from the measured arterial pressure waveform *without* measurement of blood flow; the equation is:

(from Parker *et al.*, 2011):

$$\bar{P} - P_{\infty} = ae^{-(a+b)t} \int_0^t (P(t') - P_{\infty})\, e^{(a+b)t'} dt' + e^{-(a+b)t}(\bar{P}_d - P_{\infty}) \quad \text{(Eq. 2.20)}$$

Where:

$\bar{P}$ = reservoir or Windkessel pressure
a = is a rate constant (units of s^{-1}) and is derived from the approximation that Q_{in} is proportional to the wave pressure $(P - \bar{P})$ such that $Q_{in} = \lambda(P - \bar{P})$ and that $a = \lambda/C$; λ is a constant dependent on values such as local wave speed and cross-sectional area of aortic root (Aguado-Sierra *et al.*, 2008).
$b = 1/\tau$ and is a rate constant, units of s^{-1}
$\bar{P}_d$ = pressure at the onset of cardiac ejection, or end diastolic pressure at t_0

a, b and P_{∞} are found through a Matlab fitting algorithm developed by Prof. KH Parker, using the profile of the recorded pressure pulse waveform. The diastolic exponential decay is taken from the end-systolic start of the incisura to the end-diastolic nadir coinciding with the upstroke of pressure at inception of the next systole. The Matlab algorithm of Prof. KH Parker is named 'kreservoir_v10_simpsons' (see *within* the first Matlab algorithm and second in the Appendix).

It is the later approach of calculation, to obtain reservoir pressure from only the measured arterial pressure, which is applied in this thesis, along with using the Matlab algorithm as developed by Prof. KH Parker (see in Appendix). However, as stated in Chapter 1, the aim of this thesis was to study blood pressure waveforms in the abdominal aorta, thus consideration must therefore be given to the applicability of the above calculation and Matlab algorithm for analysis of blood pressure waveforms in the abdominal aorta. Aguado-Sierra *et al*. (2008) extended the concept put forward by Wang *et al*. (2003); the latter based their concept on the relationships of blood pressure and flow in the central, i.e. the ascending, aorta whereas Aguado-Sierra *et al*. (2008) extended the theory to measurements at an arbitrary location in (large) arteries i.e. at sites distal to the ascending aorta. Aguado-Sierra *et al*. (2008) based their proposal on two observations, namely:

i) that the diastolic pressure decay part of the waveform is similar at different sites in the aorta and arterial system;
ii) that the wave pressure, Pw, measured at any aortic site is approximately proportional to the blood flow waveform (cardiac output) in the ascending aorta.

If those two observations are true, Aguado-Sierra *et al*. (2008) reason that the reservoir pressure, P_{Wk}, can be determined from the measured pressure waveform, P_T, at an arbitrary site in the arterial tree. The truth of those two observations has not been demonstrated in this thesis because in the case of the *in vivo* experiments with rabbits it was decided not to extend dissection to thoracotomy; the latter would be required for access to the ascending aorta to measure blood flow at that site. Thus, Aguado-Sierra *et al*. (2008) put forward their calculation for use at aortic, or large arterial, sites distal to the ascending aorta. With that proposition in mind, though not tested in this thesis, the calculation was used as a tool for analysis of blood pressure waveforms in the abdominal aorta of rabbits (Chapters 4 and 5) and pressure waveforms in the abdominal aorta section of the polyurethane model of the human aorta (Chapter 7). Pw was used for WIA of data obtained from the rabbits. However, in the case of experiments with the polyurethane model aorta (Chapter 7), two wave intensity analyses were carried out, one using P_W which was obtained by the calculation proposed by Aguado-Sierra *et al*. (2008), and the other using P_T which, of course, does not require the calculation and acceptance of the two untested observations.

This thesis also considers the concept of wave reflection in the arterial system. Wave reflections occur wherever the properties of an artery change; the changes can be referred to as discontinuities or impedance mismatches, which can result from change of wall elastic modulus, change of diameter (vessel taper, discontinuities at bifurcations and branching).

As the incident wave meets a discontinuity some of its energy is reflected while the remainder transmits through the discontinuity; reflection in this thesis is measured as an index, namely Wave Reflection Index (WRI), and is simply:

$$WRI = \frac{(reflected\ energy)}{(incident\ energy)} \quad \text{(Eq. 2.21)}$$

The incident and reflected wave energies were obtained from WIA.

Figures 2.1, 2.2, 2.3 and 2.4, summarise this chapter with exemplary data obtained from the abdominal aorta of an anaesthetised rabbit and show how data of this thesis were analysed. This is explained in the following paragraphs.

Figure 2.1 (top panel) illustrates Eq. 2.19, showing three pressures, namely the measured (Total) pressure, P_T, along with its component pressures, calculated from Eq. 2.20, being reservoir (Windkessel) pressure, P_{Wk} (also sometimes denoted as RP in the thesis text) and wave pressure, Pw. Also shown in Figure 2.1 (bottom panel) is the associated blood flow velocity waveform which is similar in shape to that of wave pressure, Pw.

Figure 2.2 shows pressure-velocity loops (PU Loops) using P_T (top panel) or Pw (bottom panel); it is noted that the PU loop for the former and that for the latter, respectively, plot counter-clockwise or clockwise. The direction of plot is dependent on the closeness of similarity of the waveforms, P_T or Pw, with the velocity waveform. Indeed, if the pressure waveform is very closely proportional to the velocity waveform then an almost straight line is plotted (see Figure 2 in Wang *et al*., 2003).

Figure 2.3 shows plots of wave intensity analysis (WIA); the top panel shows WIA using P_T and the bottom panel shows WIA using Pw. Interestingly there is little difference between WIA using P_T or Pw. Figure 2.3 shows for example purpose only the two WIA plots obtained using P_T and Pw from one *in vivo* rabbit experiment; however, this was not done as an analysis for the rabbit experiments but, as stated above, only for the experiments with the polyurethane model human aorta.

Figure 2.4 gives details on the WIA plot showing the two intensities considered in the analyses, namely the compression wave and the expansion wave as incident and reflected. The transit time (Tt; Figure 2.4), being the time for the incident wave to travel to a reflection site then the return of the reflected wave to the site of measurement, was measure using the foot, or initiation, of the incident compression wave intensity and reflected compression wave intensity. The foot of an incident and respective reflected intensity was subjectively judged

and mouse-clicked. The mouse-click gives a ‘ginput’ for the MATLAB algorithm which was used for calculations (see Appendix: Extra Data). Sometimes careful judgement of a foot was required on what might be artefact (i.e. “noise” of the system) near to a foot and so not be accepted as part of the wave intensity. Wave energy was also obtained from WIA plots – this is commented on under Eq. 2.4 above.

FIGURE 2.1: *Top Panel* Shows a Pulse of Measured (Total) Pressure (P_T) with its component parts, which are the Reservoir (Windkessel) Pressure (Pwk) and Wave Pressure (Pw). *Bottom Panel* shows the associated Blood Flow Velocity Pulse.
All obtained from the Abdominal Aorta of an Anaesthetised Rabbit* under Control Treatment.
Measured Diastolic Blood Pressure was 5366 Pa.

Note: i) the close fitting of the Pwk curve to the P_T curve during diastole; ii) the similarity of shape of the Pw waveform with the blood flow velocity waveform.

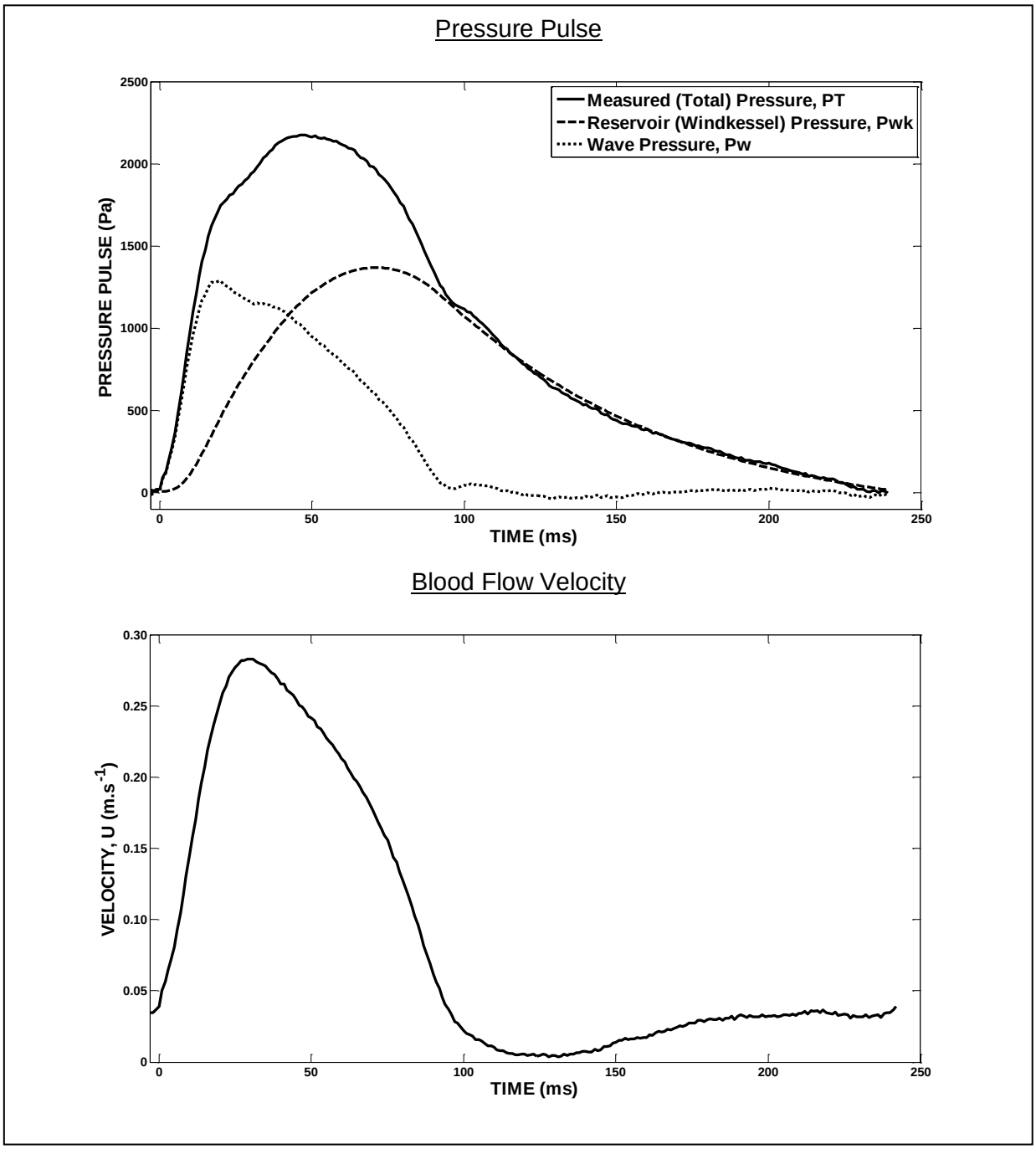

*Experiment Ref: AAEH100329(1)

FIGURE 2.2: Examples of Pressure – Velocity Loops (PU Loop)* for Measured (Total) Pressure (P_T) and Wave Pressure (Pw) plotted against Blood Flow Velocity. Data obtained from the Abdominal Aorta of an Anaesthetised Rabbit** under Control Treatment.

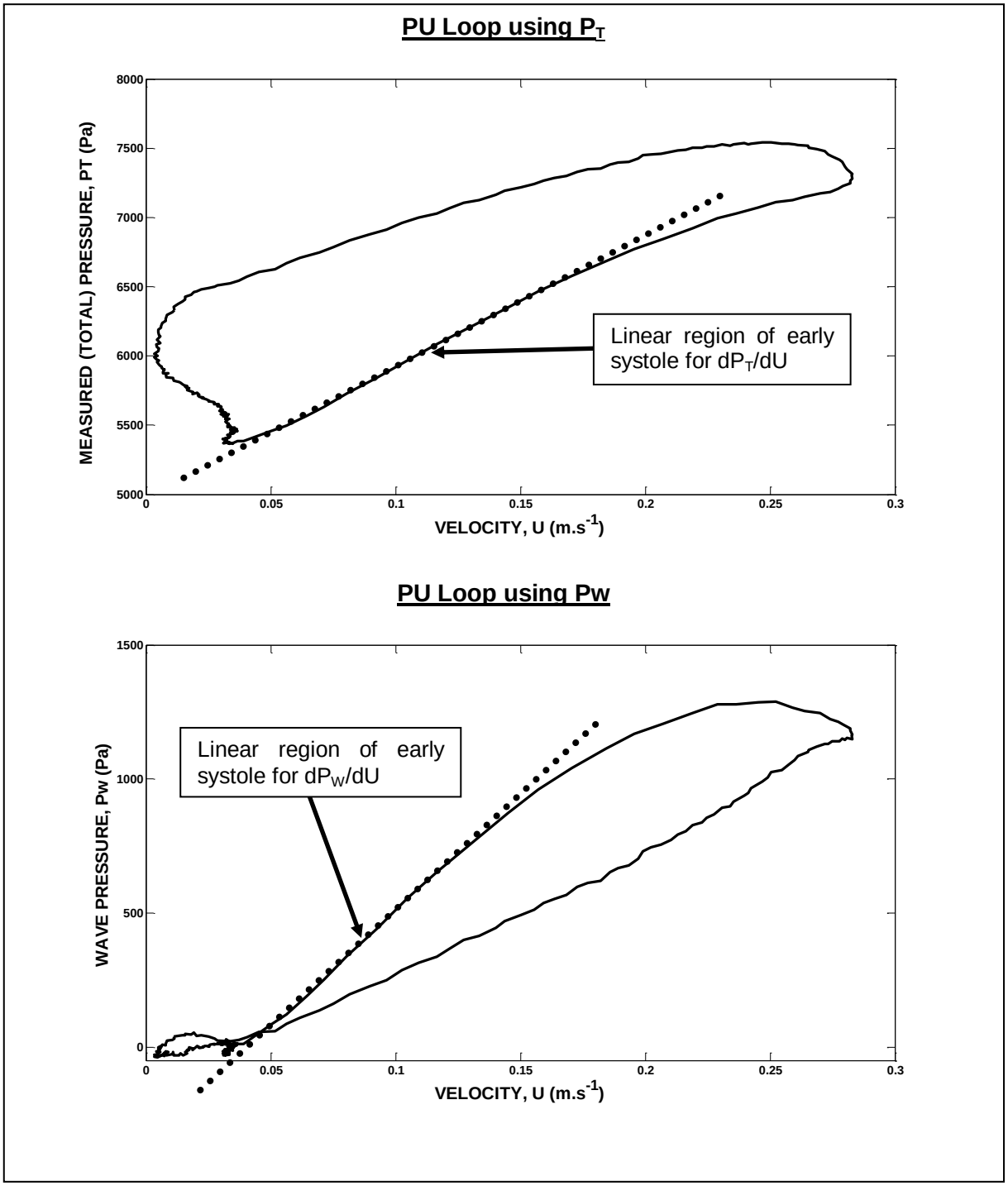

* The PU Loop using P_T is counter-clockwise whereas that using Pw is clockwise. The direction of plots is dependent on the waveform shapes of P_T or Pw and their closeness of similarity with the velocity waveform.

**Experiment Ref: AAEH100329(1)

FIGURE 2.3: *Upper Graph*: Plots of Wave Intensity Analysis (WIA) using Measured (Total) Pressure, P_T.
Lower Graph: Plots of WIA using Wave Pressure, Pw.

Both Graphs from Blood Pressure and Flow Velocity in the Abdominal Aorta of an Anaesthetised Rabbit* under Control Treatment. See Figure 2.4 for features of a WIA Plot.

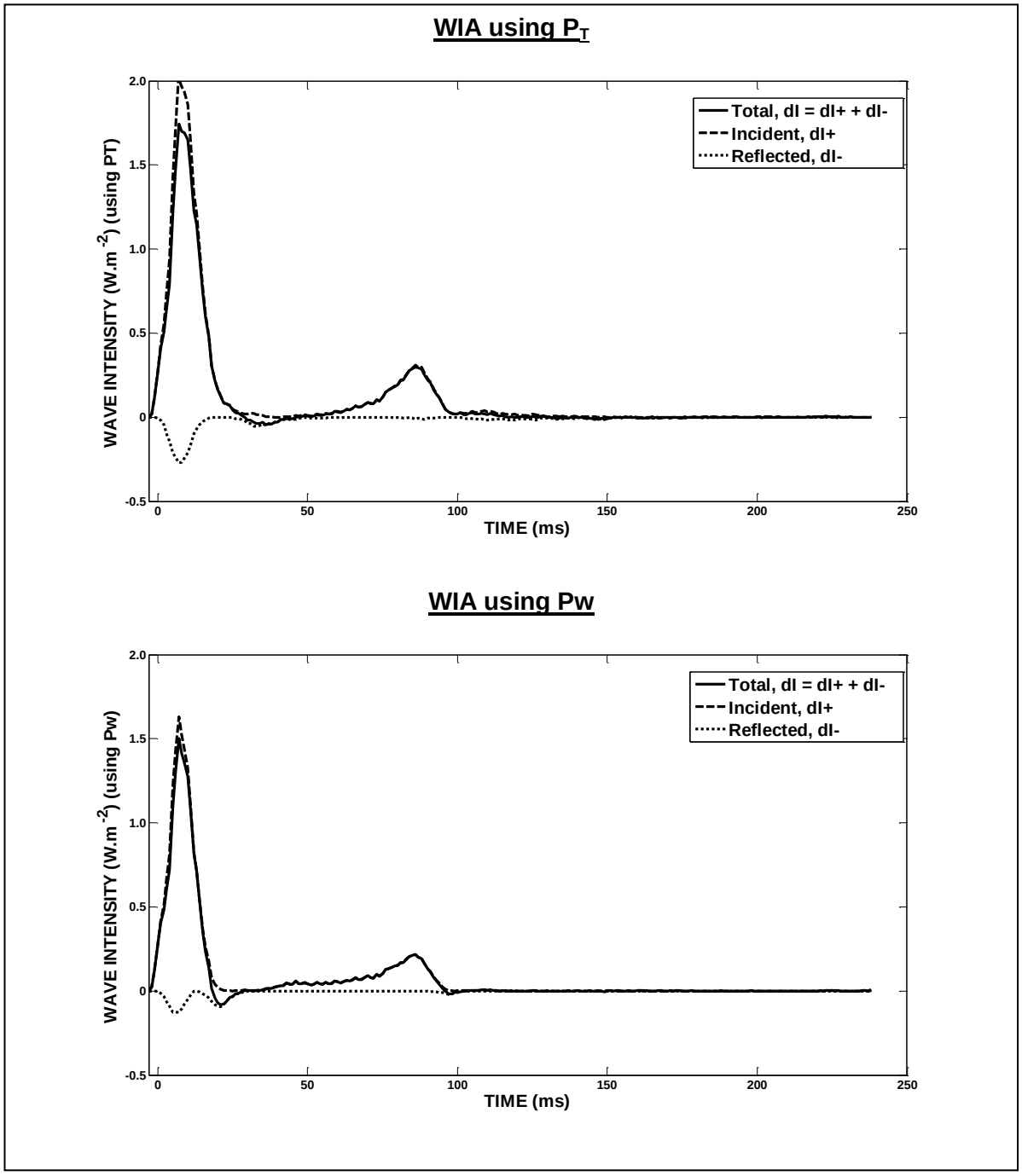

*Experiment Ref: AAEH100329(1)

FIGURE 2.4: Features of the Wave Intensity Analysis (WIA) Plot. This WIA plot is from a study different to those shown in Figure 2.3 for the reason that this shown below exhibits more reflected intensity thus helps to illustrate the main features of WIA. Data from Blood Pressure and Flow Velocity in the Abdominal Aorta of an Anaesthetised Rabbit* under Control Treatment.

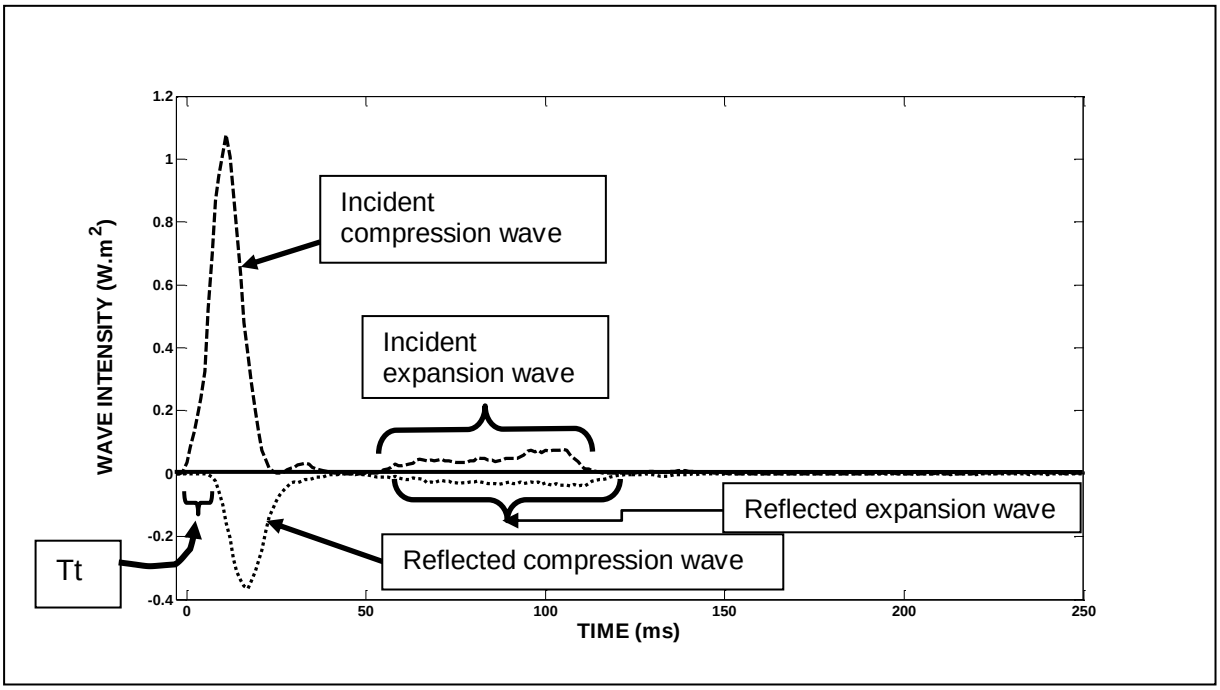

*Experiment Ref: AAEH090805(2)

Tt is the transit time for the incident compression wave arriving at the reflection site and returning as the reflected wave to site of measurement. Tt is measured between the foot of the incident and foot of the reflected compression wave intensities. Site of reflection can be calculated if wave speed is known:

$$Distance\ to\ Reflection\ site = \frac{Wave\ speed\ .Tt}{2} \quad \text{(Eq. 2.22)}$$

The integral of intensities of compression and expansion waves (incident and reflected) gives their wave energies (Eq. 2.9).

CHAPTER 3

GENERAL METHODS

This chapter gives details of the methodology common to practical aspects of Chapters 4, 5, 6 and 7; methodology specific to those chapters are dealt with under the method sections in those chapters.

3.1 Measuring Devices and Acquisition Systems

Blood Pressure Measuring Devices

- Dual sensor Millar Mikro-tip catheter transducer: model SPC-721; size 2.5F; sensors being **50mm** apart.
- Single sensor Millar Mikro-tip catheter transducer: model SPR-407; size 2F.
- Applanation Tonometer – see Chapter 4
- CWE Inc. PM1000 Amplifier for driving transducers and registration of pressure. This is an analogue amplifier, so gives an analogue output; the filter was set to 50Hz.

Millar catheters are provided with a Transducer Control Unit Model TC-510 which has a facility for electronic calibration at 100mmHg. As a check of calibration, the sensors were set up for application of 100mmHg via a mercury manometer; the reading was exactly that as given by electronic calibration for all catheters used. These catheters operate on a strain-gauge and Wheatstone bridge arrangement (Geddes, 1970; Nichols and O'Rourke, 2005).

Blood Flow Measuring Devices for Volumetric Blood Flow

- Transonic Systems Inc., Perivascular Blood Flow Probe types:

  MA4PSB (4mm diameter).

  MA20PAX (20mm diameter).

  MA14PAX (14mm diameter).

  MA10PAX (10mm diameter).

- Transonic Systems Inc. Blood Flow Meter: Model TS420; 2 Channel; Perivascular Flow Modules. Filter control set to 40Hz

This system for blood flow measurement operates on the ultrasonic transit time principle. Two transducers are contained within the blood flow probe; the flowmeter measures the transit time for a pulse of ultrasound to travel from one transducer to another at an angle across a blood vessel – the transducers alternately transmit and receive pulsed ultrasound so that ultrasound alternately travels upstream and downstream through the blood flow. The difference between the upstream and downstream transit times is a function of blood velocity which integrated gives volume flow:

(from Mills, 1972)

If $U(x) \ll C$, then

$$\Delta t = \frac{2cos\theta}{C^2} \int_0^l U(x)\, dx \quad \text{(Eq. 3.1)}$$

Where:

Δt = difference between upstream and downstream transit times
θ = angle between flow axis and line of transducer crystals
C = velocity of sound in blood
$U(x)$ = blood velocity as a function of x axially

$\int_0^l U(x)\, dx$ is the integral of blood velocities through which the ultrasound beam passes;

this is close to the true average velocity for wide transducers covering the entire diameter of the vessel which is the case with the Transonic probes used in these experiments.

The theory of operation of the transonic system is described in the manual of Transonic Systems Inc.

The statement of calibration in the manual (Transonic Systems Inc.) was accepted for this work; calibration is carried out using water, an adjustment is applied to correct for the acoustical velocity of blood vs. water. However, a simple in-house test was carried out on two flow probes (4.0mm; 4PSB945 & 4PSB1080) that were used for *in vivo* experiments with rabbits. The simple test was a gravity-fed flow system with water collected in a measuring cylinder over 1minute; the system was not driven by a constant hydrostatic head but it was accepted that for the flow rates set and for 1minute, the hydrostatic head would change only a little. Figure 3.1 shows a plot of the calibration test. The test revealed that probe 4PSB945 read lower and 4PSB1080 read higher than the volume collection (Figure 3.1). To avoid discrepancies between sets of data obtained from the same sites of measurement in

different experiments, it was decided that the two flow probes would always be placed on their own same sites on the abdominal aorta and operated from their own same channel of the flow meter; thus, flow probe 4PSB945 was always positioned on the upstream site (Figure 3.2; UpSt Site) of the abdominal aorta and operated from channel 1 of the flow meter, whereas flow probe 4PSB1080 was always positioned on the downstream site (Figure 3.2; DnSt Site) of the abdominal aorta and operated from channel 2 of the flow meter.

FIGURE 3.1: Test of Calibration for two 4mm Blood Flow Probes, 4PSB945 and 4PSB1080. System was a Gravity-Fed Flow arrangement at Room Temperature (~20°C) using Water. Line of identity is Volume Collection plotted against itself.

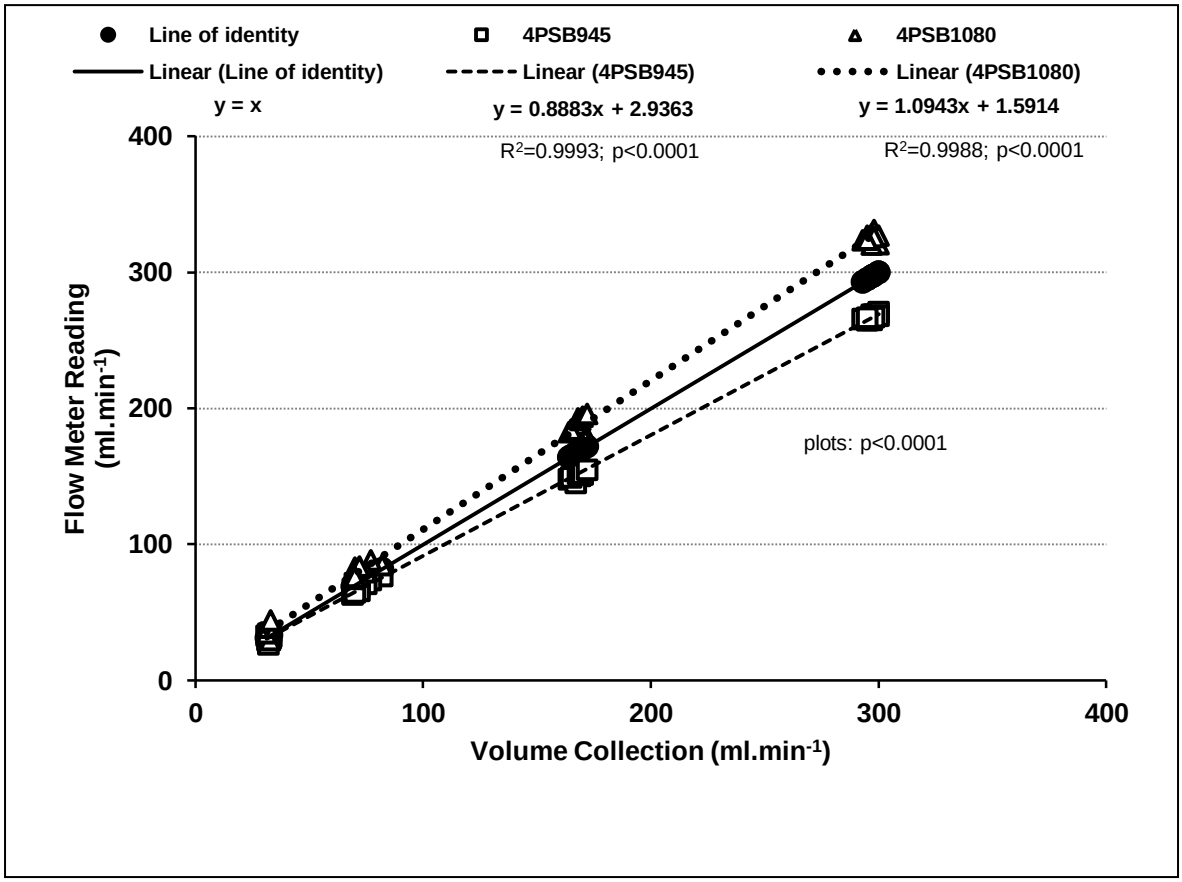

As stated in the manual (Transonic Systems Inc.) the sampling rates of Transonic flow probes are dependent on their size, ranging from 3.6 kHz for the smallest probes to 225Hz for the largest probes. It is generally held that the first ten harmonics adequately make up cardiovascular pulsatile waveforms, the fundamental being heart rate itself. Thus the filter setting on the flowmeter was set for 40Hz for *in vivo* experiments since the heart rate of anaesthetised rabbits is about 240 beats.min^{-1}.

Measurement of Aorta Diameter

- Ultrasonix system – see Chapter 4

Acquisition Systems and Data Analysis

- Notocord-HEM. Details of this software can be found at www.notocord.com

Notocord-HEM acquisition software is designed for acquisition of cardiovascular data. The acquisition digital sampling rate was set for 1kHz thus each data point would be separated by 1ms of time. Data was processed using Microsoft Excel and MathWorks MATLAB.

Statistical tests were carried out using Microsoft Excel or GraphPad Prism 5. Statistical tests applied were Student's t-test, and ANOVA, along with correlation and regression analyses; use of statistical tests is stated with displayed data; differences between measures were considered either significant when $p \leq 0.05$, or not significant (NS) when $p > 0.05$.

3.2 *In Vivo* Experiments using Anaesthetised Rabbits

All animal procedures complied with the Animals (Scientific Procedures) Act (1986).

3.2.1 Initial Procedures

Male New Zealand White (NZW) rabbits of the Harlan Interfauna strain were used; weights, ages and numbers used are stated in the chapters appropriate to experiments. Experiments commenced by first giving the rabbits a pre-medication with Hypnorm (0.1ml/kg) intramuscularly into the gluteus maximus. 10 minutes after the pre-medication, anaesthetic was administered via a butterfly needle/cannula in a marginal vein of the ear. Anaesthesia

was induced with sodium pentobarbitone (~35mg/kg i.v.) and maintained to effect with intravenous 'top-ups' of sodium pentobarbitone ('top-ups' being of the order 10-30% of full induction dose). Rabbits were artificially ventilated with a Harvard Small Animal Ventilator; respiratory rate 50 breaths/min; inflation pressure set for trough 25cmH_2O and peak 50cmH_2O. Rabbit body temperature was maintained near 39°C by placing the rabbit on a heating blanket which was controlled by a CWE Inc. TC1000 temperature controller which in turn monitored body temperature via a rectal thermistor probe. A femoral vein was exposed at the level between the knee and groin, a polythene cannula was inserted into the femoral vein and passed up into the inferior vena cava. The purpose of this cannula was for intravenous administration of saline or drugs (or anaesthetic "top-ups" should the ear vein cannula fail).

3.2.2 Measurement of Aortic Blood Pressure

A femoral artery was exposed at the same site as used for exposing the femoral vein (see previous section), the dual sensor Millar Mikro-tip catheter transducer (model SPC-721; sensors 50mm apart) was inserted into the femoral artery and passed up into the aorta. The sensor at the catheter tip (the upstream sensor, designated P1) was positioned in the abdominal aorta between the originations of the celiac and superior mesenteric arteries (Figure 3.2 – this illustration was made by use of a cast of a rabbit arterial anatomy; the Millar catheter lies alongside the aorta to represent the *in vivo* situation). The other sensor (the downstream sensor, designated P2) consequently lay 50mm downstream at a position distal to the originations of the renal arteries (Figure 3.2). The positioning of the two sensors just described is termed "UpSt Site" for Up-Stream Site in the abdominal aorta. During experiments readings were taken at the UpSt Site, and also when the Millar catheter had been withdrawn by 50mm; this latter position was termed "DnSt Site" for Down-Stream Site in the abdominal aorta. Thus, when the catheter had been withdrawn to DnSt Site, sensor P1 would then be in the previous position of P2 which itself would then be 50mm downstream of its previous position.

3.2.3 Measurement of Aortic Blood Flow

A ventral midline incision (laparotomy) was made into the abdomen; the intestinal viscera were displaced aside to allow access and blunt dissection was used to reveal the abdominal aorta at the sites of the sensors P1 and P2 situated in the UpSt Site in the aorta (see previous section 3.2.2). These sites were cleared gently of connective tissue, arterial branches carefully avoided, around the aortic structure to allow attachment of perivascular blood flow probes. However, before attachment of the blood flow probes, the external diameter of the aorta was measured at the two sites relative to P1 and P2.

The external diameters of the aorta were measured by divider and ruler; it is appreciated that this measure gives only an estimate of mean external diameter and does not determine the pulsatile diameter values. The measured value for *external* diameter was used to calculate the *internal* (or *lumen*) diameter by use of these relationships:

$$h = 0.1\left(\frac{Do}{2}\right) \quad \text{(Bergel, 1961; McDonald, 1976)} \ldots\ldots\ldots\ldots\ldots\ldots\ldots\ldots\ldots\ldots\ldots\ldots\ldots\ldots\ldots\ldots\ldots. \text{(Eq. 3.2)}$$

where:
$h =$ wall thickness
$Do =$ external diameter of aorta

The value for internal, or lumen, diameter was used to convert blood flow *volume* to cross-sectional average blood flow *velocity*, thus:

$$Mean\ Flow\ velocity = \frac{Flow\ volume}{luminal\ area\ of\ cross\ section} = \frac{Flow\ volume}{\pi\left(\frac{Di}{2}\right)^2} \ldots\ldots\ldots\ldots\ldots.. \text{(Eq. 3.3)}$$

where: $Di = Do - 2h \ldots\ldots\ldots.$ (Di is the internal, or lumen, diameter of aorta)

After measurement of the external diameters, a 4mm diameter perivascular blood flow probe (Transonic type MA4PSB) was positioned at each of the sites relative to the sensors P1 and P2 (Figure 3.2) (see details in section 3.1 for specified attachment of these flow probes). Blood flow volume was registered by use of the two channel Transonic Systems Inc. Blood Flow Meter.

After the blood flow probes had been attached to the aorta, the intestinal viscera were returned to the peritoneal cavity and the abdomen closed by clamps.

3.2.4 Simultaneous Readings of Aortic Pressure and Aortic Blood Flow

The importance of having the two sites, UpSt Site and DnSt Site, is for measurement of blood pressure and blood flow at each of the two sites which, for comparison, have their different aortic anatomies. When positioned for UpSt Site, sensor P1 is ~3mm upstream from the origin of the superior mesenteric and ~10mm and ~15mm upstream from the origin of the right and left renal arteries respectively, while sensor P2 is in a relatively straight section of the aorta ~60mm upstream from the aorto-iliac bifurcation. In the case of simultaneous measurement of pressure and flow at the upstream site, namely Millar sensor P1 at UpSt Site position, the sensor P1 was positioned *slightly* (<5mm) downstream of the flow probe; such positioning avoided interference by the sensor tip of the transonic insonation of the blood flow field within the lumen of the blood flow probe. However, such

positioning of the Millar sensor P1 at the UpSt Site does not avoid the interference by the sensor P2 where the catheter lies within the blood flow field within the lumen of the flow probe; for this reason the catheter is withdrawn by 50mm to position P1 at the DnSt Site to allow un-interfered blood flow registration at this downstream site. The other importance of having the two positions, UpSt Site and DnSt Site, is for measurement of pulse wave velocity between P1 and P2 along two different sites in the abdominal aorta; measurement of pulse wave velocity is discussed in the next section 3.2.5.

FIGURE 3.2: Positioning of the Millar catheter (thin white wire) and Flow Probes (Blue Objects – consider only those on the aorta*) on the Abdominal Aorta (aorta and arteries shown as an arterial cast).

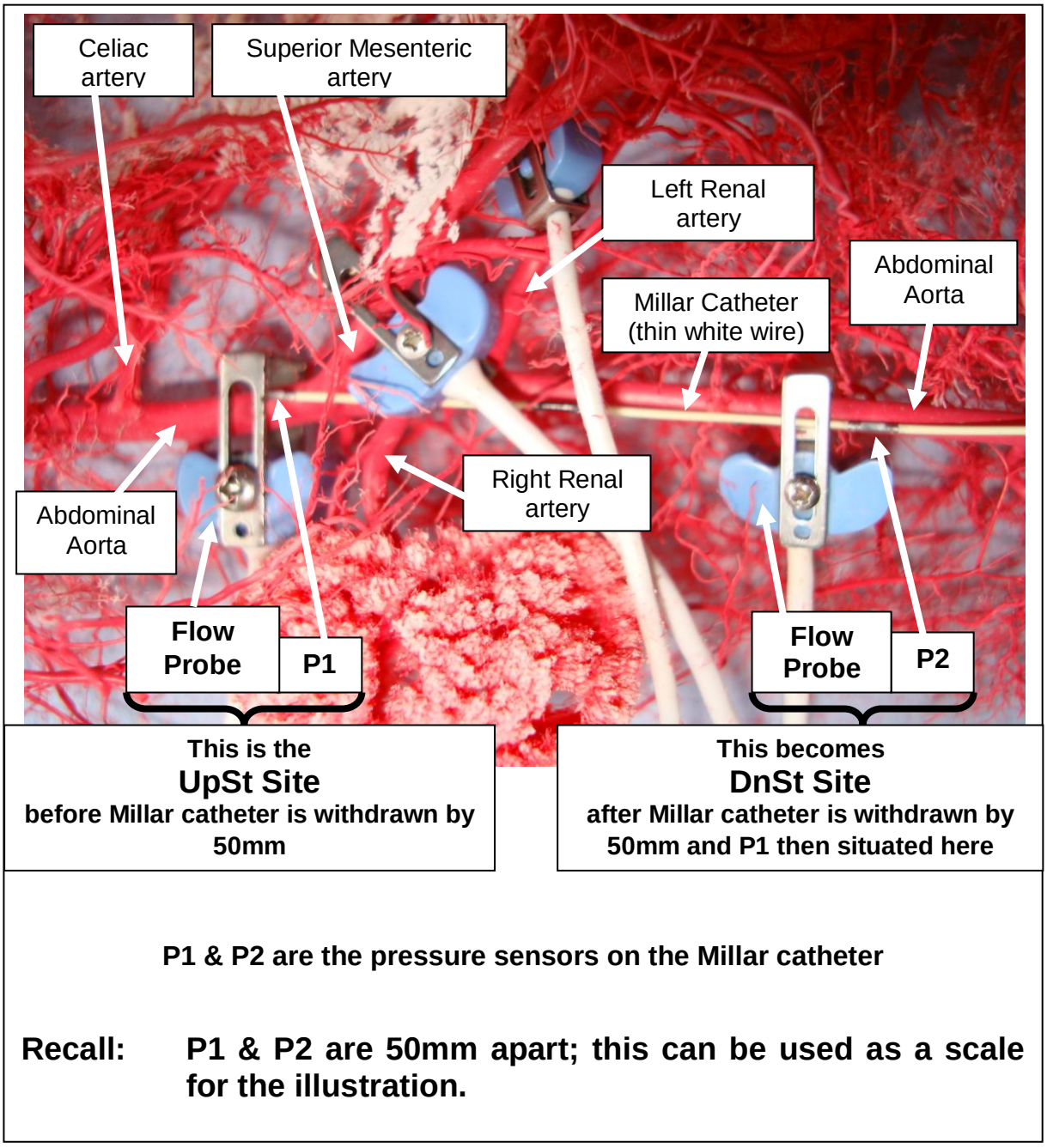

*Two other flow probes are shown, one attached to the superior mesenteric artery and the other to the left renal artery; these are not relevant to the data of this thesis.

3.2.5 Measurement of Aortic Pulse Wave Velocity (PWV)

The theoretical aspects of arterial PWV or wave speed are discussed in Chapter 2. In this section, the practical methods are considered.

Measurement of pulse wave velocity is often by a "foot-to-foot" method, of which there are several to choose from. The time of the foot of a pressure pulse wave recorded upstream is subtracted from the time of the foot of the same pulse wave recorded at a measured distance downstream; PWV is calculated as:

$$PWV = \frac{x}{\Delta t} \quad \text{(Eq. 3.4)}$$

where:
$x =$ distance between upstream and downstream recording sites
$\Delta t =$ difference between time of pulse upstream to time of pulse arrival downstream

The "foot" is that point of the pulse wave where the systolic upstroke occurs at the end of diastole, but choosing the foot of the pulse wave is not straight forward and has been, and still is, a subject of debate; identification of the foot can be subjective and hence dependent on personal judgement. This is discussed by Milnor (1989 – Chapter 9). There are many methods for determining the foot of the pressure pulse wave. Malindzak and Meredith (1970) defined the foot as the point of intercept of the diastolic portion with the systolic ascending limb of the pressure pulse. Greenwald *et al*. (1978) defined the foot as the point of intercept of a tangent drawn to half the height of the systolic ascending part of the pulse and a line parallel to the time axis passing through the minimum diastolic level of the pulse; this definition is similar to that of Ting *et al*. (1990). McDonald (1968) displayed the upstream and downstream pulse waveforms on a dual channel oscilloscope and by adjustment of the delay control aligned the early systolic ascending wave fronts of the upstream and downstream pulses over each other, thus PWV is obtained from the wave transit delay time and known transit distance. Gribbin *et al*. (1976) used corresponding points at 10% up the systolic wave fronts on the upstream and downstream pulses; similarly Arts *et al*. (1979) used points 25% up on the wave fronts. Latham *et al*. (1985 and 1987) define the foot as intersection of tangents to the end-diastolic contour and early systolic contour. Mitchell *et al*. (1997) and Fitch *et al*. (2001) compared several techniques for determining PWV by foot-to-foot technique. Algorithms have been designed for automated determination of the foot of wave fronts for measurement of PWV (Kontis and Gosling 1989; Asmar *et al*., 1995).

In addition to the issue of identifying the foot, there is also the problem of the length over which the PWV is assessed. The speed of an arterial pulse wave will be affected by the

composition of arteries encountered during its travel. So the pulse wave speed measured by the foot-to-foot method might represent that for a given artery if over a short length of artery or an average wave speed for several arteries if over a distance that includes a series of arteries; the average though is not a simple arithmetic average and would be weighted to those arteries in the series with the slowest PWV. This is pertinent if the measurement made, as is commonly done, is between a pulse wave in the ascending aorta to the arrival of that pulse wave in the femoral artery; the different make-up of the wall along the aorta, the iliac and femoral will affect the wave speed such that the speed will be an average but weighted to the proximal regions of the aorta. With this in mind for the experiments of this thesis, PWV was measured only along the abdominal aorta over two transit distances each of 50mm, namely between P1 and P2 at UpSt Site and between P1 and P2 at DnSt Site (Figure 3.2).

Data was obtained from a continuous run of ten cardiac cycles selected after treatments; the foot of each wave front of the ten pulses was marked subjectively by an event marker (a facility of the Notocord acquisition software) in accordance with either one or the other of two procedures. The two procedures adopted for determining the foot for the foot-to-foot measurement of PWV were:

Procedure 1: If the diastolic nadir of pulses was clearly defined then the method used was similar to that described by Malindzak and Meredith (1970) and Fitch *et al*. (2001 – first of three techniques described). An event marker was positioned at a point deemed the end of diastole and the start of the systolic ascent of the wave front; this point of diastolic-systolic intersection, or inflection, was selected and taken as the foot on each of the ten chosen upstream (P1) waves and likewise on each of the associated ten downstream (P2) waves (Figure 3.3).

Procedure 2: If the diastolic nadir of pulses was *not* clearly defined then the method used was similar to that described by Gribbin *et al*. (1976) and Arts *et al*. (2001). An event marker was placed on a feature (e.g. point of steep ascent) that was recognisable and exactly the same on both the upstream (P1) and downstream (P2) wave fronts but that this feature was below 50% of the height of the rising systolic wave front – this latter condition ensured selection in early systole when effects of wave reflection are believed non-existent.

Values of PWV were calculated from the ten wave fronts; a mean PWV of the ten waves was calculated along with the standard deviation of the mean. The rule adopted was to accept the mean value for PWV if the standard deviation was ≤10% of the mean. If the standard deviation was >10% of the mean, the outliers of the 10 measurements were reconsidered

and the event markers adjusted if deemed appropriate to do so. Usually it was obvious that an adjustment was required, however these adjustments were always small and had little effect on the mean value, usually at most changing the value at the second decimal place. The event markers of outliers were not adjusted if no obvious reason to do so could be observed; in this case a standard deviation of >10% of the mean was accepted and was not more than 12% of the mean. However, it must be born in mind that the resolution cannot be less than 1ms as the digital acquisition rate was 1kHz.

The event markers marking the foot of each of the ten waves (upstream and downstream) also served for marking the start and end of each cardiac cycle for ensemble averaging of the data; this process is explained in the next section 3.2.6.

3.2.6 Ensemble Averaging of Blood Pressure and Blood Flow Waves

When the foot of each of the ten pressure pulse wave fronts (P1 and associated P2) had been established for calculation of PWV, the foot of each pressure wave front was then used to assess and mark subjectively the foot of its associated blood flow pulse; the ten pressure pulses and flow pulses were ensemble averaged in an Excel spreadsheet to give one pressure pulse and one flow pulse. These ensemble waveforms were subjected to analyses as detailed in Chapter 2, namely reservoir (Windkessel) subtraction and wave intensity analysis by MATLAB algorithms.

FIGURE 3.3: Measurement of PWV (here as c) by the foot-to-foot method taking one cardiac cycle of aortic blood pressure as an example. P1 is upstream and P2 is downstream in the abdominal aorta of an anaesthetised rabbit. The Event Markers were positioned by subjective judgement by either of two procedures – see text.

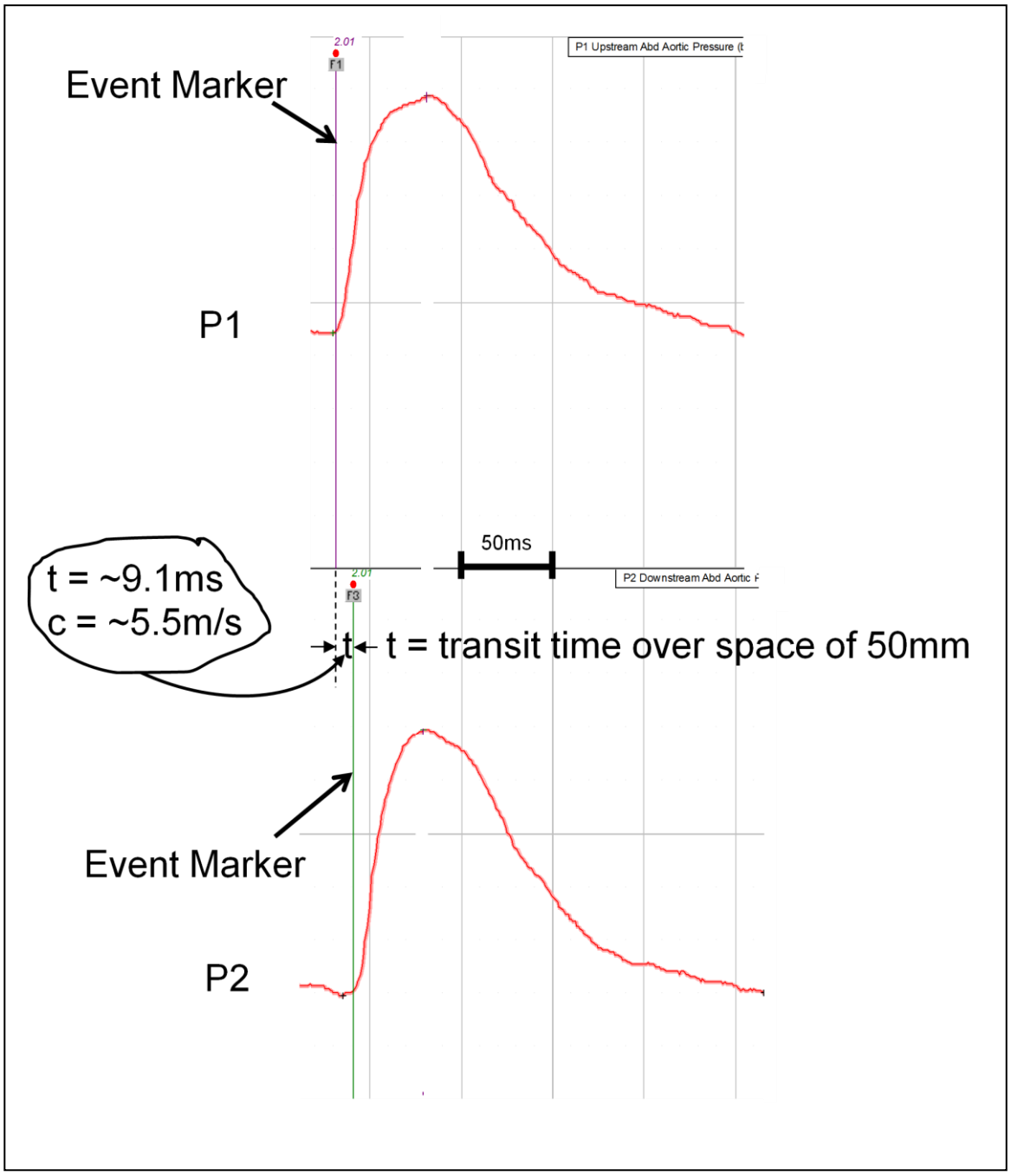

CHAPTER 4

Effects of Vascular Nitric Oxide Bioactivity on Arterial Blood Pressure and Flow Waveforms

4.1 INTRODUCTION

The effect of nitrovasodilators, e.g. nitroglycerine, on the pressure pulse waveform of peripheral arteries has been studied for many years with particular interest in the waveform during diastole and the feature of the dicrotic notch (Murrell, 1879; Imhof *et al*., 1980; Lund 1986). Nitrovasodilators lower the dicrotic notch relative to the pulse amplitude. This effect of nitrovasodilators on the dicrotic notch appears to be specific to this class of vasodilators as noted by Morikawa (1967) who compared other classes of vasodilators used in medicine at that time. Consistent with this proposed specific action of nitrovasodilators, Stengele *et al*. (1996) found nitroglycerine lowered the dicrotic notch but the calcium channel blocker vasodilator, nifedipine, did not. The effect of nitrovasodilators of lowering the dicrotic notch is specific enough for use as a measure of bioactivity and pharmokinetics of this class of vasodilators (Bass *et al*., 1989). Nitrovasodilators function as nitric oxide donors (Harrison and Bates, 1993), thus it is logical to propose that nitric oxide is specifically responsible for the effect of lowering the dicrotic notch, indeed such a proposal is supported by Weinberg *et al*. (2001) from experimental studies on the peripheral pulse waveform in the central ear artery of rabbits. Nier *et al*. (2008), also using the central ear artery of rabbits, have supported this proposal with evidence for nitric oxide bioactivity specifically affecting the dicrotic notch height while other drugs active on the cardiovascular system were without effect on the dicrotic notch. The height of the dicrotic notch is expressed as a fraction of the overall amplitude of the pulse waveform and is termed ‘the relative height of the dicrotic notch’ or RHDN. Interestingly, Sundberg and Castrén (1986) observed that prazosin, a potent α_1-adrenoceptor antagonist, not a nitrovasodilator, and not dependent on endothelial derived nitric oxide (Spokas *et al*., 1983), decreased dicrotic notch height, but because of variable bioavailability between subjects the effect was not statistically significant. However, in one subject prazosin markedly reduced the height of the dicrotic notch (Fig. 1 in Sundberg and Castrén, 1986), no explanation was given. An explanation could be that the subject was sensitive to prazosin which, due to its potent α_1-adrenoceptor antagonist property, caused

marked arteriolar vasodilatation, this in turn would likely have cause marked increased blood flow through the conduit arteries thereby increasing conduit artery wall shear stress and so stimulate release of nitric oxide; this effect is akin to the hyperaemic response on which the FMD test relies – FMD meaning flow-mediated endothelium-dependent brachial artery vasodilatation (Raitakari and Celermajer, 2000). The nitric oxide released in this way might then have decreased the height of the dicrotic notch as observed after prazosin.

Dawber *et al*. (1973) promoted observation and measurement of the dicrotic notch as a procedure for diagnosis of coronary heart disease and found that the dicrotic notch became less pronounced with increased coronary disease; furthermore they concluded that changes in the peripheral pulse waveform reflect changes in the arterial walls, including the coronary arteries, and may indicate the degree of atherosclerosis. Indeed, height of the dicrotic notch could be a useful, simple and non-invasively obtained, index of endogenous nitric oxide bioactivity and arterial health. Klemsdal *et al*. (1994), using hypercholesterolaemic rabbits, have demonstrated decreased effect of acetylcholine on lowering the dicrotic notch in these rabbits (acetylcholine stimulates nitric oxide synthesis in and release from vascular endothelial cells – see below; hypercholesterolaemia impairs function of vascular endothelial cells). Furthermore, type 2 diabetes impairs function of vascular endothelial cells and is associated with attenuation of nitric oxide release and consequential lack of effect of albuterol on height of the dicrotic notch (Chowienczyk *et al*., 1999). Thus, there is strong evidence for the height of the dicrotic notch being associated specifically with vascular nitric oxide bioavailability and arterial health; it is tenable, therefore, that simple diagnostic procedures be developed using the dicrotic notch as an index of arterial health.

The mechanisms governing the height and form of the dicrotic notch should be known if these aspects of the dicrotic notch are to be used for a rational diagnostic procedure. The mechanism(s) should be specific or unique to the character of the dicrotic notch. In the case of nitrovasodilators, or nitric oxide, their effect on the height of the dicrotic notch appears to be a mechanism specific to them; it is unlikely due to vasodilatation *per se* since other vasodilator drugs do not affect the dicrotic notch (Morikawa, 1967; Stengele *et al*., 1996; Nier *et al*., 2008). The nitrovasodilators are also venodilators (Imhof *et al*., 1980; Strohm *et al*., 1983; Westling and Andersson, 1986) so can affect cardiac preload and cardiac output. However this does not explain the effect of these agents decreasing the height of the dicrotic notch since Nier *et al*., (2008) have shown that decreasing heart rate which might have decreased cardiac output (admittedly not measured), did not affect height of the dicrotic notch; Imhof *et al*. (1980) are of the opinion that cardiac output has little or no effect on the height of the dicrotic notch. However, there is good evidence for nitrovasodilators, in addition to their venodilator properties, having a vasodilator effect selective for conduit

arteries rather than for resistance arteries or arterioles (Westling and Andersson, 1986; Harrison and Bates, 1993); furthermore, nitrovasodilators increase compliance of conduit arteries without effect on cardiac output and arterial pressure (Westling *et al*., 1984). There is convincing haemodynamic evidence for nitrovasodilators altering arterial pulse waveform by selectively increasing compliance of conduit arteries at doses that do not affect the aorta and have little or no effect on arterioles so peripheral vascular resistance and hence arterial blood pressure are unaffected (Pepine *et al*., 1979; Sauer *et al*., 1981; Babalis *et al*., 1981; Simon *et al*., 1982; Merillon *et al*., 1984; Yaginuma *et al*., 1986; Fitchett *et al*., 1988a&b; Latson *et al*., 1988). Yaginuma *et al*. (1986) proposed a mechanism whereby the increased compliance of medium to small conduit arteries attenuates wave reflection by an interaction of reflections from the arteriolar interface with negative reflections at the interface of the dilated conduit arteries with their upstream parent artery branches; negative reflections being resultant of the diameter of daughter branches being increased relative to that of the parent branch (see also Figure 24.2, p.437 in Nichols and O'Rourke, 2005). This mechanism is analogous to the concept of *wave trapping* proposed by Parker (2009).

This chapter of the thesis presents work done in an attempt to elucidate some of the haemodynamic mechanisms responsible for the change in height of the dicrotic notch of peripheral arterial pulse waveforms in response to altered vascular nitric oxide bioactivity. The work investigated the effects of pharmacologically altered nitric oxide bioactivity on aortic blood pressure and flow waveforms. The assumption taken was that the nitric oxide causing changes in blood pressure and flow waveforms is produced within the vasculature, namely produced by the vascular endothelium; the enzyme responsible for the production of this nitric oxide is endothelial nitric oxide synthase (eNOS or Type III NOS) (Shimokawa and Vanhoutte, 1997; Choate, 1998; Fleming and Busse, 1999). It must be appreciated however that nitric oxide is also produced, and has physiological function, within the central nervous system and autonomic nervous system – this nitric oxide is produced by neuronal nitric oxide synthase (nNOS or Type I NOS) (Shimokawa and Vanhoutte, 1997; Choate, 1998) and can also affect cardiovascular function. There is yet another source of nitric oxide but unlikely to be relevant in these experiments; nitric oxide production can be induced in most mammalian cells by a variety of pro-inflammatory or immunological stimuli (e.g. endotoxins, cytokines) which activate inducible nitric oxide synthase (iNOS or Type II NOS) (Shimokawa and Vanhoutte, 1997; Choate, 1998).

For these experiments two pharmacological agents were used to alter vascular nitric oxide bioactivity, the agents were acetylcholine (Ach) and N^G-nitro-L-arginine methyl ester (L-NAME). Ach stimulates muscarinic receptors on the external surface membrane of vascular endothelial cells (Rang *et al*. 2003a), stimulation of these receptors leads to activation of

eNOS which in turn produces nitric oxide (Rang *et al*. 2003b); the latter is released from the endothelial cells then to cause relaxation of vascular smooth muscle, hence vasodilatation, of the affected blood vessels. Thus, Ach increases bioactivity of nitric oxide. L-NAME reduces bioactivity of nitric oxide by inhibiting the action of eNOS thereby reducing the production of nitric oxide (Rang *et al*. 2003b); L-arginine is the natural substrate for eNOS to produce nitric oxide, L-NAME competes as a substrate but is inhibitory and is not converted to nitric oxide.

The experiments reported here were carried out in two parts: 1) to assess the changes of aortic diameter during the pharmacological treatments and, 2) to determine the effects of the pharmacological treatments on blood pressure and flow waveforms.

The Hypotheses:

- The height and form of the dicrotic notch of the pulse in the rabbit central ear artery can be explained by wave reflections from conduit arteries of the limbs and organs.
- These reflections depend on conduit artery diameter and compliance and do not depend on aortic pulse wave velocity, cardiac output, heart rate, total peripheral resistance, or blood pressure.

4.2 METHODS

Chapter 3 describes the surgical procedures for preparing anaesthetised rabbits for the experiments reported here. Furthermore, chapter 3 describes methods for acquiring the haemodynamic data.

Mature rabbits, aged between 6 – 12 months (weight range 3 – 4½kg) were used for these experiments. Pharmacological treatment was by intravenous infusion; the infusion rate and doses used for Ach or L-NAME were selected on the basis of data from Nier *et al*. (2008). It was intended that the chosen doses should not greatly affect blood pressure since interest was in the effects of the pharmacology of Ach or L-NAME on waveforms rather than due to the effects of blood pressure *per se* on waveforms. Ach and L-NAME were dissolved in saline. Intravenous infusions of saline (0.5ml/min for 5min), or Ach (1 or 2ug/kg/min for 5min) or L-NAME (100 or 200ug/kg/min for 5min) were given via a cannula inserted in the femoral vein (cannula insertion is described in section 3.2.1); the infusion volumes for solutions of Ach and L-NAME were as for saline. As a shorthand notation the doses as

stated are referred to as *'lo dose'* (Ach: 1ug/kg/min for 5min; L-NAME: 100ug/kg/min for 5min) and *'hi dose'* (Ach: 2ug/kg/min for 5min; L-NAME: 200ug/kg/min for 5min). Ach (as acetylcholine chloride) and L-NAME were obtained from ACROS Organics and SIGMA respectively.

4.2.1 Experiments to Determine by Ultrasound the Internal (Lumen) Diameter of the Abdominal Aorta during Infusions of Saline, Acetylcholine and L-NAME

For the experiments described in section 4.2.2 (see below), Transonic blood flow probes were used to measure aortic blood flow *volume*. However, as explained in section 3.2.3, measurements are required of blood flow *velocity* which can be calculated from the measured *external* diameter of the vessel under investigation (see section 3.2.3 - abdominal aortic *external* diameter measured with a divider and ruler). The calculated velocity would be such for the vessel at that measured diameter; however when the diameter changes in response to physiological or pharmacological effects then the velocity would change too which would be difficult to measure without disturbing the experiment. It would have been ideal to have obtained data for diameter *simultaneously with* pressure and flow in the experiments described in section 4.2.2, but it was technically too difficult to do this.

Four rabbits were used in the experiments described here and referred to as Rabbit 1, 2, 3, or 4. These experiments were separate from those described below in section 4.2.2, and had the purpose of determining what changes in aortic internal (luminal) diameter (and associated changes in aortic blood pressure) occur in response to *lo* and *hi doses* of Ach and L-NAME.

The data obtained for *internal* or *luminal* diameter after treatments with Ach and L-NAME was used to derive a Correction Factor that could be applied to velocity measurements where simultaneous measurements in diameter were not possible. Data for and derivation of the "correction factor" are given in the Results (section 4.3.1).

An Ultrasonix RP 500 (Ultrasonix Medical Corporation, BC, Canada) system was used for ultrasonic measurement of the abdominal aortic internal diameter. After mid-line laparotomy (as per section 3.2.3), the insonating probe was positioned to allow insonation, hence viewing an image, of the abdominal aorta in, or as near as possible to, the region of P1 at the UpSt Site position (this reference to regions or positions for measurements in the abdominal aorta is explained in section 3.2.2). Only this site was considered as it was technically very difficult to move the insonating probe from one site to the other (i.e. from P1 at the "UpSt Site" position to P1 at the "DnSt Site" position) within the time (5min) for dose infusion and without significantly disturbing the haemodynamic status.

The image of the abdominal aorta at the chosen site was of the longitudinal midline (Figure 4.0), rather than of the cross-sectional, aspect of the vessel. The insonating probe was placed approximately 2cm above the region of interest of abdominal aorta; acoustic contact between the probe and aorta was maintained by immersing the probe transmitter/receiver surface into a pool of saline made over the aorta. Insonation was adjusted so that the image of the parallel vessel walls allowed measurement of the internal diameter. Ultrasound scanning was performed in B-mode at a centre frequency of 10 MHz, and a minimum frame rate of 70 Hz. The amplification and the display setting were adjusted to maximize the contrast on the vessel boundaries. The data were recorded during several seconds in both video mode and raw-data mode to allow accurate post processing of the data set. Persistence (through time) was cancelled in order to allow a finer time analysis of the movement. A Millar catheter for measurement of pressure was inserted into a femoral artery (as per section 3.2.2). Only one pressure sensor of the (dual) Millar catheter was required and this was positioned within the abdominal aorta close to the site being viewed by ultrasound. To ensure that the sensor was close to the site of measurement of diameter, the sensor was moved into the field of insonation until its tip was viewed on the Ultrasonix monitor, the pressure sensor was then withdrawn and positioned just out of view.

When satisfactory images of the abdominal aorta were viewed (Figure 4.0) and recording of pulsatile aortic pressure was underway, infusions of saline, Ach (*lo* and *hi doses*), or L-NAME (*lo* and *hi doses*) were given via the cannula in a femoral vein; dosing for these studies were done on a cumulative basis. Because diameter and pressure were recorded by two separate acquisition systems (Ultrasonix and Notocord respectively), the data were not collected fiducially, instead initiation of recording was signalled verbally between two collaborators (A Hunt and Dr. JM Mari), thus recordings for aortic blood pressure and images of the abdominal aorta were taken as near simultaneously as possible. Recordings were taken during mid-infusion of saline and the *lo* and *hi doses* of Ach (the latter's effects for both doses were at maximum by mid-infusion). However, it was observed that the effect of the *lo* and *hi doses* of L-NAME on aortic blood pressure were slow in onset and tended to be maximal by 10-20min after the full infusion dose – readings were taken for both doses of L-NAME when their effects on blood pressure were at maximum.

Data for the ultrasound images were extracted from the Ultrasonix system files and processed by MATLAB algorithms to produce data for vessel diameter (MATLAB algorithms designed by Dr. JM Mari). The region of interest was manually localized in the first image of the raw data and then automatically processed over the rest of the images. A double parallel integral projection (PIP), a Radon based transform (Barva, *et al.*, 2004; Helgason, 2007), algorithm was applied on each data frame to identify the internal boundaries of the

imaged vessel. This algorithm is well adapted to the identification of straight lines in images, which facilitated the detection, but obliged to image and process nearly straight portions of the imaged blood vessel. In order to favour the detection of the edges, light image processing was performed on the image prior to PIP processing. The image was cleaned through a thresholding and an edge detection algorithm applied to focus the line detection algorithm on the edge of the vessel, and not on the acoustic signature of the wall itself. The detection of the positions of the internal side of both walls of the vessel allowed direct estimation of the internal diameter through time. Both pressure and diameter data were analysed and from this the "correction factor" (see earlier in this section and section 4.3.1) was derived for correcting measurements of blood flow velocity for changes in diameter in experiments where diameter cannot be measured.

FIGURE 4.0: B-Mode Image of the Rabbit Abdominal Aorta.

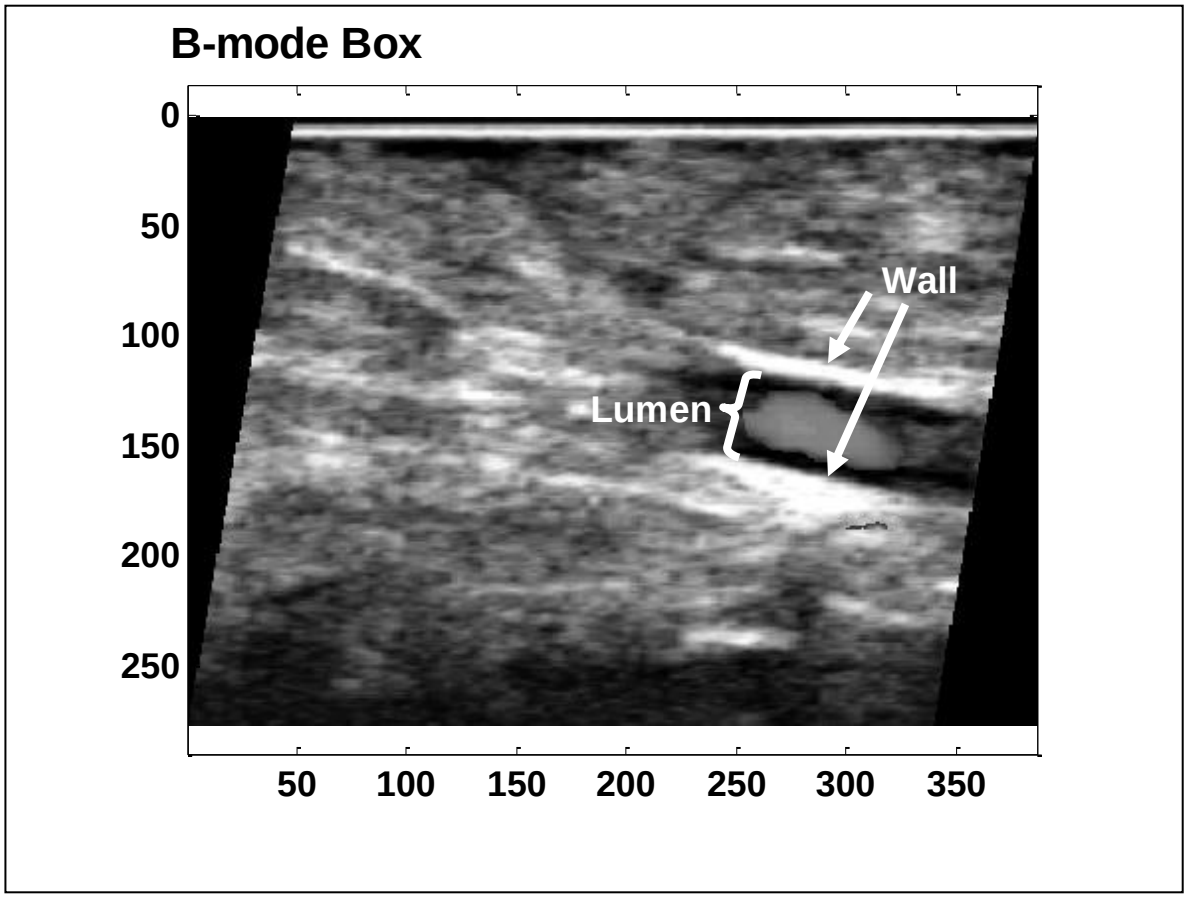

4.2.2 Pharmacological Effects of Saline, Acetylcholine and L-NAME on Abdominal Aortic Blood Pressure and Flow Waveforms

Twenty-eight rabbits were used in these experiments, grouped into sets according to the experimental requirement; numbers of rabbits for a data set are indicated by n. For these experiments, blood pressures along with associated blood flows were recorded at two sites along the abdominal aorta; these recording sites and the methodology are discussed fully in chapter 3, section 3.2.

Additionally, in some experiments, the blood pressure waveform of the central ear artery (auricular artery) was recorded by applanation tonometery; the principle and application of applanation tonometry is explained fully by Mackay *et al*. (1960), Pressman and Newgard (1963), Drzewiecki *et al*. (1983), Kelly *et al*. (1989a, b). To access the central ear artery, superficially and non-invasively, the pinna was manipulated such that the dorsal surface of the pinna was uppermost while the inner surface was placed against a firm flat surface; sufficient fur was shaved from the dorsal surface to expose the skin over the central ear artery. This superficial artery lies just under the skin and just above a central rib of cartilage which gives the mechanical support required for applanation. A tonometer probe (Millar SPT-301 NI Pulse Transducer Pen), supported by a clamp-stand was then placed, i.e. applanated, perpendicularly, gently and lightly against the artery to record the pressure waveform. This was performed with five rabbits for *lo* and *hi doses* of Ach and L-NAME along with the respective saline controls. Ten cardiac cycles were ensemble averaged for each dose. Although the tonometer measured pressure and was calibrated, it was considered that the pressure values obtained by applanation were unlikely to be exactly those that pertain within the artery; however, exact absolute readings were not necessary as readings were standardised in the manner as used by Weinberg *et al*. (2001) and as explained in section 4.3.2.

When all surgical and preparatory procedures were completed, approximately 30min was allowed for the preparation to settle and equilibrate before administration of drugs. In the experiments described here the same doses were used as previously stated, however the doses were given on a non-cumulative basis, namely sets of rabbits received saline, Ach *lo dose* and L-NAME *lo dose* and another set of rabbits received saline, Ach *hi dose* and L-NAME *hi dose*. Infusions were given via the cannula in a femoral vein. As in the experiments described in the previous section 4.2.1, readings for aortic blood pressure and blood flow were taken during mid-infusion of saline and both doses of Ach (*lo* and *hi doses* at maximum effect by mid-infusion), and at 10-20min after the full infusion of both doses of L-NAME when their effects on blood pressure were at maximum.

Data for blood flow velocity was corrected for changes in vessel diameter by application of a "correction factor" (see section 4.2.1 and 4.3.1). The data from these experiments were subjected to analysis of foot-to-foot pulse wave velocity, calculation of wave speed from the pressure and velocity pulse waveforms, reservoir (Windkessel) pressure analysis and wave intensity analysis, from the latter wave reflection can be derived. Wave speed, reservoir (Windkessel) pressure and wave intensity analysis are discussed in Chapter 2.

4.3 RESULTS

This section is set out in two parts: 1) data for determining changes in aortic diameter during the pharmacological treatments thence a derivation of a "correction factor" to correct blood flow velocity values in the event of changes in associated vessel diameter, 2) data to determine the effects of the pharmacological treatments on blood pressure and flow waveforms.

4.3.1 Experiments to Determine by Ultrasound the Internal (Lumen) Diameter of the Abdominal Aorta during Infusions of Saline, Acetylcholine and L-NAME

Figures 4.1 A – H, show recordings of pulsatile abdominal aortic blood pressure along with pulsatile abdominal aortic luminal diameters during infusions of saline, Ach *lo* and *hi doses*, and after infusions but at maximal effect of L-NAME *lo* and *hi doses*; the data for *lo dose* Ach and L-NAME are shown in Figure 4.1 A, C, E & G and data for *hi dose* are shown in Figure 4.1 B, D, F & H. The pressure and diameter recordings are as simultaneous as possible for each treatment. Saline had no effect on resting blood pressure or aortic luminal diameter and these findings with saline are taken as the control for comparison with Ach *lo* and *hi doses* and L-NAME *lo* and *hi doses*. Ach *lo* and *hi doses* caused concomitant decreases in blood pressure and aortic luminal diameter, though these effects of Ach *lo dose* were not clear in the rabbit whose data is shown in Figure 4.1 E. Conversely, L-NAME *lo* and *hi doses* caused concomitant increases in blood pressure and aortic luminal diameter. Again, the effects of L-NAME *lo dose*, like Ach *lo dose*, on blood pressure and aortic luminal diameter were not clear in Figure 4.1 E.

Mean aortic blood pressure (MAP) and mean aortic luminal diameter (mØ) were computed from the pulsatile waveforms (exemplified in Figures 4.1 A – H) of pressure and luminal diameter; the values of MAP and mØ are shown in Table 4.1. These values for each individual rabbit are shown as a scatter plot in Figure 4.2.; a wide scatter is observed. The mean±SD values of MAP and mØ from Table 4.1 are plotted in Figure 4.3 which supplements, or summarises, the data in Figure 4.2. The mean data only are plotted in

Figure 4.4 and, for simplicity, the two sets of data for the saline controls have been combined to give one control data point; a linear fit has been applied.

The data as plotted in Figure 4.4, along with the linear fit and its equation were used to derive the Correction Factor.

FIGURE4.1A: Blood Pressure & Luminal Diameter Pulsatile Waveforms of the Abdominal Aorta after Infusions of Saline, and *lo dose* Ach and L-NAME (Rabbit 1)
(Expt Ref: AAEH100119(1))

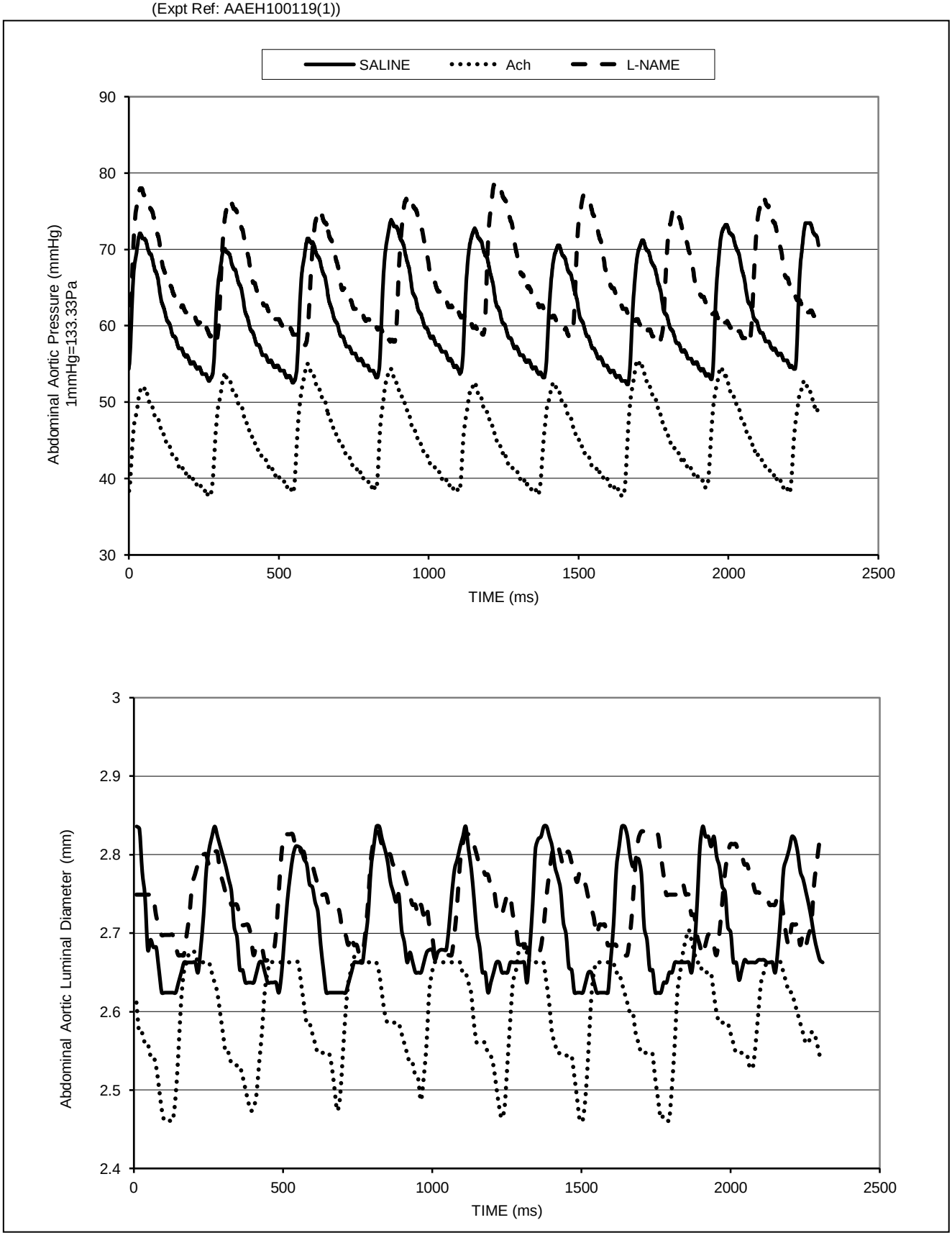

FIGURE4.1B: Blood Pressure & Luminal Diameter Pulsatile Waveforms of the Abdominal Aorta after Infusions of Saline, and *hi dose* Ach and L-NAME (Rabbit 1)
(Expt Ref: AAEH100119(1))

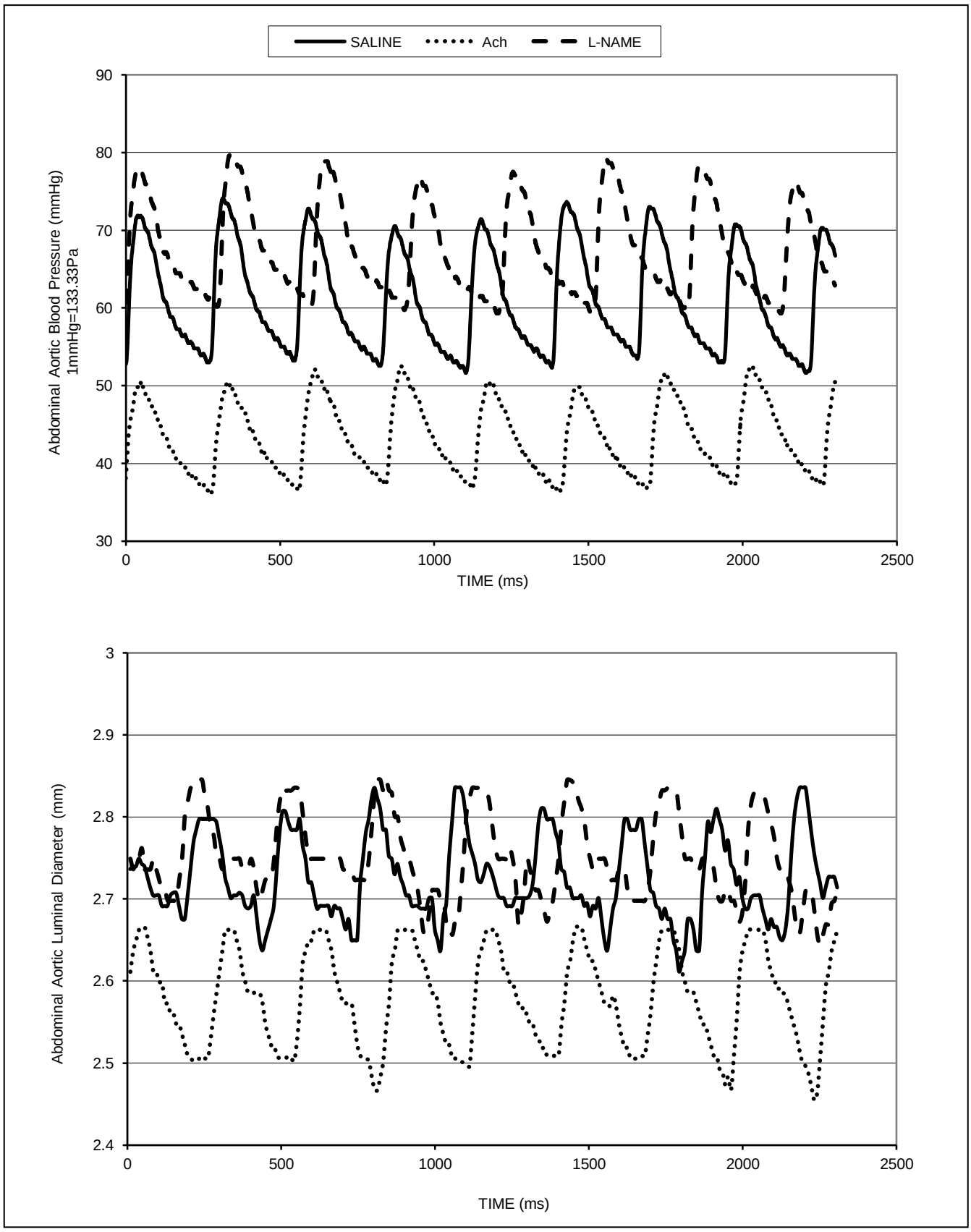

FIGURE4.1C: Blood Pressure & Luminal Diameter Pulsatile Waveforms of the Abdominal Aorta after Infusions of Saline, and *lo dose* Ach and L-NAME (Rabbit 2)
(Expt Ref: AAEH100119(2))

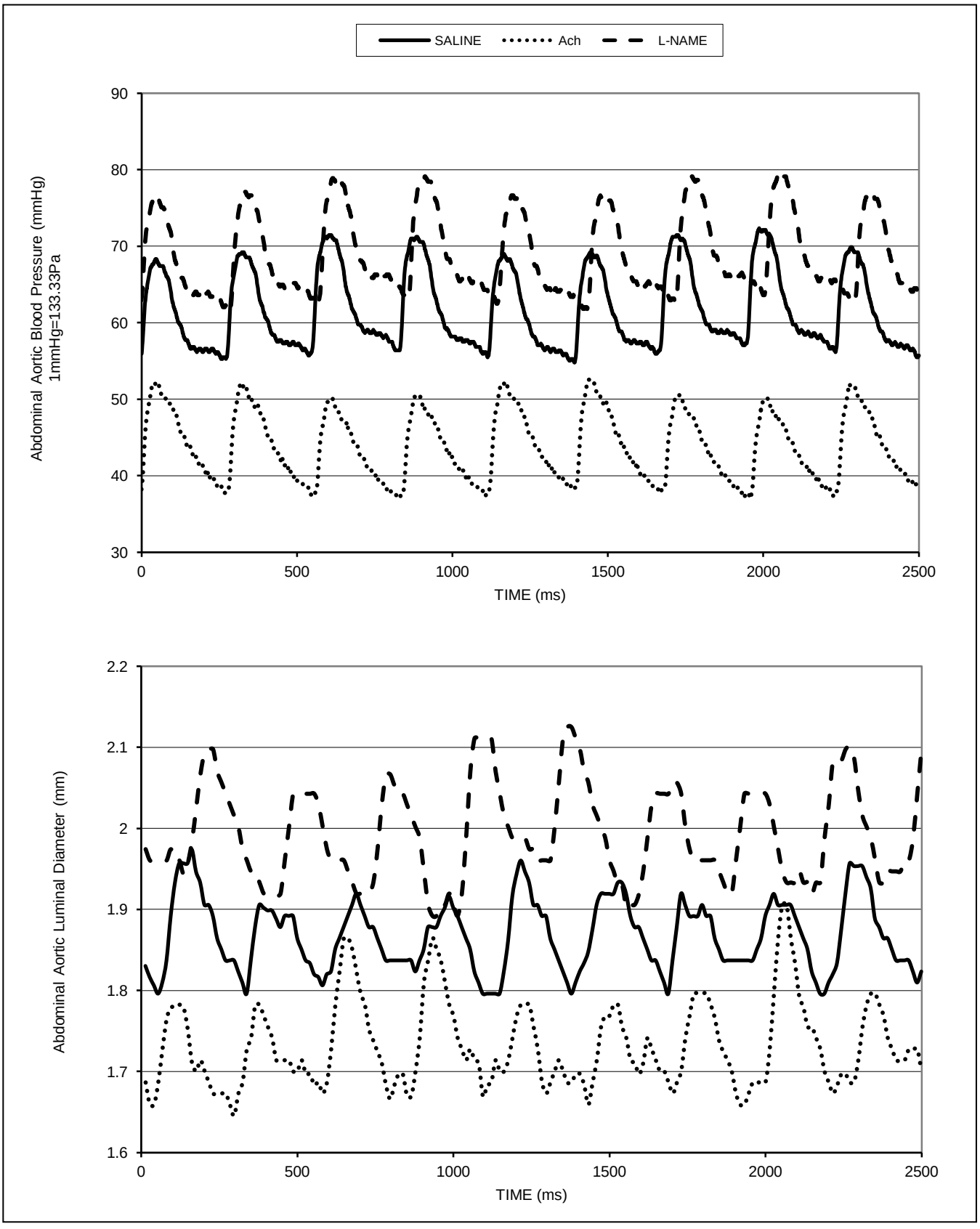

FIGURE4.1D: Blood Pressure & Luminal Diameter Pulsatile Waveforms of the Abdominal Aorta after Infusions of Saline, and *hi dose* Ach and L-NAME (Rabbit 2)
(Expt Ref: AAEH100119(2))

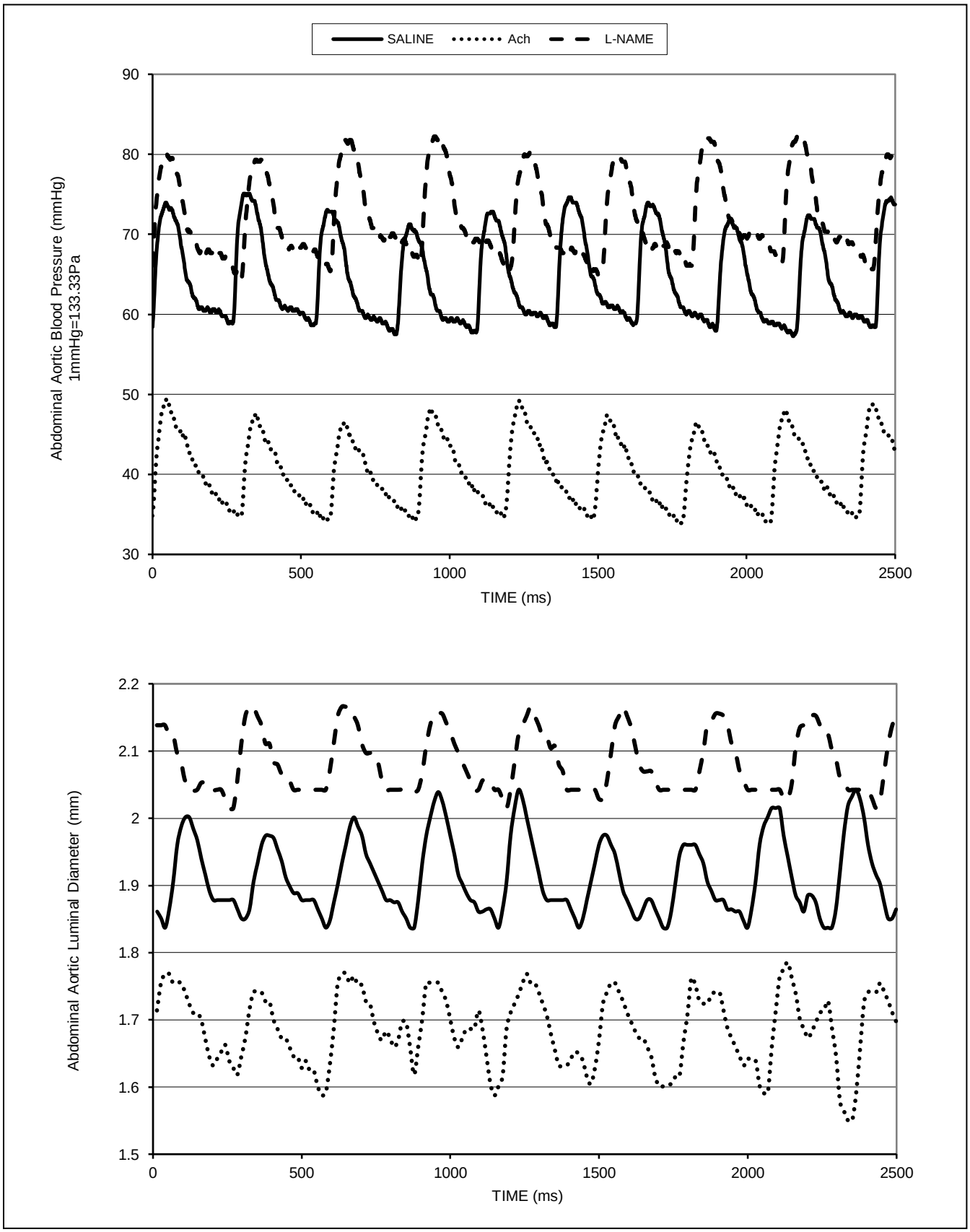

FIGURE4.1E: Blood Pressure & Luminal Diameter Pulsatile Waveforms of the Abdominal Aorta after Infusions of Saline, and *lo dose* Ach and L-NAME (Rabbit 3)
(Expt Ref: AAEH100126(1))

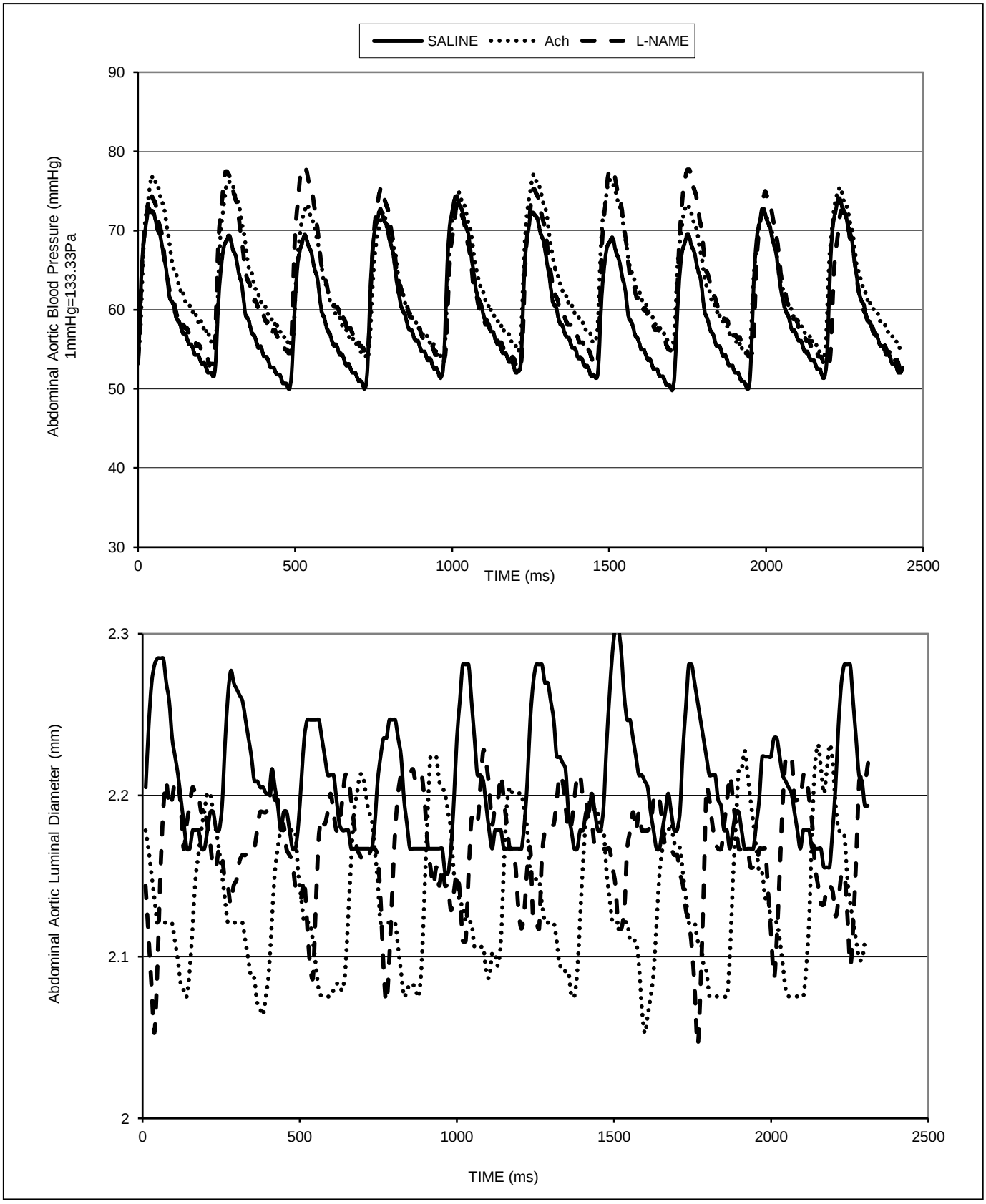

FIGURE4.1F: Blood Pressure & Luminal Diameter Pulsatile Waveforms of the Abdominal Aorta after Infusions of Saline, and *hi dose* Ach and L-NAME (Rabbit 3)
(Expt Ref: AAEH100126(1))

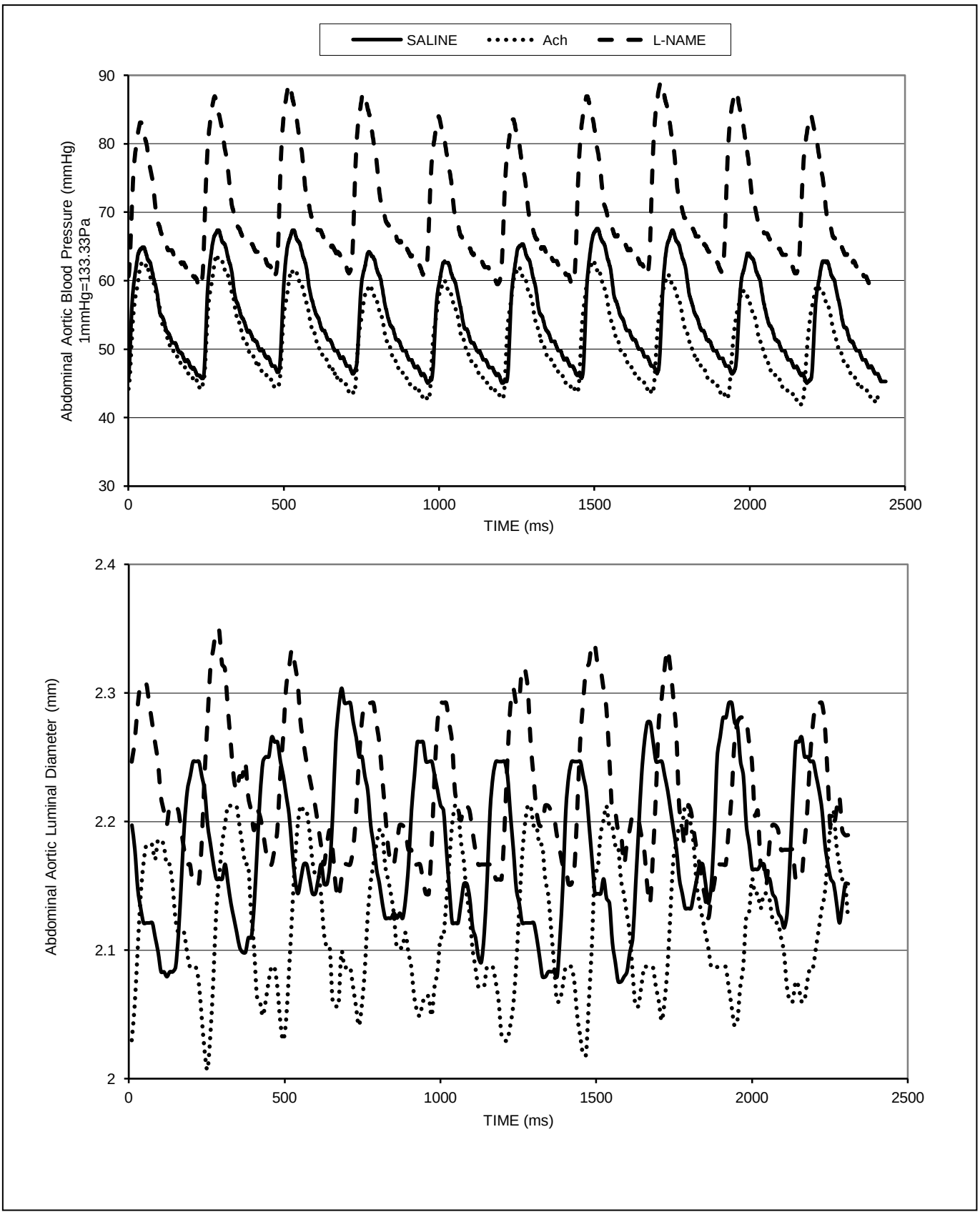

FIGURE4.1G: Blood Pressure & Luminal Diameter Pulsatile Waveforms of the Abdominal Aorta after Infusions of Saline, and *lo dose* Ach and L-NAME (Rabbit 4)
(Expt Ref: AAEH100126(2))

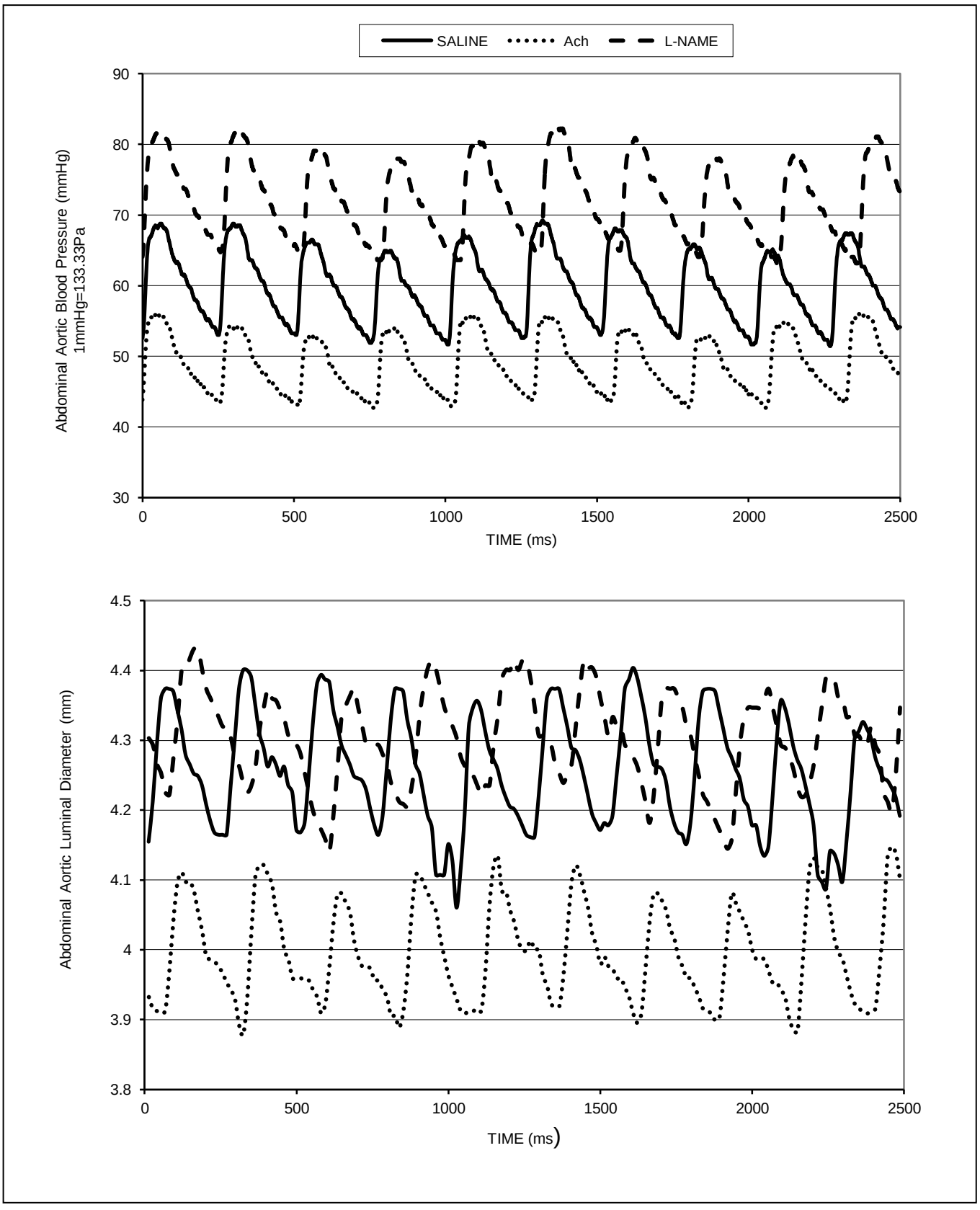

FIGURE4.1H: Blood Pressure & Luminal Diameter Pulsatile Waveforms of the Abdominal Aorta after Infusions of Saline, and *hi dose* Ach and L-NAME (Rabbit 4)
(Expt Ref: AAEH100126(2))

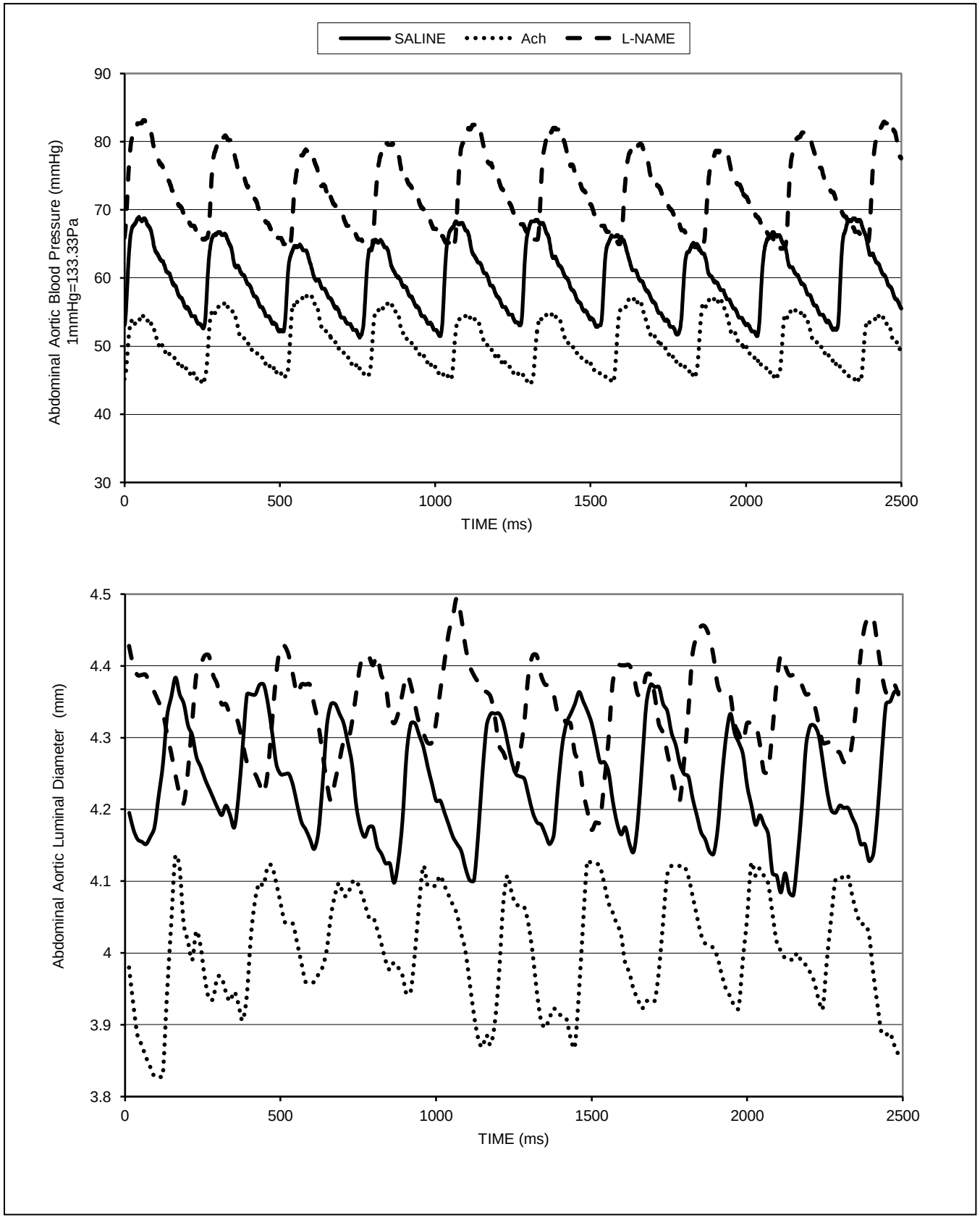

TABLE 4.1: Data from waveforms shown in Figure 4.1 A-H as Derived Mean Abdominal Aortic Blood Pressure (MAP; Pa) and Mean Abdominal Aortic Luminal Diameter (mØ; mm)

Treatment	Parameter	Rabbit 1 Fig 4.1 A&B	Rabbit 2 Fig 4.1 C&D	Rabbit 3 Fig 4.1 E&F	Rabbit 4 Fig 4.1 G&H	MEAN ±SD
Ach *hi*	MAP	5767	5358	6812	6717	6164 ±746
	mØ	2.578	1.686	2.118	4.008	2.598 ±0.791
Ach *lo*	MAP	5991	5879	8459	6508	6709 ±1038
	mØ	2.593	1.734	2.135	3.995	2.614 ±0.853
Saline for *lo*	MAP	8155	8219	7974	7992	8085 ±105
	mØ	2.706	1.87	2.209	4.255	2.760 ±0.913
Saline for *hi*	MAP	8108	8568	7251	7963	7973 ±668
	mØ	2.725	1.911	2.178	4.238	2.763 ±0.812
L-NAME *lo*	MAP	8758	9143	8332	9622	8964 ±476
	mØ	2.744	1.991	2.167	4.300	2.801 ±0.909
L-NAME *hi*	MAP	8935	9566	9358	9705	9391 ±785
	mØ	2.750	2.081	2.222	4.338	2.848 ±0.807

FIGURE 4.2: Scatter Plot of the Data from Table 4.1 of Individual Rabbits after each Treatment. Plots of Mean Abdominal Aortic Blood Pressure (MAP; Pa) and Mean Abdominal Aortic Luminal Diameter (mØ; mm)

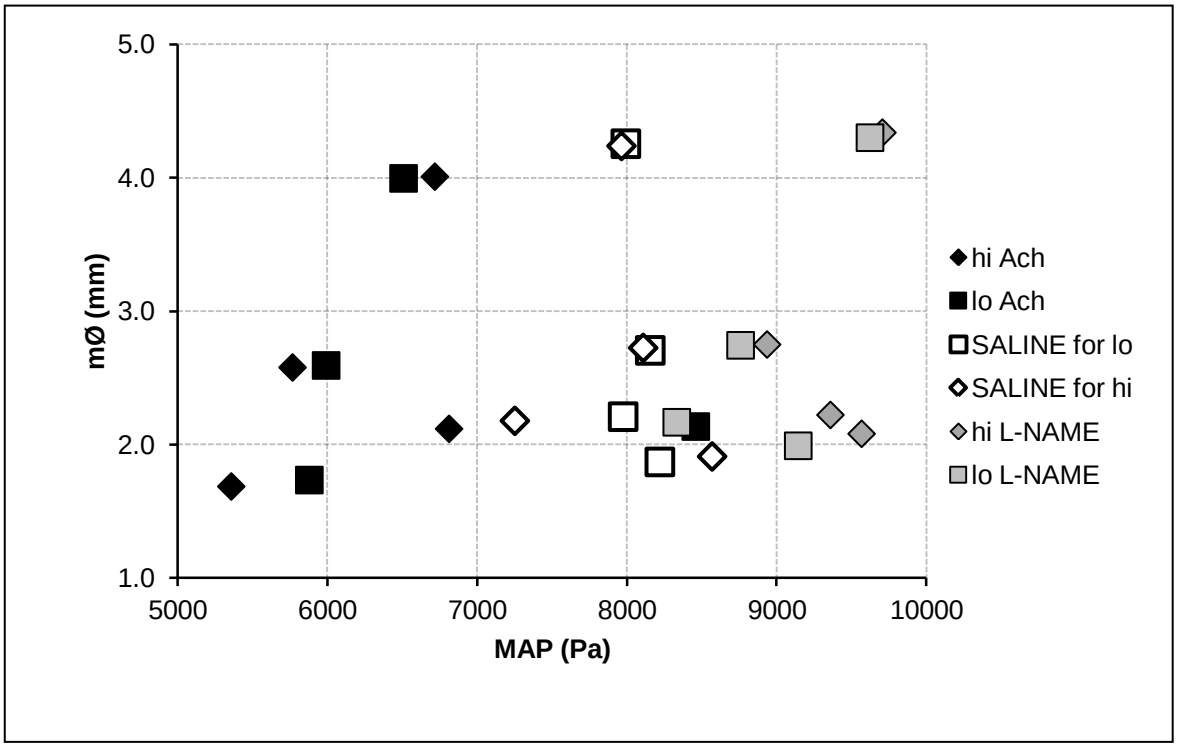

FIGURE 4.3: Plot of the Mean±SD for MAP and mØ from Table 4.1; this summarises the Data in Figure 4.2

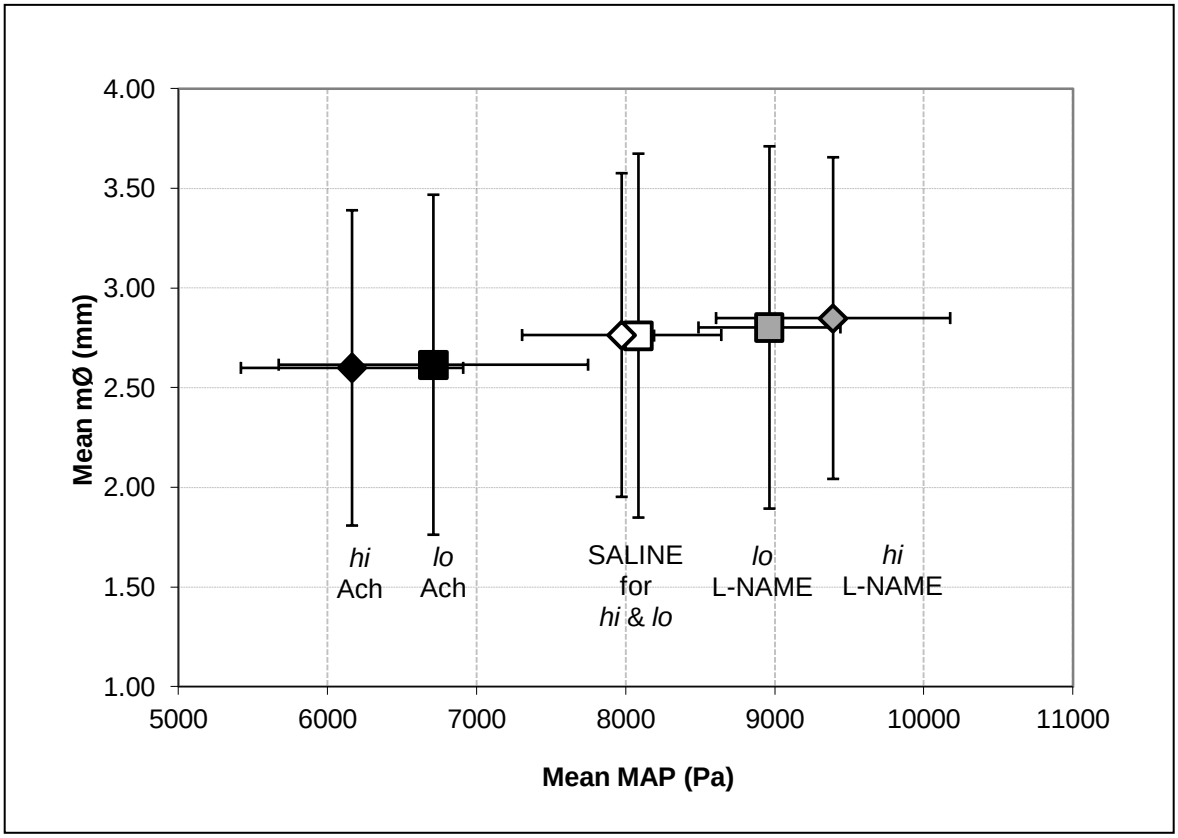

FIGURE 4.4: Re-plot of Data from Figure 4.3 but without SD and the saline data combined as one point; a linear fit is applied.

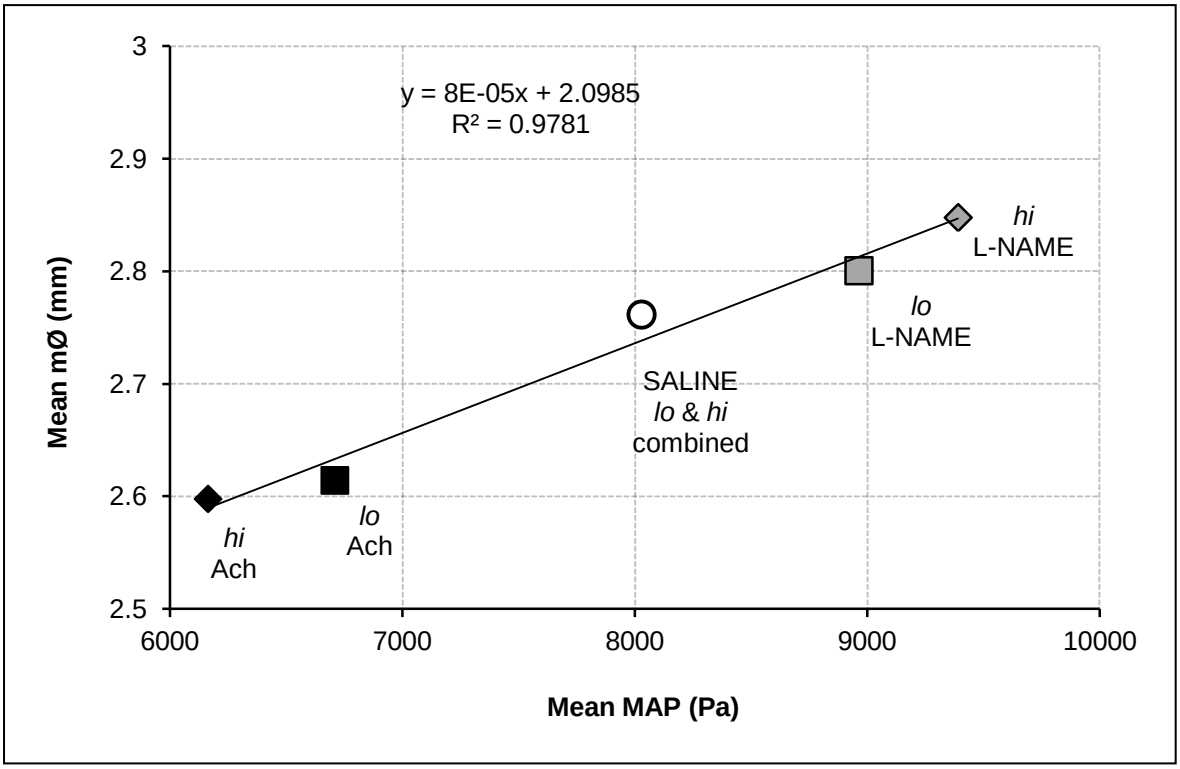

Derivation of the "Correction Factor"

The linear fit equation as shown in Figure 4.4 was used to derive a fitted value for mean mØ from the mean MAP for each treatment (Table 4.2). The fitted mean mØ values obtained for Ach *lo* & *hi doses* and L-NAME *lo* & *hi doses* were then ascribed a value relative to the fitted mean mØ value for saline (Table 4.2). The Correction Factor respective to each treatment is the *reciprocal* value of the *square* of the relative value respective to each treatment since blood flow velocity is calculated (see in section 3.2.3) as the ratio of the measured blood flow volume (numerator) to the luminal area (denominator); the latter is a function of luminal diameter to which the Correction Factor is applied. Thus the blood flow velocity data for Ach *lo* & *hi doses* and L-NAME *lo* & *hi doses* were multiplied by their respective Correction Factor.

TABLE 4.2: Data for the “Correction Factor”

Treatment	Mean MAP (Pa) (x)	*Fitted Mean mØ (mm) (y)	Relative Mean mØ	“Correction Factor”
Ach *hi*	6164	2.592	0.94556	1.1185
Ach *lo*	6709	2.635	0.96149	1.0817
SALINE	8029	2.741	1.00000	1.0000
L-NAME *lo*	8964	2.816	1.02729	0.9476
L-NAME *hi*	9391	2.850	1.03976	0.9250

*Fitting equation from Figure 4.4: $y = 8.0\times10^{-5}x + 2.0985$

$$\text{"}Correction\ Factor\text{"} = \frac{1}{(Relative\ Mean\ m\emptyset)^2}$$

Measurements of External Diameters at the Upstream UpSt Site and Downstream DnSt Site of the Abdominal Aorta

Measurements of external diameter of the abdominal aorta at the UpSt and DnSt sites were made by ruler and divider (section 3.2.3). The mean ± SD values were:

UpSt Site: 4.3±0.3 mm

DnSt Site: 3.0±0.2 mm

Thus, a decrease in diameter of some 30% occurred between the UpSt and DnSt Sites of measurement in the abdominal aorta.

4.3.2 Pharmacological Effects of Acetylcholine and L-NAME on Abdominal Aortic Blood Pressure and Flow Waveforms

Basic Data

Table 4.3 shows basic data as obtained from measurements at the upstream UpSt and downstream DnSt Sites of the abdominal aorta, data being for heart rate (HR), systolic (SBP), diastolic (DBP), pulse amplitude of measured, or total, pressure (PP_{TP}) and mean (MAP) aortic blood pressures, mean aortic blood flow (MABF) and vascular resistance (VR; VR = MAP / MABF; VR respective to the site of measurement, i.e. either UpSt or DnSt Sites in the abdominal aorta). Data were obtained during treatments with L-NAME (*lo* & *hi doses*), saline, and Ach (*lo* & *hi doses*); p-values for statistical significance of effects compared against saline data are included in Table 4.3 – effects were considered not significant (NS) when $p>0.05$. Saline itself had no discernable effects on the basal haemodynamic parameters being considered, thus the data obtained for treatments with L-NAME (*lo* & *hi doses*) and Ach (*lo* & *hi doses*) are compared to the data obtained for treatment with saline.

HR was unaffected by treatments with L-NAME (*lo* & *hi doses*) and Ach (*lo* & *hi doses*). However, L-NAME (*lo* & *hi doses*) increased, whereas Ach (*lo* & *hi doses*) decreased, SBP, DBP and MAP; these effects of L-NAME and Ach were statistically significant (Table 4.3). PP_{TP} was not affected by L-NAME (*lo* & *hi doses*) but was significantly decreased by Ach (*lo* & *hi doses*) (Table 4.3).

L-NAME (*lo dose*) and Ach (*lo dose*) both decreased MABF (Table 4.3 for p-values); this was apparent for both treatments at the UpSt Site but not so apparent for L-NAME (*lo dose*) at the DnSt Site where the decrease was not statistically significant (Table 4.3). Ach (*hi dose*) also decreased MABF as measured at UpSt and DnSt Sites but this was not the case at either site with L-NAME (*hi dose*) which did not change MABF (Table 4.3). L-NAME (*lo dose*) increased and Ach (*lo dose*) decreased VR; these effects were statistically significant as measured at the UpSt Site, but significant only for L-NAME (*lo dose*) at the DnSt Site where Ach caused, at most, a small non-significant increase in VR. L-NAME (*hi dose*) also significantly increased VR as measured at both UpSt and DnSt Sites (Table 4.3). Ach (*hi dose*) significantly decreased VR as measured at the UpSt Site but caused only a small non-significant decrease in VR as measured at the DnSt Site (Table 4.3).

Figure 4.5 summarises graphically the cardiovascular effects of L-NAME and Ach. The effects of L-NAME and Ach on MAP, VR and MABF are considered in relative terms to the data obtained for saline which is considered as zero change. It can be seen that the

increase in blood pressure (MAP) caused by L-NAME (*lo* & *hi doses*) was associated with increased VR; the latter was associated with decreased MABF after L-NAME (*lo dose*) measured at the UpSt Site but at the DnSt Site the effects L-NAME (*lo dose*) on MABF were very variable, likewise for L-NAME (*hi dose*) at UpSt and DnSt Sites. Ach (*lo* & *hi doses*) decreased blood pressure (MAP) as measured at the UpSt and DnSt Sites. This effect was associated with decreased MABF. It is clear at the UpSt Site that the decrease in MAP in response to Ach (*lo* & *hi doses*) was also associated with decreased VR; however this association was not so at the DnSt Site where variable changes in VR occurred.

Overall, the magnitudes of cardiovascular effects of L-NAME and Ach were associated with large variation as indicated by the standard deviations. The data for the two doses of L-NAME and Ach show some limited dose dependency.

TABLE 4.3: Values measured for Heart Rate (HR), Systolic (SBP), Diastolic (DBP), Pulse Pressure (PP_{TP}) and Mean (MAP) Aortic Blood Pressures, Mean Aortic Blood Flow (MABF) and Vascular Resistance (VR) at the Abdominal Aorta of Anaesthetised Rabbits. Data Compared for Treatments with L-NAME (*hi* & *lo doses*) or Ach (*lo* & *hi doses*) against their respective Saline Controls; data are Mean±SD, n=12–15; [p by paired t-test to Saline; NS=not significant p>0.05].

	UpSt Site			**DnSt Site**		
lo dose:	**L-NAME**	**SALINE**	**Ach**	**L-NAME**	**SALINE**	**Ach**
HR (beats/min)	268 ±30 [NS;p=0.48]	273 ±32	270 ±32 [NS;p=0.64]	267 ±31 [NS;p=0.85]	268 ±31	269 ±33 [NS;p=0.58]
SBP (Pa)	11769 ±1428 [p=0.004]	10860 ±1532	8842 ±1203 [p=0.0001]	12046 ±1587 [p=0.0006]	11077 ±1653	9301 ±1225 [p=0.0001]
DBP (Pa)	9089 ±1296 [p=0.0025]	8249 ±1353	6766 ±1074 [p=0.0001]	9006 ±1322 [p=0.0005]	8113 ±1336	6881 ±964 [p=0.0002]
PP_{TP} (PP_{TP}=SBP-DBP) (Pa)	2680 ±435 [NS;p=0.24]	2611 ±390	2076 ±277 [p<0.0001]	3040 ±604 [NS;p=0.21]	2964 ±578	2420 ±496 [p<0.0001]
MAP (Pa)	10312 ±1339 [p=0.003]	9548 ±1435	7851 ±1108 [p<0.0001]	10229 ±1324 [p=0.001]	9461 ±1419	7998 ±1031 [p=0.0001]
MABF $x10^{-6}$ (m^3/s)	2.08 ±0.51 [p=0.0008]	2.31 ±0.53	2.14 ±0.58 [p=0.016]	1.25 ±0.34 [NS;p=0.21]	1.31 ±0.34	1.10 ±0.32 [p<0.0001]
VR $x10^{9}$ (VR=MAP/MABF) ($N.m^{-5}.s$)	5.28 ±1.65 [p<0.0007]	4.30 ±0.99	3.87 ±1.03 [p=0.0017]	8.84 ±2.57 [p=0.0045]	7.78 ±2.35	8.23 ±3.58 [NS;p=0.34]
hi dose:	**L-NAME**	**SALINE**	**Ach**	**L-NAME**	**SALINE**	**Ach**
HR (beats/min)	255 ±31 [NS;p=0.51]	253 ±33	255 ±35 [NS;p=0.15]	254 ±31 [NS;p=0.93]	254 ±33	255 ±35 [NS;p=0.68]
SBP (Pa)	12562 ±1502 [p=0.0003]	11369 ±1489	8094 ±1134 [p<0.0001]	12874 ±1637 [p<0.0001]	11557 ±1557	8616 ±1158 [p<0.0001]
DBP (Pa)	9854 ±1229 [p=0.0002]	8745 ±1189	6292 ±984 [p<0.0001]	9874 ±1183 [p<0.0001]	8597 ±1175	6547 ±914 [p<0.0001]
PP_{TP} (PP_{TP}=SBP-DBP) (Pa)	2708 ±500 [NS;p=0.3]	2624 ±524	1802 ±280 [p<0.0001]	3000 ±616 [NS;p=0.49]	2961 ±608	2069 ±394 [p<0.0001]
MAP (Pa)	10935 ±1264 [p=0.0003]	9873 ±1247	7169 ±1044 [p<0.0001]	10971 ±1232 [p<0.0001]	9786 ±1216	7496 ±997 [p<0.0001]
MABF $x10^{-6}$ (m^3/s)	1.92 ±0.38 [NS;p=0.45]	1.98 ±0.46	1.73 ±0.46 [p=0.019]	0.99 ±0.22 [NS;p=0.56]	0.98 ±0.22	0.81 ±0.22 [p=0.003]
VR $x10^{9}$ (VR=MAP/MABF) ($N.m^{-5}.s$)	5.88 ±1.12 [p=0.013]	5.15 ±0.95	4.38 ±1.10 [p=0.0007]	11.84 ±4.18 [p=0.0002]	10.61 ±3.66	10.06 ±3.74 [NS;p=0.31]

FIGURE 4.5: Effects of L-NAME (*lo* & *hi doses*) and Ach (*lo* & *hi doses*), relative to Saline, on Mean Aortic Pressure (MAP), Vascular Resistance (VR) and Mean Aortic Blood Flow (MABF) in Anaesthetised Rabbits. Data are Mean±SD, n=12 - 15. See Table 4.3 for basal values of saline (control).

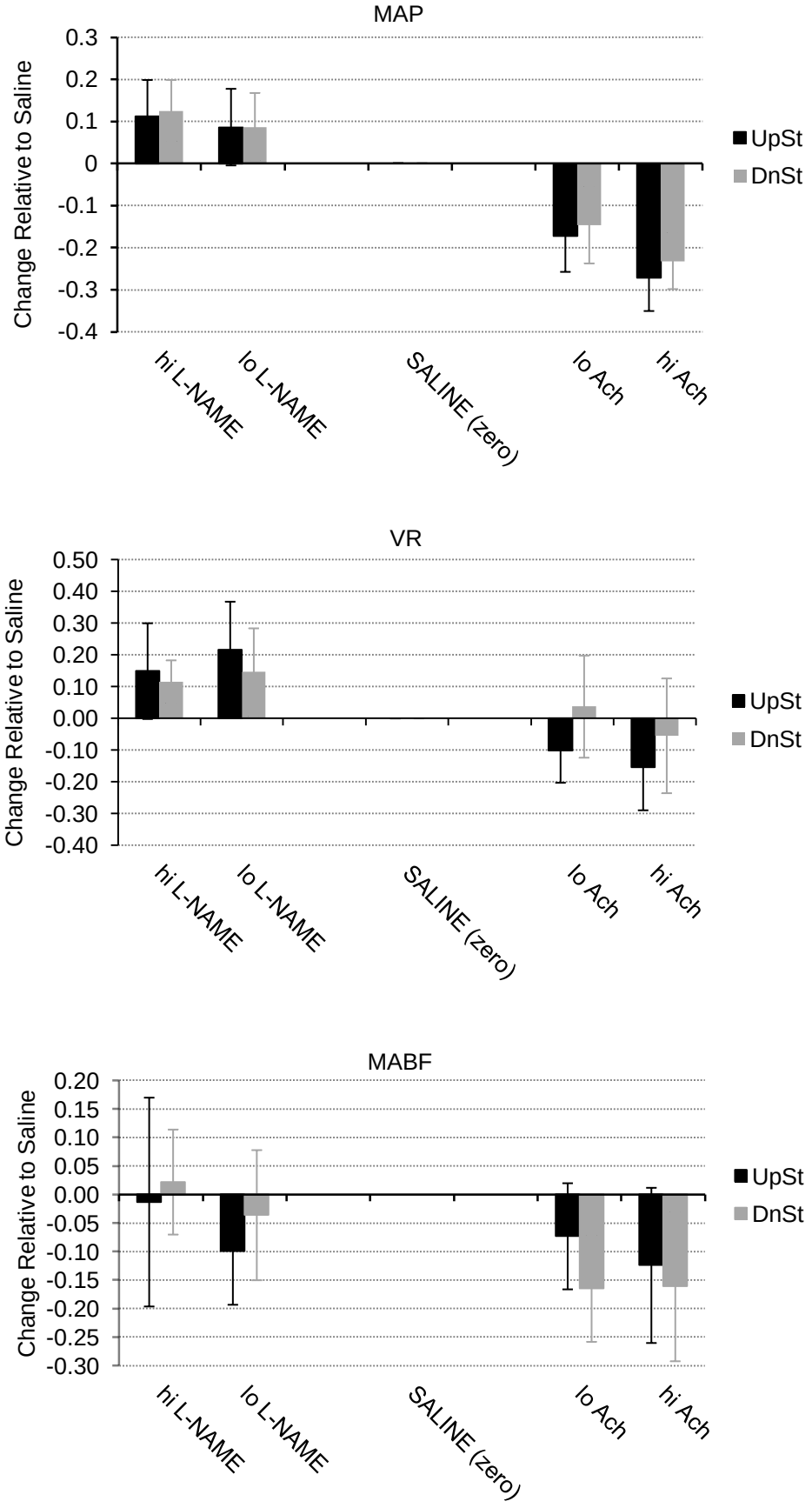

Blood Pressure and Flow Waveforms

Here consideration is given to the shapes of the blood pressure and blood flow velocity waveforms. A brief consideration is made first of the waveforms obtained from the central ear artery followed by a more detailed consideration of aortic pressure and flow waveforms.

Pressure Waveforms of the Central Ear Artery of Anaesthetised Rabbits.

These waveforms were obtained by applanation tonometery (see section 4.2.2). Although applanation tonometry data were obtained from five rabbits for each dose of L-NAME and Ach, only data from three rabbits for each dose are considered here as the data acquired from the other rabbits was of poor quality. However, before considering the data obtained by applanation tonometry, it is useful to be assured that L-NAME and Ach did pharmacologically affect vascular function and this is implied by their effects on aortic blood pressure (i.e. MAP); this is shown in Table 4.4 for the rabbits whose data have been chosen for consideration. Table 4.4 gives values of MAP and HR after infusions of L-NAME (*lo & hi doses*), saline or Ach (*lo* or *hi doses*); it can be seen in comparison to MAP during treatment with saline that L-NAME increased and Ach decreased MAP, especially after *hi doses*, thereby demonstrating pharmacological action of L-NAME and Ach on vascular function. These effects though were not large as the doses chosen were never intended to have marked effect on MAP (see section 4.2), hence taken as a group statistical significance of effects on MAP were not quite achieved by L-NAME (*hi dose*) but were achieved by Ach (*lo & hi* doses) (Table 4.4); the effects of L-NAME (*lo & hi doses*) and Ach (*lo & hi doses*) on HR were small and only that of Ach (*hi* dose), a small increase in HR, achieved statistical significance (p=0.035).

The pressure waveforms obtained from the central ear arteries by applanation tonometry are shown in Figure 4.6 where the waveform shapes are ensemble averages. They are expressed as a ratio of the maximum pulse amplitude and curves are aligned from their respective maximum systolic points; this method of data comparison is taken from Weinberg *et al*. (2001) (see also Figure 1.1). Figure 4.6 shows waveforms obtained from the rabbits after they received doses of L-NAME (*lo & hi doses*), saline, or Ach (*lo & hi doses*). Because the timing of the maximum systolic points differed between waveforms, the aligning of the maximum systolic points caused a paucity of data at the early systolic shoulders and so resulted in the unevenness seen on the curves. Ach (*lo & hi doses*) caused a broadening of the waveform as compared to that after saline infusions. L-NAME (*lo & hi doses*) caused only small changes to the waveform which remained closely similar to the control (saline) waveform. It should be noted that the line of the diastolic decay for the pressure waveform

after infusions of Ach is *above* that after infusions of saline, while the diastolic decay line after infusions of L-NAME is *below* that after infusions of saline. That the waveforms after L-NAME infusion were little different to the control might indicate that L-NAME was not active, however, as the data suggests in Table 4.4, certainly in the three rabbits that received *hi dose* L-NAME, the latter did affect aortic blood pressure by increasing it thereby demonstrating activity of L-NAME.

TABLE 4.4: Effects of L-NAME and Ach compared with saline on Abdominal Aortic Blood Pressure (MAP; Pa) and Heart Rate (HR; beats/min) in Anaesthetised Rabbits. Three rabbits, though different rabbits, for *lo* or *hi doses*. Percent Differences of MAP from Saline values are shown in parentheses.
Paired t-test, NS = Not Significant at p>0.05 compared to Saline.
Each rabbit is identified by an experiment reference number.

	L-NAME *lo dose*		**Saline**		**Ach *lo dose***	
Rabbit Expt. Ref.	MAP	HR	MAP	HR	MAP	HR
AAEH 090602	8467 (+1.9)	254	8307	259	6320 (-23.9)	254
AAEH 090624	12133(+21.5)	317	9986	311	9066 (-9.2)	319
AAEH 090710	9653 (+4.5)	238	9240	230	7627 (-17.5)	236
MEAN ± SD	10084±1871 NS;p=0.28	270±42 NS;p=0.54	9178±841	267±41	7671±1374 p=0.04	270±44 NS;p=0.54
	L-NAME *hi dose*		**Saline**		**Ach *hi dose***	
AAEH 090317(1)	10626(+18.6)	281	8960	272	6467 (-27.8)	274
AAEH 090318(1)	12560(+21.4)	250	10346	255	7147 (-30.9)	258
AAEH 090402	10360 (+7.2)	276	9666	272	7333 (-24.1)	276
MEAN ± SD	11182±1201 NS;p=0.076	269±17 NS;p=0.58	9657±693	266±10	6982±456 p=0.01	269±10 p=0.035

For conciseness the values are taken only from the upstream UpSt Site

For comparison with the pressure waveforms obtained by applanation tonometry from the central ear artery of the rabbits considered, Figures 4.7A & B show, for the same rabbits, the pressure waveforms obtained in the abdominal aorta at both the upstream, UpSt, and downstream, DnSt, Sites. The waveforms are expressed and compared in the same manner as used for Figure 4.6, namely the method of Weinberg *et al*. (2001). Note, as with the pressure waveforms of the central ear artery, in all cases of the abdominal aorta (UpSt &

DnSt Sites) the line of the diastolic decay for the pressure waveform after infusions of Ach is *above* that after infusions of saline, while the diastolic decay line after infusions of L-NAME is *below* that after infusions of saline. As explanation for Figure 4.7A at DnSt Site, the peculiar shape of the mean waveforms in early systole, especially that after saline, is due to the shape of the waveform of one rabbit – see Figure 4.8 for clarification.

FIGURE 4.6: Effects of Ach (*lo & hi doses*) and L-NAME (*lo & hi doses*) Compared to Saline Control, on the Blood Pressure Waveform of the Central Ear Artery of Anaesthetised Rabbits; n=3 for each dose; data acquired by Applanation Tonometry. Note the diastolic decay curves, after Ach they diverge up, after L-NAME they diverge down, and away from that after Saline.

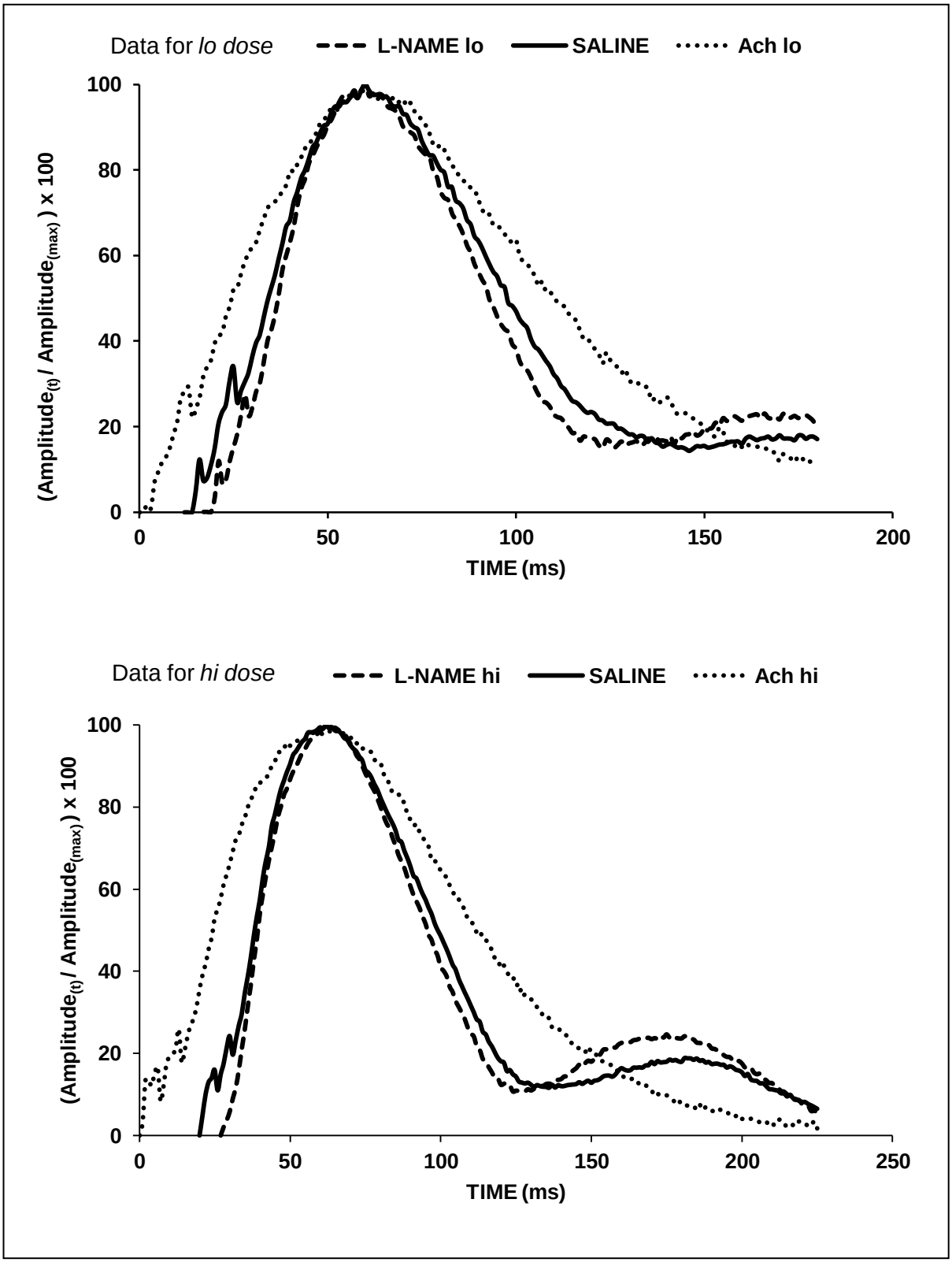

FIGURE 4.7A: Effects of Ach (*lo dose*) and L-NAME (*lo dose*) Compared to Saline Control on the Blood Pressure Waveform at the UpSt & DnSt Sites of the Abdominal Aorta of Anaesthetised Rabbits; n=3 for each dose; same rabbits as of Figure 4.6. Note the diastolic decay curves, after Ach they diverge up, after L-NAME they diverge down, and away from that after Saline.

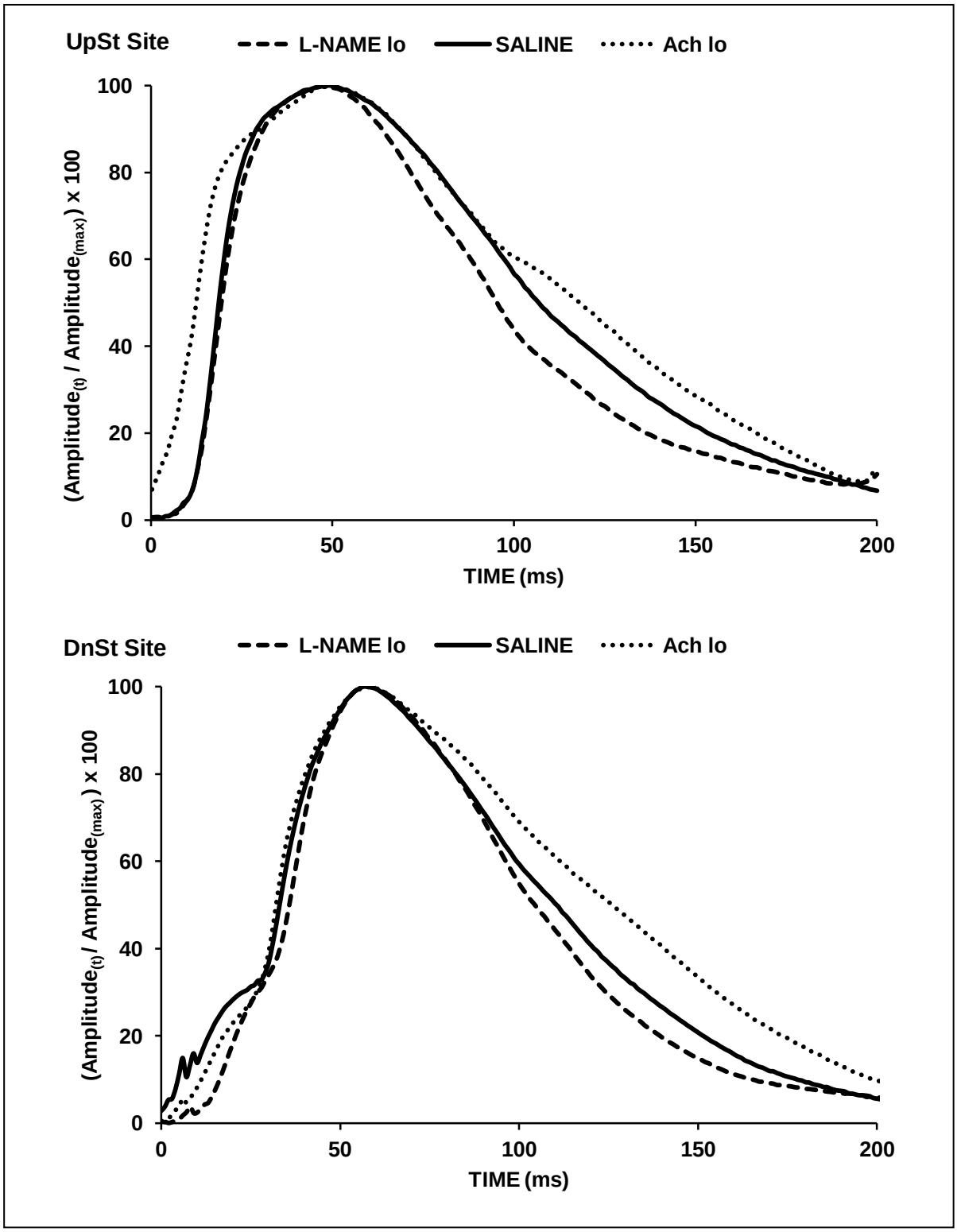

FIGURE 4.7B: Effects of Ach (*hi dose*) and L-NAME (*hi dose*) Compared to Saline Control on the Blood Pressure Waveform at the UpSt & DnSt Sites of the Abdominal Aorta of Anaesthetised Rabbits; n=3 for each dose; same rabbits as of Figure 4.6. Note the diastolic decay curves, after Ach they diverge up, after L-NAME they diverge down, and away from that after Saline.

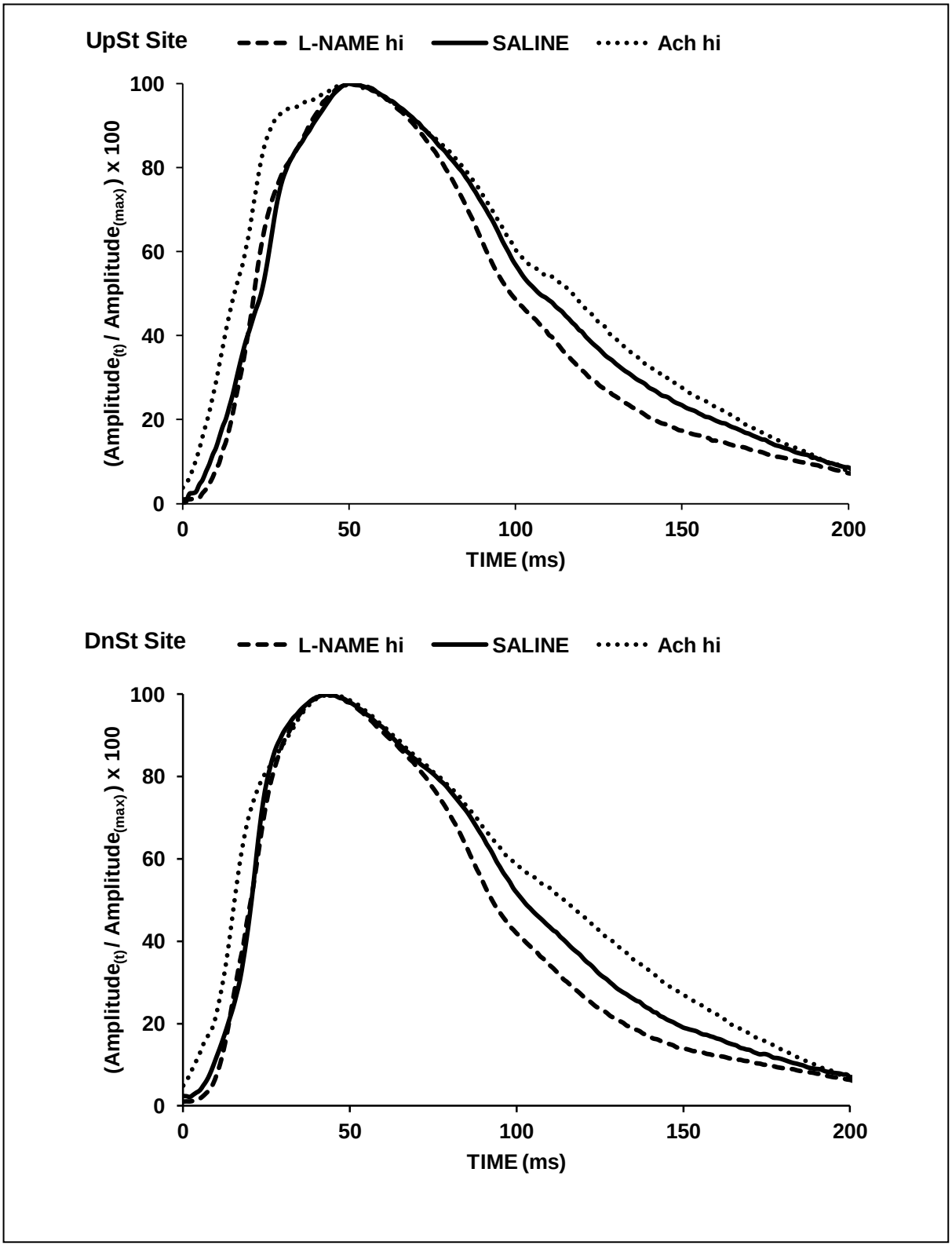

FIGURE 4.8: The Waveforms at the DnSt Site of the Abdominal Aorta after treatment with Saline shown individually for the three Rabbits considered in Figure 4.7A DnSt Site. This figure explains the shape of the mean waveform curve in early systole; the mean curve is also shown here. It is the systolic aspect of rabbit 090710 that affects the early systolic aspect of the mean waveform.

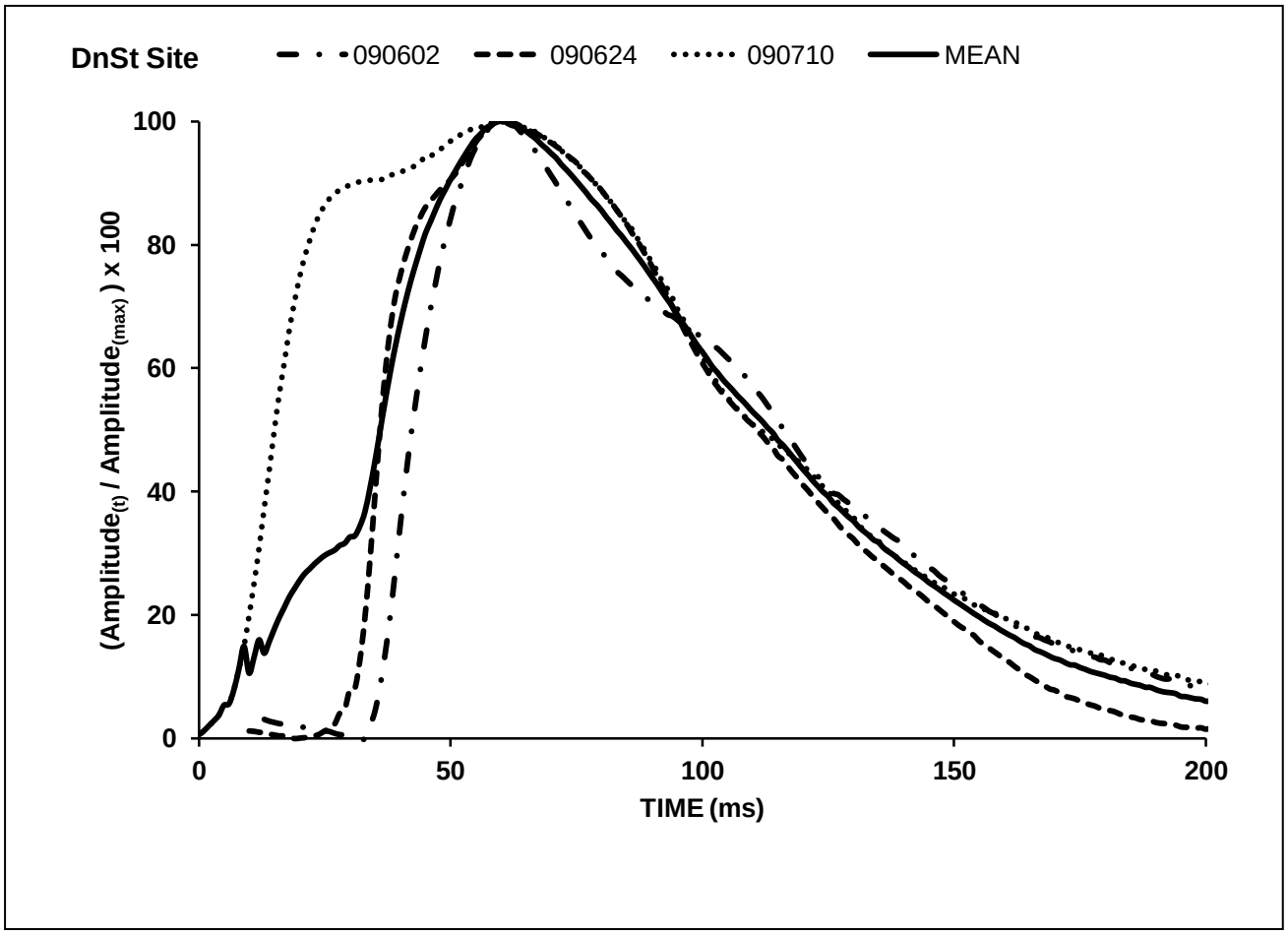

Blood Pressure and Flow Waveforms of the Abdominal Aorta of Anaesthetised Rabbits (Of all Rabbits used in these Experiments). The blood pressure waveforms for the abdominal aorta observed under control conditions appeared to be of two general types with regard to their diastolic pressure decay curves; let us refer to these as Type 1 diastolic pressure decay and Type 2 diastolic pressure decay. The two types of pressure waveform are shown in Figure 4.9. Those of Type 1 seemed to be the most often observed during control conditions and exhibited quasi-exponential decays of pressure during diastole; those of Type 2 were less often observed during control conditions and exhibited complex shaped pressure decays during diastole. Figures 4.10A & B to Figures 4.11A & B show more examples of Type 1 diastolic decay and Figures 4.12A & B to Figures 4.14A & B show examples of Type 2 diastolic decay pressure waveforms; available associated blood flow velocity waveforms are included in the figures. Figures show, for comparison, the effects of L-NAME and Ach on the waveforms. Interestingly, a Type 1 pressure waveform existing during saline control conditions can be converted by L-NAME to almost a Type 2 pressure waveform (Figure 4.11A & B). Furthermore, a Type 2 pressure waveform existing during saline control conditions is accentuated by L-NAME but converted to a Type 1-like pressure waveform by Ach (Figures 4.12A & B to 4.14A & B). Although Type 1 and Type 2 pressure waveforms can exist at similar MAP values, Type 1 tend to occur more at MAP values lower than those at which Type 2 occur (Figure 4.15A & B); the latter tend to occur more frequently above MAP of 10,000 Pa. Hence no Type 2 diastolic pressure decay waveforms occurred after treatment with Ach when MAP was reduced but Type 2 pressure waveforms did occur after treatment with L-NAME when blood pressure increased (Figure 4.15A & B). Table 4.5 presents an analysis of the data of Figures 4.15A & B. Comparisons are made in Table 4.5 of the data for mean blood pressure (MAP) associated with Type 1 and 2 waveforms from the treatment groups L-NAME (*lo & hi doses*) and saline controls, however that of Ach (*lo & hi doses*) has been omitted to avoid bias because this treatment resulted in only Type 1 waveforms. The data in Table 4.5 confirms the observation displayed in Figures 4.15A & B that Type 2 waveforms tend to occur at higher blood pressures than do the Type 1 waveforms.

The reason for drawing attention to these waveform shapes is to caution consideration of the data obtained from the diastolic fitting algorithm for reservoir (Windkessel) pressure (Chapter 2). Figure 4.16 shows an example where the reservoir (Windkessel) pressure diastolic fitting is close to the Type 1 diastolic pressure decay waveform during saline (Figure 4.16A) and Ach (Figure 4.16B) infusions but the fit is less precise when the waveform converts to a Type 2 diastolic pressure decay waveform after infusion of L-NAME (Figure 4.16C). Figure 4.17 also gives examples of the less precise diastolic fitting of the reservoir (Windkessel)

pressure to a Type 2 diastolic pressure decay waveform under control conditions of saline infusion (Figure 4.17A) and under conditions of L-NAME infusion (Figure 4.17B), but close fitting to the Type 1 curve resulting under conditions of Ach infusion (Figure 4.17C).

A relationship between the level of arterial blood pressure and Type 1 or Type 2 waveforms has been addressed above. However, as a test to determine if differences exist between data derived from Type 1 or Type 2 waveforms for other analyses (e.g. of reservoir (Windkessel) pressure, wave intensity analysis), data sets derived from Type 1 waveforms were compared to data sets derived from Type 2 waveforms. This was done for those treatment groups where the two waveforms existed, namely the treatment groups L-NAME (*lo* and *hi dose*) and saline controls; as explained previously, data was not considered for the Ach (*lo* and *hi doses*) treatment as only the Type 1 waveform occurred with this treatment. Of all the data sets derived from Type 1 or Type 2 waveforms, the two data sets that showed the most statistically significant differences across the treatments were the integral ($\int$RP) and pressure pulse amplitude (PP_{RP}) of the reservoir (Windkessel) pressure (Table 4.6). $\int$RP and PP_{RP} derived from Type 1 waveforms had values that were greater than those of $\int$RP and PP_{RP} derived from Type 2 waveforms. Otherwise, differences in the other data sets derived from Type 1 and Type 2 waveforms were sporadic and were not consistently observed across the treatments; these data sets were not therefore included in Table 4.6. Because, overall, there were no remarkable differences between data sets derived from the Type 1 and Type 2 waveforms, it was decided that data for each treatment group would be considered (pooled) as one set for each treatment; pooling included the data for $\int$RP and PP_{RP}.

Reservoir (Windkessel) Pressure: Data derived from it; its Subtraction from Measured (Total) Pressure.

As explained in Chapter 2, the reservoir (Windkessel) pressure is derived in two parts: 1) the systolic part from which the parameter A is obtained, and 2) the diastolic part (discussed above in relation to Type 1 & 2 diastolic pressure decay waveforms) from which three parameters are obtained, namely: B the decay rate constant, tau (τ) the decay time constant which is the reciprocal of B, and P infinity (P_∞).

Figure 4.9: Illustrations exemplifying the two pressure waveforms ascribed as Type 1 and Type 2 recorded in the abdominal aorta at the upstream site, UpSt, and downstream site, DnSt, in two anesthetised rabbits. Data are expressed as amplitude after subtraction of DBP at 0 time.

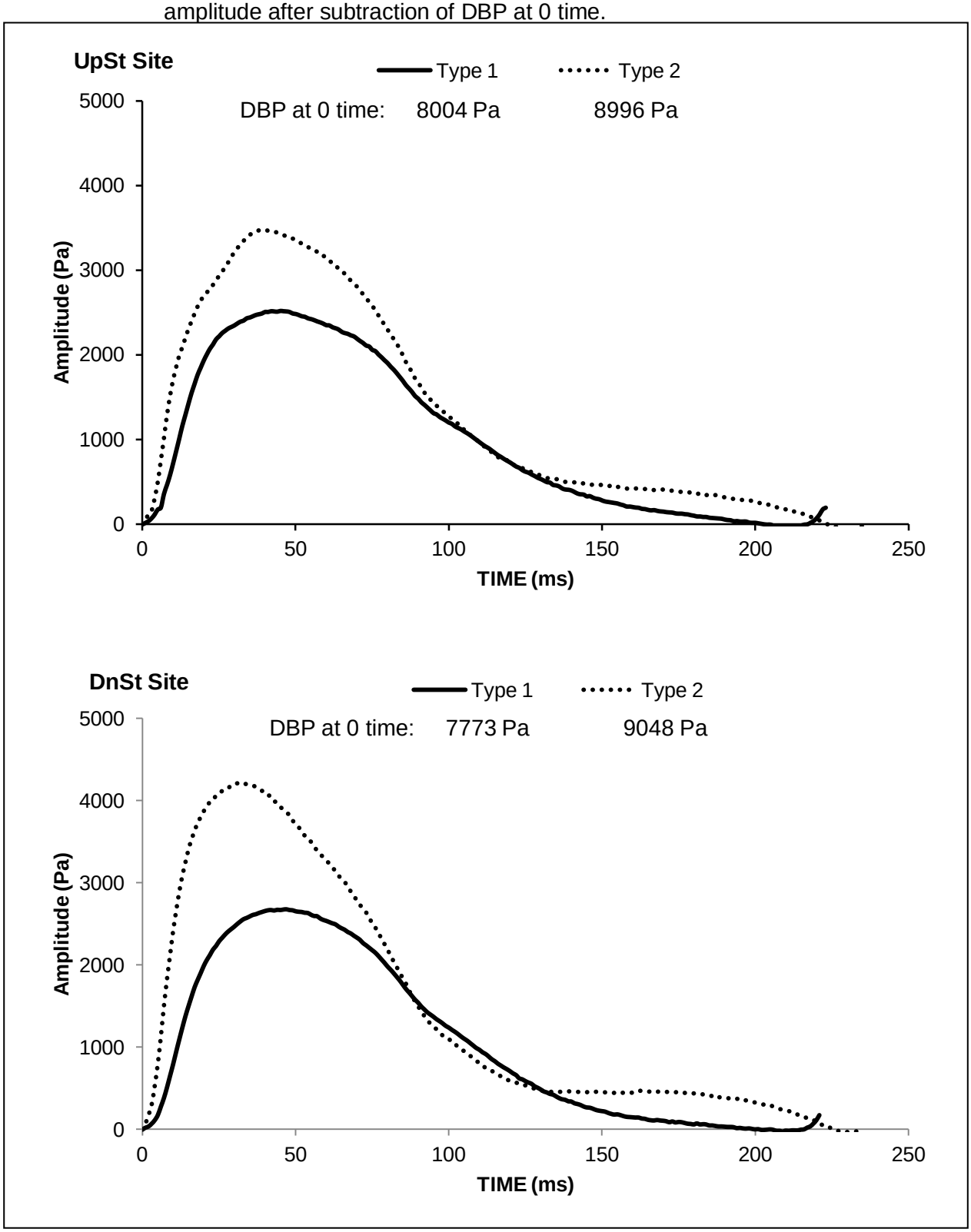

Type 1 from Rabbit Ref. AAEH 091016(2); Type 2 from Rabbit Ref. AAEH 090318(1)

FIGURE 4.10 A: **Type 1** Blood Pressure Waveform along with the Associated Blood Flow Velocity Waveform (UpSt Site in the Abdominal Aorta). Included are Waveforms after ***lo*** *doses* of L-NAME or Ach. All waveforms shown are after subtraction of their respective absolute diastolic values at time 0.
Absolute diastolic values (Pa & m/s): L-NAME curves 9086 & 0.134; Saline curves 7947 & 0.107; Ach curves 6883 & 0.059.

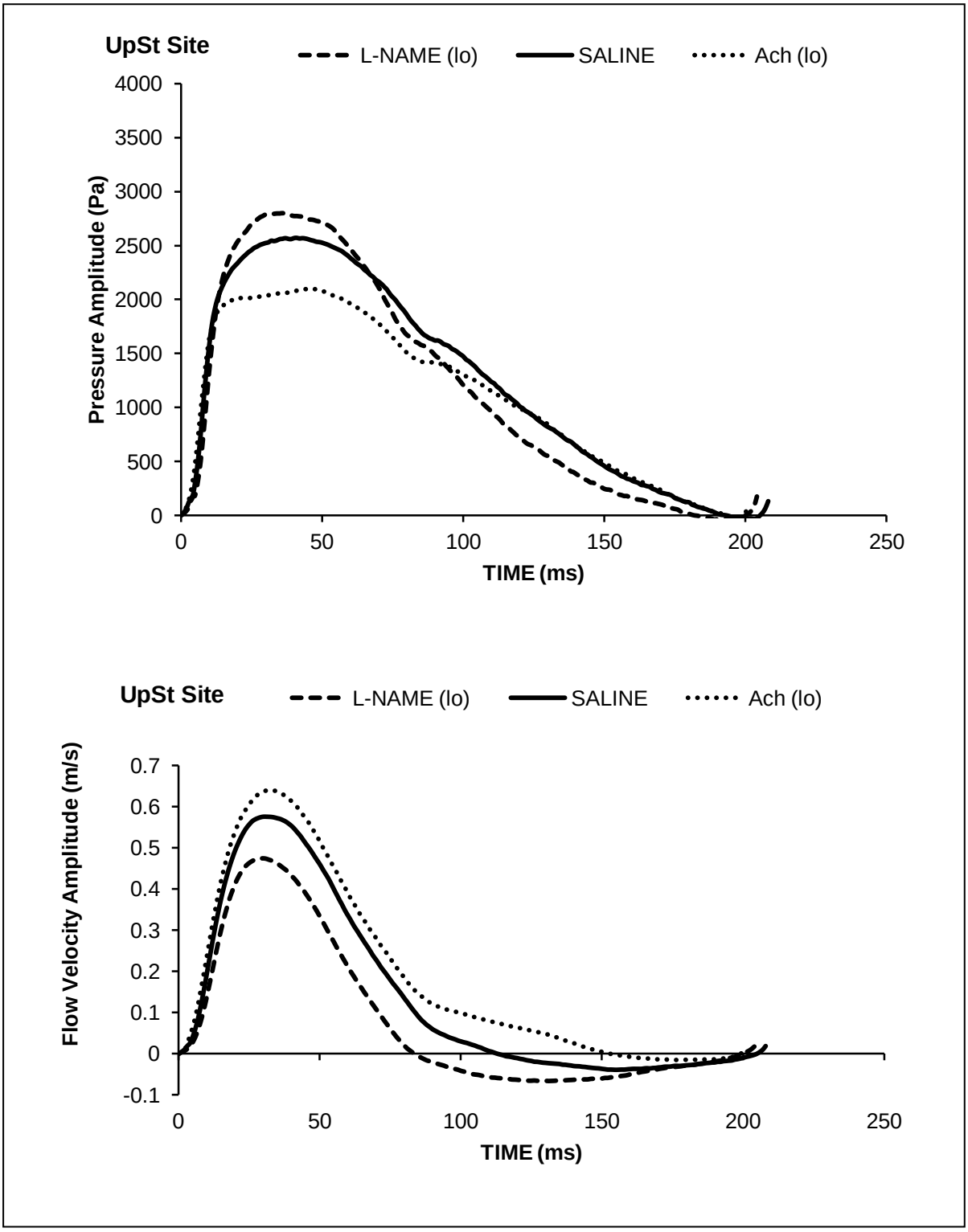

Experiment Ref.: AAEH 090616(1)

FIGURE 4.10 B: **Type 1** Blood Pressure Waveform along with the Associated Blood Flow Velocity Waveform (DnSt Site in the Abdominal Aorta). Included are Waveforms after ***Io*** *doses* of L-NAME or Ach. All waveforms shown are after subtraction of their respective absolute diastolic values at time 0.
Absolute diastolic values (Pa & m/s): L-NAME curves 8843 & 0.118; Saline curves 7809 & 0.089; Ach curves 6628 & 0.041.

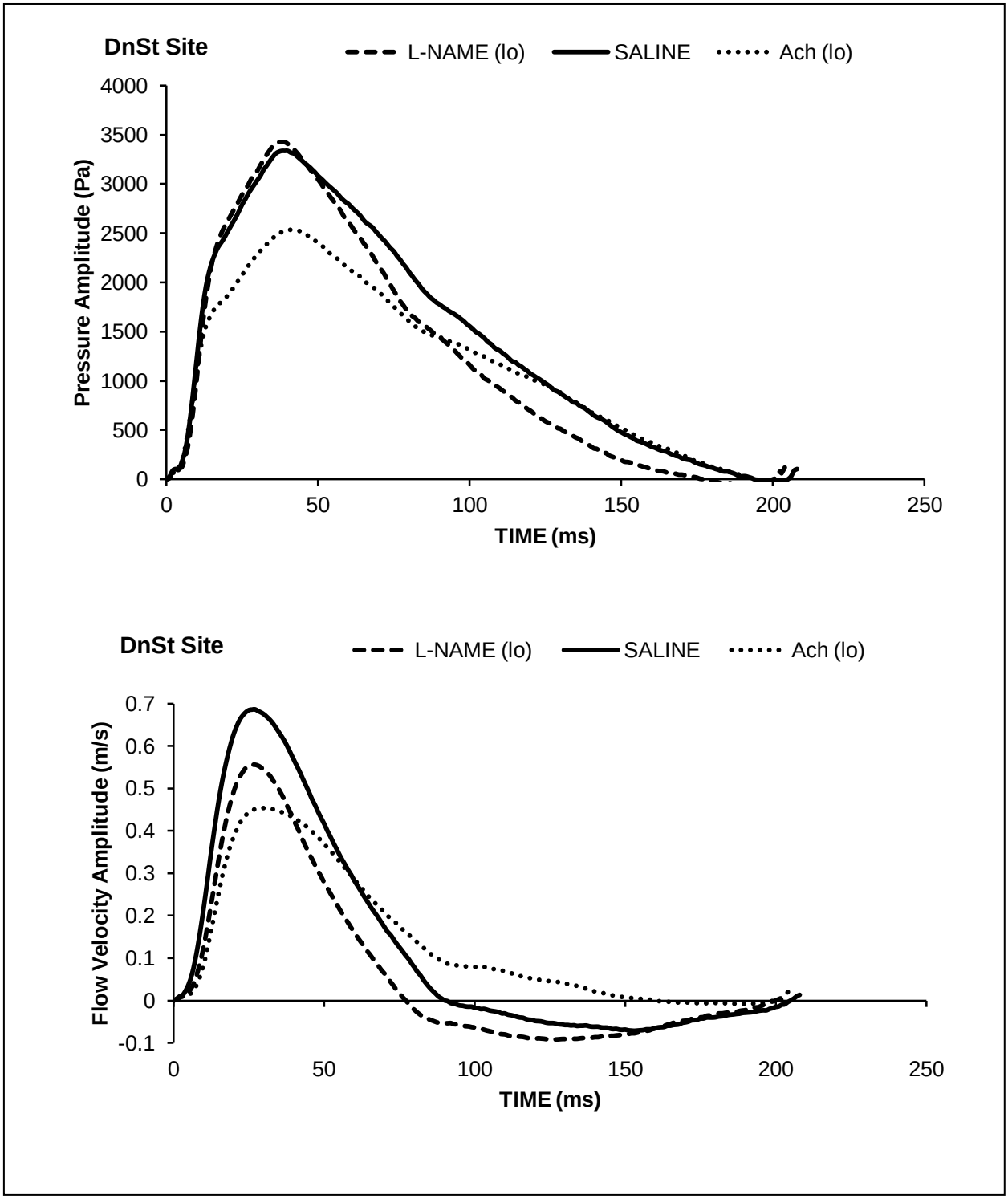

Experiment Ref.: AAEH 090616(1)

FIGURE 4.11 A: **Type 1** Blood Pressure Waveform (see saline curve) along with the Associated Blood Flow Velocity Waveform (UpSt Site in the Abdominal Aorta). Included are Waveforms after ***hi*** *doses* of L-NAME* or Ach. All waveforms shown are after subtraction of their respective absolute diastolic values at time 0.
Absolute diastolic values (Pa & m/s): L-NAME curves 9330 & 0.085; Saline curves 8028 & 0.093; Ach curves 4687 & 0.003.

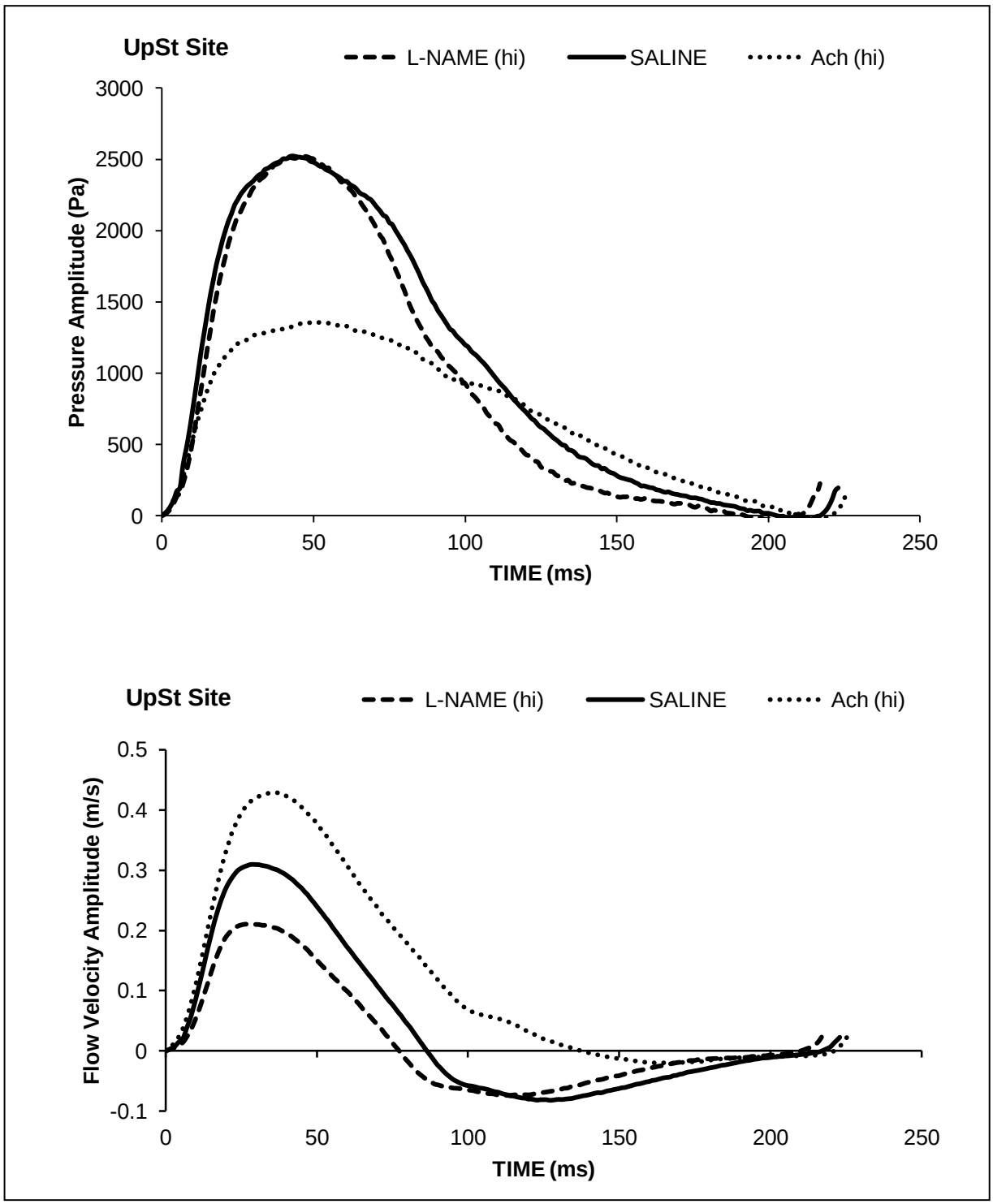

*Note: L-NAME appears to convert Type 1 almost to Type 2 (see plot of pressures).

Experiment Ref.: AAEH 091016(2)

FIGURE 4.11 B: **Type 1** Blood Pressure Waveform (see saline curve) along with the Associated Blood Flow Velocity Waveform (DnSt Site in the Abdominal Aorta). Included are Waveforms after ***hi*** *doses* of L-NAME* or Ach. All waveforms shown are after subtraction of their respective absolute diastolic values at time 0.
Absolute diastolic values (Pa & m/s): L-NAME curves 9285 & 0.204; Saline curves 7800 & 0.166; Ach curves 5545 & 0.127.

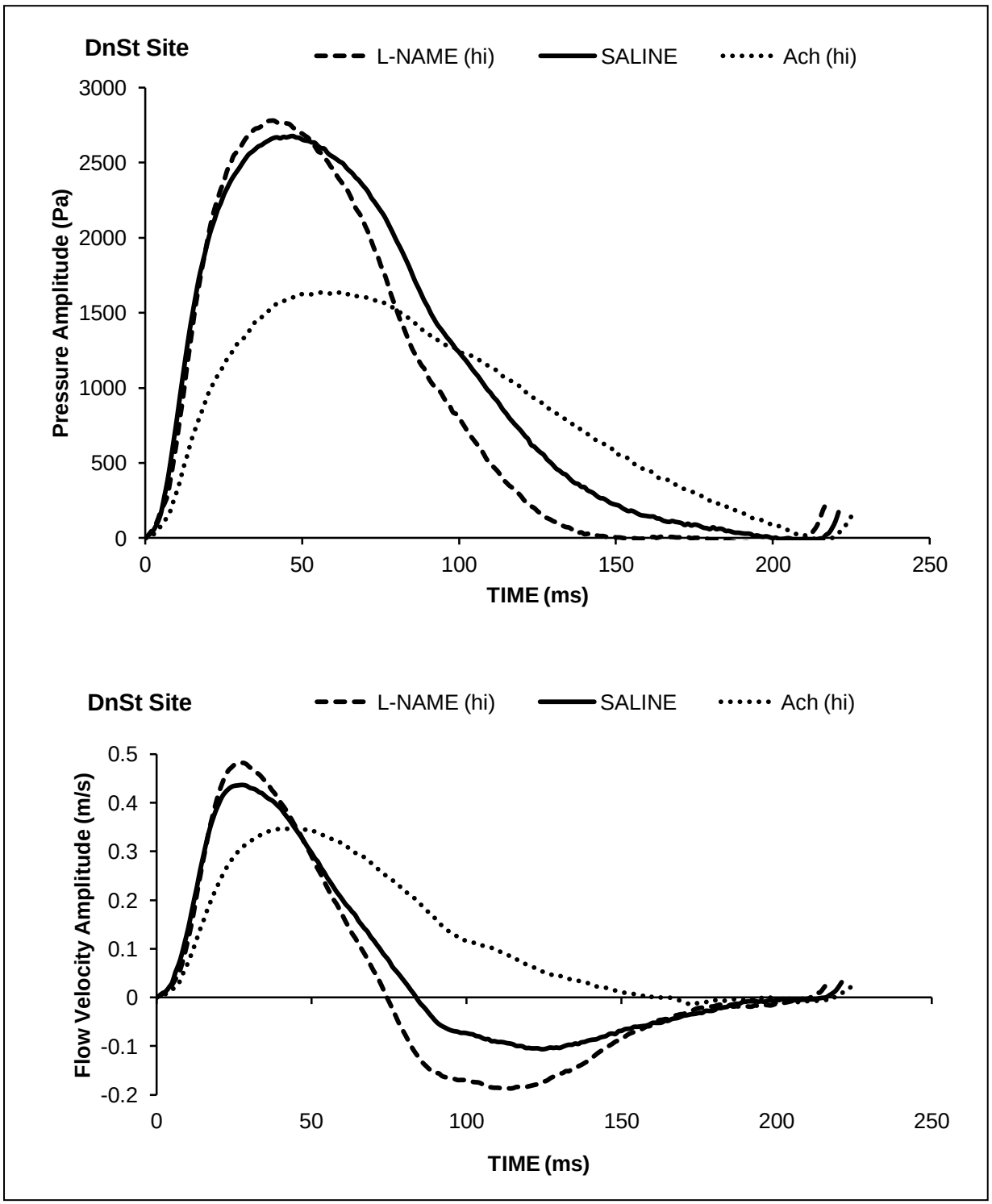

*Note: L-NAME appears to convert Type 1 almost to Type 2 (see plot of pressures).

Experiment Ref.: AAEH 091016(2)

FIGURE 4.12 A: **Type 2** Blood Pressure Waveform (see saline curve) along with the Associated Blood Flow Velocity Waveform (UpSt Site in the Abdominal Aorta). Included are Waveforms after ***lo*** *doses* of L-NAME or Ach*. All waveforms shown are after subtraction of their respective absolute diastolic values at time 0.
Absolute diastolic values (Pa & m/s): L-NAME curves 11,030 & 0.137; Saline curves 10,011 & 0.184; Ach curves 8376 & 0.205.

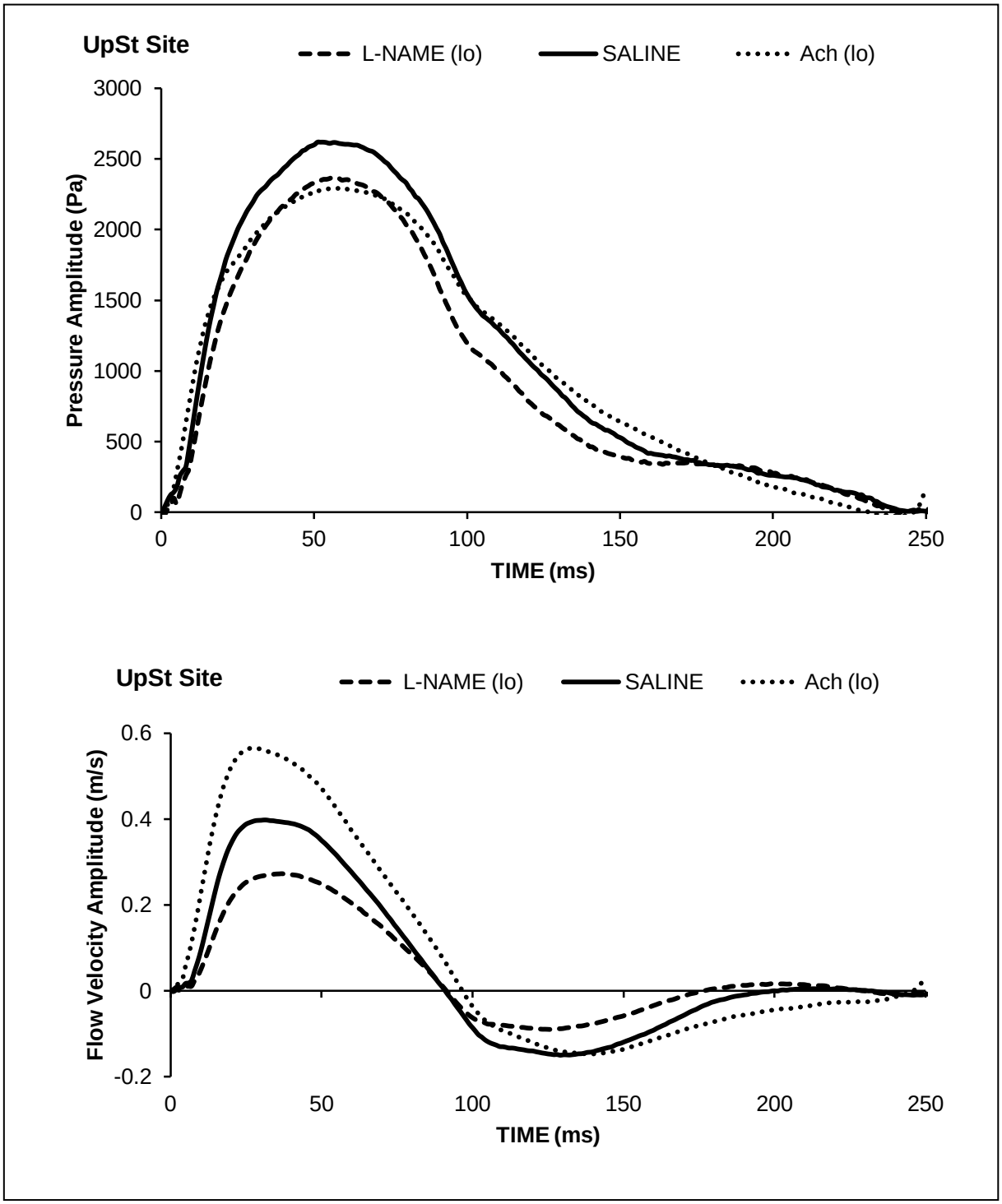

*Note: Ach appears to convert Type 2 to Type 1 (see plot of pressures).

Experiment Ref.: AAEH 091029(2)

FIGURE 4.12 B: **Type 2** Blood Pressure Waveform (see saline curve) along with the Associated Blood Flow Velocity Waveform (DnSt Site of the Abdominal Aorta). Included are Waveforms after ***lo*** *doses* of L-NAME or Ach*. All waveforms shown are after subtraction of their respective absolute diastolic values at time 0.
Absolute diastolic values (Pa & m/s): L-NAME curves 11,058 & 0.169; Saline curves 9,993 & 0.195; Ach curves 7972 & 0.150

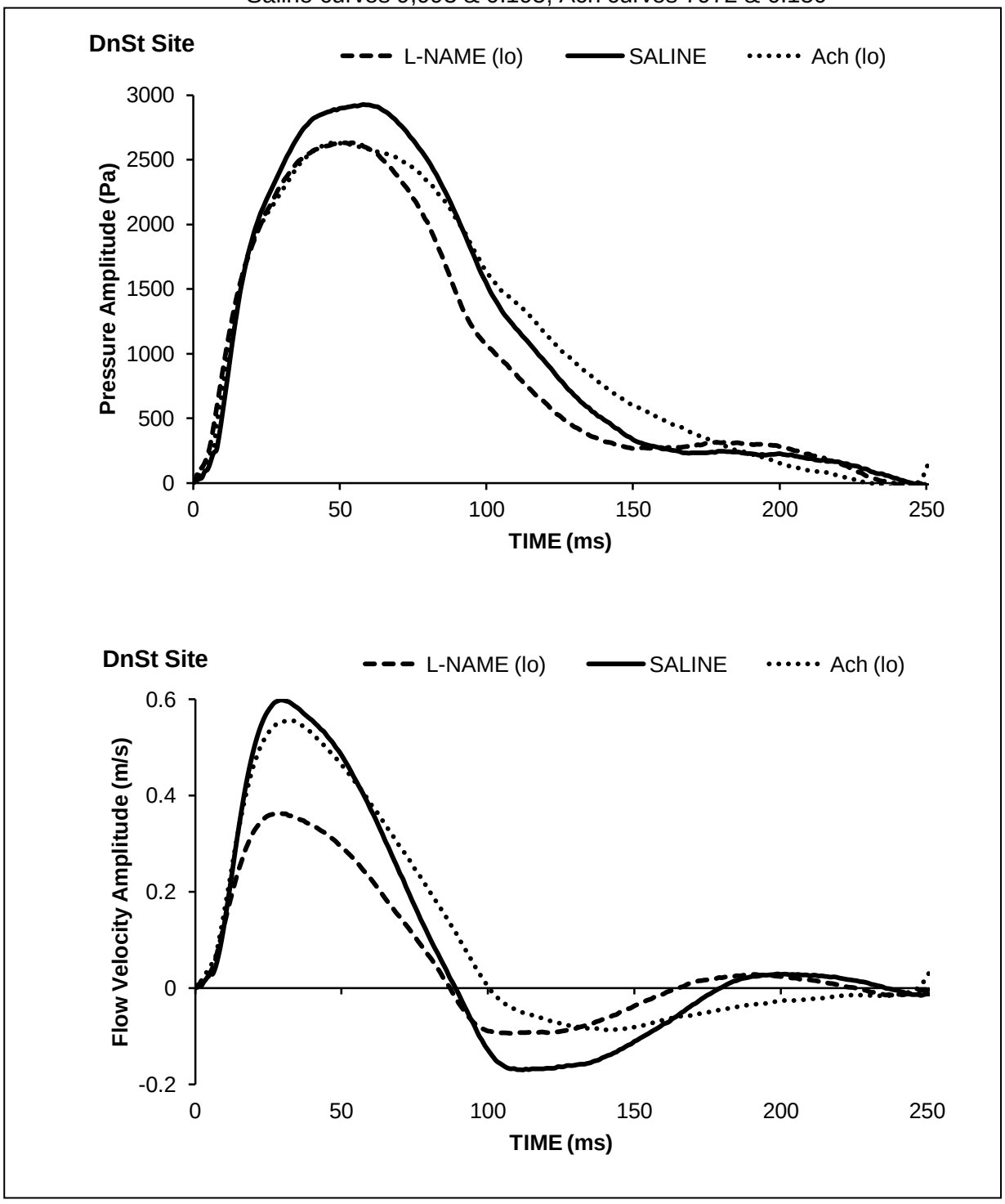

*Note: Ach appears to convert Type 2 to Type 1 (see plot of pressures).

Experiment Ref.: AAEH 091029(2)

FIGURE 4.13 A: **Type 2** Blood Pressure Waveform (see saline curve) (Blood Flow Velocity not available) (UpSt Site of the Abdominal Aorta). Included are Waveforms after ***hi*** *doses* of L-NAME or Ach*. All waveforms shown are after subtraction of their respective absolute diastolic values at time 0.

Absolute diastolic values (Pa): L-NAME curve 11,111; Saline curve 9048; Ach curve 6099.

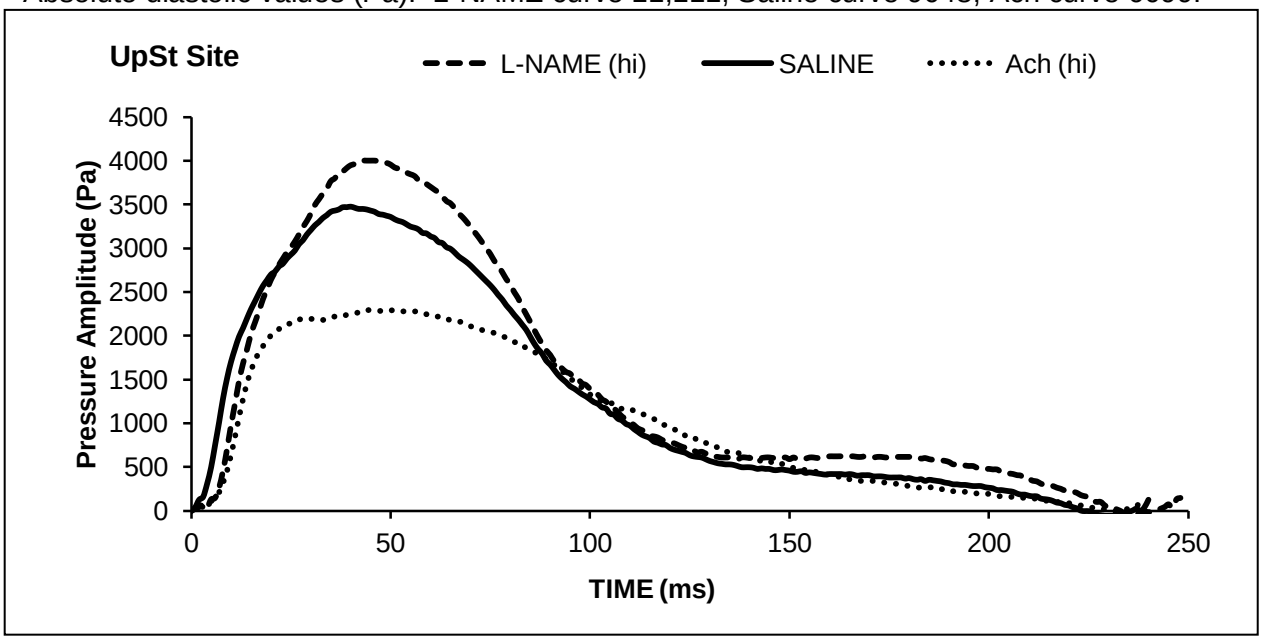

Experiment Ref.: AAEH 090318(1)

FIGURE 4.13 B: **Type 2** Blood Pressure Waveform (see saline curve) (Blood Flow Velocity not available) (DnSt Site of the Abdominal Aorta). Included are Waveforms after ***hi*** *doses* of L-NAME or Ach*. All waveforms shown are after subtraction of their respective absolute diastolic values at time 0.

Absolute values (Pa): L-NAME curve 11,384; Saline curve 9077; Ach curve 6473.

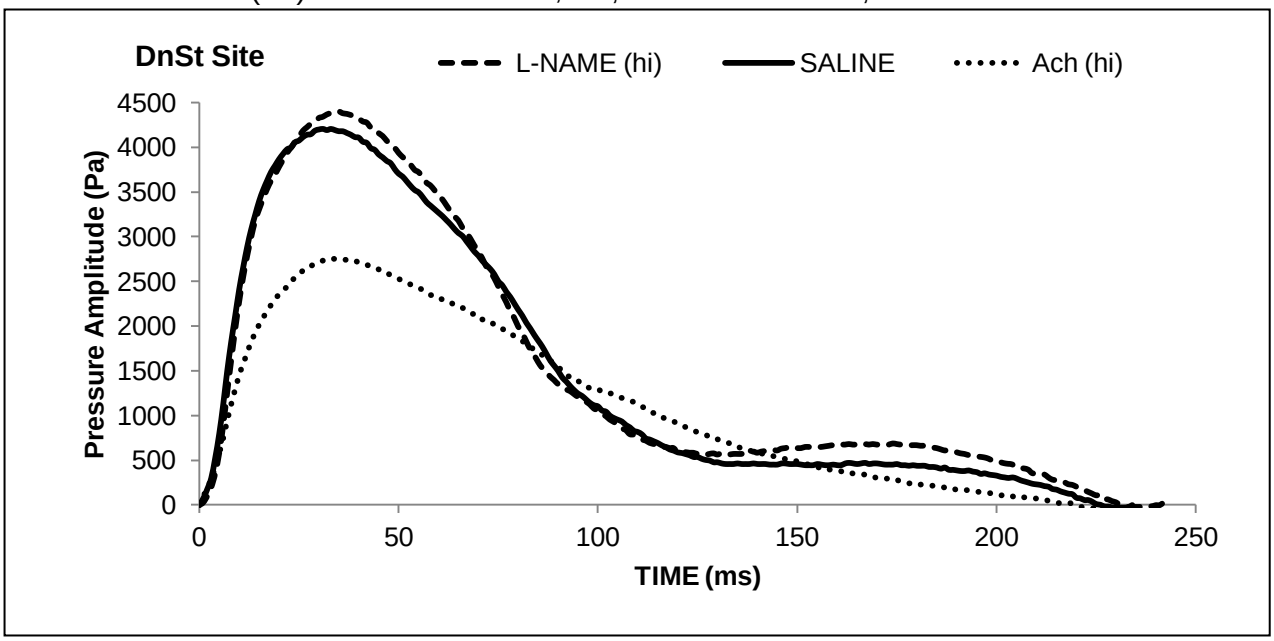

*Note: Ach appears to convert Type 2 to Type 1

Experiment Ref.: AAEH 090318(1)

FIGURE 4.14 A: **Type 2** Blood Pressure Waveform (see saline curve) along with the Associated Blood Flow Velocity Waveform (UpSt Site in the Abdominal Aorta). Included are Waveforms after ***hi*** *doses* of L-NAME or Ach*. All waveforms shown are after subtraction of their respective absolute diastolic values at time 0.
Absolute diastolic values (Pa & m/s): L-NAME curves 10,857 & 0.090; Saline curves 10,506 & 0.106; Ach curves 7269 & 0.026.

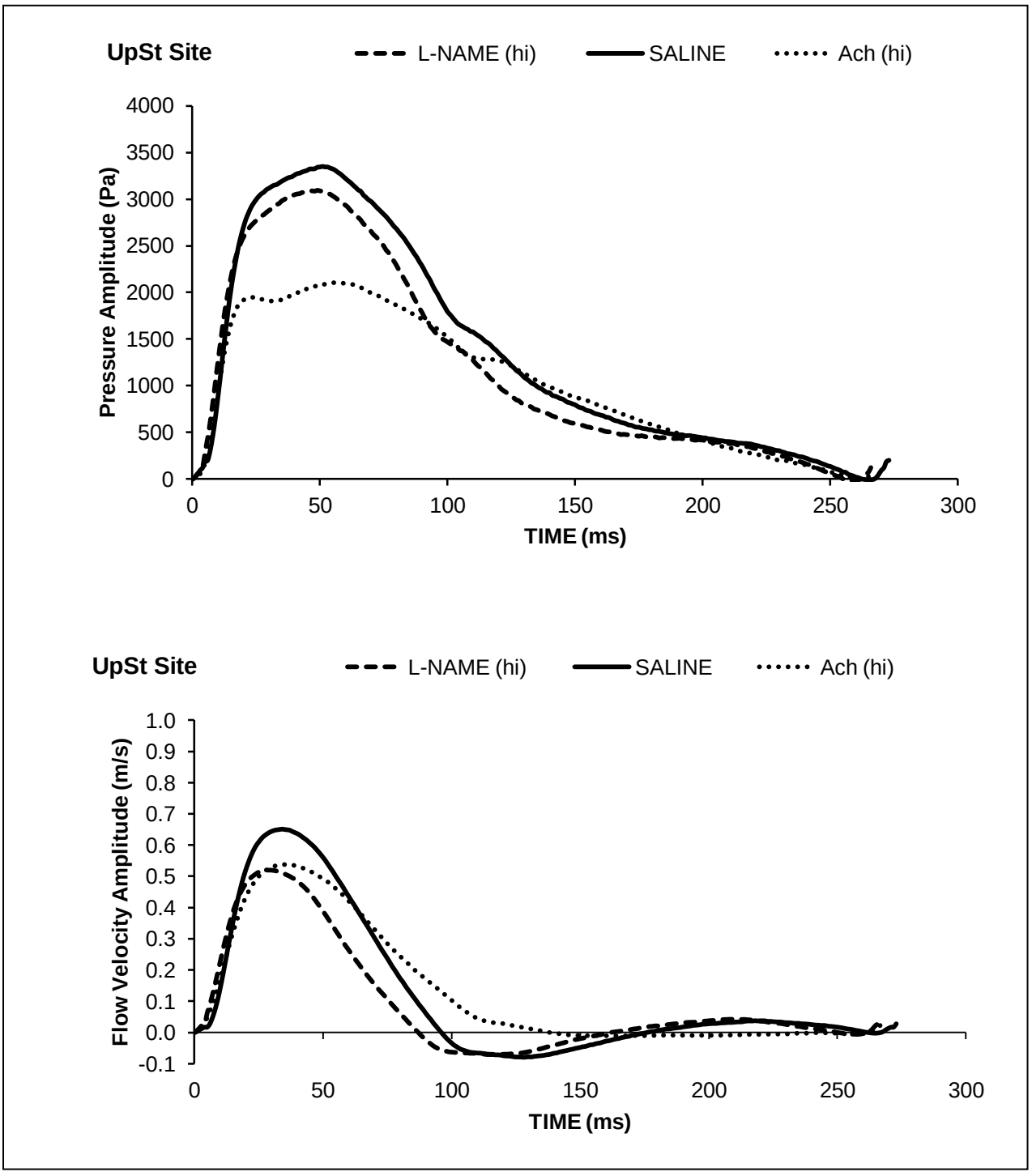

*Note: Ach appears to convert Type 2 to Type 1 (see plot of pressures).

Experiment Ref.: AAEH 091105

FIGURE 4.14 B: **Type 2** Blood Pressure Waveform (see saline curve) along with the Associated Blood Flow Velocity Waveform (DnSt Site in the Abdominal Aorta). Included are Waveforms after ***hi*** *doses* of L-NAME or Ach*. All waveforms shown are after subtraction of their respective absolute diastolic values at time 0.
Absolute diastolic values (Pa & m/s): L-NAME curves 10,791 & 0.072; Saline curves 10,239 & 0.088; Ach curves 7392 & 0.034.

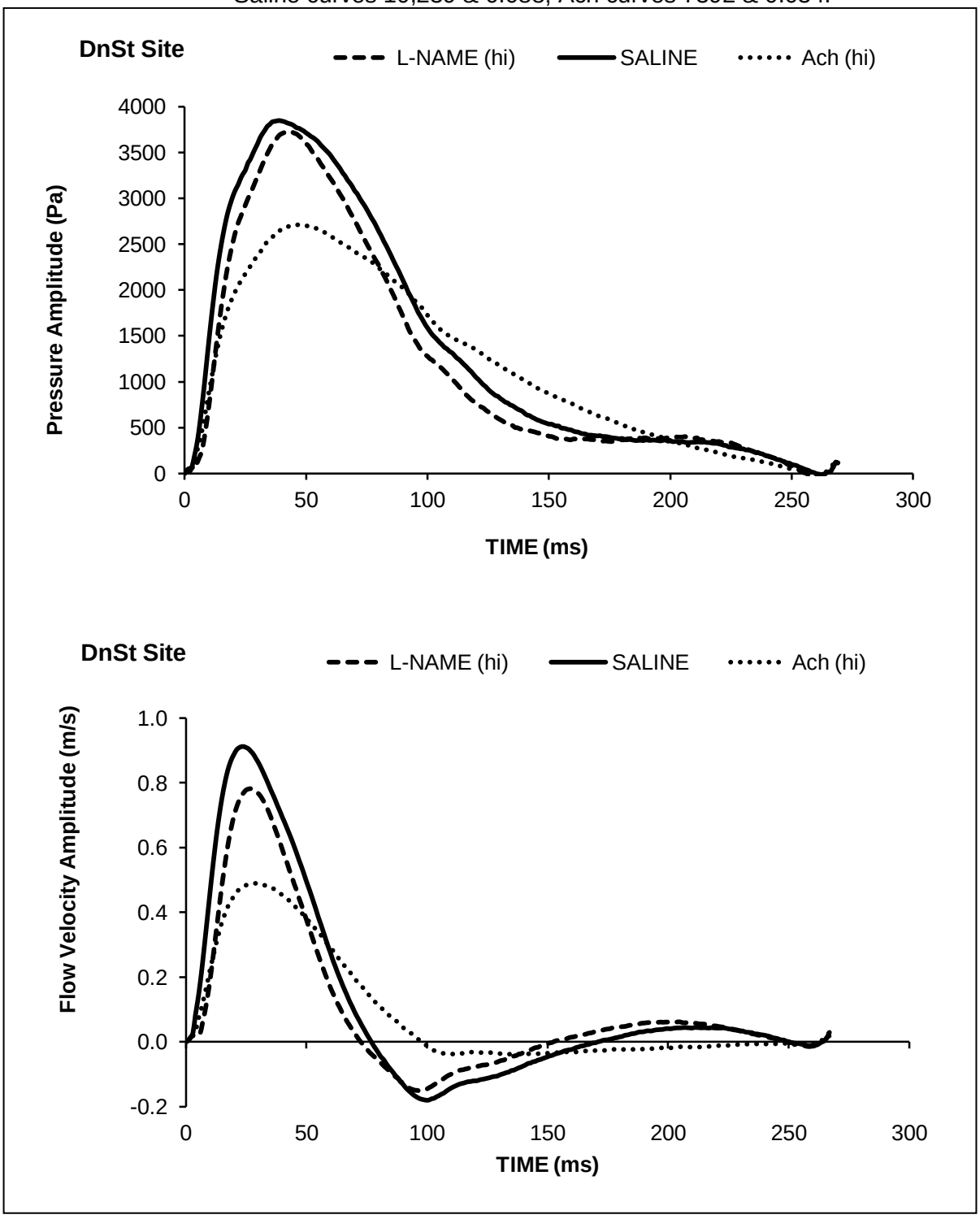

*Note: Ach appears to convert Type 2 to Type 1 (see plot of pressures).

Experiment Ref.: AAEH 091105

FIGURE 4.15A: Relationship of Mean Abdominal Aortic Blood Pressure (MAP) with Type 1 and Type 2 Pressure Waveforms **UpSt Site** in Individual Anaesthetised Rabbits. (See also Table 4.5). Note: Although Type 1 and Type 2 pressure waveforms can exist at similar MAP values, Type 1 tend to occur more at MAP values lower than those at which Type 2 occur; the latter tend to occur more frequently above MAP of 10,000 Pa.

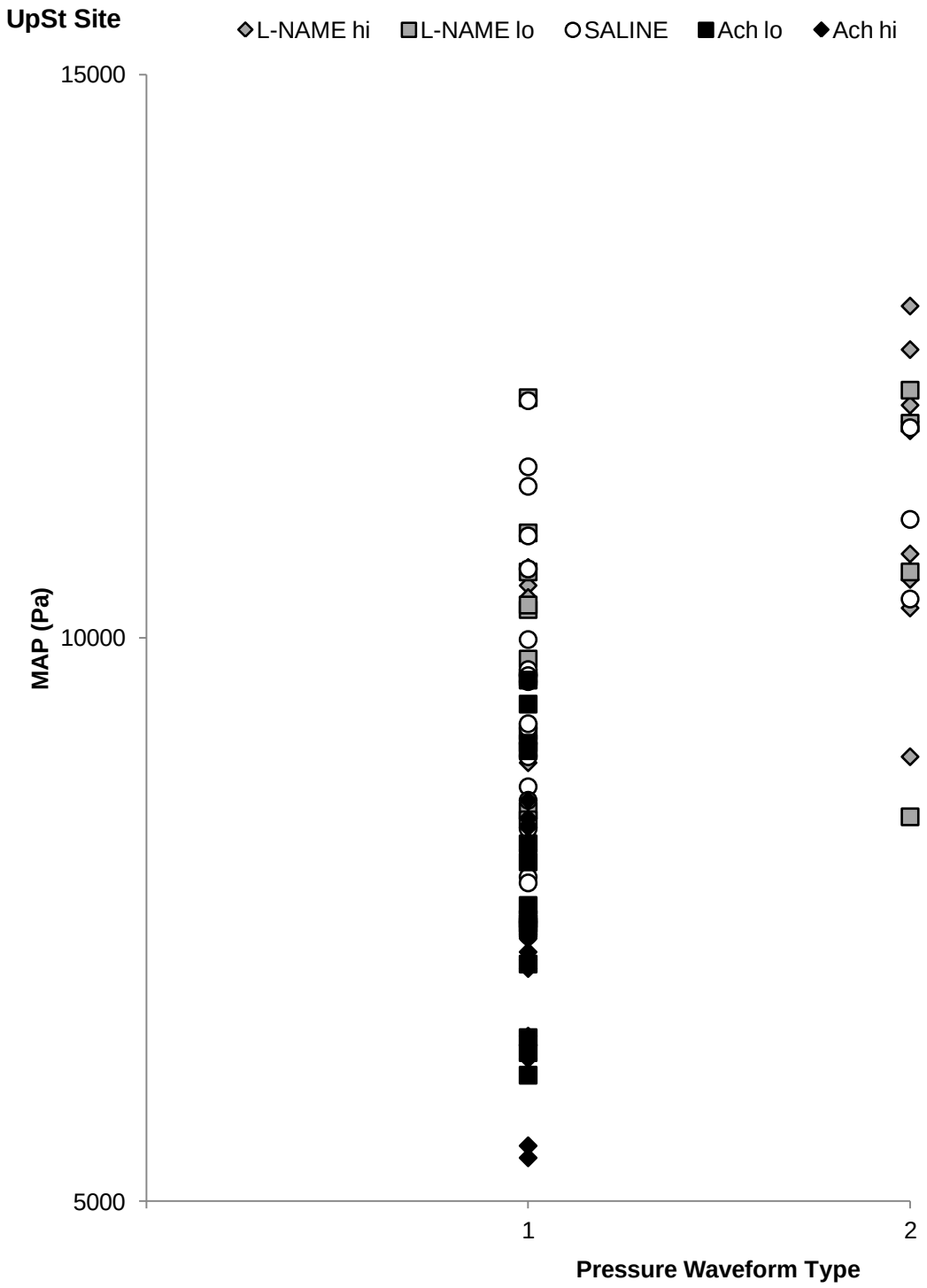

FIGURE 4.15B: Relationship of Mean Abdominal Aortic Blood Pressure (MAP) with Type 1 and Type 2 Pressure Waveforms **DnSt Site** in Individual Anaesthetised Rabbits.(See also Table 4.5). Note: Although Type 1 and Type 2 pressure waveforms can exist at similar MAP values, Type 1 tend to occur more at MAP values lower than those at which Type 2 occur; the latter tend to occur more frequently above MAP of 10,000 Pa.

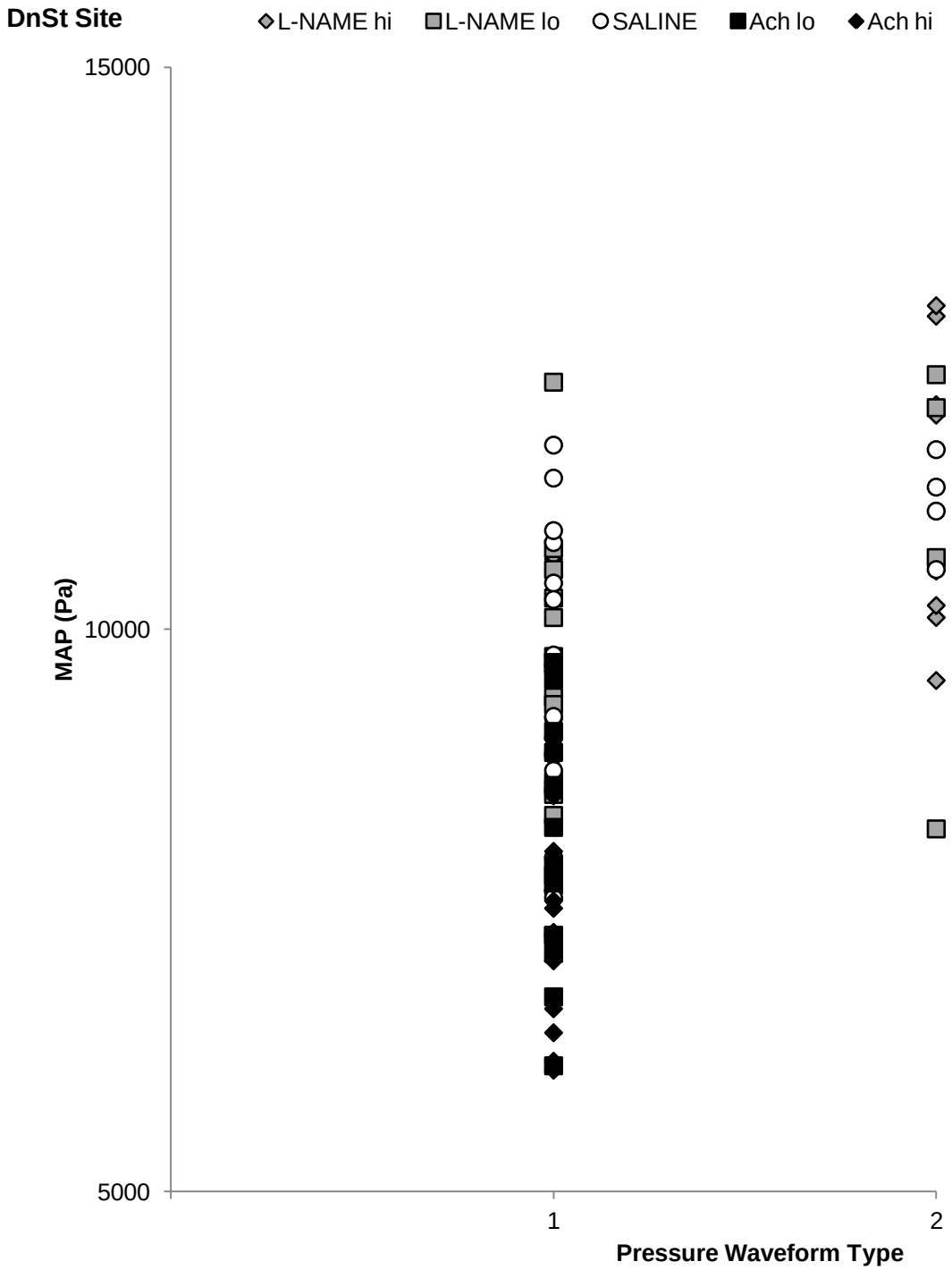

TABLE 4.5: Analysis* of Association of Type 1 and Type 2 Blood Pressure Waveforms with Mean Arterial Blood Pressure (MAP) in the Abdominal Aorta of Anaesthetised Rabbits. Mean±SD (Pa); [p by unpaired t-test, data from Type 1 vs. data from Type 2 Waveforms; NS=not significant at p>0.05].

	MAP at UpSt Site		MAP at DnSt Site	
	Type 1	Type 2	Type 1	Type 2
Saline for *hi dose*	9648 ±1179	11107 ±1075 [NS;p=0.13]	9554 ±1154	11067 ±754 [NS;p=0.11]
Saline for *lo dose*	9293 ±1367	11053 [p=n/a; n=1]	9046 ±1218	11160 ±151 [p=0.042]
Saline pooled for *lo* & *hi dose*	9456 ±1270	11089 ±761 [p=0.041]	9289 ±1217	11113 ±447 [p=0.0073]
L-NAME *hi dose*	10087 ±803	11313 ±1279 [NS;p=0.11]	10173 ±864	11326 ±1240 [NS;p=0.12]
L-NAME *lo dose*	9969 ±1140	10777 ±1725 [NS;p=0.32]	9921 ±1126	10777 ±1842 [NS;p=0.3]
L-NAME pooled *lo* & *hi dose*	10003 ±1026	11148 ±1378 [p=0.021]	9993±1032	11157 ±1394 [p=0.02]
Pooled all Saline & all L-NAME	9658 ±1201	11137 ±1264 [p=0.0002]	9555 ±1187	11147 ±1223 [p=00004]

*Analysis of data from Figures 4.15A & B

FIGURE 4.16: Example of Fitting the Reservoir Pressure Diastolic Decay to Type1 (Graphs A & B) or Type 2 (Graph C) Diastolic Pressure Decay Waveforms of Abdominal Aortic Blood Pressure (UpSt Site) in an Anaesthetised Rabbit. (Total pressure is Measured Pressure, P_T). Note: good precise fit to Type 1; not precise fit to Type 2.

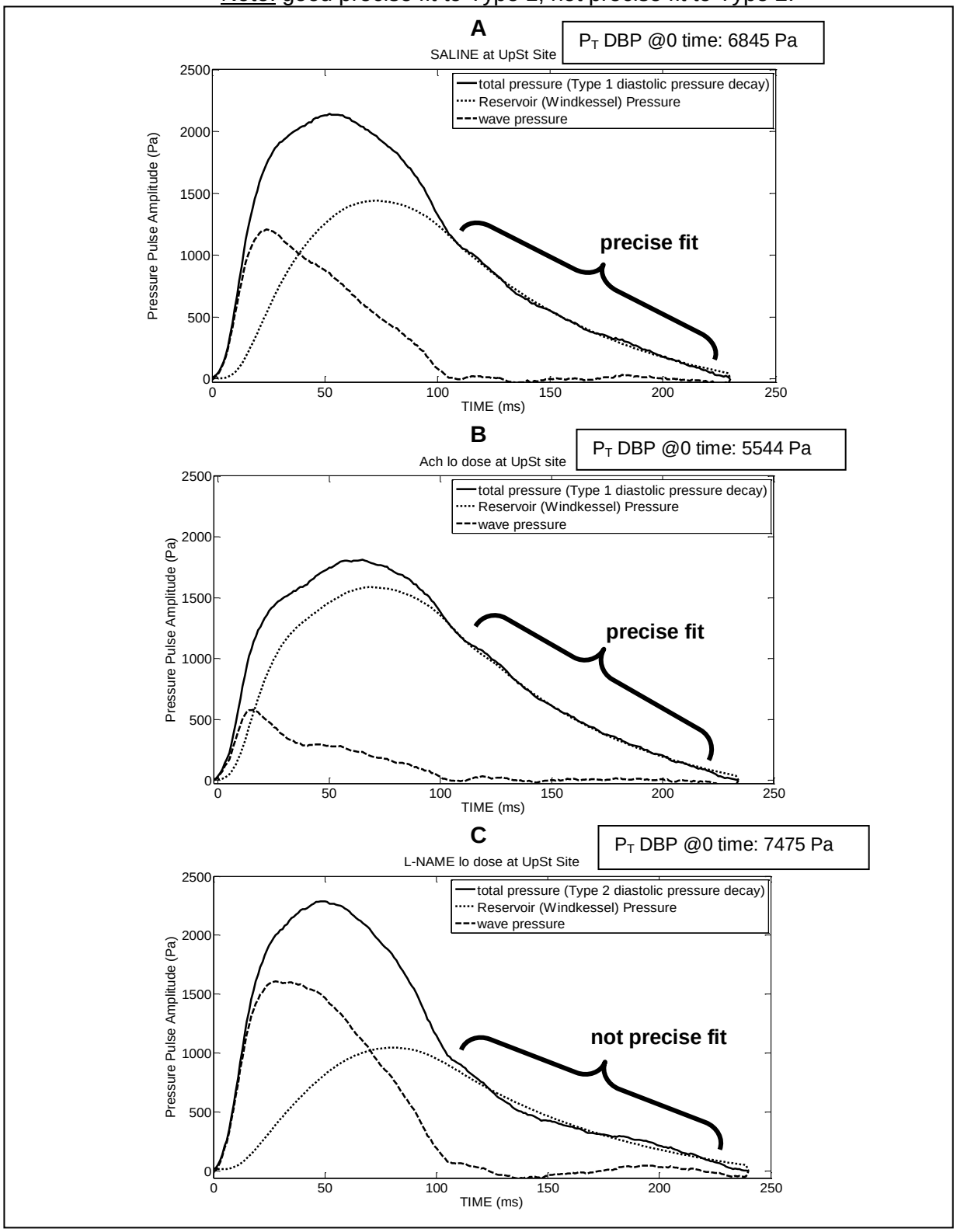

Experiment ref.: AAEH 091016(1)

FIGURE 4.17: Example of Fitting the Reservoir Pressure Diastolic Decay to Type 2 (Graphs A & B) or Type 1 (Graph C) Diastolic Pressure Decay Waveforms of Abdominal Aortic Blood Pressure (UpSt Site) in an Anaesthetised Rabbit (Total Pressure is the Measured Pressure, P_T). Note: poor fit to Type 2; good close fit to Type 1.
Experiment ref.: AAEH 091105

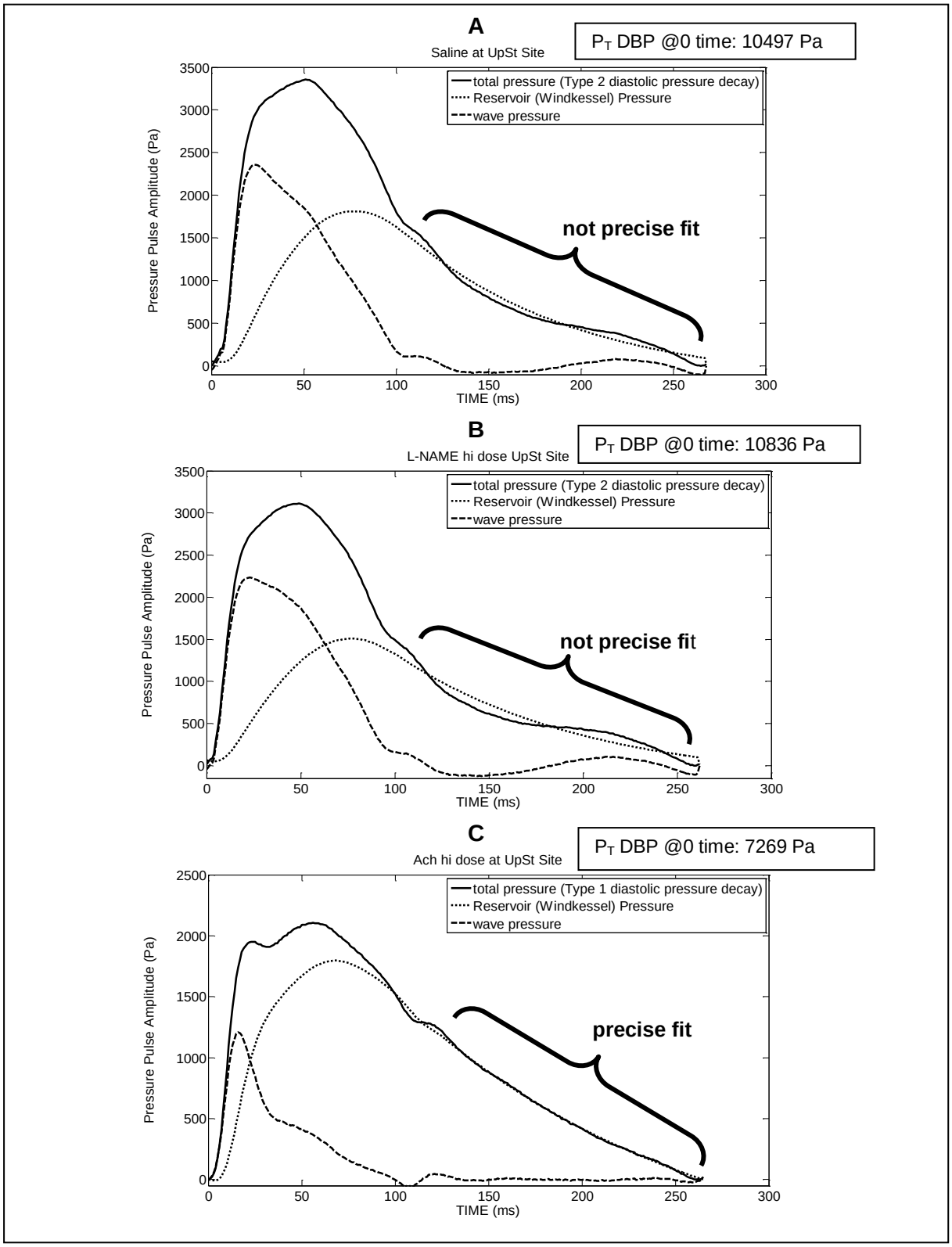

TABLE 4.6 Summarised Result of determination of differences between data sets, of ∫RP and PP_{RP}, derived from Type 1 or Type 2 Blood Pressure Pulse Waveforms. Mean±SD; n=number of samples; p by unpaired t-test for data from Type 1 vs. data from Type 2 waveforms, NS=not significant at p>0.05

	UpSt Site							
	L-NAME *lo dose*		L-NAME *hi dose*		Saline for *lo dose*		Saline for *hi dose*	
	Type 1	Type 2	Type 1	Type 2	Type 1	Type 2	Type 1	Type 2
∫RP	196 ±30 n=10	154 ±48 n=4 NS;p=0.067	201 ±35 n=4	160 ±27 n=9 p=0.04	217 ±35 n=13	194 ±0 n=1 p=n/a	206 ±32 n=11	183 ±48 n=2 NS;p=0.4
PP_{RP}	2114 ±529 n=10	1597 ±622 n=4 NS;p=0.14	2122 ±428 n=4	1532 ±379 n=9 p=0.03	2161 ±445 n=13	1801 ±0 n=1 p=n/a	1941 ±314 n=11	1580 ±292 n=2 NS;p=0.16
	DnSt Site							
∫RP	209 ±33 n=10	153 ±49 n=4 p=0.028	206 ±36 n=4	146 ±39 n=9 p=0.024	233 ±35 n=12	176 ±20 n=2 p=0.047	216 ±36 n=11	136 ±41 n=2 p=0.016
PP_{RP}	2447 ±637 n=10	1749 ±798 n=4 NS;p=0.11	2275 ±442 n=4	1496 ±599 n=9 p=0.041	2486 ±555 n=12	1937 ±565 n=2 NS;p=0.22	2184 ±376 n=11	1216 ±414 n=2 p=0.007

∫RP: Integral of the reservoir (Windkessel) pressure (Pa.s)

PP_{RP}: pressure pulse amplitude of the reservoir (Windkessel) pressure (Pa)

Despite the quality of curve fittings to, and regardless of their derivation from, either the Type 1 or Type 2 diastolic decays, values of B, τ and P_∞ are each pooled (as reasoned above) and averaged for each treatment, these are given in Tables 4.7 (*lo dose*) and 4.8 (*hi dose*); the data are derived from reservoir (Windkessel) pressures.

The data for B and τ of one rabbit have been omitted from the averaged data in Table 4.8 because poor curve-fitting to the Type 2 diastolic decay (exemplified in Figure 4.18; DnSt Site; treatments with saline and L-NAME *hi dose*) rendered spurious values (Table 4.9), namely negative values for B and τ after treatment with L-NAME (*hi dose*), along with an exceptionally small value for B which rendered an exceptionally large value for τ after treatment with saline. Interestingly, the Ach (*hi dose*) treatment resulted in a Type 1 curve to which a close (good) fit was obtained (Figure 4.18) resulting in "sensible" values for B and τ (Table 4.9).

TABLE 4.7: Data (Mean ± SD) Derived from the Calculation of Reservoir (Windkessel) Pressure in the Abdominal Aorta of Anaesthetised Rabbits (n=14). Comparison of Treatments with L-NAME (***lo*** *dose*) and Ach (***lo*** *dose*) against their respective Saline Controls. [p by paired t-test to Saline; NS=not significant at p>0.05].

	UpSt Site			DnSt Site		
Parameter	L-NAME (*lo*)	SALINE	Ach (*lo*)	L-NAME (*lo*)	SALINE	Ach (*lo*)
A	0.096 ±0.058 [p=0.004]	0.111 ±0.050	0.114 ±0.033 [NS;p=0.85]	0.126 ±0.075 [NS;p=0.59]	0.130 ±0.052	0.123 ±0.027 [NS;p=0.64]
B	0.019 ±0.009 [NS;p=0.14]	0.016 ±0.005	0.010 ±0.004 [p=0.0005]	0.029 ±0.023 [NS;p=0.11]	0.022 ±0.011	0.012 ±0.004 [p=0.004]
τ	63.2 ±24.7 [NS;p=0.32]	68.2 ±20.5	130.7 ±83.7 [p=0.012]	48.8 ±23.1 [NS;p=0.17]	55.7 ±21.6	103.9 ±56.6 [p=0.003]
P_∞	8928 ±1401 [p<0.0001]	7984 ±1479	5822 ±1536 [p<0.0001]	8920 ±1388 [p=0.0004]	7915 ±1484	6165 ±1306 [p<0.0001]

Where: A = rate constant (s^{-1}); B = Rate constant for diastolic decay (s^{-1});
τ = time (s) constant for diastolic decay ($\tau = 1/B$); P_∞ = P infinite (Pa);

TABLE 4.8: Data (Mean ± SD) Derived from the Calculation of Reservoir (Windkessel) Pressure in the Abdominal Aorta of Anaesthetised Rabbits (n=12-13). Comparison of Treatments with L-NAME (***hi*** *dose*) and Ach (***hi*** *dose*) against their respective Saline Controls. [p by paired t-test to Saline; NS=not significant at p>0.05].

	UpSt Site			DnSt Site		
Parameter	L-NAME (*hi*)	SALINE	Ach (*hi*)	L-NAME (*hi*)	SALINE	Ach (*hi*)
A	0.069 ±0.056 [NS;p=0.24]	0.079 ±0.050	0.081 ±0.042 [NS;p=0.85]	0.085 ±0.074 [NS;p=0.3]	0.096 ±0.059	0.101 ±0.048 [NS;p=0.64]
B	0.018 ±0.010 [NS;p=0.15]	0.016 ±0.006	0.009 ±0.002 [p=0.0016]	0.025 ±0.021 [NS;p=0.24]	0.020 ±0.010	0.010 ±0.003 [p=0.0011]
τ	73.3 ±37.5 [NS;p=0.85]	74.6 ±30.2	124.5 ±34.9 [p<0.0016]	64.1 ±39.2 [NS;p=0.78]	61.2 ±29.1	117.6 ±42.8 [p=0.0005]
P_∞	9480 ±1251 [p=0.0017]	8517 ±1256	5772 ±890 [p<0.0001]	9655 ±1152 [p<0.0001]	8399 ±1351	6004 ±1042 [p<0.0001]

Where: A = rate constant (s^{-1}); B = Rate constant (s^{-1}) for diastolic decay;
τ = time (s) constant for diastolic decay ($\tau=1/B$); P_∞ = P infinite (Pa);

TABLE 4.9: Data Derived from Calculation of Reservoir (Windkessel) Pressure resulting from poor curve-fitting (see Figure 4.18). Data are spurious under conditions of Treatments with L-NAME (***hi*** *dose*) and Saline, but "sensible" after treatment with Ach (***hi*** *dose*) in one Anaesthetised Rabbit at DnSt Site in the Abdominal Aorta; spurious data were omitted from the Averaged data of Table 4.6 DnSt Site. (Rabbit Expt. Ref.: AAEH 090318(1))

	DnSt Site		
Parameter	L-NAME (*hi*)	SALINE	Ach (*hi*)
B	-0.0098 *	0.00075 **	0.015 ***
τ	-101.96 *	1,326.06 **	69.1 ***

Where: B = Rate constant (s^{-1}) for diastolic decay;
τ = time (s) constant for diastolic decay ($\tau=1/B$)

(*) spurious '–ve' values; (**) spurious magnitudes; (***) "sensible" values

FIGURE 4.18: Illustration of Poor Fitting of the Reservoir Pressure to Type 2 Diastolic Pressure Decay resulting in spurious data (see Table 4.7) after Treatments with L-NAME (*hi dose*) and Saline but Good Fitting of the Reservoir Pressure to Type 1 Diastolic Pressure Decay resulting in "sensible" data (see Table 4.7) after Treatment with Ach (*hi dose*) (DnSt Site) in an Anaesthetised Rabbit*- data of Abdominal Aorta.

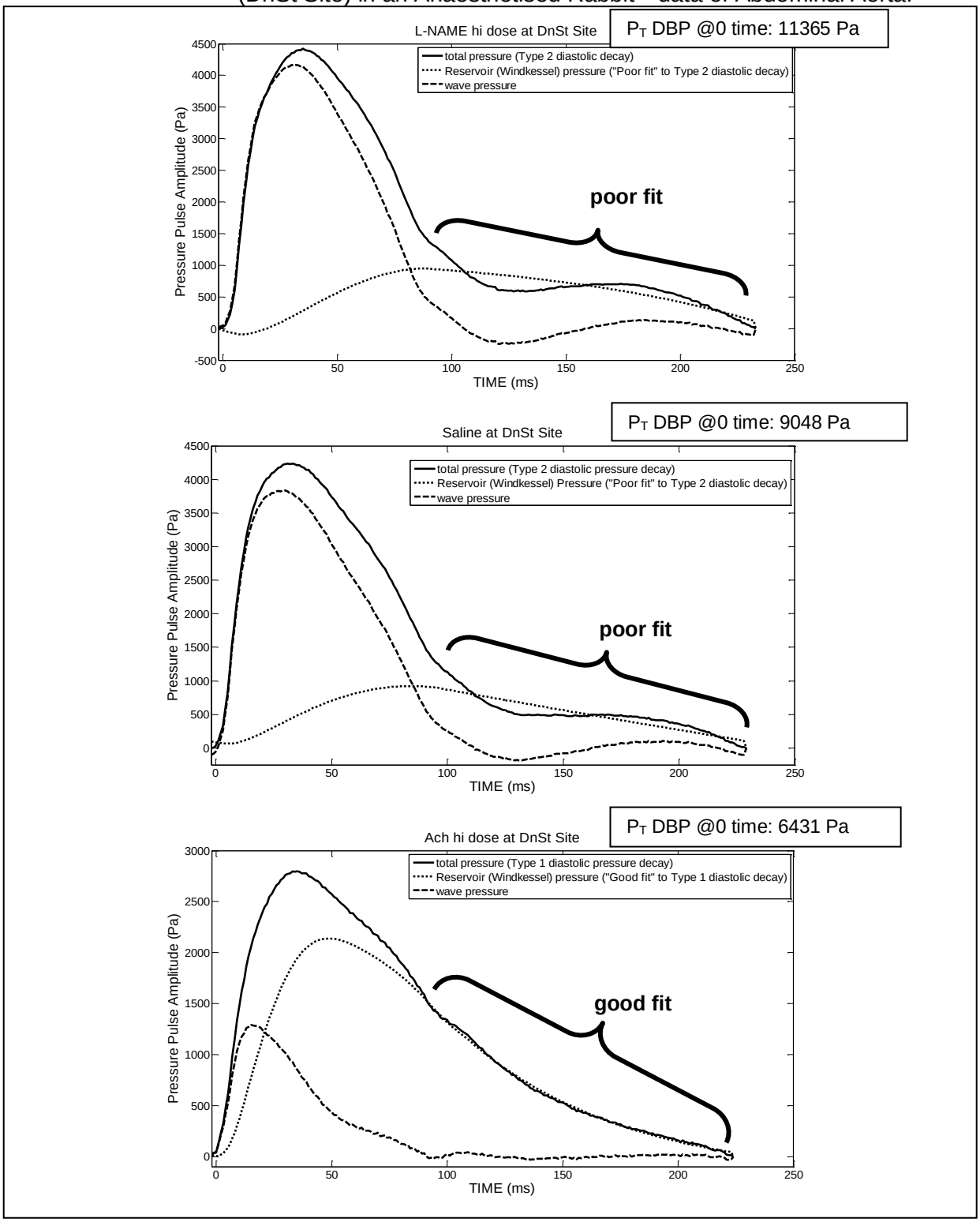

*Experiment Ref.: AAEH 090318(1)

Ach (*lo & hi doses*) caused no statistically significant change of values of parameter A from those during saline treatment (Tables 4.7 & 4.8); L-NAME (*lo dose*) at the UpSt Site caused a significant decrease ($p=0.004$) in value of parameter A below that of the saline control (Table 4.7) but otherwise was without effect on parameter A (Tables 4.7 & 4.8). Parameters B and τ were significantly (ranging $0.02>p>0.0001$) affected only by Ach which decreased B below, and consequently increased τ, above, the values during saline treatment (Tables 4.7 & 4.8). P_∞ was significantly (ranging $0.002 \geq p<0.0001$) increased by L-NAME over, and decreased ($p<0.0001$) by Ach below, the values during saline treatment (Tables 4.7 & 4.8).

Arterial compliance (AC) can be calculated as the ratio of τ / VR. Figure 4.19A&B and Figure 4.20A&B show AC plotted against MAP in treatment sets (Figures 4.19A & 4.20A) and pooled to show an exponential fit (Figures 4.19B & 4.20B), at the UpSt and DnSt Sites. The treatments do not appear to cause separate AC vs. MAP curves, instead all the data points cluster and distribute along one apparently exponential curve. The treatment data as shown in Figures 4.19A and 4.20A are again shown graphically in Figure 4.21 but separated into treatment groups. Thus Figure 4.21 shows the effects of L-NAME (*hi* & *lo doses*), saline controls, and Ach (*hi* & *lo doses*) on AC. As measured at the UpSt Site, L-NAME (*hi* & *lo doses*) significantly decreased whereas Ach (*hi* & *lo doses*) significantly increased AC; the same was observed at the DnSt Site but the effects L-NAME (*hi* & *lo doses*) on AC did not reach statistical significance.

Other data obtained from the reservoir (Windkessel) pressure curve are the pulse amplitude (PP_{RP}) and the integral ($\int RP$) of the curve; these are considered as indices of arterial compliance, Table 4.10 gives this data. Interestingly, both L-NAME (*lo & hi dose*) and Ach (*lo & hi dose*) appeared to have the same effect on PP_{RP} and $\int RP$ by decreasing them to values below those during saline treatment; the trend of these effects reached statistical significance in several cases (Table 4.10).

TABLE 4.10: Data (Mean ± SD) for Pulse Amplitude (PP_{RP}) and integral ($\int RP$) Derived from the Reservoir (Windkessel) Pressure in the Abdominal Aorta (UpSt & DnSt Sites of measurement) of Anaesthetised Rabbits (n=13-14). Comparison of Treatments with L-NAME (*lo* & *hi dose*) and Ach (*lo* & *hi dose*) against their respective Saline Controls. [p by paired t-test to Saline; NS = Not Significant at p>0.05].

	UpSt Site			DnSt Site		
	L-NAME (*lo*)	SALINE	Ach (*lo*)	L-NAME (*lo*)	SALINE	Ach (*lo*)
PP_{RP} (Pa)	1966 ±585 [p=0.02]	2135 ±438	1829 ±248 [p=0.0063]	2247 ±731 [NS;p=0.059]	2408 ±570	2108 ±418 [p=0.025]
$\int RP$ (Pa.s)	184 ±39 [p<0.0001]	215 ±34	202 ±24 [NS;p=0.15]	193 ±45 [p<0.0001]	225 ±39	218 ±33 [NS;p=0.57]
	L-NAME (*hi*)	SALINE	Ach (*hi*)	L-NAME (*hi*)	SALINE	Ach (*hi*)
PP_{RP} (Pa)	1713 ±471 [NS;p=0.074]	1886 ±328	1465 ±243 [p=0.002]	1736 ±654 [p=0.039]	2035 ±514	1696 ±356 [NS;p=0.085]
$\int RP$ (Pa.s)	173 ±34 [p=0.0033]	202 ±33	172 ±27 [p=0.012]	164 ±46 [p=0.0048]	204 ±46	191 ±35 [NS;p=0.46]

Table 4.11 shows linear correlation coefficients (r) for MAP vs. AC, PP_{RP} and $\int RP$, also AC vs. PP_{RP} and $\int RP$; for exploring those relationships, the correlation assessments were carried out with data pooled from the treatments. Although in Figures 4.19 and 4.20, AC appears exponentially related to MAP, a determination of linear correlation was carried out here in Table 4.11 which shows a significant negative linear correlation between MAP and AC at the UpSt (r=-0.442; p<0.001) and at the DnSt (r=-0.637; p<0.001) sites of measurement (Table 4.11); the r values being negative since, as expected, AC decreases with increasing MAP. As stated earlier, PP_{RP} and $\int RP$ are considered as indices of AC, thus a test of correlation of PP_{RP} and $\int RP$ with MAP and also with AC was done; the results are shown in Table 4.11. PP_{RP} correlated positively with MAP at the UpSt Site (r=0.252; 0.05>p>0.02) but showed no significant correlation with MAP at the DnSt Site; the positive correlation of PP_{RP} with MAP at the UpSt Site suggests that PP_{RP} increases with increasing blood pressure. In the case of $\int RP$ however this did not correlate linearly with MAP. The

correlation assessments of PP_{RP} and $\int RP$ using pooled data do not reveal the apparent findings in Table 4.10, where Ach which decreased MAP also decreased PP_{RP} and $\int RP$, but L-NAME which increased MAP actually *decreased* PP_{RP} and $\int RP$; thus Ach and L-NAME, despite their opposite effects on blood pressure, they both decreased PP_{RP} and $\int RP$. This is further explored with the treatment groups by regression analyses for MAP vs. PP_{RP} and for MAP vs. $\int RP$ at the UpSt and DnSt Sites in the abdominal aorta; for brevity, the analyses are shown just for the UpSt Site in Figure 4.22i and Figure 4.22ii. The analyses are shown graphically where regression lines are plotted for the treatment groups (Figures 4.22i A & 4.22ii A). Regression analysis showed that with Ach (*lo* & *hi dose* data pooled) an expected positive and significant (p=0.002) correlation was found for MAP with PP_{RP} (Figure 4.22i A) or $\int RP$ (Figure 4.22ii A), but unexpectedly such a correlation was not found for MAP vs. PP_{RP} (Figure 4.22i A) or MAP vs. $\int RP$ (Figure 4.22ii A) with saline (for *lo* and *hi doses* pooled) or with L-NAME (*lo* & *hi dose* data pooled) – with the latter, the correlation appeared negative (not significant). Thus, this illustrates the findings in Table 4.10. Considering the pooled data (Figures 4.22i B & 4.22ii B) it can be seen that the pooled data for MAP vs. PP_{RP} and MAP vs. $\int RP$ either fit a linear regression or fit a quadratic (2^{nd} order polynomial fit) relationship. This quadratic relationship is consistent with the data of Table 4.10 which is re-expressed as plots in Figures 4.22i C and 4.22ii C. The same analyses were done for the DnSt Site; quadratic relationships were found for MAP vs. PP_{RP} and for MAP vs. $\int RP$ but not shown here for conciseness. PP_{RP} correlated negatively with AC but this was significant only at the DnSt Site ($r=-0.297$; $0.02>p>0.01$); the negative correlation indicating, as expected, that PP_{RP} decreased with increasing AC. $\int RP$ showed no significant correlations with AC. PP_{RP} and $\int RP$ correlated significantly with each other (Table 4.11). Following from example by Davies *et al*. (2009), tests of correlation were also done for AC, $\int RP$ and PP_{RP} against the square of pulse wave velocity, $C_{ft\text{-}ft}^2$ (Table 4.11); the latter is inversely related to the distensibility of the aorta and so should correlate with AC and indices of AC. Pulse wave velocities etc. are discussed below under "*Pulse Wave Velocities (PWV) and Wave Speeds*". AC and $\int RP$ correlated negatively and significantly with $C_{ft\text{-}ft}^2$, but PP_{RP} did not correlate at all (Table 4.11).

FIGURE 4.19: Plots of Arterial Compliance (AC) against Mean Arterial Blood Pressure (MAP) at the UpSt Site in the Abdominal Aorta of Anaesthetised Rabbits. A) Plots data from each of the treatments; B) Plots the data as pooled.

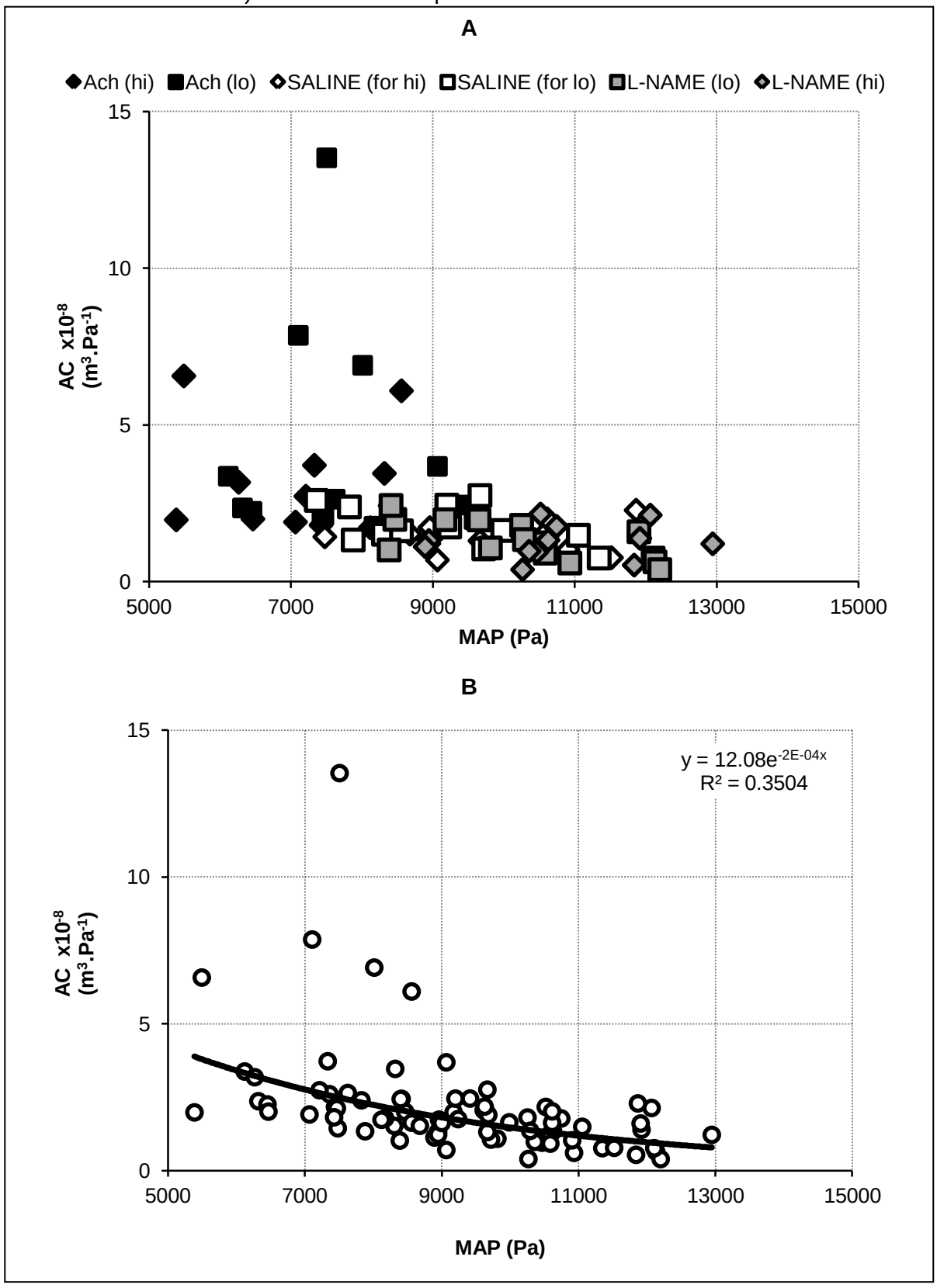

FIGURE 4.20: Plots of Arterial Compliance (AC) against Mean Arterial Blood Pressure (MAP) at the DnSt Site in the Abdominal Aorta of Anaesthetised Rabbits. A) Plots data from each of the treatments; B) Plots the data as pooled.

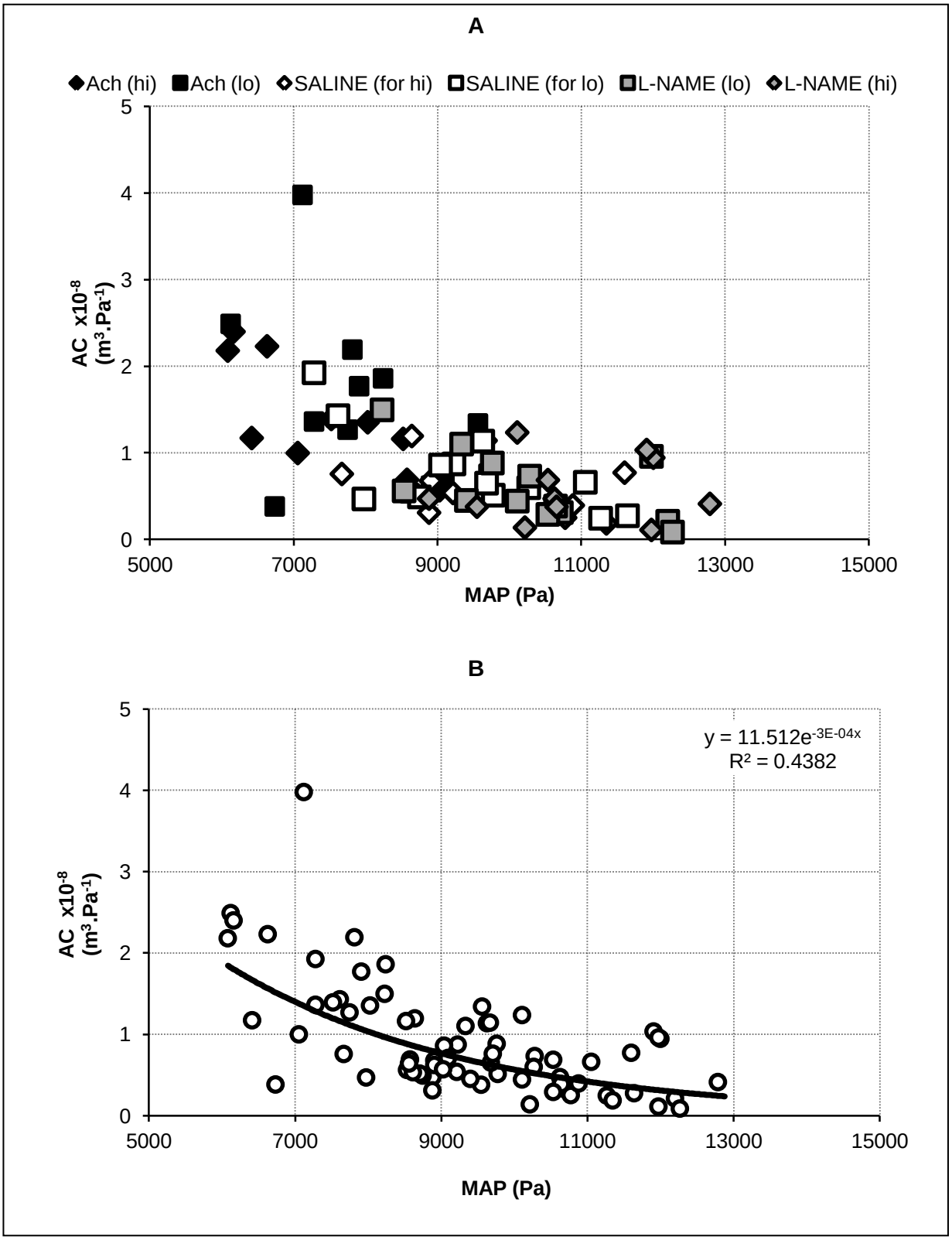

FIGURE 4.21: Values (Mean±SD) of Calculated Arterial Compliance (AC) for the UpSt & DnSt Sites in the Abdominal Aorta of Anaesthetised Rabbits (n=11-14) after Treatment with L-NAME (*hi* & *lo doses*) or Ach (*hi* & *lo doses*). Treatments Compared to their respective Saline Controls; p by paired t-test, NS=not significant at p>0.05. For supplement data see p138 of pp138-142.

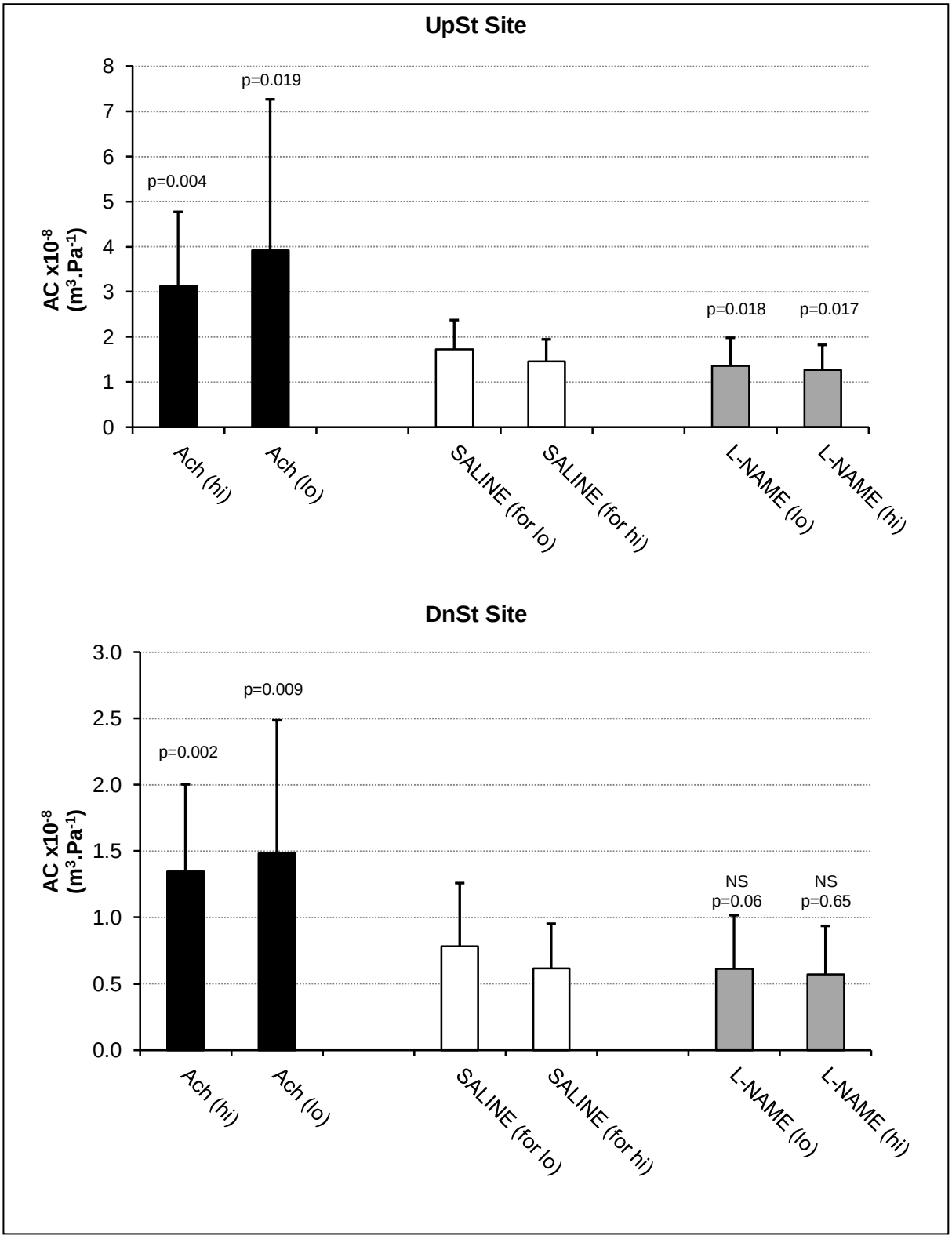

TABLE 4.11: Linear Correlation Coefficients (r) for Pulse Amplitude (PP_{RP}) and Integral ($\int RP$) vs. Mean Arterial Blood Pressure (MAP) or Arterial Compliance (AC) or the Square of Pulse Wave Velocity ($(C_{ft\text{-}ft})^2$)*****. Data are pooled from the Treatments in Anaesthetised Rabbits at the UpSt & DnSt Sites of measurement in the Abdominal Aorta.
(Regression x: abscissa; y: ordinate; NS=not significant at p>0.05)

	UpSt Site		DnSt Site	
MAP (x) vs.	r	p	r	p
AC (y)	-0.442	<0.001	-0.637	<0.001
PP_{RP} (y)	0.252	0.05>p>0.02	0.094	NS 0.5>p>0.2
$\int RP$ (y)	0.01	NS p>0.8	-0.217	NS 0.1>p>0.05
AC (x) vs.	r	p	r	p
PP_{RP} (y)	-0.209	NS 0.1>p>0.05	-0.297	0.02>p>0.01
$\int RP$ (y)	0.052	NS 0.8>p>0.5	0.017	NS p>0.8
PP_{RP} (x) vs. $\int RP$ (y)	0.748	<0.001	0.767	<0.001
*****$(C_{ft\text{-}ft})^2$ (y) vs.	r	p	r	p
AC (x)	-0.355	0.005>p>0.002	-0.384	0.001
PP_{RP} (x)	0.036	NS 0.8>p>0.5	0.0097	NS p>0.8
$\int RP$ (x)	-0.267	0.05>p>0.02	-0.359	0.005>p>0.002

*See below for $C_{ft\text{-}ft}$ data under: *Pulse Wave Velocities (PWV) and Wave Speeds*

FIGURE 4.22 i: Analysis (A&B) of Mean Arterial Blood Pressure (MAP) vs. Pulse Pressure of the Reservoir (Windkessel) Pressure (PP_{RP}) in the Abdominal Aorta at the UpSt Site in Anaesthetised Rabbits. C) Comparison between Treatments and respective Saline Controls - p by paired t-test to Saline; NS = Not Significant at p>0.05

A: Treatments (with trendlines for each treatment)

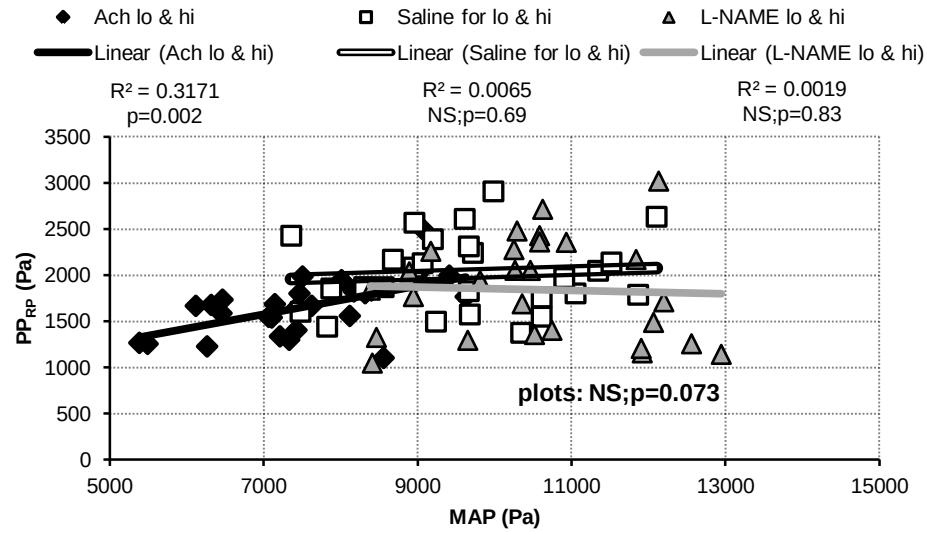

B: Pooled (note the quadratic curve fit)

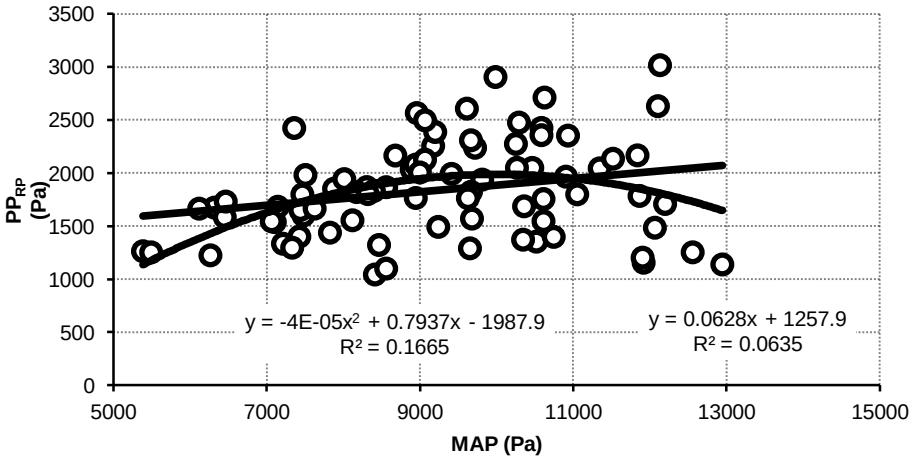

C: Treatment Groups (data from Table 4.10)

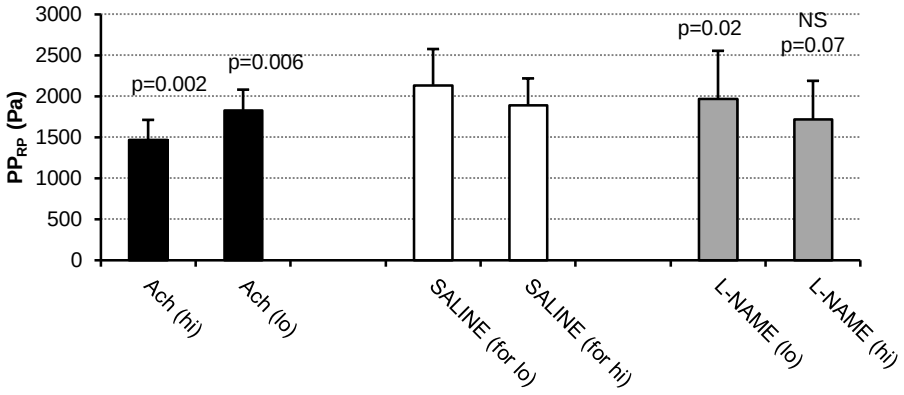

FIGURE 4.22 ii: Analysis (A&B) of Mean Arterial Blood Pressure (MAP) vs. Integral (∫RP) of the Reservoir (Windkessel) Pressure at the UpSt Site in the Abdominal Aorta of Anaesthetised Rabbits. C) Comparison between Treatments and respective Saline Controls - p by paired t-test to Saline; NS = Not Significant at p>0.05

A: Treatments (with trendlines for each treatment)

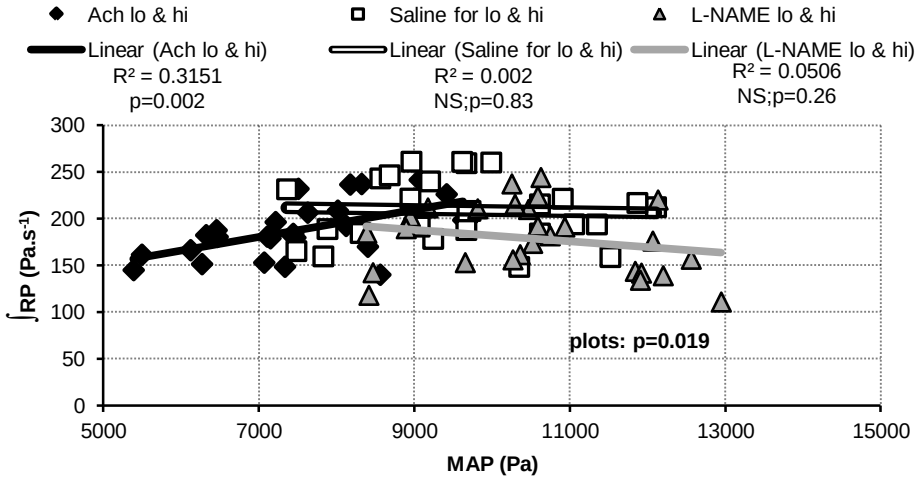

B: Pooled (note the quadratic curve fit)

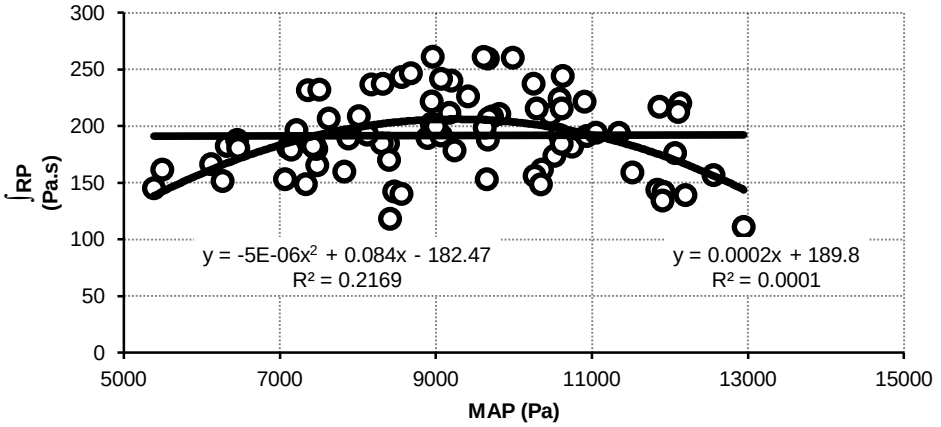

C: Treatment Groups (data from Table 4.10)

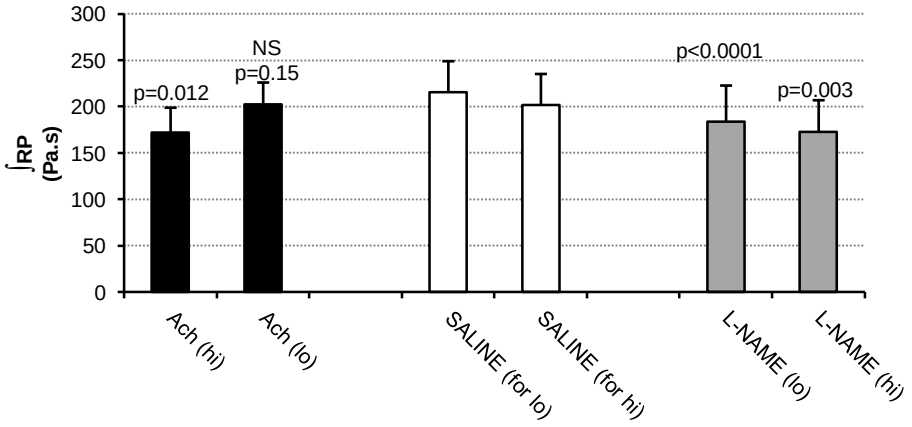

Relative Height of the Dicrotic Notch (RHDN) obtained from the Measured (Total) Blood Pressure Waveform of the Abdominal Aorta.

The term “dicrotic notch” referred to here for RHDN, is a position on the pressure pulse decay where an inflection occurs when the associated blood flow ceases its forward direction; the latter is determined by inspection of the recorded blood flow waveform. The RHDN is the “height” or pressure of this inflection above end-diastolic pressure as a fraction of the pulse pressure.

Table 4.12 gives data for RHDN, along with the time (Tn) of the inflection after end-diastole (end-diastole being the start of systole). L-NAME (*lo & hi dose*) at UpSt and DnSt Sites decreased values of RHDN and Tn to below those values obtained for saline treatment; these effects were statistically significant (Table 4.12) except for that of L-NAME (*hi dose*) at UpSt Site for RHDN. Ach (*lo & hi dose*) at UpSt and DnSt Sites increased values of RHDN and Tn (*hi dose* only) over those obtained for saline; statistical significance of these effects are given in Table 4.12).

Wave Pressure.

Subtraction of the Reservoir (Windkessel) pressure from the measured (or total) pressure gives the wave pressure; the latter is exemplified in Figures 4.16, 4.17 & 4.18. The wave pressure is used for calculating one of the estimates of wave speed, and for wave intensity analysis (WIA); wave speed and WIA are the next to be discussed.

Pulse Wave Velocities (PWV) and Wave Speeds

PWV was measured by the “foot-to-foot” method explained in Chapter 3 (section 3.2.5) and is ascribed here as $C_{ft\text{-}ft}$.

Table 4.13 gives the mean data for $C_{ft\text{-}ft}$ within the abdominal aortas (UpSt & DnSt Sites) of rabbits that each received the treatments of L-NAME (*lo & hi doses*), saline and Ach (*lo & hi doses*). At both sites in the abdominal aorta, L-NAME (*lo & hi doses*) increased, while Ach ((*lo & hi doses*) decreased, $C_{ft\text{-}ft}$; these effects were statistically significant (Table 4.13). Comparison of the saline controls shows that $C_{ft\text{-}ft}$ increased by some 10-18% between the upstream, UpSt, and downstream, DnSt, Sites (Table 4.13), indicating that the pulse wave accelerates as it travels from upstream to downstream along the aorta; this was statistically significant for the controls of the *hi dose* experiments.

Figure 4.23A supplements Table 4.13, showing $C_{ft\text{-}ft}$ plotted against MAP in the abdominal aorta of the individual rabbits whose averaged data is shown in Table 4.13. All the data

points in Figure 4.23A appear to cluster on, or distribute along, one curve where low and high values of $C_{ft\text{-}ft}$ tend to associate respectively with low and high values of MAP. Significant ($p<0.001$) correlation coefficients (r) are found if the data are considered as one pooled set (rather than treatment sets): r=0.642 & r=0.48 for UpSt & DnSt Sites respectively. If the data are considered in treatment sets (Figure 4.23B), only the saline data at the UpSt Site show a significant (p=0.028) linear correlation (r=0.448); the slopes of the three regression lines are not significantly different at the UpSt and DnSt Sites. However, although the data do not show marked separation between regression lines for each of the treatments, the intercept values were significantly different (p=0.01 UpSt Site; p=0.002 DnSt Site) which indicates that Ach and L-NAME might have affected smooth muscle tone, hence the elastic properties, of the aorta wall.

Another determination, referred to as *wave speed*, is the value obtained from the plot of pressure (P) and flow velocity (U) pulses; the plot is a loop (PU loop) but with a linear part during early systole – the ratio of the slope of the linear part to blood density gives the wave speed (Chapter 2). Two wave speed values were obtained, a value ascribed as C_{Tpu} from the measured (Total) pressure and another value ascribed as C_{Wpu}, from the wave pressure - wave pressure results from subtraction of the Reservoir (Windkessel) pressure from the measured (Total) pressure (exemplified in Figures 4.16, 4.17 & 4.18).

Data for $C_{ft\text{-}ft}$, C_{Tpu}, and C_{Wpu} are compared in Table 4.14, however these data are only for those rabbits where all three measurements were obtained; in several experiments C_{Tpu} and C_{Wpu} could not be measured. Table 4.14, like Table 4.13, shows L-NAME to increase and Ach to decrease $C_{ft\text{-}ft}$; this trend was found with C_{Tpu}, and C_{Wpu} though there were inconsistencies where the trend was in some cases reversed but such inconsistencies were not statistically significant (Table 4.14).

Theoretically, the null hypothesis is that $C_{ft\text{-}ft} = C_{Tpu} = C_{Wpu}$ because the values of these are obtained during early systole when reflected waves are believed not to exist. Table 4.15 displays the t-test results for this, where comparisons are made: $C_{ft\text{-}ft}$ with C_{Tpu}, $C_{ft\text{-}ft}$ with C_{Wpu} and C_{Tpu} with C_{Wpu}; in Table 4.15, the symbol '#' indicates that being compared against. In Table 4.15, the null hypothesis is supported where there are "complete sets" of no significant differences (NS); complete sets of NS indicate that all comparisons show $C_{ft\text{-}ft} = C_{Tpu} = C_{Wpu}$. It can be seen that the null hypothesis is not consistently supported, furthermore, there are NS findings where p-values are close to significance of p=0.05.

TABLE 4.12: Data for RHDN* and Tn** (Mean ± SD) from Anaesthetised Rabbits (n=13-14) at the UpSt & DnSt Sites of measurement in the Abdominal Aorta. Comparisons made for Treatments L-NAME (lo & *hi dose)* and Ach (lo & *hi dose*) against their respective Saline Controls. [p by paired t-test to Saline; NS = not significant at p>0.05]

	UpSt Site			DnSt Site		
	L-NAME (*lo*)	SALINE	Ach (*lo*)	L-NAME (*lo*)	SALINE	Ach (*lo*)
RHDN	0.55 ±0.09 [p=0.0007]	0.60 ±0.08	0.66 ±0.06 [p=0.0003]	0.51 ±0.11 [p=0.0062]	0.56 ±0.11	0.64 ±0.09 [p=0.0012]
Tn (ms)	89.2 ±8.3 [p=0.0005]	93.8 ±8.4	94.5 ±9.8 [NS;p=0.51]	88.3 ±8.4 [p=0.0063]	92.9 ±9.7	91.7 ±9.1 [NS;p=0.24]
	L-NAME (*hi*)	SALINE	Ach (*hi*)	L-NAME (*hi*)	SALINE	Ach (*hi*)
RHDN	0.54± 0.07 [NS;p=0.14]	0.57 ±0.09	0.60 ±0.07 [NS;p=0.11]	0.47 ±0.12 [p=0.034]	0.51 ±0.12	0.60 ±0.09 [p=0.015]
Tn (ms)	92.5 ±10.9 [p=0.0001]	98.9 ±10.3	104.2 ±11.2 [p=0.0002]	91.8 ±9.5 [p=0.0001]	98.1 ±8.8	102.4 ±11.0 [p=0.0004]

*RHDN: Relative Height of the Dicrotic Notch.
**Tn: time of notch from onset of systolic upstroke of the pressure pulse.

TABLE 4.13: Data for $C_{ft\text{-}ft}$* (m/s) (Mean ± SD) in the Abdominal Aorta at the UpSt & DnSt Sites of measurement in Anaesthetised Rabbits (n=10-12). Comparisons made for Treatments L-NAME (lo & *hi dose*) and Ach (*lo & hi dose*) against their respective Saline Controls. [p by paired t-test to Saline]

	UpSt Site			DnSt Site		
	L-NAME	SALINE	Ach	L-NAME	SALINE	Ach
$C_{ft\text{-}ft}$ (*lo dose*)	5.92 ±0.96 [p=0.015]	5.47 ±0.69	4.65 ±0.58 [p<0.0001]	6.56 ±0.84 [p=0.039]	6.00 ±0.94	5.12 ±0.49 [p=0.0078]
$C_{ft\text{-}ft}$ (*hi dose*)	5.81 ±0.86 [p<0.0001]	5.15 ±0.87	3.97 ±0.48 [p<0.0001]	7.12 ±1.19 [p=0.0034]	6.04 ±0.77 [p=0.021]**	4.72 ±0.53 [p<0.0001]

*$C_{ft\text{-}ft}$: pulse wave velocity by foot-to-foot.
**[Unpaired t-test to saline data UpSt Site]

FIGURE 4.23A: $C_{ft\text{-}ft}$ plotted against MAP in the Abdominal Aorta (UpSt & DnSt Sites) after Treatments with L-NAME (*lo & hi dose*), Saline and Ach (*lo & hi dose*) for each of 12 Anaesthetised Rabbits.
Linear regression of pooled data: UpSt Site r=0.642, p<0.001; DnSt Site r=0.480, p<0.001.

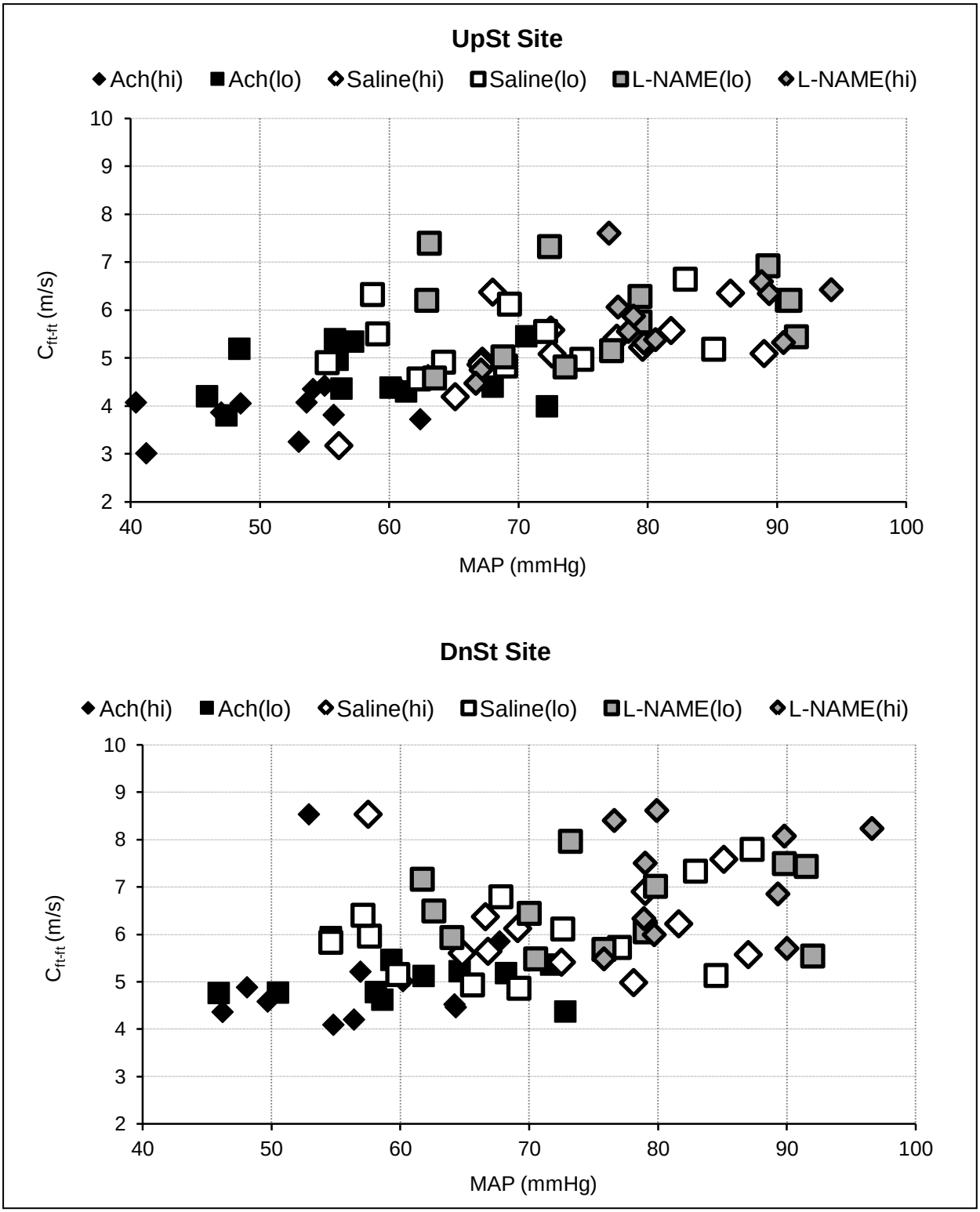

FIGURE 4.23B: $C_{ft\text{-}ft}$ plotted against MAP in the Abdominal Aorta (UpSt & DnSt Sites). Plots and Linear Regressions are shown for Treatments with L-NAME, Saline and Ach. Data for *lo & hi dose* pooled for each treatment of 12 Anaesthetised Rabbits.
Note: for UpSt & DnSt Sites, regression lines not significantly different but their intercepts are, thereby indicating effect of Ach & L-NAME on the relationship of $C_{ft\text{-}ft}$ vs. MAP – see text.

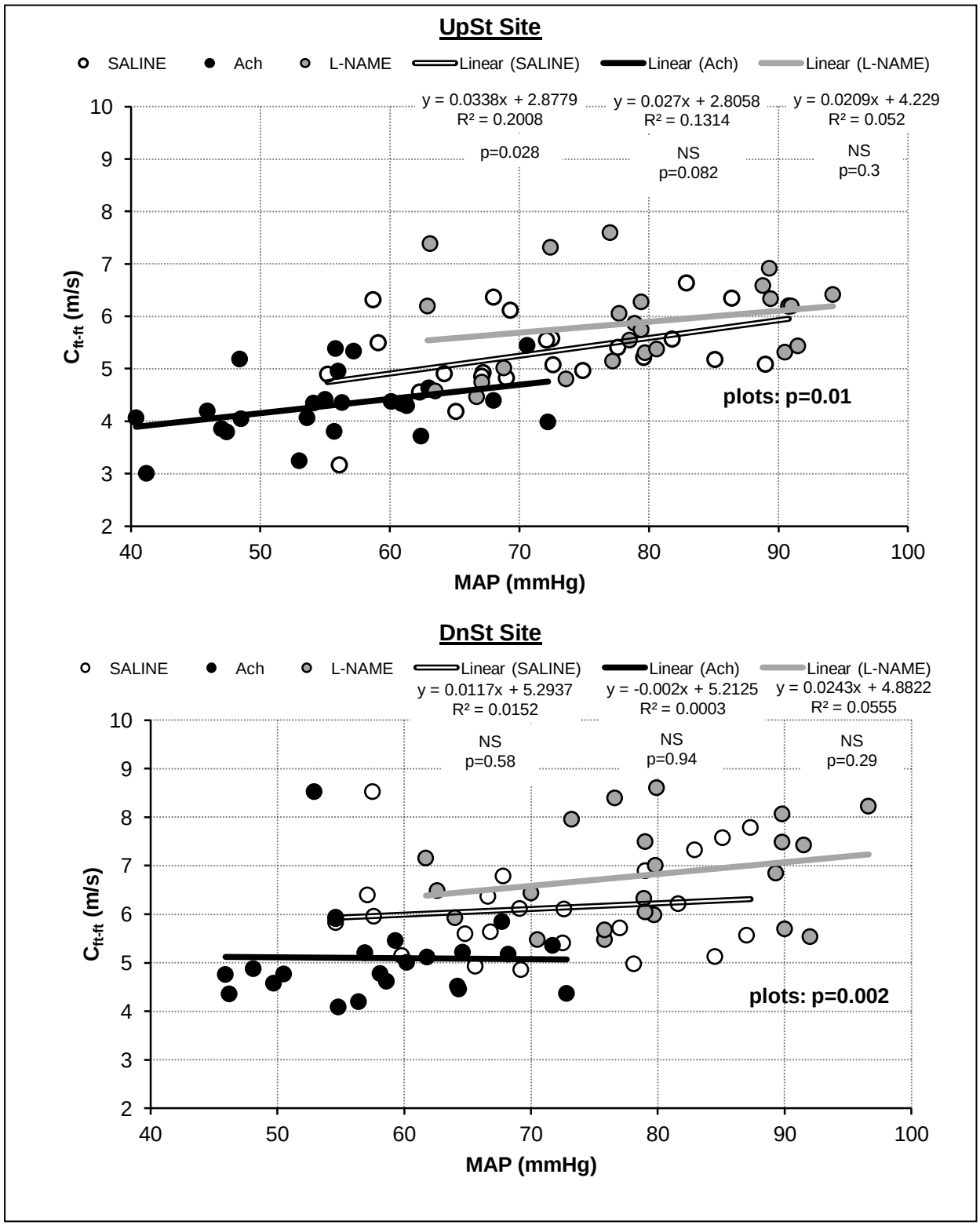

TABLE 4.14: Data for C_{ft-ft}, C_{Tpu} and C_{Wpu} (all m/s) (Mean ± SD) at the UpSt & DnSt Sites of measurement in the Abdominal Aorta of Anaesthetised Rabbits. Comparisons made for Treatments L-NAME (lo & *hi dose*) and Ach (lo & *hi dose*) against their respective Saline Controls. [n*]; [p by paired t-test; NS = Not Significant for p>0.05].

See also notes at foot of table.

	UpSt Site			DnSt Site		
	L-NAME (*lo*)	SALINE	Ach (*lo*)	L-NAME (*lo*)	SALINE	Ach (*lo*)
C_{ft-ft}	5.92 ±0.96 [12] [p=0.015]	5.47 ±0.69 [12]	4.65± 0.58 [12] [p<0.0001]	6.56 ±0.88 [11] [NS;p=0.058]	6.00 ±0.99 [11]	5.05 ±0.44 [11] [p=0.007]
C_{Tpu}	7.42 ±2.21 [12] [p=0.0029]	6.36 ±1.79 [12]	6.23 ±2.60 [12] [NS;p=0.78]	6.22 ±2.11 [11] [NS;p=0.12]	5.63 ±2.02 [11]	6.91 ±4.45 [11] [NS;p=0.22]
C_{Wpu}	5.88 ±1.71 [12] [p=0.002]	4.71 ±1.09 [12]	4.54 ±2.11 [12] [NS;p=0.70]	4.72 ±2.07 [11] [NS;p=0.09]	4.16 ±1.71 [11]	4.87 ±3.53 [11] [NS;p=0.41]
	L-NAME (*hi*)	SALINE	Ach (*hi*)	L-NAME (*hi*)	SALINE	Ach (*hi*)
C_{ft-ft}	5.85 ±1.20 [6] [p=0.013]	5.12 ±1.26 [6]	3.84 ±0.63 [6] [p=0.01]	7.26±1.23[4] [NS;p=0.14]	6.85±1.19[5] 6.44±0.84[4]	5.65±1.70[5] [p=0.002]
C_{Tpu}	5.57 ±1.38 [6] [NS;p=0.23]	4.76 ±1.51 [6]	4.57 ±1.79 [6] [NS;p=0.22]	4.83±1.62[4] [NS;p=0.68]	4.98±1.33[5] 4.98±1.54[4]	5.24±1.55[5] [NS;p=0.53]
C_{Wpu}	4.26 ±1.27 [6] [NS;p=0.23]	2.78 ±0.68 [6]	3.17 ±1.55 [6] [NS;p=0.075]	3.69±1.16[4] [NS;p=0.77]	3.64±0.92[5] 3.88±0.86[4]	3.15±1.15[5] [NS;p=0.31]

C_{ft-ft}: pulse wave velocity by foot-to-foot

C_{Tpu}: wave speed by PU loop using measured (Total) pressure (P_T)

C_{Wpu}: wave speed by PU loop using wave pressure (Pw).

*[n]: difficulties with poor acquisition quality was experienced in some cases, hence the comparisons with different numbers of animals.

TABLE 4.15: Comparisons between $C_{ft\text{-}ft}$, C_{Tpu} and C_{Wpu} as measured at the UpSt & DnSt Sites in the Abdominal Aorta of Anaesthetised Rabbits under conditions of Treatments with L-NAME (lo & *hi dose*), Saline, and Ach (lo & *hi dose*); p by unpaired t-test to #. See Table 4.14 for values of $C_{ft\text{-}ft}$, C_{Tpu}, and C_{Wpu}.

	UpSt Site			DnSt Site		
	$C_{ft\text{-}ft}$	C_{Tpu}	C_{Wpu}	$C_{ft\text{-}ft}$	C_{Tpu}	C_{Wpu}
L-NAME (*lo*)	#	p=0.043	NS [p=0.94]	#	NS [p=0.63]	p=0.014
		#	NS [p=0.07]		#	NS [p=0.11]
Saline (for *lo*)	#	NS [p=0.13]	NS [p=0.053]	#	NS [p=0.59]	p=0.006
		#	p=0.013		#	NS [p=0.081]
Ach (*lo*)	#	NS [p=0.052]	NS [p=0.87]	#	NS [p=0.18]	NS [p=0.87]
		#	NS [p=0.094]		#	NS [p=0.25]
L-NAME (*hi*)	#	NS [p=0.71]	NS [p=0.051]	#	NS [p=0.055]	p=0.006
		#	NS [p=0.12]		#	NS [p=0.3]
Saline (for *hi*)	#	NS [p=0.88]	NS [p=0.13]	#	p=0.046	p=0.001
		#	NS [p=0.087]		#	NS [p=0.1]
Ach (*hi*)	#	NS [p=0.37]	NS [p=0.35]	#	NS [p=0.71]	p=0.026
		#	NS [p=0.18]		#	p=0.042

$C_{ft\text{-}ft}$: pulse wave velocity by foot-to-foot; C_{Tpu}: wave speed by PU loop of measured (Total) pressure; C_{Wpu}: wave speed by PU loop of wave pressure

NS: not significant i.e. p>0.05; complete sets of NS support the null hypothesis that $C_{ft\text{-}ft} = C_{Tpu} = C_{Wpu}$

p≤0.05 conflicts with the null hypothesis.

Values for $C_{ft\text{-}ft}$ were used for the determination of wave intensity since values for C_{Tpu} and C_{Wpu} are very sensitive to the fidelity of acquisition of the systolic part of the pressure (P) and velocity (U) waveforms.

Wave Intensity Analysis (WIA)

Chapter 2 explained the theoretical aspects of WIA and pointed out the features of the wave intensity plot. Figure 4.24 (bottom row three panels) shows an example of wave intensity plots from an experiment.

Figure 4.24 shows a study when a Type 1 (saline) waveform was converted to a Type 2 waveform by L-NAME. It is notable that the diastolic (dicrotic) wave late in diastole (100-250ms) of the Type 2 waveform is not associated at this time with any remarkable features of wave intensity – the wave intensity is quiescent (Figure 4.24 – under L-NAME).

Data for WIA were obtained from the wave intensity plots; these plots were integrated to give wave energy as J/m^2. Figures 4.25 & 4.26 give data, in terms of wave energy, for compression and expansion waves (incident and reflected in both cases) at UpSt (Figure 4.25) and DnSt (Figure 4.26) Sites in the abdominal aorta of anaesthetised rabbits, under treatments with L-NAME (*lo* & *hi doses*), saline and Ach (*lo* & *hi doses*).

At the UpSt Site (Figure 4.25), neither L-NAME nor Ach had effects on incident compression wave energy; this was also the case for incident expansion wave energy except for one observation only where Ach (*lo dose*) decreased the energy ($p=0.002$). In the case of reflected compression wave energy, L-NAME significantly decreased while Ach significantly increased this energy. Reflected expansion wave energy was unaffected by Ach and little affected by L-NAME, only L-NAME (*lo dose*) caused a statistically significant ($p=0.002$) decrease in this energy.

At the DnSt Site (Figure 4.26), both L-NAME and Ach appeared to decrease incident compression wave energy but these effects were statistically significant only for L-NAME (*lo dose*) and Ach (*lo dose*). Incident expansion wave energy was unaffected by L-NAME but Ach decreased it significantly at *lo dose* but not significantly at *hi dose*. Both L-NAME and Ach decreased reflected compression wave energy, though this effect of L-NAME (*hi dose*) did not reach statistical significance. Reflected expansion wave energy was unaffected by L-NAME but was significantly decreased by Ach. These effects of Ach causing decreased reflected wave energies (compression or expansion) were in comparison to saline treatment; however the reflected wave energies were not decreased when considered in proportion to their respective incident wave energies (see next paragraph and Figure 4.28).

FIGURE 4.24: Examples of Wave Intensity Plots (bottom row three panels). Top row gives details of Pulse Amplitude (PP) for Total Pressure (PPtp), Reservoir (Windkessel) Pressure (PPrp) and Wave Pressure (PPwp). Middle row shows the associated Blood Flow Velocity. Legends on Saline panels are applicable to all. Data are from the Abdominal Aorta (UpSt Site) of an Anaesthetised Rabbit.

DBP at 0 time: L-NAME 10824 Pa; Saline 9679 Pa; Ach 7149 Pa

Note: the diastolic (dicrotic) wave late in diastole (100-250ms) of the Type 2 waveform (see under L-NAME) is not associated at this time with any remarkable features of wave intensity – the wave intensity is quiescent.

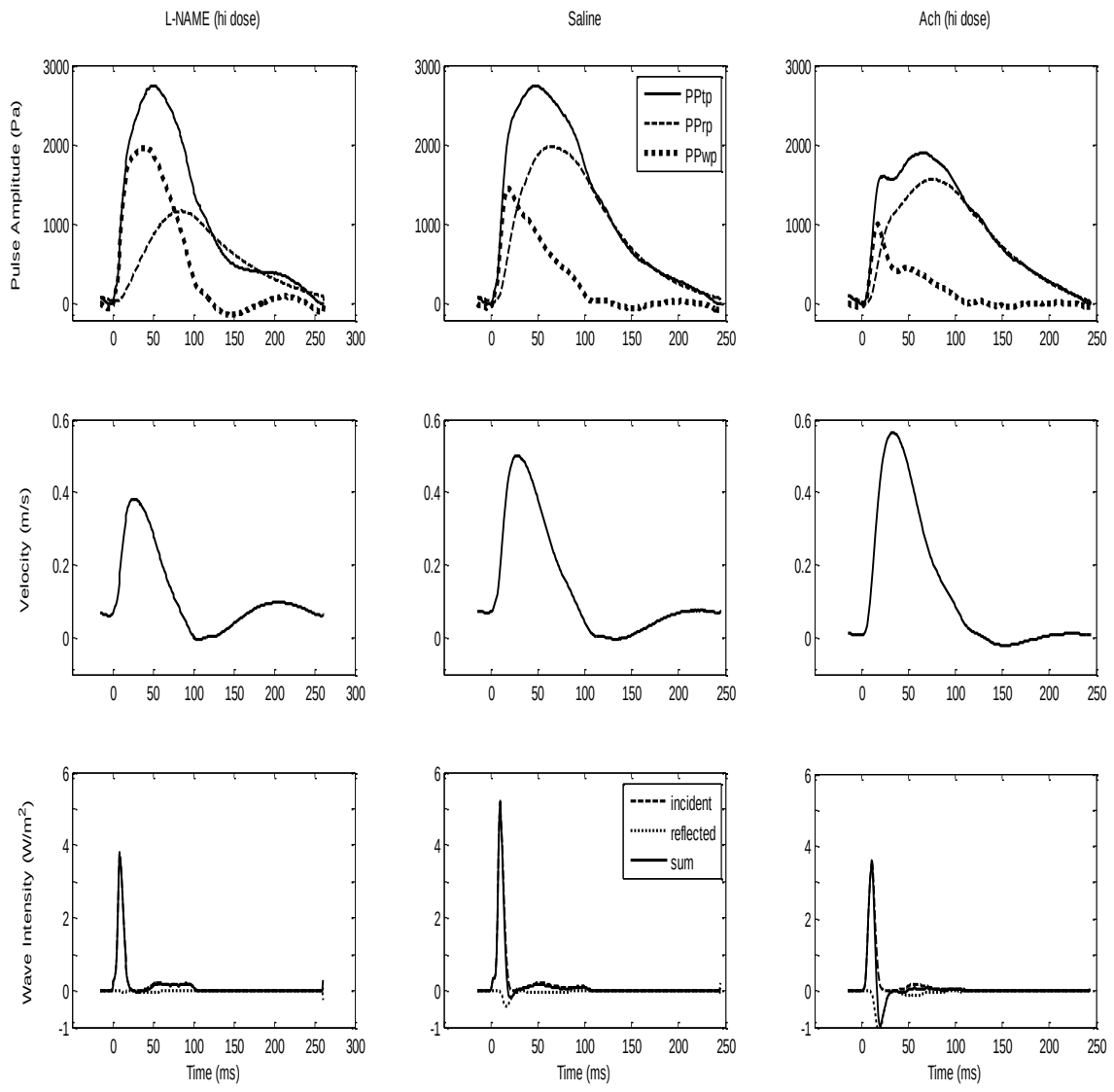

Experiment Ref.: AAEH 091112

By considering the data in terms of wave reflection indices (WRI), namely considering the reflected wave energies in proportion to their respective incident wave energies (i.e. reflected energy / incident energy), treatment-related effects are apparent for L-NAME and Ach on compression and expansion wave energies at the UpSt Site (Figure 4.27). At this site, the lack of effect of L-NAME or Ach on incident compression or expansion wave energies (Figure 4.25) when considered with their significant effects on the respective reflected wave energies gives WRI shown in Figure 4.27; these WRI confirm that L-NAME significantly decreased whereas Ach significantly increased reflections of compression waves; the same trend occurs for expansion waves, though not all WRI are statistically significant from control (Figure 4.27). Treatment-related effects on WRI for compression and expansion waves at the DnSt Site are not marked (Figure 4.28), but are of a trend similar to those at the UpSt Site (c.f. Figure 4.27).

Figures 4.29 (UpSt Site) and 4.30 (DnSt Site) explore, by regression analysis, a possible relationship between WRI and RHDN. At the UpSt Site of measurement in the abdominal aorta (Figure 4.29), positive and significant correlations between compression wave WRI and RHDN were found with treatments L-NAME ($r=0.602$; $p=0.008$), saline ($r=0.731$; $p=0.0006$) and Ach ($r=0.596$; $p=0.009$); the plots did not differ significantly from each other. Expansion wave WRI also correlated positively and significantly with RHDN (Figure 4.29) with treatments L-NAME ($r=0.699$; $p=0.001$), saline ($r=0.745$; $p=0.0004$) and Ach ($r=0.561$; $p=0.015$); again the plots did not differ significantly from each other. At the DnSt Site of measurement in the abdominal aorta (Figure 4.30) positive correlations, though not always significant, were again found between compression wave WRI and RHDN with treatments L-NAME ($r=0.475$; NS $p=0.054$), saline ($r=0.435$; NS $p=0.08$) and Ach ($r=0.714$; $p=0.001$); the plots differed significantly ($p=0.0002$). It was found similarly for expansion wave WRI and RHDN (Figure 4.30) with treatments L-NAME ($r=0.442$; NS $p=0.08$), saline ($r=0.381$; NS $p>0.1$) and Ach ($r=0.589$; $p=0.013$); the plots differed significantly ($p=0.0004$). Thus, RHDN appears to be affected by reflections, increasing with increased reflections; Ach appears to enhance this while L-NAME does the opposite – this is consistent with the data in Table 4.12.

Another ratio considered is that of the incident expansion wave energy to the incident compression wave energy. The data for this is shown in Figure 4.31. The energy ratios appear to follow a trend of L-NAME increasing while Ach decreasing the values. L-NAME increased the values significantly, whereas the decreases caused by Ach were mostly not statistically significant; significance was achieved only for Ach *lo dose* DnSt Site.

The distance of reflection sites from the sites of recording can be deduced from the wave intensity curves (see Chapter 2); these distances are plotted in Figure 4.32. Under saline control conditions, the distance of reflection sites were approximately 2.5cm and 1.5cm from the UpSt and DnSt Sites respectively (estimated from the saline control plots in Figure 4.30). L-NAME had no statistically significant effect on the distance to the reflection sites from the UpSt or the DnSt Sites of recording (Figure 4.32). On the other hand, Ach (*lo & hi dose*) appeared to reduce the distance of the reflection site from the UpSt Site of recording; this effect of both doses was statistically significant (Figure 4.32). However, Ach (*lo & hi dose*) had no statistically significant effect on the distance to the reflection site from the DnSt Site of recording.

FIGURE 4.25: Data for WIA on Compression (CW) and Expansion Waves (EW) at the UpSt Site of measurement in the Abdominal Aorta of Anaesthetised Rabbits. Comparison for Treatments with L-NAME (*lo & hi dose*) and Ach (*lo & hi dose*) against their respective Saline controls. Values are Mean ± SEM (J/m^2); p by paired t-test to saline, NS=not significant at p>0.05; *lo dose* n=12, *hi dose* n=6. For supplement data see pp138-139 of pp138-142.

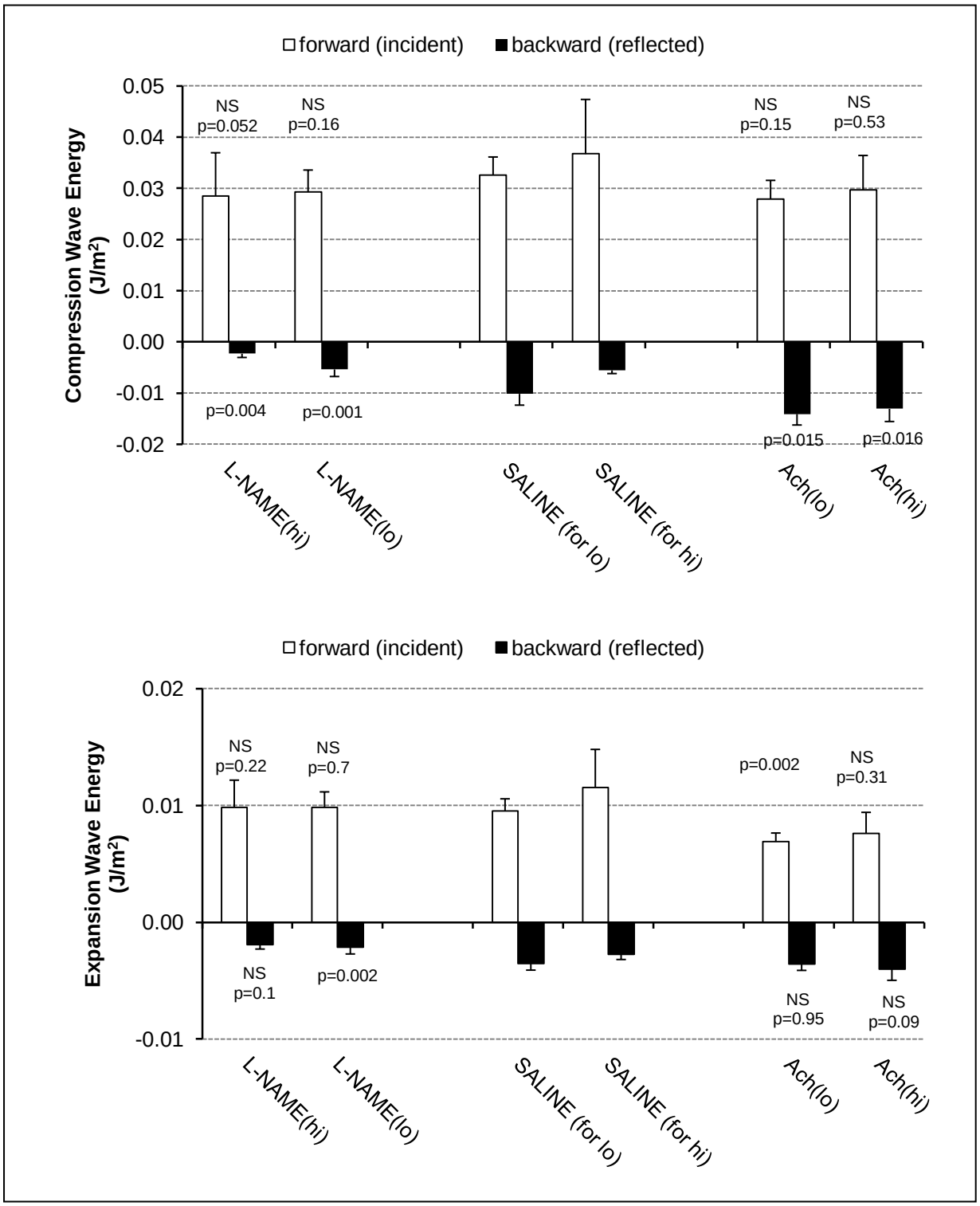

FIGURE 4.26: Data for WIA on Compression (CW) and Expansion Waves (EW) at the DnSt Site of measurement in the Abdominal Aorta of Anaesthetised Rabbits. Comparison of Treatments with L-NAME (*lo* & *hi dose*) and Ach (*lo* & *hi dose*) against their respective Saline controls. Values are Mean ± SEM (J/m^2); p by paired t-test to saline, NS=not significant at p>0.05; *lo dose* n=11, *hi dose* n=6. For supplement data see pp139-140 of pp138-142.

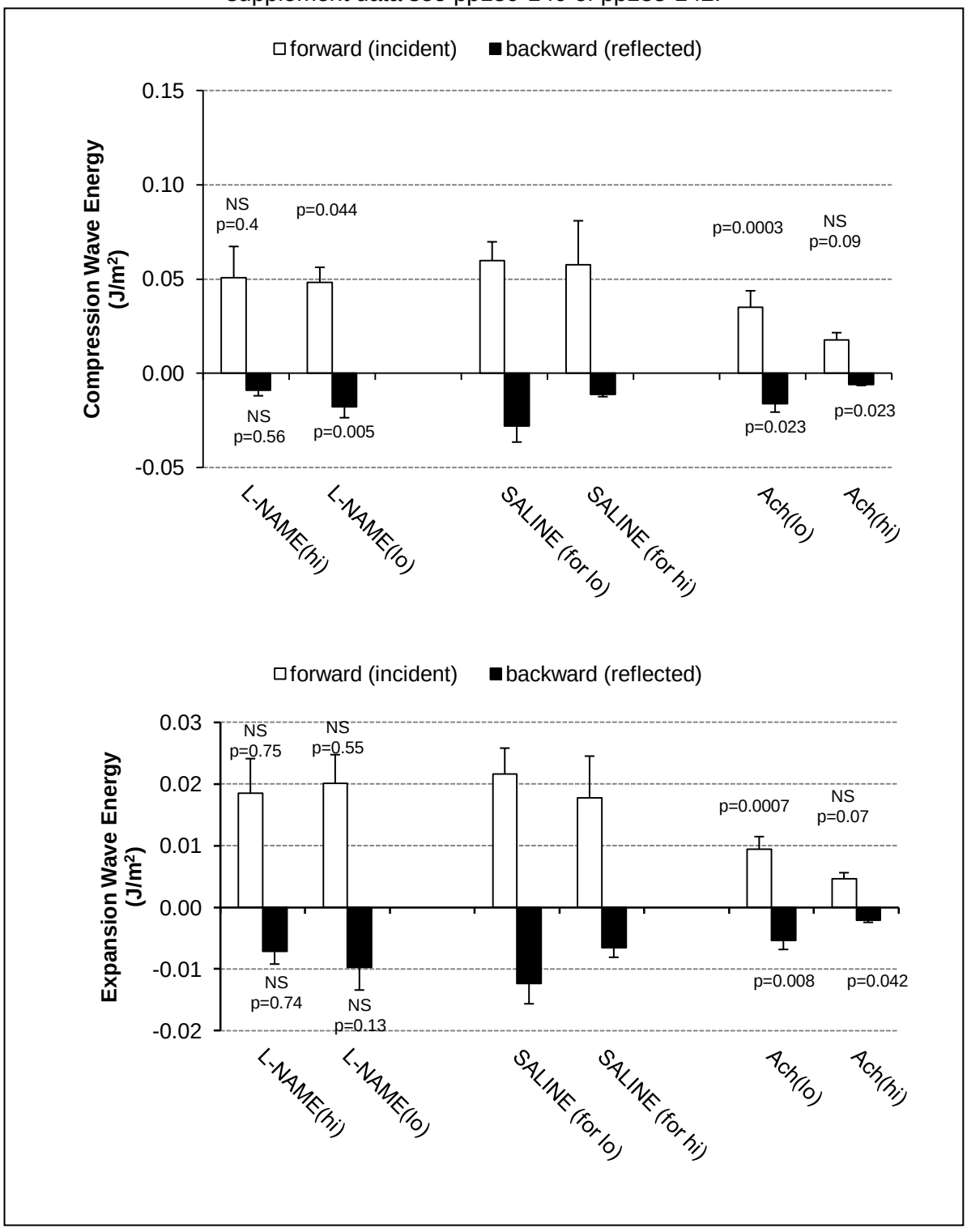

FIGURE 4.27: Wave Reflection Indices (WRI) for Compression and Expansion Waves in the Abdominal Aorta (UpSt Site) of Anaesthetised Rabbits. Comparison of Treatments with L-NAME (*lo & hi dose*) and Ach (*lo & hi dose*) against their respective Saline Controls. Plots of Mean ± SEM; p by paired t-test to saline; NS=not significant at p>0.05.
(*lo dose* n=12; *hi dose* n=6)
(WRI = Reflected Energy / Incident Energy). For supplement data see p140 of pp138-142.

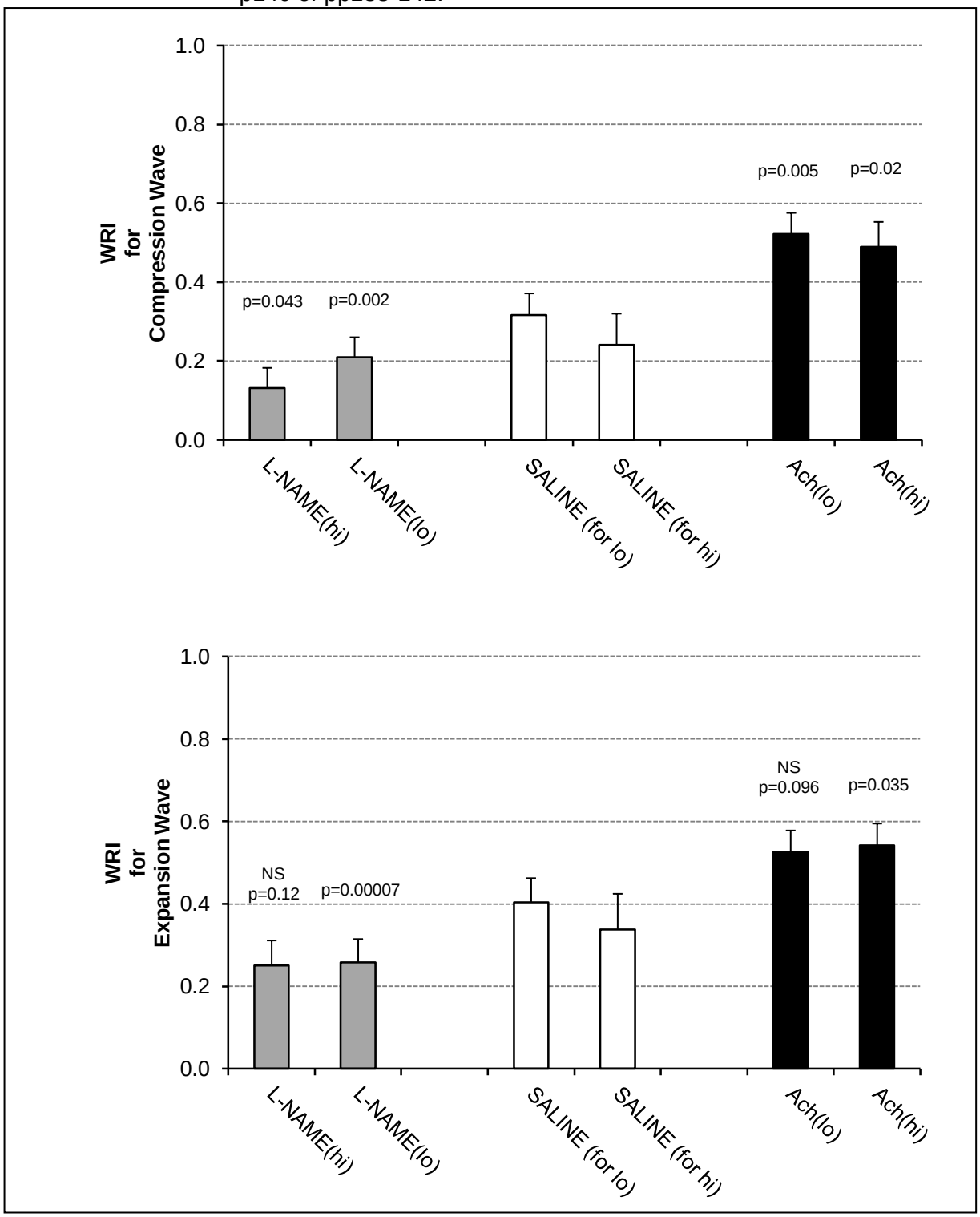

FIGURE 4.28: Wave Reflection Indices (WRI) for Compression and Expansion Waves in the Abdominal Aorta (DnSt Site) in Anaesthetised Rabbits. Comparison of Treatments with L-NAME (*lo & hi dose*) and Ach (*lo & hi dose*) against their respective Saline Controls.. Plots of Mean ± SEM; p by paired t-test to saline, NS=not significant at p>0.05.
(*lo dose* n=11; *hi dose* n=6)
(WRI = Reflected Energy / Incident Energy). For supplement data see p141 of pp138-142.

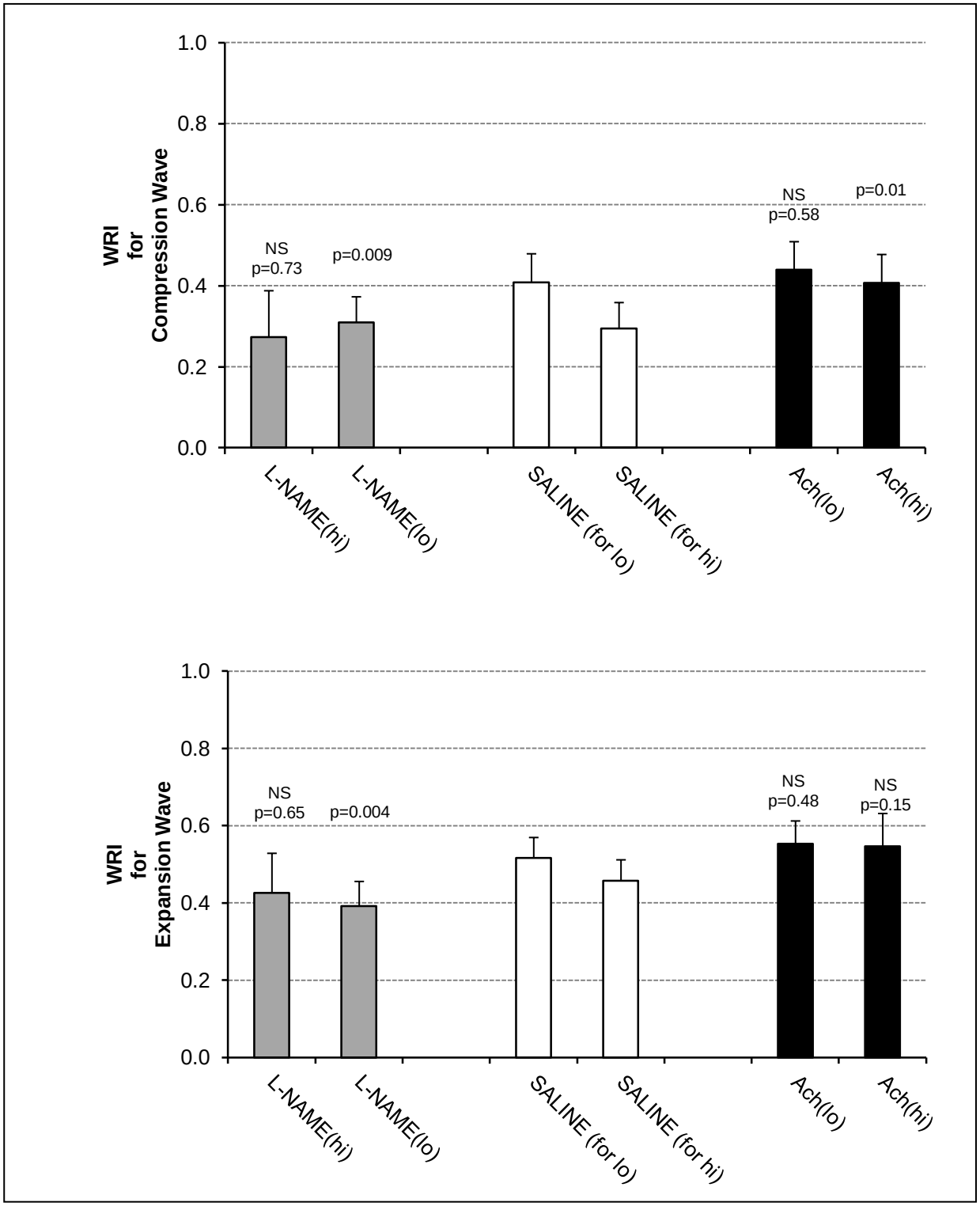

FIGURE 4.29: Relationship Between Wave Reflection Index (WRI) for Compression and Expansion Waves with RHDN in the Abdominal Aorta (UpSt Site) of Anaesthetised Rabbits after Treatments with L-NAME (*lo & hi dose*), Saline and Ach (*lo & hi dose*). NS=not significant at p>0.05.

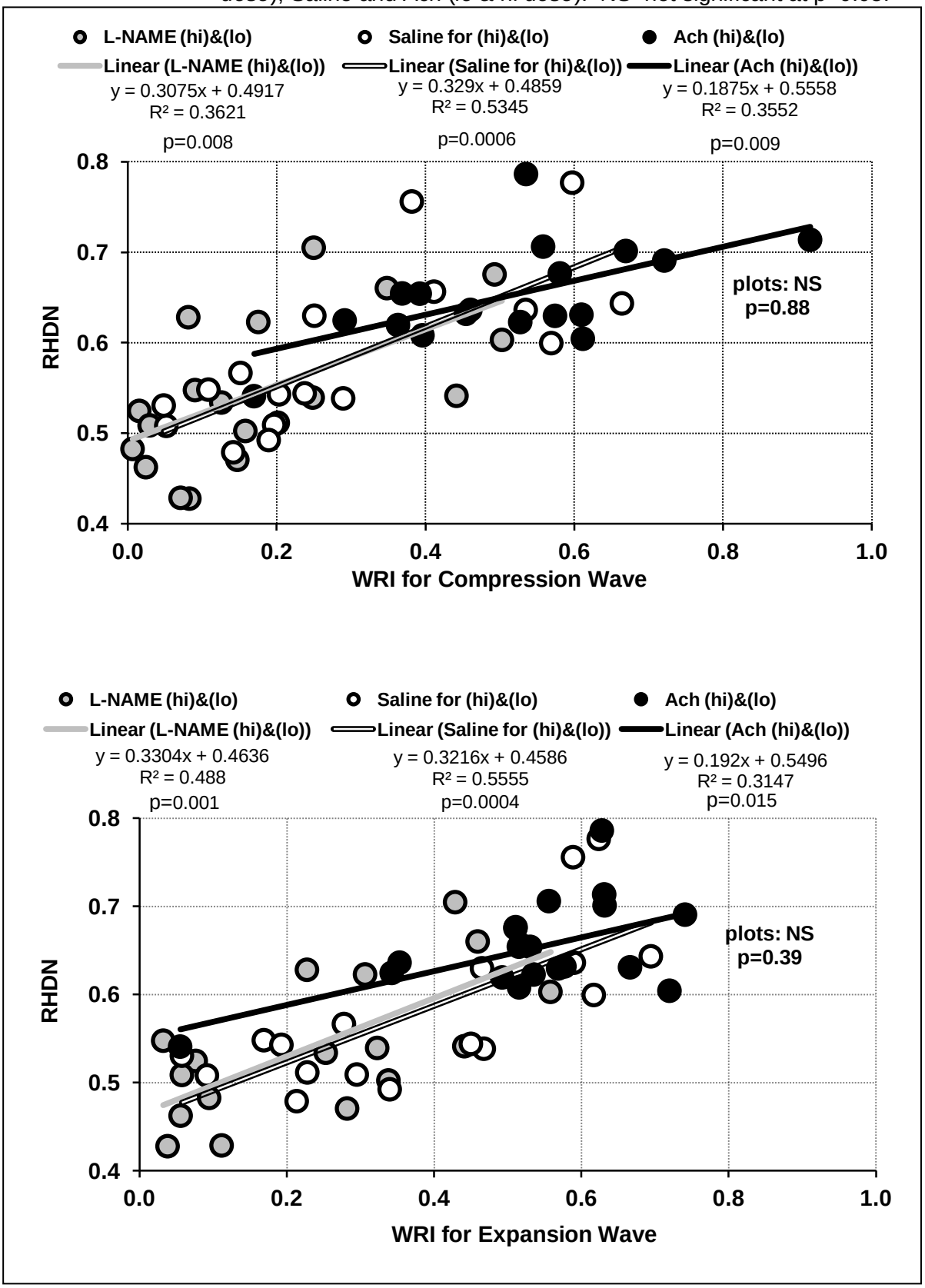

FIGURE 4.30: Relationship Between Wave Reflection Index (WRI) for Compression and Expansion Waves with RHDN in the Abdominal Aorta (DnSt Site) of Anaesthetised Rabbits after Treatments with L-NAME (*lo & hi dose*), Saline and Ach (*lo & hi dose*). NS=not significant at p>0.05.

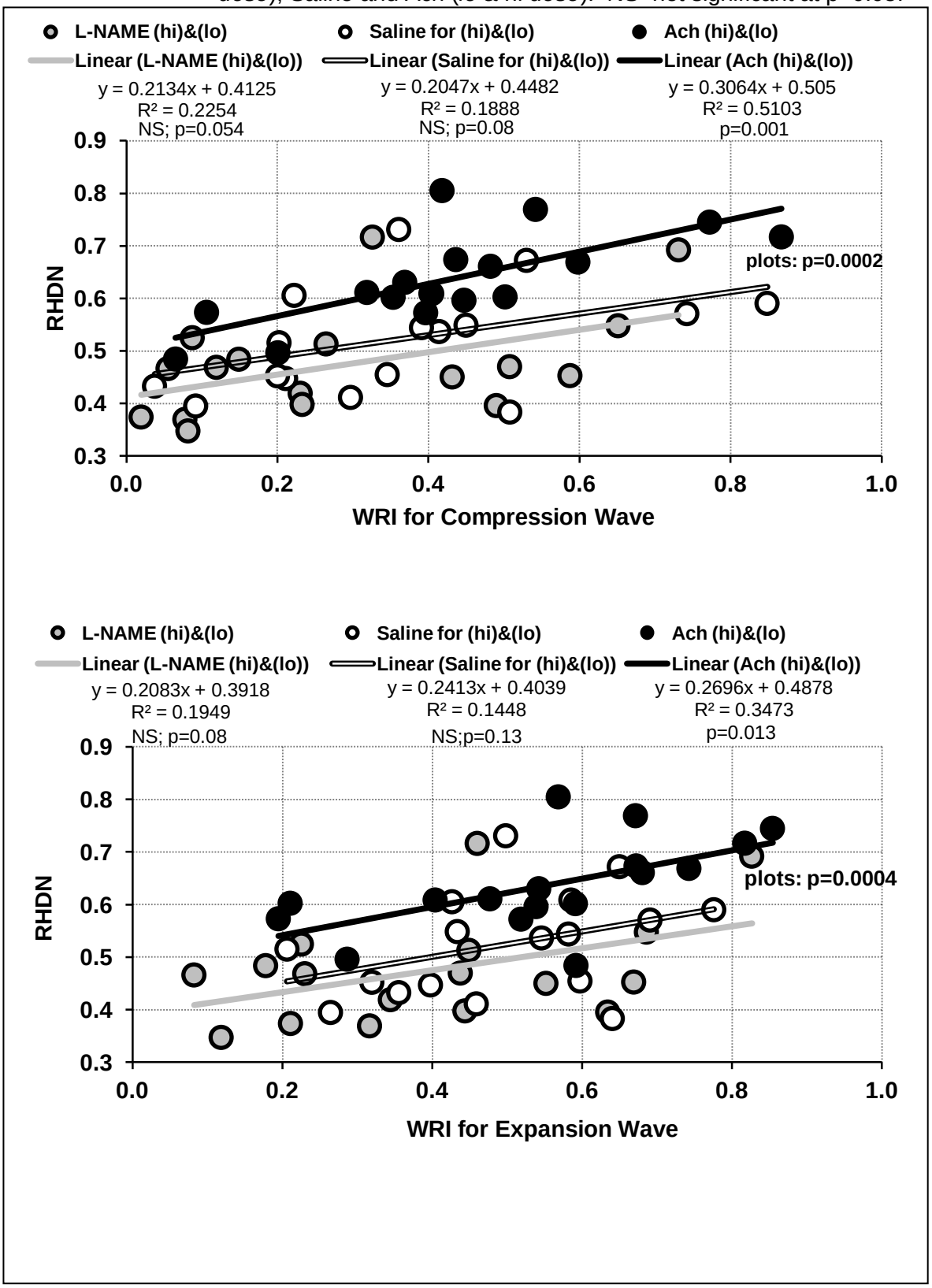

FIGURE 4.31: Ratios for Incident Expansion to Incident Compression Waves in the Abdominal Aorta (UpSt & DnSt Sites) of Anaesthetised Rabbits. Comparison of Treatments with L-NAME (*lo & hi dose*) and Ach (*lo & hi dose*) against their respective Saline Controls. Plots of Mean ± SEM (*lo dose* n=11-12; *hi dose* n=6); p by paired test to saline, NS=not significant at p>0.05. For supplement data see p141 of pp138-142.

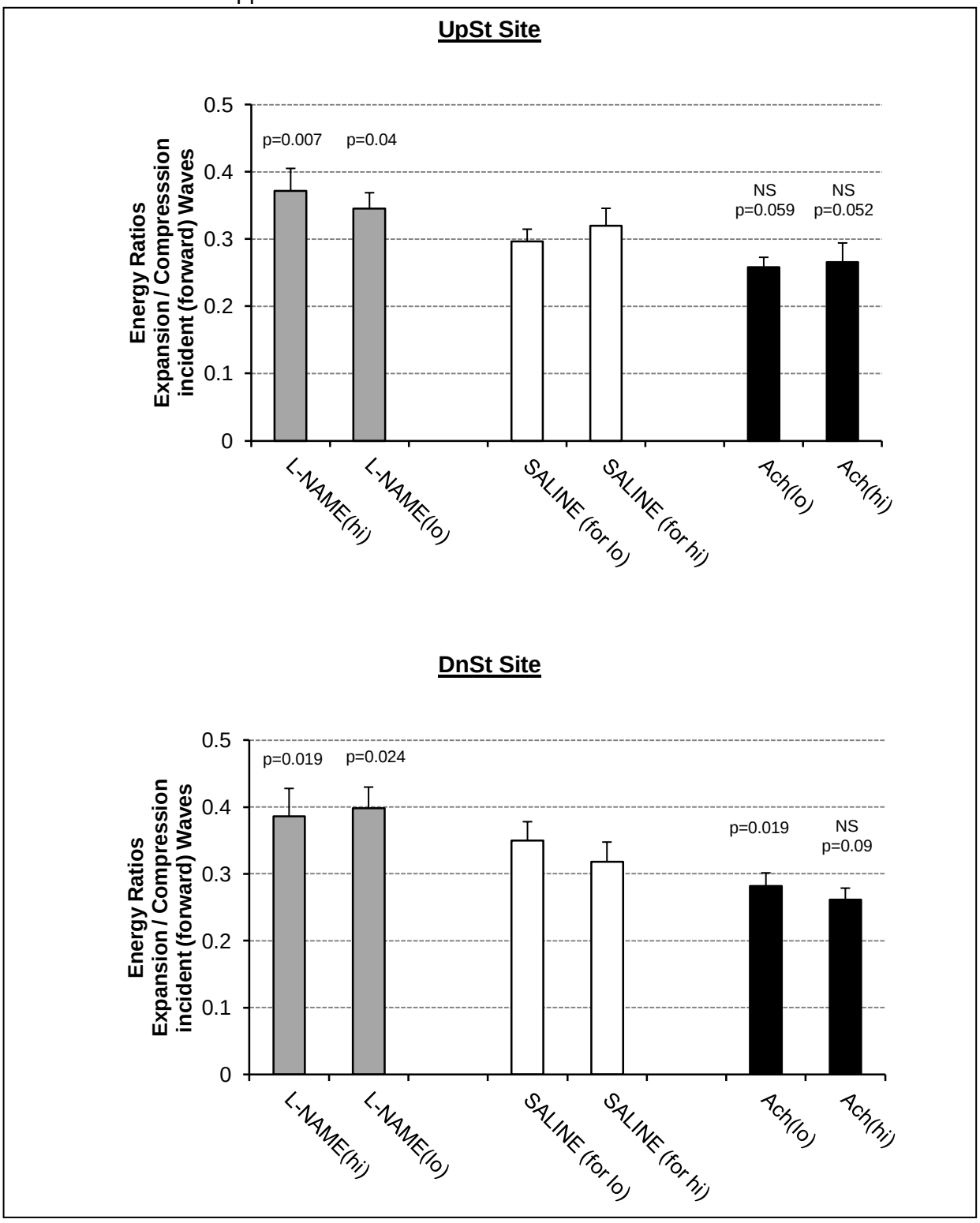

FIGURE 4.32: Distances of Reflection Site from the Sites of Recording (i.e. UpSt & DnSt Sites) as estimated from the time lapse between Incident and Reflected Intensities of the Compression Wave in the Abdominal Aorta of Anaesthetised Rabbits. Comparison of Treatments with L-NAME (*lo & hi dose*) and Ach (*lo & hi dose*) against their respective Saline Controls. Values are Mean ± SEM; p by paired test to saline, NS=not significant at p>0.05. For supplement data see p142 of pp138-142.

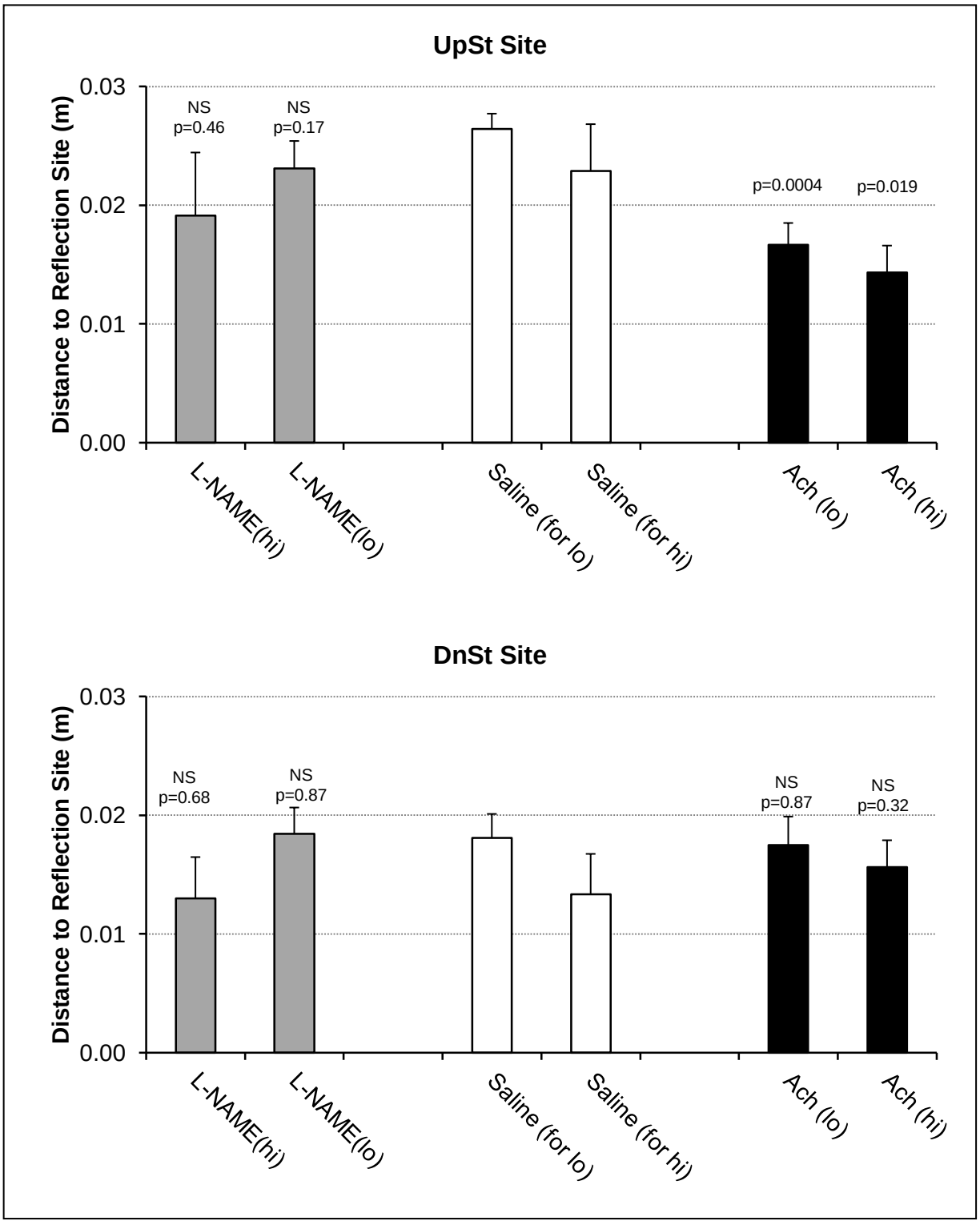

Supplement to Figures 4.21, 4.25 – 4.28, 4.31, 4.32

Table cells are tinted where disagreement occurs for p-values indicating significant or not significant for group values or Δ% values – Statistical Type I or Type II errors might arise.

Figures	Detail	Treatment	Bar Value Mean± SEM (±SD indicated) (see Figure for units etc.)	p-value as stated on Figure (compared to Saline)	Δ as % of Saline Control Mean±SD	t-value	p-value
4.21	UpSt	Ach (*hi*)	3.13±1.64(SD)	0.004	130±111	4.036	0.002
		Ach (*lo*)	3.92±3.35(SD)	0.019	125±143	3.252	0.006
		Saline (*lo*)	1.72±0.65(SD)	-	-	-	-
		Saline (*hi*)	1.46±0.49(SD)	-	-	-	-
		L-NAME (*lo*)	1.36±0.62(SD)	0.018	-20±29	2.540	0.025
		L-NAME (*hi*)	1.27±0.55(SD)	0.017	-15±21	2.481	0.031
	DnSt	Ach (*hi*)	1.35±0.67(SD)	0.002	159±128	4.115	0.002
		Ach (*lo*)	1.48±1.00(SD)	0.009	110±117	3.385	0.005
		Saline (*lo*)	0.78±0.48(SD)	-	-	-	-
		Saline (*hi*)	0.62±0.34(SD)	-	-	-	-
		L-NAME (*lo*)	0.61±0.41(SD)	0.06	-21±34	2.153	0.052
		L-NAME (*hi*)	0.57±0.36(SD)	0.65	-0.6±64	0.031	0.98
4.25 (UpSt)	Compression Incident	L-NAME (*hi*)	0.0285±0.0084	0.052	-18±25	1.760	0.14
		L-NAME (*lo*)	0.0293±0.0043	0.16	-13±21	2.208	0.049
		Saline (*lo*)	0.0326±0.0035	-	-	-	-
		Saline (*hi*)	0.0367±0.0107	-	-	-	-
		Ach (*lo*)	0.0279±0.0037	0.15	-13±25	1.868	0.09
		Ach (*hi*)	0.0297±0.0068	0.53	-2±54	0.096	0.93
	Compression Reflection	L-NAME (*hi*)	−0.0023±0.0007	0.004	-61±27	5.505	0.003
		L-NAME (*lo*)	−0.0054±0.0014	0.001	-50±20	8.738	<0.0001
		Saline (*lo*)	−0.0101±0.0022	-	-	-	-
		Saline (*hi*)	−0.0055±0.0006	-	-	-	-
		Ach (*lo*)	−0.0141±0.0021	0.015	91±137	2.299	0.042
		Ach (*hi*)	−0.0131±0.0025	0.016	135±75	4.416	0.007

Supplement to Figures Continued:

Figures	Detail	Treatment	Bar Value Mean± SEM (see Figure for units etc.)	p-value as stated on Figure (compared to Saline)	Δ as % of Saline Control Mean±SD	t-value	p-value
4.25 cont. (UpSt)	Expansion Incident	L-NAME (*hi*)	0.0098±0.0023	0.22	-4±32	0.297	0.77
		L-NAME (*lo*)	0.0098±0.0014	0.70	0.7±22	0.110	0.91
		Saline (*lo*)	0.0095±0.0010	-	-	-	-
		Saline (*hi*)	0.0116±0.0032	-	-	-	-
		Ach (*lo*)	0.0069±0.0008	0.002	-26±18	4.889	0.0005
		Ach (*hi*)	0.0076±0.0018	0.31	-14±57	0.587	0.58
	Expansion Reflection	L-NAME (*hi*)	−0.0019±0.0004	0.10	-27±27	2.489	0.055
		L-NAME (*lo*)	−0.0022±0.0006	0.002	-41±34	4.166	0.002
		Saline (*lo*)	−0.0035±0.0006	-	-	-	-
		Saline (*hi*)	−0.0028±0.0004	-	-	-	-
		Ach (*lo*)	−0.0036±0.0005	0.95	32±125	0.883	0.40
		Ach (*hi*)	−0.0040±0.0010	0.09	43±50	2.102	0.09
4.26 (DnSt)	Compression Incident	L-NAME (*hi*)	0.0508±0.0165	0.40	2±33	0.166	0.87
		L-NAME (*lo*)	0.0483±0.0079	0.044	-10±36	0.945	0.37
		Saline (*lo*)	0.0598±0.0099	-	-	-	-
		Saline (*hi*)	0.0577±0.0232	-	-	-	-
		Ach (*lo*)	0.0350±0.0087	0.0003	-44±19	7.600	<0.0001
		Ach (*hi*)	0.0176±0.0039	0.09	-59±21	7.028	0.0009
	Compression Reflection	L-NAME (*hi*)	−0.0091±0.0030	0.56	-13±75	0.424	0.69
		L-NAME (*lo*)	−0.0177±0.0060	0.005	-13±100	0.452	0.66 *****
		Saline (*lo*)	−0.0281±0.0085	-	-	-	-
		Saline (*hi*)	−0.0112±0.0013	-	-	-	-
		Ach (*lo*)	−0.0161±0.0046	0.023	-37±19	6.485	<0.0001
		Ach (*hi*)	−0.0059±0.0007	0.023	-43±25	4.155	0.009

Supplement to Figures Continued:

Figures	Detail	Treatment	Bar Value Mean± SEM (see Figure for units etc.)	p-value as stated on Figure (compared to Saline)	Δ as % of Saline Control Mean±SD	t-value	p-value
4.26 cont. (DnSt)	Expansion Incident	L-NAME (*hi*)	0.0185±0.0056	0.75	27±55	1.190	0.29
		L-NAME (*lo*)	0.0202±0.0046	0.55	3±42	0.226	0.83
		Saline (*lo*)	0.0216±0.0042	-	-	-	-
		Saline (*hi*)	0.0178±0.0068	-	-	-	-
		Ach (*lo*)	0.0094±0.0021	0.0007	-54±14	12.589	<0.0001
		Ach (*hi*)	0.0046±0.0010	0.07	-63±28	5.604	0.003
	Expansion Reflection	L-NAME (*hi*)	−0.0072±0.0020	0.74	24±89	0.655	0.54
		L-NAME (*lo*)	−0.0098±0.0036	0.13	-28±31	3.005	0.013
		Saline (*lo*)	−0.0123±0.0033	-	-	-	-
		Saline (*hi*)	−0.0066±0.0015	-	-	-	-
		Ach (*lo*)	−0.0054±0.0014	0.008	-50±20	8.403	<0.0001
		Ach (*hi*)	−0.0021±0.0003	0.042	-56±33	4.155	0.009
4.27 (UpSt)	WRI for Compression	L-NAME (*hi*)	0.131±0.052	0.043	-49±41	2.98	0.031
		L-NAME (*lo*)	0.209±0.052	0.002	-41±26	5.424	0.0002
		Saline (*lo*)	0.316±0.056	-	-	-	-
		Saline (*hi*)	0.240±0.080	-	-	-	-
		Ach (*lo*)	0.522±0.054	0.005	137±186	2.539	0.028
		Ach (*hi*)	0.489±0.064	0.02	205±173	2.908	0.035
	WRI for Expansion	L-NAME (*hi*)	0.250±0.060	0.12	-20±34	1.481	0.20
		L-NAME (*lo*)	0.258±0.057	<0.0001	-41±30	4.815	0.0005
		Saline (*lo*)	0.404±0.058	-	-	-	-
		Saline (*hi*)	0.338±0.086	-	-	-	-
		Ach (*lo*)	0.526±0.051	0.096	95±219	1.505	0.16
		Ach (*hi*)	0.542±0.052	0.035	119±116	2.503	0.054

Supplement to Figures Continued:

Figures	Detail	Treatment	Bar Value Mean± SEM (see Figure for units etc.)	p-value as stated on Figure (compared to Saline)	Δ as % of Saline Control Mean±SD	t-value	p-value
4.28 (DnSt)	WRI for Compression	L-NAME (*hi*)	0.273±0.115	0.73	-22±48	1.133	0.31
		L-NAME (*lo*)	0.310±0.063	0.009	-16±51	1.025	0.33 *
		Saline (*lo*)	0.408±0.070	-	-	-	-
		Saline (*hi*)	0.294±0.064	-	-	-	-
		Ach (*lo*)	0.440±0.069	0.58	23±48	1.573	0.15
		Ach (*hi*)	0.407±0.070	0.01	43±32	3.250	0.023
	WRI for Expansion	L-NAME (*hi*)	0.426±0.102	0.65	-9±34	0.664	0.54
		L-NAME (*lo*)	0.391±0.064	0.004	-27±27	3.346	0.007
		Saline (*lo*)	0.517±0.052	-	-	-	-
		Saline (*hi*)	0.457±0.054	-	-	-	-
		Ach (*lo*)	0.553±0.058	0.48	13±38	1.120	0.29
		Ach (*hi*)	0.546±0.085	0.15	18±33	1.306	0.25
4.31	UpSt	L-NAME (*hi*)	0.372±0.033	0.007	16±9	4.403	0.007
		L-NAME (*lo*)	0.346±0.023	0.04	19±27	2.379	0.037
		Saline (*lo*)	0.297±0.018	-	-	-	-
		Saline (*hi*)	0.320±0.026	-	-	-	-
		Ach (*lo*)	0.258±0.014	0.059	-11±20	1.826	0.095
		Ach (*hi*)	0.266±0.028	0.052	-17±17	2.469	0.057
	DnSt	L-NAME (*hi*)	0.386±0.042	0.019	21±14	3.739	0.013
		L-NAME (*lo*)	0.398±0.032	0.024	15±18	2.856	0.017
		Saline (*lo*)	0.350±0.028	-	-	-	-
		Saline (*hi*)	0.318±0.029	-	-	-	-
		Ach (*lo*)	0.282±0.019	0.019	-16±18	2.981	0.014
		Ach (*hi*)	0.261±0.017	0.09	-16±18	2.147	0.085

Supplement to Figures Continued:

Figures	Detail	Treatment	Bar Value Mean± SEM (see Figure for units etc.)	p-value as stated on Figure (compared to Saline)	Δ as % of Saline Control Mean±SD	t-value	p-value
4.32	UpSt	L-NAME (*hi*)	0.0191±0.0053	0.46	-20±42	1.146	0.30
		L-NAME (*lo*)	0.0231±0.0023	0.17	-12±30	1.387	0.19
		Saline (*lo*)	0.0264±0.0013	-	-	-	-
		Saline (*hi*)	0.0229±0.0040	-	-	-	-
		Ach (*lo*)	0.0167±0.0018	0.0004	-36±23	5.453	0.0002
		Ach (*hi*)	0.0143±0.0023	0.019	-33±18	4.479	0.007
	DnSt	L-NAME (*hi*)	0.0130±0.0035	0.68	50±86	1.149	0.33
		L-NAME (*lo*)	0.0184±0.0022	0.87	8±41	0.666	0.52
		Saline (*lo*)	0.0181±0.0020	-	-	-	-
		Saline (*hi*)	0.0133±0.0034	-	-	-	-
		Ach (*lo*)	0.0175±0.0024	0.87	18±94	0.641	0.54
		Ach (*hi*)	0.0156±0.0022	0.32	99±189	1.048	0.37

* Figures 4.26 & 4.28: the differing p-values were due to one and the same outlier rabbit but no obvious correct reason to exclude from the data.

4.4 DISCUSSION

Determination of internal diameter of the abdominal aorta was necessary for these studies since calculation of blood flow velocity from blood flow volume was required; the latter was measured. Changes in vessel diameter affect flow velocity within the vessel and this is pertinent to studies on effects of L-NAME and Ach on haemodynamics of blood flow since L-NAME and Ach, by altering blood pressure, effect alterations in aortic diameter; this being a passive response of the aorta to pressure. The passive response of aortic diameter to pressure is in addition to pharmacological effects that L-NAME and Ach might have on the smooth muscle of the aorta. For these experiments it was technically too difficult to measure aortic diameter simultaneously with pressure and blood flow so a Correction Factor was derived to allow corrections for diameter changes and hence the blood flow velocity. The technique required opening the abdominal cavity to allow access to the abdominal aorta for close ultrasonic imaging of the vessel (section 4.2.1); this is invasive surgery and certainly would impact on the physiological status of the anaesthetised rabbit. It is likely that the invasiveness of the surgery was responsible for the variability of the data obtained (Figures 4.2 & 4.3), however it is reassuring that the effects L-NAME and Ach on diameter and blood pressure were dose-related and so a Correction Factor could be derived (Figure 4.4 and Table 4.2); the Correction Factor allowed calculation of blood flow velocity under treatments with L-NAME and Ach. That L-NAME and Ach did increase or decrease respectively the diameter of the abdominal aorta is an important observation for analysis of pulse wave mechanics of the aorta; changes in aortic diameter have consequences on aortic wall distensibility, hence aortic compliance, and pulse wave reflections (Nichols and O'Rourke, 2005).

The data on basic haemodynamics showed clearly that the *lo* and *hi doses* used of L-NAME and Ach had effects on the cardiovascular system of anaesthetised rabbits (Table 4.3; Figure 4.5). These effects were measured from two sites, namely the UpSt and DnSt Sites, within the abdominal aorta (Figure 3.1). The UpSt Site was between the celiac and superior mesenteric arteries, so the downstream major arterial vasculatures would be those of the superior mesenteric artery, renal arteries and all those included in the distal continuation of the abdominal aorta. The DnSt Site was some 35mm downstream (distal) of the renal arteries, so the downstream major arterial vasculatures would be all those arteries off the distal abdominal aorta including the inferior mesenteric artery and the aorto-iliac bifurcation with the iliac arteries leading into the femoral arteries which feed mainly the muscular beds of the hind-limbs. Aortic blood pressure, in terms of mean aortic blood pressure (i.e. MAP), in a normally functioning aorta differs little between the two sites (Milnor, 1989; Nichols and

O'Rourke, 2005), however the vascular resistances will differ according to the vascular beds supplied by the different sections along the aorta.

Ach decreased blood pressure; this effect was measured at both UpSt and DnSt Sites (Figure 4.5) and was dose-dependent. At both sites, the decreased blood pressure was accompanied by decreased MABF (Figure 4.5); however the response of VR was different at the two sites: VR decreased consistently at the UpSt Site but changed variably at the DnSt Site. In the case of the UpSt Site, VR is influenced by the visceral and renal vasculatures along with those supplied by the aorta distal to the UpSt Site. The decrease in VR was expected as Ach is a known vasodilator by way of its effect of increasing nitric oxide bioavailability. Vasodilatation in turn decreased MAP, the magnitude of decrease dependent on the magnitude of compensatory (baroreflex induced) increase in cardiac output; the latter was not measured but probably decreased as implied by the decreased MABF – if cardiac output did decrease then this would have been due to decreased stroke volume as heart rate was unchanged (Table 4.3). In the case of the DnSt Site, VR is largely influenced by the vasculature of the hind-limb muscles. The effects of Ach on VR were variable (Figure 4.5); the large standard deviations indicate that VR increased in some rabbits but decreased in others. The reasons for this are not clear. A suggestion for this could be that the vasculature of the hind-limbs was variably sensitive to Ach depending on what local physiological influences pertained in the hind-limbs of the rabbits used to obtain the data; anaesthesia and physiological status would be important factors. Local influences in the hind-limb vasculature of some rabbits suited the effect of Ach to reduce hind-limb VR, i.e. the expected vasodilator effect of Ach. Alternatively, in the hind-limbs of other rabbits local physiological influences nullified the vasodilator effects of Ach so VR either remained unchanged, or elevated as a consequence of overriding local vasoconstrictor effects; these latter effects might be in response, say, to decreased MAP resulting from vasodilatation of other beds, e.g. the viscera.

Ach stimulates muscarinic receptors on the external surface membrane of vascular endothelial cells (refs in section 4.1), stimulation of these receptors initiates a cascade of intracellular events to produce nitric oxide; the latter is released from the endothelial cells to cause relaxation of vascular smooth muscle, hence vasodilatation, so decreasing VR of the affected blood vessels. If a given vascular bed has a high endothelial production rate of nitric oxide thus endowing that vasculature with high nitric oxide bioactivity, it is possible that pharmacological doses of Ach might have little further effect on VR of such a vascular bed – this could have been the status in the hind-limb vasculature of some of the rabbits where Ach did not alter hind-limb VR. In hind-limb vasculatures with low endothelial production of nitric oxide, hence low nitric oxide bioactivity, Ach could cause vasodilatation, but if nitric

oxide bioactivity is suppressed by high sympathetic drive, the latter causing vasoconstriction, in that vasculature, then Ach might either compete with the sympathetic drive and cause vasodilatation, or would not surmount the vasoconstrictor effect of high sympathetic drive and so a net balance of increased VR would result; this is a possible circumstance if vasodilatation elsewhere has decreased MAP thereby causing reflex-mediated increase in sympathetic activity. The point made on high sympathetic drive brings into consideration the importance of anaesthesia and how it might affect these experiments. For the rabbit experiments of this thesis, anaesthesia was induced and maintained using sodium pentobarbitone (section 3.2.1); barbiturate anaesthetics, such as sodium pentobarbitone, are thought to increase sympathetic drive (Page and McCubbin, 1965; Lokhandwala *et al*., 1973).

L-NAME increased blood pressure (MAP) and this was clearly due to increased VR, i.e. a vasoconstrictor effect, and was measurable at the UpSt and DnSt Sites (Figure 4.5), indicating that the majority of vascular beds would likely have been affected. This vasoconstrictor effect was likely due to L-NAME decreasing the production, hence bioactivity, of nitric oxide, resulting in decrease vasodilatation (refs in section 4.1) of the small arteries of narrow lumen which because of their size are resistive in function. The effects of the vasoconstrictor action of L-NAME on MABF were variable; MABF increased in some rabbits, remained unchanged or decreased in other rabbits. In these circumstances MABF would be governed by MAP and VR. Cardiac output was not measured so compensatory changes in cardiac output can only be implied by changes in MABF; heart rate was not affected by treatment with L-NAME.

Thus, the basic haemodynamic data obtained in these experiments gives assurance that the doses used of L-NAME and Ach were pharmacologically active in the vasculature and affected VR which implies altered function of resistance vessels; the latter do impact on arterial pulse wave reflections (Nichols and O'Rourke, 2005) which affect waveform shape, so have relevance to this thesis.

Limited data was obtained, by use of applanation tonometry, for the pressure waveform of the central ear artery of anaesthetised rabbits (Figure 4.6). However, of these data, the treatments with L-NAME or Ach changed the waveforms in a manner that did not resemble those observed by Weinberg *et al*. (2001) (c.f. Figure 1.1). The details of the waveforms are very different to those observed by Weinberg *et al*. (2001) in that they had no clearly defined dicrotic notch, or that the dicrotic notch, if indeed it was such, was extraordinarily low in the waveform. Weinberg *et al*. (2001) and Nier *et al*. (2008) used photoplethysmography to detect and record the pulse waveform from the central ear artery of rabbits; their

experiments found that in comparison to control, L-NAME was observed to raise, and Ach to lower, the diastolic decay part of the waveform along with the dicrotic notch, the latter measured as RHDN (Figure 1.1). In the experiments described in this thesis, the opposite was found, namely that, in comparison to the saline control, L-NAME lowered and Ach raised the diastolic decay part of the waveform; RHDN for the arterial pulse of the central ear artery was not measured as it was difficult to discern precisely the dicrotic notch on the waveforms, especially with treatment by Ach (Figure 4.6). Furthermore, in the abdominal aorta, L-NAME and Ach had the same profile of effects on the pressure waveforms as they had on the pressure waveform of the central ear artery. The effects of L-NAME and Ach on the blood pressure waveforms of the abdominal aorta are discussed below. At this point it should be added that the broadening of the pulse in response to Ach (Figure 4.6 UpSt & DnSt Sites and 4.7 UpSt Site) was not due to an effect of bradycardia which did not occur - HR was little affected by Ach, at most a very small tachycardia occurred perhaps reflexly mediated in response to decreased MAP.

The changes in waveform in response to Ach, and, indeed, nitro-vasodilators, as observed by Weinberg *et al*. (2001) are considered characteristic of and specific for the action of nitric oxide on the vasculature, especially on the conduit arteries (Morikawa, 1967; Weinberg *et al.,* 2001; Nier *et al.,* 2008; see references in section 4.1). Part of the work of this thesis sought to determine what haemodynamic changes occur in response to changes in nitric oxide bioactivity to cause the changes in the peripheral arterial pulse waveform as observed by Weinberg *et al.* (2001) and Nier *et al.* (2008). However, this aspect of the work was confounded by the very different response of the central ear arteries to L-NAME and Ach as to the central ear arteries observed by Weinberg *et al*. (2001) and Nier *et al*. (2008). A reason for this disagreement could be that the experiments of Weinberg *et al*. (2001) and Nier *et al*. (2008) used conscious awake rabbits, whereas barbiturate-anaesthetised rabbits were used in the experiments of this thesis. As noted above, barbiturates enhance sympathetic tone and this might affect peripheral arterial response to nitric oxide bioactivity. Alastruey *et al*. (2009) applied computational modelling to seek an explanation for the effects of nitric oxide bioactivity on the peripheral arterial pulse waveform of the central ear artery as observed by Weinberg *et al*. (2001) and Nier *et al*. (2008). This modelling indicated that RHDN and the diastolic decay limb of the waveform could be altered by single or combined alterations of blood viscosity, peripheral (vascular) resistance and compliance, and elasticity of conduit arteries.

As explained below, when correctly used RHDN is a measure of the height of the dicrotic notch of the pulse in peripheral arteries (rabbit central ear artery; human digital artery). However, in the studies of this thesis, when considering pulse waveforms in the rabbit

abdominal aorta, the term RHDN (Table 4.12) refers to the inflection which occurs on the pressure pulse decay at the end of systole when the associated blood flow ceases its forward direction; the latter is determined by inspection of the recorded blood flow waveform. This inflection is actually the *incisura* as discussed in the next paragraph. So, RHDN in the context of the studies in this thesis when considering the aortic pulse waveform, is not strictly the same as that defined by Weinberg *et al*. (2001) who were measuring RHDN from the true *dicrotic notch* of a peripheral arterial pulse, namely that of the rabbit central ear artery. It was observed in the studies of this thesis that the diastolic decay curves of pressure pulses were decrease by L-NAME and increased by Ach to below and above respectively the saline control diastolic decay curve (Table 4.12). It is because of these effects on diastolic decay that L-NAME decreased, while Ach increased RHDN. Irrespective of the definitions for RHDN, the findings here for the pressure waveform of the abdominal aorta conflict with the findings of Weinberg *et al*. (2001) and Nier *et al*. (2008) for the pressure waveform of the central ear artery. Tn is defined as the time of the inflection (incisura) after end-diastole (end-diastole being the start of systole). The effects of L-NAME and Ach on Tn (Table 4.12) could have been a consequence of their effects on the diastolic decays; by decreasing the diastolic decay curve, L-NAME effectively decreased Tn, whereas Tn was effectively increased by Ach raising the diastolic decay curve – this can be seen pictorially in Figures 4.7A&B expressed as a ratio of the maximum pulse amplitude and curves are aligned from their respective maximum systolic points, but without correction to pulse amplitude systolic maximum in Figures 4.10A&B, 4.11A&B, 4.12A&B, and 4.14A&B.

Two features of the arterial pressure pulse waveform that are important in the studies of this thesis are the **incisura** (prominent feature of the central aortic pulse) and the **dicrotic notch** (prominent feature of the peripheral arterial pulse); these terms are often *mistakenly* thought of as synonymous but are actually manifestations of two separate and unrelated events. O'Rourke (1982), Nichols and O'Rourke (2005) define the incisura as "the high frequency wavelet on an arterial pressure wave due to sudden closure of the aortic or pulmonary valve", and define the dicrotic notch as "the foot of the dicrotic or diastolic wave due to peripheral wave reflection". Weinberg *et al*. (2001) point out this difference as a caution for defining their measurement of RHDN. With the features incisura, dicrotic notch and RHDN in mind, the pressure waveforms in the abdominal aorta of anaesthetised rabbits were examined. The pressure waveforms observed in this work appeared to be of two general types with regard to their diastolic pressure decay curves; these are referred to as Type 1 and Type 2 for the sake of discussion in this thesis (Figure 4.9). The Type 1 waveform resembles the pulse waveform of the proximal aorta, e.g. the ascending (c.f. Avolio *et al.*, 1976 – Fig 4; O'Rourke 1982 – Fig 9.1 of rabbit, reproduced in Nichols and O'Rourke, 1990

– Fig 8.2A). The pressure pulse waveform of the proximal aorta and the Type 1 pressure pulse share the feature of a quasi-exponential diastolic decay. However the pulse of the proximal aorta being close to its point of propagation, i.e. near the aortic valves, has a well defined incisura (see in Avolio *et al.*, 1976 – Fig 4; O'Rourke 1982 – Fig 9.1 of rabbit, reproduced in Nichols and O'Rourke, 1990 – Fig 8.2A); this feature is not always so well defined on the Type 1 waveform at UpSt or DnSt Sites of measurement in the abdominal aorta, presumably due to the pulse undergoing a change in its waveform as it propagates along the aorta (McDonald, 1974; Milnor, 1989; Nichols and O'Rourke, 1990, 1998, 2005). It seems that at the UpSt or DnSt Sites, the Type 1 pulse often has a feature that is a *remnant* incisura (Figure 4.33). In the case of the Type 2 waveform, this resembles that of a peripheral arterial pulse where the dicrotic notch and dicrotic (diastolic) wave are becoming defined, or prominent, and the incisura has often become truly remnant if not vanished (Figure 4.34). Interestingly, the peripheral pulse waveform in the central ear artery in these experiments (Figure 4.6) is similar to a Type 2 waveform. Thus, at the level of the abdominal aorta at the UpSt and DnSt Sites, depending on the physiological status of the animal while under anaesthesia, as the pressure pulse propagates along the aorta, its waveform transforms from that of upstream to either a Type 1 waveform, or a Type 2 waveform which resembles a peripheral waveform; the Type 2 pulse waveform was observed most often in the abdominal aorta when MAP was ≥10,000 Pa (75mmHg) (Figure 4.15A&B; Table 4.5). Interestingly, the examples given by McDonald (1974: Figs 13.2 & 13.4) of pulse waveforms of the abdominal aorta, resemble Type 2 and are scaled at MAP >75mmHg (reproduced in: Milnor 1989 - Fig 6.5; Nichols and O'Rourke, 1990 – Fig 8.1; 1998 – Fig 8.1; 2005 - Fig 9.1). The diastolic, or dicrotic, wave appearing in late diastole (after 100ms) of the Type 2 waveform is not associated with any obvious incident or reflected wave intensities (Figure 4.24; bottom panel under L-NAME); the cause of this dicrotic wave is not clear and is not explainable in terms of wave reflections.

FIGURE 4.33: Features of a Type 1 Pressure Pulse Waveform. The incisura is clearly defined on some but not all Type 1 waveforms - less clear when remnant.

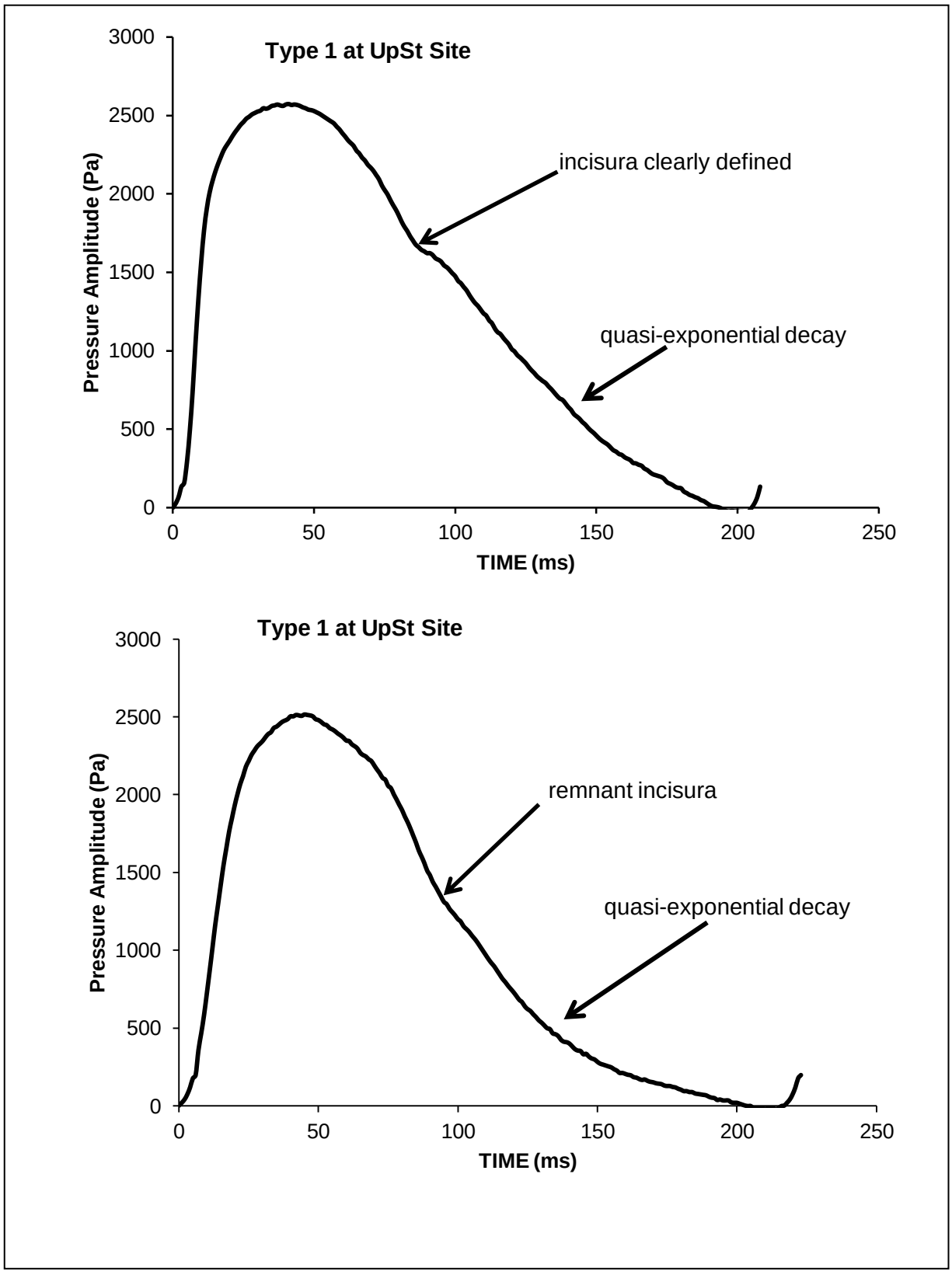

FIGURE 4.34: Features of a Type 2 Pressure Pulse Waveform – the incisura is remnant and the dicrotic notch and wave become prominent.

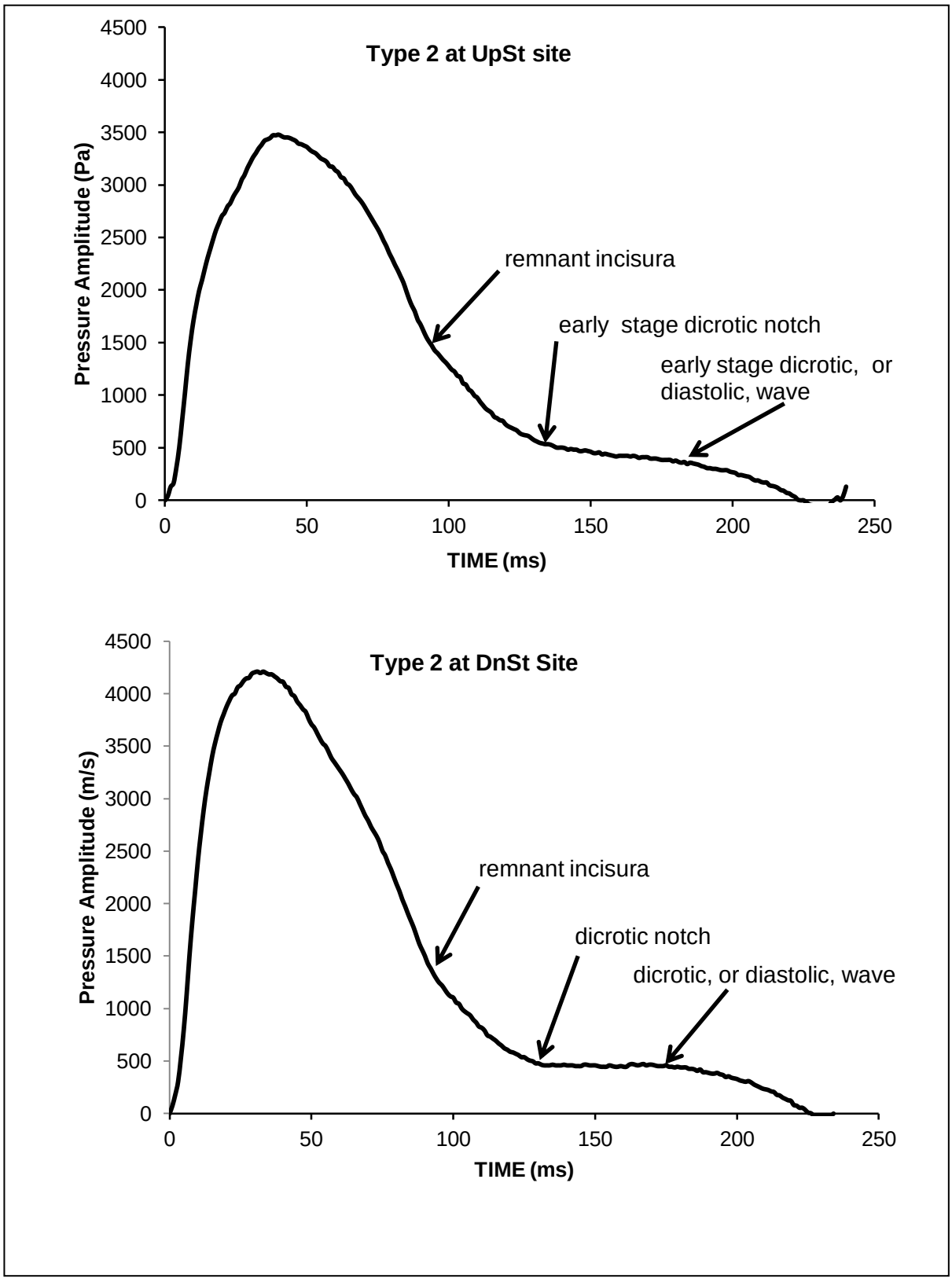

Appreciation of Type 1 and Type 2 waveforms as observed in these experiments is important because the algorithm for calculating the reservoir (Windkessel) pressure requires a point on the pulse that is end of systole; this would be a clear-cut incisura on a pulse waveform near the cardiac valves in, say, the ascending aorta or aortic arch. The incisura was definable on Type 1 waveforms though often a remnant incisura had to be accepted, but an incisura was often much more difficult to discern on a Type 2 waveform when the incisura was truly remnant. The algorithm curve-fitting was reasonably accurate for the diastolic decay of a Type 1 waveform which is exponential-like, but the curve-fitting was not so precise for the diastolic decay of a Type 2, because: i) the selection of the incisura (remnant of) might not be accurate, and ii) the Type 2 diastolic decay is not at all exponential-like.

Implicit in their absence from Table 4.6, the parameters A, B, τ and P_∞ were not dependent on which of the two waveforms, Type 1 or Type 2, they were derived from by the diastolic curve fit algorithm.

Parameter A is a rate constant and its value determines the continuity of fit of the systolic part to the diastolic part of commencement of the exponential decay of the reservoir (Windkessel) pressure (Davies *et al.*, 2007; Aguado-Sierra *et al*., 2008; Parker *et al*., 2011). Parameter A was largely unaffected by L-NAME or Ach (Tables 4.7 & 4.8). Only L-NAME (*lo dose*) had a significant effect on parameter A, so it is difficult to suggest that this effect was a true pharmacological effect. Parameter A is dependent on the diastolic waveform since it is found by minimising the square error between the reservoir pressure calculated over the whole of diastole (Parker *et al*., 2011). It is not surprising that L-NAME had little effect on Parameter A since L-NAME had no effect on Parameter B (hence τ) which is also dependent on the waveform during diastole. However, it is interesting that parameter A was not affected by Ach (*lo & hi doses*) which did significantly alter parameter B (hence τ) by increasing it.

The literature has not reported an *established* physiological definition for P_∞. However, P_∞ is the asymptotic pressure of the diastolic exponential decay at which, it is suggested, flow from the arteries to the veins ceases (Wang *et al.*, 2003); it has also been proposed that P_∞ is not venous pressure but is a pressure associated with the waterfall or mean circulatory pressure (Wang *et al.*, 2006; Aguado-Sierra *et al*., 2008), or furthermore, it could relate to the interstitial pressure through the waterfall effect (Parker *et al*., 2011). Thus, the values of P_∞ would be in the order of: if equivalent to right atrial pressure ±1mmHg; if venous pressure 3-5mmHg; if mean circulatory pressure 6-10 mmHg (Guyton *et al*., 1954,; Guyton and

Greganti, 1956; Guyton and Jones, 1973; Caro *et al*., 1978; Rothe, 1993). However, it was found in the studies of this thesis that the values of P_∞ were much greater than those expected for, say, mean circulatory pressure. In fact the values for P_∞ were very close to DBP, if not greater than DBP in some animals; this is shown in Figure 4.35 below. On further consideration, P_∞ might be closely related to, if not *the*, critical closing pressure; Shrier *et al*. (1993) measured critical closing pressure in the hindlimb of anaesthetised dogs and report control values of ~40mmHg (5333Pa) - ~50mmHg (6667Pa) – those values are close to the DBP values measured in some rabbits of experiments in this thesis, especially in rabbits after treatment with Ach (c.f. Figure 4.35). However, if P_∞ is related closely to critical closing pressure, then some separation should have occurred between DBP and P_∞ with L-NAME treatment when mean DBP was increased to ~9100Pa (68mmHg) or ~9900Pa (74mmHg) (*lo & hi dose* L-NAME respectively in Figure 4.35) while P_∞ be expected to remain at 40-50mmHg but instead increased closely with DBP. Perhaps P_∞ is nitric oxide dependent, though this is questionable because Shrier *et al*. (1993) implied that P_∞ is controlled by vessels close to the level of arterioles, such distal vessels are likely more dependent on endothelium-derived hyperpolarising factor (EDHF) than on nitric oxide (Félétou and Vanhoutte, 1999; Mombouli and Vanhoutte, 1999). Another consideration for (erroneous) values obtained for P_∞ is perhaps that the attempted extrapolation to the asymptote was not performed correctly by the algorithm because of the high heart rates of anaesthetised rabbits – the higher the heart rate the shorter the diastolic period and this affects the algorithm fitting process (Parker *et al*., 2011).

AC was derived from the ratio of τ / VR. The use of τ = AC x VR for cardiovascular haemodynamic studies is well known (Liu *et al*., 1986; Laskey *et al*., 1990; Stergiopulos *et al*., 1995). The relationship of AC to MAP shown in Figures 4.19 & 4.20 is as expected, namely that AC decreased with increased MAP and that this relationship is quasi-exponential. It is interesting to note from Figures 4.19A and 4.20A that the treatments do not cause separate AC vs. MAP curves but, instead, the data hold to a general curve which suggests that the treatments *per se* do not alter AC but that they alter AC only through their effects on blood pressure. The treatments are considered in their separate entities in Figure 4.21, which shows L-NAME (*hi & lo doses*) decreased whereas Ach (*hi & lo doses*) increased AC; however, these effects on AC are likely, as just stated, to be due to their effects on blood pressure, and not to any direct pharmacological effect on the elasticity of

the arteries. The effect of blood pressure on AC is well known; AC is greater at low blood pressure and decreases as blood pressure increases; this is indicated in Table 4.11 which shows a significant negative correlation between AC and MAP. Increased arterial pressure distends arterial walls, especially the walls of large elastic arteries, which decreases arterial compliance as a function of increased vessel wall elastic modulus. This property of, certainly the large elastic, arteries is due to the elastic nature residing in the elastin elements of the vessel wall at low pressures and then as the vessel distends, the elastic properties transfer to reside in the stiffer collagenous elements (Roach and Burton, 1957).

FIGURE 4.35: Comparisons of Diastolic Blood Pressure (DBP) with P_∞.

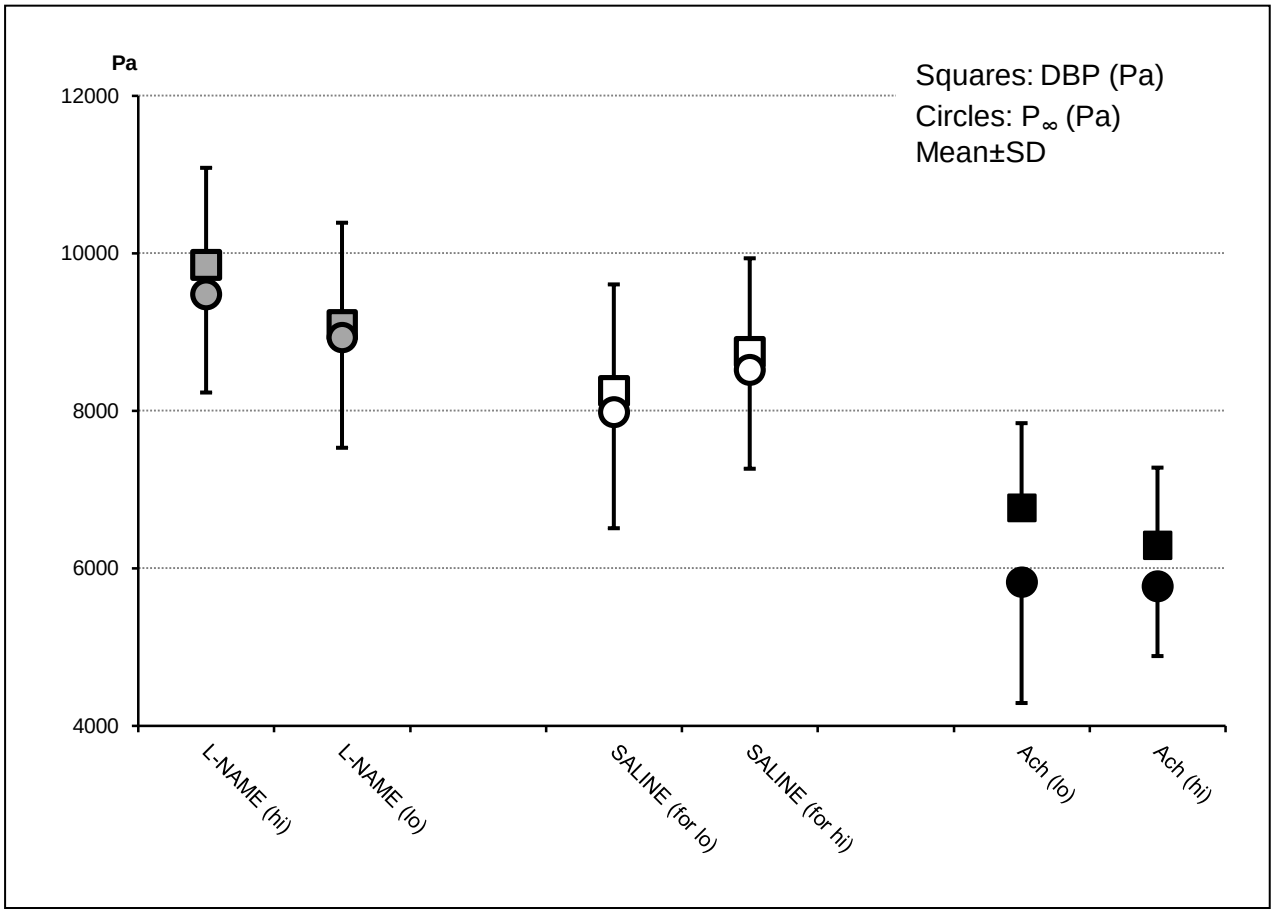

As indicated by their presence in Table 4.6, $\int$RP and PP_{RP} were to some extent dependent on which of the two waveforms, Type 1 or Type 2, they were derived from. $\int$RP and PP_{RP} derived from Type 1 waveforms had values that were greater than those of $\int$RP and PP_{RP} derived from Type 2 waveforms (Table 4.6). The reason for these differences likely lies in the fact that $\int$RP and PP_{RP} are derived from the reservoir (Windkessel) pressure which is itself derived from the algorithm fit to the waveform; the algorithm fit is much more precise on the Type 1 waveform than on the Type 2 waveform and so will influence the resulting reservoir (Windkessel) pressure waveform. Despite this, it was decided that data for each treatment group would be considered (pooled) as one set for each treatment, regardless of their origin from Type 1 or Type 2 waveforms.

$\int$RP and PP_{RP} are considered as possible indices of AC; the values of PP_{RP} and $\int$RP would be expected to decrease as AC increases. If this is so then there should be correlations between $\int$RP and PP_{RP} with AC and, furthermore, correlation with factors, e.g. MAP, that affect AC. As already mentioned, AC had a significant negative correlation with MAP (Table 4.11). However there was no correlation between $\int$RP and MAP or with AC itself (Table 4.11); thus with this data it is difficult to support the contention that $\int$RP is an index of AC. PP_{RP} showed limited correlations with MAP (only UpSt Site) and AC (only DnSt Site), so the data only weakly supports the view that PP_{RP} is an index of AC. Not surprisingly PP_{RP} and $\int$RP do correlate significantly since they are arithmetically related. That PP_{RP} can be considered an index of AC is supported by Davies *et al.* (2010) who found that the magnitude of aortic reservoir pressure (i.e. PP_{RP}) related closely to aortic pulse wave velocity squared ($C_{ft\text{-}ft}^2$), which in turn relates inversely to aortic distensibility, hence aortic compliance; they also found that the magnitude of aortic reservoir pressure increased with aortic ageing (stiffening). Following Davies *et al.* (2010), tests of correlation with $C_{ft\text{-}ft}^2$ were carried out and in contradiction to Davies *et al.* (2010) this thesis found that PP_{RP} did not correlate with $C_{ft\text{-}ft}^2$ but that $\int$RP did; AC correlated with $C_{ft\text{-}ft}^2$ as expected. Although linear correlations were not found between MAP and PP_{RP} or $\int$RP, the plots of MAP vs. PP_{RP} or MAP vs. $\int$RP appear to fit a quadratic relationship (Figures 4.22i B & 4.22ii B) which is consistent with the findings shown in Table 4.10, namely that Ach and L-NAME, despite their opposite effects on blood pressure, both decreased PP_{RP} and $\int$RP; this observation is not understood but Figure 4.36 illustrates the parameters that affect $\int$RP.

FIGURE 4.36: Parameters that Affect the Integral ($\int$RP) of Reservoir (Windkessel) Pressure (P_{RP}).

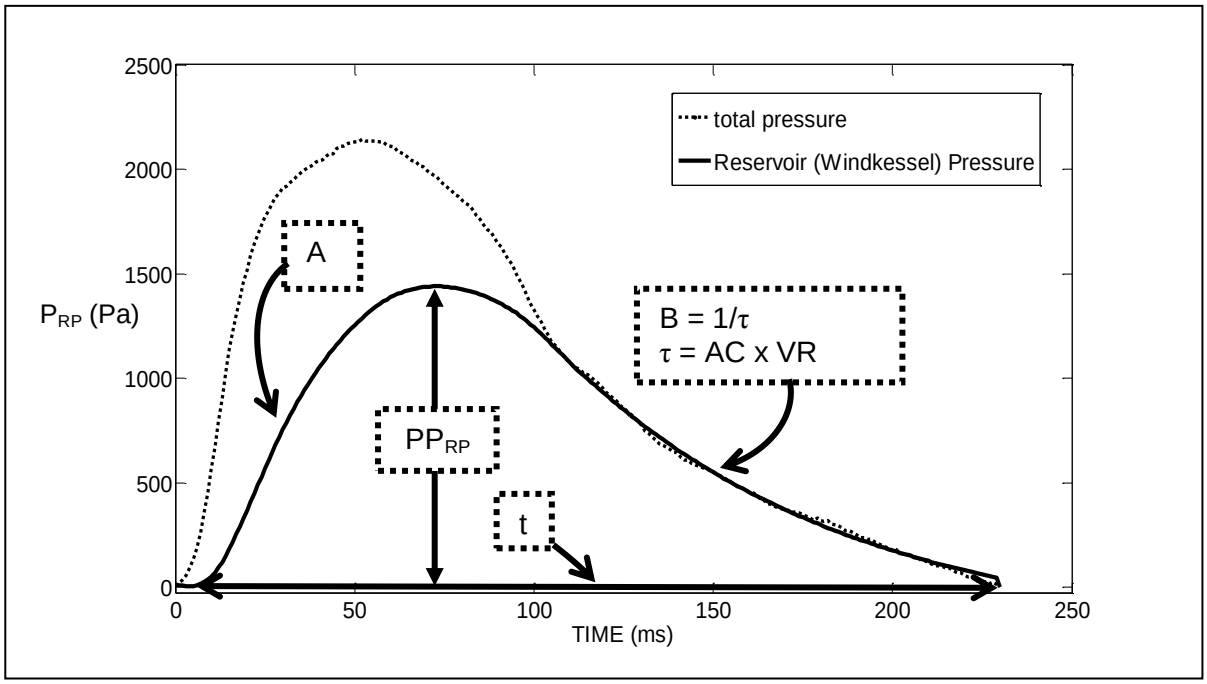

Pulse wave velocity, or $C_{ft\text{-}ft}$, is defined by the time it takes a wave to propagate from one site to another and the distance between the two sites (50mm in these studies). The measurement indicates an average wave speed over the distance between the sites of measurement. Vessel structures which influence $C_{ft\text{-}ft}$ may vary between the sites. Khir *et al*. (2001) propose measurement of local wave speed as a preferable measurement, using the simultaneous measurement of pressure and velocity at the same site in the artery; two such wave speeds were determined in this thesis and ascribed as C_{Tpu} and C_{Wpu}. The accuracy of all these measures of wave speed depends on the absence of reflected waves at the point of time on the waveforms from where the measures are taken. Blood pressure waveforms are commonly assumed to be free of reflected waves during the last two thirds of diastole into very early systole. Theoretically, in a reflection-free state $C_{ft\text{-}ft}$, C_{Tpu}, C_{Wpu}, should be equal; however such equivalence was not consistently found (Table 4.15). It is possible that reflected waves were present to distort the pulse wave during early systole; also the fidelity of acquisition might not have been adequate in some experiments though care was taken to position the measuring devices optimally. With regard to reflected waves, these may well have been present at the sites of measurements as the sites were close to bifurcations; certainly this was the case for the UpSt Site which is near the origins of the superior mesenteric and renal arteries. The aorto-iliac bifurcation might have affected the DnSt Site of measurement. As expected, $C_{ft\text{-}ft}$ increased as the pulse wave propagated along the aorta between the UpSt and DnSt Sites, an increase of 10 -18% in the control $C_{ft\text{-}ft}$

occurred which was likely, in part, a consequence of the 30% decrease in diameter of the abdominal aorta between the two sites. The $C_{ft\text{-}ft}$ values were used to substitute into the algorithm for WIA.

AC and $C_{ft\text{-}ft}$ are inter-related since $C_{ft\text{-}ft} = 1/\sqrt{\rho D}$ where D is the vessel distensibility, the latter relates directly to AC. In the literature there are reports of direct effects of vascular endothelial nitric oxide on aortic and arterial compliances and pulse wave velocities (Wilkinson *et al*., 2004). In the studies of this thesis Ach and L-NAME did not appear to cause separation of the MAP vs. AC (Figures 4.19 & 4.20) but perhaps caused a small separation of MAP vs. $C_{ft\text{-}ft}$ (Figure 4.23B) curves; separation of curves would indicate a direct effect (via Ach) or lack of effect (via L-NAME) of nitric oxide on the smooth muscle, hence elastic properties, of the abdominal aorta and arterial vasculature. These effects, if they occurred, were overshadowed by the passive response of the aorta to the decrease (Ach) or increase (L-NAME) in blood pressure and so the data for AC or $C_{ft\text{-}ft}$ appeared to distribute along one curve (Figures 4.19, 4.20 & 4.23A). There are other experimental designs used to get around the confounding effects of changes in blood pressure and so reveal the effects of nitric oxide on elastic properties of the aorta or conduit arteries; such experiments control for pressure changes (Hu *et al*., 1997; Fitch *et al*., 2001; Stewart *et al*., 2003) or administer drug doses close-arterially *in vivo*, i.e. into the arterial segment of interest *in situ* (Wilkinson *et al*., 2002). Interestingly, despite controlling for pressure change, Stewart *et al*. (2003) concluded that effects of inhibition of basal nitric oxide release on carotid-femoral PWV were due to changes in MAP rather than to effects of inhibition of nitric oxide on the aorta.

L-NAME had little to no effect on incident compression or expansion wave energies (Figures 4.24 – 4.28). The lack of effect of the vasoconstrictor, L-NAME, on incident compression wave energy contrasts with the findings of Jones *et al*. (2002) who found that vasoconstriction (by methoxamine) decreased incident compression wave intensity; however, in agreement with Jones *et al*. (2002), vasoconstriction – in the case of this thesis with L-NAME - did not affect incident expansion wave energy. Jones *et al*. (2002) did not comment on reflected wave intensities. Surprisingly, the work of this thesis found that L-NAME appeared to decrease reflected compression wave energy (Figures 4.24 – 4.28). The opposite might be expected since decreased diameter of small arteries and arterioles, i.e. vasoconstriction, is believed to cause wave reflection (Nichols and O'Rourke, 2005). With regard to a state of increased nitric oxide bioactivity, Jones *et al*. (2002) observed that nitroglycerine (a nitric oxide donating vasodilator) decreased both incident compression and incident expansion wave intensities. In this respect, the findings of this thesis are ambiguous in that Ach (a stimulator of nitric oxide production and release) had little or no

effect on incident compression and expansion wave energies at the UpSt Site, yet did at the DnSt Site, in agreement with Jones *et al*. (2002) (Figures 4.24 – 4.28). Another surprising finding of the work of this thesis was that Ach increased reflected wave energy, certainly at the UpSt Site (Figure 4.24 & 4.27) though this effect is not remarkable at the DnSt Site (Figure 4.28). This is a surprising finding since Ach caused vasodilatation and increased arterial compliance which are states in which wave reflections generally decrease (Nichols and O'Rourke, 2005). An explanation for the unexpected findings of L-NAME decreasing and Ach increasing reflected wave energies is that L-NAME increased whereas Ach decreased the diameter of the abdominal aorta; these diameter changes respectively favour reduced or increased wave reflection.

It is notable that WRI for compression and expansion waves correlated positively with RHDN (Figures 4.29 & 4.30). RHDN as discussed above for the abdominal aorta actually refers to the *incisura*, which is the inflection on the pressure pulse decay of the abdominal aortic blood pressure waveform when the associated blood flow ceases its forward direction. Abdominal aortic RHDN increases with increasing WRI which implies that RHDN in the abdominal aorta is affected by wave reflections travelling in this vessel.

Another measure used is the ratio of the incident expansion wave energy to the incident compression wave energy. To appreciate the meaning of this ratio it is necessary to understand the natures of incident compression and expansion wave intensities or energies. They result from different events in systole. The incident compression wave results from events occurring in early systole, namely cardiac ventricular contraction, stroke volume ejection, acceleration of blood and so is likened to the initial ventricular impulse (Rushmer, 1964 – quoted by Parker *et al*., 1988). The incident expansion wave results from events that are not yet clearly defined but occur near the end of systole, namely ventricular inactivation with reduced rate of shortening of ventricular major axis, and speculated to be the primary determinant of aortic blood flow deceleration mediated in part by left ventricular wall movement, aortic blood flow reversal, aortic valve closure and end-systolic ventricular volume (Parker *et al*., 1988; Parker and Jones, 1990; Jones *et al*., 2002; Page *et al*., 2010). Incident compression wave intensity is affected by the contractility (e.g. left ventricular Max dP/dt), or inotropic, state of the myocardium and so is sensitive to the effects of positive or negative inotropic agents which respectively increase or decrease incident compression wave intensity (Jones *et al*., 2002); incident expansion wave intensity is not affected by inotropic state (Jones *et al*., 2002). Furthermore incident compression wave intensity is sensitive to changes in cardiac preload and afterload; venodilatation (preload reduction) or vasoconstriction (afterload increase) both decrease incident compression wave intensity as does reduced afterload by vasodilatation, but incident expansion wave intensity is decreased

only by vasodilatation (Jones *et al*., 2002). Incident compression and expansion wave intensities are decreased in chronic heart failure (Curtis *et al*., 2007). The ratio of the incident expansion wave energy to the incident compression wave energy (Figure 4.31) could therefore be used to give a measure of the balance of influence of early and late systolic cardiac function on wave intensities in aortic haemodynamics.

With reference to Figures 4.25, 4.26, and 4.31, although effects (separately) of L-NAME and Ach on incident expansion and incident compression waves were small, their effects on the ratio were much larger and more consistent. This is difficult to explain, thus the effects of L-NAME and Ach on cardiac parameters requires further exploration.

Distances to sites of reflection were estimated from the time lapse between incident and reflected intensities of compression waves (Figure 4.32). Sites of reflection were close to the sites of recording: 2 – 3cm from UpSt Site and 1 – 2cm from DnSt Site. The ostia of major vessels, e.g. superior mesenteric and renal arteries exist within the 2 – 3cm from the UpSt Site, so these are likely causes of reflection. The site of reflection 1 – 2cm from the DnSt Site is not obvious but could be an unrecognised change in aortic diameter or compliance (the aorto-iliac bifurcation is ~60mm downstream of the DnSt Site). Ach (*lo* and *hi dose*) at the UpSt Site had the effect of shortening this distance. An explanation for this could be an effect of decreased diameter of the aorta in passive response to the effect of Ach decreasing MAP. Changes in vessel diameter affect wave propagation and wave reflection (Milnor, 1989; Nichols and O'Rourke, 2005).

In conclusion, three inter-related haemodynamic parameters can be considered: i) diameter of the aorta and of conduit arteries, ii) compliance of the aorta and of conduit arteries, and iii) wave reflections in the aorta and conduit arteries. Ach decreased blood pressure and thereby decreased the diameter of the aorta along with perhaps diameters of conduit arteries. Ach increased arterial compliance, mainly as a consequence of decreased diameter of the aorta and conduit arteries, and perhaps in part with pharmacological effect of increased nitric oxide bioactivity induced by Ach. Ach increased wave reflection, a net effect of two properties of the aorta or conduit arteries, namely decreased aortic or conduit arterial diameter increases wave reflection and/or arterial compliance; the latter attenuates wave reflection. L-NAME had the opposite effects to those of Ach: it increased blood pressure and so increased aortic diameter, it decreased arterial compliance and decreased wave reflection.

The Hypotheses - supported or not supported:

- *Hypothesis*: The height and form of the dicrotic notch of the pulse in the rabbit central ear artery depends on wave reflections from conduit arteries of the limbs and organs.

  Findings: It was not possible to measure RHDN of the central ear artery, however the form of the diastolic decay of the pulse was considered along with that of the pulse in the abdominal aorta. Ach increased and L-NAME decreased wave reflection which had the effect of respectively raising or lowering the diastolic decay curve of both the central ear artery pulse and the abdominal aorta pulse, with the consequence of raising or lowering the abdominal aortic RHDN. However, the treatments changed the diameter of the aorta: Ach decreased and L-NAME increased aortic diameter. These changes in aortic diameter would have impacted on wave reflections from conduit arteries and cause uncertainty as to the origin of the reflections – some may emanate from the aorta as a result of its changes in diameter; the experimental ideal is for constancy of aortic geometry despite the treatments.

  Support: This thesis supports the hypothesis that wave reflections affect the diastolic features of the rabbit central ear artery. However, the findings of this thesis are the inverse of the findings of Weinberg *et al*., (2001) and Nier *et al*., (2008) who found that Ach lowered and L-NAME raised the diastolic decay curve, hence respectively decreased or increased the RHDN.

- *Hypothesis*: These reflections depend on conduit artery diameter and compliance and do not depend on aortic pulse wave velocity, cardiac output, heart rate, total peripheral resistance, or blood pressure.

  Findings: The lack of constancy of aortic geometry with treatments confounded explanation for involvement of conduit artery diameter. Aortic pulse wave velocity ($C_{ft\text{-}ft}$) decreased with Ach but increased with L-NAME and this is consistent with effects of these treatments on blood pressure and arterial compliance but not on reflections. Ach increased arterial compliance (inclusive of aortic and conduit), a condition that should favour attenuation of reflections but the reverse was found. L-NAME decreased arterial compliance (inclusive of aortic and conduit) favouring increased reflections but the reverse was found. Cardiac output was not measured,

heart rate was unaffected by Ach or L-NAME. Total peripheral resistance was not measured but vascular resistance (VR) was measured at two sites in the abdominal aorta. There were no associations of reflections with VR; reflections are expected to increase with increased VR, this did not happen as Ach decreased VR but increased reflections, L-NAME increased VR but decreased reflections. The same applies to blood pressure.

Support: This thesis cannot support the hypothesis that reflections depend on conduit artery diameter and compliance but can support the hypothesis that reflections are not dependent on aortic pulse wave velocity, heart rate, total peripheral resistance.

Limitations of experiment are discussed in Chapter 8.

CHAPTER 5

Effects of Fructose Feeding on Arterial Blood Pressure and Flow Waveforms in Immature and Mature Rabbits

5.1 INTRODUCTION

Chapter 1 introduced the concept of vascular ageing being partly a result of time-dependent, non-enzymatic, glycosylation (or glycation; Figure 1.2) of proteins in walls of arteries, especially walls of large elastic conduit arteries (Bierhaus *et al*., 1998; Ulrich and Cerami, 2001). Reducing sugars (e.g. glucose, fructose) can react with the protein chains of collagen and elastin to form protein-protein cross-links (Figure 1.2); this 'stiffens' the collagen and elastin structures (Brownlee *et al*., 1988; Reddy, 2004; Brüel and Oxland, 1996). Cross-linked proteins are known as advanced glycation end products (AGEs). AGEs of collagenous structures are stable and long-lived, so as the glycation process continues in time, the vasculature becomes progressively stiffer.

The experiments described in this chapter intended to model the AGE component of vascular ageing by inducing AGE formation in large artery walls in rabbits. Fructose was used for this purpose as it is more potent than glucose as a producer of AGEs (Schalkwijk *et al*., 2004). A diet of high fructose causes non-enzymatic increase in AGEs in the walls of the large elastic arteries (e.g. the aorta) of rats and rabbits, and there are many experimental protocols for treating rats or rabbits with fructose; all protocols having different intended outcomes (Dai and McNeill, 1995; Naka *et al*., 1998; Lin *et al*., 2004; Tokita *et al*., 2005; Akira *et al*., 2006; Chang *et al*., 2007; Mikulíková *et al*. 2008). As a point of interest, Vlassara *et al*. (1995) adopted a protocol of 4months of daily *intravenous* administration of AGE-modified rabbit serum to normal (non-diabetic) rabbits. This treatment promoted expression of the adhesion molecules, VCAM-1 and ICAM-1, and atheroma formation in otherwise normal aortas. Although this study demonstrated *in vivo* a causal relationship between chronic AGE accumulation and atherosclerosis, the model could be useful as one for vascular ageing providing data for haemodynamics and vessel mechanics along with development of atherosclerosis.

Mikulíková *et al*. (2008) treated rats for three weeks with 10% fructose solution in their drinking supply and observed in the aortas of the rats a tenfold increase in the AGE, pentosidine. Because such a large increase in pentosidine had occurred in the aortas after a short treatment time, one can reason that a shorter treatment time might still cause a significant increase in pentosidine, or other AGEs, in aortas perhaps even of rabbits. Lin *et al*. (2004) used a 2 week period of administration of 10% fructose solution to rats and observed significantly altered haemodynamic status (elevated aortic characteristic impedance and decreased wave transit time) in fructose treated rats compared to water treated controls. A short treatment time is convenient for quick throughput of experiments. So, based on the studies of Lin *et al*. (2004) and Mikulíková *et al*. (2008), a short period of 2 weeks treatment with 10% fructose solution was chosen for the experiments with rabbits reported in this thesis.

The Hypotheses

- Dietary supplementation with fructose will decrease arterial compliance and increase aortic pulse wave velocity.
- Fructose supplements will increase pressure pulse reflection in the aorta.
- Immature rabbits will have greater arterial compliance and lower aortic pulse wave velocity than mature rabbits.
- Immature rabbits will have lower pressure pulse reflection in their aortas than do mature rabbits.

5.2 METHOD

Experiments were carried out with mature rabbits aged 8 - 10 months and immature rabbits aged 3 – 3½ months. Rabbits were divided into two groups of Test Group and Control Group:

TEST GROUP:

Group sizes were: 8 mature rabbits; 6 immature rabbits. Rabbits received a solution of 10% fructose in tap water for two weeks and then this was changed to tap water for another two weeks. The two week period of water drinking after the 10% fructose drink was a "washout" period to clear the rabbits of fructose; this was done with the belief that AGEs formed in blood vessel walls would remain as AGEs because the latter result from an irreversible non-enzymic reaction process (Figure 1.2; Bierhaus *et al.*, 1998).

CONTROL GROUP:

As with the test group, group sizes were: 8 mature rabbits; 6 immature rabbits. Rabbits received tap water for 2 + 2 weeks to mimic the Test Group.

Terminal Surgical Procedures.

When the period for treatment with 10% fructose solution or water was over, the rabbits were prepared for terminal studies using the procedures as described in section 3.2.

Identification of Rabbits.

Rabbits with their data are identified by sets of letters which are unique to the individual rabbit. For example, the series A – H along with the letters in parenthesis make unique identities; M indicates Mature and Im indicates Immature, while W indicates of the Water Drinking Group and F indicates of the Fructose Drinking Group. For example, taking the letter A:

A(MW) is rabbit A, is Mature, and is of the Water Drinking Group

A(MF) is rabbit A, is Mature, and is of the Fructose Drinking Group

A(ImW) is rabbit A, is Immature, and is of the Water Drinking Group

A(ImF) is rabbit A, is Immature, and is of the Fructose Drinking Group

i.e. A(MW), A(MF), A(ImW), A(ImF) are 4 different rabbits.

5.3 RESULTS

Data were obtained from all mature rabbits, i.e. 8 water fed rabbits and 8 fructose fed rabbits. Data were obtained from all 6 immature rabbits of the water fed group but from only 5 of 6 of immature rabbits in the fructose fed group because 1 died early during the surgical procedure for the terminal study.

Data will be considered in two ways:

- *First,* in section 5.3.1, consideration will be given to the effects of the two treatments, i.e. effects of Water- or Fructose-drinking, on haemodynamics of mature and immature rabbits.

- *Second,* in section 5.3.2, an age comparison will be made between haemodynamics of immature and mature rabbits.

5.3.1 Effects of Water- or Fructose-Drinking Treatments

Basic Data

Table 5.1 shows basic data on heart rate (HR), systolic (SBP), diastolic (DBP), pulse (PP_{TP}) and mean (MAP) aortic arterial blood pressures, mean aortic blood flow (MABF), vascular resistance (VR; VR = MAP / MABF) and external diameter, at the UpSt and DnSt Sites in the abdominal aorta of anaesthetised rabbits of each treatment group; Table 5.1 includes the p-values for statistical significance of differences by Student's unpaired t-test – NS meaning no significant difference for $p>0.05$.

The data in Table 5.1 show for the mature and immature rabbits that there were no significant differences between the water- or fructose-treated groups. However, although not statistically significant (but close for SBP, DBP & MAP; Table 5.1), heart rate (HR) and blood pressure as an average were slightly higher in the mature fructose-treated rabbits compared with the mature controls. For the immature rabbits, blood pressure was lower in the fructose-treated group compared to controls but again the differences were not statistically significant.

TABLE 5.1: Basic Data (Mean±SD) for Heart Rate (HR), Systolic (SBP), Diastolic (DBP), Pulse Pressure (PP_{TP})* Mean (MAP) Aortic Arterial Blood Pressures, Mean Aortic Blood Flow (MABF), Vascular Resistance (VR) and External Diameter ($Ø_{Ext}$) at the UpSt and DnSt Sites in the abdominal aorta of Mature and Immature anaesthetised rabbits for each treatment group. Comparisons made to respective Water Controls; p by unpaired t-test to Water; NS=not significant p>0.05. $Ø_{Ext}$, mm; HR, beats/min; SBP, Pa; DBP, Pa; MAP, Pa; PP_{TP}, Pa; MABF m^3/s; VR, $N.m^{-5}.s$

	UpSt Site		DnSt Site	
MATURE	Water	Fructose	Water	Fructose
n	8	8	8	8
$Ø_{Ext}$	4.25±0.27	4.31±0.26 NS;p=0.76	2.81±0.26	3.00±0.27 NS;p=0.18
HR	226±24	243±18 NS;p=0.13	228±25	249±21 NS; p=0.08
SBP	9438±1925	11149±1192 NS; p=0.051	9941±2276	11401±1504 NS;p=0.15
DBP	7263±1729	8657±673 NS; p=0.052	7472±2054	8593±752 NS
PP_{TP} (PP_{TP}=SBP-DBP)	2175±368	2493±620 NS;p=0.23	2469±455	2808±840; NS;p=0.33
MAP	8242±1790	9707±845 NS; p=0.055	8517±2136	9683±966 NS;p=0.18
MABF $x10^{-6}$	2.17±0.52	2.54±0.71 NS;p=0.26	0.87±0.35	1.13±0.32 NS;p=0.14
VR $x10^9$ (VR=MAP/MABF)	3.89±0.88	4.02±0.88; NS;p=0.76	11.67±6.38	9.52±4.09 NS;p=0.44
IMMATURE				
n	6	5	6	5
$Ø_{Ext}$	4.00±0.00	4.05±0.11 NS;p=0.3	2.67±0.26	2.70±0.45 NS;p=0.88
HR	215±27	241±23 NS;p=0.13	220±27	243±22 NS;p=0.16
SBP	10551±1886	9108±2233 NS;p=0.28	10628±1720	9373±2306 NS;p=0.33
DBP	8119±1863	6927±1923 NS;p=0.33	7945±1746	6965±1893 NS;p=0.4
PP_{TP} (PP_{TP}=SBP-DBP)	2432±312	2181±428 NS;p=0.29	2683±378	2409±580 NS;p=0.37
MAP	9127±1850	7848±1994 NS;p=0.3	8996±1712	7899±1979 NS;p=0.35
MABF $x10^{-6}$	1.85±0.63	1.53±0.50 NS;p=0.38	0.62±0.17	0.77±0.33 NS;p=0.38
VR $x10^9$ (VR=MAP/MABF)	5.28±1.36	5.23±0.61 NS;p=0.94	16.42±5.27	11.11±3.05 NS; p=0.087

*PP_{TP} is pulse amplitude pressure of the measured (Total) pressure waveform.

Blood Pressure and Flow Waveforms

In Chapter 4, two types of blood pressure waveform were discussed; these were referred to as Type 1 and Type 2 waveforms. The two types of pressure waveform are shown in Figure 4.9; during diastole, Type 1 exhibit quasi-exponential decays of pressure, and Type 2 exhibit complex shaped decays of pressure. These waveform types were also observed in these experiments with mature and immature rabbits after water- or fructose-drinking treatments. As observed in the experiments discussed in Chapter 4, the two types of waveform appear to relate to blood pressure, such that Type 1 waveforms tend to occur at lower MAP than do Type 2 waveforms but this was not found statistically significant here (Table 5.2); this was not the case with the mature fructose-treated rabbits where the opposite occurred. As explained in Chapter 4, cautious consideration of the waveforms is required for algorithm fitting for calculating the reservoir (Windkessel) pressure and derivation of parameters from it.

TABLE 5.2: Association of Type 1 and Type 2 Waveforms with Mean Arterial Blood Pressure (MAP) at the UpSt and DnSt Sites of Measurement in the Abdominal Aorta of Anaesthetised Rabbits. Mean±SD (Pa); p by unpaired t-test, Type 1 vs. Type 2 Waveforms; NS=not significant at p>0.05.

Treatment	MAP (Pa) at UpSt Site		MAP (Pa) at DnSt Site	
MATURE	Type 1	Type 2	Type 1	Type 2
Water	7796±1801 n=6	9580±1197 n=2 NS;p=0.25	7784±2443 n=5	9716±668 n=3 NS;p=0.24
Fructose	9757±719 n=5	9622±1205 n=3 NS;p=0.85	9715±926 n=5	9631±1244 n=3 NS;p=0.92
IMMATURE				
Water	7973±2395 n=2	9703±1570 n=4 NS;p=0.33	6547±0 n=1	9485±1365 n=5
Fructose	6769±1734 n=3	9467±1075 n=2 NS;p=0.15	6867±2206 n=2	8587±1904 n=3 NS;p=0.42

Reservoir (Windkessel) Pressure: Data derived from it; its Subtraction from Measured (Total) Pressure.

Algorithm fitting for subtraction of reservoir (Windkessel) pressure from the measured (total) pressure was affected by the waveform type; good fit was observed with Type 1 but not with Type 2 waveforms (Figure 5.1A&B). This algorithm fitting is discussed in Chapter 4. The mean±SD of values of parameters derived from the reservoir (Windkessel) pressure where good algorithm fitting was achieved are given in Table 5.3; this table omits spurious data resulting from poor fitting to Type 2 waveforms. Table 5.4 shows the spurious data which are from individual rabbits – 1 mature and 6 immature rabbits.

As explained in Chapter 2, the reservoir (Windkessel) pressure is derived in two parts: 1) the systolic part from which the parameter A is obtained, and 2) the diastolic part (discussed above in relation to Type 1 & 2 diastolic pressure decay waveforms) from which three parameters are obtained, namely: B the decay rate constant, tau (τ) the decay time constant which is the reciprocal of B, and P infinity (P_∞). Two other measures of the reservoir (Windkessel) pressure are its integral, $\int$RP, and its pulse amplitude, PP_{RP}.

Of the **mature rabbits**, at the UpSt Site, B, τ and P_∞ were significantly different between the treatments but B only was significantly different between treatments at the DnSt Site (Table 5.3). The other parameters, namely A, $\int$RP and PP_{RP} were not significantly different between treatments. Arterial compliance (AC) was calculated from τ as AC = τ / VR. Table 5.5 gives data for calculated AC; no significant differences for AC were found between treatment groups with mature rabbits though the group mean AC was lower in the fructose-drinking group. Regression analysis was applied to MAP vs. AC as obtained from the UpSt and DnSt Sites in the abdominal aorta; plots are not shown but results are stated here. At the UpSt Site, the regression analysis revealed that plots of MAP vs. AC each for water- or fructose- drinking treatments showed non-significant ($p>0.05$) negative correlations (water: $r=-0.555$ & fructose: $r=-0.176$); furthermore, the two regression plots were not significantly different to each other, indicating that AC was not affected by fructose-drinking compared to control. Findings were similar at the DnSt Site in the abdominal aorta, though here the regression only for MAP vs. AC of the water controls correlated ($r=-0.88$) significantly ($p=0.009$) but not for the fructose-drink group: $r=-0.503$; NS $p>0.05$; the two regression plots were not significantly different from each other thus confirming the same finding at the UpSt Site that fructose-drink treatment was without effect on AC. Plotting the pooled data of water and fructose treatments (Figure 5.2) at the UpSt Site gave a significant ($p=0.018$) negative correlation ($r=-0.6$) (Figure 5.2A) and at the DnSt Site pooled data gave a negative

correlation (r=-0.778) that was significant (p=0.0006) (Figure 5.2B); thus the data indicate the expected relationship of AC decreasing with increasing MAP (Figure 5.2 A&B).

Of the **immature rabbits**, none of the parameters stated in Table 5.3 at UpSt or DnSt Sites were significantly different between treatments. No significant differences for calculated AC were found between treatment groups with immature rabbits though at the UpSt Site the group mean AC was lower in the fructose-drinking group (Table 5.5). Due to paucity of data not considered spurious due to poor algorithm fitting of the Type 2 waveforms, no data was available for the DnSt Site. Analysis of the relationship of MAP vs. AC was difficult with few values to consider. At the UpSt Site there were only three and four data points for control and fructose-drinking treatment respectively; at the DnSt Site only one and four data points were available for control and fructose-drinking treatment respectively. In all cases where regression analysis was attempted with the limited data, there were no significant correlations for MAP vs. AC, and no significant differences were observed between regression plots for the treatments.

FIGURE 5.1: Illustration of Fitting of Reservoir (Windkessel) Pressure to Type1 (Graph A; good fit) or Type 2 (Graph B; poor fit) Diastolic Pressure Decay in the Abdominal Aorta of Anaesthetised Rabbits.

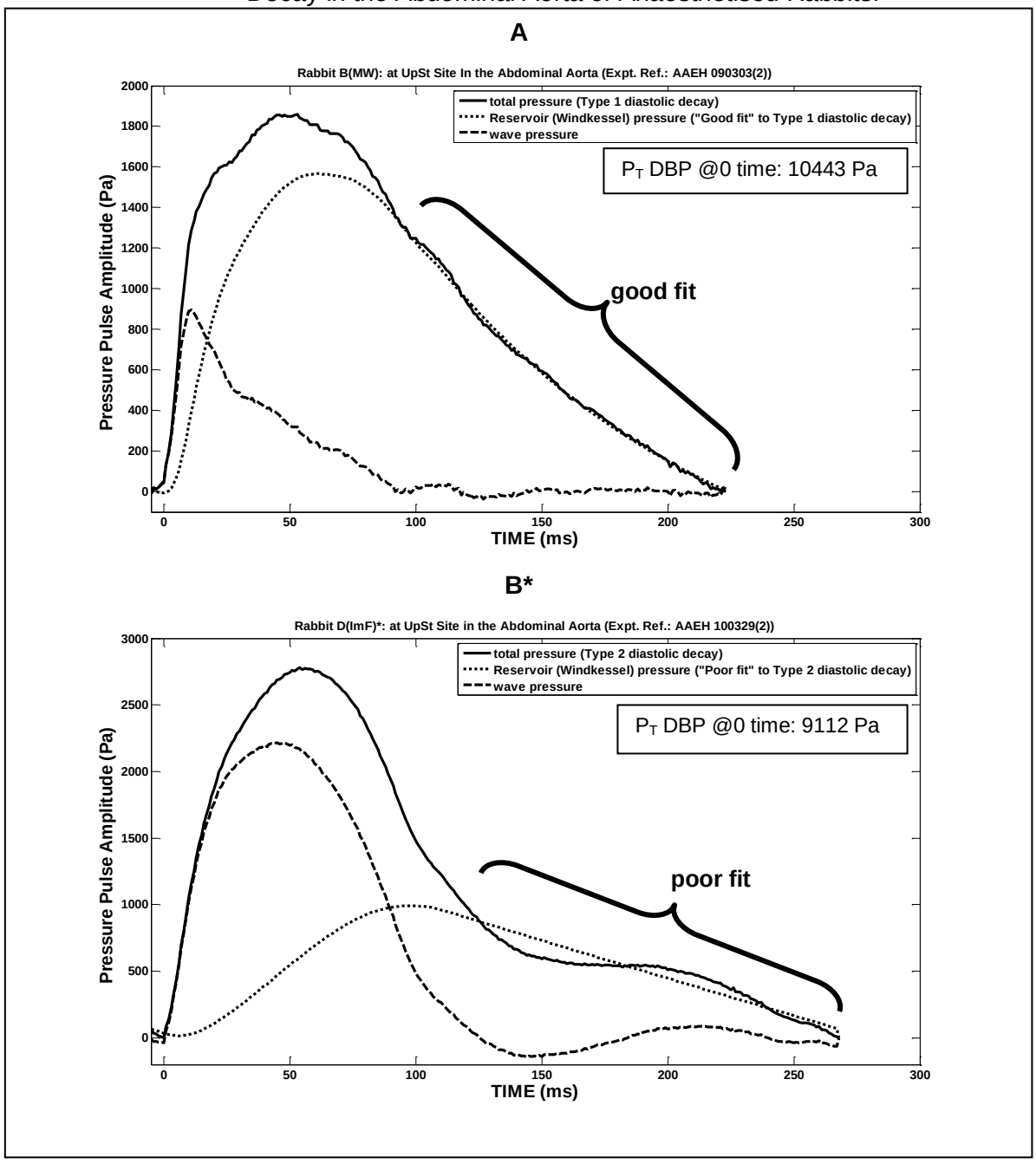

*See Table 5.4 for spurious data of Rabbit D(ImF) resulting from poor fit by algorithm.

TABLE 5.3: Data Derived from the Calculation of Reservoir (Windkessel) Pressure from the Aortic Pressure at the UpSt and DnSt Sites of Measurement in the Abdominal Aorta of Anaesthetised Mature and Immature Rabbits following Treatments with Water- or Fructose-Drinking. Mean±SD; Comparisons between Fructose Treatment and respective Water Controls; p by unpaired t-test to Water; NS=not significant p>0.05
Spurious data omitted but placed in Table 5.4

MATURE	UpSt Site		DnSt Site	
Parameters	Water	Fructose	Water	Fructose
A	0.084±0.053 n=8	0.071±0.039 n=8 NS;p=0.6	0.095±0.068 n=8	0.082±0.055 n=8 NS;p=0.67
B	0.010±0.003 n=7	0.017±0.005 n=8; p=0.007	0.013±0.004 n=7	0.020±0.006 n=8; p=0.029
τ	105.9±35.9 n=7	63.8±22.1 n=8; p=0.016	86.4±37.9 n=7	55.0±20.4 n=8; NS; p=0.063
P_∞	6550±1874 n=8	8534±747 n=8; p=0.015	7138±2183 n=7	8582±808 n=8 NS;p=0.1
$\int RP$	204±39 n=8	183±24 n=8 NS;p=0.23	204±50 n=8	175±29 n=8 NS;p=0.19
PP_{RP}	1606±364 n=8	1740±299 n=8 NS;p=0.44	1707±515 n=8	1780±449 n=8 NS;p=0.77
IMMATURE	Water	Fructose	Water	Fructose
A	0.014±0.010 n=6	0.044±0.043 n=5 NS;p=0.14	0.012±0.009 n=6	0.039±0.044 n=5 NS;p=0.17
B	0.007±0.006 n=3	0.011±0.004 n=4 NS;p=0.28	0.015; n=1	0.012±0.003 n=4; p=n/a
τ	234.2±159.4 n=3	98.8±31.2 n=4 NS;p=0.15	65.5; n=1	88.7±22.5 n=4; p=n/a
P_∞	6970±1560 n=3	6077±1751 n=4 NS;p=0.52	3488±2809; n=2	6165±1622 n=4 NS;p=0.2
$\int RP$	150±35 n=6	147±23 n=5 NS;p=0.87	141±48 n=6	133±18 n=5 NS;p=0.72
PP_{RP}	1055±212 n=6	1252±166 n=5 NS;p=0.13	972±247 n=6	1165±187 n=5 NS;p=0.19

Where: A = rate constant (s^{-1}); B = rate constant for diastolic decay (s^{-1});
τ = time (s) constant for diastolic decay (t=1/B); P_∞ = P infinite (Pa);
$\int RP$ =Integral of reservoir (Windkessel) pressure (Pa.s);
PP_{RP} = pulse amplitude of reservoir (Windkessel) pressure (Pa).

TABLE 5.4: Spurious Data Derived from Calculation of Reservoir (Windkessel) Pressure resulting from poor Algorithm Curve-Fitting of Aortic Pressure at the UpSt & DnSt Sites in the Abdominal Aorta of Anaesthetised Mature and Immature Rabbits following Treatments of Water- or Fructose-Drinking. (See Figure 5.1B for example of poor fitting).

		UpSt Site				DnSt Site			
Rabbit ID	Treatment	B	τ	P_∞	DBP	B	τ	P_∞	DBP
E(MW)	Water	0.002	620**			-0.002*	-440*	10683#	8011
A(ImW)	Water					-0.0004*	-2561*	19343#	9419
B(ImW)	Water	-0.002*	-485*	13598#	10624	-0.0031*	-322*	12247#	10307
C(ImW)	Water	-0.003*	-318*	9123#	7090	0.0001**	11307**	-47078*	6847
D(ImF)	Fructose	0.0003**	3579**	-10595*	9112	-0.0006*	-1773*	18012#	9304
E(ImW)	Water	-0.004*	-236*	9606#	7550	-0.0170*	-59*	8097#	7160
F(ImW)	Water					0.0007**	1440**		

Where: B = rate constant for diastolic decay (s^{-1});
τ = time (s) constant for diastolic decay (t=1/B); P = P infinite (Pa);
DBP = Diastolic Blood Pressure (Pa);

(*) spurious '–ve' values; (**) spurious magnitudes; (#) P_∞>DBP is "not sensible"

TABLE 5.5: Data for Calculated Arterial Compliance (AC) UpSt & DnSt Sites of Measurement in the Abdominal Aorta of Mature and Immature Anaesthetised Rabbits. Mean±SD ($x10^{-8}$ $m^3.Pa^{-1}$); comparison between Fructose Treatment and respective Water Controls, p by unpaired t-test to Water; NS=not significant p>0.05

Treatments	UpSt Site		DnSt Site	
	Water	Fructose	Water	Fructose
Mature	3.08±1.74 $x10^{-8}$ n=7	1.73±0.87 $x10^{-8}$ NS; p=0.07 n=8	0.96±0.55 $x10^{-8}$ n=7	0.67±0.42 $x10^{-8}$ NS; p=0.27 n=8
Immature	4.65±3.11 $x10^{-8}$ n=3	1.88±0.74 $x10^{-8}$ NS; p=0.14 n=4	No data	0.78±0.06 $x10^{-8}$ n=4

FIGURE 5.2: Regression on Pooled Data of Water- and Fructose-Drink Treatment. Plots of Mean Arterial Pressure (MAP) vs Arterial Compliance (AC) at the UpSt Site (A) and DnSt Site (B) in the Abdominal Aorta of Anaesthetised Mature Rabbits. Correlation not significant p>0.05

Note: Regressions of treatments individually were unremarkable but the pooled data as shown indicate the expected relationship of AC decreasing with increasing MAP – see text.

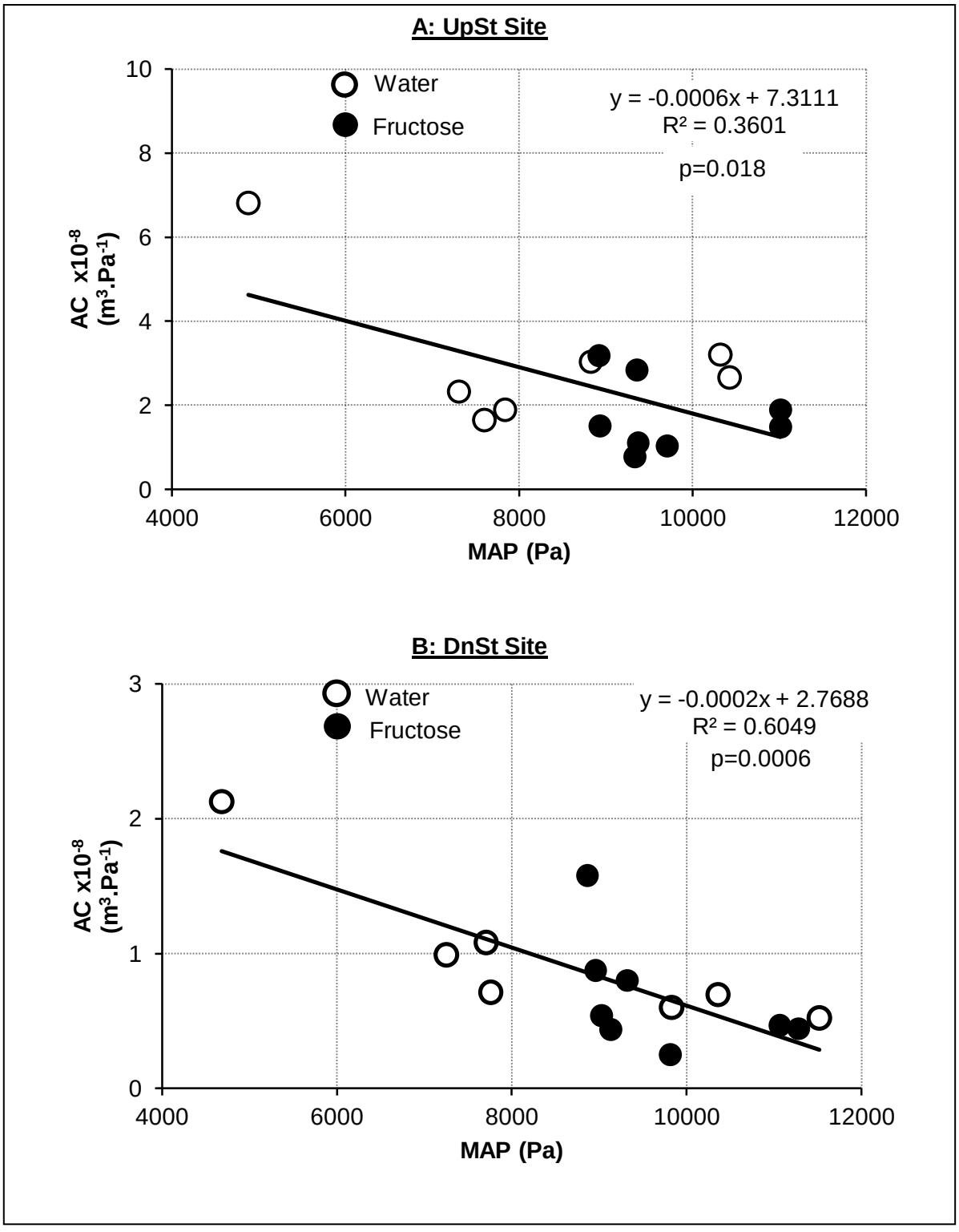

Relative Height of the Dicrotic Notch (RHDN) obtained from the Measured (Total) Blood Pressure Waveform of the Abdominal Aorta.

The term “dicrotic notch” referred to here for RHDN, is discussed fully in Chapter 4.

Table 5.6 gives data for RHDN, along with the time (Tn) of the incisura inflection timed from end-diastole (i.e. start of systole). Fructose-drinking treatment had no significant effect on RHDN or Tn compared to control in mature or immature anaesthetised rabbits.

TABLE 5.6: Data (Mean ± SD) for RHDN and Tn at the UpSt and DnSt Sites of Measurement in the Abdominal Aorta of Water and Fructose-drinking Treated Mature and Immature Anaesthetised Rabbits. Comparisons between Fructose and respective Water Controls, p by unpaired t-test to Water, NS = not significant at p>0.05.

	UpSt Site		DnSt Site	
MATURE	Water	Fructose	Water	Fructose
n	8	8	8	8
RHDN	0.62±0.10	0.57±0.06 NS;p=0.19	0.58±0.13	0.51±0.09 NS;p=0.24
Tn (ms)	104.8±8.4	100.3±8.6 NS;p=0.31	102.9±9.2	100.8±10.7 NS;p=0.68
IMMATURE				
n	6	5	6	5
RHDN	0.50±0.04	0.55±0.08 NS;p=0.17	0.42±0.06	0.51±0.09 NS; p=0.066
Tn (ms)	108.3±14.2	97.6±8.4 NS;p=0.17	106.8±13.6	93.6±6.4 NS; p=0.081

RHDN: Relative Height of the Dicrotic Notch.
Tn: time of notch from onset of systolic upstroke of the pressure pulse.

Wave Pressure.

Subtraction of the Reservoir (Windkessel) pressure from the measured (total) pressure gives the wave pressure; the latter is exemplified in Chapter 4 (Figures 4.16, 4.17 & 4.18) and in this chapter (Figure 5.1). The wave pressure is used for calculating one of the estimates of wave speed, and for wave intensity analysis which is discussed below.

Pulse Wave Velocities (PWV) and Wave Speeds

PWV was measured by the "foot-to-foot" method (see section 3.2.5) and, as in Chapter 4, is ascribed here as $C_{ft\text{-}ft}$.

Table 5.7 gives mean data for $C_{ft\text{-}ft}$ at the UpSt and DnSt Sites in the abdominal aortas of anaesthetised mature and immature rabbits of the water- (control) and fructose-drinking treatment groups. Of the mature rabbits, group mean $C_{ft\text{-}ft}$ as measured at the UpSt Site was not significantly different between the two treatment groups (Table 5.7), but at the DnSt Site group mean $C_{ft\text{-}ft}$ was significantly (p=0.043) higher in the fructose-drinking treated group compared to control group. *Vice versa* for the immature rabbits, where the group mean $C_{ft\text{-}ft}$ was lower in the fructose-drinking group compared with control but the difference was not statistically significant.

TABLE 5.7: Data for $C_{ft\text{-}ft}$ (m/s) (Mean ± SD) at the UpSt & DnSt Sites of Measurement in the Abdominal Aorta in Anaesthetised Mature and Immature Rabbits of Water- and Fructose-Drinking Treatment Groups. Comparisons between Fructose and respective Water Controls, p by unpaired t-test to Water; NS = not significant at p>0.05.

	$C_{ft\text{-}ft}$ at UpSt Site		$C_{ft\text{-}ft}$ at DnSt Site	
	Water	Fructose	Water	Fructose
MATURE (n)	5.27±0.66 (8)	5.58±0.45 (8) NS; p=0.3	5.28±0.62 (8)	6.04±0.74 (8) p=0.043
IMMATURE (n)	6.34±1.24 (6)	5.57±1.09 (5) NS; p=0.31	7.58±0.85 (6)	6.38±1.27 (5) NS; p=0.35

$C_{ft\text{-}ft}$ is plotted against MAP for mature (Figure 5.3) and immature (Figure 5.4) rabbits, along with associated regression plots. In the case of mature rabbits (Figure 5.3) at the UpSt and DnSt Sites, the correlations were not significant and the regression plots were not

significantly different between treatments; furthermore, regression analysis of pooled data of the two treatments revealed no significant correlation (at UpSt & DnSt Sites, pooled data, r=0.204 & r=0.387 respectively; both p>0.05). Thus, at the UpSt and DnSt Sites of measurement in the abdominal aorta of mature rabbits, fructose-drinking had no effect on the relationship of MAP with $C_{ft\text{-}ft}$, a relationship where $C_{ft\text{-}ft}$ is expected to increase with increasing MAP but this also was not evident from the regression of pooled data. In the case of immature rabbits (Figure 5.4), at the UpSt Site, regression analysis showed significant correlations for MAP vs. $C_{ft\text{-}ft}$ for both treatment groups but the regression plots were not significantly different between the treatments indicating no effect of fructose-drinking on the MAP vs. $C_{ft\text{-}ft}$ relationship. At the DnSt Site, the MAP vs. $C_{ft\text{-}ft}$ plot correlated significantly for the control group but not for the fructose-drinking group; the two regression plots were not significantly different, again indicating no effect of fructose-drinking on the MAP vs. $C_{ft\text{-}ft}$ relationship. At both the UpSt and DnSt Sites, pooling the data of the controls with fructose-drinking groups gives significant correlations: at UpSt Site r=0.8996 p=0.0002; at DnSt Site r=0.763 p=0.006. This shows the expected relationship that $C_{ft\text{-}ft}$ increases with increasing MAP; this contrasts with mature rabbits.

The term *wave speed* refers to values obtained by plotting pressure (P) and flow velocity (U) pulses to obtain a PU loop (see Chapters 2 and 4); the ratio of the slope of the linear part of the PU loop to blood density gives wave speed. Wave speeds ascribed as C_{Tpu} or C_{Wpu} are obtained by plotting the measured (Total) pressure or wave pressure respectively, against flow velocity.

PU loop data were not available from four mature rabbits (2 of control and 2 of fructose-drinking group), their IDs are: A(MW); B(MW); A(MF); B(MF). Thus, data for $C_{ft\text{-}ft}$, C_{Tpu} and C_{Wpu} are compared between six mature rabbits in the control group and six in the fructose-drinking group. Of the immature rabbits, PU loop data was not available from one rabbit (which died) of the fructose-drinking group and one control rabbit, D(ImW), for the DnSt Site. Mean data for $C_{ft\text{-}ft}$, C_{Tpu} and C_{Wpu} are shown in Table 5.8 (mature rabbits) and Table 5.9 (immature rabbits). In mature and immature rabbits, fructose-drinking treatment had no significant effect on $C_{ft\text{-}ft}$, C_{Tpu} and C_{Wpu} as compared with control at the UpSt and DnSt Sites in the abdominal aorta of the rabbits. In the case of $C_{ft\text{-}ft}$ it is noted that here in mature rabbits of this smaller group size (Table 5.8), at the DnSt Site, the difference of $C_{ft\text{-}ft}$ between the two treatment groups is not significance (p=0.08) in contrast to the larger group size when $C_{ft\text{-}ft}$ differed significantly (p=0.043) between the two treatment groups (Table 5.7). Theoretically, values for $C_{ft\text{-}ft}$, C_{Tpu} and C_{Wpu} should not differ significantly; this was discussed in Chapter 4, where the null hypothesis is proposed that $C_{ft\text{-}ft} = C_{Tpu} = C_{Wpu}$. Data in Tables 5.8 and 5.9 support the null hypothesis where it is shown by one-way ANOVA (including by

repeated measures) that there were no significant differences between the means of $C_{ft\text{-}ft}$, C_{Tpu} and C_{Wpu} in mature and immature rabbits at both UpSt and DnSt Sites in the abdominal aorta; though for the water-drinking control data differences in variance are detected for mature (UpSt & DnSt Sites) and immature (DnSt Site) rabbits. As in Chapter 4, values for $C_{ft\text{-}ft}$ were used for the determination of wave intensity since values for C_{Tpu} and C_{Wpu} are very sensitive to fidelity of acquisition of the systolic part of the pressure (P) and velocity (U) waveforms for plot of the PU loop.

FIGURE 5.3: Plots of $C_{ft\text{-}ft}$ with Mean Arterial Blood Pressure (MAP) at the UpSt and DnSt Sites of Measurement in the Abdominal Aorta of each Anaesthetised *Mature* Rabbit of the Water- and Fructose-Drinking Treatment Groups. NS = not significant at p>0.05.
Note: No significant correlations or differences between plots – see text.

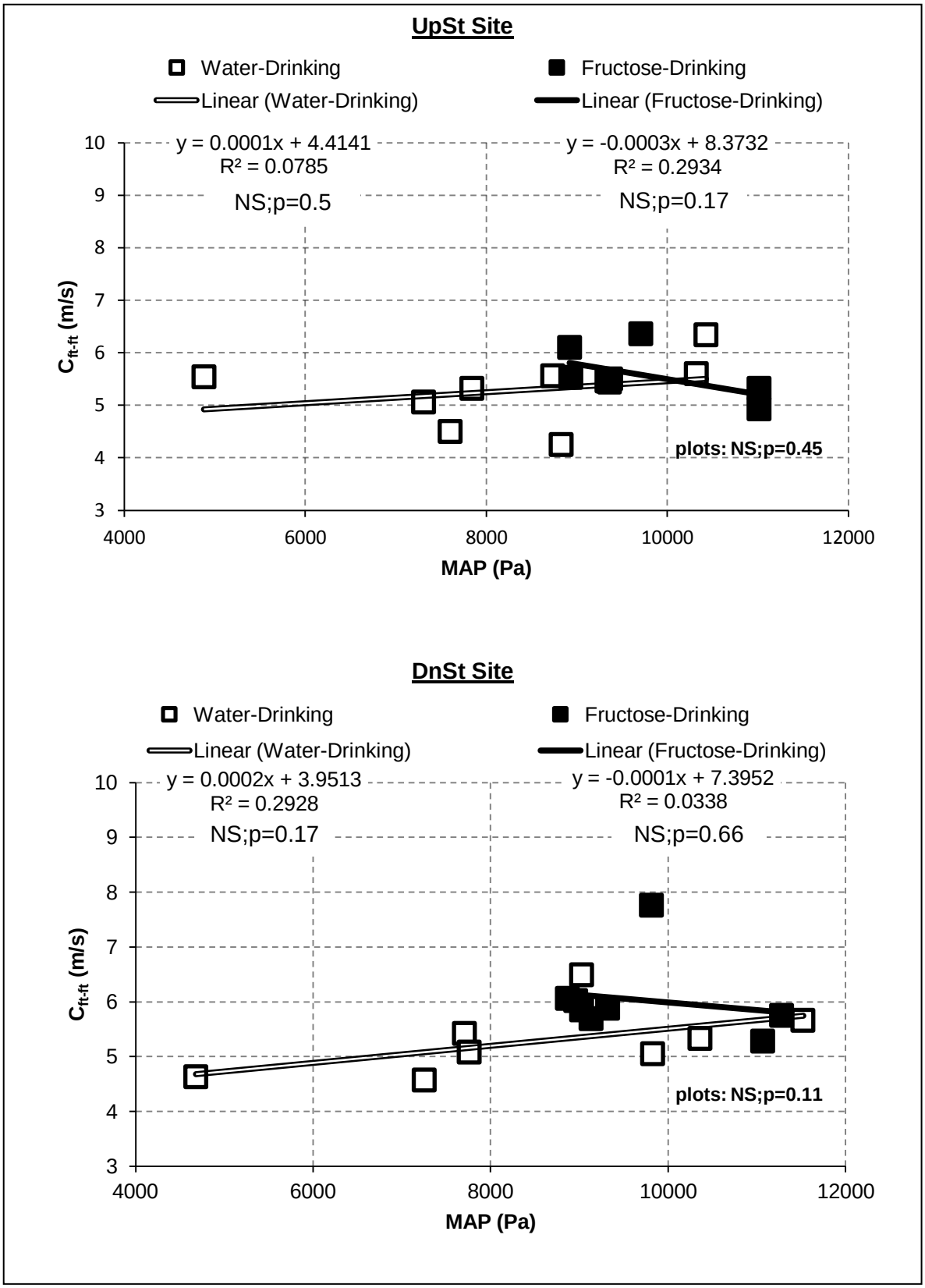

FIGURE 5.4: Plots of $C_{ft\text{-}ft}$ with Mean Arterial Blood Pressure (MAP) at the UpSt and DnSt Sites of Measurement in the Abdominal Aorta of each Anaesthetised *Immature* Rabbit of the Water- and Fructose-Drinking Treatment Groups.
NS = not significant at p>0.05.
Note: significant correlations revealed but not with fructose DnSt Site; no significant difference between plots – see text.

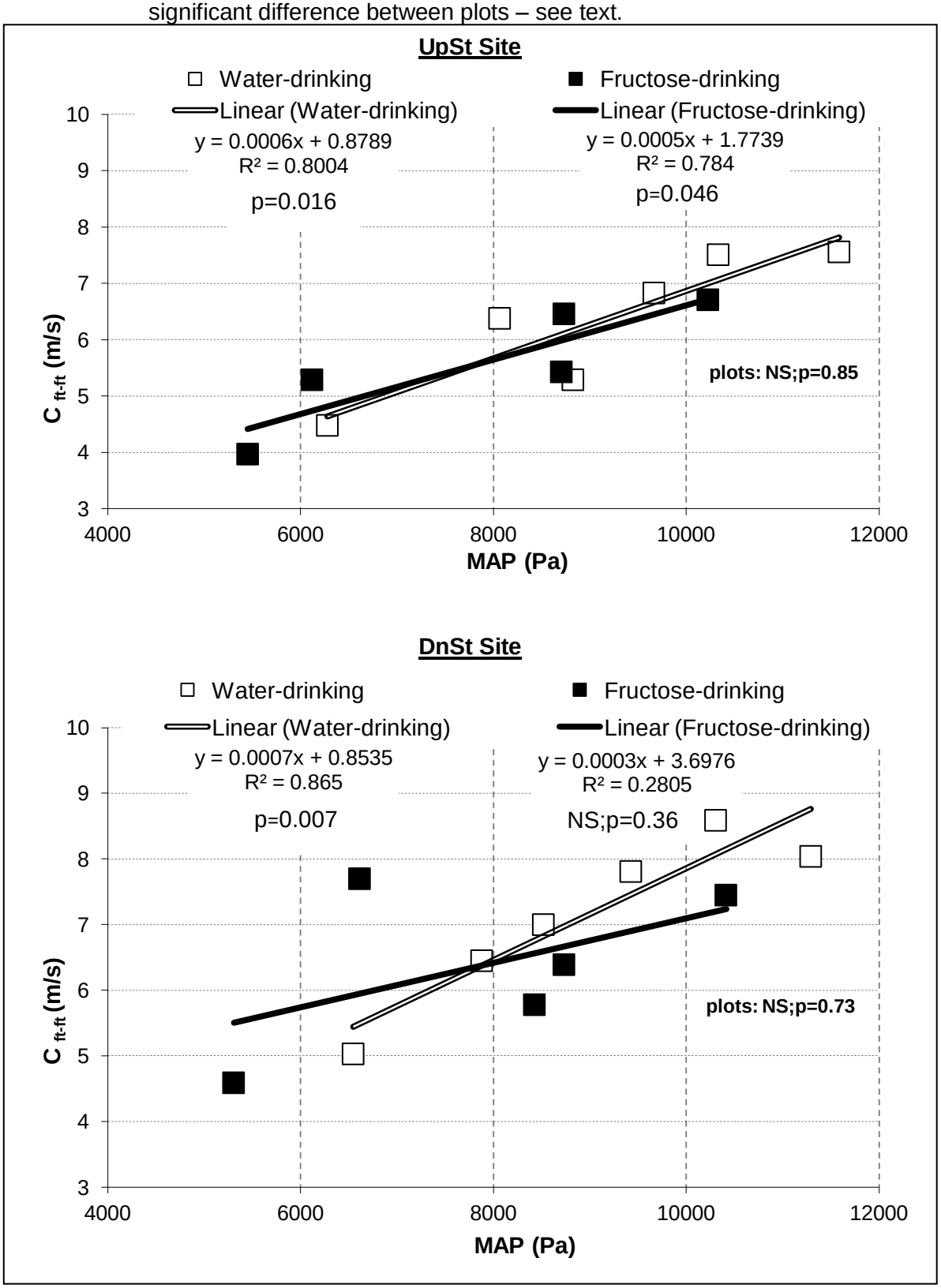

TABLE 5.8: Comparisons between $C_{ft\text{-}ft}$, C_{Tpu} and C_{Wpu} (Mean ± SD) measured at the UpSt & DnSt Sites in the Abdominal Aorta of Anaesthetised *Mature* Rabbits from Treatment Groups of Water- or Fructose-Drinking. Statistical Comparisons using unpaired t-test (t) made against respective water control (#) and One-Way ANOVA (& Repeated Measures, RM) - differences of means ($\bar{x}$), differences of variances (*var*); NS=not significant at p>0.05

UpSt Site						DnSt Site					
Water (n=6)			Fructose (n=6)			Water (n=6)			Fructose (n=6)		
$C_{ft\text{-}ft}$	C_{Tpu}	C_{Wpu}	$C_{ft\text{-}ft}$	C_{Tpu}	C_{Wpu}	$C_{ft\text{-}ft}$	C_{Tpu}	C_{Wpu}	$C_{ft\text{-}ft}$	C_{Tpu}	C_{Wpu}
5.39 ±0.61 #	6.31 ±1.68 #	5.77 ±2.63 #	5.62 ±0.52 (t)NS p=0.3	5.88 ±1.09 (t)NS p=0.61	6.13 ±1.28 (t)NS p=0.77	5.25 ±0.70 #	5.76 ±3.02 #	4.58 ±3.25 #	6.12 ±0.85 (t)NS p=0.08	4.79 ±2.25 (t)NS p=0.55	4.43 ±2.10 (t)NS p=0.93
($\bar{x}$) NS;p=0.69 (*var*) p=0.022			($\bar{x}$) NS;p=0.69 (*var*) NS;p=0.19			($\bar{x}$) NS;p=0.73 (*var*) p=0.014			($\bar{x}$) NS;p=0.28 (*var*) NS;p=0.13		
RM ($\bar{x}$) NS;p=0.45			RM ($\bar{x}$) NS;p=0.58			RM ($\bar{x}$) NS;p=0.49			RM ($\bar{x}$) NS;p=0.08		

TABLE 5.9: Comparisons between $C_{ft\text{-}ft}$, C_{Tpu} and C_{Wpu} (Mean ± SD) measured at the UpSt & DnSt Sites in the Abdominal Aorta of Anaesthetised *Immature* Rabbits from Treatment Groups of Water- or Fructose-Drinking. Statistical Comparisons using unpaired t-test (t) made against respective water control (#) and One-Way ANOVA (& Repeated Measures, RM) - differences of means ($\bar{x}$), differences of variances (*var*); NS=not significant at p>0.05; see text for explanation of n.

UpSt Site						DnSt Site					
Water (n=6)			Fructose (n=5)			Water (n=5)			Fructose (n=5)		
$C_{ft\text{-}ft}$	C_{Tpu}	C_{Wpu}	$C_{ft\text{-}ft}$	C_{Tpu}	C_{Wpu}	$C_{ft\text{-}ft}$	C_{Tpu}	C_{Wpu}	$C_{ft\text{-}ft}$	C_{Tpu}	C_{Wpu}
6.34 ±1.24 #	5.94 ±1.89 #	6.14 ±1.50 #	5.57 ±1.09 (t)NS p=0.31	6.07 ±0.78 (t)NS p=0.89	5.37 ±1.12 (t)NS p=0.37	7.58 ±0.85 #	9.18 ±4.18 #	9.16 ±4.08 #	6.38 ±1.27 (t)NS p=0.35	5.92 ±2.75 (t)NS p=0.18	4.92 ±2.11 (t)NS p=0.07
($\bar{x}$) NS;p=0.91 (*var*) NS;p=0.69			($\bar{x}$) NS;p=0.54 (*var*) NS;p=0.76			($\bar{x}$) NS;p=0.7 (*var*) p=0.027			($\bar{x}$) NS;p=0.56 (*var*) NS;p=0.38		
RM ($\bar{x}$) NS;p=0.9			RM ($\bar{x}$) NS;p=0.35			RM ($\bar{x}$) NS;p=0.57			RM ($\bar{x}$) NS;p=0.55		

Wave Intensity Analysis (WIA)

The theoretical aspects of WIA are explained in Chapter 2, where also the features of the wave intensity plot are pointed out. Wave Intensity Analysis (WIA) here, as in Chapter 4, was achieved by integrating the wave intensity plots to give data in terms of wave energy (J/m^2). With regard to terminology, incident waves are forward-going waves travelling from proximal (upstream) to distal (downstream); whereas, reflected waves are backward-going waves travelling distal to proximal.

Figures 5.5 (mature rabbits) and 5.6 (immature rabbits) show group mean wave energies of incident and reflected compression and expansion waves. For mature and immature rabbits, no statistically significant differences between control and fructose-drinking treatments were observed for incident or reflected compression or expansion wave energies. Wave reflection indices (WRI) (i.e. reflected wave energy / incident wave energy) for compression and expansion waves are shown graphically in Figures 5.7 and 5.8; there were no significant differences for reflection coefficients between water- and fructose-drinking treatment groups. Although the mean values between the treatment groups are not significantly different, there appears a trend for fructose-drinking treatment to increase or decrease WRI in mature or immature rabbits respectively. The large standard deviation of the data (UpSt Site; Figure 5.8) for the fructose-drinking immature group was due to one rabbit having WRI of some 10 fold of the others for compression and expansion waves.

The distance of reflection sites from the sites of recording were estimated from the time lapse between incident and reflected intensities of the compression wave (see Chapter 2); these distances are plotted in Figures 5.9 (mature and immature rabbits). Distances of reflection sites were not affected significantly by fructose-drinking treatment compared to control.

FIGURE 5.5: Wave Energies (Mean±SD) of Incident and Reflected Compression and Expansion Waves, at the UpSt and DnSt Sites of Measurement in the Abdominal Aorta of Anaesthetised *Mature* Rabbits of Water- or Fructose-Drinking Treatment Groups. Comparisons made between Fructose and respective Water Controls, p by unpaired t-test, NS = not significant at p>0.05; n=6 each treatment.

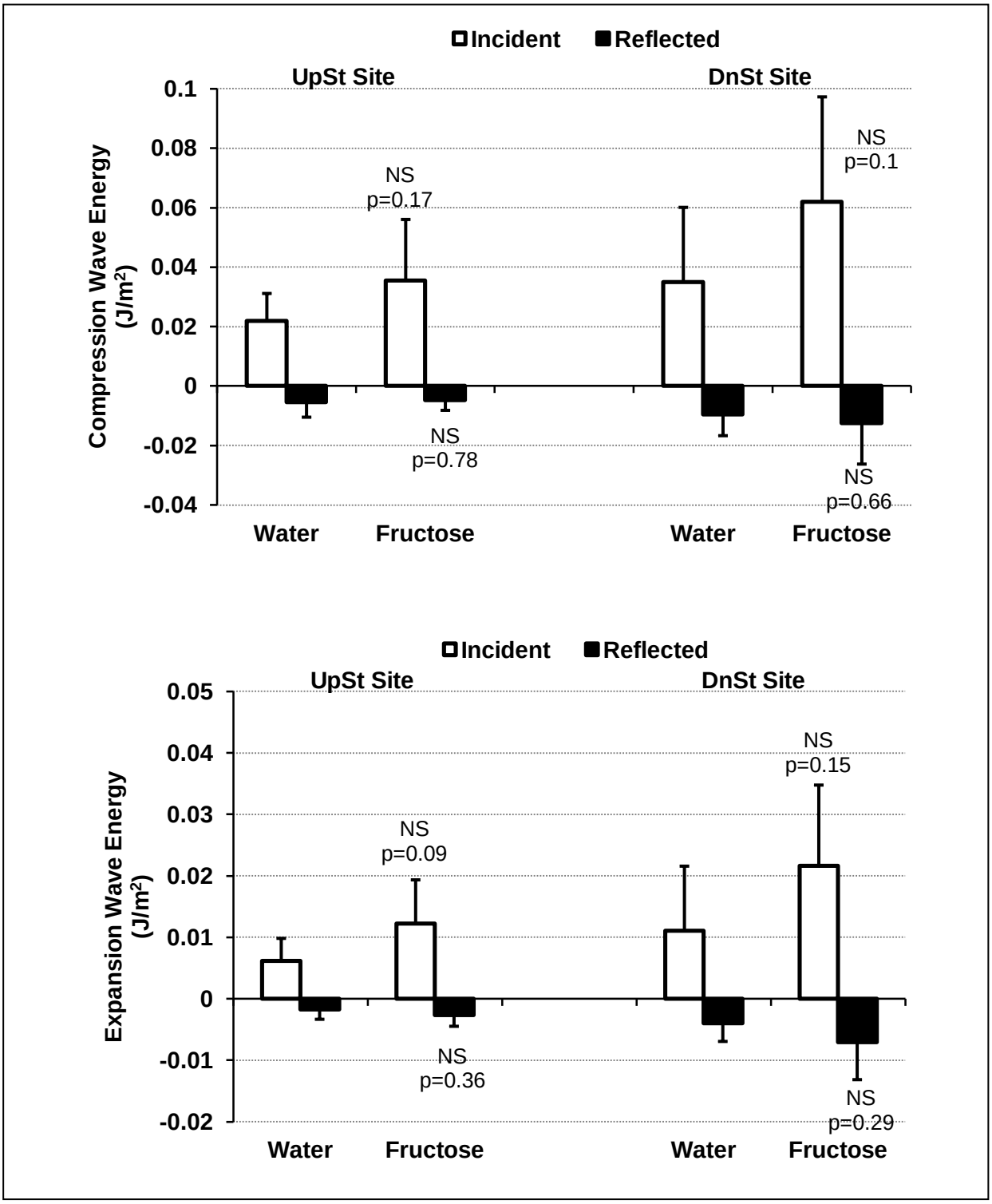

FIGURE 5.6: Wave Energies (Mean±SD) of Incident and Reflected Compression and Expansion Waves, at the UpSt and DnSt Sites of Measurement in the Abdominal Aorta of Anaesthetised *Immature* Rabbits of Water- or Fructose-Drinking Treatment Groups. Comparisons made between Fructose and respective Water Controls, p by unpaired t-test, NS = not significant at p>0.05; n inserted in figure.

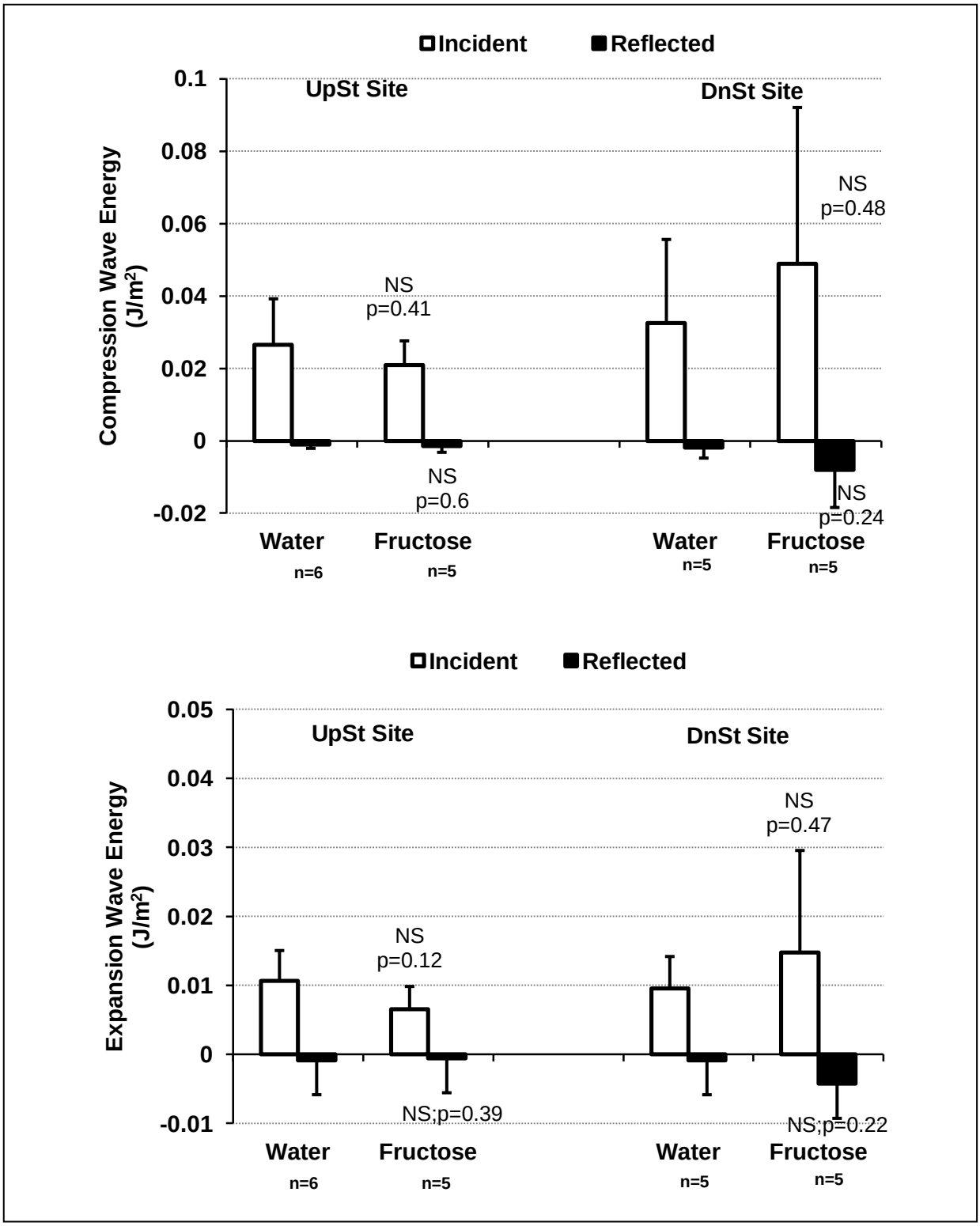

FIGURE 5.7: Wave Reflection Indices (WRI) (Mean±SD) for Compression and Expansion Waves at the UpSt and DnSt Sites of Measurement in the Abdominal Aorta of Anaesthetised *Mature* Rabbits of Water- or Fructose-Drinking Treatment Groups. Comparisons made between Fructose and respective Water Controls, p by unpaired t-test, NS = not significant at p>0.05; n=6 each treatment.

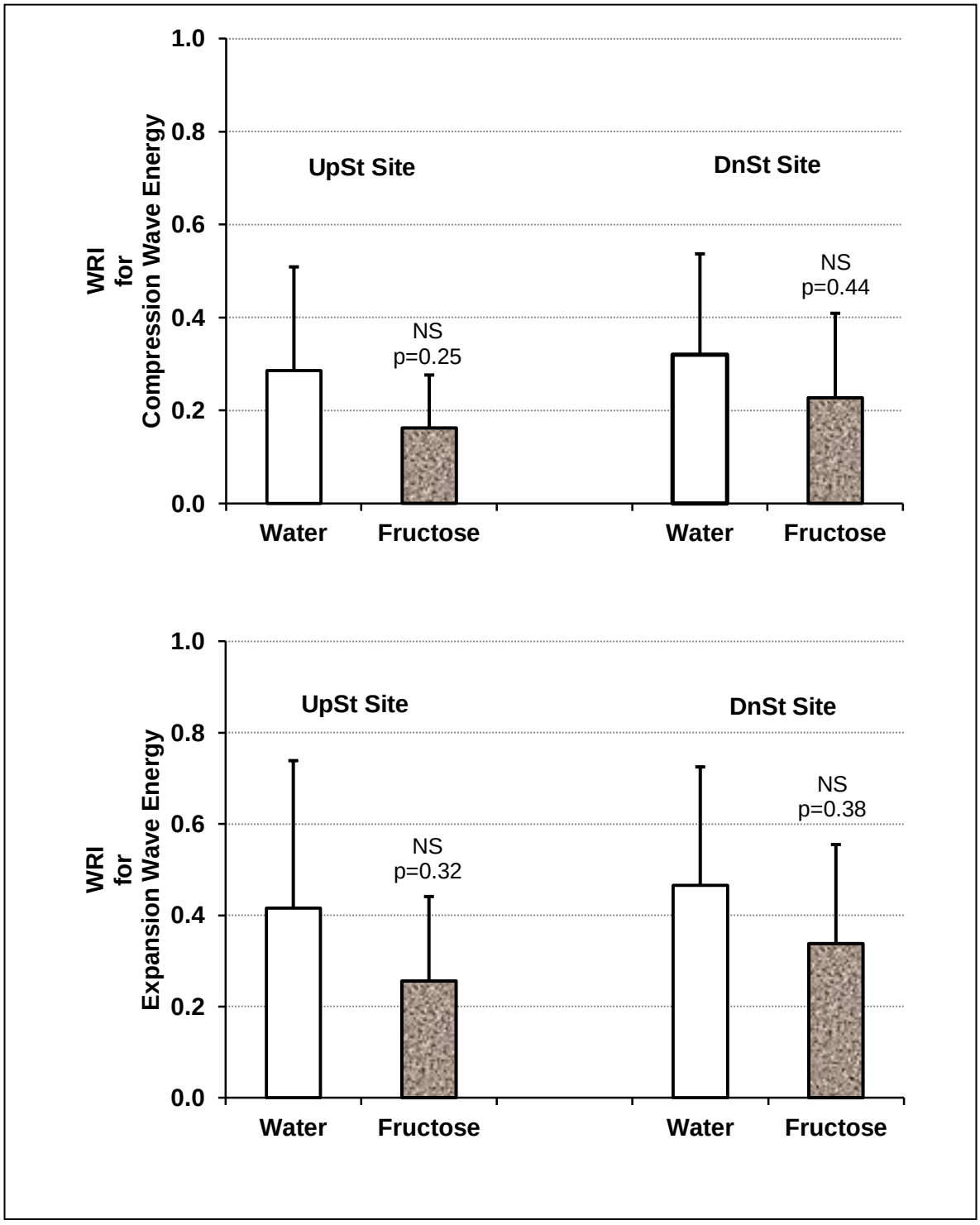

FIGURE 5.8: Wave Reflection Indices (WRI) (Mean±SD) for Compression and Expansion Waves at the UpSt and DnSt Sites of Measurement in the Abdominal Aorta of Anaesthetised *Immature* Rabbits of the Water- or Fructose-Drinking Treatment Groups. Comparisons made between Fructose and respective Water Controls; p by unpaired t-test, NS = not significant at p>0.05; n inserted in figure.

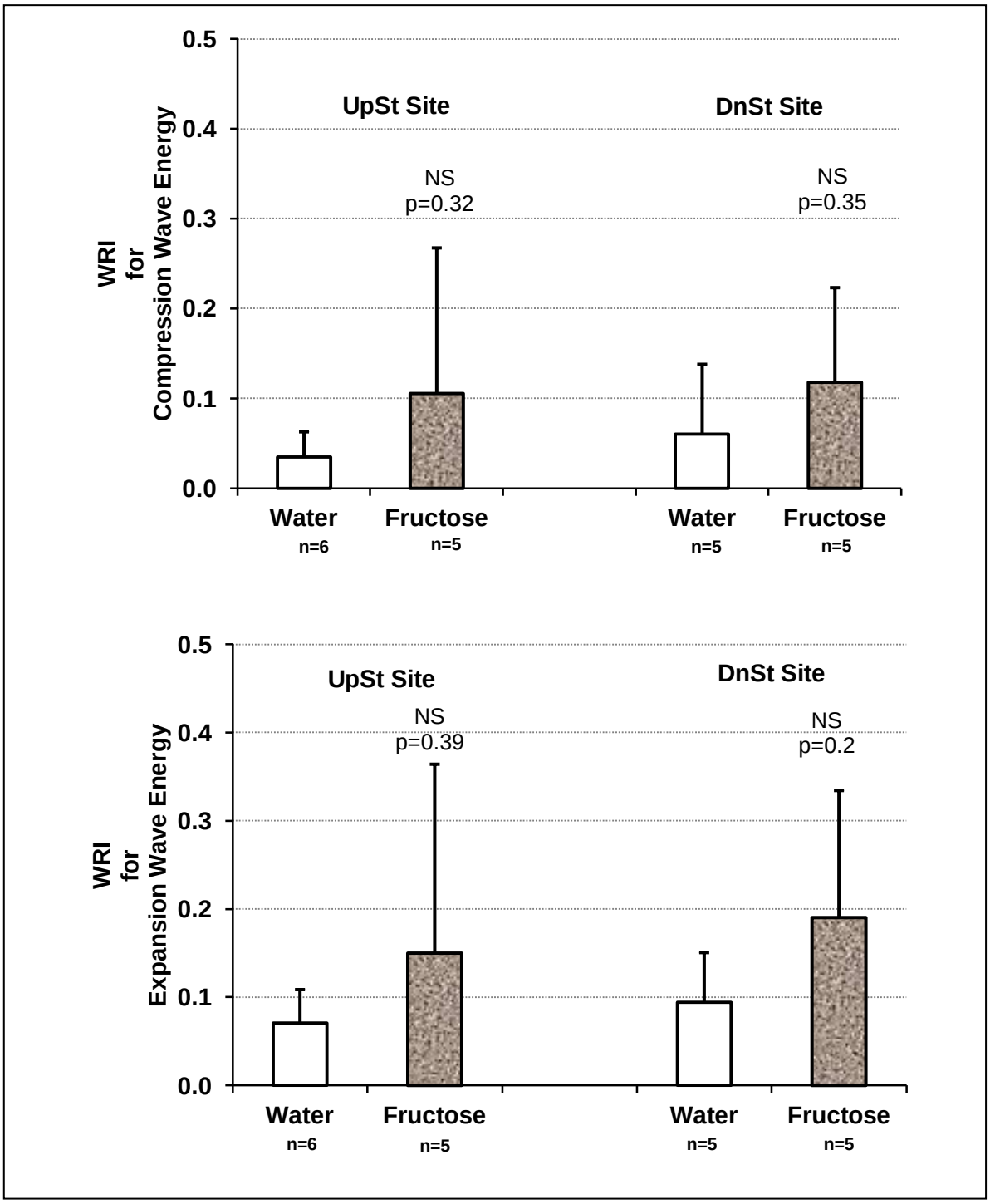

FIGURE 5.9: Distances of Reflection Site from the Sites of Recording (i.e. UpSt & DnSt Sites) (Mean±SD) as estimated from the time lapse between Incident and Reflected Intensities of the Compression Wave in the Abdominal Aorta of Anaesthetised *Mature and Immature* Rabbits from Water- and Fructose-Drinking Treatments. Comparisons made between Fructose and respective Water controls, p by unpaired t-test, NS = not significant at p>0.05; n=6 for Mature, n inserted in figure for Immature.

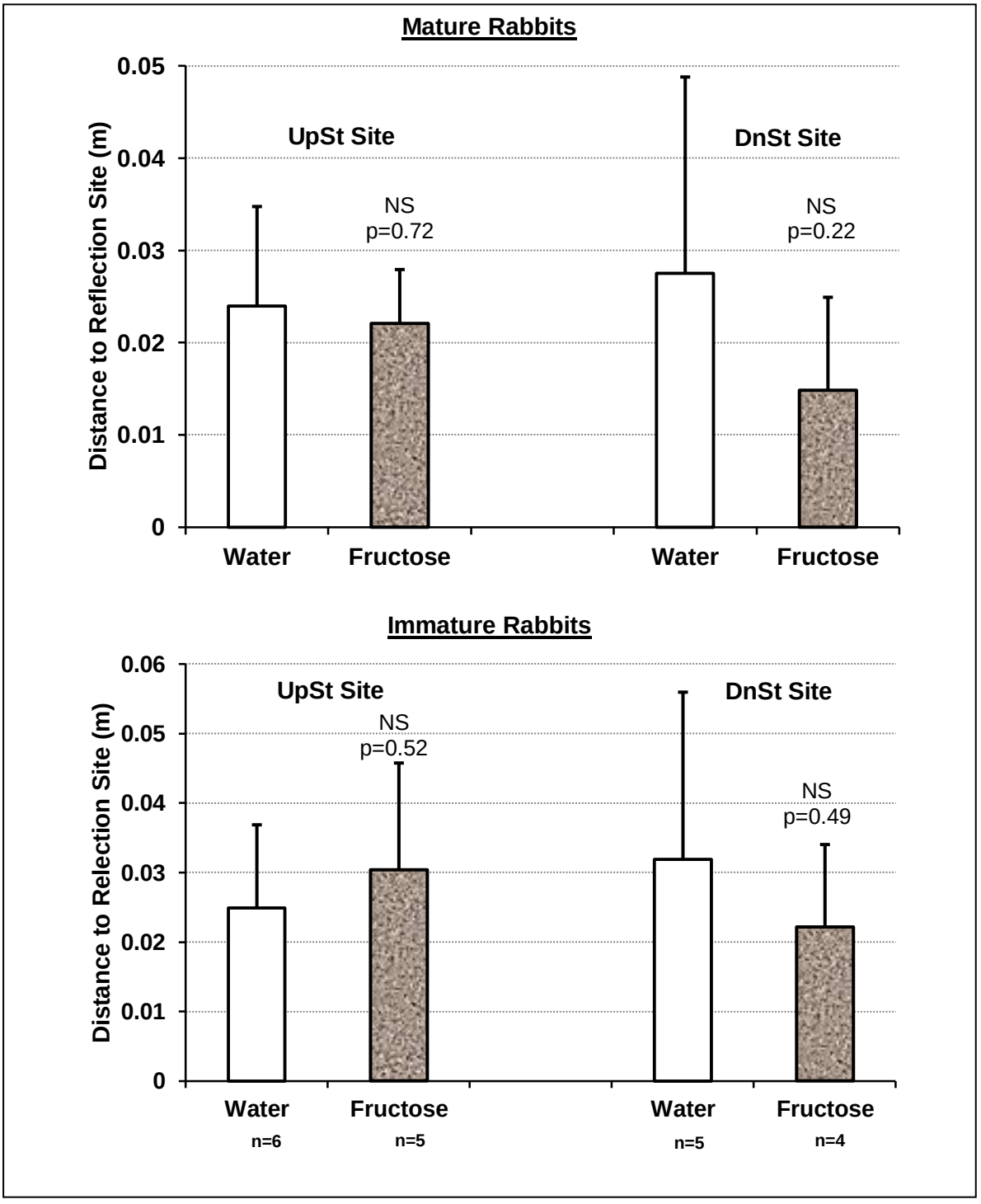

5.3.2 Comparison of Haemodynamic Parameters between Immature and Mature Rabbits

The statements above and data so far shown, all reveal that with immature rabbits control and fructose-drinking treatments did not differ significantly in their effects which indicates that fructose-drinking treatment did not cause vascular ageing-like effects in immature rabbits. Furthermore, the data indicates that, overall, fructose-drinking treatment had effects little different to control treatment in mature rabbits, thus little conclusive evidence for vascular ageing-like effects by fructose-drinking in mature rabbits.

In this section, data from immature rabbits are compared to those of mature rabbits. Because fructose-drinking treatment had little or no effect on vascular function and so was little different to water-drinking control treatment within immature and within mature rabbits, it is taken that all immature rabbits and all mature rabbits, regardless of their treatment groups, constitute two homogenous populations, namely an immature or a mature population. Thus, the data from the two treatments are pooled for each population for consideration in the analyses discussed in this section. Comparison between only the water-treated immature and water-treated mature rabbits would be ideal (referred to as the 'ideal comparison'), since fructose might have had effects that were not measurable in these experiments; however, that both immature and mature groups would include data from fructose-treatment means that the populations were balanced and that the increased group sizes would be advantageous for the analyses of immature vs. mature rabbit haemodynamic data. However, before deciding to pool data and for assurance of the validity of pooling the data, preliminary comparisons were made with the four treatment groups, immature water-treated (ImW), mature water-treated (MW); immature fructose-treated (ImF) and mature fructose-treated (MF); preliminary comparisons were thus:

ImW vs. MW (both groups supposedly normal rabbits receiving water only – the 'ideal comparison')

ImF vs. MF

ImF vs. MW

ImW vs. MF

As a summary, data of *some* of just the preliminary 'ideal comparison' for ImW vs. MW are shown in Tables 5.10 and 5.11. The full details of *all* the preliminary 'ideal comparison' for ImW vs. MW and the other combinations of preliminary comparisons are not shown (for conciseness) but were made with the data in section 5.3.1.

TABLE 5.10: Comparisons between Anaesthetised Rabbits of ImW vs. MW Groups, for Blood Pressure (MAP) and $C_{ft\text{-}ft}$ at the UpSt and DnSt Sites of Measurement in the Abdominal Aorta. NS = Not Significant for p>0.05

UpSt Site	Immature	Mature	Unpaired t-test
n	6	8	
MAP (Pa)	9127±1850	8242±1790	NS;p=0.38
$C_{ft\text{-}ft}$ ($m.s^{-1}$)	6.34±1.24	5.27±0.66	NS; p=0.058
DnSt Site			
n	6	8	
MAP (Pa)	8996±1712	8517±2136	NS;p=0.66
$C_{ft\text{-}ft}$ ($m.s^{-1}$)	7.58±0.85	5.28±062	p=0.003

TABLE 5.11: Comparisons between Anaesthetised Rabbits of ImW vs. MW Groups, for Wave Reflection Indices (WRI) of Compression and Expansion Waves at the UpSt and DnSt Sites of Measurement in the Abdominal Aorta. Not Significant for p>0.05

UpSt Site	Immature	Mature	Unpaired t-test
n	6	6	
WRI for Compression	0.035±0.028	0.286±0.222	p=0.021
WRI for Expansion	0.071±0.038	0.416±0.322	p=0.026
DnSt Site			
n	5	6	
WRI for Compression	0.060±0.078	0.320±0.217	p=0.032
WRI for Expansion	0.094±0.056	0.466±0.257	p=0.012

Some findings from the 'ideal comparison' of ImW vs. MW were interesting. Table 5.10 shows $C_{ft\text{-}ft}$ as greater in immature than in mature rabbits, the differences were nearly significant at the UpSt Site and reached significance at the DnSt Site. Furthermore, Table 5.11 shows reflection coefficients for compression and expansion waves at the UpSt and DnSt Sites as being significantly greater in mature than in immature rabbits. The results of *all* (i.e. ImW, MW, ImF, & MF) the combinations of comparisons between immature vs. mature revealed significant differences for many of the haemodynamic parameters measured; this is in marked contrast to the comparisons between fructose- and water-treated rabbits *within* the immature (no significant differences found) and *within* the mature (very few significant differences found) groups. Thus a possible age-effect exists in terms of immature vs. mature. With this in mind, along with the interesting findings from the 'ideal comparison' between ImW vs. MW (Tables 5.10 & 5.11), especially the unexpected finding of $C_{ft\text{-}ft}$ being greater in immature than in mature rabbits (Table 5.10), it was reasoned as valid to increase the immature and mature sample sizes by combining groups as discussed above. So data was pooled within the immature group and within the mature group, i.e. the immature group is ImW pooled with ImF; the mature group is MW pooled with MF.

Table 5.12 gives the basic pooled data. The external diameter ($Ø_{Ext}$) of the abdominal aorta at the UpSt Site is significantly greater in mature than that in immature rabbits – this is not surprising since the mature rabbits are physically larger than the immature ones; however, although the mean value of $Ø_{Ext}$ at the DnSt Site is also greater in mature than in immature rabbits, the difference does not reach statistical significance (Table 5.12). HR, SBP, DBP, PP_{TP}, and MAP are not significantly different between immature or mature rabbits. However, MABF measured at both UpSt and DnSt Sites in the abdominal aorta is significantly greater in mature than in immature rabbits, while VR is greater in the immature than in the mature rabbits - significant at the UpSt but not at the DnSt Site (Table 5.12).

The analysis for comparing immature vs. mature rabbits here by pooling data from water- and fructose-drinking treatments is perhaps not appropriate when considering parameters B, τ and P_∞ because these are the few parameters that did appear to be affected by fructose-drinking in mature rabbits (Table 5.3). However, these parameters were found not significantly different in the preliminary 'ideal comparison' between ImW vs. MW. Parameter A was not affected by fructose-drinking (Table 5.3) but its pooled data does differ significantly between immature and mature rabbits (Table 5.13); this was the case also when compared between immature and mature rabbits that had received only water-drinking treatment.

$\int$RP and PP_{RP} are discussed in Chapter 4 and stated as being indices of arterial compliance; however their relationship to MAP was not understood. Figure 5.10 compares the mean values of $\int$RP and PP_{RP} between immature and mature rabbits; the mean values of $\int$RP and PP_{RP} differ significantly between immature and mature rabbits; this was also found in the preliminary 'ideal comparison' between ImW vs. MW. Figure 5.11 and 5.12 show regression plots for MAP vs. $\int$RP (Figure 5.11) and MAP vs. PP_{RP} (Figure 5.12). $\int$RP did not correlate significantly with MAP at the UpSt or DnSt Sites in immature or mature rabbits, however at both sites the regression plots for MAP vs. $\int$RP in immature and mature rabbits were significantly different to each other (UpSt Site: $p=0.0004$; DnSt Site: $p=0.0007$; Figure 5.11), thus confirming the significant differences found for the mean values of $\int$RP between immature and mature groups (Figure 5.10). PP_{RP} correlated negatively and significantly with MAP in immature rabbits at the UpSt Site ($r=-0.808$; $p=0.003$) and at the DnSt Site ($r=-0.847$; $p=0.001$) (Figure 5.12); however, no significant correlation exists for MAP vs. PP_{RP} at the UpSt or DnSt Sites in mature rabbits (Figure 5.12). At both sites, the regression plots for MAP vs. PP_{RP} in immature and mature rabbits were significantly different to each other (UpSt Site: $p<0.0001$; DnSt Site: $p=0.0001$; Figure 5.12), thus confirming the significant differences found for the mean values of PP_{RP} between immature and mature groups (Figure 5.10). Data for calculated AC (re: $AC = \tau / VR$) are shown in Figure 5.13 which shows no significant difference for AC between immature and mature rabbits. This analysis was made difficult due to paucity of data resulting from poor algorithm fitting to Type 2 blood pressure waveforms (section 5.3.1; Table 5.4). Figure 5.14 shows regression analysis for MAP vs. AC of immature and mature rabbits at the UpSt Site of measurement; analysis was not attempted at the DnSt Site due to paucity of data as just explained. The correlation coefficients for MAP vs. AC were statistically significant for immature rabbits ($r=0.886$; $p=0.019$) and mature rabbits ($r=-0.600$; $p=0.018$). The correlation coefficient was positive for immature rabbits; this is surprising since AC is expected to decrease with increasing MAP as is observed for the mature rabbits for which a negative correlation was found.

TABLE 5.12: Basic Data (Mean±SD) for Age, Body Weight (BW), External Aorta Diameter ($Ø_{Ext}$), Heart Rate (HR), Systolic (SBP), Diastolic (DBP), Pulse Pressure (PP_{TP}) Mean (MAP) Aortic Arterial Blood Pressures, Mean Aortic Blood Flow (MABF), and Vascular Resistance (VR) at the UpSt and DnSt Sites of Measurement in the Abdominal Aorta of Immature and Mature Anaesthetised Rabbits. Data are pooled from Treatment Groups. Comparisons made between Immature and Mature at respective UpSt Site or DnSt Site; p by unpaired t-test; NS=not significant at p>0.05.

	UpSt Site		DnSt Site	
	Immature	Mature	Immature	Mature
n	11	16	11	16
Age (month)	3.28±0.05	8.97±0.66 p<0.0001	-	-
BW (kg)	2.76±0.26	3.88±0.52 p<0.0001	-	-
$Ø_{Ext}$ (mm)	4.02±0.08	4.28±0.26 p=0.003	2.68±0.34	2.91±0.27 NS;p=0.07
HR (beats/min)	227±28	234±22 NS;p=0.46	231±27	239±25 NS;p=0.44
SBP (Pa)	9895±2084	10294±1782 NS;p=0.6	10059±2009	10671±2010 NS;p=0.44
DBP (Pa)	7578±1898	7960±1457 NS;p=0.56	7500±1794	8032±1602 NS;p=0.43
PP_{TP} (PP_{TP}=SBP-DBP) (Pa)	2318±373	2334±519 NS;p=0.93	2558±476	2639±675 NS;p=0.74
MAP (Pa)	8545±1936	8974±1550 NS;p=0.53	8497±1833	9100±1711 NS;p=0.39
MABF $x10^{-6}$ (m^3/s)	1.71±0.57	2.35±0.63 p=0.01	0.69±0.26	1.00±0.35 p=0.03
VR $x10^9$ (VR=MAP/MABF) ($N.m^{-5}.s$)	5.25±1.03	3.95±0.85 p=0.002	13.76±4.93	10.59±5.30 NS;p=0.14

TABLE 5.13: Data (Mean±SD) for Parameter A Derived from Calculation of Reservoir (Windkessel) Pressure from Aortic Pressure at the UpSt and DnSt Sites of Measurement in the Abdominal Aorta of Anaesthetised Immature and Mature Rabbits. Data pooled from Treatments. Comparisons made between Immature and Mature; p by unpaired t-test; not significant p>0.05

	UpSt Site		DnSt Site	
Parameter	Immature	Mature	Immature	Mature
A	0.028±0.0319 n=11	0.078±0.045 p=0.004 n=16	0.024±0.032 n=11	0.088±0.060 p=0.004 n=16

Where: A = rate constant (s^{-1})

FIGURE 5.10: $\int$RP and PP_{RP} (Mean±SD) at the UpSt & DnSt Sites of Recording in the Abdominal Aorta of Immature and Mature Anaesthetised Rabbits. Data Pooled from Treatments. Comparisons made between Immature and Mature, p by unpaired t-test. not significant p>0.05

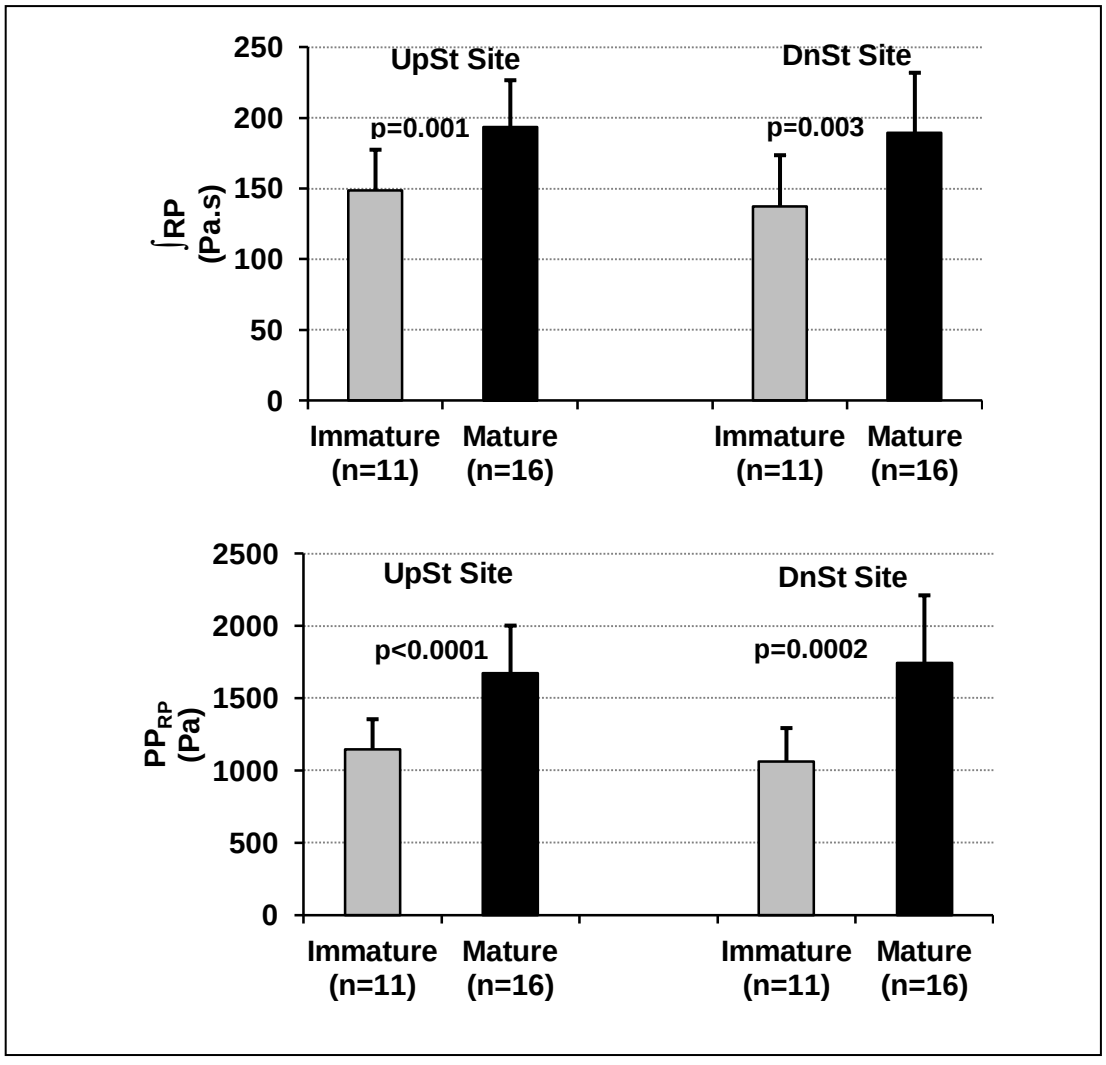

FIGURE 5.11: Comparisons of Regression Plots for ∫RP at the UpSt & DnSt Sites of Measurement in the Abdominal Aorta of Immature and Mature Anaesthetised Rabbits. Data Pooled from Treatments. Test of Correlation: NS not significant for p>0.05
Note: correlations not significant but regression plots are significantly different – see text.

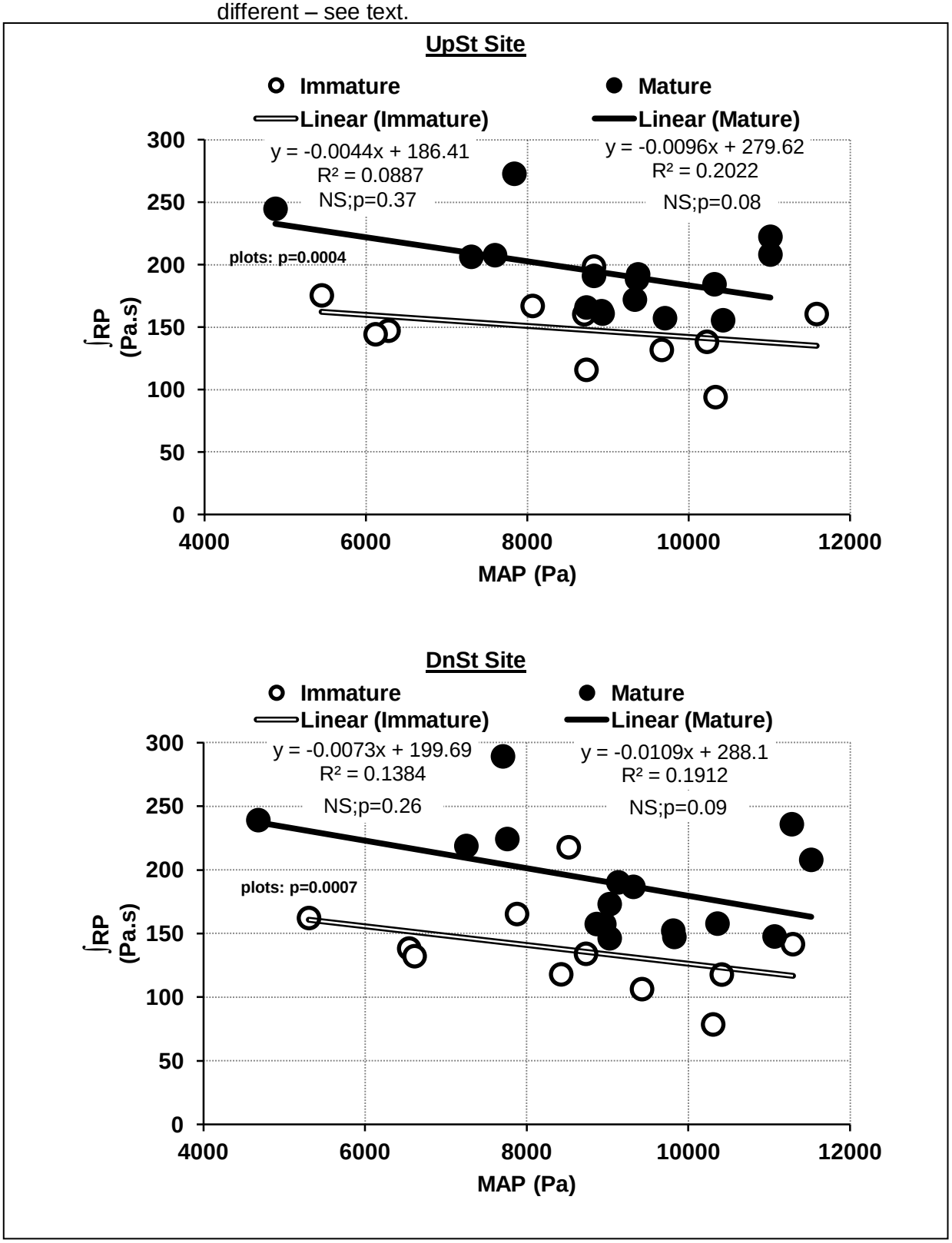

FIGURE 5.12: Comparisons of Regression Plots for PP_{RP} at the UpSt & DnSt Sites of Measurement in the Abdominal Aorta of Immature and Mature Anaesthetised Rabbits. Data Pooled from Treatments. Test of Correlation: NS not significant at p>0.05

Note: correlations significant only for Immature Rabbits but regression plots differ significantly – see text.

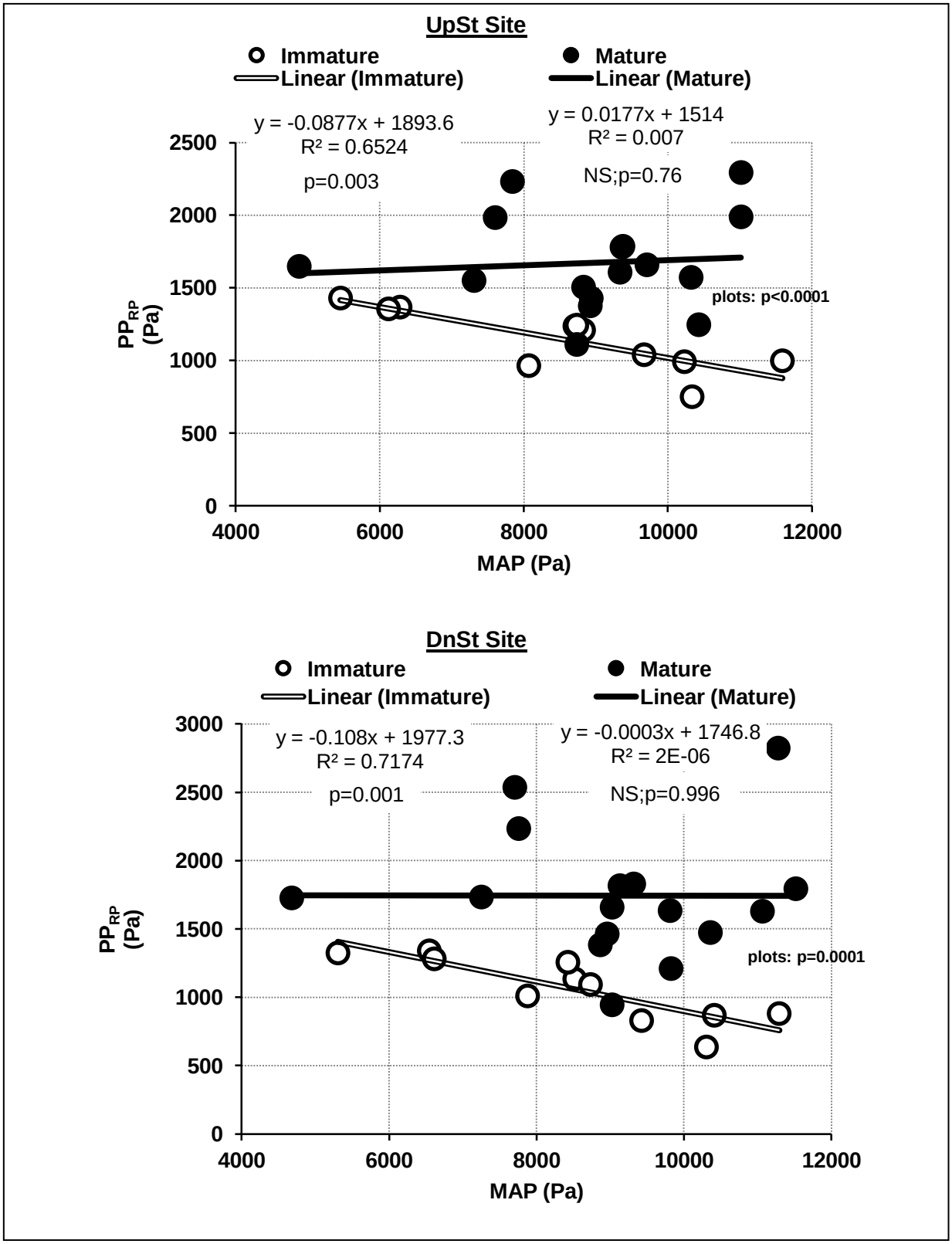

FIGURE 5.13: Data (Mean±SD) for Calculated Arterial Compliance (AC) at the UpSt and DnSt Sites of Measurement in the Abdominal Aorta of Immature* and Mature Anaesthetised Rabbits. Data Pooled from Treatments; Comparisons made between Immature and Mature; p by unpaired t-test; NS=not significant at p>0.05

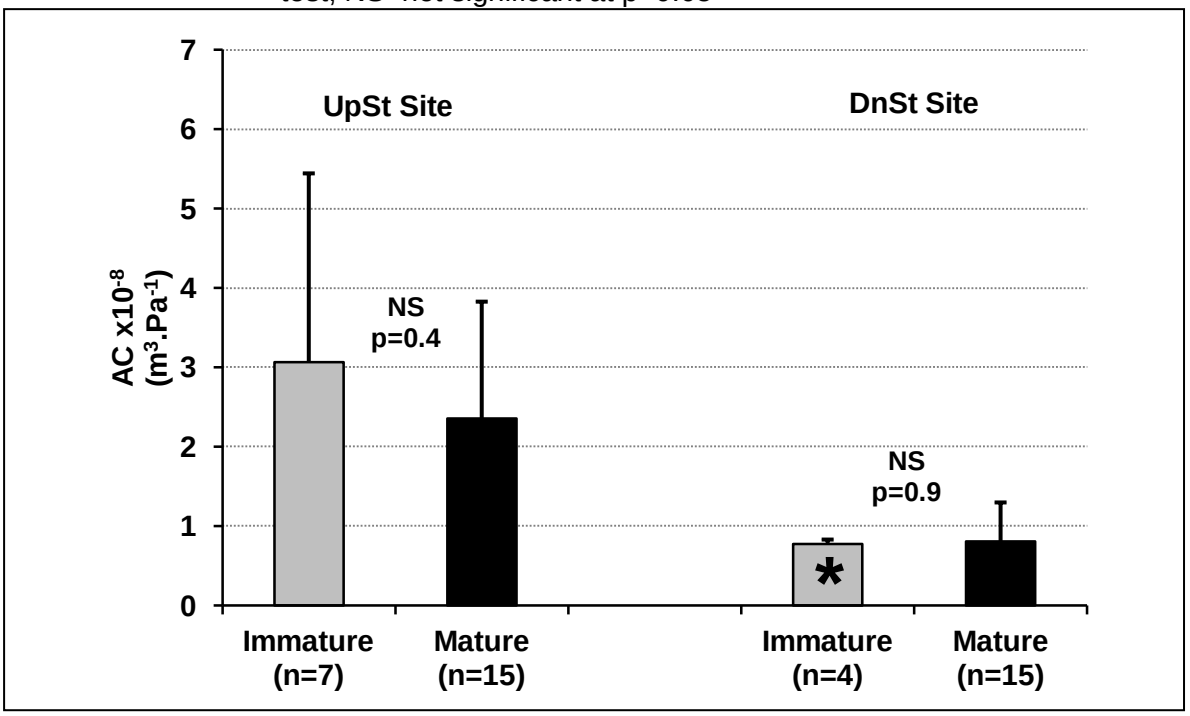

*Data sparse for Immature at DnSt Site having only data from fructose treatment; this is included but is not appropriate for true comparisons.

FIGURE 5.14: Comparisons of Regression Plots for Arterial Compliance (AC) at the UpSt Site of Measurement in the Abdominal Aorta of Immature and Mature Anaesthetised Rabbits. Data Pooled from Treatments. Test of Correlation: not significant at p>0.05

Note: correlations significant but positive regression plot for Immature is surprising – see text.

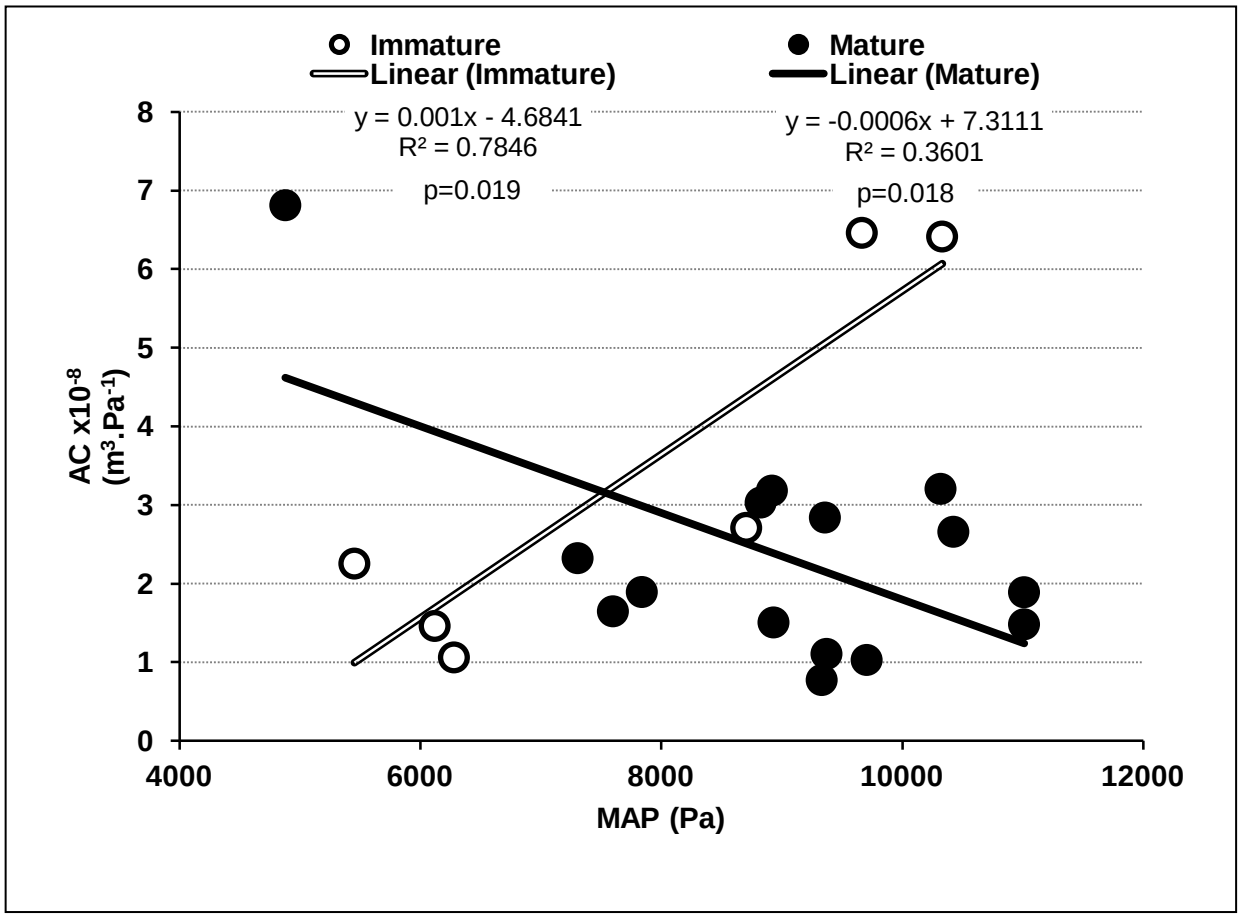

Figure 5.15 gives mean data for RHDN (this term is discussed fully in Chapter 4), and Table 5.14 gives mean values for the time (Tn) of the incisura inflection after end-diastole (end-diastole being the start of systole). The mean value for RHDN is significantly higher in mature rabbits than that in immature rabbits; Tn is not significantly different between immature and mature rabbits. These findings for RHDN and Tn were true also in the preliminary 'ideal comparison' of ImW vs. MW.

Group mean $C_{ft\text{-}ft}$ was not significantly different between immature and mature rabbits at the UpSt Site of measurement in the abdominal aorta (Figure 5.16). However, at the DnSt Site, $C_{ft\text{-}ft}$ was significantly greater ($p=0.007$) in immature than in mature rabbits (Figure 5.16). These findings for $C_{ft\text{-}ft}$ of the pooled data agree with those of the preliminary 'ideal comparison' of ImW vs. MW (Table 5.10). Regression plots for MAP vs. $C_{ft\text{-}ft}$ at the UpSt and DnSt Sites of measurement are shown in Figure 5.17. MAP vs. $C_{ft\text{-}ft}$ correlated significantly in immature rabbits at the UpSt ($r=0.8995$; $p=0.0002$) and at the DnSt Site ($r=0.763$; $p=0.006$) but not in mature rabbits at either site (Figure 5.17); regression plots differed significantly at the UpSt ($p=0.002$) and DnSt Sites ($p=0.0005$).

The three wave speeds, $C_{ft\text{-}ft}$, C_{Tpu} and C_{Wpu} were compared (Figure 5.18) *within* immature rabbits and *within* mature rabbits. In both groups the rabbits considered were only those in which the three wave speeds had been measured. Furthermore, comparison of the three wave speeds was made *between* the immature and mature groups. The statistical comparisons were made using two-way ANOVA separately for the UpSt Site and DnSt Site. It was found that *within* both the immature and mature groups, at both the UpSt and DnSt Sites, there was no statistically significant difference between the three wave speeds, thus supporting the null hypothesis that $C_{ft\text{-}ft}$, C_{Tpu} and C_{Wpu} do not differ. However, the two-way ANOVA comparison test indicated a difference *between* immature and mature rabbits at the DnSt Site, where unpaired t-test confirmed a significant difference only for $C_{ft\text{-}ft}$ between immature and mature rabbits, $C_{ft\text{-}ft}$ being greater in the immature group than in the mature group (Figure 5.18); this agrees with the data in Figure 5.16 with additional mature rabbits, and also agrees with the data in Table 5.10 for the preliminary 'ideal comparison' of ImW vs. MW.

FIGURE 5.15: RHDN (Mean±SD) at the UpSt and DnSt Sites of Measurement in the Abdominal Aorta of Immature and Mature Anaesthetised Rabbits. Data Pooled from Treatments. Comparisons made between Immature and Mature; p by unpaired t-test; not significant at p>0.05

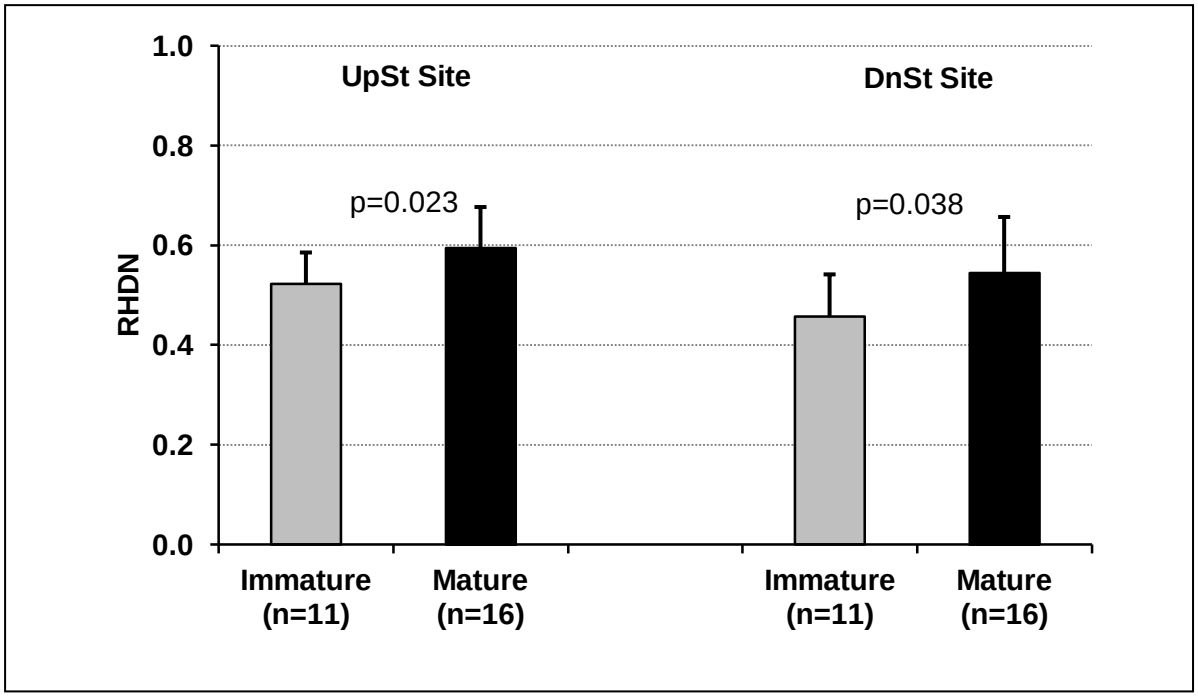

TABLE 5.14: Data for Tn in Immature and Mature Anaesthetised Rabbits at the UpSt and DnSt Sites of Measurement in the Abdominal Aorta. Data pooled from Treatments. Values are Mean ± SD; p by unpaired t-test Immature vs. Mature, NS = not significant at p>0.05.

Tn (ms)			
UpSt Site		DnSt Site	
Immature (n=11)	Mature (n=16)	Immature (n=11)	Mature (n=16)
103.4±12.7	102.6±8.5 NS;p=0.83	100.8±12.5	101.9±9.7 NS;p=0.8

Tn: time of the incisura inflection after end-diastole

FIGURE 5.16: C_{ft-ft} (Mean±SD) at the UpSt and DnSt Sites of Measurement in the Abdominal Aorta of Immature and Mature Anaesthetised Rabbits. Data Pooled from Treatments. Comparisons made between Immature and Mature; p by unpaired t-test; NS=not significant at p>0.05

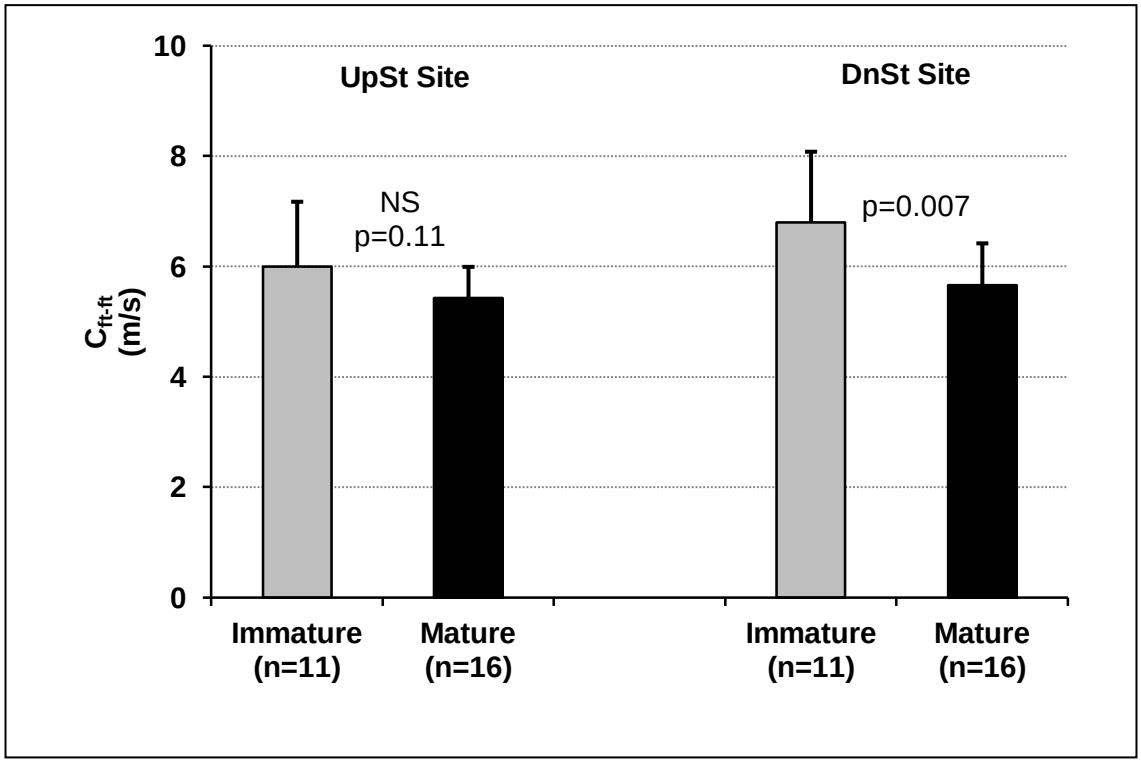

FIGURE 5.17: Comparisons of Regression Plots for C_{ft-ft} vs. MAP at the UpSt and DnSt Sites of Measurement in the Abdominal Aorta of Immature and Mature Anaesthetised Rabbits. Data Pooled from Treatments. Test of Correlation and Differences between Regression Plots:
NS = Significant at p>0.05

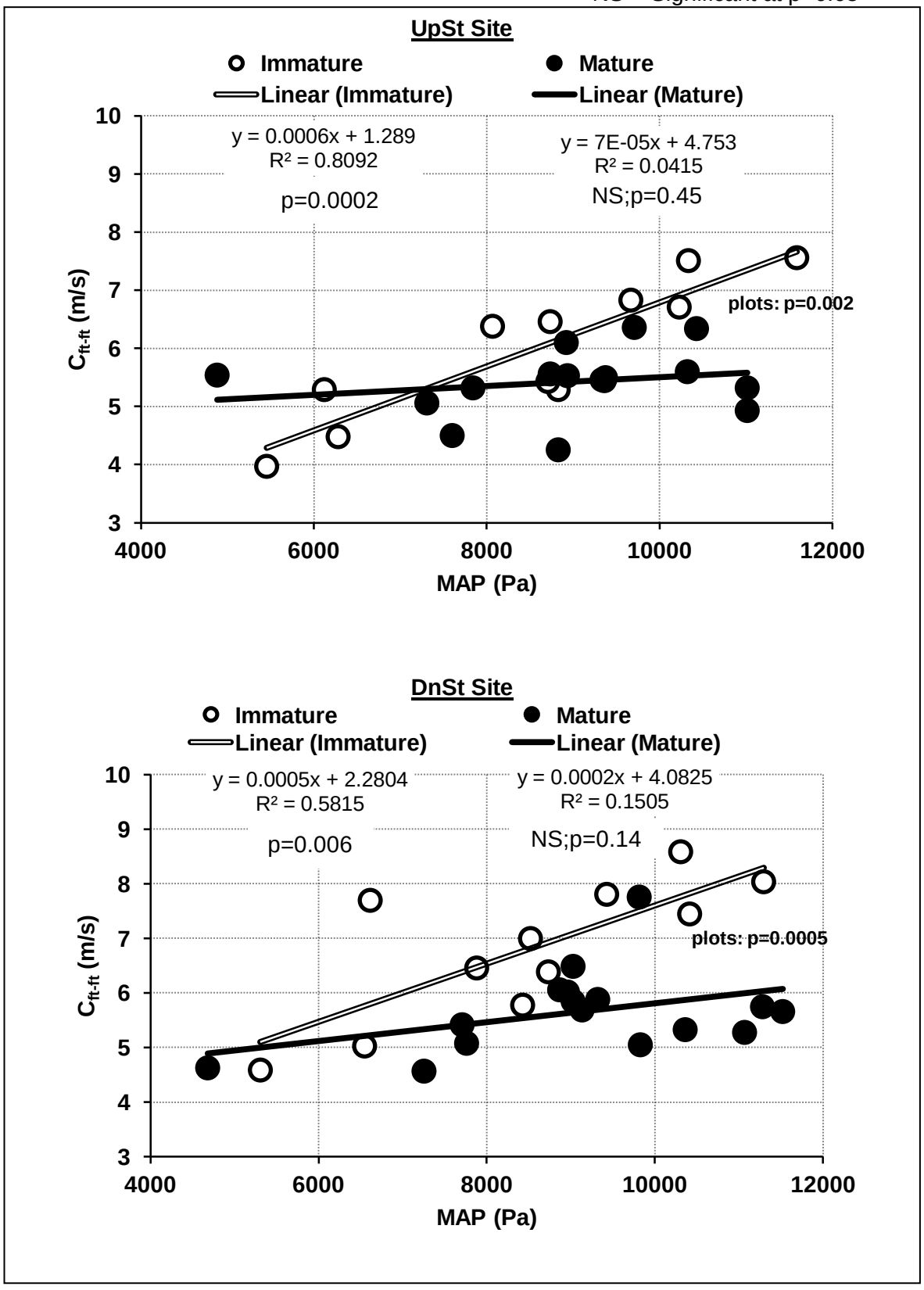

FIGURE 5.18: Comparisons made between $C_{ft\text{-}ft}$, C_{Tpu} and C_{Wpu} (Mean±SD) at the UpSt and DnSt Sites of Measurement in the Abdominal Aorta of Anaesthetised Immature and Mature Rabbits; Data pooled from Treatment Groups; Statistical Comparisons made with unpaired t-test and Two-Way ANOVA; NS = not significant at p>0.05
Rabbits considered were those in which all three wave speeds were measured.

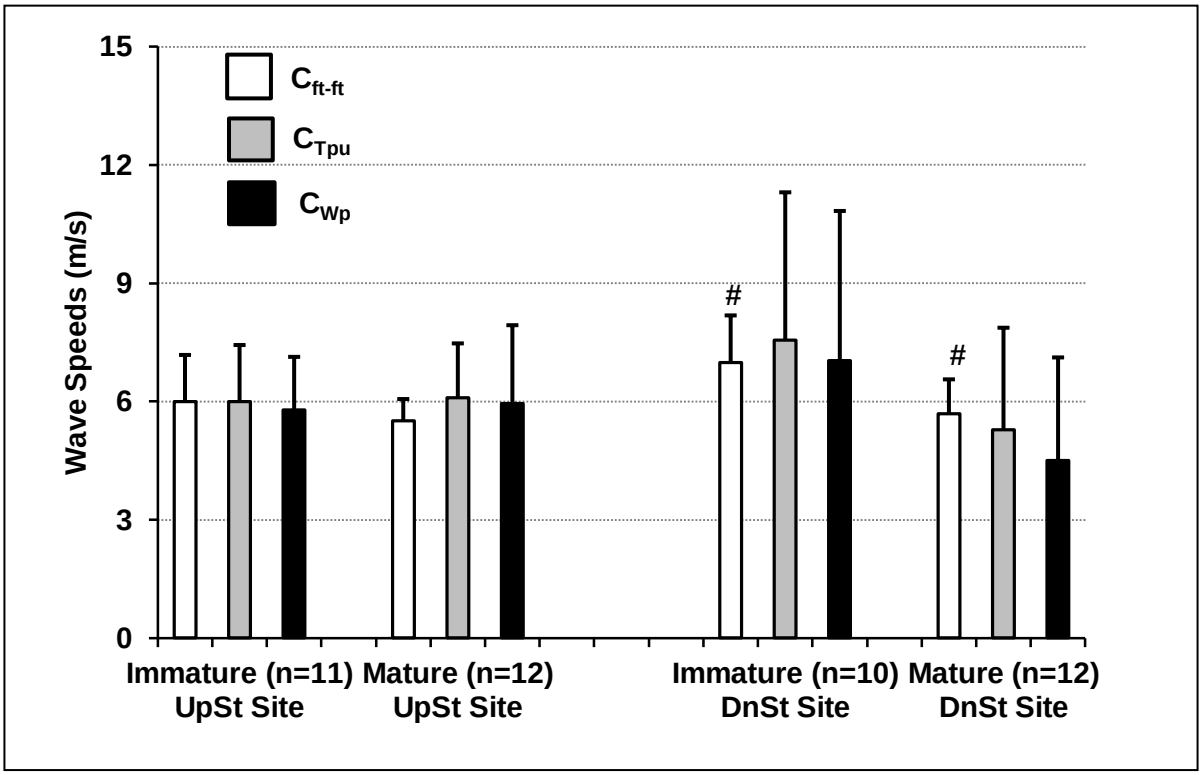

Only at DnSt Site and only for $C_{ft\text{-}ft}$, Immature vs. Mature p=0.008 by unpaired t-test, all others were NS i.e. p>0.05.

Note: UpSt and DnSt Sites, *within* Immature group and *within* Mature group, comparison by two-way ANOVA of $C_{ft\text{-}ft}$ vs. C_{Tpu} vs. C_{Wpu} showed NS i.e. p>0.05, thus indicating that $C_{ft\text{-}ft}$ = C_{Tpu} = C_{Wpu} at both sites and this supports the null hypothesis that the three wave speeds are not different. Two-way ANOVA *between* Immature and Mature groups detected the difference for $C_{ft\text{-}ft}$ DnSt Site.

Analysis by 2-way ANOVA:

	UpSt Site	DnSt Site
Interaction p-value	NS; 0.68	NS; 0.72
Column Factor p-value	NS; 0.75	NS; 0.69
Row Factor p-value	NS; 0.81	0.003 (confirms #)

Wave intensity analysis (WIA) revealed no significant difference between immature and mature rabbits for incident compression and incident expansion waves at the UpSt and DnSt Sites of measurement in the abdominal aorta (Figure 5.19); whereas there was a significant difference between immature and mature rabbits for reflected compression and reflected expansion waves at the UpSt Site but not at the DnSt Site of measurement (Figure 5.19). However, wave energy data expressed as wave reflection indices (WRI) (i.e. reflected wave energy / incident wave energy – Figure 5.20) revealed differences between immature and mature rabbits in that immature rabbits have significantly less reflections of compression and expansion waves than do mature rabbits (Figure 5.20); this was also found for the preliminary 'ideal comparison' of ImW vs. MW (Table 5.11).

The relationship between compression and expansion WRI with RHDN (RHDN is defined in Chapter 4) in the abdominal aorta of immature and mature rabbits is explored in Figures 5.21 (UpSt Site) and 5.22 (DnSt Site). At the UpSt Site of measurement (Figure 5.21), compression WRI correlated positively and significantly with RHDN in immature ($r=0.746$; $p=0.008$) and mature ($r=0.757$; $p=0.004$) rabbits but the plots for immature and mature rabbits did not differ significantly. A similar relationship was found for expansion WRI with RHDN in immature ($r=0.662$; $p=0.027$) and mature ($r=0.713$; $p=0.009$) rabbits – again the plots for immature and mature did not differ significantly (Figure 5.21). At the DnSt Site of measurement (Figure 5.22), positive correlations were found between compression WRI with RHDN though not significant in immature ($r=0.423$; NS $p>0.05$) but significant in mature ($r=0.731$; $p=0.007$) rabbits; the plots did not differ significantly between immature and mature rabbits. Expansion WRI correlated positively with RHDN at the DnSt Site, though not significantly in immature ($r=0.263$; NS $p>0.05$) but significantly in mature ($r=0.733$; $p=0.007$) rabbits; here the plots did differ significantly ($p=0.02$) between immature and mature rabbits (Figure 5.22). Correlations between WRI with RHDN are more convincing in mature than in immature rabbits; in the former the data points spread more widely whereas in the latter the data points cluster at the lower values (Figures 5.21 & 5.22). The relationships are not remarkably different between immature and mature rabbits. As was found in Chapter 4, RHDN in the abdominal aorta is affected by wave reflections in this vessel, such that abdominal aortic RHDN increases with increased reflections.

Distances to reflection sites (Figure 5.23) at the UpSt and DnSt Sites of measurement in the abdominal aorta did not differ significantly between immature and mature rabbits, despite the difference in body size.

FIGURE 5.19: Compression and Expansion Wave Energies (Mean±SD) at the UpSt and DnSt Sites of Measurement in the Abdominal Aorta of Anaesthetised Immature and Mature Rabbits. Data Pooled from Treatment Groups. Comparisons made between Immature and Mature; p by unpaired t-test; NS = not significant at p>0.05

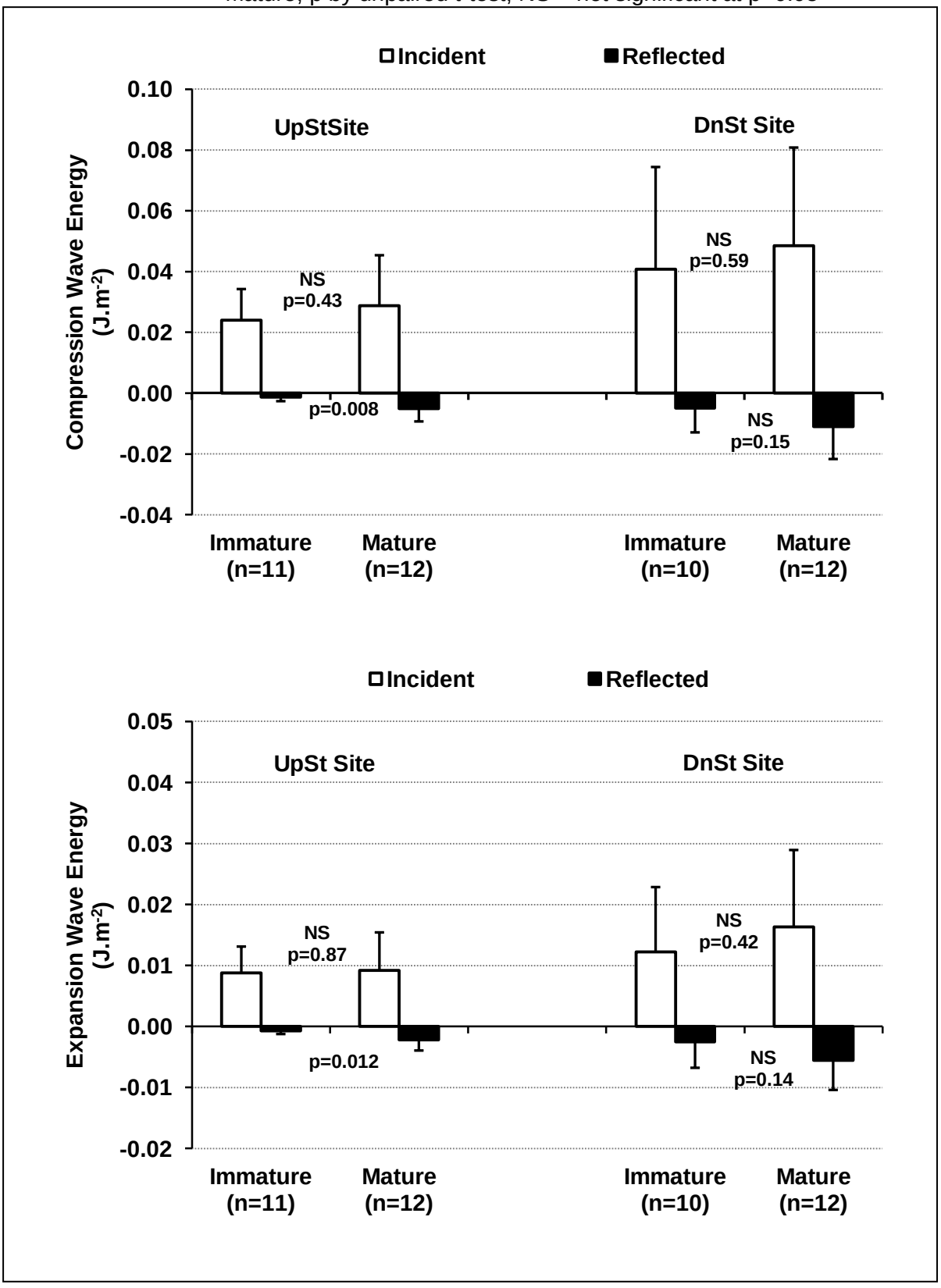

FIGURE 5.20: Wave Reflection Indices (WRI) (Mean±SD) for Compression and Expansion Waves at the UpSt and DnSt Sites of Measurement in the Abdominal Aorta of Anaesthetised Immature and Mature Rabbits. Data Pooled from Treatment Groups. Comparisons made between Immature and Mature; p by unpaired t-test; not significant at p>0.05

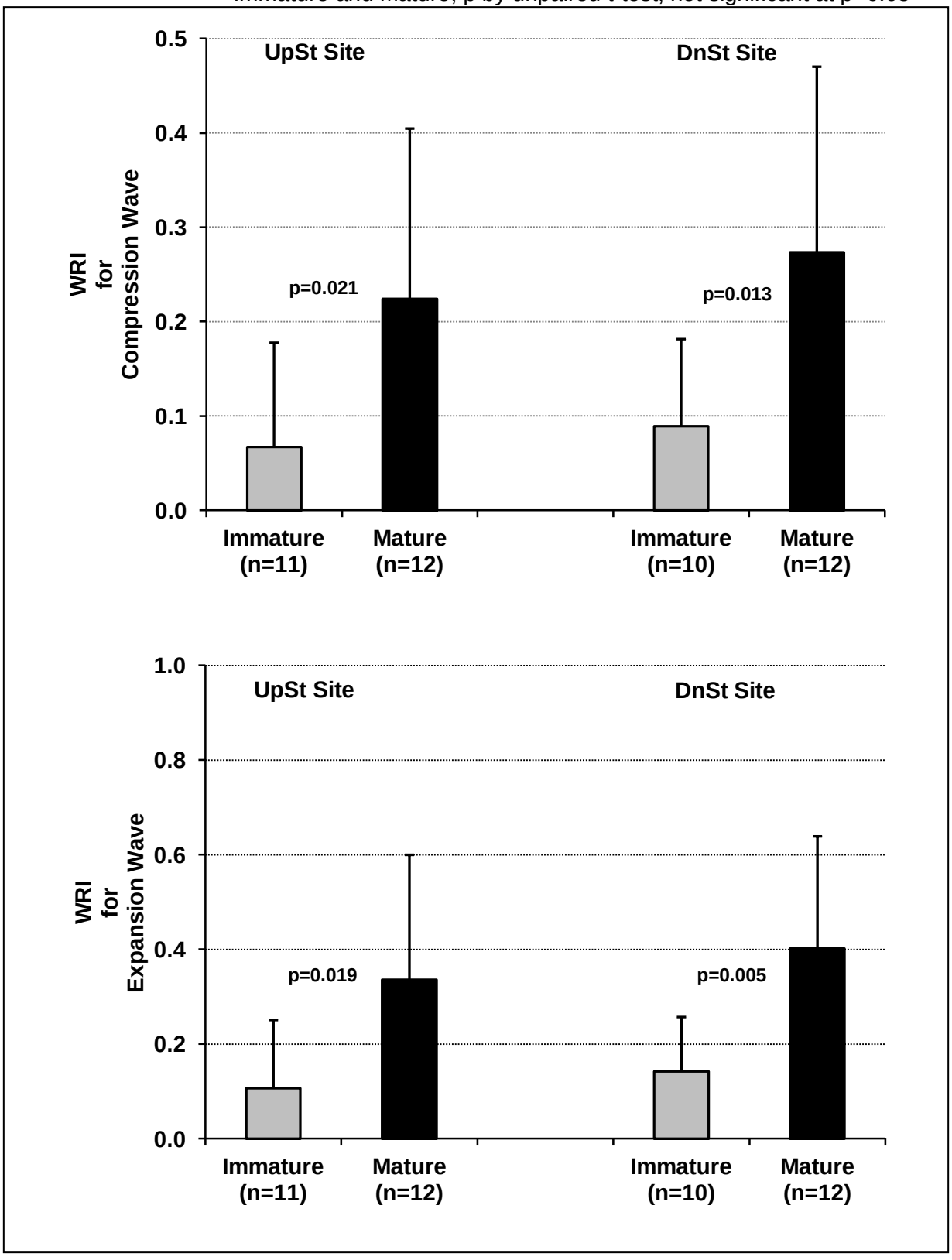

FIGURE 5.21: Relationship Between Wave Reflection Indices (WRI) for Compression and Expansion Waves with RHDN at the UpSt Site in the Abdominal Aorta of Anaesthetised Immature and Mature Rabbits; NS = not significant at p>0.05

Note: significant correlations but regression plots are not significantly different between Immature and Mature rabbits – see text.

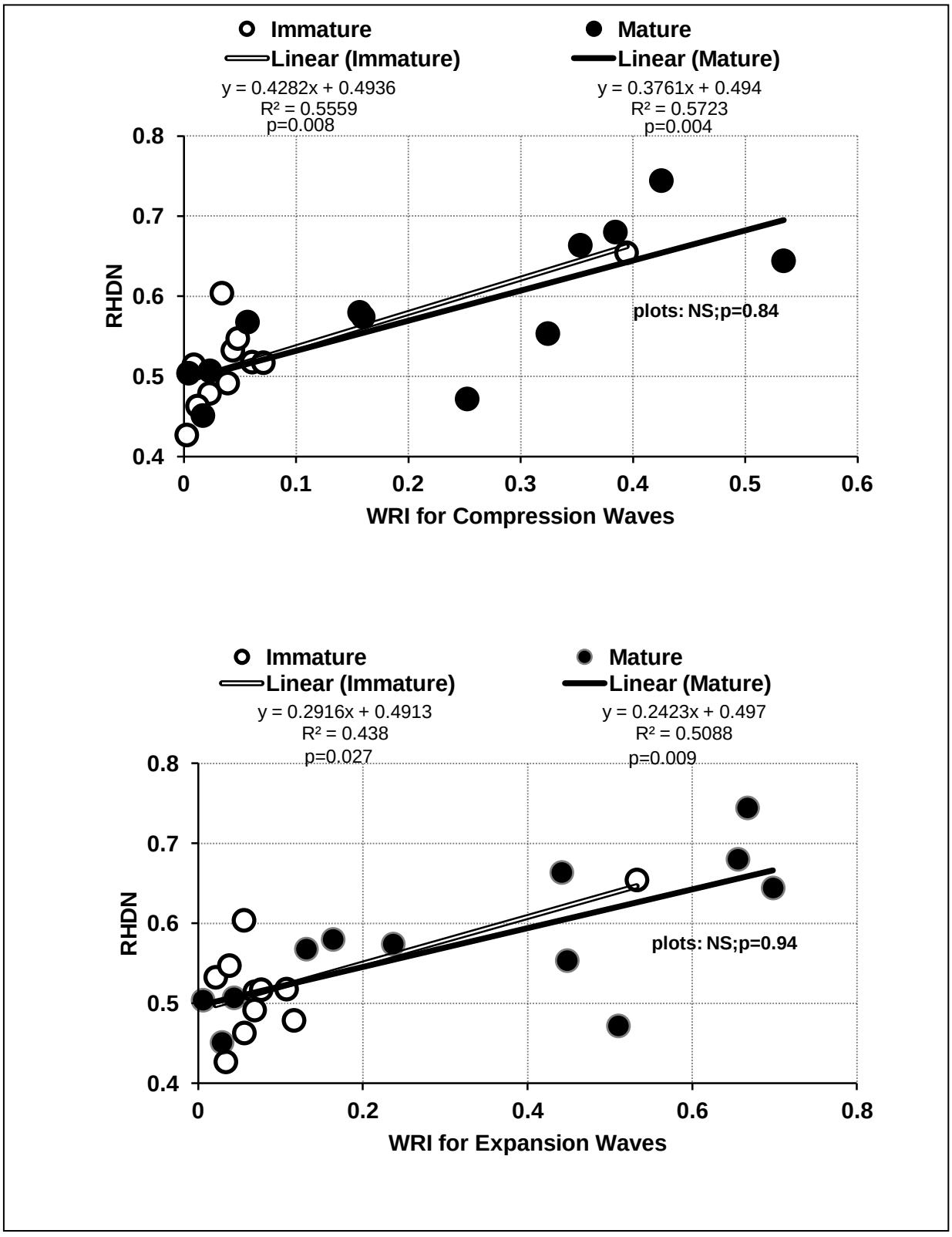

FIGURE 5.22: Relationship Between Wave Reflection Indices (WRI) for Compression and Expansion Waves with RHDN at the DnSt Site in the Abdominal Aorta of Anaesthetised Immature and Mature Rabbits; NS is not significant at p>0.05

Note: correlations significant for Mature rabbits; regression plots significantly different for expansion waves between Immature and Mature rabbits – see text.

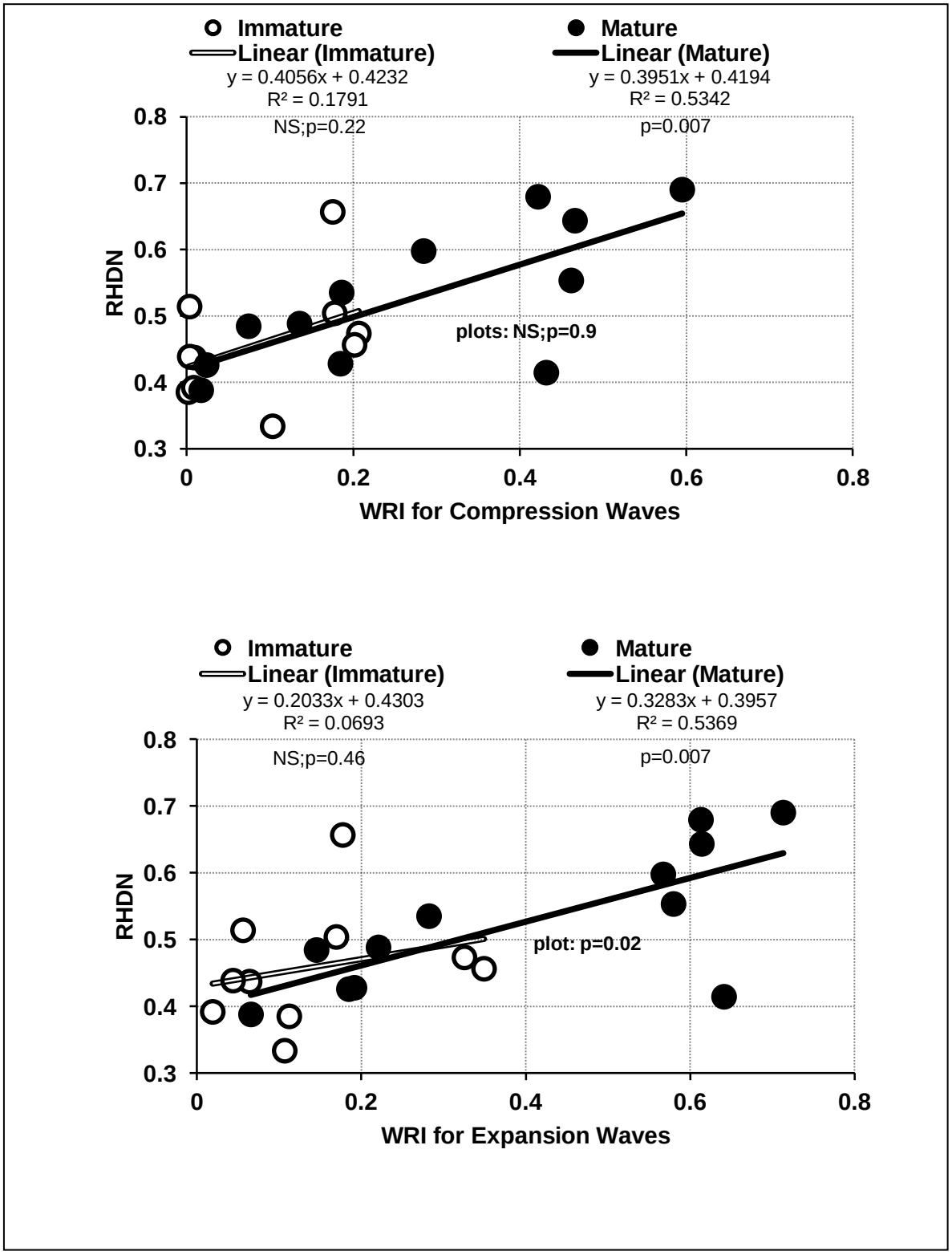

FIGURE 5.23: Distances (Mean±SD) of Reflection Sites from Sites of Recording (i.e. UpSt & DnSt Sites) as estimated from the time lapse between Incident and Reflected Intensities of the Compression Wave in the Abdominal Aorta of Anaesthetised Immature and Mature Rabbits. Data Pooled from Treatment Groups. Comparisons made between Immature and Mature; p by unpaired t-test; NS = not significant at p>0.05

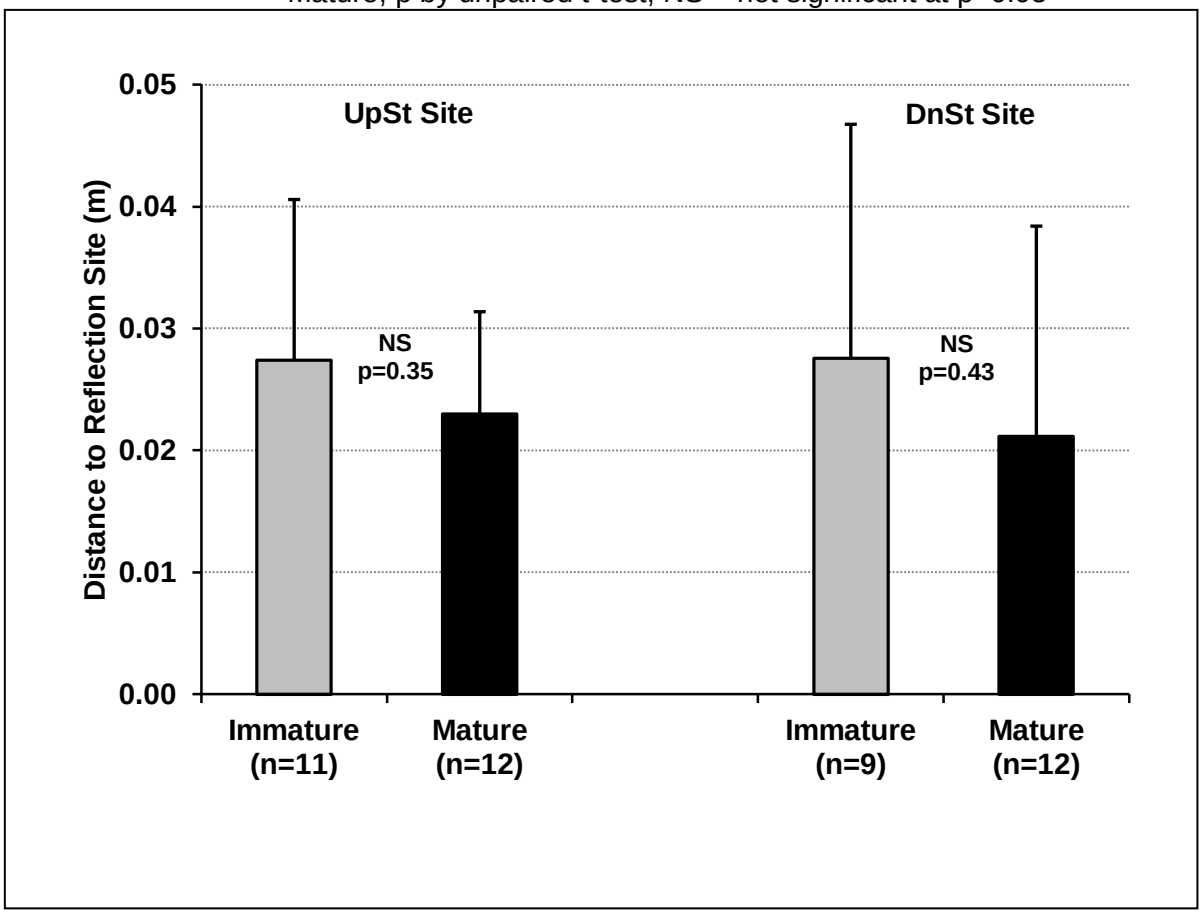

5.4 DISCUSSION

The experimental protocol applied a 2 week period of administration of fructose solution (10% w/v aq.) followed by a 2 week period off fructose solution when the latter was replaced with drinking water – this served as a period of washout. Lin *et al*. (2004) used a 2 week period of administration of 10% fructose solution to rats, though did not then use a 2 week period off fructose, and observed significantly altered haemodynamic status (e.g. increased aortic characteristic impedance and decreased wave transit time) in fructose treated rats compared to water treated controls. As already stated in the Introduction (section 5.1), Mikulíková *et al*. (2008) treated rats for three weeks with 10% fructose solution in their drinking supply which resulted in tenfold increase in the AGE, pentosidine, in the aortas of the treated rats. Thus, it appears that short, namely 2 – 3 week, periods of treatment of rats with fructose causes haemodynamic changes indicative of stiffened arteries and AGE formation. A protocol of short-term (2 weeks) fructose treatment of immature and mature rabbits was attempted for this thesis.

Treatment of mature rabbits with fructose had no statistically significant effect on most of the parameters measured. The few affected parameters were B, τ, P_∞ (Table 5.3 UpSt Site) and B (Table 5.3 DnSt Site); in one data set $C_{ft\text{-}ft}$ appeared affected by fructose treatment (Table 5.7 DnSt Site) but in another data set (Table 5.8 DnSt Site) the effect was not statistically significant. Treatment of immature rabbits with fructose had no statistically significant effect on any of the parameters measured. With both mature and immature rabbits there were a few parameters where fructose might have had effect on them but the effects did not quite reach statistical significance where p was $0.1>p>0.05$, or fructose did have a significant effect, or effects were of a trend but, whichever, deserve further investigation; these were blood pressure (Table 5.1), τ (Table 5.3), P_∞ (Table 5.3), calculated AC (Table 5.5), RHDN (Table 5.6), $C_{ft\text{-}ft}$ (Table 5.7) and PU loop derived wave speeds (Tables 5.8 & 5.9).

It could be argued for the lack of effect of fructose that 10% fructose solution was not sufficient for adequate exposure to the vascular system. However, there is abundant evidence in the literature that 10% fructose solution is an effective treatment for changing haemodynamic and vascular wall function in rats (Dai and McNeill, 1995; Lin *et al*., 2004; Chang *et al*., 2007; Mikulíková *et al*. 2008) and rabbits (Naka *et al*., 1998; Tokita *et al*., 2005; Akira *et al*., 2006). The overall lack of effect of fructose might be explained by the fact that fructose treatment was withdrawn for the two weeks prior to haemodynamic measurements. Dai and McNeill (1995) have shown that hypertension induced by 10% fructose drinking is

short-lived in rats; after withdrawal of fructose treatment, normal blood pressure returned rapidly. In the studies of this thesis, fructose was required for formation of AGEs in the aortic and conduit vessel walls. Fructose is a potent producer of AGEs (Akira *et al*., 2006; Schalkwijk *et al*., 2004). It was assumed, based on reports from the literature (Brownlee *et al*., 1988), that formation of AGEs is a non-reversible process and so it was believed that AGEs would still be present after two weeks washout period. Perhaps formation of AGEs did occur in the walls of the aorta and conduit arteries in the fructose treated rabbits (mature and immature) but not sufficiently enough over two weeks to have had impact on haemodynamic function. Tokita *et al*. (2005) and Akira *et al*. (2006) treated rabbits for eight weeks with 10% fructose solution for deposition of AGEs in the aortic walls.

Although the results for fructose-drinking treatment of mature and of immature rabbits were inconclusive, the studies were extended to comparisons of haemodynamic data between immature and mature rabbits. The four treatment groups, immature water-treated (ImW), mature water-treated (MW); immature fructose-treated (ImF) and mature fructose-treated (MF) were compared in combinations of immature vs. mature – these comparisons were referred to as *preliminary* comparisons.

As stated in section 5.3.2, comparison between the water-treated immature and water-treated mature rabbits is ideal (ImW vs. MW - referred to as the 'ideal comparison'), thereby omitting unknown and unmeasured effects of fructose. This 'ideal comparison' was carried out as a preliminary comparison along with the other preliminary comparisons. Data from *only* the 'ideal comparison' is summarised in Tables 5.10 & 5.11 which revealed differences between immature and mature rabbits for $C_{ft\text{-}ft}$ (greater in immature) and reflection coefficients (greater in mature). The other preliminary comparisons between the different age groups, i.e. immature vs. mature, revealed significant differences for many of the haemodynamic parameters measured (not listed for conciseness); this is in marked contrast to the comparisons between fructose- and water-treated rabbits *within* the immature and *within* the mature groups where no (immature rabbits) or very few (mature rabbits) significant differences were found. Thus, it is reasoned that age has an effect on those parameters that differed between immature and mature rabbits, i.e. those parameters changed as a function of age rather than a function of treatment. It was decided therefore, since fructose-treatment had virtually no significant effects, to pool the data of the two treatment groups within immature and within mature groups, i.e. the immature group is ImW pooled with ImF; the mature group is MW pooled with MF. Since both immature and mature groups would include data from fructose-treatment, it was accepted that the populations were balanced and that the increased group sizes would confer advantage to the analyses.

Of the basic haemodynamic parameters (Table 5.12), MABF was significantly less in immature than in mature rabbits, however this is likely a function of difference of physical size, or weight, between immature and mature rabbits. If the mean values (Table 5.12) of MABF are divided by the mean values of body weight, coefficients obtained at the UpSt Site of measurement are 0.62×10^{-6} for immature and 0.61×10^{-6} for mature rabbits and at the DnSt Site 0.25×10^{-6} and 0.26×10^{-6} for immature and mature rabbits respectively. The similarities of these coefficients indicate no difference in MABF between immature and mature rabbits when corrected for body weight. VR is greater in immature than in mature rabbits ($p=0.002$ at UpSt Site; NS at DnSt Site) and this is likely related to the arteriolar cross-sectional area being smaller in immature than in mature rabbits, since the latter are physically larger rabbits and so will have a greater arteriolar network (Milnor, 1989).

Parameter A (Table 5.13), which is a rate constant for fitting the systolic increase of reservoir (Windkessel) pressure, had a significantly smaller value in immature than in mature rabbits; this is difficult to explain. However, parameter A being associated with reservoir (Windkessel) pressure is thus associated with $\int RP$ and PP_{RP}, the values of which were also significantly less in immature than mature rabbits (Figure 5.10).

That $\int RP$ and PP_{RP} were significantly less in immature than mature rabbits (Figure 5.10) is of interest since $\int RP$ and PP_{RP} are considered indices of arterial compliance in that they are inversely related to arterial compliance (Chapter 4). PP_{RP} increases with age in humans (Davies *et al*., 2010) indicating a reduction of arterial compliance with increasing age; this appears likewise here with rabbits where PP_{RP}, like $\int RP$, increased with age (i.e. immature age to mature age); however, it must be emphasised that here with rabbits it is transition from immaturity to maturity, <u>*not*</u> as in the human studies of Davies *et al*. (2010) of transition from young (~35years) to elderly (~73years). As in Chapter 4, the relationship of $\int RP$ and PP_{RP} with blood pressure is not understood as regressions of $\int RP$ and PP_{RP} should show the two parameters increasing with increasing blood pressure but this was not found (Figures 5.11 & 5.12). However, an explanation could be that as MAP increased so the aortic diameter might have increased too as the aorta distends in passive response to the increased MAP – increasing aortic diameter decreases aortic characteristic impedance and so decreases pulse pressure (Hu *et al*., 1997; Mitchell, 2009); thus PP_{RP} would decrease too as it is a component of pulse pressure – the other component being wave pressure. The quadratic-like relationship of $\int RP$ and PP_{RP} with MAP (Figure 4.22) was not seen in these experiments with immature or mature rabbits. The regression analyses in Figures 5.11 &

5.12 for $\int RP$ and PP_{RP} respectively, show regression plots that are significantly different between immature and mature rabbits; the two plots lie within the same range of MAP, yet the plot for immature rabbits lies within values of $\int RP$ and PP_{RP} which are below those values of the plot for mature rabbits so confirming the finding in Figure 5.10 and implying that immature rabbits have a greater arterial compliance than do mature rabbits.

The lack (see section 5.3.1) of data for calculated AC makes it difficult to analyse this parameter, save to say that AC is expected to be greater in immature than in mature rabbits as is suggested in Figure 5.13 for the UpSt Site of measurement, and to decrease with increasing blood pressure (Figure 5.14 – mature rabbits); the positive regression plot of MAP vs. AC for immature rabbits is likely spurious due to too few data points (Figure 5.14 – immature rabbits).

All wave speeds, namely $C_{ft\text{-}ft}$, C_{Tpu} and C_{Wpu} (Figure 5.18) did not differ significantly between each other and did not differ significantly between immature and mature rabbits at the UpSt Site of measurement. The finding that $C_{ft\text{-}ft}$, C_{Tpu} and C_{Wpu} did not differ between each other supports the concept of deriving wave speed by PU loop during early systole. At the DnSt Site, $C_{ft\text{-}ft}$, C_{Tpu} and C_{Wpu} appeared faster in immature than in mature rabbits, however this was statistically significant only for $C_{ft\text{-}ft}$ (Figures 5.16 & 5.18). This is an unexpected finding since wave speed, or pulse wave velocity, is usually higher in older than in younger individuals (Nichols and O'Rourke, 2005; Greenwald, 2007), why it is higher in immature than in mature rabbits is not understood but this has been observed in humans; Laogun and Gosling (1982) found that PWV is high in early childhood (1-5 years) decreasing to a minimum at ~8 years then to increase again and on through adulthood. The regression plots for MAP vs. $C_{ft\text{-}ft}$, (Figure 5.17) show the expected increase of $C_{ft\text{-}ft}$ with increasing MAP in immature rabbits but not in mature rabbits where the regression plot is almost horizontal with correlation coefficient not significantly different from r=0; this finding is difficult to explain – one expects a marked positive correlation for MAP vs. $C_{ft\text{-}ft}$ in mature rabbits with a slope greater than that in immature rabbits as the latter would presumably have aortas with lower wall elastic modulus (i.e. greater wall distensibility) than that of mature rabbits.

Wave intensity analysis (WIA) (Figures 5.19 & 5.20) revealed no significant differences for incident compression or incident expansion waves between immature and mature rabbits (Figure 5.19) indicating that systolic and early diastolic cardiac ventricular-vascular interactions are similar in both immature and mature rabbits. However, wave reflections of compression and expansion waves were significantly greater in mature than in immature rabbits as measured at the UpSt Site (Figure 5.19); when wave reflections are expressed as

wave reflection indices (WRI) (i.e. reflected wave energy / incident wave energy), it can be seen that reflections were significantly greater in mature than in immature rabbits for compression and expansion waves at both UpSt and DnSt Sites of measurement in the abdominal aorta. This finding suggests that arterial branches and bifurcations are better matched for forward wave transmission in immature rabbits than in mature rabbits. It is interesting to speculate whether this has any bearing on the age-dependent location of atherosclerotic lesions in rabbits; the distribution of atherosclerosis in the rabbit aorta changes at maturity (Barnes and Weinberg, 1998; Staughton *et al*., 2001; Weinberg, 2002, 2004).

Further to discussion on wave reflection, distances to reflection sites were estimated from WIA plots (estimates given in Figures 5.9 & 5.23). The distances (2-3cm) to reflection sites from the UpSt Site of measurement in the abdominal aorta indicate reflections arising from regions near the ostia of the superior mesenteric and renal arteries (likewise as noted in Chapter 4). The distances to reflection sites from the DnSt Site of measurement in the abdominal aorta do not indicate any obvious site at 1-3cm but data show large standard deviations; of the data spread, the high value distances measured might indicate a site of reflection being the aorto-iliac bifurcation which is some ~6cm downstream of the DnSt Site of measurement in the abdominal aorta. It is noted in section 5.3.2 that estimated distances (Figure 5.23) did not differ significantly between immature and mature rabbits despite the difference in body size.

Another interesting finding was the correlation of RHDN with WRI (Figure 5.21 & 5.22); this was discussed also in Chapter 4, where also RHDN was defined fully. In the context of this thesis, RHDN refers to the incisural inflection on the abdominal pressure pulse waveform. From Figures 5.21 & 5.22 it can be concluded that RHDN is affected by reflected waves in the abdominal aorta whereby RHDN increases with increased wave reflection. The plot of this correlation for mature rabbits is not remarkably different to that of immature rabbits; however mean RHDN (Figure 5.15) differs significantly between immature and mature rabbits with mean RHDN being the greater in the latter. This difference in mean values of RHDN appears to relate to the data of RHDN for immature rabbits being clustered at low values and that of mature rabbits being more widely distributed and so achieving a higher mean value (Figures 5.21 & 5.22); even so, this relates to WRI which does distribute to high values in mature rabbits (Figures 5.21 & 5.22), thus mature rabbits exhibit greater wave reflection in the abdominal aorta than do immature rabbits. RHDN in the abdominal aorta could perhaps serve as an indicator of vascular health or vascular ageing; if the RHDN of the abdominal aorta relates haemodynamically to the RHDN in a peripheral artery (e.g. human digital artery) then the latter could likewise be used as an indicator of vascular health.

The Hypotheses - supported or not supported:

- *Hypothesis*: Fructose diet will decrease arterial compliance and increase aortic pulse wave velocity.

  Findings: Fructose diet in immature and mature rabbits had no conclusive statistically significant effects on indices of arterial compliance: $\int$RP, PP_{RP} or AC. With regard to pulse wave velocity, $C_{ft\text{-}ft}$, in one data set for the DnSt Site of measurement, fructose treatment appeared to increase it but in another data set the effect was not significant. Wave speeds C_{Tpu} and C_{Wpu} were not significantly affected by fructose treatment.

  Support: The data of this thesis do not conclusively support the hypothesis that fructose diet decreases arterial compliance and increases aortic pulse wave velocity.

- *Hypothesis*: Fructose diet will increase pressure pulse reflection in the aorta.

  Findings: Fructose diet caused no significant effects on reflections of compression or expansion waves in the aorta of immature or mature rabbits.

  Support: The data of this thesis do not support the hypothesis that fructose diet increases pressure pulse reflection in the aorta.

- *Hypothesis*: Immature rabbits will have greater arterial compliance and lower aortic pulse wave velocity than mature rabbits.

  Findings: The indices of arterial compliance, $\int$RP and PP_{RP} were significantly different between immature and mature rabbits; the differences indicate a greater arterial compliance in immature than in mature rabbits. The data for AC was inconclusive, though at the UpSt Site of measurement the trend (not statistically significant) suggests greater AC in immature rabbits than in mature rabbits. Pulse wave velocity, $C_{ft\text{-}ft}$, is not significantly different between immature and mature rabbits at the UpSt Site of measurement. However, at the DnSt Site, $C_{ft\text{-}ft}$ is significantly greater in immature rabbits than in mature rabbits – contrary to the proposed hypothesis. Wave speeds, C_{Tpu} and C_{Wpu}, were not significantly different between immature and mature rabbits, though a trend to greater values at the DnSt Site of measurement in immature compared to mature rabbits – contrary to the proposed hypothesis.

Support: The data of this thesis support the hypothesis that immature rabbits have greater arterial compliance than do mature rabbits but the data does not support the hypothesis that aortic pulse wave velocity is lower in immature than in mature rabbits – the contrary was found.

- *Hypothesis*: Immature rabbits will have lower pressure pulse reflection in their aortas than do mature rabbits.

  Findings: Reflections of compression and expansion waves in the aorta of immature rabbits are significantly less than those occurring in the aorta of mature rabbits. RHDN of the abdominal aortic pressure pulse wave is significantly less in immature compared to mature rabbits – abdominal aortic RHDN appears directly affected by wave reflections in the aorta.

  Support: The data of this thesis support the hypothesis that immature rabbits have lower pressure pulse reflection in their aortas than do mature rabbits.

Limitations of experiment are discussed in Chapter 8.

CHAPTER 6

The Polyurethane Model of the Human Aorta: Manufacture

6.1 INTRODUCTION

Early examples of experiments with models were described by Westerhof *et al*., (1971) and Sipkema *et al*., (1990). The polyurethane aorta used in this thesis is similar to that described by Segers *et al*. (1998), Segers and Verdonck (2000) and Matthys *et al*. (2007) and is an exact duplicate of that used by Kolyva *et al*., (2010).

6.2 METHODS

6.2.1 Development of the Polyurethane Aorta Model

The polyurethane aorta model was manufactured by Ranier Technologies Ltd, Cambridge, U.K. to our specification.

The polyurethane model is a 1:1 replica of the human aorta along with the main conduit arteries bifurcating off it (see Figure 7.1 & 7.2), these being: left and right coronary arteries; innominate artery bifurcating to the right subclavian and right carotid arteries; left carotid artery; left subclavian artery; celiac artery; superior mesenteric artery; left and right renal arteries; aorto-iliac bifurcation leading to left and right iliac arteries which each bifurcate to the inner and outer femoral arteries.

Mandrels were manufactured out of aluminium and lathed to diameters, tapers and bifurcation angles specified for the aorta and conduit arteries. The dimensions and geometry for this model were taken from a human aorta and its associated bifurcating conduit arteries. The mandrels were immersed into a polyurethane compound by a process of precision dipping. The dipping process was done sufficiently to layer the polyurethane on to the mandrels to a specified thickness. The polyurethane was left to cure; the curing process was carried out in a way to ensure that the polyurethane coating was of even thickness throughout the entire vessel being fabricated. The fabricated vessel was then

taken off the mandrels; the polyurethane component vessels (i.e. conduit arteries) were then assembled to make the complete polyurethane aorta model.

Before making the model aorta, the chemical and physical nature of the polyurethane had to be evaluated; this is discussed in the next section.

6.2.2 Evaluation of Material for Construction of the Model Aorta

Preliminary work was carried out to assess suitability of polyurethane materials for the aorta model; assessment of suitability included measures of wave speed – ideal wave speeds would be those expected for the human aorta. Assessments were carried out on specimens of two different polyurethanes: Z1D1 and SG-80A (Tecoflex); the specimens were in the form of tubes: Internal Diam.18mm; length170-180mm. Wall thicknesses of the tubes are stated below in Table 6.1 – wall thickness measurements stated by the manufacturers Ranier Technologies Ltd. For all but one tube (No. 2 of SG-80A, Tecoflex) wall thicknesses were uneven along the length of the tubes and are expressed in Table 6.1 as left hand side (LHS), Mid-section (MID) and right hand side (RHS) of the tubes as related to their assembly in the test system (Figure 6.1), where the LHS end was connected to the hydrostatic head of the test system and the RHS end was clamped shut (Figure 6.1).

TABLE 6.1: Wall Thicknesses* (µm) of Polyurethane Tubes Submitted for Assessments. Tube Lengths were 170mm (Z1D1) & 180mm (SG-80A Tecoflex), all with Internal Diameter of 18mm.
NOTE: Tube numbers are as labelled by Ranier Technologies Ltd., the supplier of the tubes, and do not relate to the wall thickness of the tubes.

Polyurethane	Tube No.	LHS	MID	RHS
Z1D1**	6	130	120	90
	5	160	170	170
	4	230	260	270
	3	180	190	165
	2	250	270	260
SG-80A*** (Tecoflex)	5	190	190	200
	6b	280	260	250
	4	320	335	360
	2	400	400	400

*Wall thicknesses of the tubes (excepting No. 2 of SG-80A, Tecoflex) were uneven along the length of the tubes and are expressed in the table from left hand side (LHS), Mid-section (MID), right hand side (RHS), of the tubes as related to their assembly in the test system (Figure 6.1), where the LHS end was connected to the hydrostatic head of the test system and the RHS end was clamped shut (Figure 6.1).
****For Z1D1**, tube order of wall thickness is: tube 6 < 5 < 3 < 4 < 2
*****For SG-80A (Tecoflex)**, tube order of wall thickness: tube 5<6b<4<2

As illustrated in Figure 6.1, the polyurethane tubes of length 170-180mm were set up in a bath of water at room temperature (20°C) and allowed to soak in the bath over night before the study. It is important to soak the tubes thoroughly in water before the assessments because the state of hydration of the material affects the elastic properties (Bembridge, 2007). The polyurethane tubes were connected to a polythene tube; the latter tube being much more rigid than the polyurethane tubes. The other end of the latter was connected to a burette. The burette and tubes were filled with water at room temperature (20°C); the burette contained the hydrostatic head of water. Pressure within the polyurethane tubes was measured using a Millar Mikro-tip catheter transducer (model SPR-407; size 2F) that was positioned approximately half way within the tube (Figure 6.1).

Pressure-Volume measurements

Initially the hydrostatic head was raised such that the pressure within the polyurethane tube was 5mmHg; this was taken as the initial value since the tube was little stressed but sustained a strain which maintained its tubular form of 18mm diameter. The hydrostatic head was then raised to apply 10mmHg of pressure, and then subsequently the hydrostatic head was raised by sequential increments of 10mmHg to a pressure of 100mmHg. At 100mmHg the hydrostatic head was ~1.35m above the polyurethane tube under test. As the burette, namely the hydrostatic head, was raised, water was displaced from the burette into the polyurethane tube as it distended in response to the increased pressure; the volume of displaced water was measured from the burette (Figure 6.1).

Values of compliance, distensibility and calculated wave speed (by the equation of Bramwell and Hill 1922) for the polyurethane tubes were calculated using these formulae:

$$Compliance = \frac{\Delta V}{\Delta P} \quad \text{(Eq. 6.1)}$$

$$Distensibility = \frac{\Delta V}{\Delta P} \cdot \frac{1}{V} \quad \text{(Eq. 6.2)}$$

$$Calculated\ wave\ speed = \frac{1}{\sqrt{\rho \cdot Distensibility}} \quad \text{(Eq. 6.3)}$$

Where:

ΔP = incremental increases of applied pressure within tube

ΔV = incremental inreases of volume within tube after each applied ΔP

V = the tube volume before each ΔP; ρ = density of water: 1000kg.m^{-3}

Circumferential incremental Young's modulus (E_{inc}) for the polyurethane tubes was calculated using an equation first proposed by Love (1927) and applied by Bergel (1961):

$$E_{inc} = \frac{\Delta P}{\Delta R_o} \cdot \frac{2(1-\sigma^2)R_i^2 R_o}{\left(R_o^2 - R_i^2\right)} \ldots\ldots\ldots\ldots\ldots\ldots\ldots\ldots\ldots\ldots\ldots\ldots\ldots\ldots\ldots\ldots\ldots\ldots\ldots\ldots\ldots .. \text{(Eq. 6.4)}$$

where:

(Values for R_o and R_i were calculated from values of volume with constant tube length)

$\Delta P =$ incremental step change of applied pressure within tube

$\Delta R_o =$ incremental step change of external or outer radius of tube after each applied ΔP

$R_o =$ external or outer radius of tube

$R_i =$ inner (luminal)radius of tube

$\sigma =$ Poisson's ratio is 0.5 for changes in tube wall strain occurring isovolumically − this is assumed here − furthermore, the tube length is held constant.

As calculated in the manner of Bergel (1961), ΔP and associated ΔR_o are the differences between alternate measurements of pressure; Einc is taken as between the measurements as are $R_i^2 R_o$ but not $\left(R_o^2 - R_i^2\right)$ since this remains constant if changes in wall strain are isovolumic.

Wave speed was also calculated using the Moens-Kortweg equation adapted with a correction factor proposed by Bergel (1960); this correction is discussed fully by McDonald (1976), Nichols and O'Rourke (2005) and Milnor (1989):

$$Wave\ speed = \sqrt{\frac{Eh}{2\rho R_o(1-\sigma^2)}} \ldots\ldots\ldots\ldots\ldots\ldots\ldots\ldots\ldots\ldots\ldots\ldots\ldots\ldots\ldots\ldots\ldots .. (Eq.\ 6.5)$$

where:

$E =$ circumferential elastic modulus of tube, here values of E_{inc} are used

$h =$ tube wall thickness; initial wall thickness taken as mean wall thickness for tube − see Table 6.1; tube wall thickness were uneven

$R_o =$ external or outer radius of tube

$\rho =$ density of water: $1000 kg.m^{-3}$

$\sigma =$ Poisson's ratio of 0.5

$(1-\sigma^2)$ is Bergel's correction

FIGURE 6.1: Diagrammatic Illustration of the Pressure-Volume Test System (not to scale).

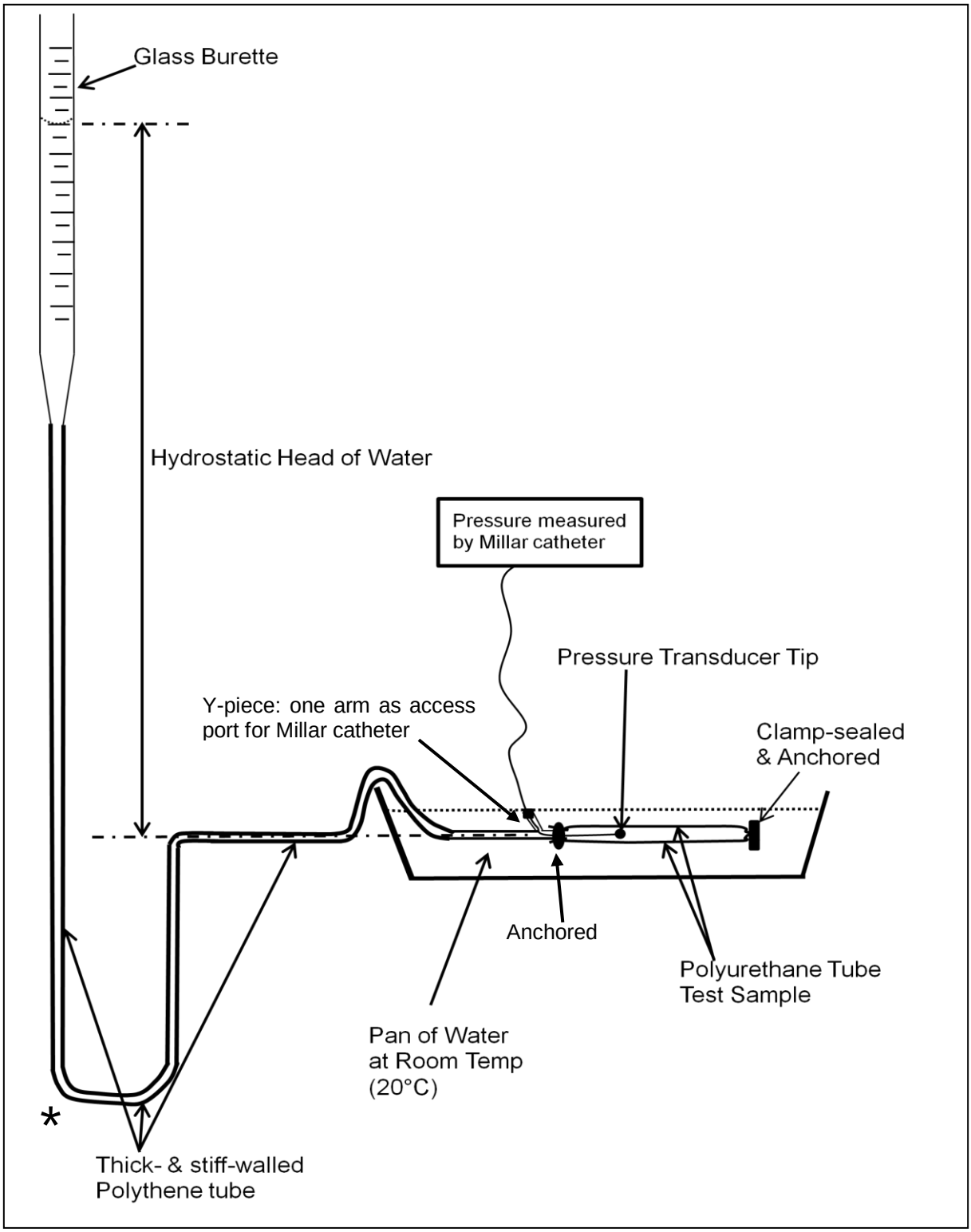

* The loop of the tube gives length to allow elevation of the burette to increase the hydrostatic head. A hydrostatic head of ~1.35m is required for a pressure of 100mmHg in the polyurethane tube test sample.

High Pressure Test

The High Pressure Test was simply the application of 175mmHg pressure to check that the tubes could withstand this pressure without ballooning or rupture.

6.3 RESULTS

Pressure-volume measurements for tubes made from the polyurethanes Z1D1 and SG-80A (Tecoflex) are shown respectively in Figures 6.2A and 6.2B. The length (170-180mm) of the tubes did not alter during the pressure-volume procedure – the tubes were anchored at both ends – length was checked against a ruler; increases in volume were therefore a function of increases in diameter. Tube 6 of polyurethane Z1D1 (Figure 6.2A) is of least wall thickness (Table 6.1) and shows a curvi-linear relationship but, on 2nd testing, departs from the general relationship at 100mmHg. At this pressure, tube 6 ballooned at the thin region of wall thickness (i.e. 90µm), and when tested at 175mmHg (high pressure test – section 6.2.2) it ballooned progressively without reaching a stable pressure; the 175mmHg applied stress on tube 6 was ceased lest the tube ruptured. The other tubes of polyurethane Z1D1 had thicker walls than Tube 6 and so had pressure-volume curves that were more linear and more stable than that of Tube 6; furthermore, the wall thicknesses of Tubes 5 & 3 were close in value to each other as were those of Tubes 4 & 2 to each other (Table 6.1), and so the data of Tubes 5 & 3 grouped together as did that of Tubes 4 & 2 (Figures 6.2A, 6.3A, 6.4A, 6.5A). Tubes of the polyurethane SG-80A (Tecoflex) had almost linear pressure-volume curves (Figure 6.2B) and these were influenced by tube wall thickness – the thinner the wall the steeper the slope of the curve. Furthermore, for the SG-80A (Tecoflex) tubes, no ballooning but instead a stable pressure occurred at 175mmHg (high pressure test – section 6.2.2).

The pressure-volume data are further analysed to give measures of compliance (Figures 6.3A&B) and distensibility (Figures 6.4A&B). Other than Tube 6 on its 2nd test (Figure 6.3A; Z1D1), when ballooning occurred, tubes of polyurethane Z1D1 maintained constant compliance values over the pressure range 10 – 100mmHg. Tubes 2, 3, 4, 5 of polyurethane Z1D1 have compliances of the same order of magnitude as the compliances of the tubes of SG-80A (Tecoflex) (Figures 6.3A&B); tube 5 of SG-80A (Tecoflex) showed an increase in compliance at pressures above 50mmHg (40% at 100mmHg). The data for distensibility (Figures 6.4A&B) of tubes of both polyurethanes follow trends similar to that of data for compliance. In all cases, for Z1D1 and for SG-80A (Tecoflex), tube wall thickness has an inverse influence on both tube compliance and tube distensibility (Figures 6.3 and 6.4).

Values for circumferential incremental Young's modulus (E_{inc}) are shown in Figures 6.5A&B. The values of E_{inc} were of similar order of magnitude for both polyurethanes, Z1D1 and SG-80A (Tecoflex) and were little affected by incremental increases in pressure, except in the case of Z1D1 Tube 6 (Figure 6.5A) where E_{inc} departed from the general values at pressures above 50mmHg; this did not happen with any of the SG-80A (Tecoflex) Tubes. The values for E_{inc} are used to calculate wave speed by the Moens-Kortweg equation.

Wave speeds calculated by use of the Bramwell and Hill equation are shown in Table 6.2 and also represented graphically in Figures 6.6A&B; wave speeds calculated by use of the Moens-Kortweg equation incorporating Bergel's correction factor are shown in Figures 6.7A&B). The two procedures for calculating wave speed gave closely matching values. (Interestingly, in preliminary calculations, it was found that calculating wave speed by use of the Moens-Kortweg equation *without* incorporating Bergel's correction resulted in wave speed values of ~1m/s less than those calculated by the Bramwell and Hill equation). The calculated values for wave speed appear to change little with incremental increases in pressure. However, the calculated wave speed for Z1D1 polyurethane Tube 6 (Z1D1; Figures 6.6A and 6.7A) decreased with incremental increases in pressure; this effect is associated with increasing compliance (Figure 6.3A) and distensibility (Figure 6.4A) along with decreasing E_{inc} (Figure 6.5A). Calculated wave speeds of the tubes of polyurethane SG-80A (Tecoflex) appear little affected by the incremental changes in pressures (Figure 6.6B). In all cases, for Z1D1 and for SG-80A (Tecoflex), the wave speeds are influenced by tube wall thickness; the thicker the wall the greater the wave speed.

TABLE 6.2: Data for Calculated Wave Speeds ($m.s^{-1}$) at different Applied Pressures. See also Figures 6.5A & 6.5B

Polyurethane	Tube No.	Applied Pressures (mmHg)									
		10	20	30	40	50	60	70	80	90	100
Z1D1	6 (1^{st})	5.66	6.27	5.98	5.76	5.73	5.23	4.81	4.41	4.20	3.78
	6(2^{nd})	6.00	6.06	5.98	5.62	5.47	4.87	4.62	4.51	3.80	2.38
	5	6.00	7.31	7.76	7.16	7.95	7.04	7.14	6.97	6.41	6.16
	4	7.59	8.05	8.63	9.31	8.77	8.85	8.92	8.05	8.57	8.20
	3	7.59	7.64	7.73	7.45	7.54	7.30	7.10	6.93	6.38	6.48
	2	8.49	8.53	9.20	8.68	8.75	8.83	8.39	8.47	8.55	8.19
SG-80A (Tecoflex)	5	7.64	8.10	8.18	7.84	7.92	7.63	7.39	7.19	7.28	7.10
	6b	8.74	8.27	9.47	8.93	9.00	9.07	8.62	8.25	8.33	8.41
	4	7.13	9.40	9.47	10.3	10.3	9.66	9.73	9.80	9.87	9.29
	2	8.74	9.38	10.6	10.7	10.3	10.3	10.4	10.5	10.5	9.86

FIGURE 6.2: Pressure – Volume Data for Tubes of:
(A) Polyurethane Z1D1; (B) Polyurethane SG-80A (Tecoflex)

A) Polyurethane Z1D1:
Tube Order of Wall Thickness (Table 6.1): Tube 6 < 5 < 3 < 4 < 2

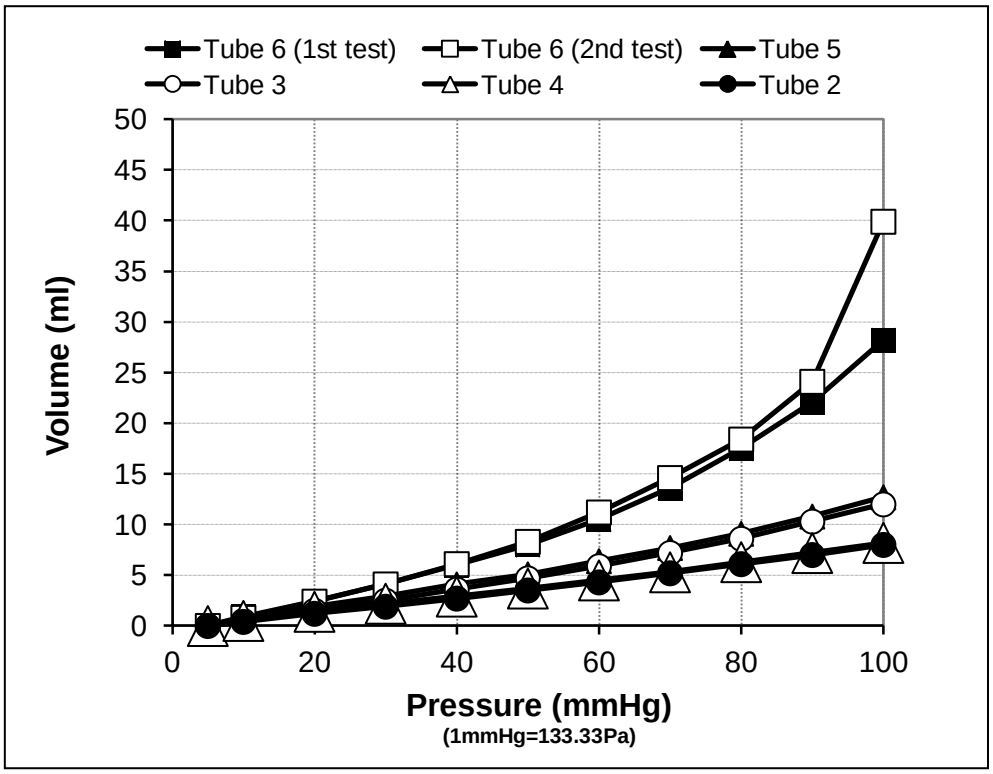

B) Polyurethane SG-80A (Tecoflex):
Tube Order of Wall Thickness (Table 6.1): Tube 5 < 6b < 4 < 2

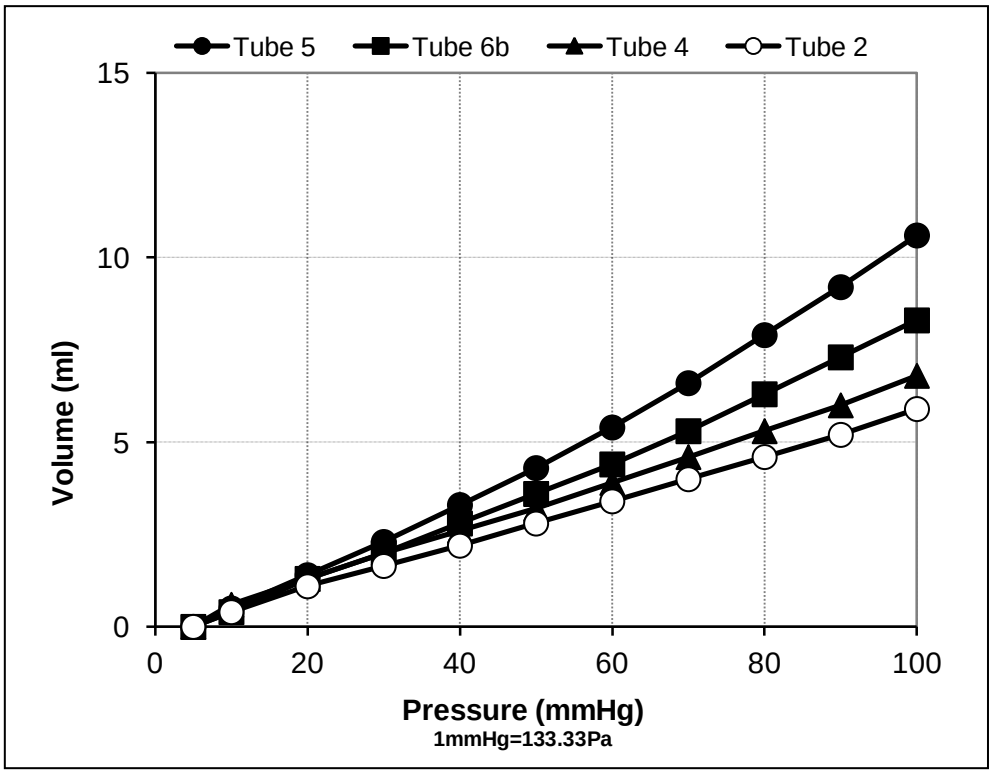

FIGURE 6.3: Compliance Data for Tubes of:
(A) Polyurethane Z1D1; (B) Polyurethane SG-80A (Tecoflex)

A) Polyurethane Z1D1:
Tube Order of Wall Thickness (Table 6.1): Tube 6 < 5 < 3 < 4 < 2

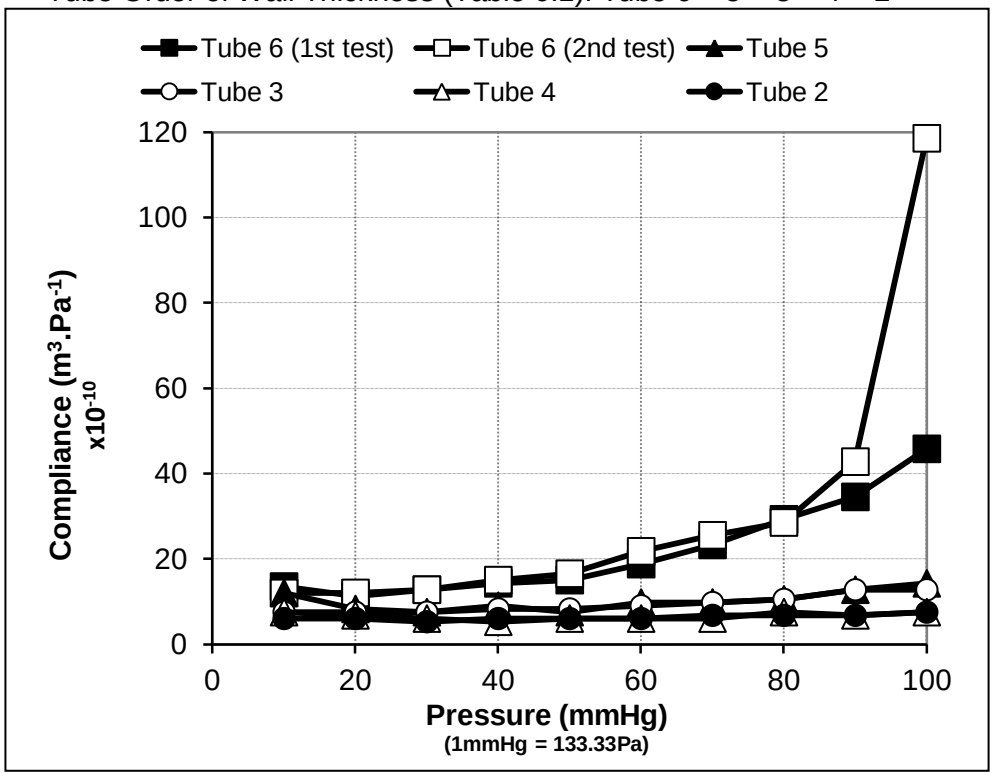

B) Polyurethane SG-80A (Tecoflex):
Tube Order of Wall Thickness (Table 6.1): Tube 5 < 6b < 4 < 2

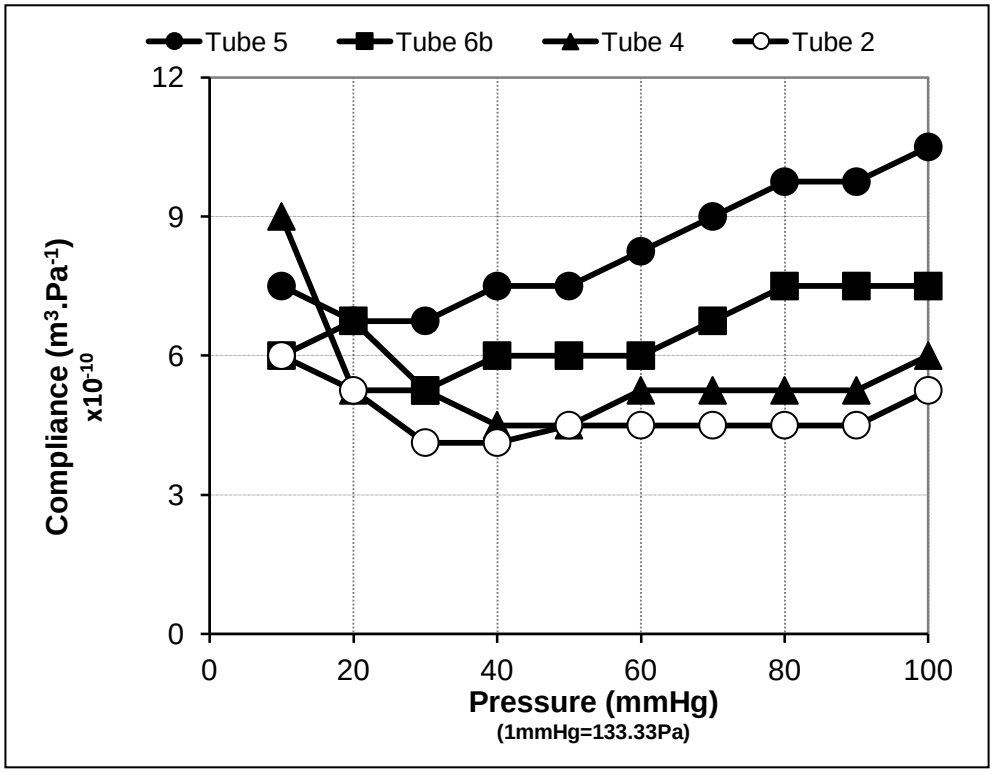

FIGURE 6.4: Distensibility Data for Tubes of:
(A) Polyurethane Z1D1; (B) Polyurethane SG-80A (Tecoflex)

A) Polyurethane Z1D1:
Tube Order of Wall Thickness (Table 6.1): Tube 6 < 5 < 3 < 4 < 2

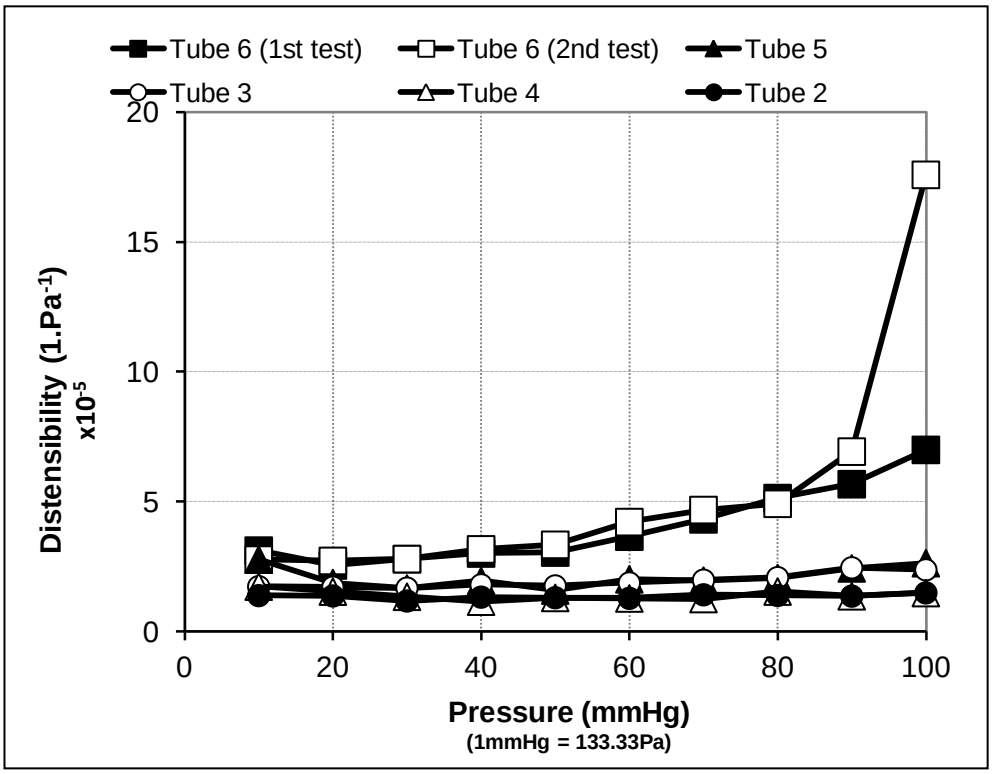

B) Polyurethane SG-80A (Tecoflex):
Tube Order of Wall Thickness (Table 6.1): Tube 5 < 6b < 4 < 2

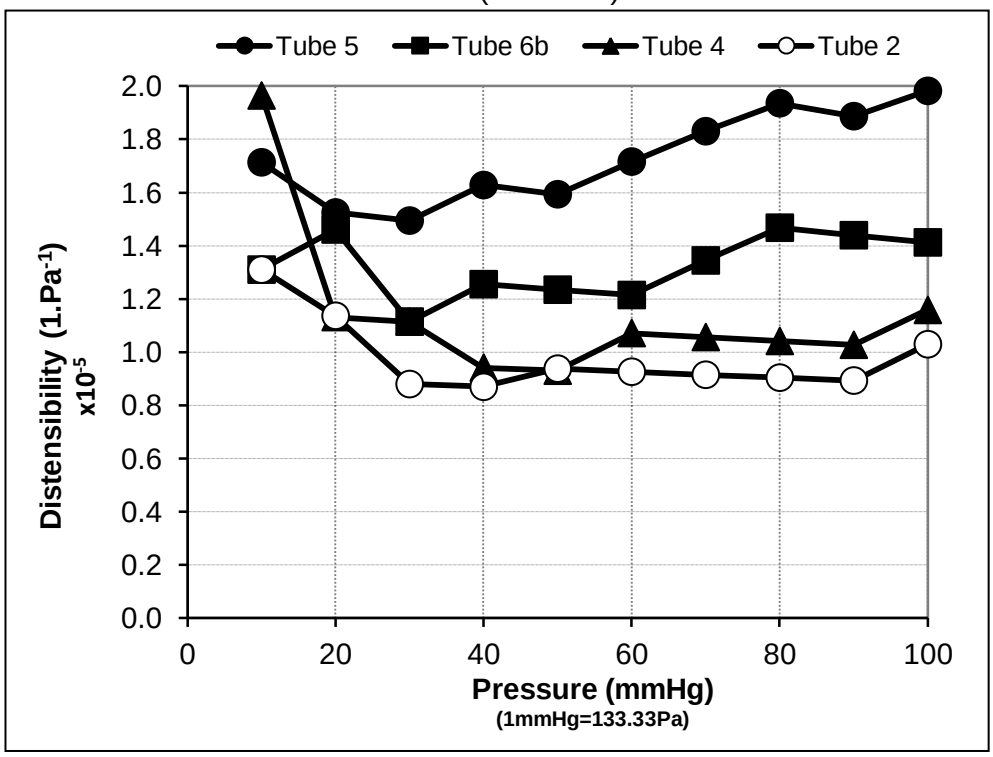

FIGURE 6.5: Circumferential Incremental Young's Modulus (E_{inc}) for:
(A) Polyurethane Z1D1; (B) Polyurethane SG-80A (Tecoflex)

A) Polyurethane Z1D1:
Tube Order of Wall Thickness (Table 6.1): Tube 6 < 5 < 3 < 4 < 2

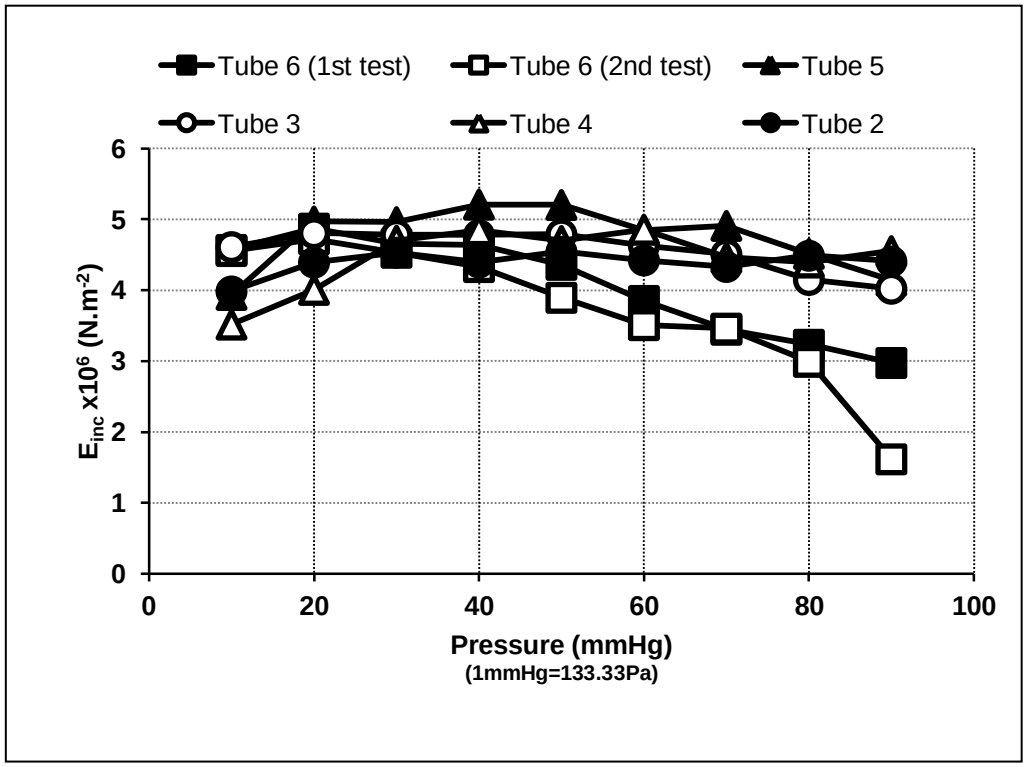

B) Polyurethane SG-80A (Tecoflex):
Tube Order of Wall Thickness (Table 6.1): Tube 5 < 6b < 4 < 2

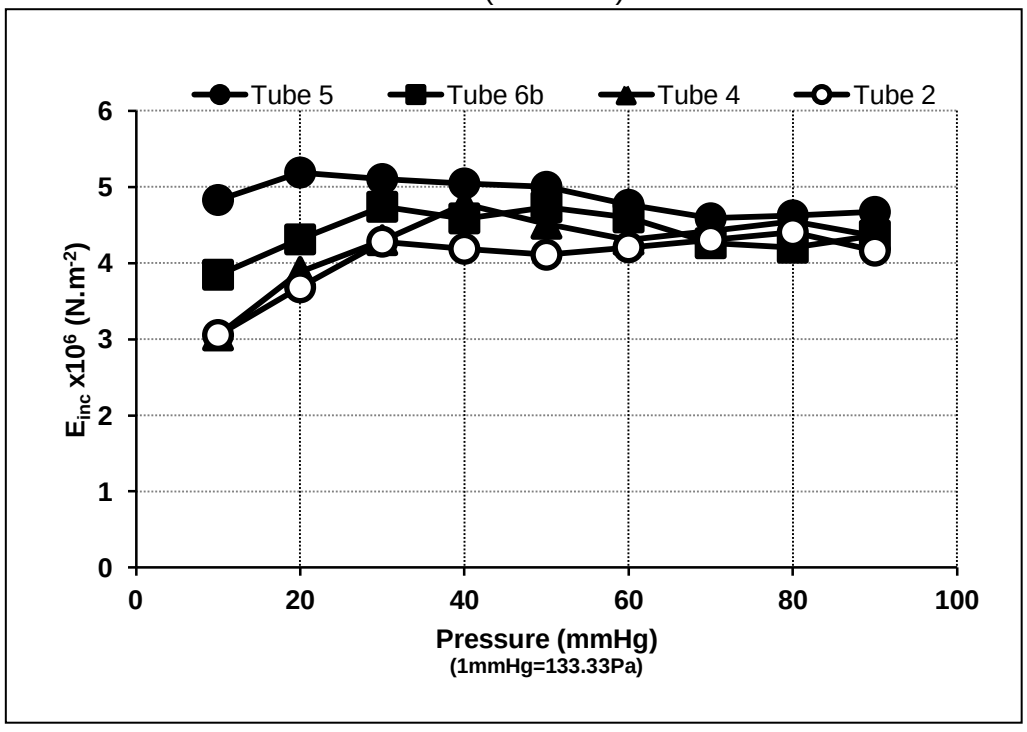

FIGURE 6.6: Calculated Wave Speed* Data (see Table 6.2) for Tubes of: (A) Polyurethane Z1D1; (B) Polyurethane SG-80A (Tecoflex)

A) Polyurethane Z1D1:
Tube Order of Wall Thickness (Table 6.1): Tube 6 < 5 < 3 < 4 < 2

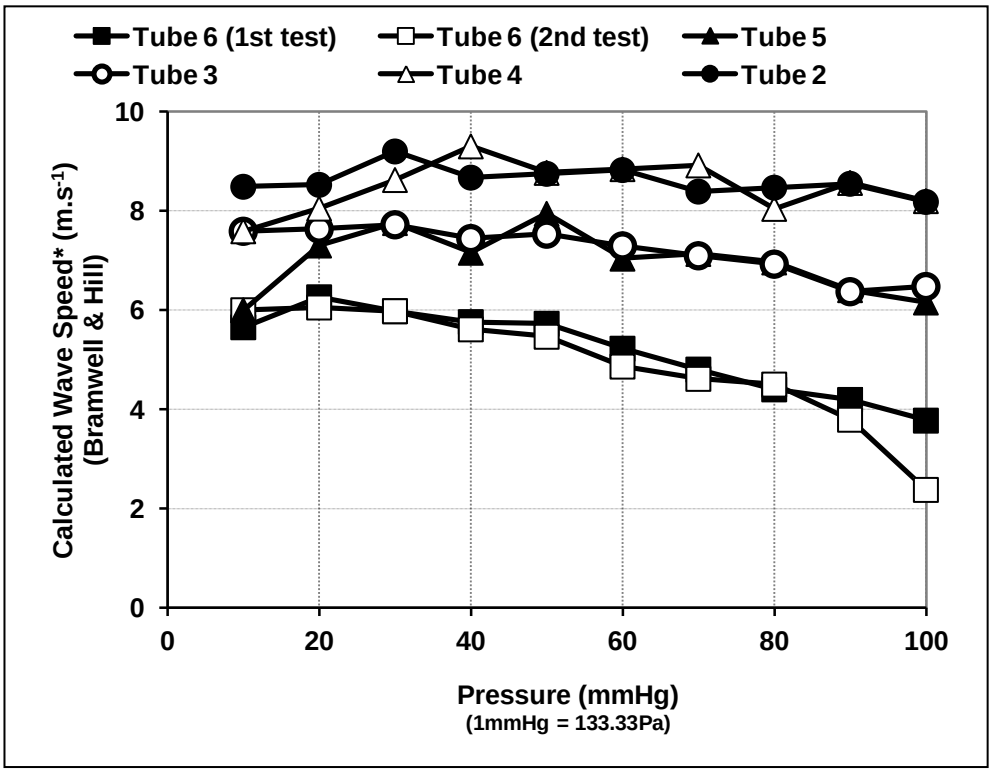

B) Polyurethane SG-80A (Tecoflex):
Tube Order of Wall Thickness (Table 6.1): Tube 5 < 6b < 4 < 2

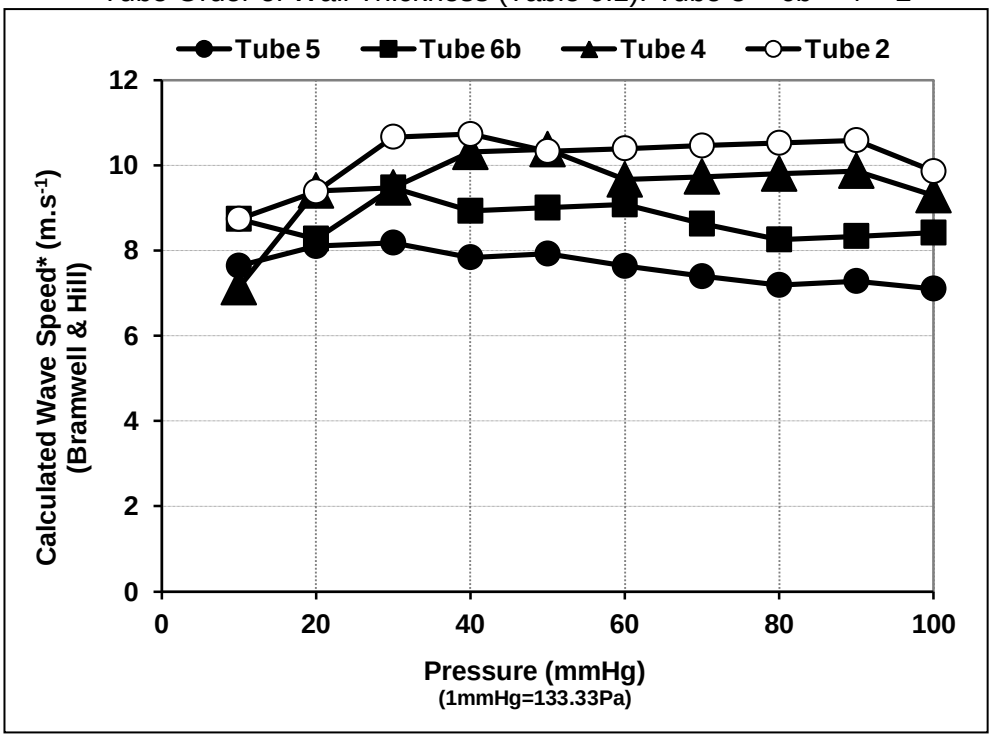

*wave speed calculated by use of the Bramwell and Hill equation.

FIGURE 6.7: Calculated Wave Speed* Data for Tubes of:
(A) Polyurethane Z1D1; (B) Polyurethane SG-80A (Tecoflex)

A) Polyurethane Z1D1:
Tube Order of Wall Thickness (Table 6.1): Tube 6 < 5 < 3 < 4 < 2

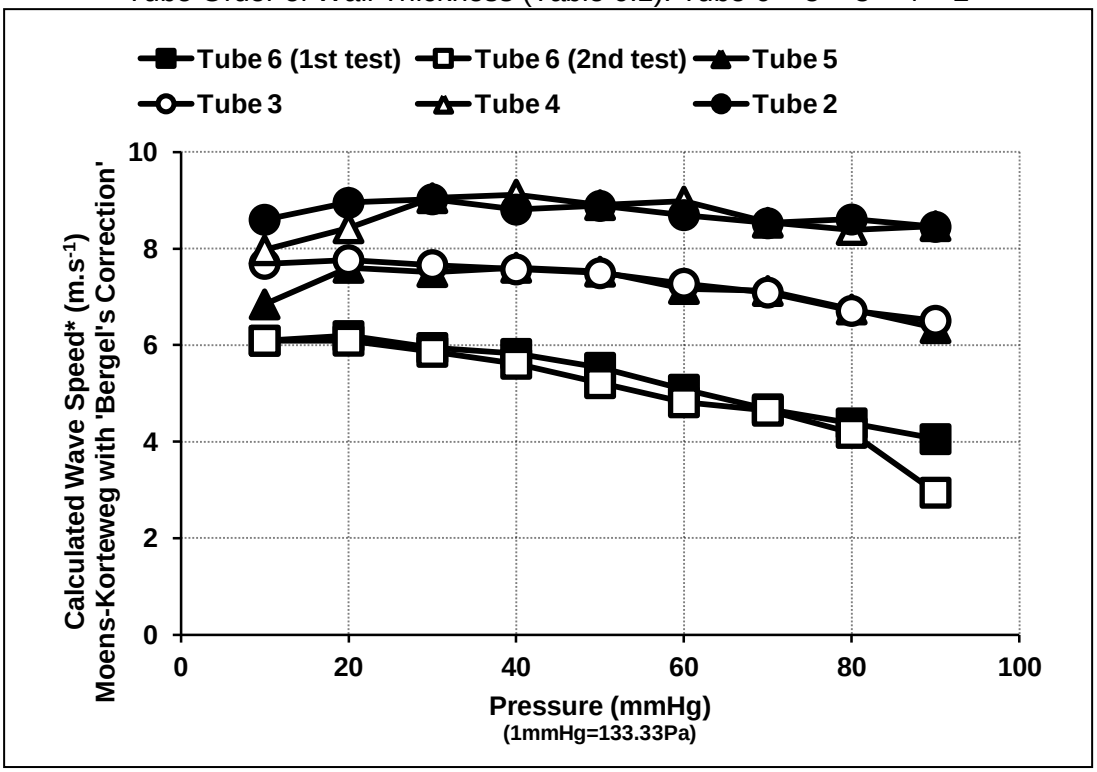

B) Polyurethane SG-80A (Tecoflex):
Tube Order of Wall Thickness (Table 6.1): Tube 5 < 6b < 4 < 2

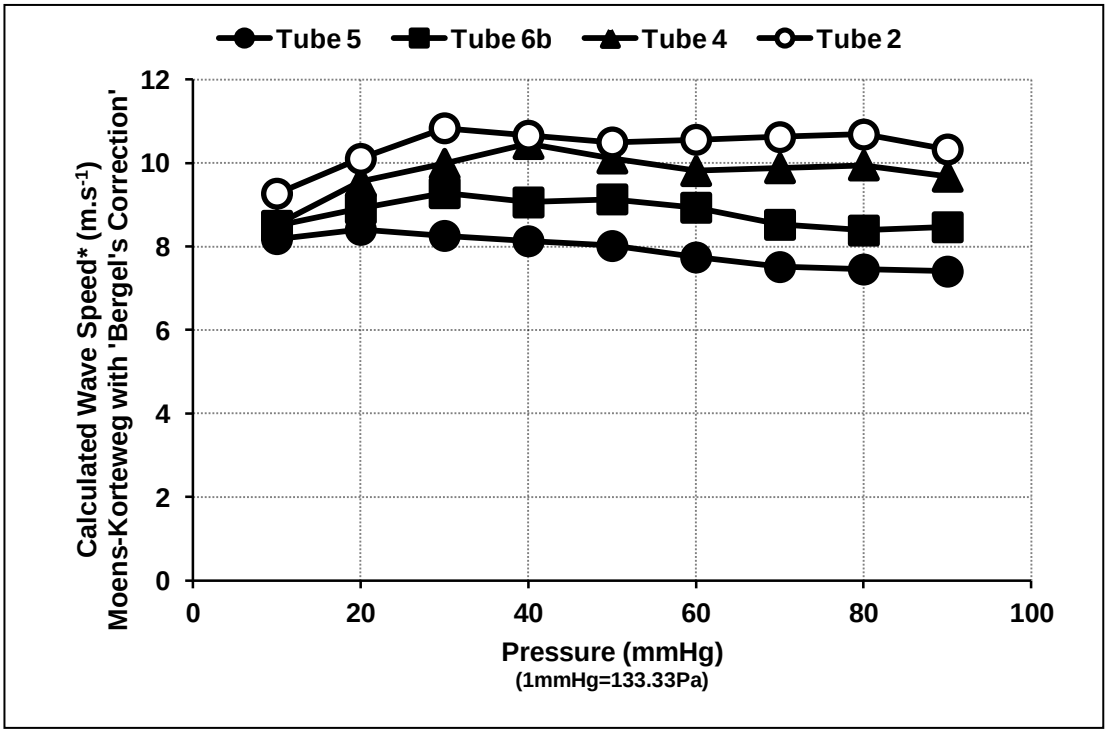

*wave speed calculated by use of the Moens-Kortweg equation with ‘Bergel’s correction’.

6.4 DISCUSSION

The findings of the pressure-volume tests on the polyurethane tubes (Figure 6.2) were not typical of those found for blood vessels. Pressure-volume curves of blood vessels are curvi-linear with the curve becoming plateau-like at high pressure when volume increments decrease for given increments of pressure at high pressure. This is due to heterogeneous elastic structure of blood vessels. The reason for this is that at low pressure the strain, or distension, of blood vessels engages elastin elements of the wall structure. Elastin has an elastic modulus which is lower than that of the other wall structural element, collagen; the latter engages at high pressures and limits the distension (Roach and Burton, 1957; Bergel, 1961). Thus, the compliance and distensibility of arteries decreases with increased pressure-volume induced distension. The mechanics of stress-strain in arteries is comprehensively discussed in *Blood Flow in Arteries* (McDonald, 1960; 1976; Nichols and O'Rourke, 1990; 1998; 2005), *The Mechanics of the Circulation* (Caro *et al*., 1978) and *Hemodynamics* (Milner, 1982; 1989). The pressure-volume curves up to 100mmHg for the polyurethane tubes were perhaps like those of the aorta of young people where no plateau occurred (Hallock and Benson, 1937); in the case of elderly people, the plateau does begin to occur within the range to 100mmHg (Hallock and Benson, 1937). Furthermore, the compliances (Figure 6.3) and distensibilities (Figure 6.4) of the tubes remained somewhat constant over the pressure range 10-100mmHg, though for some tubes (tube 6 of Z1D1 and tube 5 of SG-80A), contrary to how arteries behave, compliance and distensibility actually *increased* over the pressure range 50-100mmHg.

Data for circumferential Young's modulus, E_{inc}, (Figure 6.5) of the polyurethane tubes give more evidence for the difference of elastic behaviour of the polyurethane tubes from the elastic behaviour of blood vessels in that the E_{inc} for most tubes (except tube 6 of Z1D1) remained constant over the pressure range 10 – 100mmHg; this is not the case with blood vessels where E_{inc} increases with increasing pressure, as was shown by Bergel (1961) over the same pressure range of 10 – 100mmHg. Constancy of E_{inc} with increasing pressure, hence increasing strain, is expected of materials of homogeneous substance which presumably was the case with these polyurethane tubes (except tube 6 of Z1D1 – see end of this paragraph). Blood vessel walls are heterogeneous where their elastic nature comprises vascular smooth muscle, elastin and collagen – all with their different elastic moduli values (Bergel 1961; McDonald, 1960; 1976; Nichols and O'Rourke, 1990; 1998; 2005; Caro *et al*., 1978; Milner, 1982; 1989). The *decrease* (contrary to blood vessel behaviour) of E_{inc} of tube 6 of Z1D1 (Figure 6.5A) suggests that the Z1D1 polyurethane of

this tube changed its elastic nature at high strain thus increasing the tube's compliance and distensibility.

As expected, calculated wave speeds (Figures 6.6 and 6.7) for all tubes related directly to tube wall thickness and inversely to tube compliance and distensibility. Such relationships are consistent with the equations, namely the Bramwell and Hill equation and the Moens-Kortweg equation, used for calculation of wave speed. The calculated wave speeds for the tubes were of similar order of magnitude to those measured for the distal mammalian aorta and conduit arteries (c.f. values in McDonald, 1960; 1976; Nichols and O'Rourke, 1990; 1998; 2005; Caro *et al*., 1978; Milner, 1982; 1989) but E_{inc} calculated for the tubes was 10-40 fold that found by Bergel (1961) for thoracic and abdominal aorta or femoral and carotid arteries over the same pressure range of 10 – 100mmHg. Despite the high values of E_{inc} for the polyurethane tubes, the tube wave speeds are not greatly different to wave speeds of the distal aorta and conduit arteries because the wall thickness ratio, h/R_o, is less for the tubes than for large blood vessels. For natural aortic and conduit vessels, h/R_o is of the order 0.105 – 0.132 (Bergel, 1961) but for the polyurethane tubes it is less, namely for Z1D1 tubes 0.009 – 0.028 and for SG-80A (Tecoflex) tubes 0.016 – 0.043. Thus, for the tubes their low h/R_o values counter their high E_{inc} values thereby rendering tube wave speeds comparable to wave speeds of natural large blood vessels.

In conclusion, the elastic behaviour of the polyurethane tubes is not typical of blood vessels but the tubes gave wave speeds comparable to those of the distal aorta and conduit arteries. The decision for which polyurethane material to use for the model aorta rested on: i) the polyurethane, ii) the calculated wave speed, and iii) the wall thickness. By the time the model aorta was manufactured, the Z1D1 polyurethane was no longer available so the choice had to be for SG-80A (Tecoflex). Of the SG-80A (Tecoflex) series, Tubes 5 and 6b gave ranges of calculated wave speeds (7-8m/s and 8-9m/s respectively) that were closest to wave speeds for the aorta (5-6m/s – abdominal aorta; Nichols and O'Rourke, 2005). The range of wave speeds of the other two tubes, namely Tubes 4 and 2 (9-10m/s and 9-11m/s respectively) was higher. Thus, Tube 5 could be a candidate. A decision was then required on the wall thickness for the model aorta. The manufacturer deemed that the wall thickness of Tube 5 (190-200µm; Table 6.1) would probably be too thin and fragile for reliable long-term use of the model aorta. So the decision was taken to have a wall thickness close to that of Tube 6b, namely 250µm (see Table 6.1 for Tube 6b range of wall thickness), even though the range of calculated wave speeds for Tube 6b was slightly higher than that for Tube 5.

In summary, the model aorta was made of SG-80A (Tecoflex) polyurethane with a wall thickness of 250μm, representing a compromise between a calculated wave speed slightly higher than would be expected for the aorta and a material that gives sufficient robustness for routine use.

CHAPTER 7

The Polyurethane Model of the Human Aorta: Simulation of Aortic Physiology & Pathology

7.1 INTRODUCTION

The model aorta used here is a 1:1 replica of the human aorta (Figure 7.1A) and is an exact duplicate of that used by Kolyva *et al*. (2010). The model comprises the aorta with the main conduit arteries bifurcating off it (Figure 7.1A), as described in the previous chapter.

The model aorta was used to simulate wall stiffening as is thought to occur in the ageing aorta, a consequence of this is isolated systolic hypertension.

Objectives and Hypotheses

Objectives

- To ascertain that decreased compliance of the model aorta increases: wave speed, pressure pulse amplitude (by increasing systolic pressure while decreasing diastolic pressure), and reservoir (Windkessel) pressure.
- To ascertain that decreased compliance of the model aorta increases wave reflection in the model.

Hypotheses

- Decreased compliance of the model aorta increases RHDN
- Application of distal compliances attenuates the effects of decreased compliance of the model aorta.

7.2 METHODS

The model of the human aorta (dimensions in Figure 7.1B) was laid out in a plastic trough (Figure 7.2); the latter served to contain leaked circulating fluid or fluid released by occasional disconnections at joints. Water was used for the circulating fluid. The terminations of the conduit arteries off the aorta were connected by use of stiff plastic Y-piece tubes into a wide bore polythene tube which was a ring circuit around the model aorta

FIGURE 7.1A: The Polyurethane Model of the Human Aorta with Conduit Arteries.

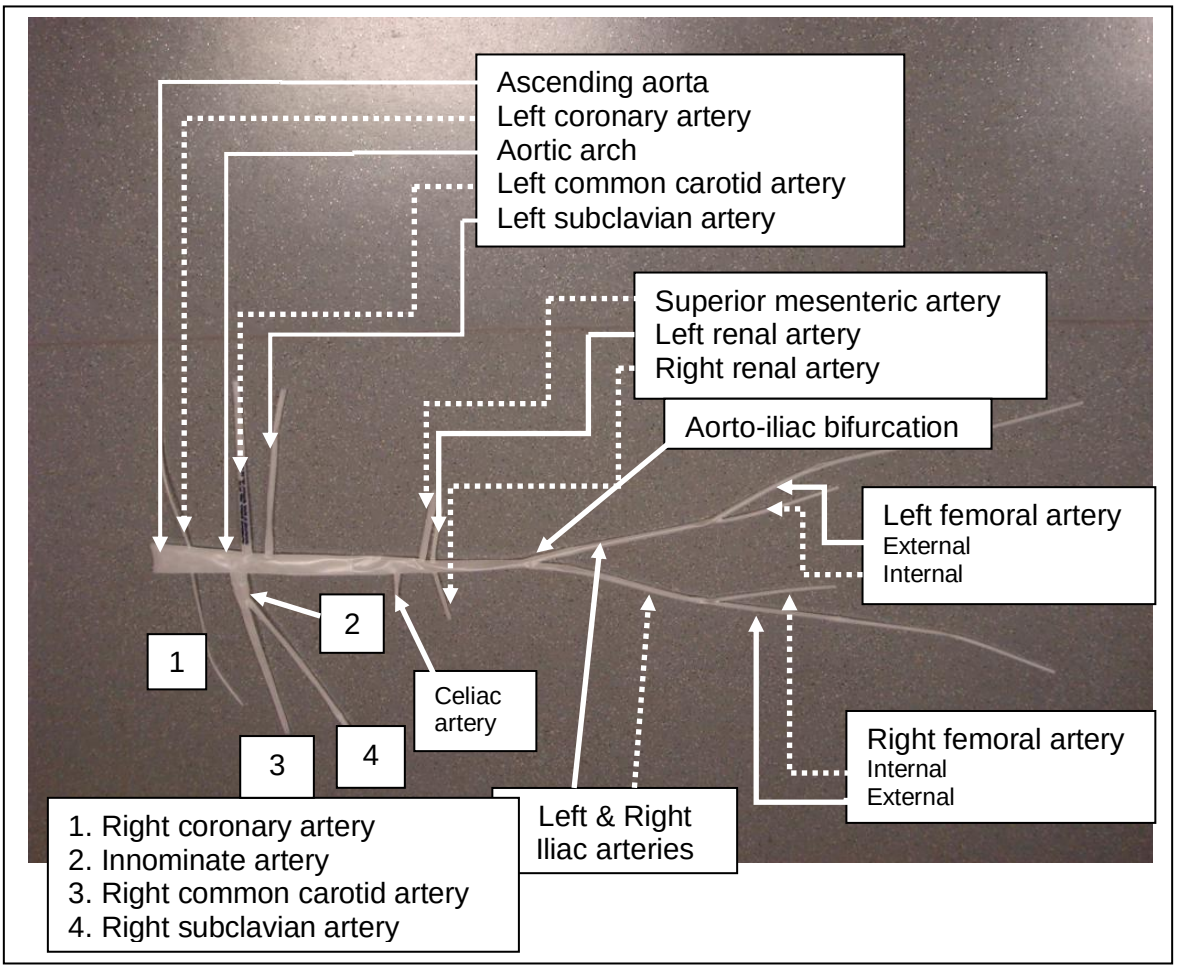

FIGURE 7.1B: Dimensions of the Polyurethane Model of the Human Aorta with Conduit Arteries.

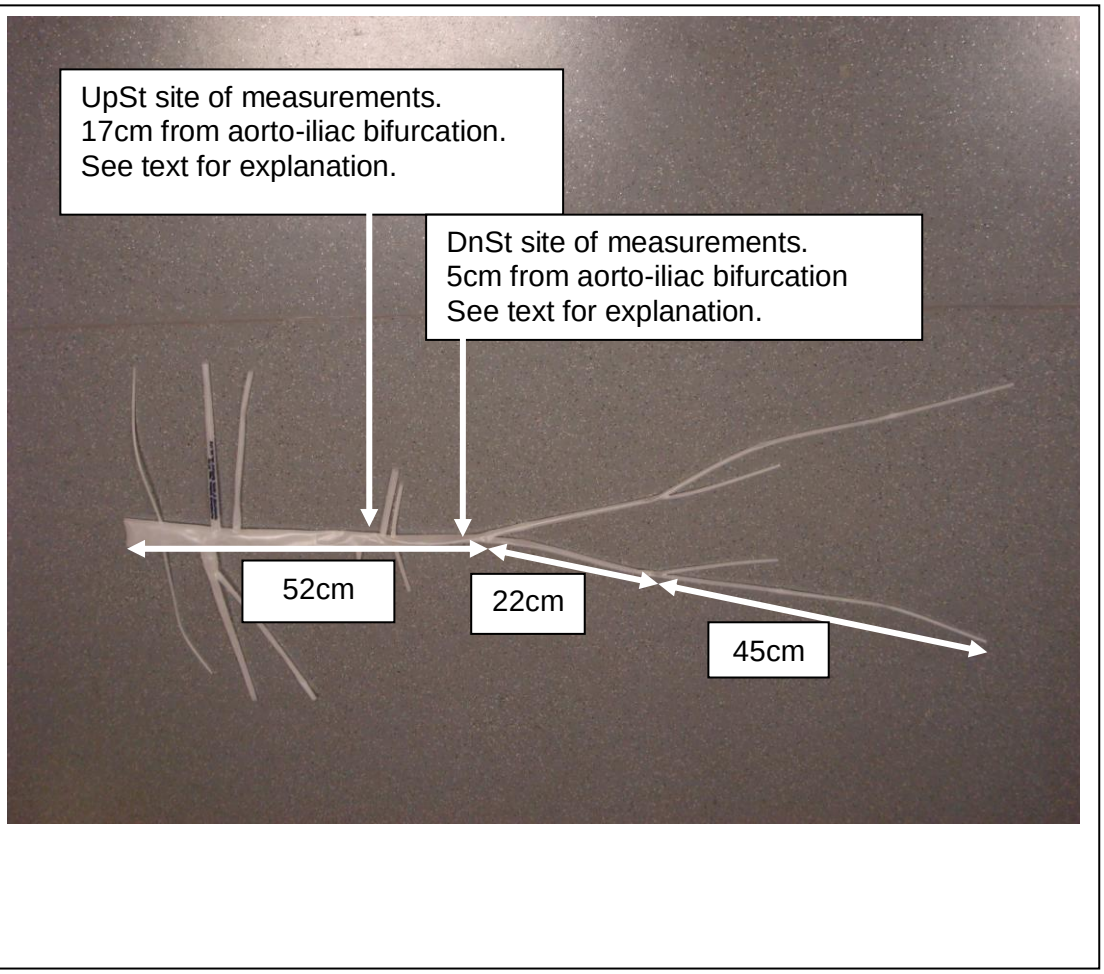

FIGURE 7.2: Lay out of Model Aorta in black plastic Trough-like Container.

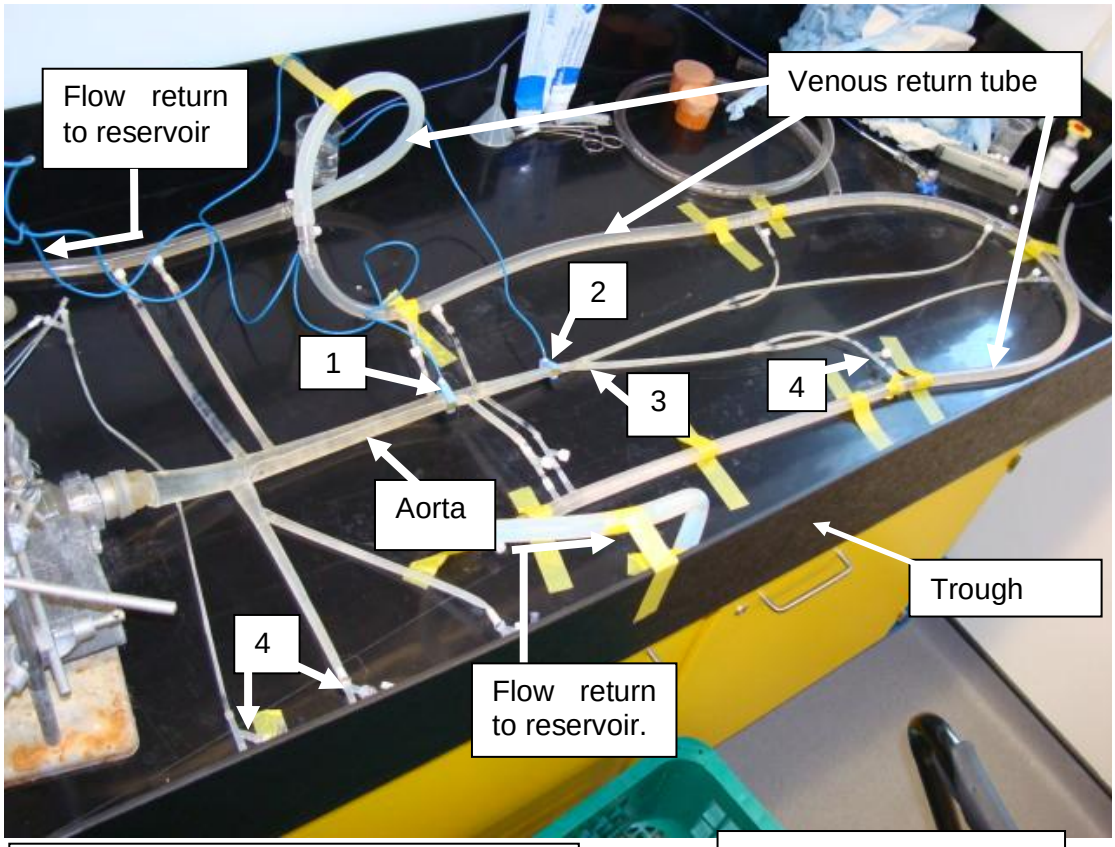

See text for explanation:
1. Upstream flow probe – UpSt site.
2. Downstream flow probe – DnSt site

3. Aorto-iliac bifurcation

4. Examples of Stiff plastic Y-pieces

and served as the venous system returning the fluid to a reservoir, referred to as the venous reservoir (Figure 7.2 and 7.8 show the venous return tube). The distal stiff plastic Y-piece tubes and connectors were of a bore that did not present hydraulic resistances sufficient to maintain the mean arterial pressure at the desired working pressure of 90-100mmHg, so a variable clamp was placed on the venous return tube at its exit into the venous reservoir. The variable clamp could be adjusted to give the required pressure.

The hydrostatic head of the venous reservoir was maintained at 13.6cmH_2O (≡10mmHg) above the model circulation; the hydrostatic head is referred to as venous pressure (VP). The circulation was driven by a left ventricular assist device (LVAD – see below) which itself was hydraulically driven by a pump (described below). For all experiments the pump was set to deliver a stroke volume (SV) of 50ml at 60 pump cycles per minute (i.e. 1Hz; referred to as heart rate or HR) thus delivering an output, referred to as cardiac output (CO), of 3000ml.min^{-1} (5.01x10^{-5} m^3.s^{-1}). The pump cycle period of 1s comprised a systolic ejection time of 320ms and diastolic filling period of 680ms; these timings are based on data for human cardiac function (Figure 7.3; Nelson *et al*., 1974; Yaginuma *et al*., 1972). Total peripheral resistance (TPR) was calculated as TPR=(MAP-VP)/CO.

FIGURE 7.3: Human Cardiac Ejection Times with Heart Rate.
Data from Nelson *et al*., (1974); Yaginuma *et al*., (1972).

Equation of linear fit: $y = -1.5083x + 408.78$; ($R^2 = 0.8201$)

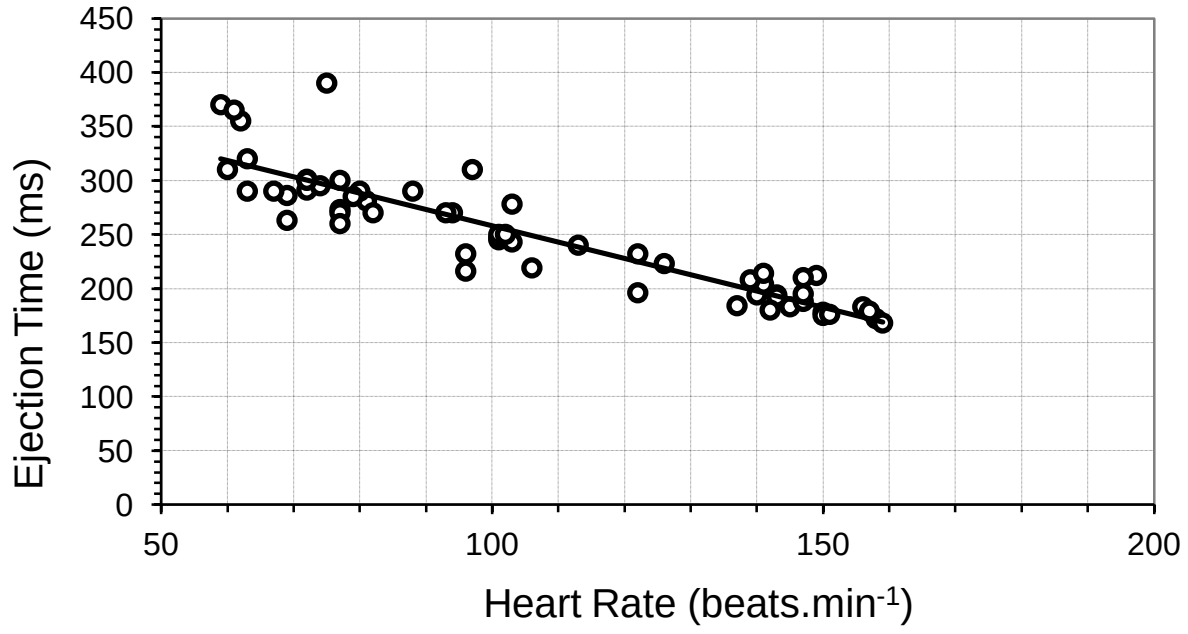

A) The Left Ventricular Assist Device (LVAD)

The LVAD (model ABIOMED BVS 5000) is made of Perspex (Figure 7.4) and designed as an extracorporeal blood circulator to assist the heart during surgical procedures on the heart, or to assist the latter during cardiac failure. The device has two chambers in series, the upstream chamber acts as the left atrium while the downstream chamber acts as the left ventricle. For the experiments detailed in this chapter, the upstream chamber (left atrium) was not activated and filled passively from the venous reservoir; the downstream chamber (left ventricle) was actively and hydraulically pumped (see B, next below). Figure 7.6 also shows an LVAD set up for an experiment with a model aorta. Figure 7.5 is a simple diagram of the LVAD device but illustrating *only* the downstream left ventricular chamber function used for the model aorta. The LVAD has capacity to deliver a stroke volume of 100ml; however 50ml was used for these experiments as preliminary assessments of pump-function found that the system did not operate smoothly with stroke volumes, e.g. 90ml, much greater than 50ml at the chosen pump frequency of 1Hz.

FIGURE 7.4: The Left Ventricular Assist Device (LVAD; Model ABIOMED BVS 5000)

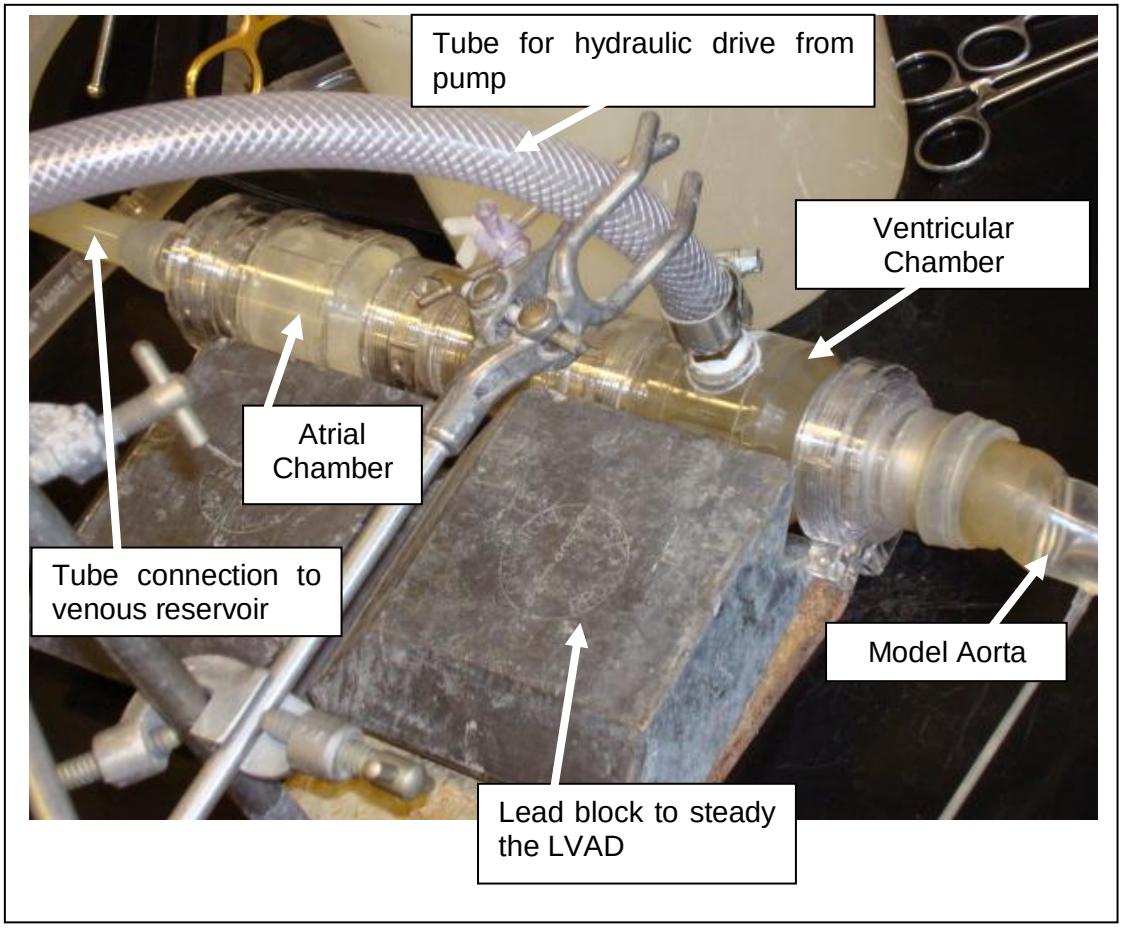

FIGURE 7.5: A simple diagram of function of the Left Ventricular Assist Device (LVAD; model ABIOMED BVS 5000) illustrating *only* the Ventricular Aspect of the LVAD Function.

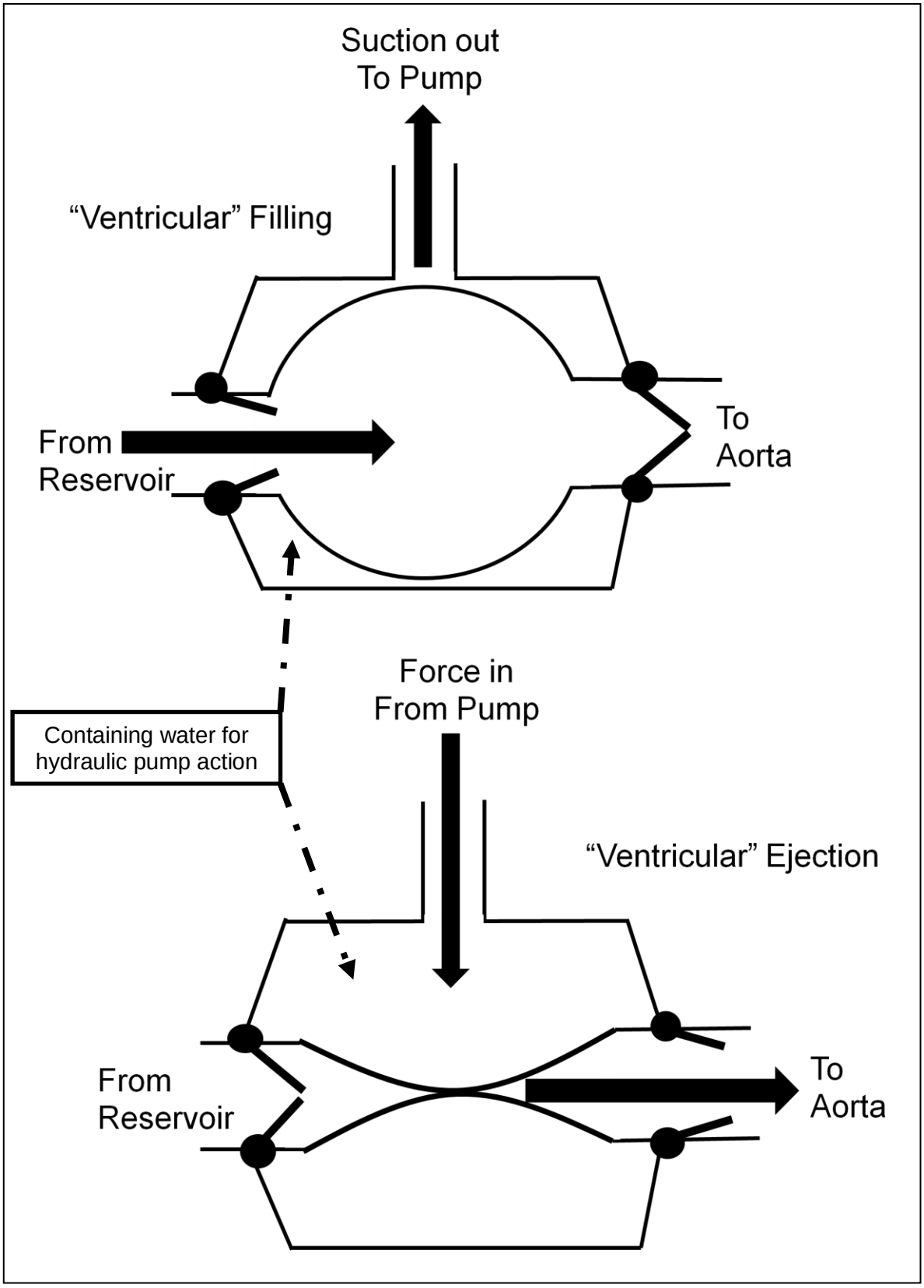

B) The Pump for driving the LVAD

The pump (Figure 7.6 and 7.7) is named the Imperial College London Heart Simulator Pump (PP212-003-07). The pump was constructed by Placepower UK Ltd. The pump action is driven by a stepper motor; the latter is driven by an intelligent stepper drive which is controlled from a PC with the appropriate software designed by Easitools, Parker Hannifin PLC (also Parker Automation). The software enables control of stroke volumes, timing of systolic ejection and diastolic filling periods, as well as flow waveforms. Fully detailed instruction manuals were supplied with the pump and an Excel spread sheet provided for calculation of the required pump characteristics.

FIGURE 7.6: The Heart Simulator Pump: External Details.

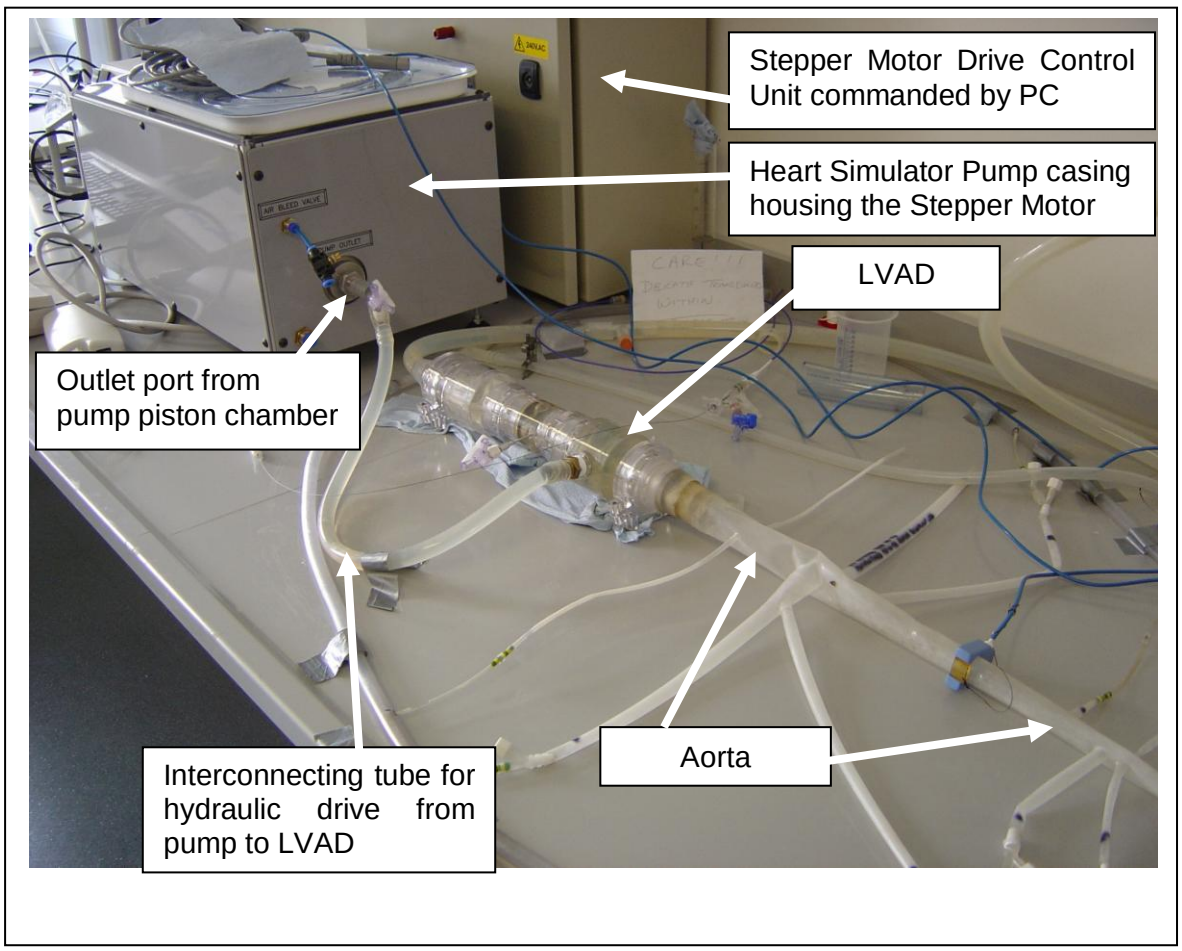

FIGURE 7.7: The Heart Simulator Pump: Internal Details showing Stepper Motor and Piston Chamber.

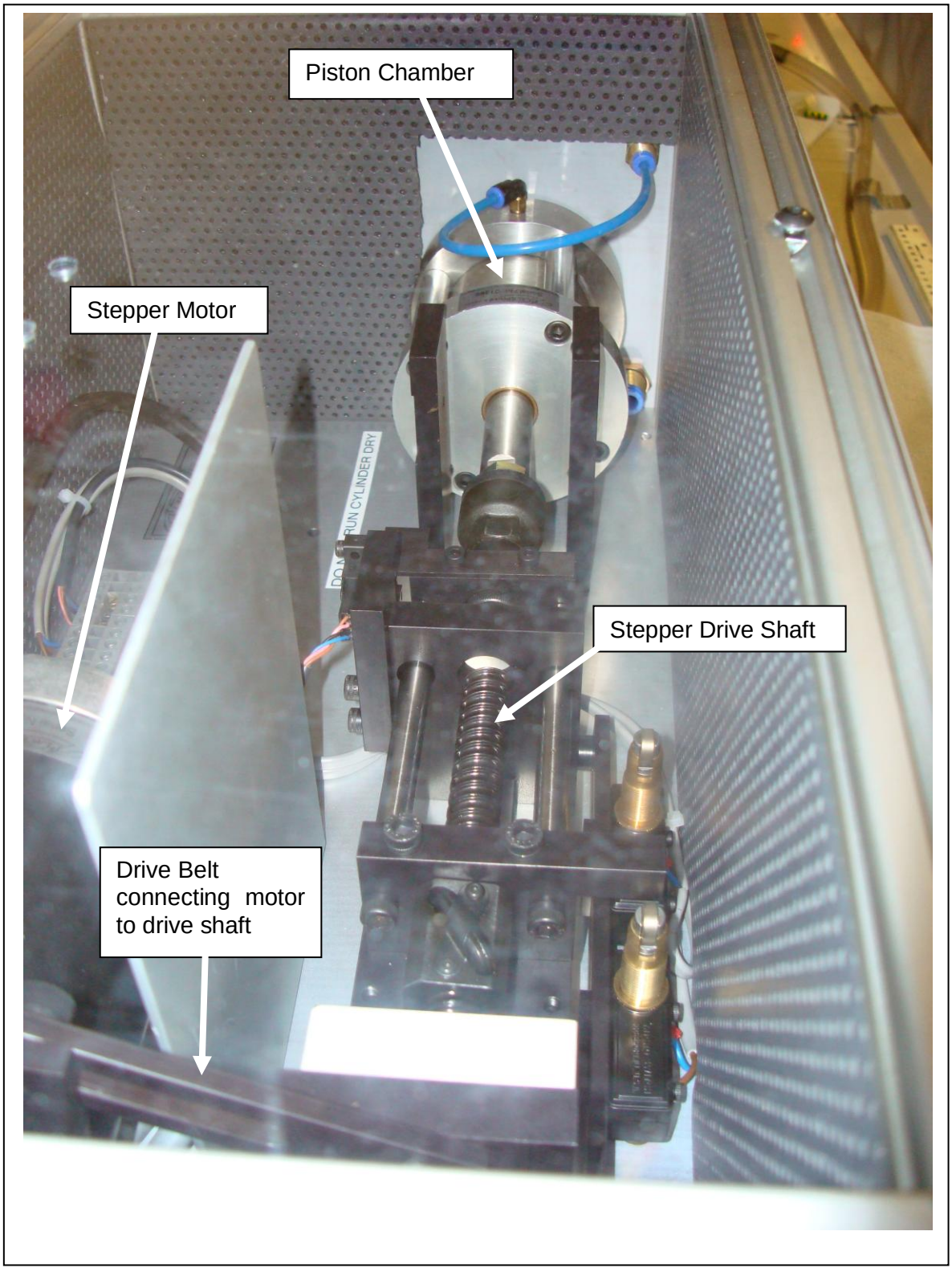

C) Experimental Procedures

All experiments were performed at room temperature (~20°C); water was used as the circulating fluid.

The model aorta was subjected to pressure-volume measurements to determine its compliance (distensibility). The method used was that described by Segers *et al*. (1998). This was done by sealing the terminal outlets of the conduit arteries, filling the aorta and conduit arteries with water (ensuring exclusion of all air bubbles) and then sealing the inlet of the aorta by using a rubber bung secured firmly into the inlet. Water was injected into the aorta and conduit arteries by syringe via one of the coronary arteries until the aorta and conduit arteries were at a low stress (~5mmHg) sufficient for a strain maintaining their tubular and tapered form; this was taken as the basal condition from which the pressure-volume curve was constructed. A Millar catheter (SPR 407) was used to measure pressure within the aorta model at the position of the ascending aorta. Incremental 5ml volumes of water were delivered by syringe into the model aorta and the associated incremental increases in pressure were recorded; this was termed *loading*. Approximately 10s were allowed between each injected 5ml increment for viscoelastic responses of the polyurethane aorta to settle. Loading with incremental 5ml volumes was continued to a total cumulated volume of 80ml which resulted in a pressure of ~150mmHg (~20kPa). This was followed by withdrawal of 5ml increments from the model aorta to return to the basal condition; this was termed *unloading*. This procedure of loading and unloading was carried out 4 times; the readings were averaged to construct a pressure-volume curve (Figure 7.17 in section 7.3). Incremental compliance was calculated from the four pressure-volume curves and also averaged to construct a compliance curve for the model aorta (Figure 7.17 in section 7.3). Compliance was calculated using Eq. 6.1 (see page 208).

For the haemodynamic-type experiments with the model aorta, pressures were measured using two Millar catheters, model SPR 407 & SPC 721; the latter is a dual sensor model but its proximal sensor was not used due to damage but instead the damaged sensor acted as a marker against which to place the SPR 407 sensor. Their active sensors were place (unless stated otherwise) 50mm apart from each other for measurements of PWV; this measure was made at prescribed positions within the model aorta. Two sites on the abdominal section of the model aorta were chosen for measurement of aortic blood flow and pressure. These two sites are indicated as UpSt (namely upstream) and DnSt (namely downstream) in Figure 7.1B. The UpSt site lies between the arteries representing the celiac and superior mesenteric arteries and is 17cm upstream of the aorto-iliac bifurcation (Figure 7.1B); the DnSt site lies downstream of the arteries representing the renal arteries but 5cm upstream of

the aorto-iliac bifurcation (Figure 7.1B). This arrangement for UpSt and DnSt sites of measurement on the abdominal section of the model aorta approximately mimics the arrangement used for the *in vivo* experiments with anaesthetised rabbits (see Chapter 4) but data obtained is not intended to be comparable with the *in vivo* data since anaesthetised rabbits and the model polyurethane aorta are very different systems. The attachment of the two Transonic blood flow probes are indicated in Figure 7.2; one flow probe (type MA14PAX - 14 mm) at UpSt (indicated as '1' in Figure 7.2), the other (type MA10PAX - 10mm) at DnSt (indicated as '2' in Figure 7.2). PWV was measured by the "foot-to-foot" ($C_{ft\text{-}ft}$) and PU loop method at both these sites, namely UpSt and DnSt sites; furthermore, a "foot-to-foot" measurement of PWV was taken for the aorta length from a position in the ascending aorta adjacent to the coronary arteries to the aorto-iliac bifurcation – over a distance of 46.5cm measured by tape measure.

As a simple model of aortic ageing, part of the model was "stiffened" by wrapping it in Clingfilm. The entire length of the aorta and both iliac arteries were wrapped as closely and as tightly as possible while the aorta was subjected to a pressure of 10mmHg; this pressure gave turgidity to the aorta and iliac arteries while maintaining their circular forms. Using the method as described above for the normal aorta, the "stiffened" aorta was subjected to pressure-volume measurements to determine its compliance (distensibility); an average pressure-volume curve was constructed (Figure 7.18 in section 7.3). Incremental compliance was calculated from the pressure-volume curves to give an averaged compliance curve (Figure 7.18 in section 7.3). Compliance was calculated using Eq. 6.1 (see page 208).

The effect of distal compliances on the pressure pulse was also determined in the "stiffened" aorta. The distal compliances were 10ml syringes containing air with the syringe plunger secured by polythene tape (Figure 7.8); a distal compliance, i.e. a syringe, was fixed into a port of each of the 13 stiff plastic Y-piece tubes where the terminal conduit arterial branches from the aorta connected into the venous return tube (Figure 7.8).

Segers *et al*. (1998), Segers and Verdonck (2000) and Kolyva *et al*. (2010) have also used air filled syringes for distal compliances in their model circulations. Calibration was carried out by subjecting a 10ml syringe to a pressure-volume evaluation. The nozzle of the distal compliance syringe was inserted into a port of a stiff plastic Y-piece. Water was contained in the Y-piece and into the syringe nozzle. Another syringe containing water was inserted into a second port of the Y-piece while the sensor of a Millar pressure transducer was positioned in the centre of the Y-piece via the third port of the Y-piece. The plunger of the 10ml syringe being used as the distal compliance was secured in place at set volumes of air within the

syringe; the set volumes of air were 2.5, 5.0, 7.5, 10ml as at 0mmHg (the pressure transducer was set as 0mmHg at atmospheric pressure). Incremental 0.05ml volumes of water were delivered from the water filled syringe to the distal compliance syringe, and the pressure developed was recorded. Four or more pressure-volume evaluations were carried out for each setting of air volume in the distal compliance syringe, the values were averaged to construct pressure-volume and compliance curves (see Figures 7.20 in section 7.3). This calibration was done as an alternative to calculation by the gas law relationship, pv=constant (Segers *et al*., 1998; Kolyva *et al*., 2010), because the syringe compliance system is not a perfectly constant chamber as the plunger seal is compressible; furthermore the air within the syringe is not perfectly dry.

For this model circulation, the distal compliances could be varied, though only the 10ml air volume was used. However distal resistances were not designed to vary so remained constant. If required, variable resistances could be constructed in several ways, e.g. Westerhof *et al*. (1971), Segers *et al*. (1998), and Kolyva *et al*. (2010).

Two sets of experiments were carried out as follows:

1st Expt.	#1:	normal aorta
	#1+Cf:	aorta wrapped in Clingfilm (Cf)
2nd Expt.	#2:	normal aorta
	#2+Cf:	aorta wrapped in Clingfilm (Cf)
	#2+Cf+Cd:	aorta wrapped in Clingfilm + 13 distal compliances (Cd)

The 13 distal compliances were summed as compliances in parallel and summed likewise with the compliance of the “stiffened” aorta to deduce the total compliance of the model (as per Segers *et al*., 1998).

FIGURE 7.8: The Syringe Compliance Assembly for Distal Compliance.

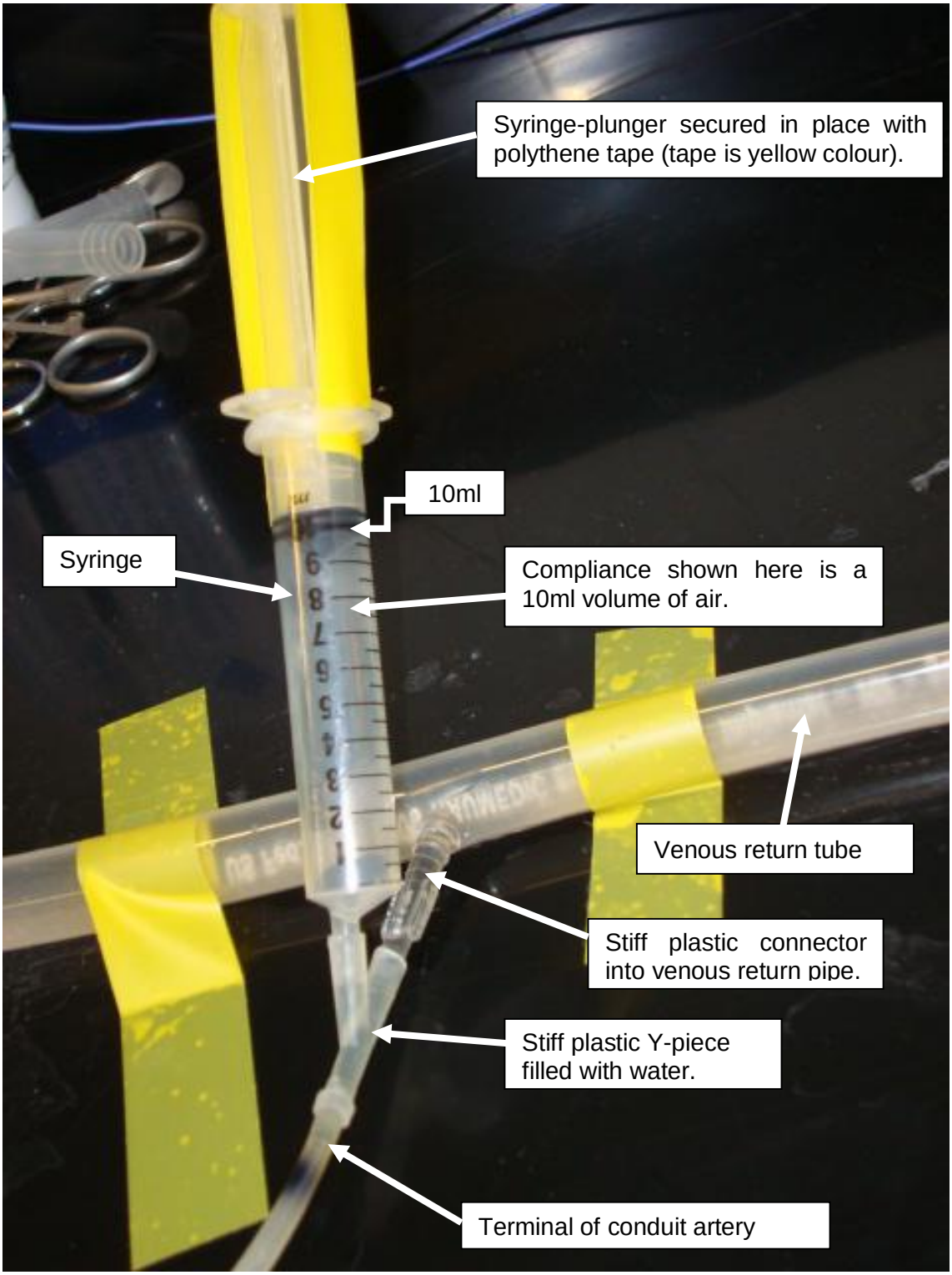

7.3 RESULTS

Basic Data

Examples of pressure and flow pulses from the normal model aorta (e.g. #1) are shown in Figures 7.9 (UpSt site) and 7.10 (DnSt site). The vertical broken line, AB, in Figures 7.9 and 7.10 marks the end of systole – point A is the pressure inflection of the incisura and point B is the flow inflection at the end of systolic flow. At these levels, namely UpSt and DnSt sites, in the model aorta line AB indicates a systolic time of 220ms, though the Heart Simulator Pump was set for a systolic ejection time of 320ms.

Figure 7.11 shows the apportionment of CO along the aorta at the UpSt and DnSt sites of measurement (see Figure 7.2 for UpSt and DnSt sites) for abdominal aortic flow (MABF); Figure 7.11 also shows values of the vascular resistance (VR) sectors of TPR at the UpSt and DnSt sites. In this model, as setup for this thesis, it is assumed that half of the cardiac output is distributed to the coronaries, common carotids, subclavians and the celiac artery. Of the other half of the cardiac output, half of this is assumed to be distributed to the superior mesenteric artery and renal arteries and the other half distributed downstream (iliacs, femorals) of the DnSt site of measurement. The values shown in Figure 7.11 are close for experiments #1 and #2, the differences (Δ %) shown in Figure 7.11 are due to inadvertent inconsistencies in set-up of the two experiments; for each experiment CO was always set the same (i.e. 3000ml.min^{-1}) from the heart simulator pump. Figure 7.12 shows that mean aortic pressure (MAP) at the UpSt abdominal aortic site for the normal aorta model was 12.36kPa (~93mmHg) for #1 and 14.35kPa (~108mmHg) for #2; the values for MAP, as expected, are little different downstream at the DnSt site of the abdominal aorta, the values being 12.24kPa (~92mmHg) for #1 and 14.42kPa (~108mmHg) for #2.

Wrapping the aorta and iliac arteries in Clingfilm had, as expected, little or no effect on MAP (Figure 7.12), MABF (Figure 7.13), VR (Figure 7.14) and TPR (Figure 7.15 – TPR as calculated from MAP at UpSt and DnSt sites) but did have a marked effect of increasing systolic (SBP) and decreasing diastolic (DBP) pressures thereby markedly increasing (widening) the pulse pressure (Figure 7.16).

FIGURE 7.9: Example of Pressure and Flow Pulses at the UpSt Site of Measurement in the Abdominal Aorta section of the Normal Model Aorta #1.

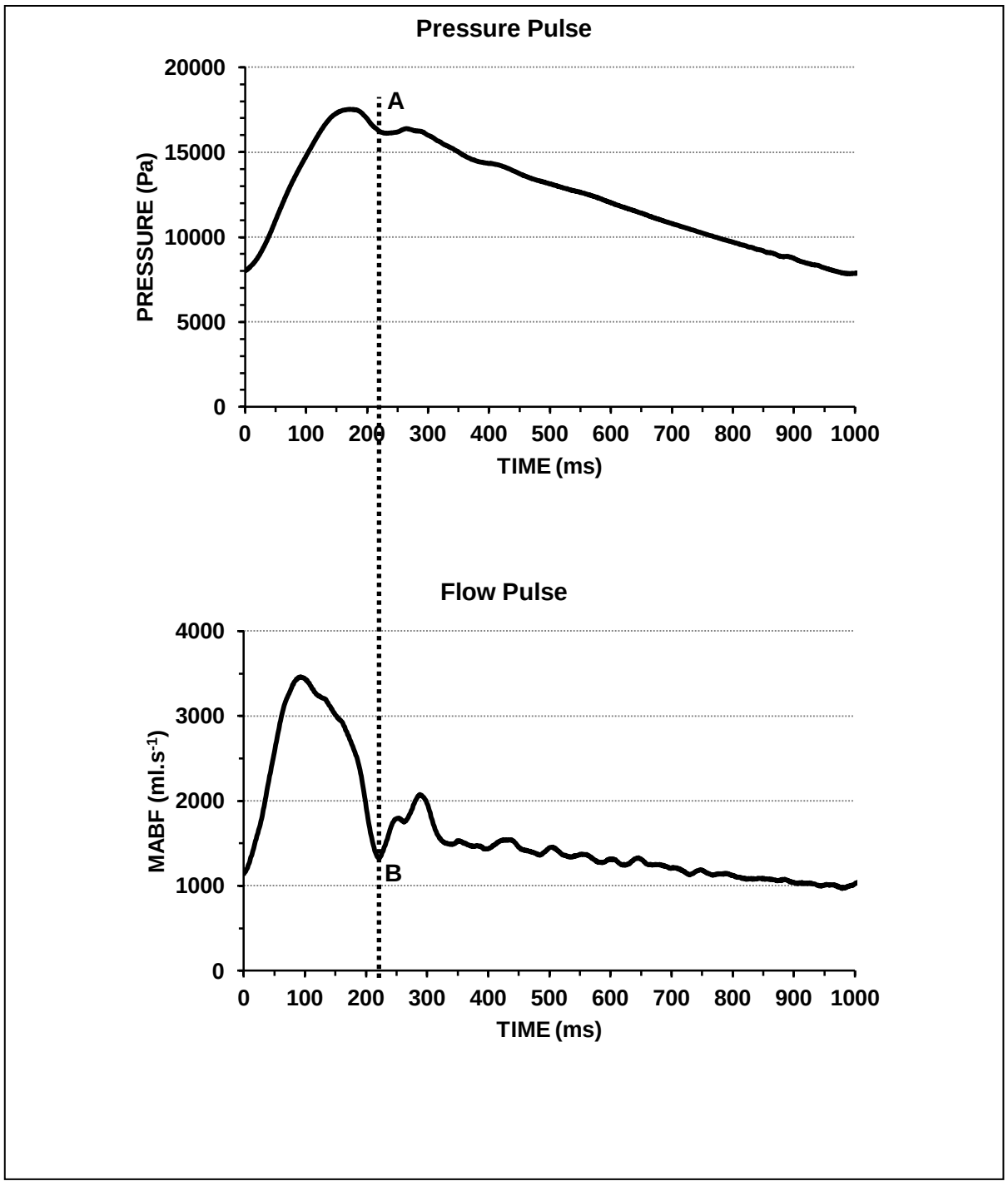

AB broken vertical line indicates time of end of systole. Pressure inflection at point A is the incisura; flow inflection at point B is end of systolic flow.

FIGURE 7.10: Example of Pressure and Flow Pulses at the DnSt Site of Measurement in the Abdominal Aorta section of the Normal Model Aorta #1.

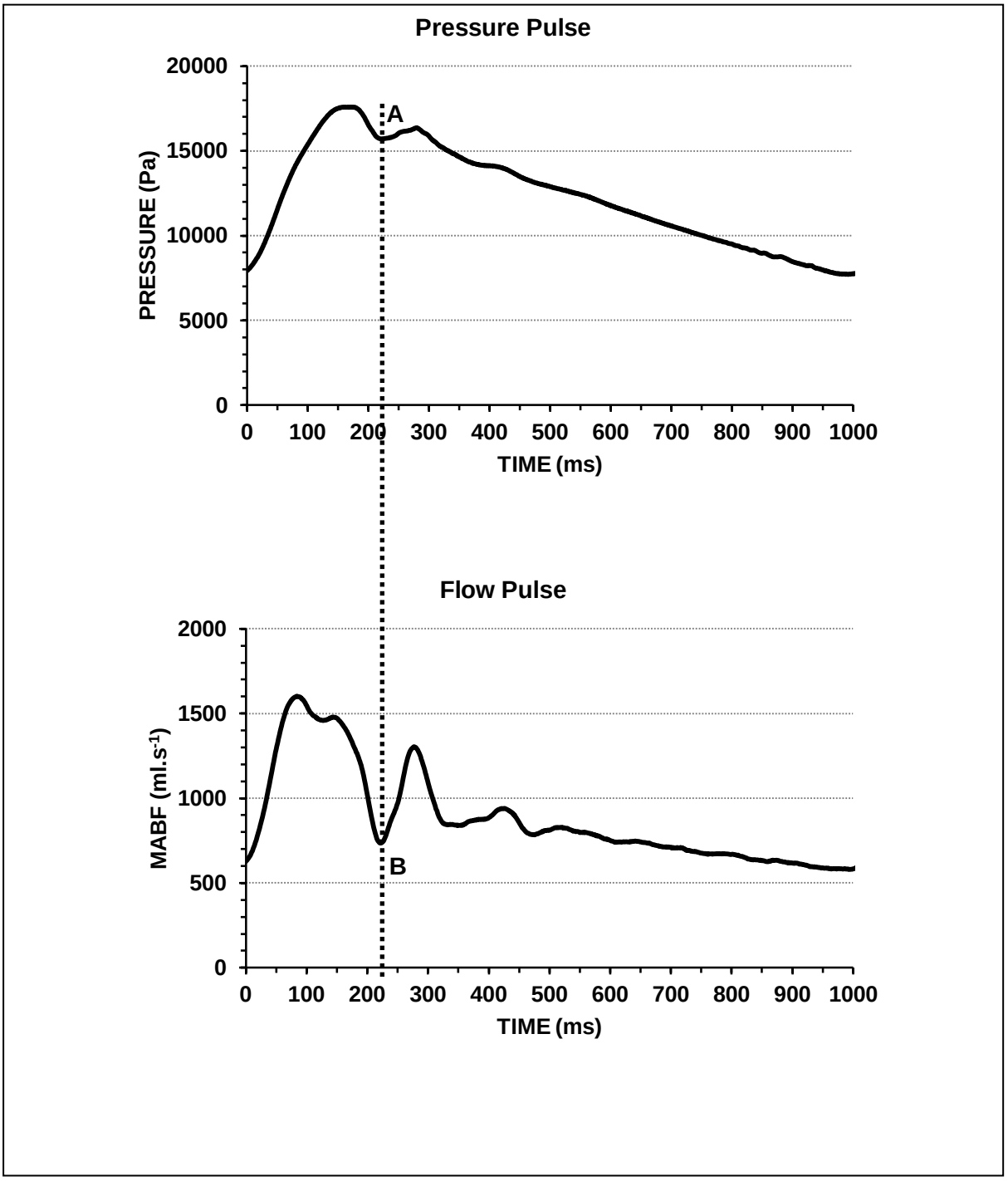

AB broken vertical line indicates time of end of systole. Pressure inflection at point A is the incisura; flow inflection at point B is end of systolic flow.

FIGURE 7.11: Apportionment of Cardiac Output (CO) and Total Peripheral Resistance (TPR) into Vascular Resistances (VR) along the Aorta at the UpSt and DnSt Sites of Measurement in the Abdominal Aorta section, for the Two Experiments #1 and #2.

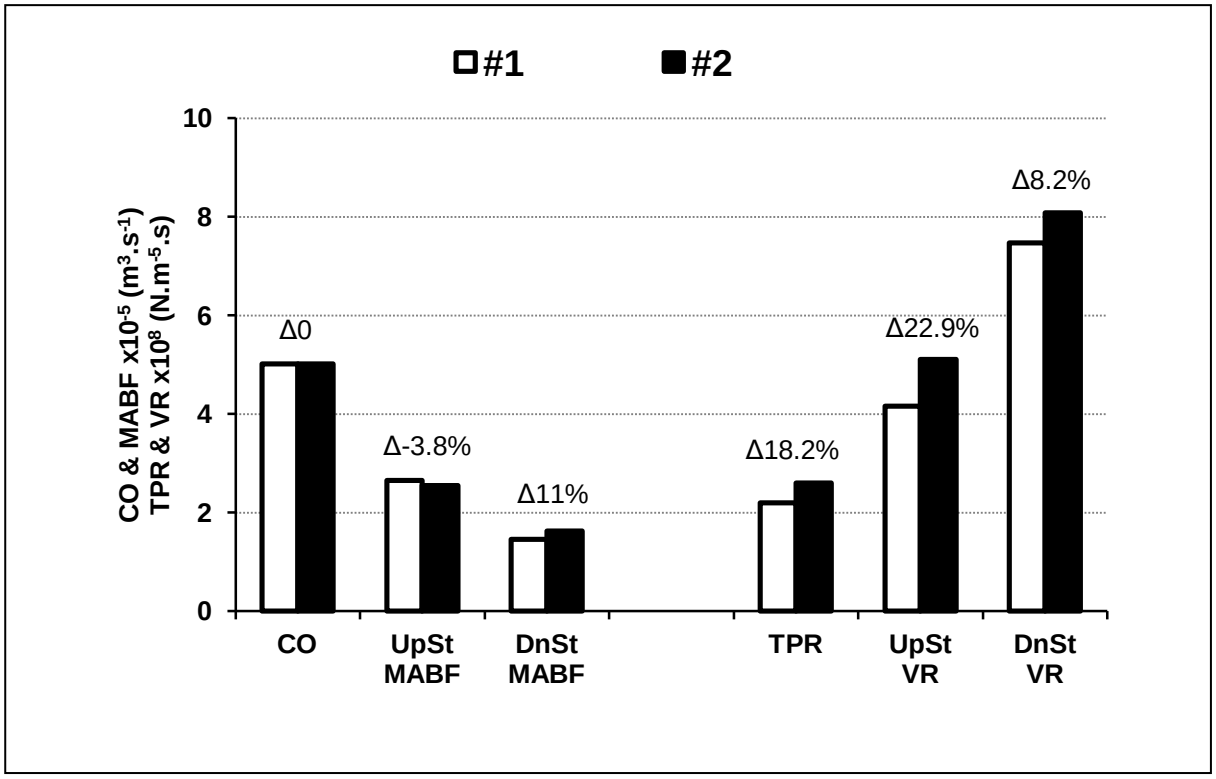

Δ values are differences between #1 and #2 as a % of the value for #1

Cardiac output (CO) is 5.0×10^{-5} $m^3.s^{-1}$ = $3 L.min^{-1}$

FIGURE 7.12: Mean Aortic Pressure (MAP) before (#1 & #2) and after (#1+Cf & #2+Cf) wrapping the Model Aorta and Iliac Arteries in Clingfilm. Also included is the application of the distal compliances (#2+Cf+Cd). Measurements made at the UpSt & DnSt Sites in the Abdominal Aorta of the Model.

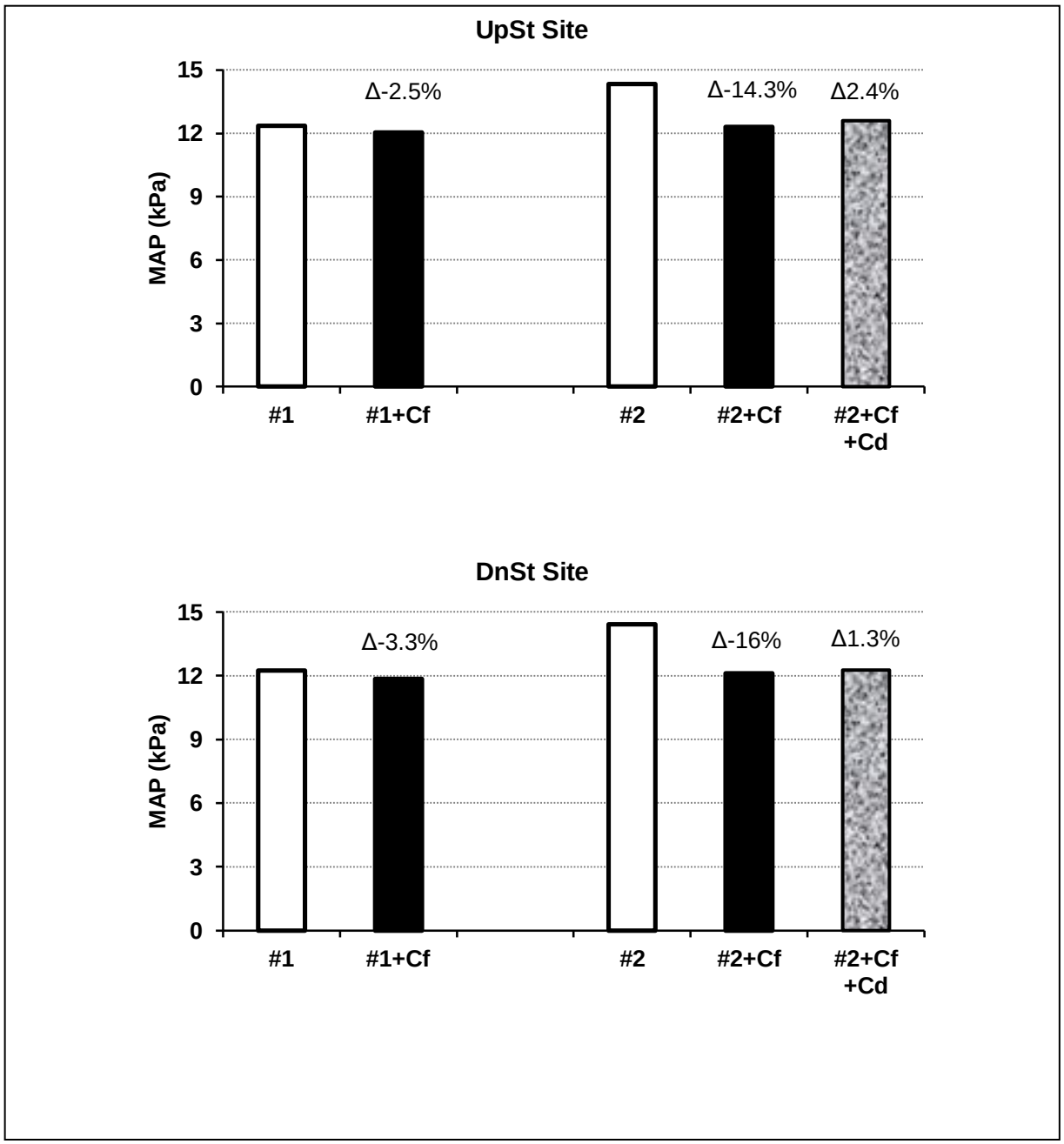

Δ values are the differences between:

#1 and #1+Cf as a % of #1,
#2 and #2+Cf as a % of #2.
#2+Cf and #2+Cf+Cd as a % of #2+Cf

FIGURE 7.13: Mean Abdominal Aortic Blood Flow (MABF) before (#1 & #2) and after (#1+Cf & #2+Cf) wrapping the Model Aorta and Iliac Arteries in Clingfilm. Also included is the application of the distal compliances (#2+Cf+Cd). Measurements made at the UpSt & DnSt Sites in the Abdominal Aorta of the Model.

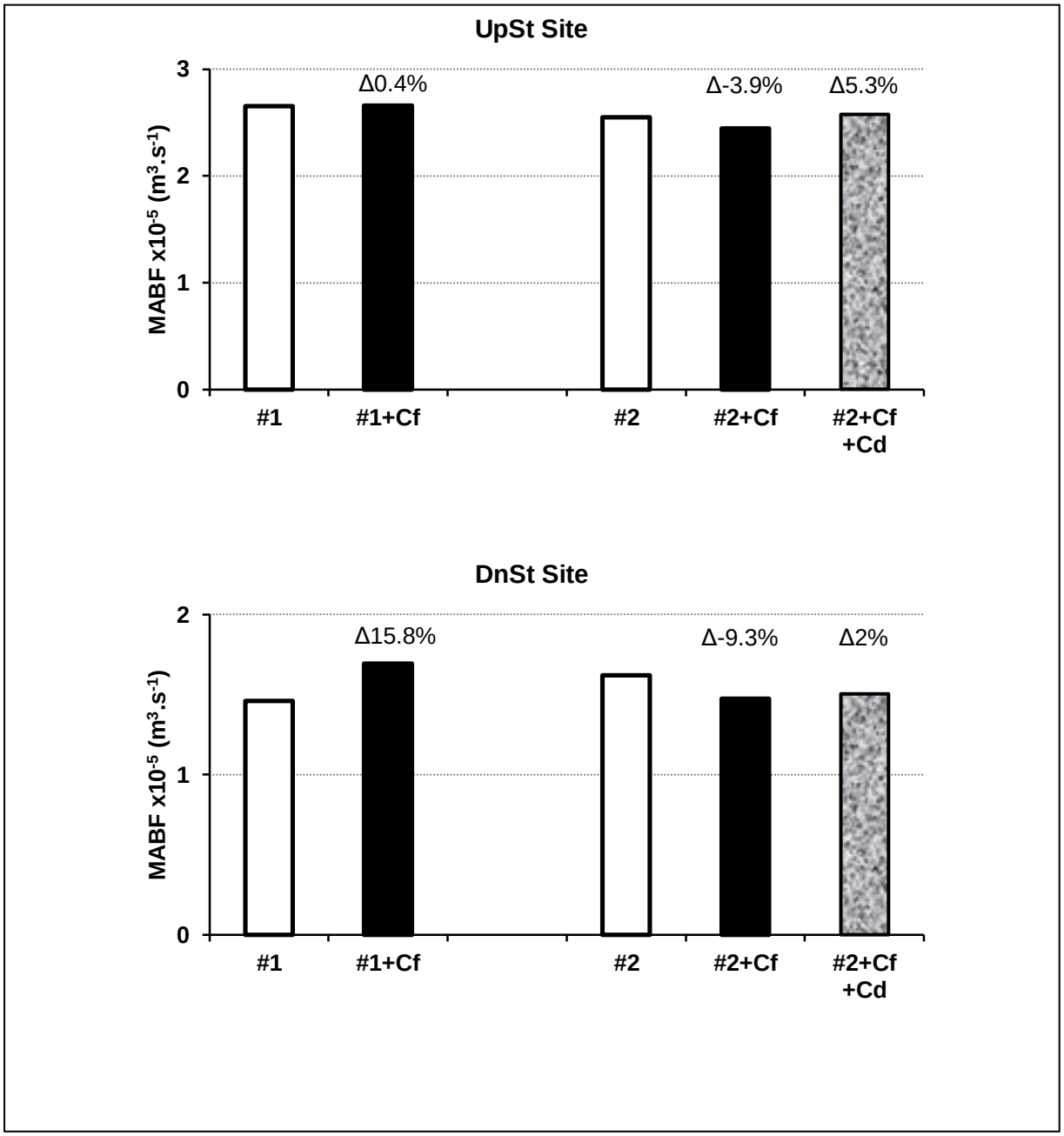

Δ values are the differences between:

#1 and #1+Cf as a % of #1,
#2 and #2+Cf as a % of #2.
#2+Cf and #2+Cf+Cd as a % of #2+Cf

FIGURE 7.14: Vascular Resistances (VR) before (#1 & #2) and after (#1+Cf & #2+Cf) wrapping the Model Aorta and Iliac Arteries in Clingfilm. Also included is the application of the distal compliances (#2+Cf+Cd). Measurements made at the UpSt & DnSt Sites in the Abdominal Aorta of the Model.

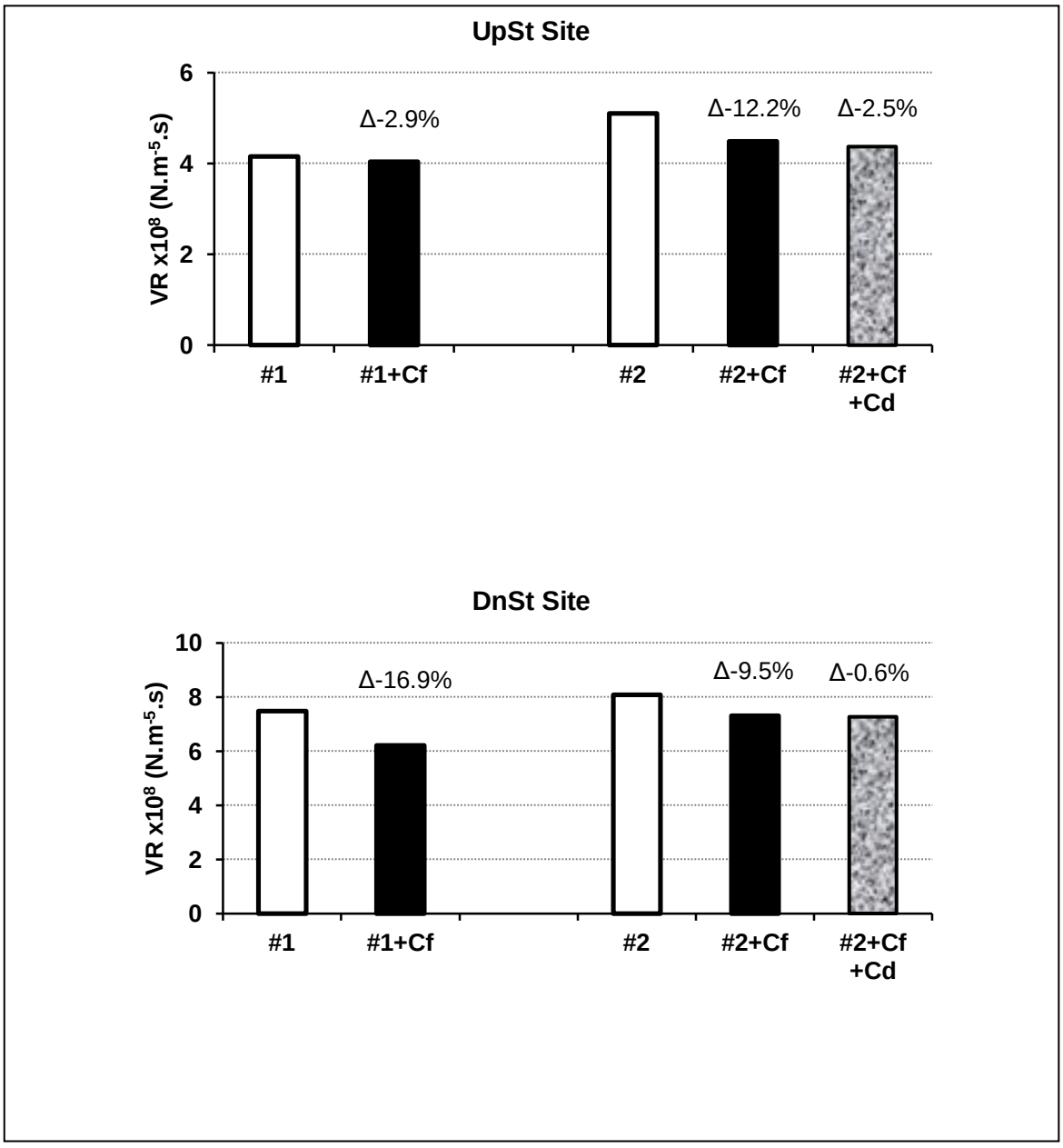

Δ values are the differences between:

#1 and #1+Cf as a % of #1,
#2 and #2+Cf as a % of #2.
#2+Cf and #2+Cf+Cd as a % of #2+Cf

FIGURE 7.15: Total Peripheral Resistance (TPR)* before (#1 & #2) and after (#1+Cf & #2+Cf) wrapping the Model Aorta and Iliac Arteries in Clingfilm. Also included is the application of the distal compliances (#2+Cf+Cd). Measurements made at the UpSt & DnSt Sites in the Abdominal Aorta of the Model.

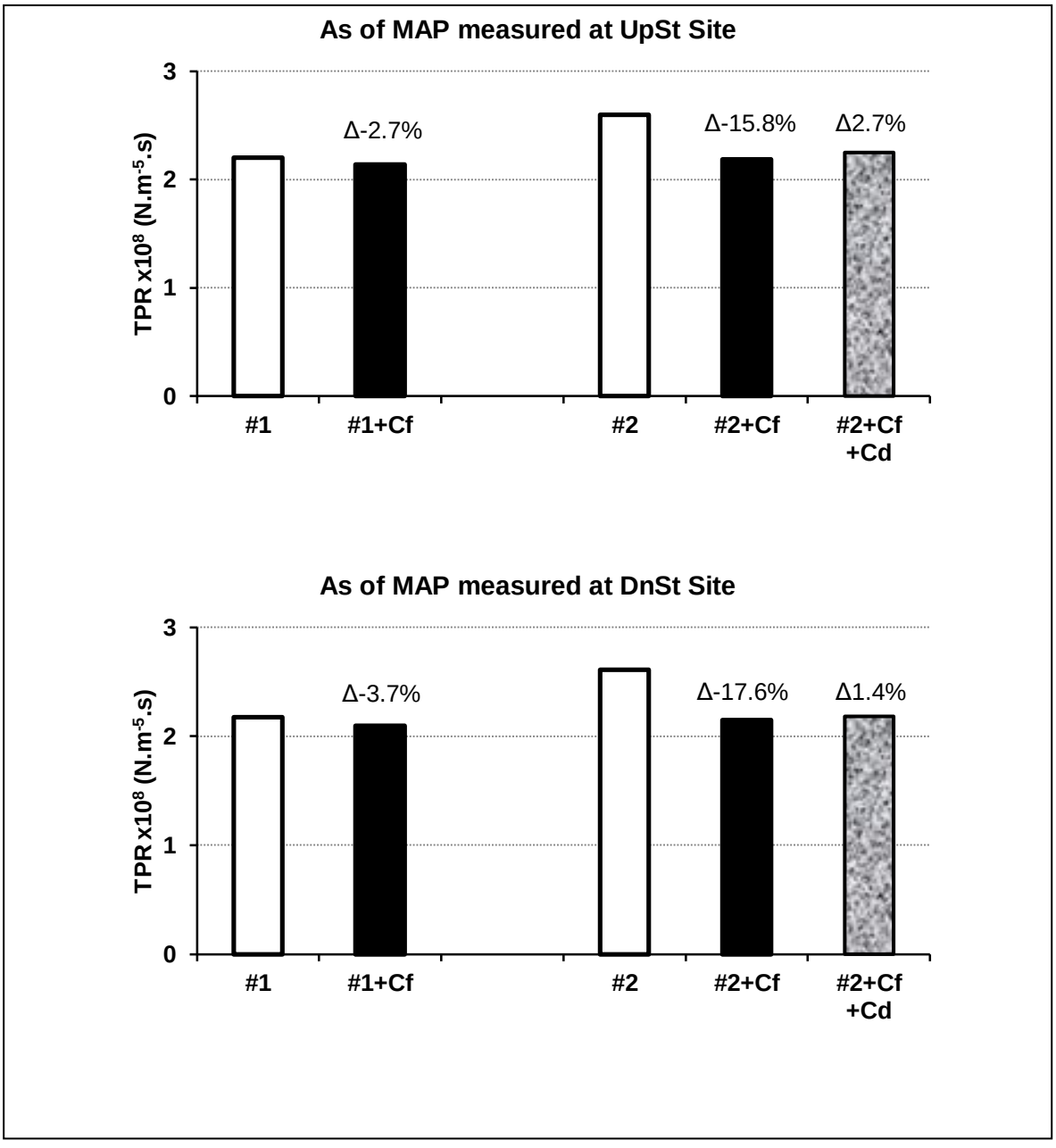

*TPR as calculated from MAP of UpSt and DnSt sites. MAP is expected to be little different between the two sites but changing the Millar transducer positions might have caused a small disturbance hence MAP of #2+Cf UpSt is slightly more than DnSt (see Figure 7.10).

Δ values are the differences between:

#1 and #1+Cf as a % of #1,
#2 and #2+Cf as a % of #2.
#2+Cf and #2+Cf+Cd as a % of #2+Cf

FIGURE 7.16: Systolic (SBP; top of columns), Diastolic (DBP; bottom of columns) and Pulse Pressure (bar length) before (#1 & #2) and after (#1+Cf & #2+Cf) wrapping the Model Aorta and Iliac Arteries in Clingfilm. Also included is the application of the distal compliances (#2+Cf+Cd). Measurements made at the UpSt & DnSt Sites in the Abdominal Aorta of the Model

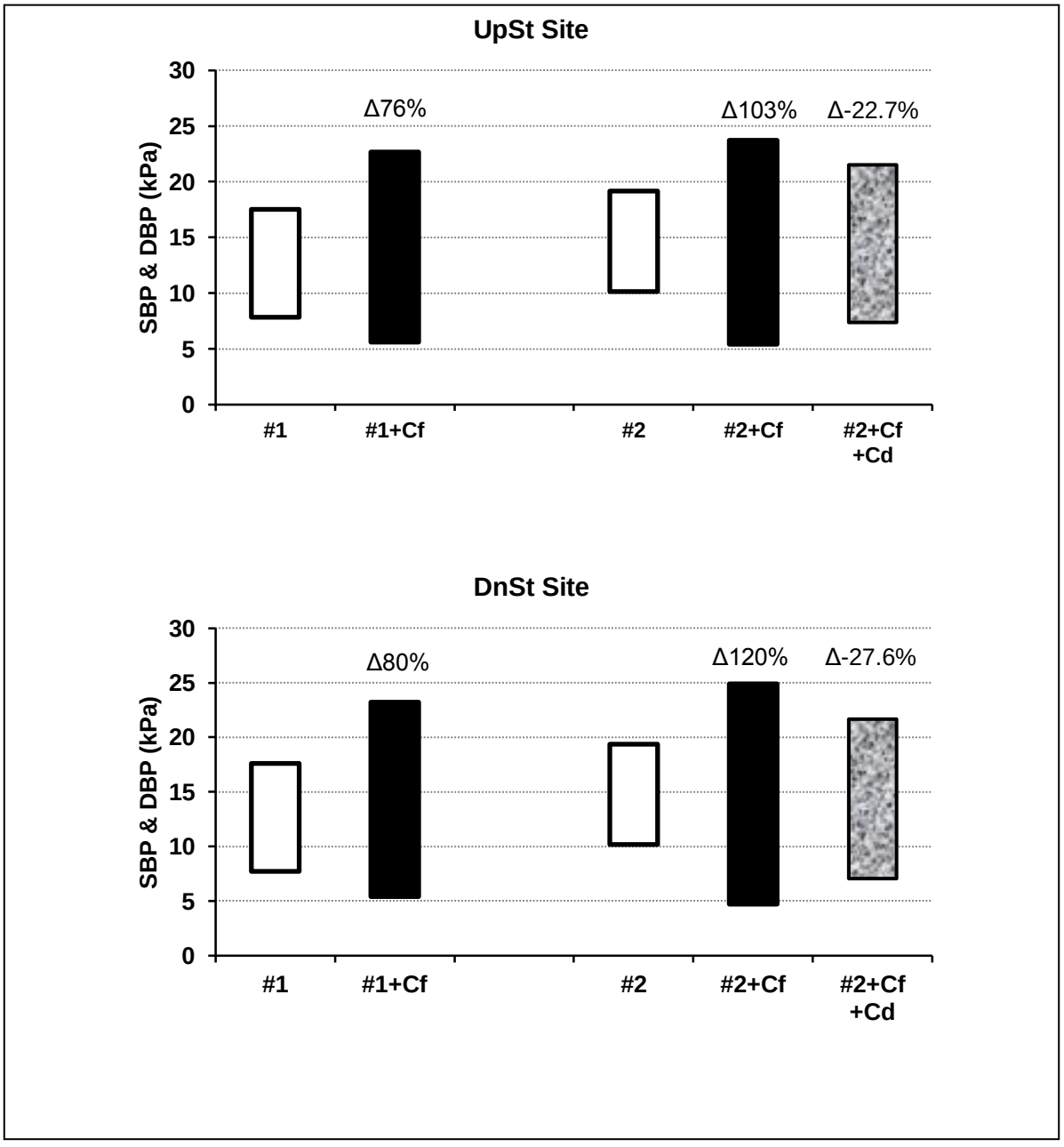

Δ values are the differences of bar lengths (pulse) between:
#1 and #1+Cf as a % of #1,
#2 and #2+Cf as a % of #2.
#2+Cf and #2+Cf+Cd as a % of #2+Cf

The inclusion of the distal compliances (13x 10ml air volume in syringes) to the Clingfilm-wrapped model aorta had little consistent or no effects on MAP (Figure 7.12), MABF (Figure 7.13), VR (Figure 7.14) and TPR (Figure 7.15) but did decrease SBP and increased DBP, thereby decreasing the pulse pressure (Figure 7.16). The function of compliance on the aorta model is now considered further.

Compliance of the Model Aorta

Pressure-volume curves and the derived compliance curves were plotted for loading and unloading the normal aorta model (Figure 7.17) and Clingfilm-wrapped aorta model (Figure 7.18). It can be seen that hysteresis occurs for the pressure-volume curves in that the unloading curve diverges from the loading curve; this hysteresis results from the visco-elastic nature of the polyurethane material of the model aorta. For purpose of comparison between the normal and Clingfilm-wrapped aorta models, their loading/unloading curves for pressure-volume and for compliance have been re-plotted in Figure 7.19 where the loading/unloading data are combined into one curve for the pressure-volume data and one curve for the compliance data, thus allowing curves of best fit be constructed for the data points (equations for the curves of best fit are shown only for the compliance curves in Figure 7.19). Thus plotted, it can be seen in Figure 7.19 that both the pressure-volume and compliance curves for the normal model diverge upwards away from those curves of the Clingfilm-wrapped model.

The *combined* loading/unloading curves for compliance in Figure 7.19 were chosen for calculating compliance at given pressures by use of the equations for curve of best fit. Thus, knowing the MAP of either the normal model aorta or the Clingfilm-wrapped model aorta, the compliance of either model (aorta plus conduit arteries) can be obtained from the compliance curves plotted in Figure 7.19, thus:

Model	MAP (as of UpSt in Figure 7.12)	Compliance (obtained from Figure 7.19)
#1	12.36kPa [93mmHg]	3.59×10^{-9} $m^3.Pa^{-1}$ [0.48ml.$mmHg^{-1}$]
#1+Cf	12.05kPa [90mmHg]	2.33×10^{-9} $m^3.Pa^{-1}$ [0.31ml.$mmHg^{-1}$]
#2	14.35kPa [108mmHg]	3.95×10^{-9} $m^3.Pa^{-1}$ [0.53ml.$mmHg^{-1}$]
#2+Cf	12.30kPa [92mmHg]	2.32×10^{-9} $m^3.Pa^{-1}$ [0.31ml.$mmHg^{-1}$]

The above compliance values are plotted in Figure 7.21. It is clear from Figure 7.21 that the compliance of the Clingfilm-wrapped model aorta is much less than that of the normal model aorta – decreases of -35.1% (#1 to #1+Cf) and -41.3% (#2 to #2+Cf).

Pressure-volume curves and derived compliances for a distal compliance (a 10ml syringe) set at various initial air volumes are shown in Figure 7.20. Distal compliances with initial air volume of 10ml were applied to the Clingfilm wrapped aorta (#2+Cf+Cd). At a given MAP, the compliance of a distal compliance with initial 10ml volume of air can be calculated from Figure 7.20, using the equation for curve of best fit. Thus, at the MAP of 12.60kPa (95mmHg; UpSt in Figure 7.12) for model #2+Cf+Cd, one distal compliance is 0.789×10^{-10} $m^3.Pa^{-1}$. This value is multiplied by 13, as 13 such distal compliances were used, to give the sum distal compliance of 1.026×10^{-9} $m^3.Pa^{-1}$ ($0.137 ml.mmHg^{-1}$) which is of the 13 distal compliances in parallel; compliances are in a parallel arrangement in the model (c.f. Segers *et al*., 1998). The total compliance value for the model #2+Cf+Cd is the sum of the distal compliances in parallel with the compliance of the Clingfilm-wrapped aorta, thus:

#2+Cf at MAP of 12.60kPa (95mmHg) has compliance of:	2.31×10^{-9} $m^3.Pa^{-1}$
13x Cd at MAP of 12.60kPa has compliance of:	1.03×10^{-9} $m^3.Pa^{-1}$
#2+Cf+Cd at MAP of 12.60kPa has total compliance of:	3.34×10^{-9} $m^3.Pa^{-1}$ [$0.45 ml.mmHg^{-1}$]

The compliance of the #2+Cf+Cd model is plotted in Figure 7.21; the summation of the 13 distal compliances to the compliance of the Clingfilm-wrapped model #2+Cf increases the compliance by 44% over that of #2+Cf.

The compliances obtained from the pressure-volume plots are for the models in their static state. In their functioning, or dynamic, state fluid is pumped and circulated in a pulsatile manner, so the functioning compliance, or arterial compliance (AC), can be calculated. AC of the functioning model is calculated from the time constant, tau (τ), of the diastolic decay of the pressure pulses ($AC = \tau / VR$); τ is the reciprocal of B (or b in Eq. 2.20 of Chap. 2) which is the diastolic decay rate constant (see Chap. 2). Values of AC for the functioning normal and Clingfilm-wrapped aortic models are plotted in Figure 7.22. The trend of this data in Figure 7.22 is consistent with that of Figure 7.21 in that AC of the Clingfilm-wrapped model aorta is much lower than that of the normal model aorta; differences (Figure 7.22) in AC were -71.6% (UpSt) or -66.5% (DnSt) for #1 to #1+Cf, and -84.4% (UpSt) or -81.9% (DnSt) for #2 to #2+Cf. The effect of adding the distal compliances to the functioning Clingfilm-wrapped model increased its compliance by 33% (UpSt Site) or 37% (DnSt Site) (Figure 7.22), a

change similar to that (44%) for the summed value of Clingfilm-wrapped + distal compliance as shown in Figure 7.21 for #2+Cf+Cd. It is notable that the calculated values of AC (Figure 7.22) for the functioning normal and Clingfilm-wrapped models are some 1000 fold greater than the compliance values obtained from the compliance plots (Figures 7.19 & 7.20) for the two models when they static.

FIGURE 7.17: Pressure-Volume and Compliance Curves for Volume Loading and Volume Unloading of the Normal Model Aorta. Curves shown are the average of four curves; majority of standard deviation bars are within the data point markers. (Pressure measured in the section equivalent to the ascending aorta).

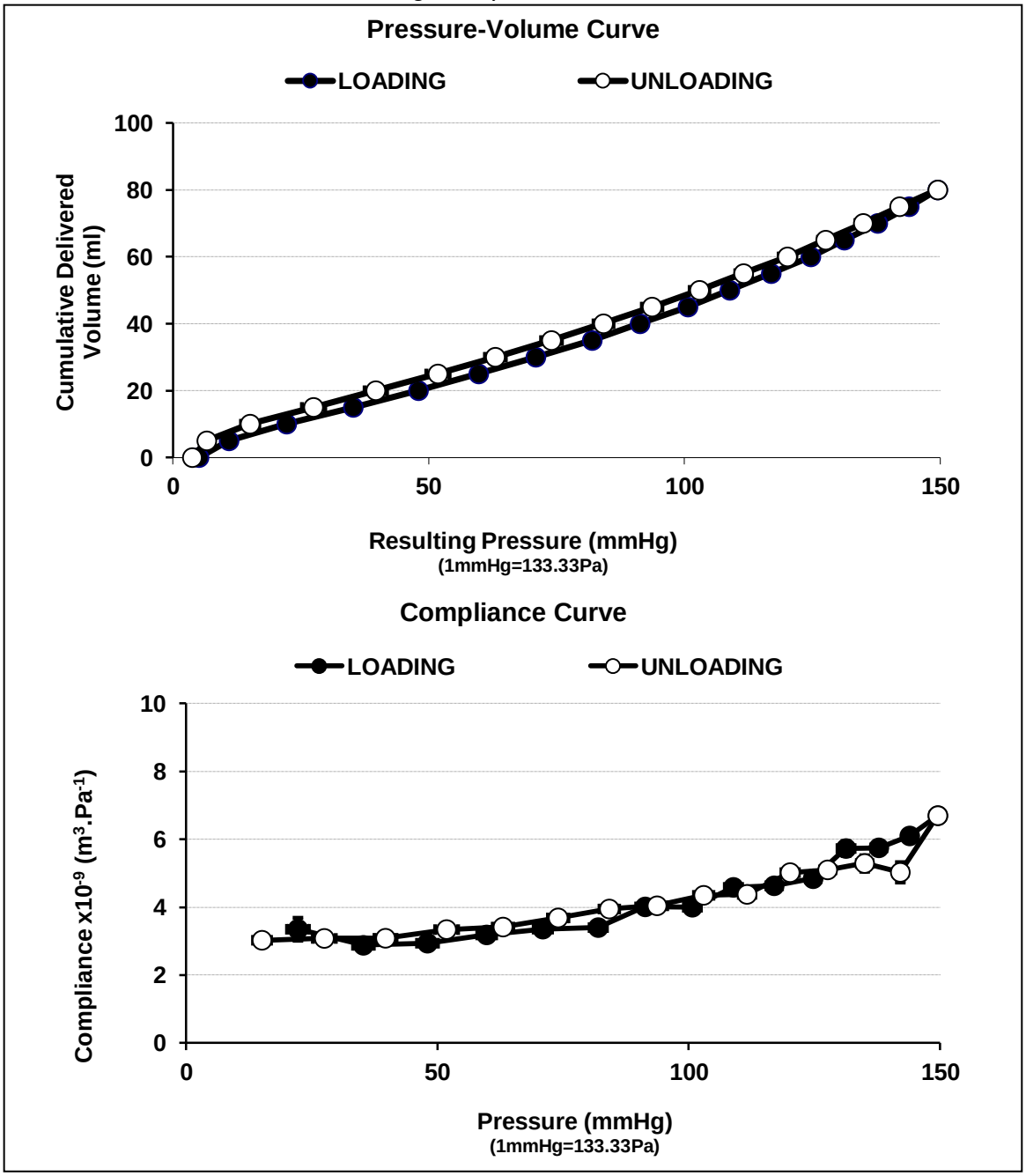

FIGURE 7.18: Pressure-Volume and Compliance Curves for Volume Loading and Volume Unloading of the Clingfilm-Wrapped Model Aorta. Curves shown are the average of four curves; some of the standard deviation bars are within the data point markers. (Pressure measured in the section equivalent to the ascending aorta).

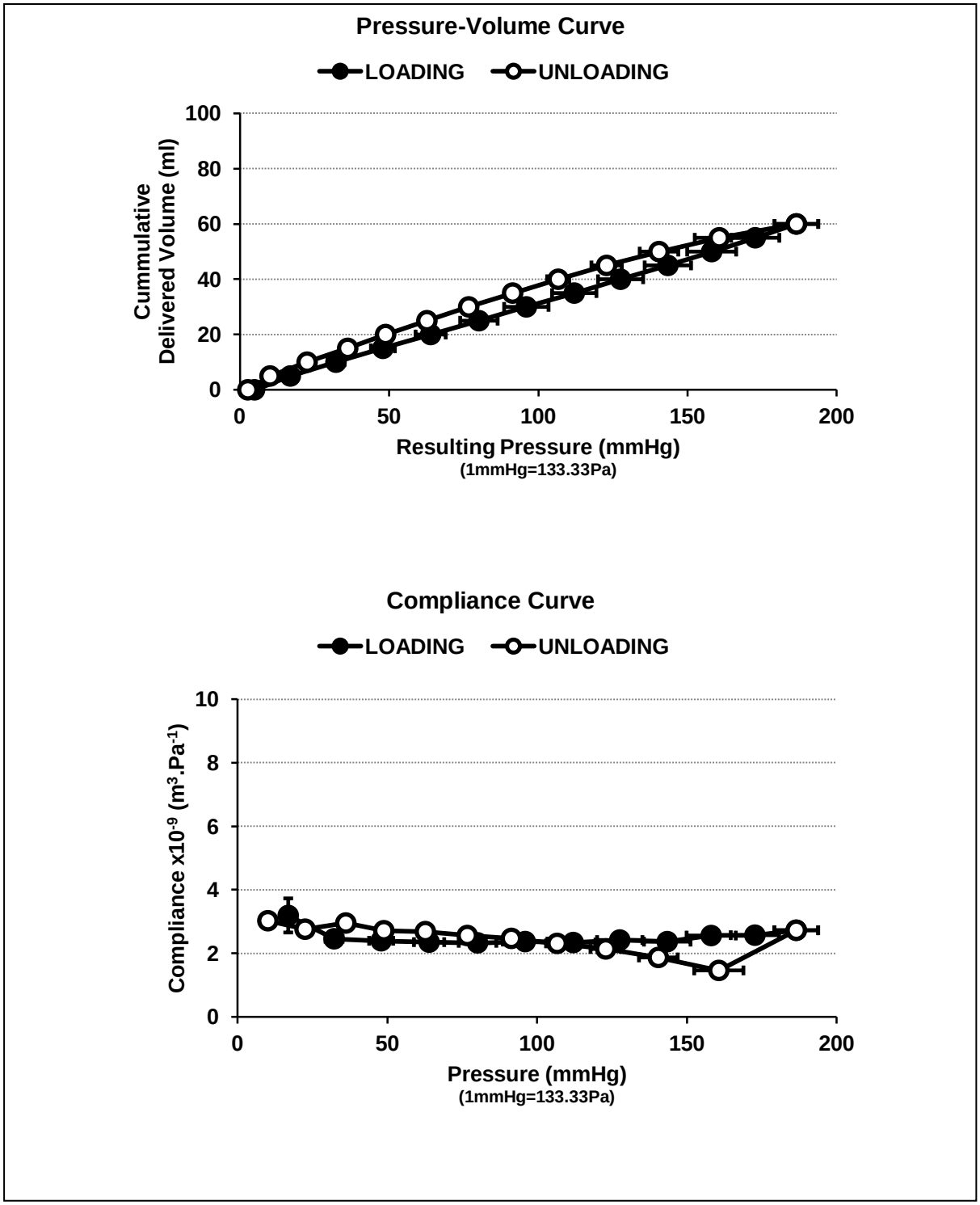

FIGURE 7.19: Mean Pressure-Volume Loading/Unloading Curves Combined and Respective Mean Compliance Loading/Unloading Curves Combined and Compared between the Normal and Clingfilm-Wrapped Model Aorta. (Curves of best fit have been constructed; Equations shown only for Compliance Curves). (Pressure measured in the section equivalent to the ascending aorta).

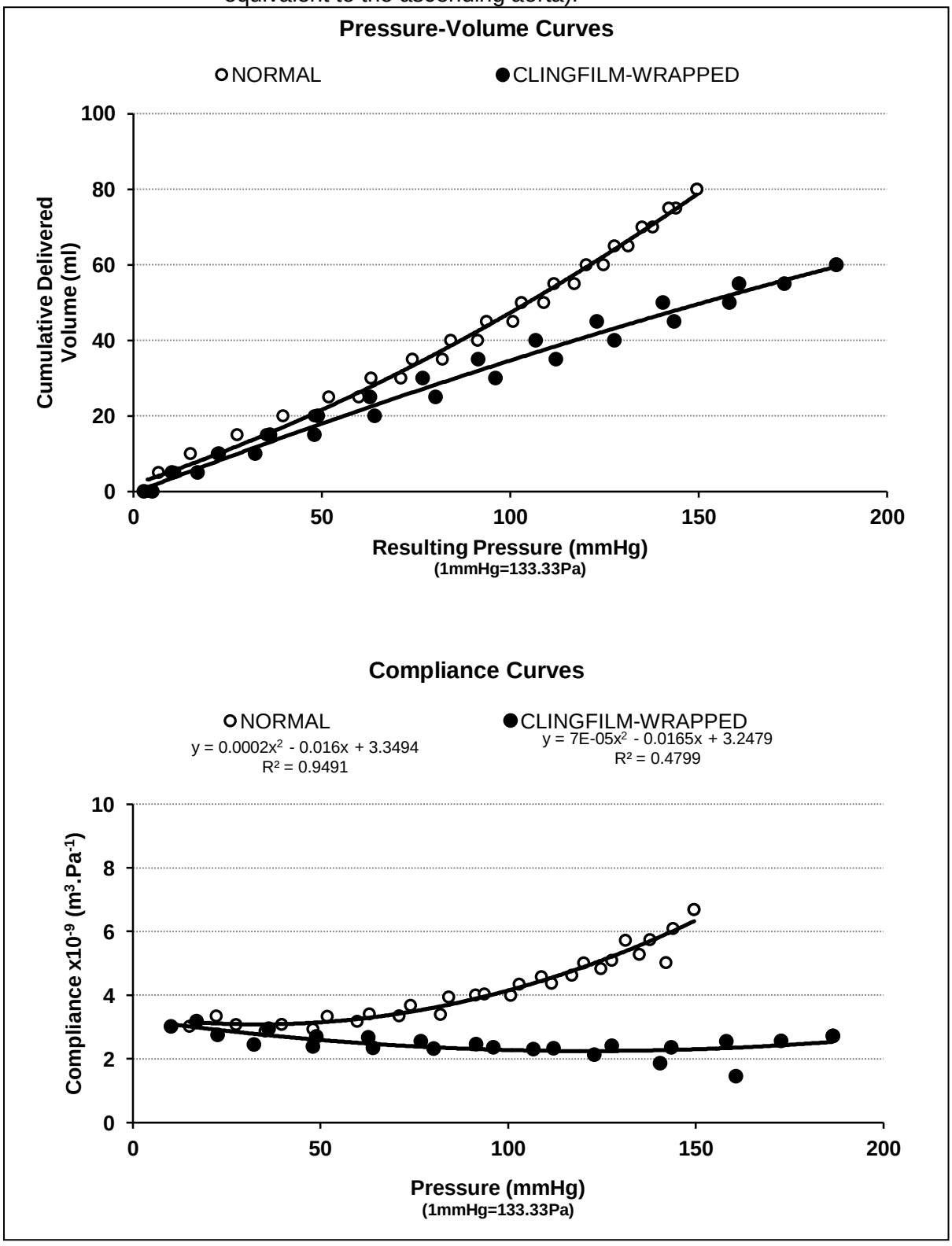

FIGURE 7.20: Pressure-Volume and Compliance Curves for a Distal Compliance Syringe set at initial volumes of air of 2.5, 5.0, 7.5 and 10ml*. Curves shown are the average of four or more curves. Some standard deviation bars are within the data point markers; for clarity standard deviations are included only for @2.5ml and @10ml curves in the compliance curves. Equation for compliance curve fit shown only for @10ml since this Distal Compliance only was used in experiments.

* 2.5, 5.0, 7.5 and 10ml at 0mmHg setting of pressure transducer at atmospheric pressure.

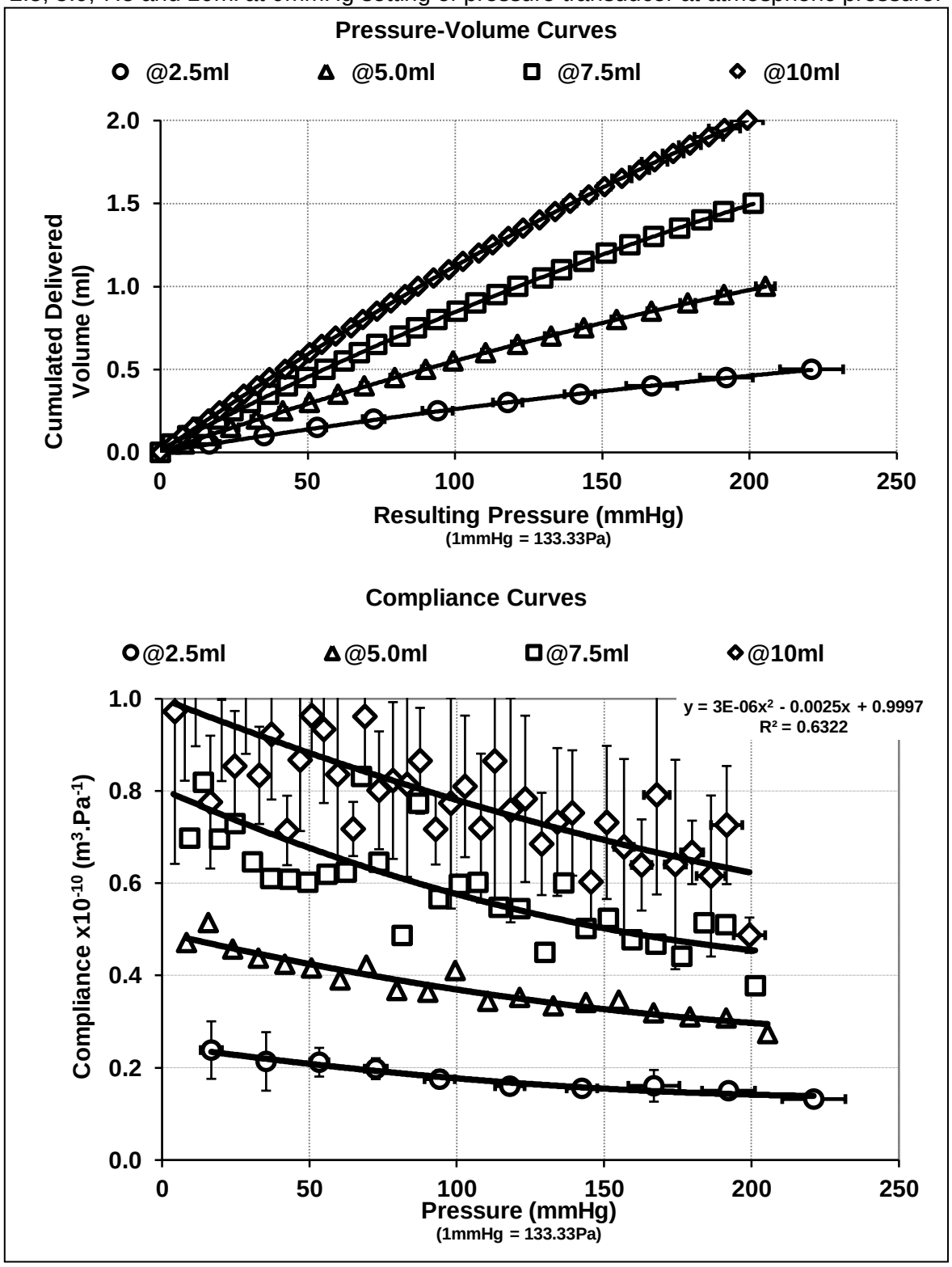

FIGURE 7.21: Compliance Values as Obtained from Plots in Figure 7.19 at MAP values* used for the Normal and Clingfilm-Wrapped Model Aorta, before (#1 & #2) and after (#1+Cf & #2+Cf) wrapping the Model Aorta and Iliac Arteries in Clingfilm. Also included is the application of the distal compliances (#2+Cf+Cd).

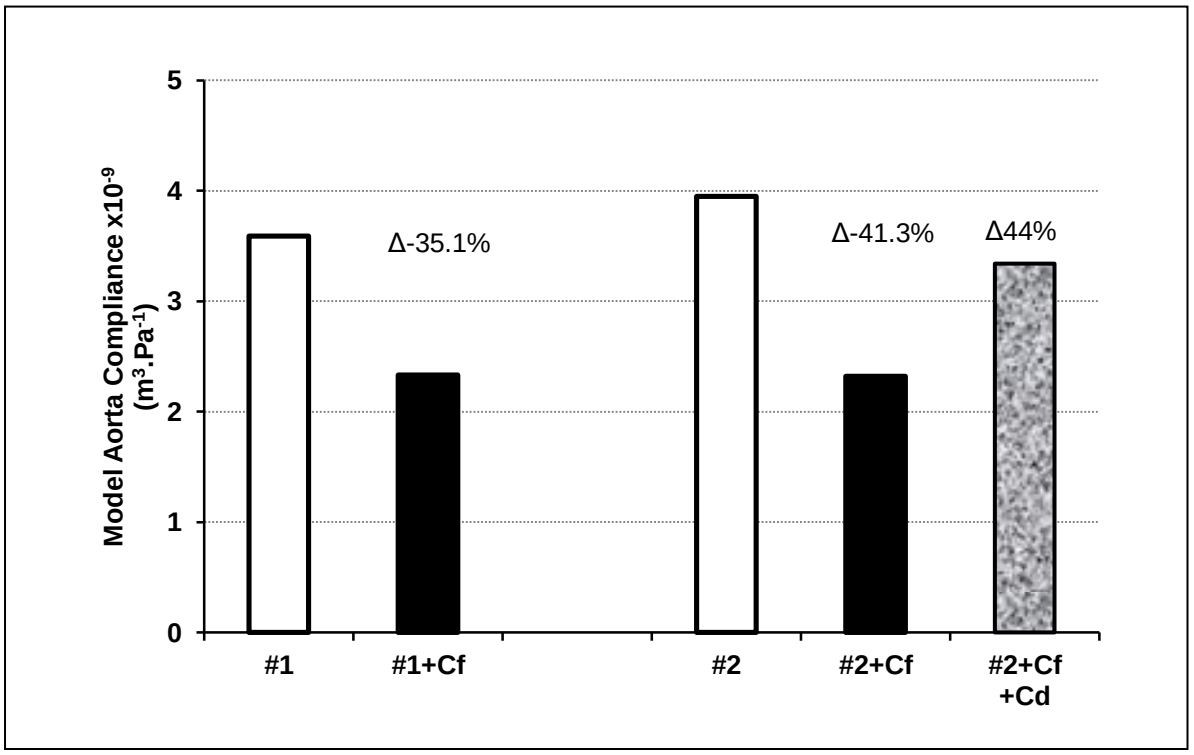

* UpSt MAP values used from Figure 7.12: #1 at 12.36kPa; #1+Cf at 12.05kPa; #2 at 14.35kPa; #2+Cf at 12.30kPa; #2+Cf+Cd at 12.60kPa.

Δ values are the differences between:

#1 and #1+Cf as a % of #1,
#2 and #2+Cf as a % of #2.
#2+Cf and #2+Cf+Cd as a % of #2+Cf

FIGURE 7.22: Arterial Compliance (AC) calculated from τ (see text and Eq. 2.20) of the Pulse Diastolic Decay. AC= τ / VR, measured at the UpSt & DnSt Sites in the Abdominal Aorta section of the Model before (#1 & #2) and after (#1+Cf & #2+Cf) wrapping the Model Aorta and Iliac Arteries in Clingfilm. Also included is the application of the distal compliances (#2+Cf+Cd).

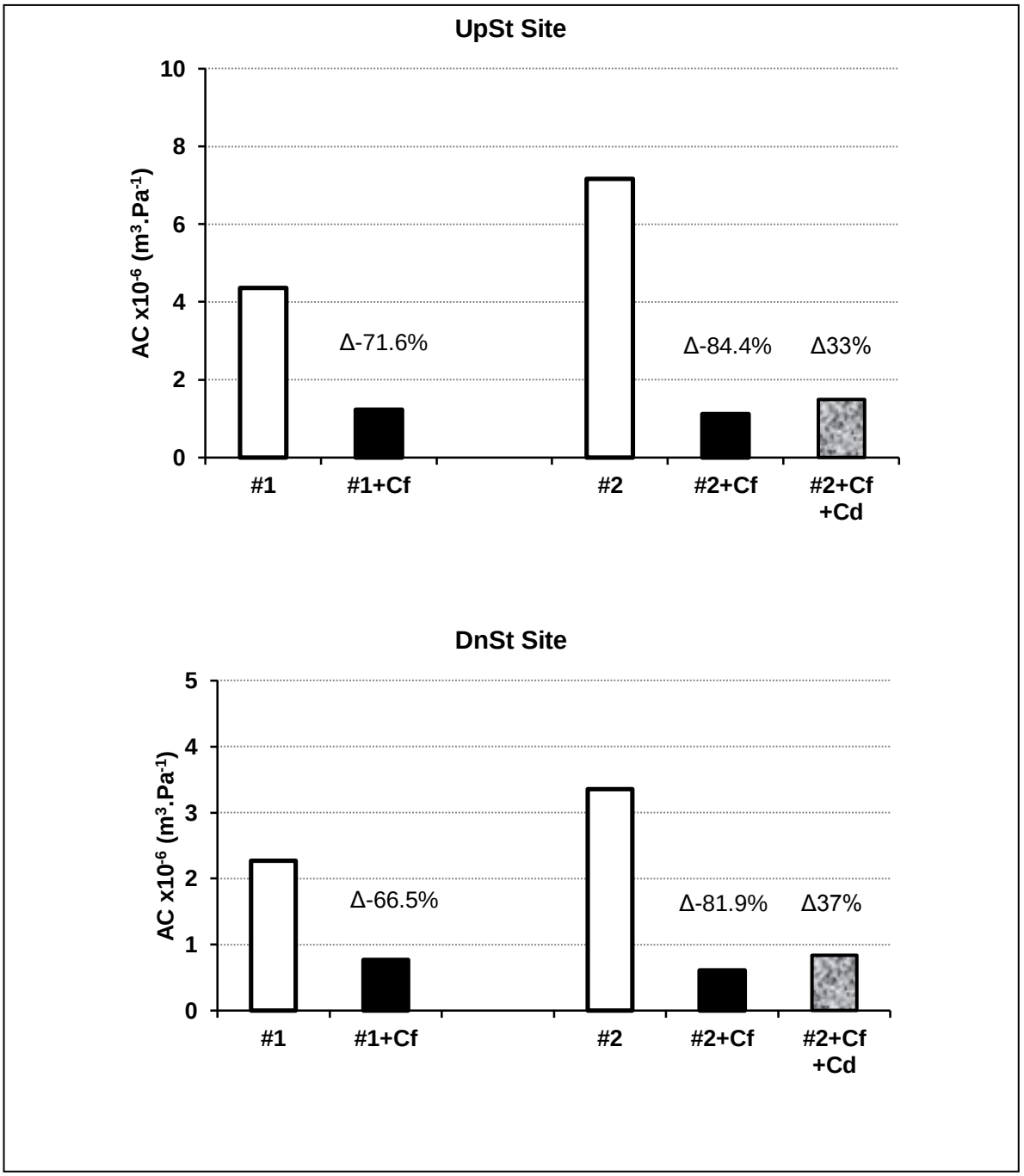

Δ values are the differences between:

#1 and #1+Cf as a % of #1,
#2 and #2+Cf as a % of #2.
#2+Cf and #2+Cf+Cd as a % of #2+Cf

Two other parameters that are thought to relate inversely to arterial compliance are $\int$RP and PP_{RP} (see in Chapters 4 & 5); these are respectively the integral and amplitude of the reservoir (Windkessel) pressure pulse (RP). Reservoir (Windkessel) pressure is discussed in Chapters 2, 4 and 5; it is derived from the measured pressure waveform by use of a MATLAB algorithm. Data for $\int$RP and PP_{RP} are shown in Figures 7.23 and 7.24 respectively. From Figures 7.23 and 7.24, it can be seen that $\int$RP and PP_{RP} relate inversely to compliance (Figure 7.21) and calculated AC (Figure 7.22) of the model aorta.

P infinity (P_∞)

As discussed in Chapters 2, 4 and 5, P_∞ is another parameter obtained from the MATLAB algorithm deriving reservoir (Windkessel) pressure from the measured pressure pulse waveform. P_∞ is an asymptote value of pressure that would be reached after cessation of cardiac function. The concept of P_∞ is discussed in Chapter 4. Figure 7.25 gives data on measures of P_∞ as obtained by the algorithm. It can be seen that large negative values of P_∞ are obtained with the normal model aorta but revert to positive values after Clingfilm-wrapping. The large negative values of P_∞ might be considered spurious; indeed, in Chapters 4 and 5, the opinion was stated that spurious values result from poor fitting by the algorithm to the pulse diastolic decay. However, poor fit by the algorithm does not appear to be the case here. Figures 7.26 and 7.27 show the fittings of the reservoir (Windkessel) pressure to the diastolic curves for pulses at the UpSt site before and after Clingfilm wrapping; the same is shown in Figures 7.28 and 7.29 for the DnSt site. In all cases the fit of the reservoir (Windkessel) pressure in diastole is very close to the diastolic decay of the pressure pulse. In the case of the waveforms before Clingfilm wrapping, the diastolic decay appears as a linear decline but is actually exponential with an exceptionally long time constant, τ; however, after Clingfilm wrapping, τ is much reduced along with a diastolic decay resembling an exponential decay. The values of τ before and after Clingfilm wrapping are plotted in Figures 7.30. Since TPR, hence VR, were held constant in the models, it follows that τ changed as a consequence of changed compliance (re: τ =compliance x resistance) which in these models has a marked influence on P_∞. Aside from the measurement of P_∞, it is interesting to note that in the case of experiment #2+Cf, at the UpSt (Figure 7.27) and DnSt (Figure 7.29) sites, Clingfilm wrapping altered the waveforms to resemble those found *in vivo.*

FIGURE 7.23: ∫RP before (#1 & #2) and after (#1+Cf & #2+Cf) wrapping the Model Aorta and Iliac Arteries in Clingfilm. Also included is the application of the distal compliances (#2+Cf+Cd). Measurements made at the UpSt & DnSt Sites in the Abdominal Aorta section of the Model.

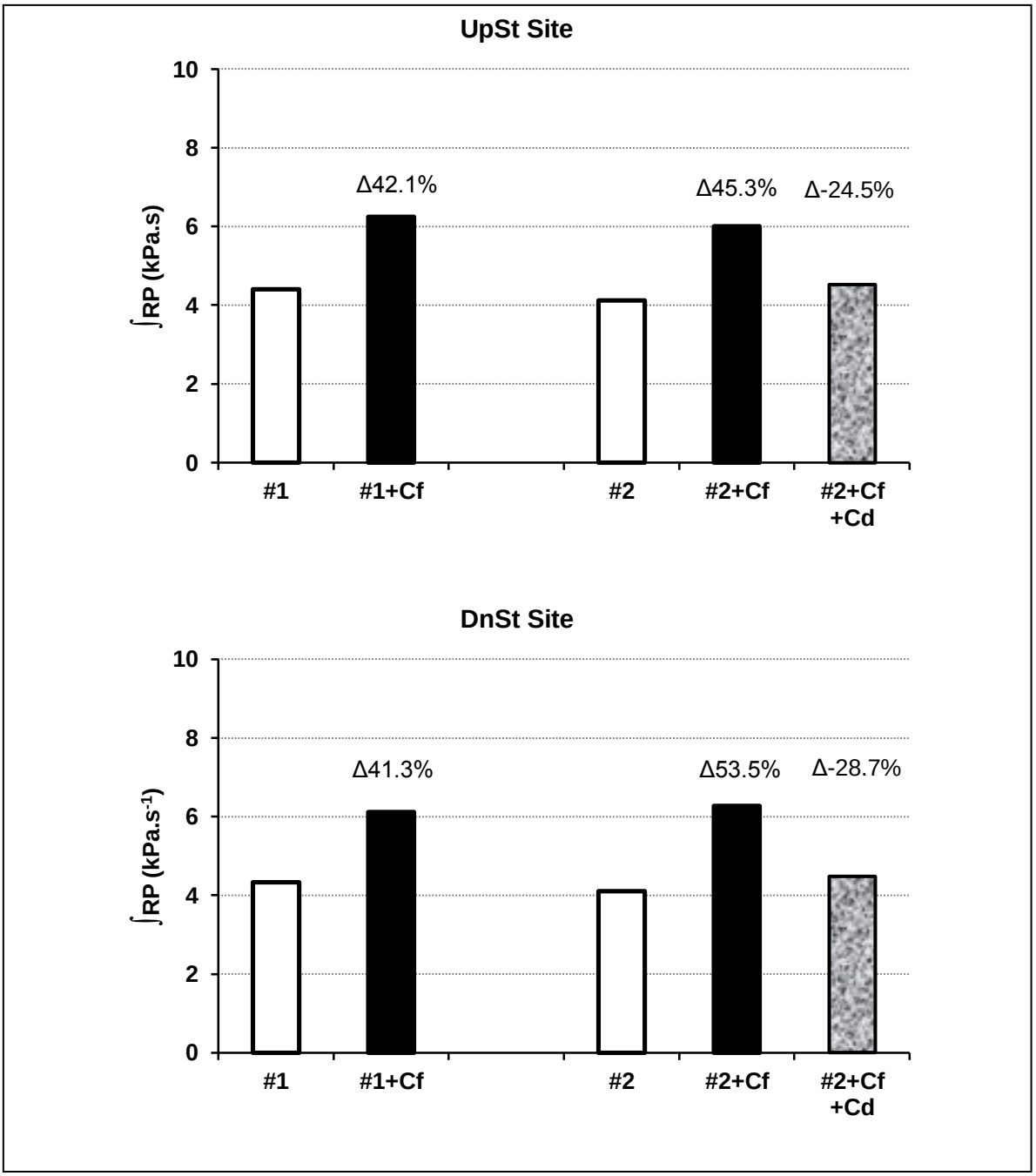

Δ values are the differences between:

#1 and #1+Cf as a % of #1,
#2 and #2+Cf as a % of #2.
#2+Cf and #2+Cf+Cd as a % of #2+Cf

FIGURE 7.24: PP_{RP} before (#1 & #2) and after (#1+Cf & #2+Cf) wrapping the Model Aorta and Iliac Arteries in Clingfilm. Also included is the application of the distal compliances (#2+Cf+Cd). Measurements made at the UpSt & DnSt Sites in the Abdominal Aorta section of the Model.

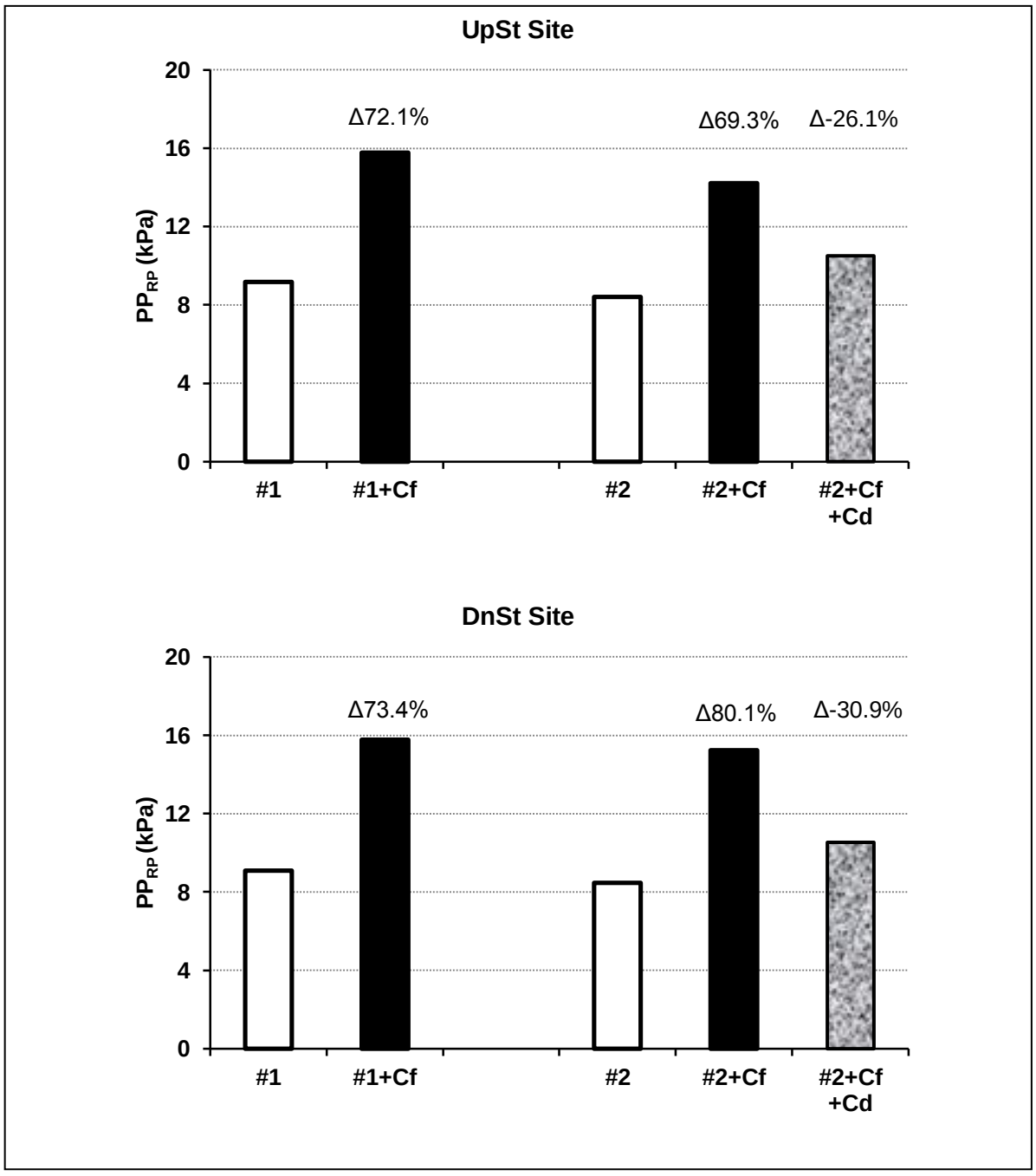

Δ values are the differences between:

#1 and #1+Cf as a % of #1,
#2 and #2+Cf as a % of #2.
#2+Cf and #2+Cf+Cd as a % of #2+Cf

FIGURE 7.25: P_∞ before (#1 & #2) and after (#1+Cf & #2+Cf) wrapping the Model Aorta and Iliac Arteries in Clingfilm. Also included is the application of the distal compliances (#2+Cf+Cd). Measurements made at the UpSt & DnSt Sites in the Abdominal Aorta section of the Model.

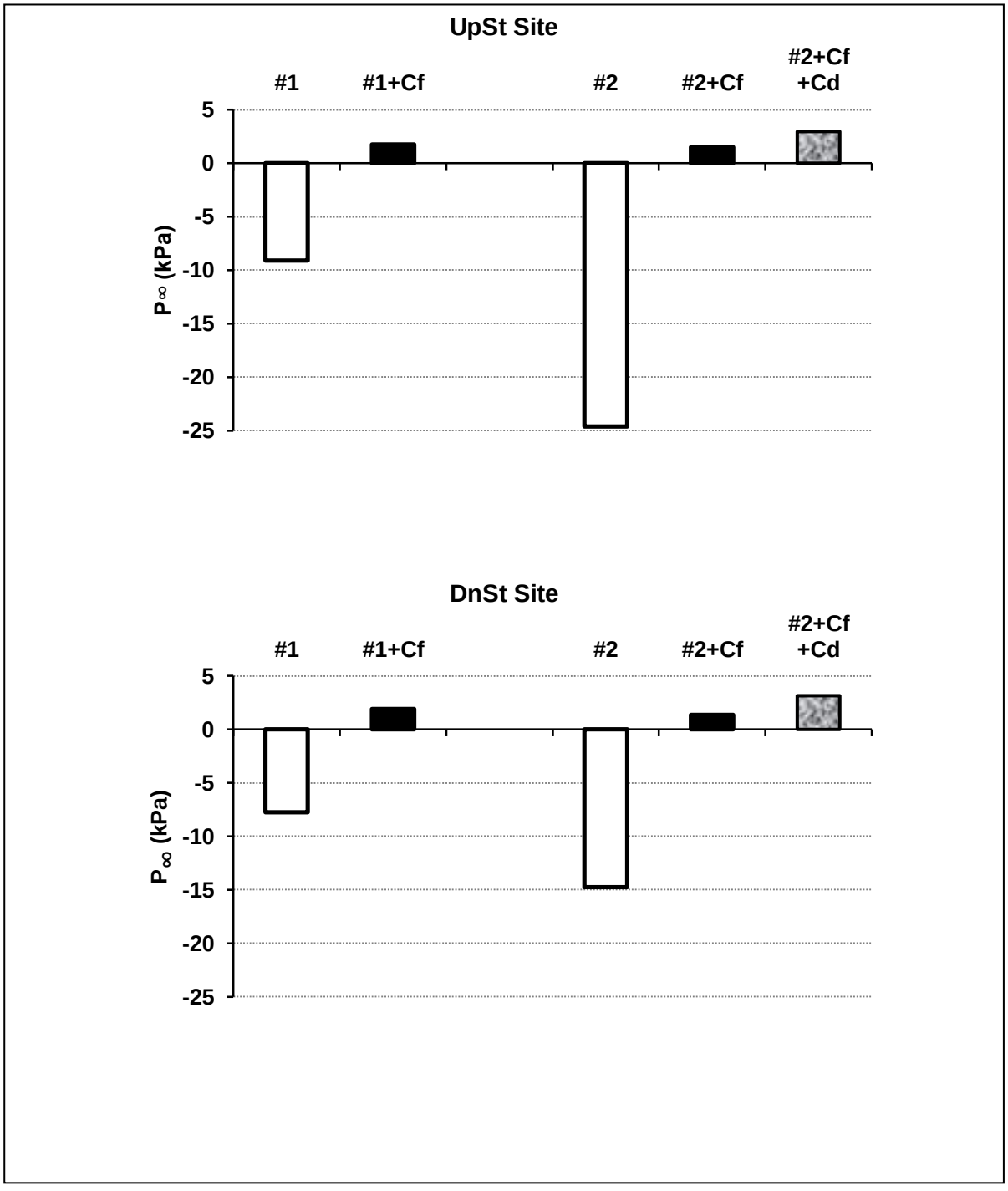

FIGURE 7.26: Pressure Pulse Waveforms at the UpSt Site of the Abdominal Aorta section of the Model before (#1) and after (#1+Cf) Clingfilm Wrapping of the Model Aorta (Expt. Ref.: AAEH100428). Note the increase in pulse pressure caused by Clingfilm wrapping. Values are given for DBP of Total Measured Pressure (P_T DBP) at 0 time.

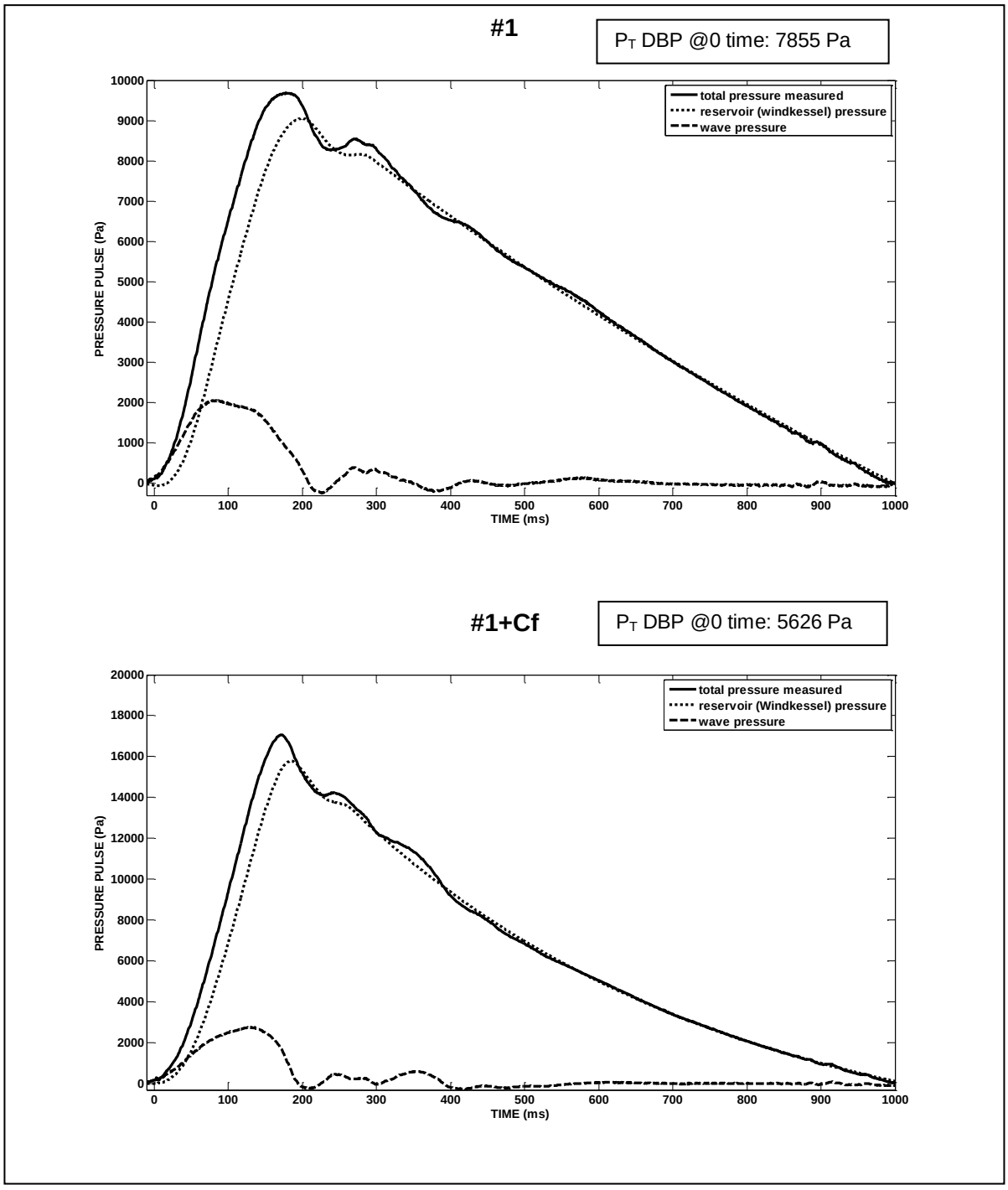

FIGURE 7.27: Pressure Pulse Waveforms at the UpSt Site of the Abdominal Aorta section of the Model before (#2) and after (#2+Cf) Clingfilm Wrapping of the Model Aorta (Expt. Ref.: AAEH100429). Note: i) the increase in pulse pressure caused by Clingfilm wrapping; ii) the conversion of the waveform to one that is similar to those found *in vivo*. Values are given for DBP of Total Measured Pressure (P_T DBP) at 0 time.

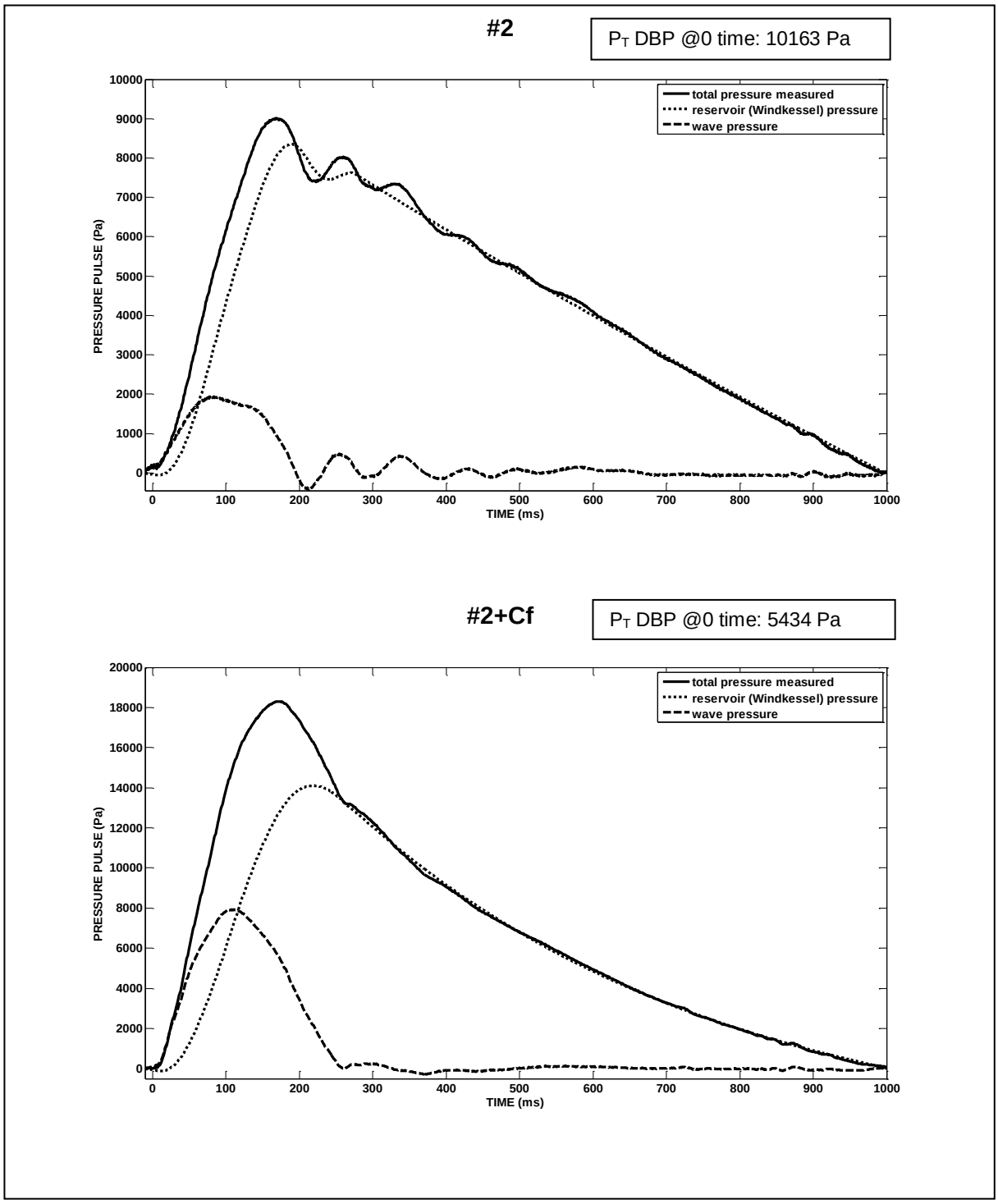

FIGURE 7.28: Pressure Pulse Waveforms at the DnSt Site of the Abdominal Aorta section of the Model before (#1) and after (#1+Cf) Clingfilm Wrapping of the Model Aorta (Expt. Ref.: AAEH100428). Note the increase in pulse pressure caused by Clingfilm wrapping. Values are given for DBP of Total Measured Pressure (P_T DBP) at 0 time.

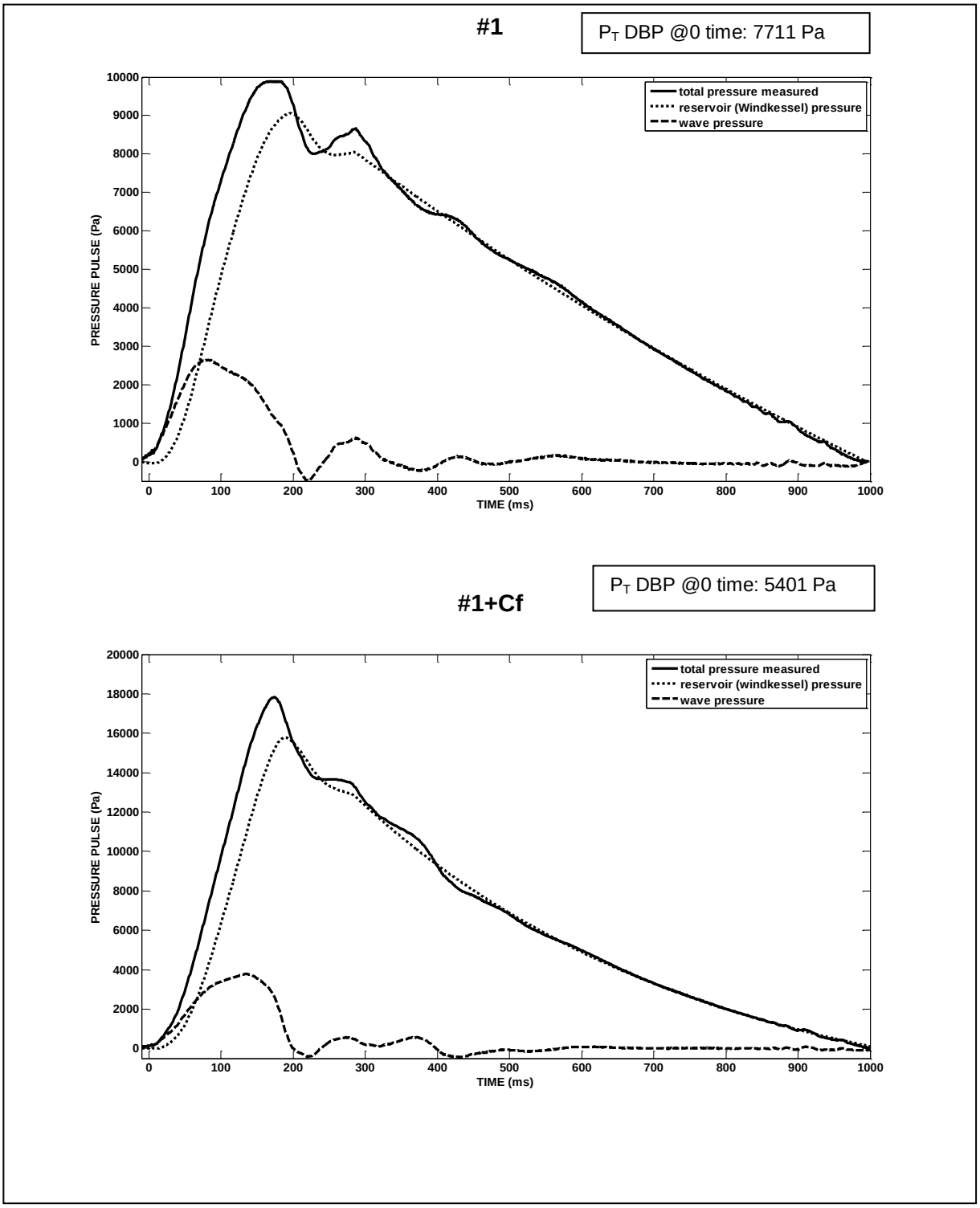

FIGURE 7.29: Pressure Pulse Waveforms at the DnSt Site of the Abdominal Aorta section of the Model before (#2) and after (#2+Cf) Clingfilm Wrapping of the Model Aorta (Expt. Ref.: AAEH100429). Note: i) the increase in pulse pressure caused by Clingfilm wrapping; ii) the conversion of the waveform to one that is similar to those found *in vivo*. Values are given for DBP of Total Measured Pressure (P_T DBP) at 0 time.

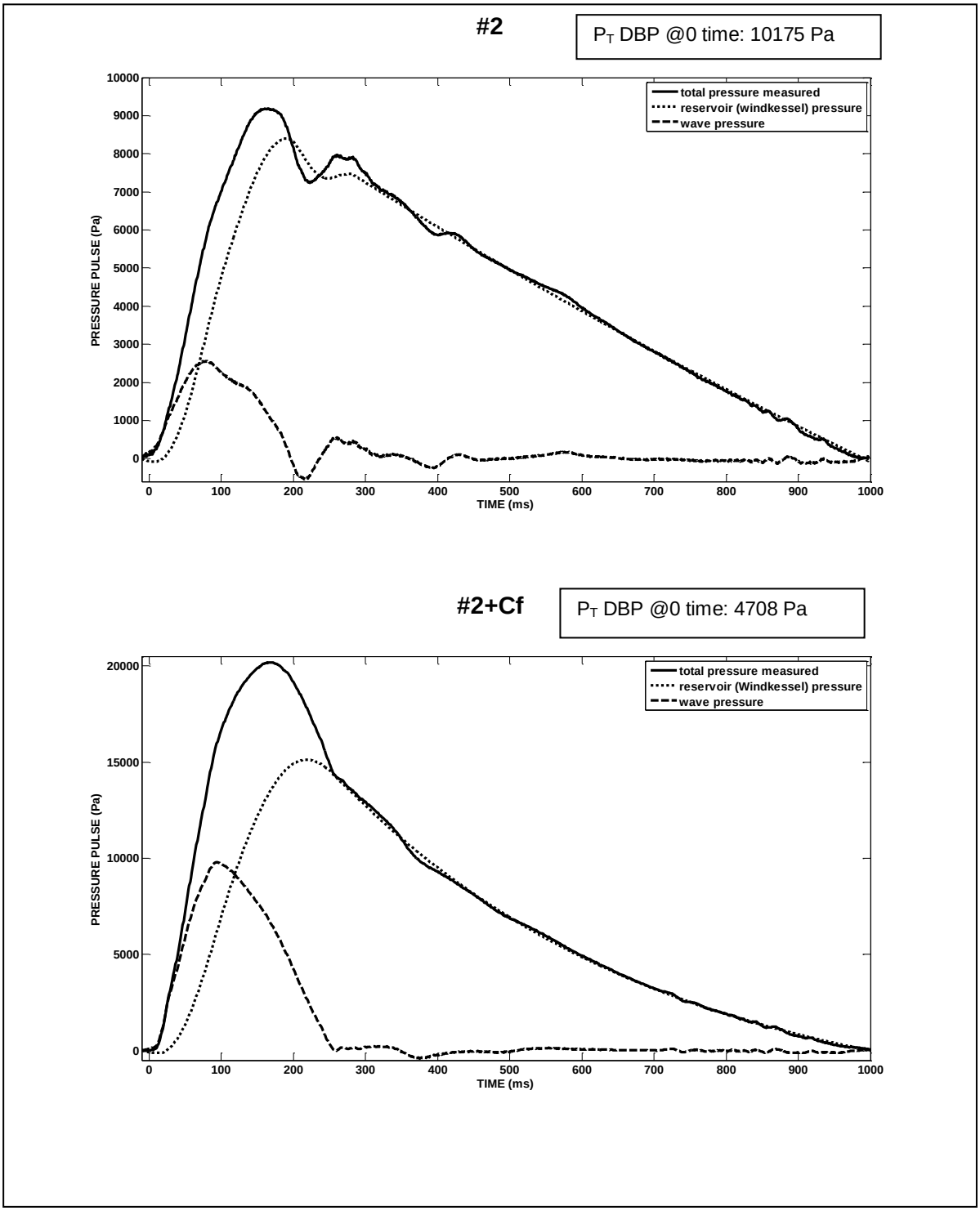

FIGURE 7.30: Diastolic Decay Time Constant, τ, before (#1 & #2) and after (#1+Cf & #2+Cf) wrapping the Model Aorta and Iliac Arteries in Clingfilm. Also included is the application of the distal compliances (#2+Cf+Cd). Measurements made at the UpSt & DnSt Sites in the Abdominal Aorta section of the Model.

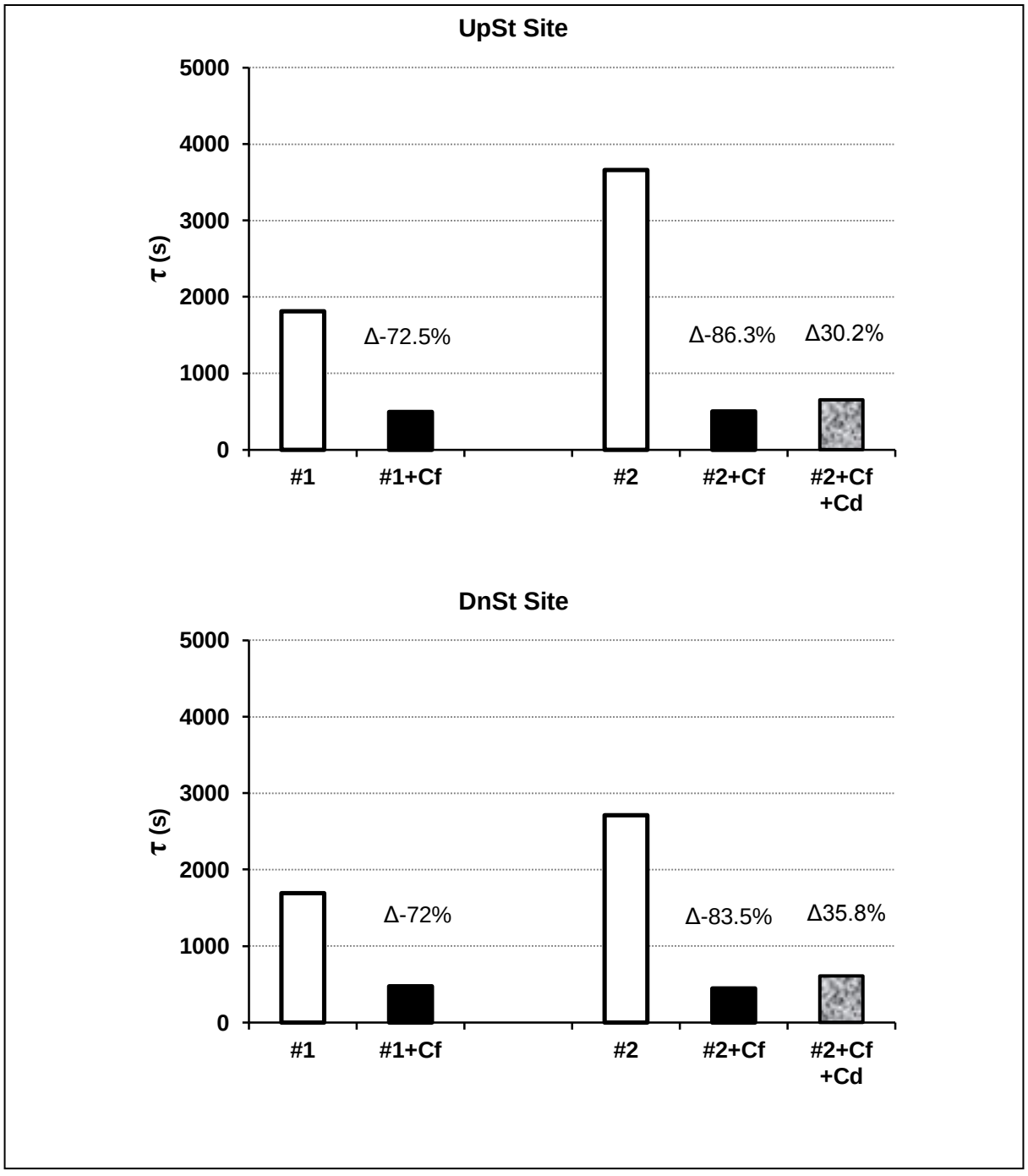

Δ values are the differences between:

#1 and #1+Cf as a % of #1,
#2 and #2+Cf as a % of #2.
#2+Cf and #2+Cf+Cd as a % of #2+Cf

Relative Height of the Dicrotic Notch (RHDN) obtained from the Measured (Total) Pressure Pulse Waveform in the Model Aorta at the UpSt and DnSt Sites of Measurement.

The term “dicrotic notch” is discussed fully in Chapter 4 where it is explained that the notch as seen in pressure waveforms of the aorta is the incisura; the incisura as indicated by ‘A’ in Figures 7.9 and 7.10 is used for measurement of RHDN in the model aorta.

Figure 7.31 and 7.32 show data for RHDN and Tn respectively; the latter is the time of the notch, or incisura, from onset of the systolic upstroke of the pressure pulse. RHDN and Tn were little affected by Clingfilm wrapping in the first experiment, namely #1 vs. #1+Cf, but RHDN and Tn were decreased and increased respectively by Clingfilm wrapping in the second experiment, namely #2 vs. #2+Cf; in the latter experiment RHDN was further decreased by application of distal compliances, namely #2+Cf+Cd (Figure 7.31), though this did not alter Tn from its value attained after Clingfilm wrapping (Figure 7.32). To illustrate the change in RHDN, Figure 7.33 shows the UpSt pulse waveform before (#2) and after Clingfilm wrapping (#2+Cf) and then after application of distal compliances (#2+Cf+Cd).

FIGURE 7.31: RHDN before (#1 & #2) and after (#1+Cf & #2+Cf) wrapping the Model Aorta and Iliac Arteries in Clingfilm. Also included is the application of the distal compliances (#2+Cf+Cd). Measurements made at the UpSt & DnSt Sites in the Abdominal Aorta section of the Model.

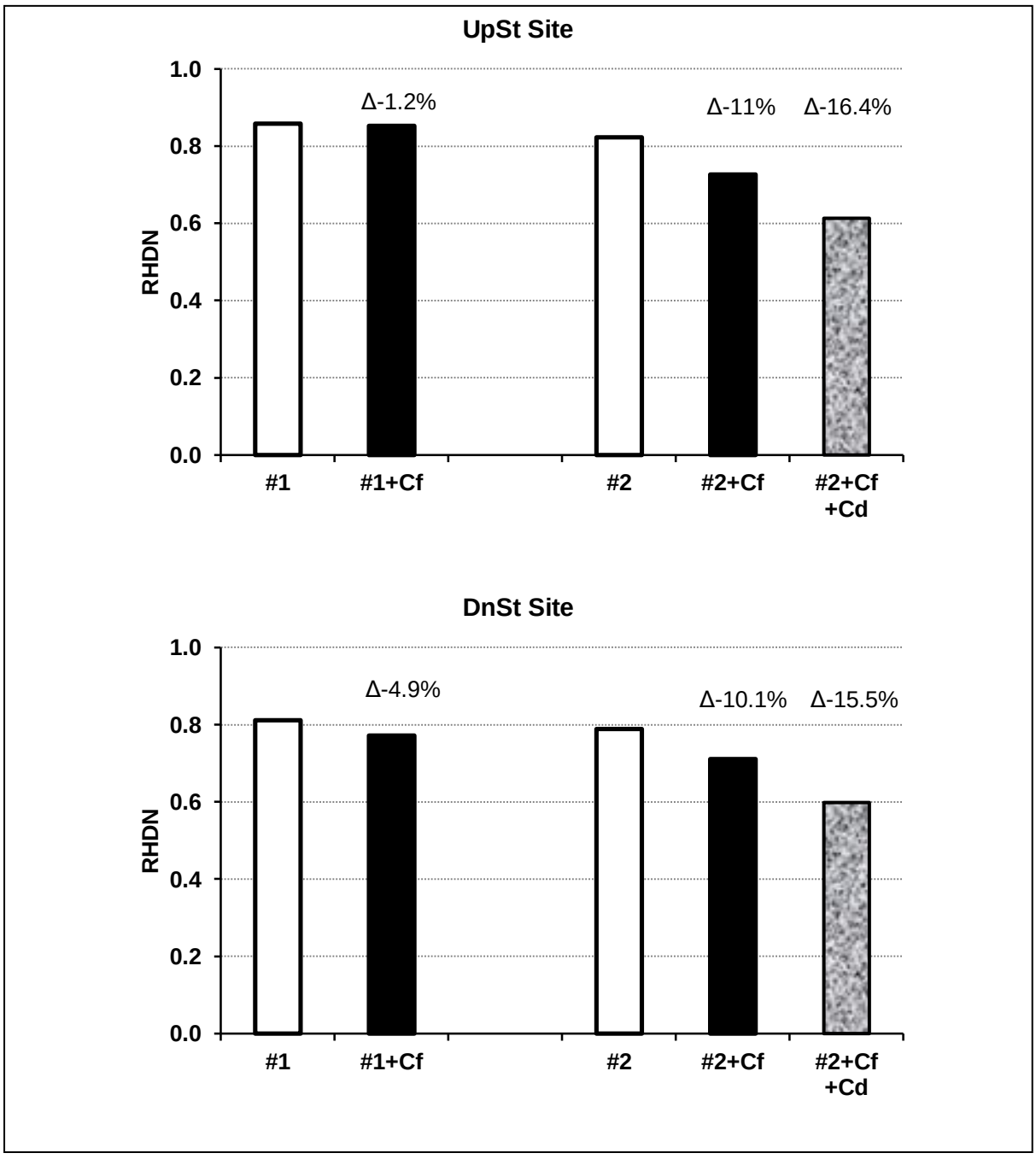

Δ values are the differences between:

#1 and #1+Cf as a % of #1,
#2 and #2+Cf as a % of #2.
#2+Cf and #2+Cf+Cd as a % of #2+Cf

FIGURE 7.32: Tn before (#1 & #2) and after (#1+Cf & #2+Cf) wrapping the Model Aorta and Iliac Arteries in Clingfilm. Also included is the application of the distal compliances (#2+Cf+Cd). Measurements made at the UpSt & DnSt Sites in the Abdominal Aorta section of the Model.

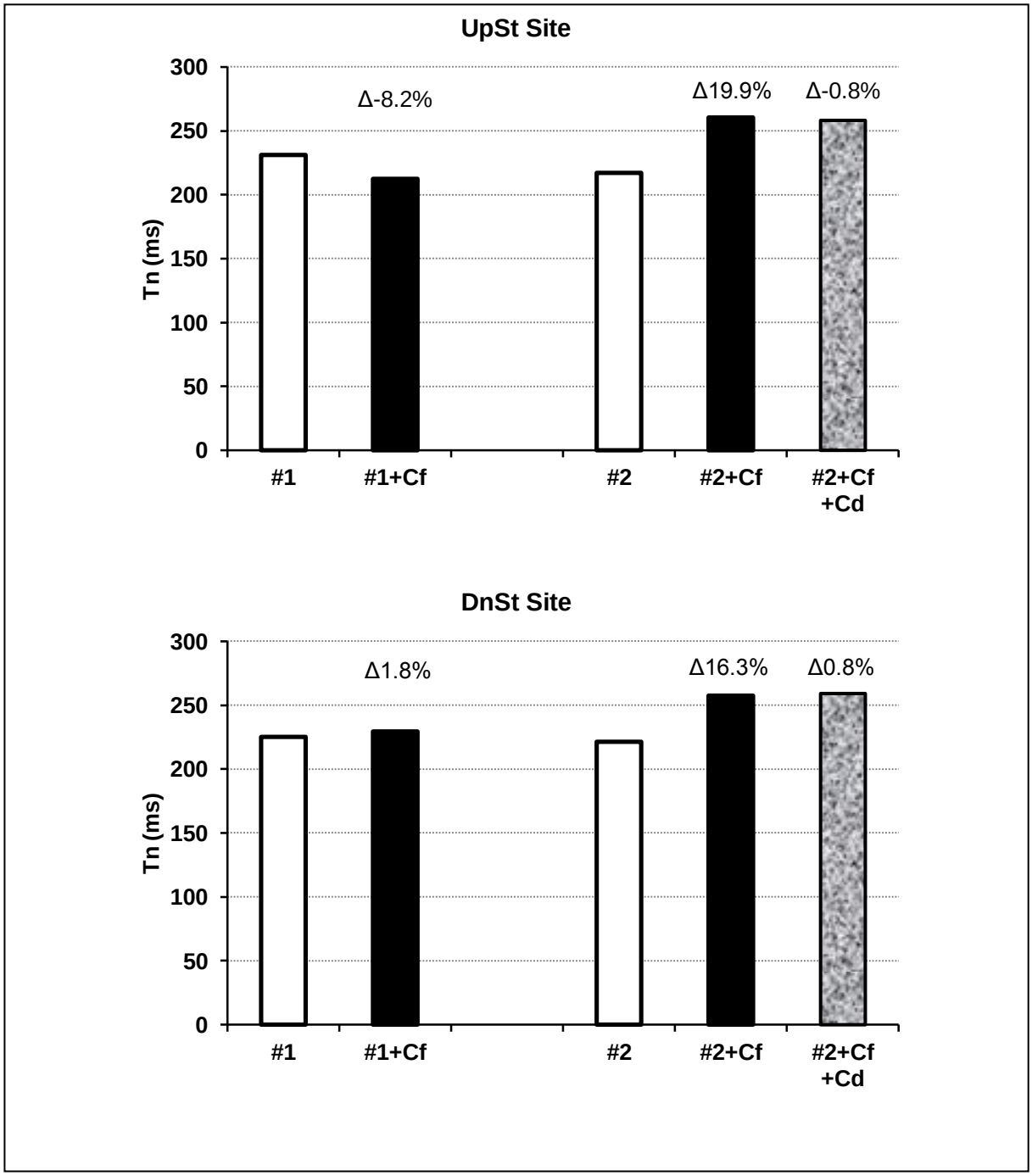

Δ values are the differences between:

#1 and #1+Cf as a % of #1,
#2 and #2+Cf as a % of #2.
#2+Cf and #2+Cf+Cd as a % of #2+Cf

FIGURE 7.33: Pressure Pulse Waveform to Illustrate Change of RHDN before (#2) and after Clingfilm wrapping (#2+Cf) and then after application of distal compliances (#2+Cf+Cd). Measurements made at the UpSt Site in the Abdominal Aorta section of the Model.

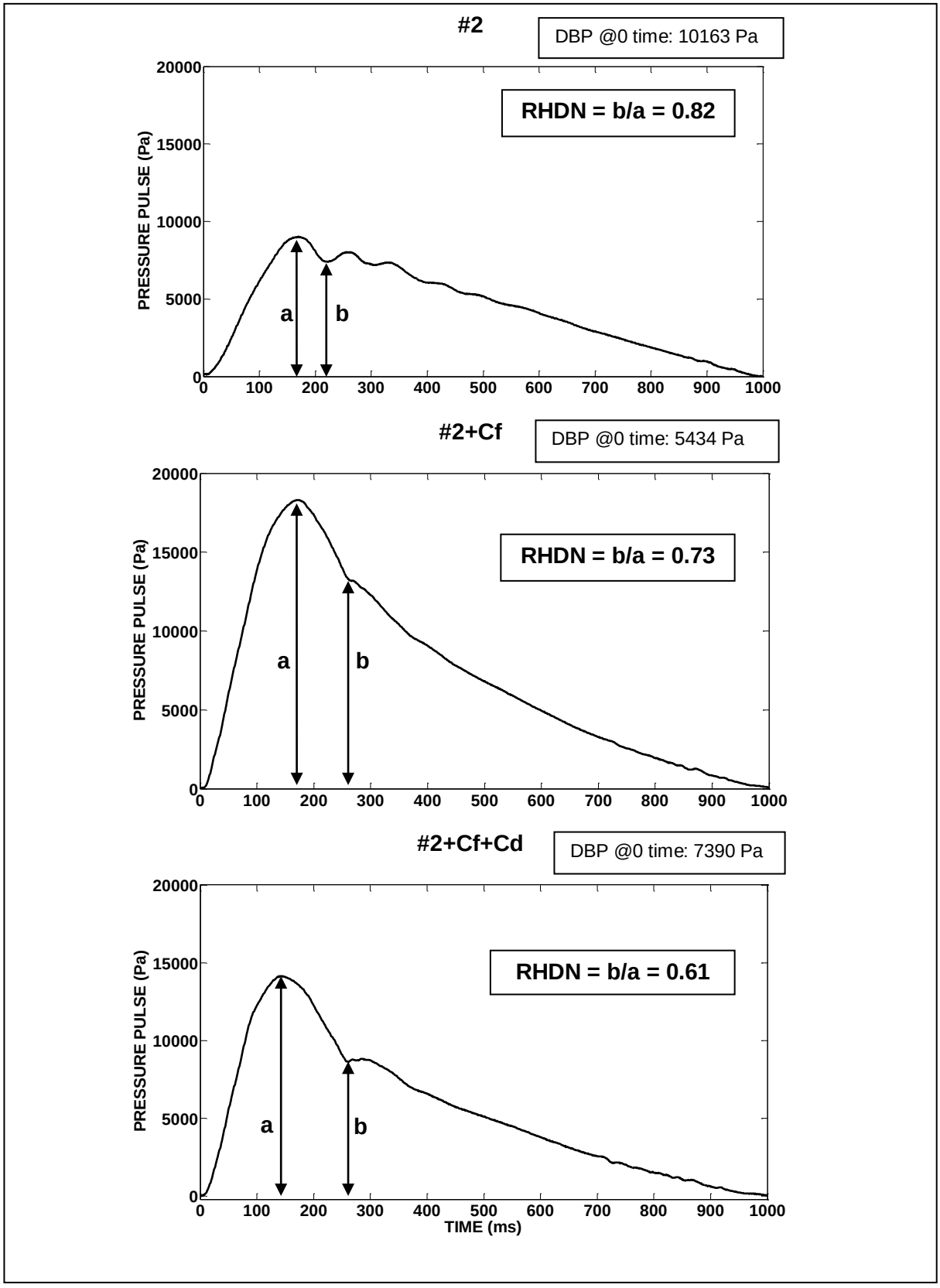

Pulse Wave Velocities (PWV) and Wave Speeds

As described in previous chapters, PWV was measured by the foot-to-foot method (see section 3.2.5) and, as in Chapters 4 and 5, is ascribed here as $C_{ft\text{-}ft}$. Also as explained in previous chapters, the term *wave speed* refers to values obtained by plotting pressure (P) against flow velocity (U) to obtain a PU loop (see Chapters 2 and 4); the ratio of the slope of the linear part of the PU loop to blood density gives wave speed. Wave speeds ascribed as C_{Tpu} or C_{Wpu} are obtained respectively by plotting the measured (Total) pressure or wave pressure against flow velocity. Figure 7.34 gives comparative data of $C_{ft\text{-}ft}$, C_{Tpu} and C_{Wpu}. Furthermore, PWV was measured by foot-to-foot method for the aorta length from a position in the ascending aorta adjacent to the coronary arteries to the aorto-iliac bifurcation – over a distance of 46.5cm; the data for this is shown in Figure 7.35.

$C_{ft\text{-}ft}$ was a little over 10m.s^{-1} at the UpSt site and approximately double that, i.e. a little over 20m.s^{-1} at the DnSt site (Figure 7.34). Values of C_{Tpu} ranged between 12-22 m.s^{-1} at the UpSt site and 18-25m.s^{-1} at the DnSt site, these values being greater than those of $C_{ft\text{-}ft}$ at the UpSt site but the values of the two were close to each other at the DnSt site. C_{Wpu} has some values close to either $C_{ft\text{-}ft}$ or C_{Tpu} at the UpSt or DnSt sites. Overall, the values of $C_{ft\text{-}ft}$, C_{Tpu} and C_{Wpu} did not consistently agree with each other. Furthermore, values of $C_{ft\text{-}ft}$, C_{Tpu} and C_{Wpu} were not consistently affected by Clingfilm wrapping or by the subsequent application of distal compliances in all experiments. As discussed above, Clingfilm wrapping decreased compliance of the model aorta which would be expected to increase PWV, or wave speed, in the model. This was observed for C_{Wpu} at both the UpSt and DnSt sites of measurement for the second set of experiments, namely #2 vs. #2+Cf (Figure 7.34), where Clingfilm wrapping increased C_{Wpu}; interestingly, this increase was attenuated by the application of distal compliances. PWV (foot-to-foot) along the length (46.5cm) of the aorta from a position in the ascending aorta adjacent to the coronary arteries to the aorto-iliac bifurcation was ~12m.s^{-1} and increased to ~15m.s^{-1} after Clingfilm wrapping – an expected effect of decreased aortic compliance (Figure 7.35); the latter speed was little changed by subsequent application of distal compliances.

FIGURE 7.34: $C_{ft\text{-}ft}$, C_{Tpu} and C_{Wpu} before (#1 and #2) and after Clingfilm wrapping (#1+Cf and #2+Cf) and then after application of distal compliances (#2+Cf+Cd). Measurements made at the UpSt & DnSt Sites in the Abdominal Aorta section of the Model.

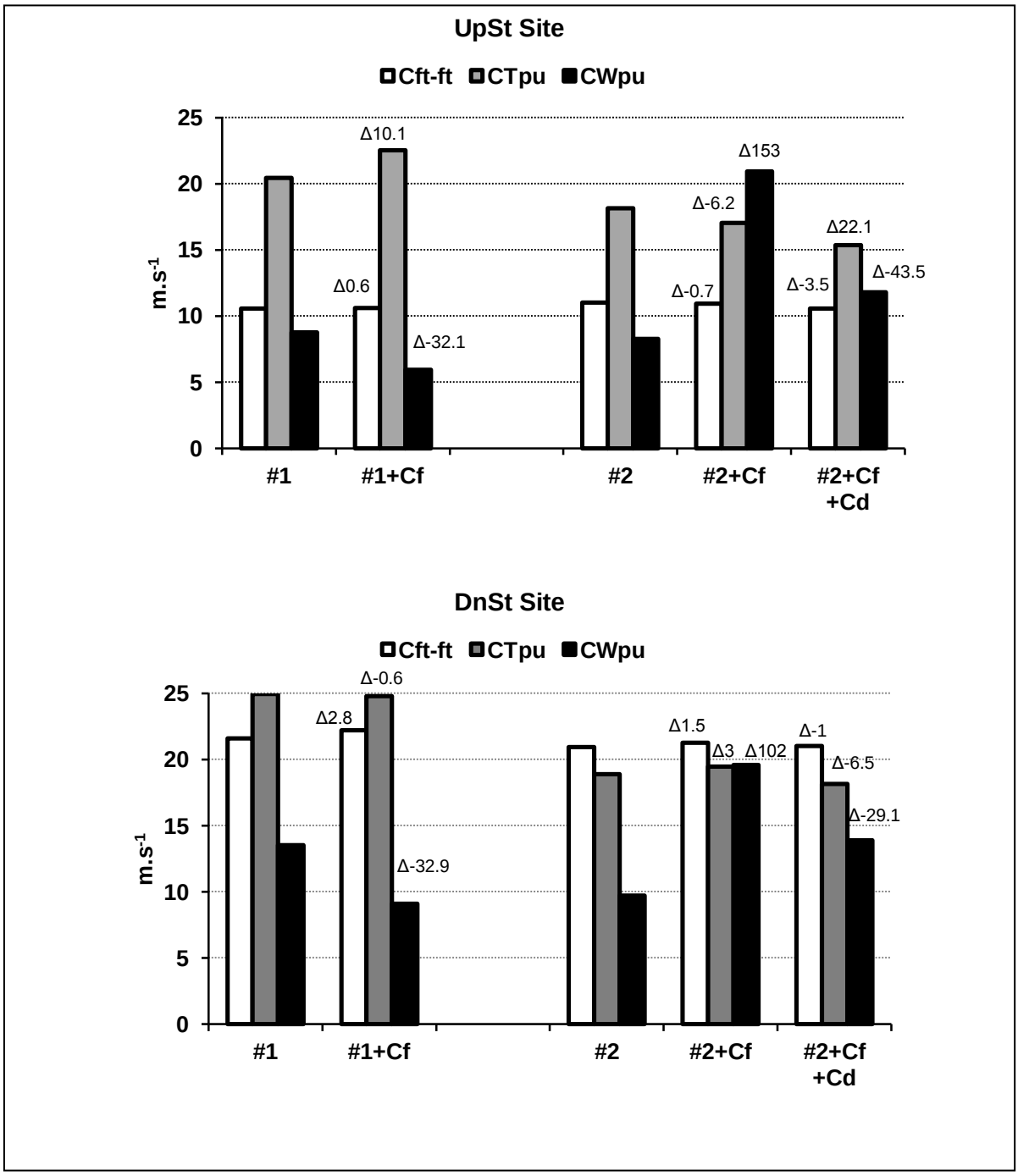

Δ values are the differences between:

#1 and #1+Cf as a % of #1,
#2 and #2+Cf as a % of #2.
#2+Cf and #2+Cf+Cd as a % of #2+Cf

FIGURE 7.35: PWV over the Length of the Model Aorta from Ascending Aorta to Aorto-iliac Bifurcation (45.6cm), before (#1 and #2) and after Clingfilm wrapping (#1+Cf and #2+Cf) and then after application of distal compliances (#2+Cf+Cd).

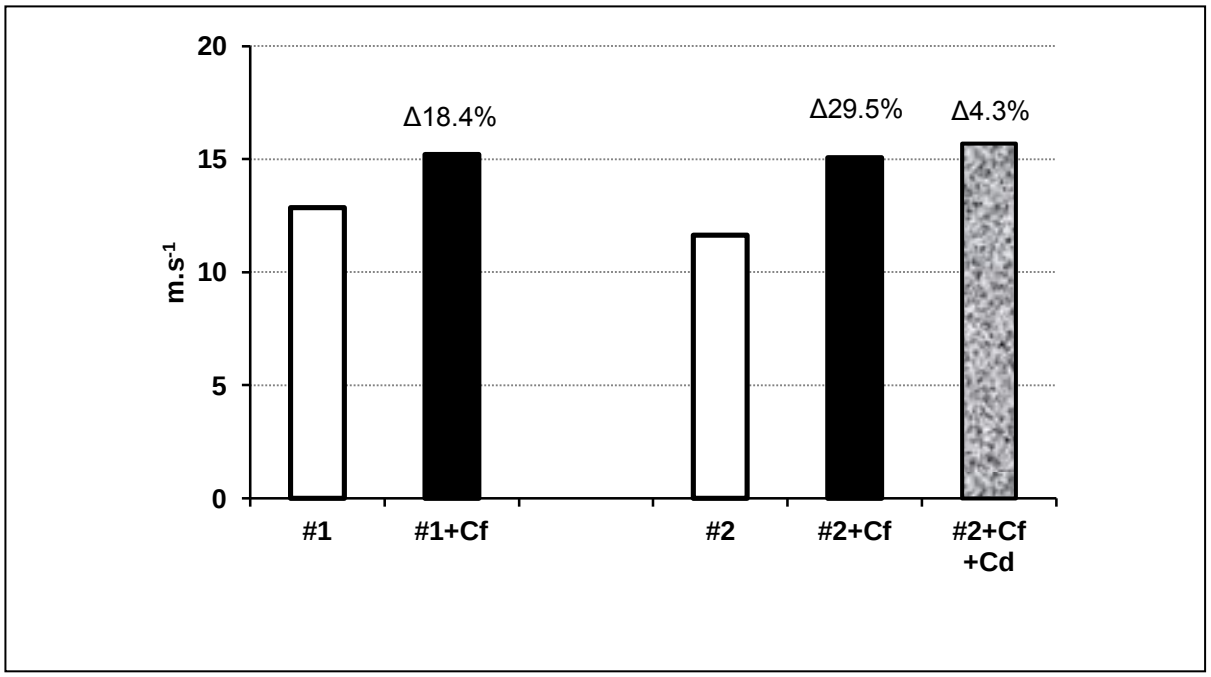

Δ values are the differences between:

#1 and #1+Cf as a % of #1,
#2 and #2+Cf as a % of #2.
#2+Cf and #2+Cf+Cd as a % of #2+Cf

Wave Intensity Analysis (WIA)

WIA is explained in Chapter 2 and is also a topic of Chapters 4 & 5. For the work on the model aorta, two separated WIA were carried out, one using wave pressure (P_W) and the other using total pressure (P_T). Values for PWV measured for the length of the aorta, namely ascending aorta to the aorto-iliac bifurcation (Figure 7.35), are used for both WIA; reasons for this are given in the section for discussion (section 7.4). For WIA the compression and expansion wave *energies* – incident and reflected – were obtained by integration of the compression and expansion wave intensities (see Chapter 2).

WIA using Wave Pressure (P_W)

Wave pressure was obtained by subtraction of the reservoir (Windkessel) pressure from the measured (total) pressure; this is explained in Chapter 2 and exemplified in Figures 7.26 – 7.29 inclusively.

Examples of plots for WIA using wave pressure are given in Figures 7.36 (UpSt site; #1 and #1+Cf) and 7.37 (UpSt site; #2, #2+Cf and #2+Cf+Cd); for conciseness, the figures show WIA only for the UpSt site. In Figure 7.36 it appears that Clingfilm wrapping increases the amplitude of the expansion wave and converts it to a spike-like feature. In Figure 7.37, Clingfilm wrapping appears to convert the WIA plot of #2 to a plot similar to those observed *in vivo* (#2+Cf) and remaining so after application of distal compliances (#2+Cf+Cd).

Clingfilm wrapping of the model aorta increased both incident and reflected compression wave energies. The increase in incident compression wave energy was much less in #1+Cf (Δ80-90%; UpSt or DnSt in Figure 7.38) than in #2+Cf (Δ~700%; UpSt or DnSt in Figure 7.38). Reflected energies were small compared with incident energies in both experiments (Figure 7.38; UpSt & DnSt sites); their increases after Clingfilm wrapping were likely consequential of the increased respective incident energies, though the magnitudes of increases were large in terms of Δ% (Figure 7.38; #1+Cf: Δ >200% UpSt & DnSt; #2+Cf: Δ >200% UpSt & Δ >3000% DnSt). Wave reflection index (WRI) (i.e. reflected wave energy / incident wave energy) for compression wave energy at the UpSt site (Figure 7.39; UpSt) was either increased (Δ ~76% for #1 vs. #1+Cf) or decreased (Δ -50% for #2 vs. #2+Cf) by Clingfilm wrapping of the model aorta. However, at the DnSt site Clingfilm wrapping increased WRI in both models (Figure 7.39, DnSt: Δ 88% for #1 vs. #1+Cf and Δ 271% for #2 to #2+Cf).

Clingfilm wrapping of the model aorta increased incident expansion wave energies (Figure 7.40; UpSt & DnSt sites) and most reflected expansion wave energies, though not for that of #2 to #2+Cf UpSt where reflected expansion wave energy was decreased (Δ-45%; Figure

7.40 UpSt). WRI (Figure 7.41; UpSt & DnSt) for expansion wave energies were generally similar to the findings for WRI of compression wave energies (c.f. Figure 7.39) though values and Δ% magnitudes differed; an exception being the WRI of the expansion wave of #2+Cf (Figure 7.41; DnSt) which decreased (Δ-23.5%) after Clingfilm wrapping (c.f. Figure 7.39; DnSt – showing Δ 271% increase WRI of compression wave of #2+Cf).

The overall trend of effects of Clingfilm wrapping was to increase incident compression and incident expansion wave energies along with *mainly* increasing reflected wave energies of both wave types. However, trends for WRI are equivocal – WRI either increased or decreased after Clingfilm wrapping.

With regard to the model #2+Cf, distal compliances were applied subsequent to Clingfilm wrapping making the model #2+Cf+Cd. Distal compliances had little effect on incident compression wave energy, either increasing (Δ 20.5%; Figure 7.38 - UpSt) or slightly decreasing it (Δ -7.8%; Figure 7.38 - DnSt). Reflected compression wave energies were of small magnitude compared to the respective incident energies and were little affected by distal compliances (Figure 7.38: Δ -6.8% UpSt; Δ 9% DnSt). Distal compliances appeared to increase incident and reflected expansion wave energies (Figure 7.40; UpSt & DnSt). With regard to WRI, distal compliances decreased WRI for compression (Figure 7.39) and expansion (Figure 7.41) waves, at the UpSt site. However, at the DnSt site, Clingfilm wrapping increased WRI for the compression wave (Δ 18.1%; Figure 7.39 DnSt) and decreased WRI for the expansion wave (Δ -53.3%; Figure 7.41 DnSt).

FIGURE 7.36: Plots of Wave Intensity Analysis (WIA), using P_W for WIA, at the UpSt Site of Measurement in the Abdominal Aorta section of the Model before (#1) and after Clingfilm wrapping (#1+Cf).

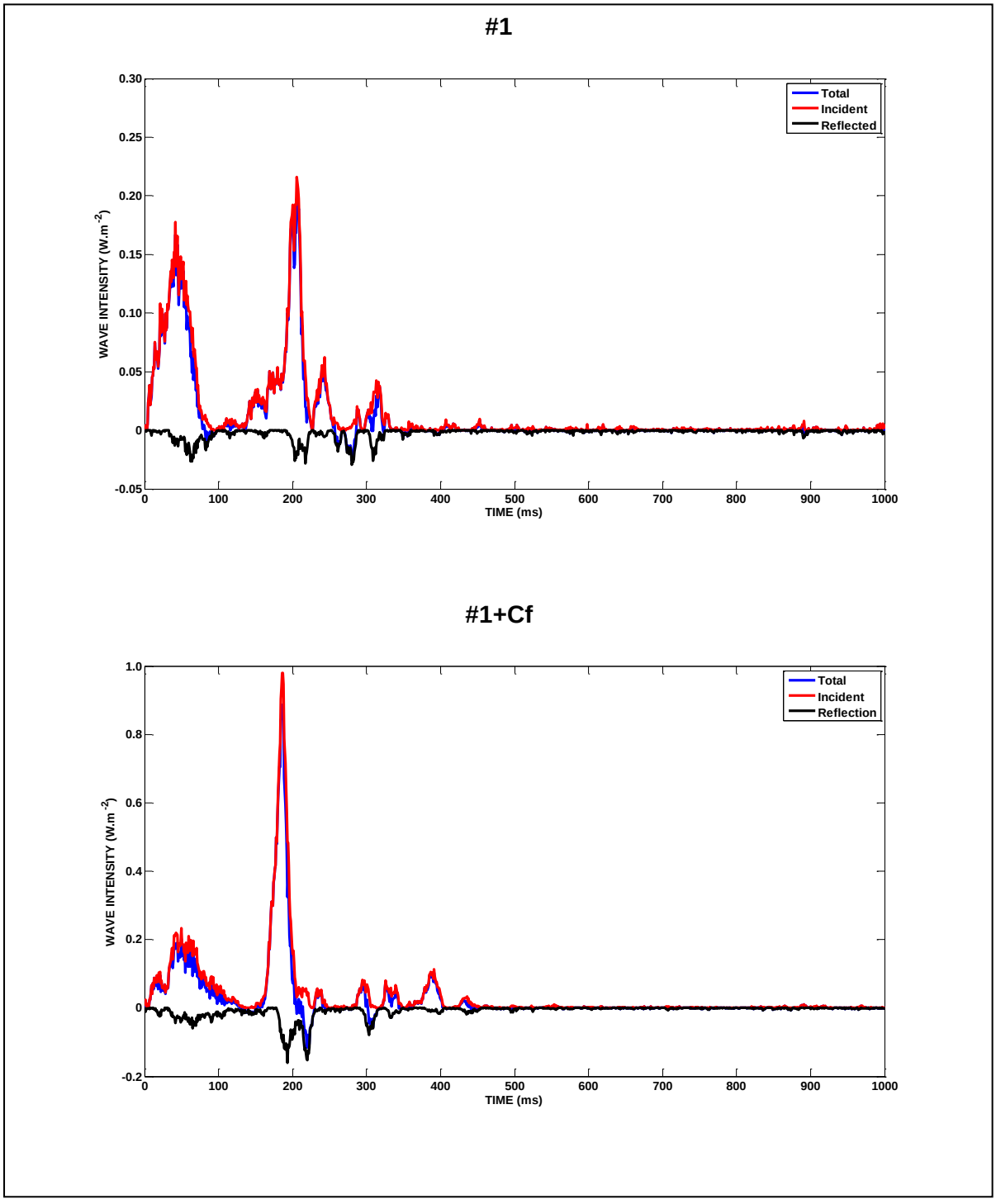

FIGURE 7.37: Plots of Wave Intensity Analysis (WIA), using P_W for WIA, at the UpSt Site of Measurement in the Abdominal Aorta section of the Model before (#2) and after Clingfilm wrapping (#2+Cf) and then after application of distal compliances (#2+Cf+Cd).

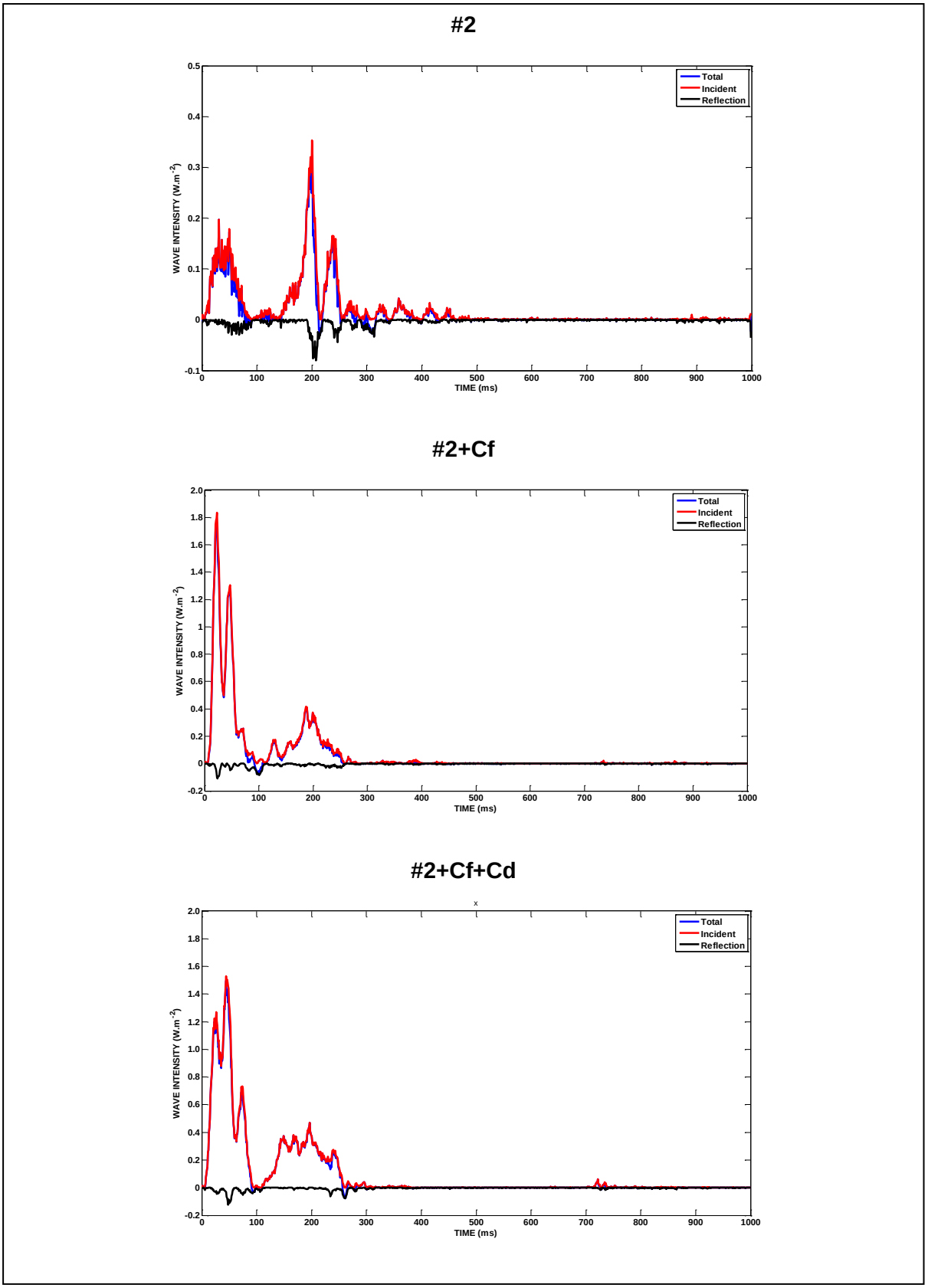

FIGURE 7.38: Compression Wave Energy, using P_W for WIA, before (#1 and #2) and after Clingfilm wrapping (#1+Cf and #2+Cf) and then after application of distal compliances (#2+Cf+Cd). Measurements made at the UpSt & DnSt Sites in the Abdominal Aorta section of the Model.

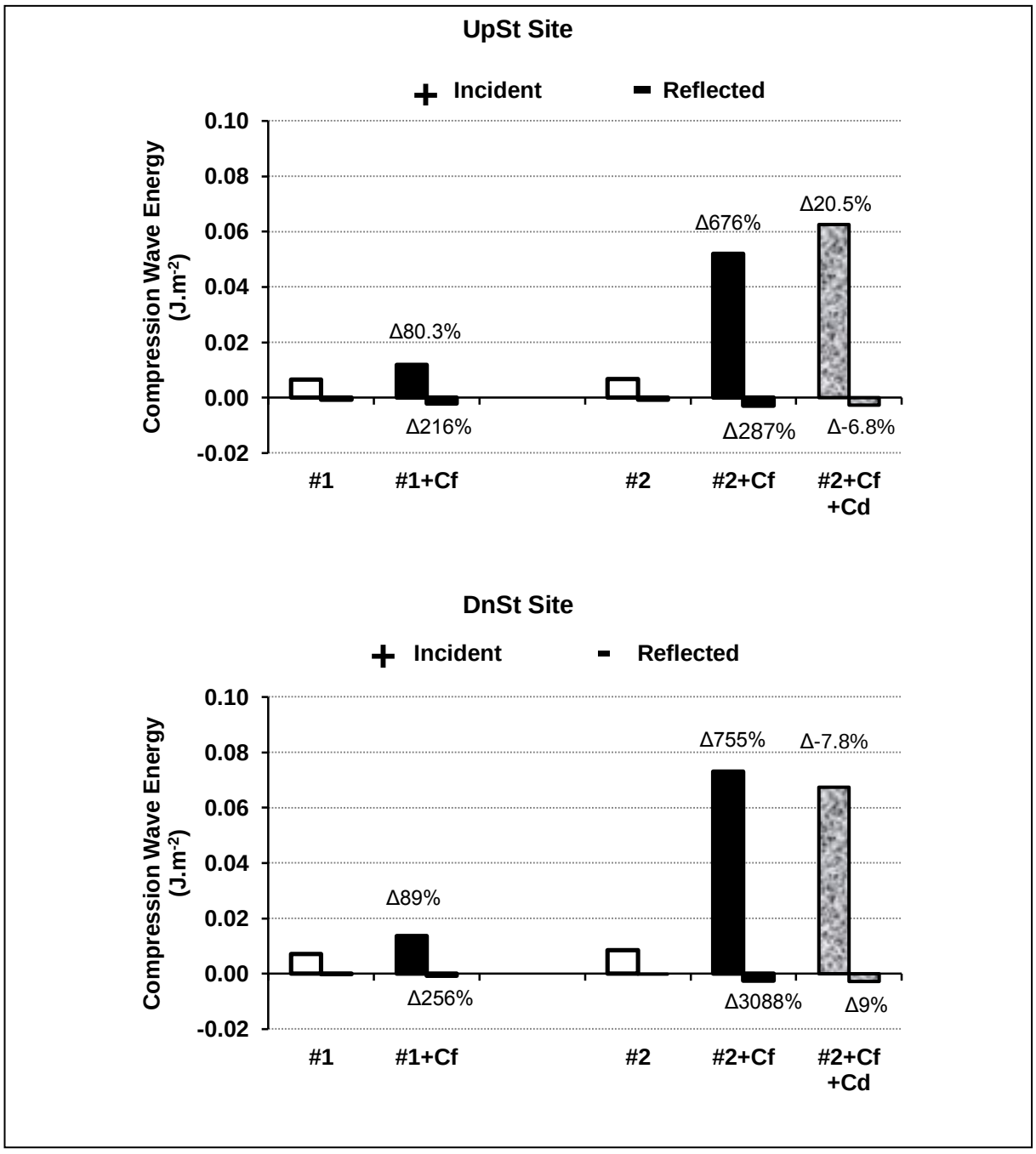

Δ values are the differences between:

#1 and #1+Cf as a % of #1,
#2 and #2+Cf as a % of #2.
#2+Cf and #2+Cf+Cd as a % of #2+Cf

FIGURE 7.39: Wave Reflection Index (WRI), using P_W for WIA, for Compression Wave Energy before (#1 and #2) and after Clingfilm wrapping (#1+Cf and #2+Cf) and then after application of distal compliances (#2+Cf+Cd). Measurements made at the UpSt & DnSt Sites in the Abdominal Aorta section of the Model.

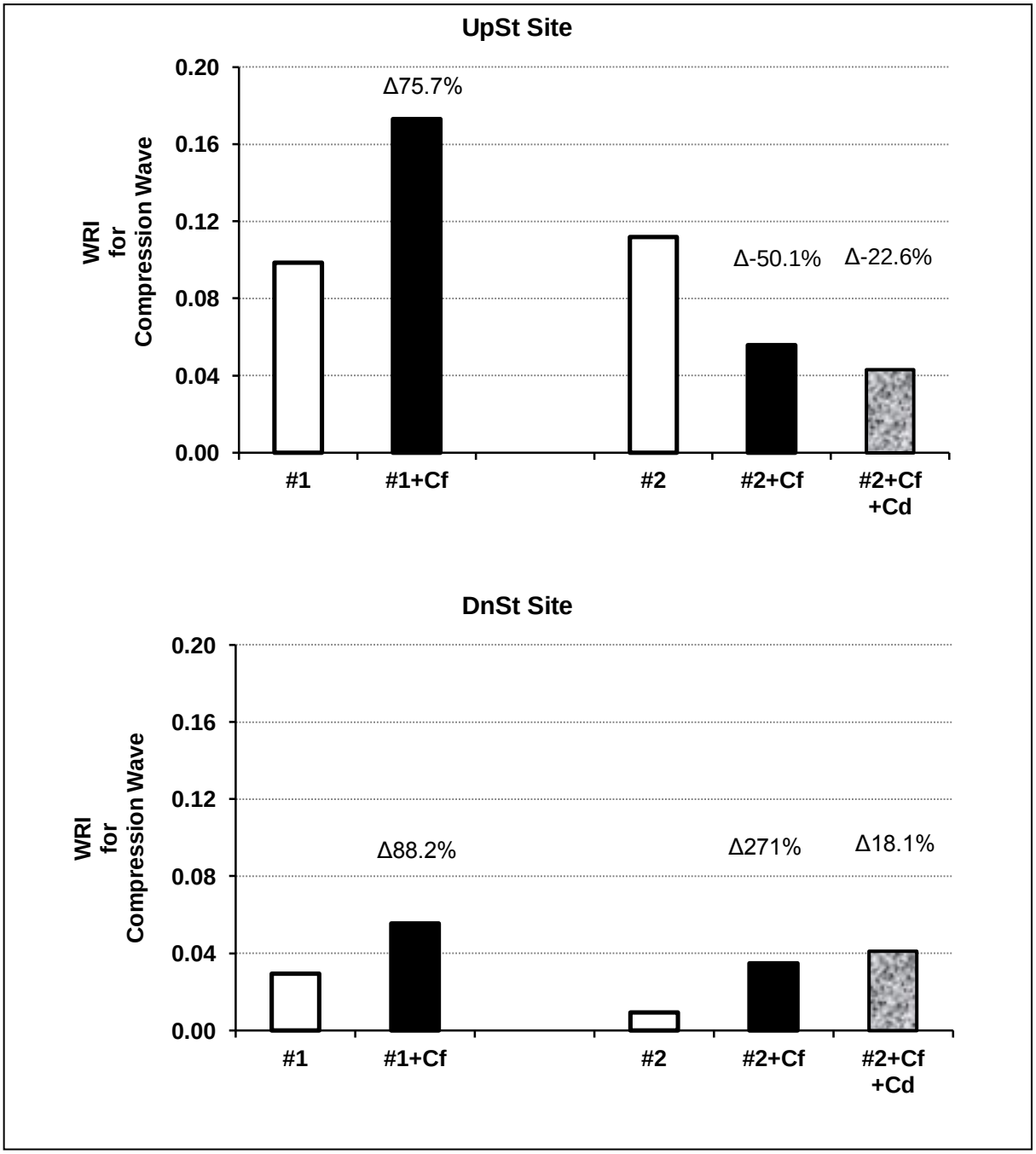

Δ values are the differences between:

#1 and #1+Cf as a % of #1,
#2 and #2+Cf as a % of #2.
#2+Cf and #2+Cf+Cd as a % of #2+Cf

FIGURE 7.40: Expansion Wave Energy, using P_W for WIA, before (#1 and #2) and after Clingfilm wrapping (#1+Cf and #2+Cf) and then after application of distal compliances (#2+Cf+Cd). Measurements made at the UpSt & DnSt Sites in the Abdominal Aorta section of the Model.

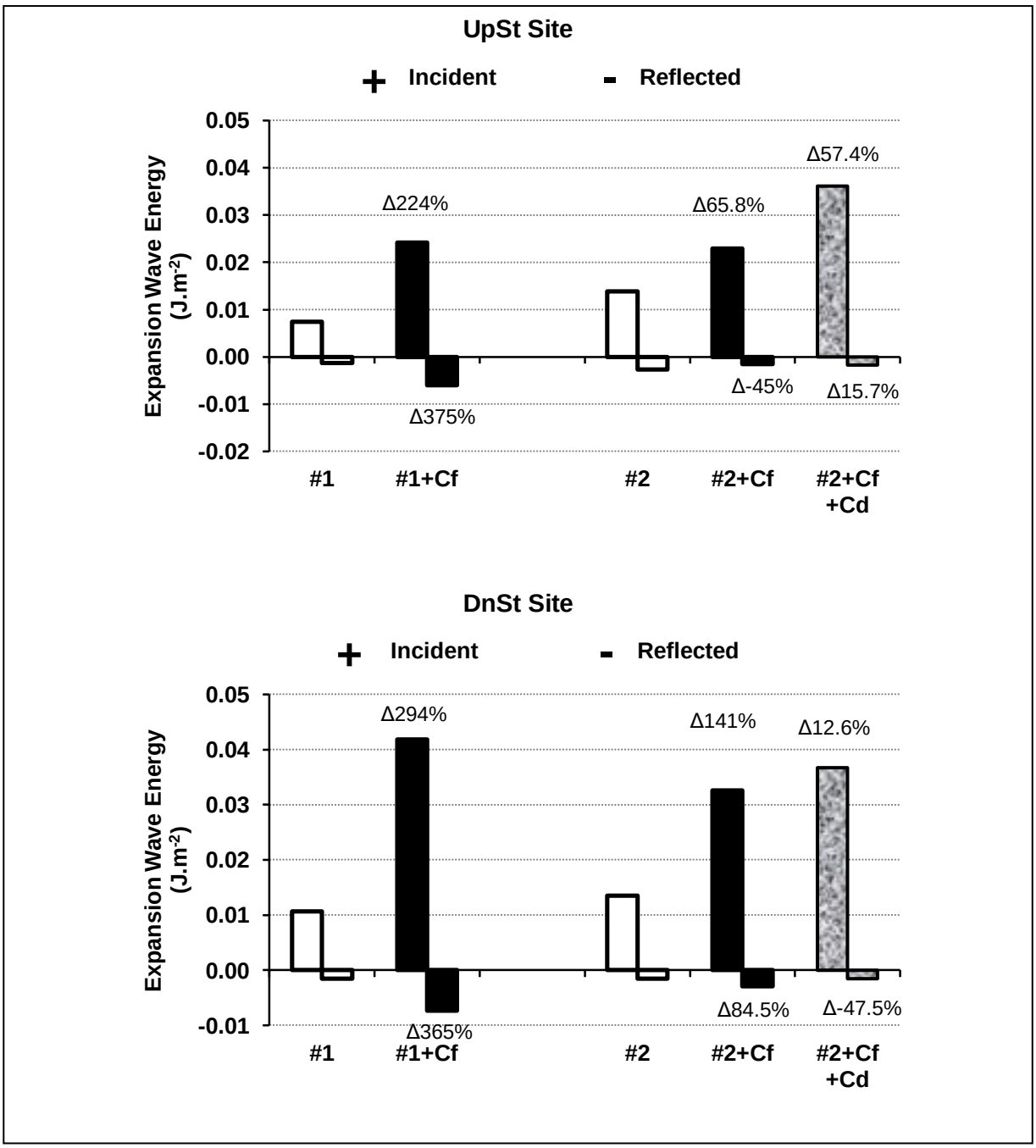

Δ values are the differences between:

#1 and #1+Cf as a % of #1,
#2 and #2+Cf as a % of #2.
#2+Cf and #2+Cf+Cd as a % of #2+Cf

FIGURE 7.41: Wave Reflection Index (WRI), using P_W for WIA, for Expansion Wave Energy before (#1 and #2) and after Clingfilm wrapping (#1+Cf and #2+Cf) and then after application of distal compliances (#2+Cf+Cd). Measurements made at the UpSt & DnSt Sites in the Abdominal Aorta section of the Model.

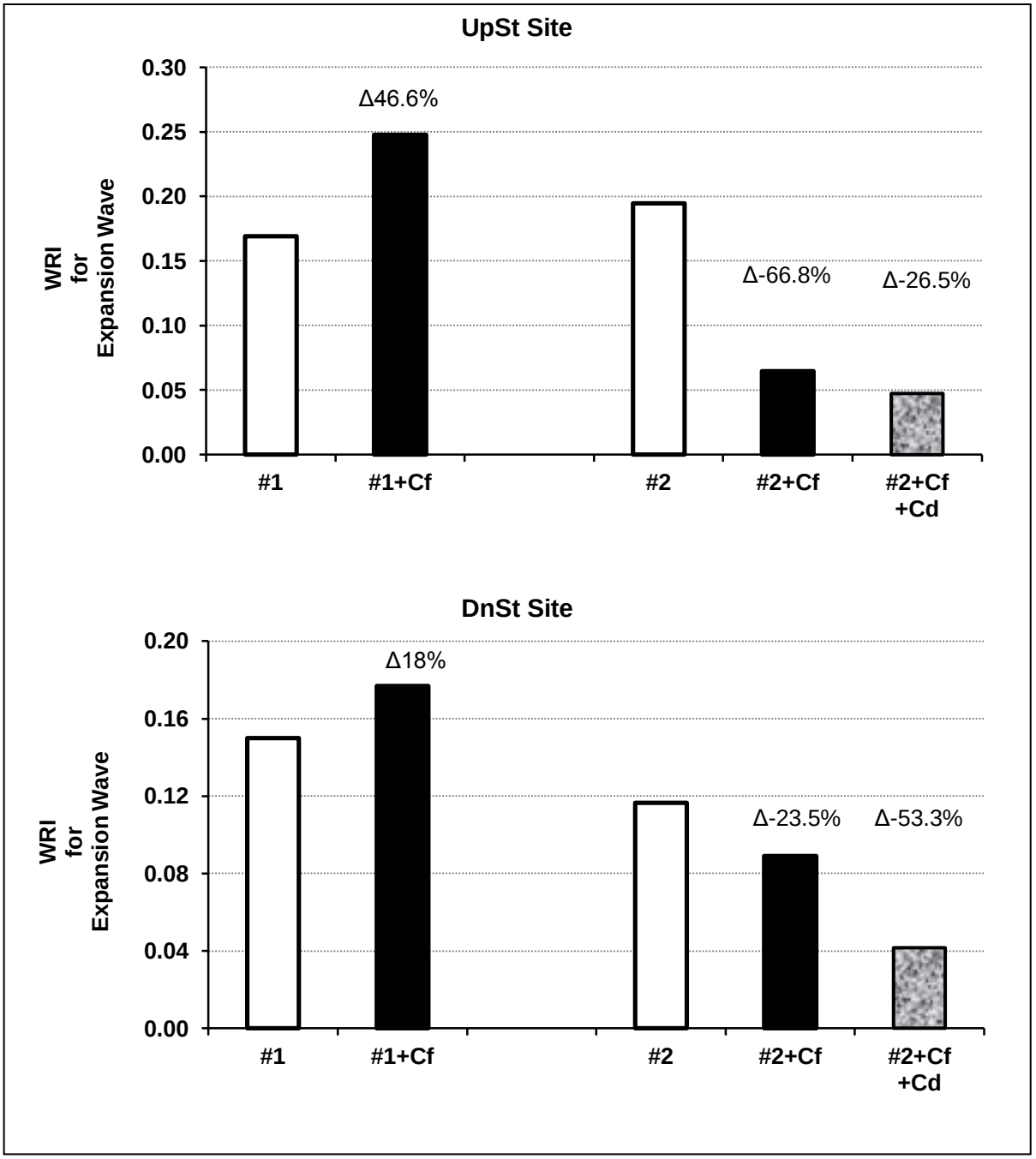

Δ values are the differences between:

#1 and #1+Cf as a % of #1,
#2 and #2+Cf as a % of #2.
#2+Cf and #2+Cf+Cd as a % of #2+Cf

WIA using Total Pressure (P_T)

In figures of this section, where comparison is made between data obtained using either Pw or P_T for WIA, the data from WIA using Pw has been copied from the previous section, i.e. the data here is not from repeated experiments.

Examples of plots for WIA using total pressure, P_T, are given in Figures 7.42 (UpSt site; #1 and #1+Cf) and 7.43 (UpSt site; #2, #2+Cf and #2+Cf+Cd); for conciseness, the figures show WIA only for the UpSt site and can be compared to Figures 7.36 (UpSt site; #1 and #1+Cf) and 7.37 (UpSt site; #2, #2+Cf and #2+Cf+Cd) which are of WIA using wave pressure, P_W. The incident and reflected compression waves were larger for #1 (Figures 7.42) and #2 (Figures 7.43) using P_T for WIA than for #1 (Figures 7.36) and #2 (Figures 7.37) when P_W was used for WIA. This is discussed further in the next paragraph.

Values for, or magnitudes of, incident and reflected compression wave energy (Figure 7.44) and respective WRI (Figure 7.45) were very much greater when total pressure, P_T, rather than when wave pressure, P_W, was used for WIA; this was found for both the UpSt (incident Δ ~200%; reflected Δ ~1000%; WRI Δ ~200%) and DnSt (incident Δ ~200%, reflected Δ 3000-10,000%; WRI Δ 1000 - ~4000%) sites of measurement in the abdominal aorta section of the normal model aorta. In contrast, values for incident and reflected expansion wave energy (Figure 7.46) and respective WRI (Figure 7.47) were little different between use of P_T or P_W for WIA (all Δ values <100%).

Although *magnitudes* of wave intensity tended to be greater using P_T rather than P_W for WIA (e.g. compression wave energy – previous paragraph), there were no remarkable differences observed for *trend* of effect of Clingfilm wrapping on wave intensity as revealed by WIA using either P_W or P_T (Models #1+Cf & #2+Cf; comparative data not shown for conciseness).

The addition of distal compliances to #2+Cf to make #2+Cf+Cd decreased reflected compression wave energy but had little effect on incident compression wave energy (Figures 7.43 & 7.48; model #2+Cf+Cd; UpSt site). This effect of distal compliances was marked when P_T was used for WIA compared to that shown by data of WIA by P_W; the latter showed little effect by distal compliances on reflected compression wave energy (Figure 7.48). Distal compliances also decreased reflected compression wave energy as measured at the DnSt site (data not shown for conciseness). Distal compliances also decreased reflected expansion wave energy; again an effect that was clearer when P_T was used for WIA (data not shown for conciseness).

FIGURE 7.42: Plots of Wave Intensity Analysis (WIA), using P_T for WIA, at the UpSt Site of Measurement in the Abdominal Aorta section of the Model before (#1) and after Clingfilm wrapping (#1+Cf).

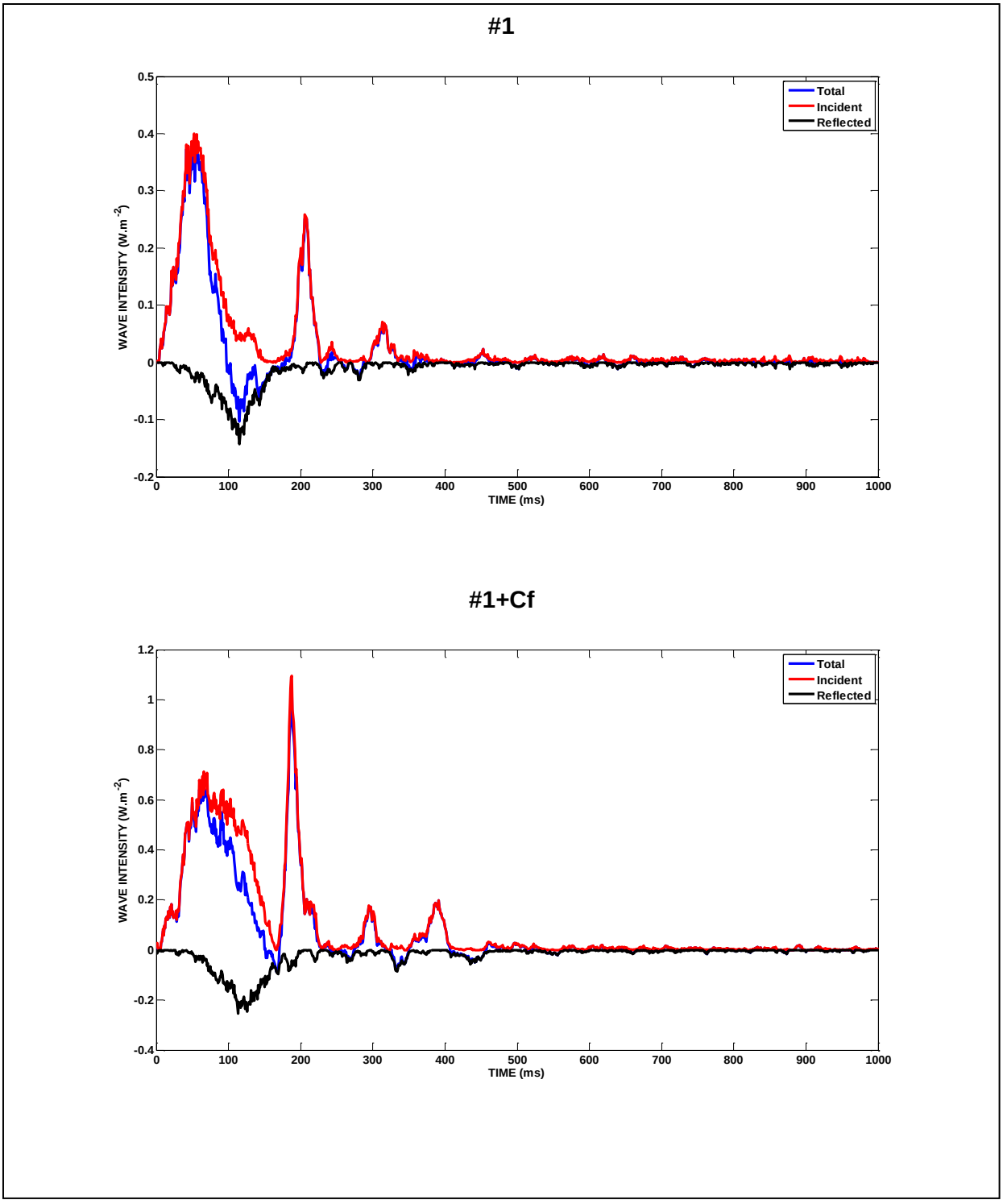

FIGURE 7.43: Plots of Wave Intensity Analysis (WIA), using P_T for WIA, at the UpSt Site of Measurement in the Abdominal Aorta section of the Model before (#2) and after Clingfilm wrapping (#2+Cf) and then after application of distal compliances (#2+Cf+Cd).

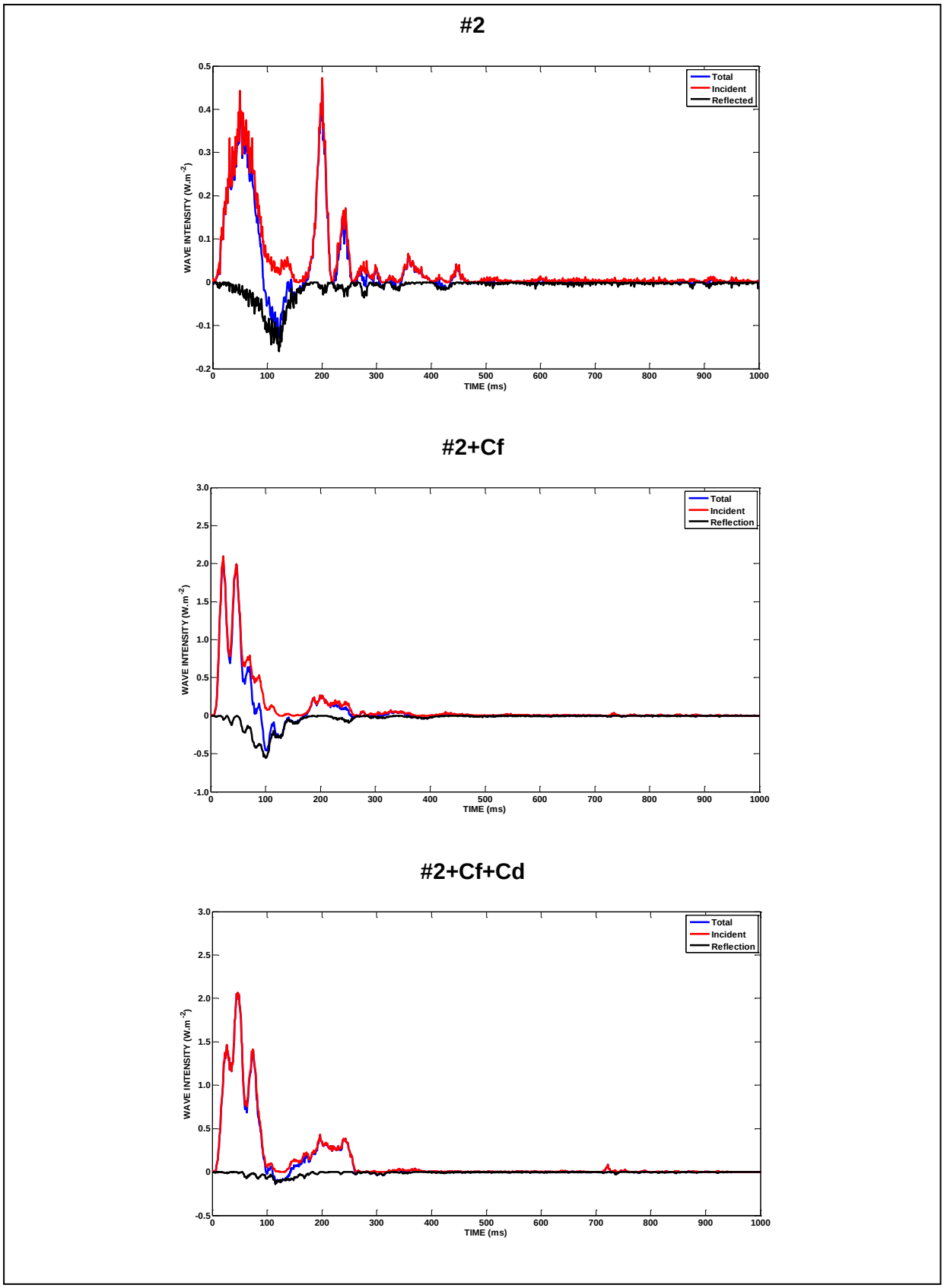

FIGURE 7.44: Compression Wave Energy compared between use of P_W or P_T (i.e. models #1P_W vs. #1P_T and #2P_W vs. #2P_T) for WIA. Measurements made at the UpSt & DnSt Sites in the Abdominal Aorta section of the Model Normal Aorta.

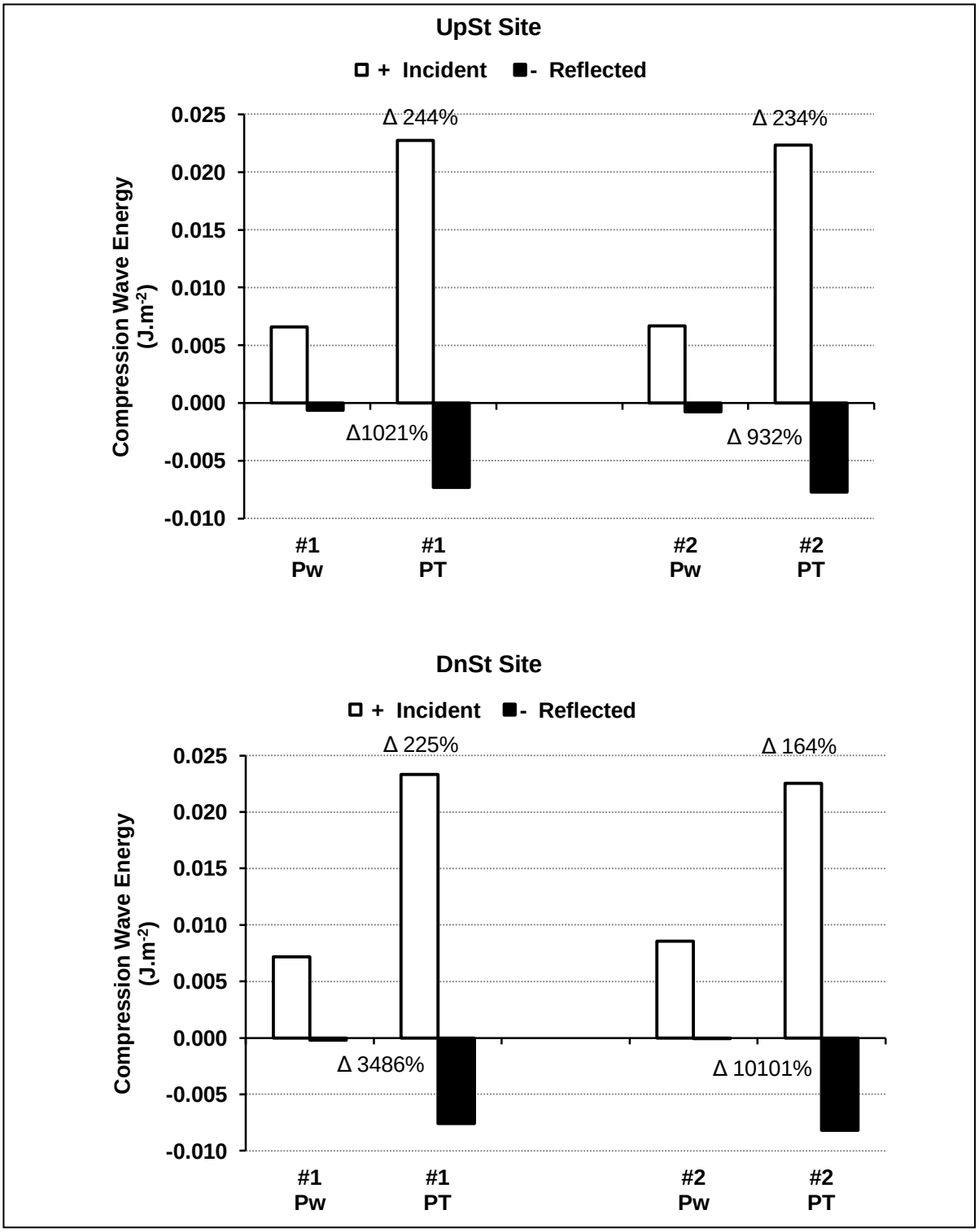

Δ values are the differences between:

#1P_W and #1P_T as a % of #1P_W
#2P_W and #2P_T as a % of #2P_W

Note the large Δ values, all much >100%.

FIGURE 7.45: Wave Reflection Index (WRI) for Compression Wave compared between use of P_W or P_T (i.e. models #1P_W vs. #1P_T and #2P_W vs. #2P_T) for WIA. Measurements made at the UpSt & DnSt Sites in the Abdominal Aorta section of the Model Normal Aorta.

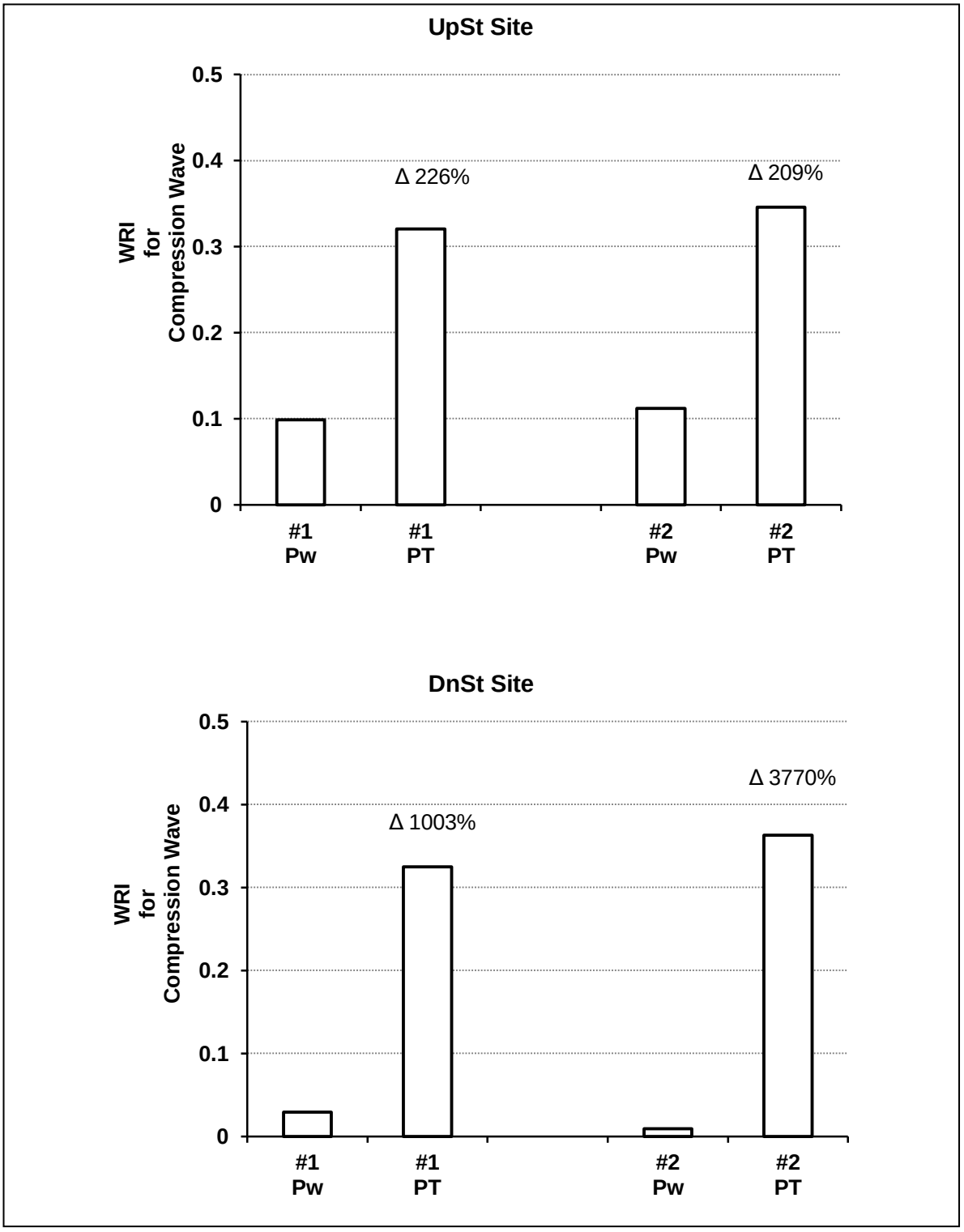

Δ values are the differences between:

#1P_W and #1P_T as a % of #1P_W
#2P_W and #2P_T as a % of #2P_W

Note the large Δ values, all much >100%.

FIGURE 7.46: Expansion Wave Energy compared between use of P_W or P_T (i.e. models #1P_W vs. #1P_T and #2P_W vs. #2P_T) for WIA. Measurements made at the UpSt & DnSt Sites in the Abdominal Aorta section of the Model Normal Aorta.

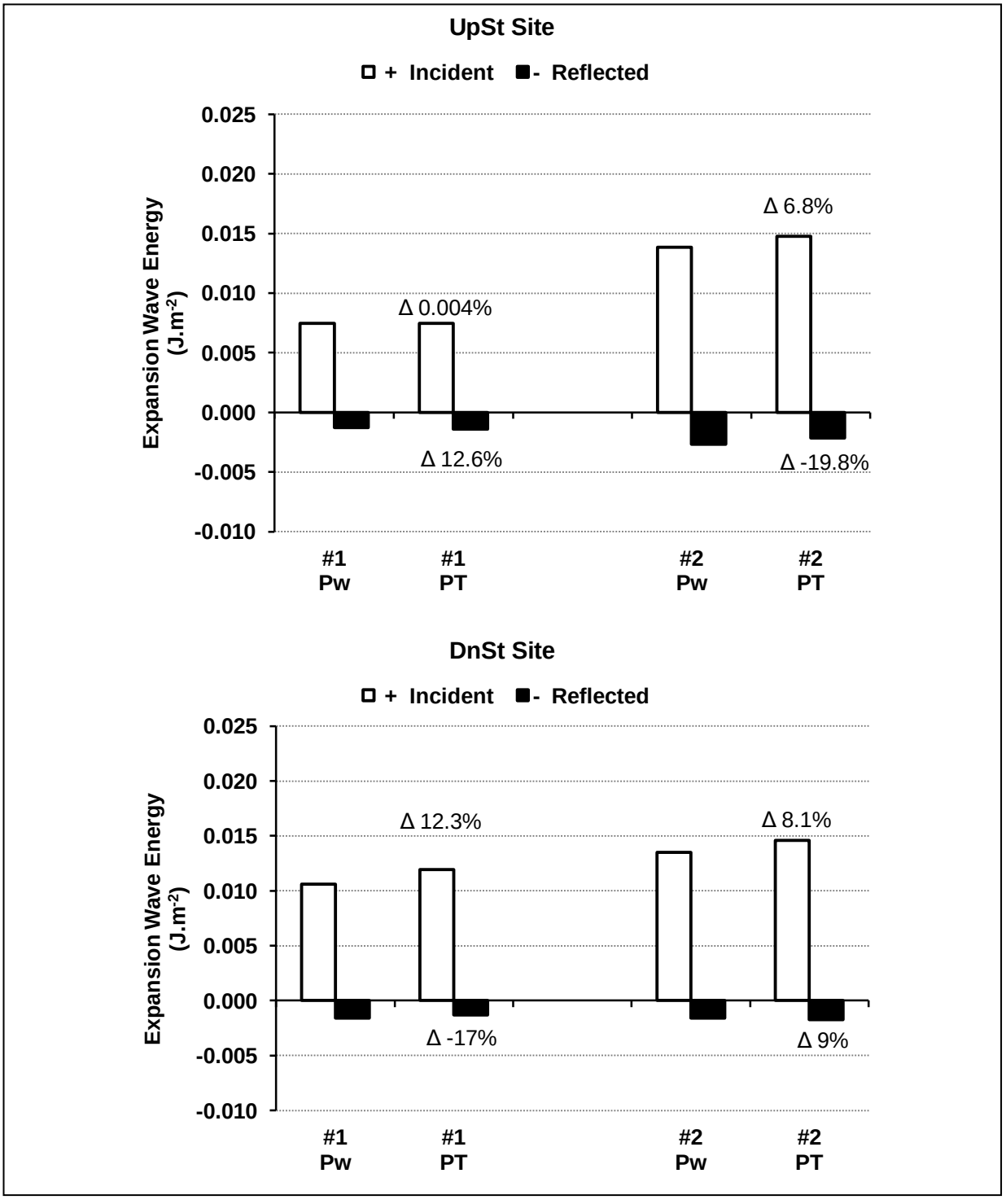

Δ values are the differences between:

#1P_W and #1P_T as a % of #1P_W
#2P_W and #2P_T as a % of #2P_W

Note the small Δ values, all <100%.

FIGURE 7.47: Wave Reflection Index (WRI) for Expansion Wave compared between use of P_W or P_T (i.e. models #1P_W vs. #1P_T and #2P_W vs. #2P_T) for WIA. Measurements made at the UpSt & DnSt Sites in the Abdominal Aorta section of the Model Normal Aorta.

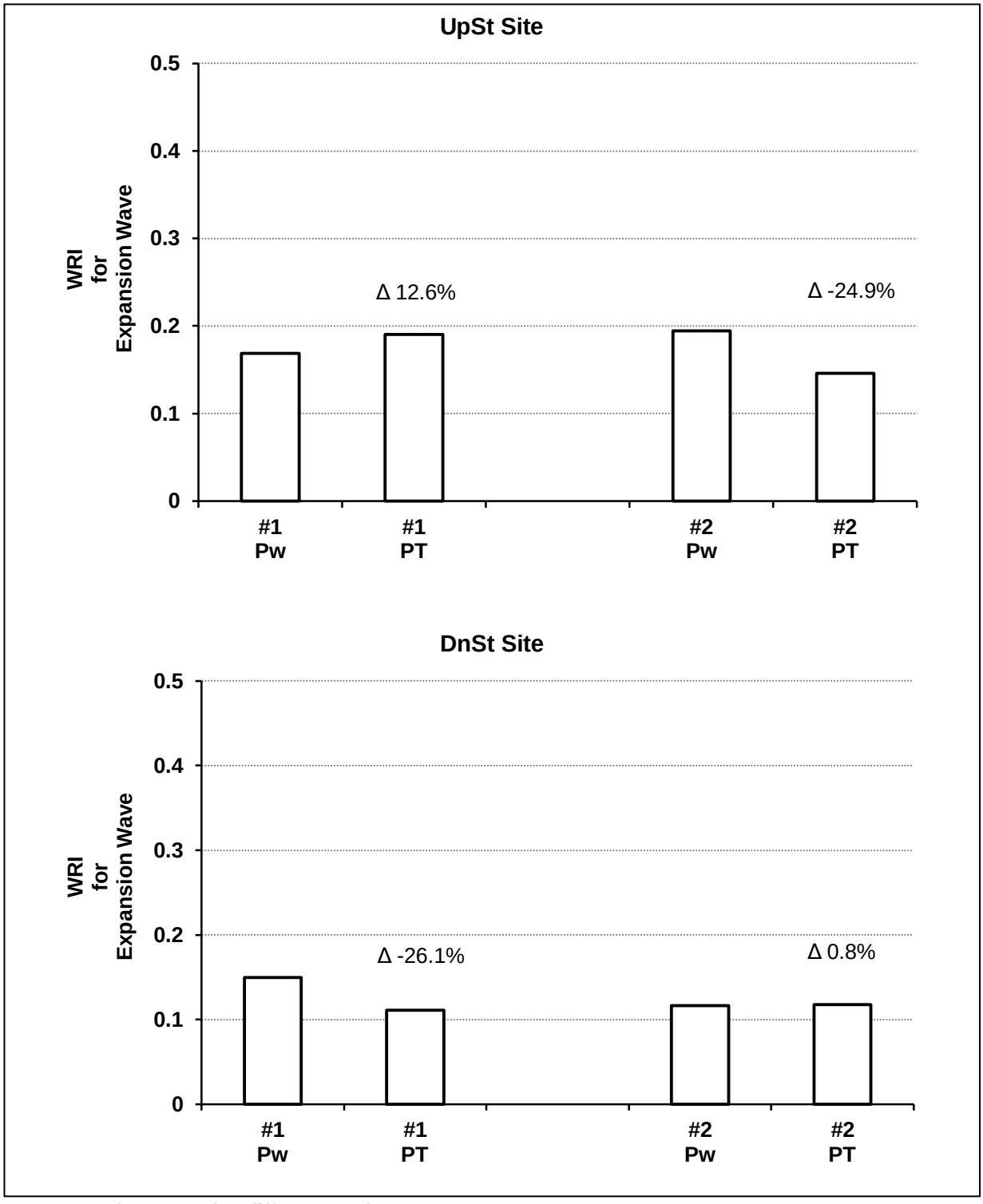

Δ values are the differences between:

#1P_W and #1P_T as a % of #1P_W
#2P_W and #2P_T as a % of #2P_W

Note the small Δ values, all <100%.

FIGURE 7.48: Compression Wave Energy and Wave Reflection Index (WRI), from WIA using P_W or P_T, before (#2) and after Clingfilm wrapping (#2+Cf) and then after application of distal compliances (#2+Cf+Cd). Measurements made at the UpSt Site in the Abdominal Aorta section of the Model Aorta.

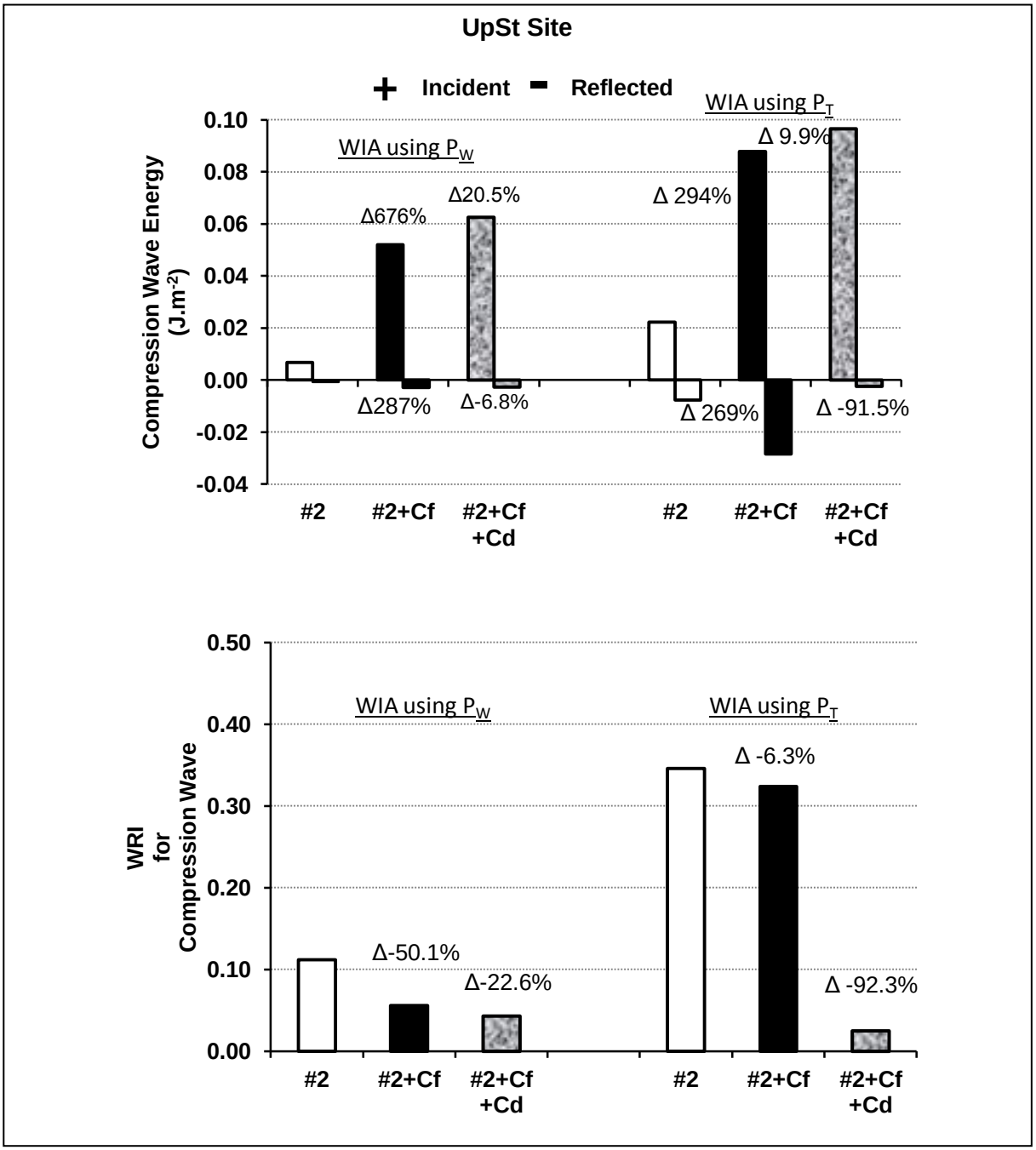

Δ values are the differences between:

#2 and #2+Cf as a % of #2.
#2+Cf and #2+Cf+Cd as a % of #2+Cf

Note: the addition of distal compliances to #2+Cf to make #2+Cf+Cd decreased reflected energy, this effect (compression wave energy Δ -91.5%; WRI Δ -92.3%) is clear when P_T is used for WIA. Incident energy is little affected by distal compliance.

WIA for Estimating position of Sites of Reflection

Sites of reflection were estimated from wave intensity plots; these estimates are shown in Figure 7.49. The precision of estimates is dependent on accuracy of measured wave speed and, importantly, on the clarity of wave intensity plots for the start, or foot, of the incident and reflected compression wave intensities; the time period between the foot of the incident and foot of the reflected intensities gives the incident-reflected wave transit time (Tt in Chapter 2 – Figure 2.3) with which the position of the reflection site can be calculated (Chapter 2 – Figure 2.3). The foot of both intensities was subjectively judged and mouse-clicked, thus using a MATLAB routine for calculations (see Appendix: Extra Data). Figures 7.36, 7.37, 7.42 and 7.43 give examples of the feet of incident and reflected compression wave intensities. Judgement must also be made on what might be artefact near to a foot and so not accepted as part of the compression wave intensity.

In the case of measurements of distances to reflection sites from the UpSt site (Figure 7.49), those obtained using Pw for WIA tended to be lower than those obtained using P_T for WIA; though #1 was an exception where *vice versa* was observed, and the two values for #2 almost agreed (11.3cm & 11.9cm). For the DnSt site (Figure 7.49), values from use of P_W were higher (#1; #2; #2+Cf) or lower (#1+Cf; #2+Cf+Cd) than those values from use of P_T. Thus, with overall consideration of UpSt or DnSt sites, no consistent trend of difference was found for sites of reflection as estimated from WIA using either P_W or P_T.

Figure 7.50 shows the Model Aorta along with distances, measured with a tape-measure, between the sites of measurement (i.e. UpSt or DnSt sites) and downstream bifurcations and terminals of the lower limb conduit arteries. The data from Figure 7.49 along with the measurements given in Figure 7.50 allow an anatomical reckoning of sites of reflection.

From the UpSt site, with Figures 7.49 and 7.50 in mind, the values for #1 (Pw: 18.7cm or P_T: 12.4cm) and 2# (Pw: 11.3cm or P_T: 11.9cm) indicate, though not precisely, the aorto-iliac bifurcation being the nearby site of reflection. The aorto-iliac bifurcation is also indicated as the site of reflection from values for #1+Cf (Pw: 18.8cm) and #2+Cf (P_T: 17.0cm), the latter of 17cm is precise. The other values for #1+Cf (P_T: 27.8cm) and #2+Cf (Pw: 8.1cm) are not clear in their indication of a reflection site; the former indicates a site between the aorto-iliac and iliac-femoral bifurcations and the latter indicates a site between the UpSt site of measurement and the aorto-iliac bifurcation.

From the DnSt site, with Figures 7.49 and 7.50 in mind, the value for #1 of 11.1cm (P_T) indicates the aorto-iliac bifurcation as the nearby reflection site, while for #2 of 23.1cm (Pw) indicates the iliac-femoral bifurcations as reflection sites, but these indications are not

precise. The values for #1 of 20.7cm (Pw) and for #2 of 15.6cm (P_T) are ambiguous in their indications since the values lead to sites almost mid-way between the aorto-iliac bifurcation and iliac-femoral bifurcations. The values for #1+Cf (Pw: 23.7cm or P_T: 27.0cm) and #2+Cf (Pw: 29.2cm) indicate, but imprecisely, the iliac-femoral bifurcations as sites of reflection. The value for #2+Cf of 20.2cm (P_T) is ambiguous in its indication leading to a site mid-way between the aorto-iliac bifurcation and iliac-femoral bifurcations.

The case for #2+Cf+Cd is that the intensity of reflected compression wave energy was small especially when the intensity was obtained from WIA using P_T. It could be argued that under the condition of applied distal compliances, no reflection sites exist hence the small, if any, reflected energy; what was considered as reflected wave intensity might have been artefact or general “noise” of the system. The values obtained for #2+Cf+Cd, UpSt (Pw: 8.4cm or P_T: 39.7cm) or DnSt (Pw: 29.5cm or P_T: 68.4cm) are widely disparate, thus measurement might have been made from artefacts rather than genuine wave intensities. However, if the values are taken as indicators of sites of reflection, then for #2+Cf+Cd, UpSt, 39.7cm (P_T) indicates the iliac-femoral bifurcations as the site of reflection; the value 8.4cm (Pw) is ambiguous. For #2+Cf+Cd, DnSt, 29.5cm (Pw) and 68.4cm (P_T) indicate sites of reflection, respectively, at the iliac-femoral bifurcations and termination of the external femoral arteries.

Other than the distance 17cm (P_T: #2+Cf; UpSt) which was precise for the aorto-iliac bifurcation, no other distances precisely indicated sites of reflection at the bifurcations, instead the distance were either close to such sites or between two sites. Use of Pw or P_T for WIA showed neither to be best for accurate measurement of distance to sites of reflection.

FIGURE 7.49: Distances* to Reflection Sites from the Sites of Recording (i.e. UpSt & DnSt Sites in the Abdominal Aorta Section of the Model Aorta) as estimated from the time lapse between Incident and Reflected Intensities of Compression Waves before (#1 and #2) and after Clingfilm wrapping (#1+Cf and #2+Cf) and then after application of distal compliances (#2+Cf+Cd). Data from WIA using Pw and P_T.

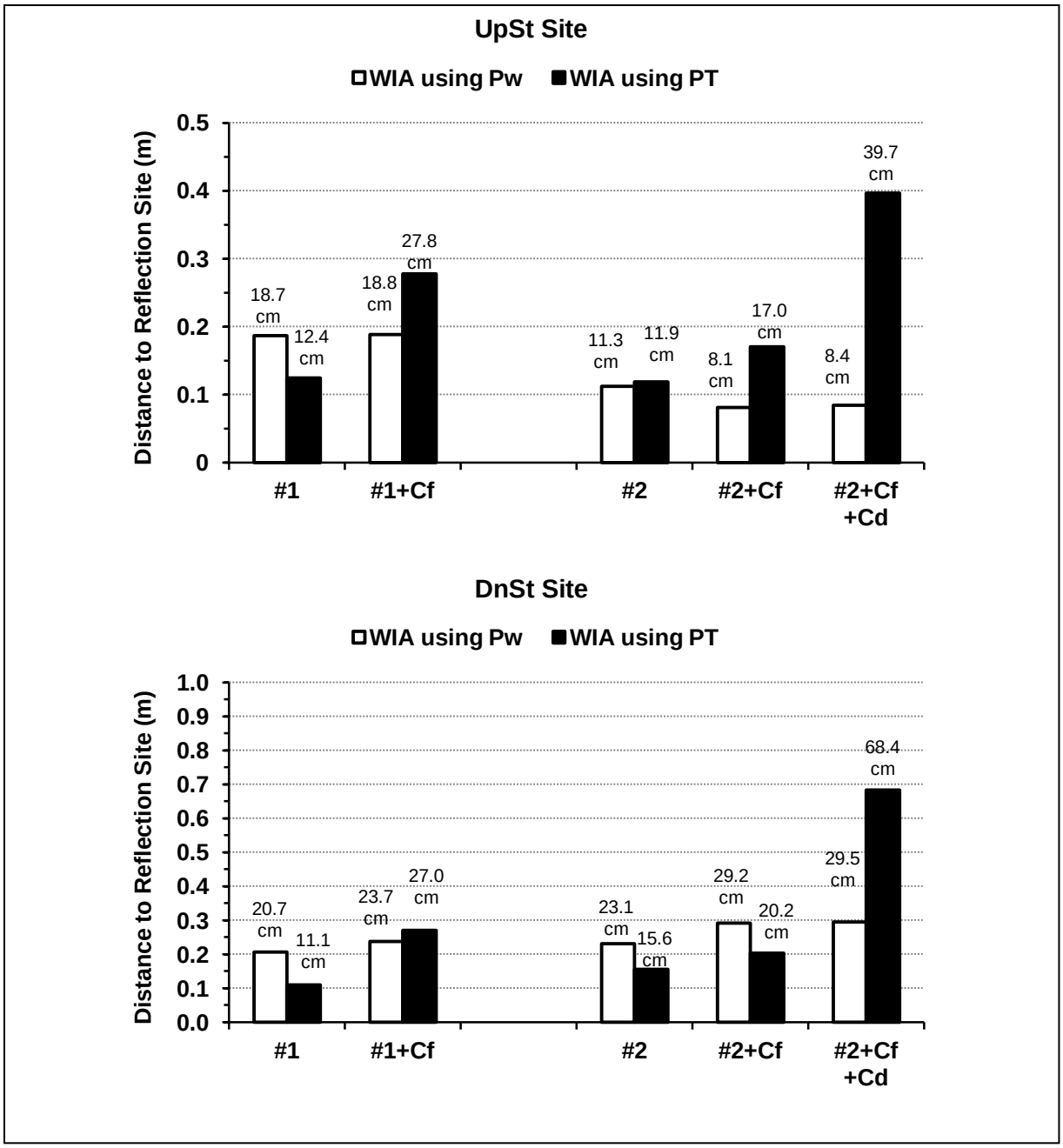

* Distances in cm are given for the value above each respective bar.

FIGURE 7.50: The Model Aorta and Distances, Measured with a Tape-measure, between the Sites of Measurement (i.e. UpSt or DnSt Sites) and Downstream Bifurcations and Terminals of Lower Limb Conduit Arteries.

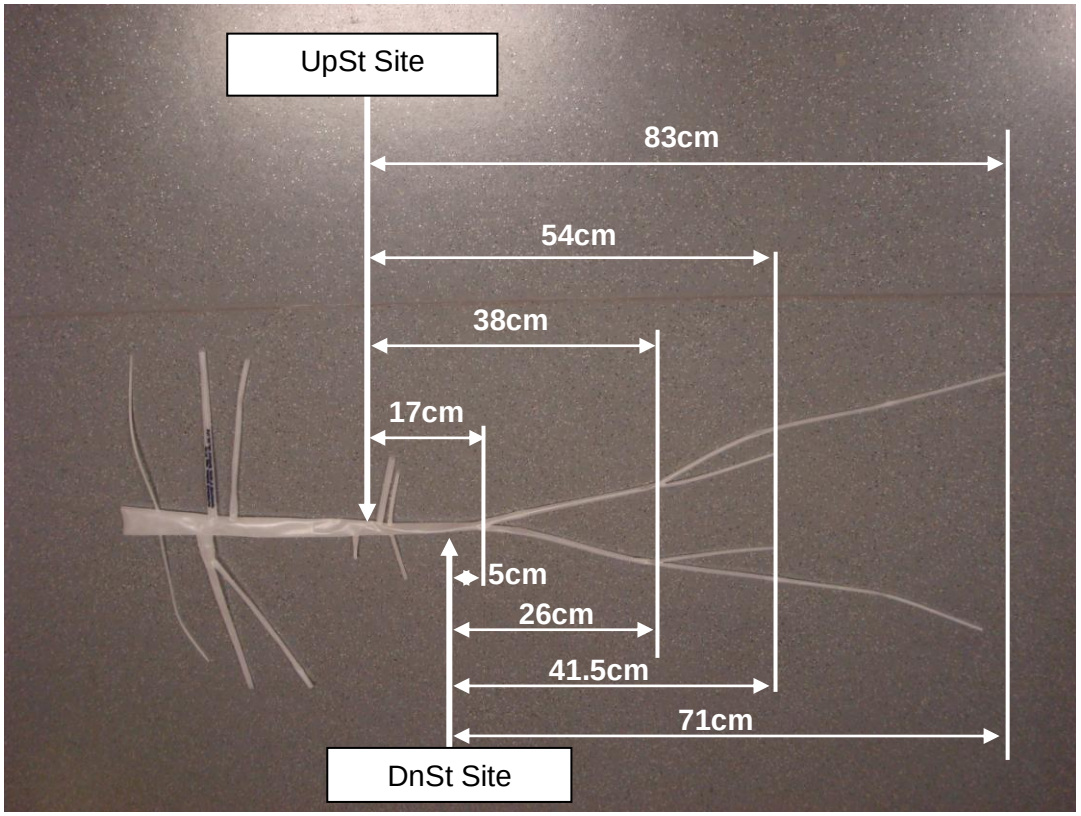

This figure, along with data from Figure 7.49, allows an anatomical reckoning of sites of reflection.

7.4 DISCUSSION

The pressure waveforms in the normal model aorta as shown in Figures 7.9 and 7.10 are comparable with those observed by others using a similar model (Segers *et al*., 1998; Segers and Verdonck, 2000) or exact replica (Kolyva *et al*., 2010), though the flow waveforms of this work were measured in the abdominal aorta, not in the ascending aorta. The distribution of the cardiac output (Figure 7.11) was closely similar to that as observed by others with a similar model (Segers *et al*., 1998).

The model aorta was converted into a model of aortic stiffening by wrapping the model in Clingfilm. The effect of this was to raise systolic and decrease diastolic pressure thereby increasing the pulse pressure (Figure 7.16). This effect does not yet appear to be reported in the published literature on this model aorta but the effect has been demonstrated in an early model of the circulation (Wiggers, 1944). Clingfilm wrapping did not greatly affect MAP or TPR which is interesting since this is often the case with isolated systolic hypertension in the elderly (Safar, 1993; Izzo, 2004; Mitchell, 2009), where SBP is certainly increase with little or no increase, if not a small decrease, in DBP. It is understood that isolated systolic hypertension results from loss of distensibility (i.e. stiffening) of the aorta (Safar, 1993; Izzo, 2004; Greenwald, 2007; Mitchell, 2009). The ageing aorta compensates for loss of distensibility by increased diameter to maintain compliance (Mitchell, 2009), though in time this too decreases. An observation made during the experiments with the Clingfilm wrapped aorta was that although pulsatile radial distension was restrained by the Clingfilm, pulsatile axial extension was free to occur and did so; this might be an explanation for tortuosity of the aged aorta where perhaps stiffening is unevenly distributed along the aorta causing a bending effect that overcomes the adventitial tethering at less stiff parts of the aorta.

Pressure-volume determinations for the model aorta were done to establish that Clingfilm wrapping did stiffen the model aorta and reduce its compliance and thus explain the observation of increased pulse pressure. The pressure-volume curve obtained for the normal model aorta (Figure 7.17) was comparable to that found by Kolyva *et al*. (2010); this is not surprising since, as already noted, the model aorta used by Kolyva *et al*. (2010) is an exact replica of the one used for the work of this thesis. Furthermore, the pressure-volume curve was close to that obtained by Segers *et al*. (1998) who used a very similar model. As with the workers here referenced, hysteresis was observed between the loading and unloading curves; hysteresis is the viscoelastic property of the polyurethane material of the model aorta wall. Compliance of the aorta models was derived from the pressure-volume determinations. Compliance for the normal aorta model without distal compliances was

found to be 0.48ml.mmHg^{-1} (model #1 at 93 mmHg) and 0.53ml.mmHg^{-1} (model #2 at 108 mmHg). The compliance calculated by Kolyva *et al*. (2010) for their model without distal compliances (referred to as C_{prox}) was 0.64ml/mmHg (at 70-120mmHg), some 20%-30% higher than those values for the model (#1 or #2) used for this thesis; the value found by Segers *et al*. (1998) for their model without distal compliances (referred to as C_p) was greater still at 0.85ml.mmHg^{-1} (at 90mmHg). It must be noted that the compliance curve for the normal aorta model (Figure 7.17 or 7.19) is not typical of the *in vivo* or *ex vivo* aorta whose compliance decreases with increasing pressure (see discussion, Chapter 6).

Pressure-volume determinations were also carried out for the model aorta wrapped in Clingfilm (Figure 7.18); hysteresis was again observed between the loading and unloading curves. As with the normal aorta model, compliance of the Clingfilm wrapped model was derived from its pressure-volume curve; compliance remained almost constant as pressure increased (Figure 7.18 or 7.19). The loading pressure-volume curves and the derived compliance curves for the normal and Clingfilm wrapped model aorta are compared in Figure 7.19 where it can be seen that the curves for the two models diverge, thus demonstrating that the Clingfilm wrapped aorta has less compliance than the normal one. Indeed, it is clearly shown in Figure 7.21 where, within the MAP range of 90-110mmHg, the compliance of the normal aorta is greater than that of the Clingfilm wrapped aorta. In support of these findings on compliance, calculated arterial compliance (AC) was also found to be much greater in the normal than Clingfilm wrapped aorta (Figure 7.22). In addition to pulse pressure (Figure 7.16) being increased by decreased aortic compliance, the same was observed for $\int$RP (Figure 7.23) and PP_{RP} (Figure 7.24) which were increased in the Clingfilm wrapped aorta. $\int$RP and PP_{RP} are inversely related to compliance and are measures of reservoir (Winkessel) function; the majority of this function resides in the ascending aorta, arch and much of the proximal thoracic aorta (Nichols and O'Rourke, 2005; Mitchell, 2009). PP_{RP} increases with age in humans (Davies *et al*., 2010). Thus, the Clingfilm wrapped aorta could be taken as a model of aortic ageing and hence demonstrate haemodynamic and vascular pathology pertaining to isolated systolic hypertension.

Another feature of the modelling to discuss is that of the distal compliances. The distal compliances are intended to simulate the compliance of medium level conduit arteries as well as more peripheral vessels. It can be seen from Figures 7.21 that summing the distal compliance with the compliance of the Clingfilm wrapped model aorta almost restores the compliance to that of the normal aorta. Application of the distal compliances to the Clingfilm wrapped aorta caused a small increase in AC (Figure 7.22) and decreased $\int$RP (Figure 7.23) and PP_{RP} (Figure 7.24). Thus, this model demonstrates that compliance of medium

level conduit arteries can influence haemodynamic events in the aorta as indicated by the reductions in $\int RP$ and PP_{RP}. The medium level conduit arteries (e.g. brachial arteries) have smooth muscle which is a feature potentially enabling control of systemic arterial compliance – medium level conduit arteries tend not to age drastically like the aorta and so could be important as a compliance to compensate for reduced compliance of the ageing aorta (Boutouyrie *et al*., 1992; Bortolotto *et al*., 1999; van der Heijden-Spek *et al*., 2000).

The concept of P_∞ is discussed in Chapter 4; values found for it *in vivo* in the rabbit experiments were surprisingly high, namely close to diastolic blood pressure, whereas expected values are between mean circulatory filling pressure (7-10mmHg) and right atrial pressure (±1mmHg). The value for P_∞ is very dependent on the algorithm for calculating reservoir (Windkessel) pressure by fit to the measured pressure pulse diastolic decay curve. In the experiments with the model aorta, very low values, in fact negative values, of P_∞ were obtained from the normal aorta (Figure 7.25) where τ long, 1700-3700s (Figure 7.30); Clingfilm wrapping decreased τ greatly to 450-500s resulting in P_∞ values of 10-14mmHg which would be expected as these are close to the venous reservoir hydrostatic head of 10mmHg. Since vascular resistance, VR, was not changed by Clingfilm wrapping then the decrease in τ is due to decreased compliance, thus in this model estimated P_∞ was dependent on compliance. The diastolic decay curves of the normal aorta model, although probably quasi-exponential, appear to have a linear decline and so give the large τ and negative values of P_∞ (Figures 7.26-7.29); Clingfilm wrapping converts the diastolic decay to one resembling an exponential decay of a shorter τ, (Figures 7.26-7.29) and, in the case of the 2nd experiment, a shape much more resembling the *in vivo* physiological form with a clearly defined incisura at ~250ms (Figures 7.27 and 7.29). This observation in the 2nd experiment is interesting and requires further exploration for an understanding of what occurred to produce the realistic pressure waveform; to reproduce this realistic waveform consistently would be useful for modelling haemodynamics.

It is hypothesised in Chapter 4 that the RHDN of a peripheral arterial pressure pulse waveform is modified specifically by nitric oxide produced in the large to medium size conduit arteries as a result of the nitric oxide increasing the compliance of those arteries. In the studies of this thesis, RHDN refers to the incisura – see Chapter 4. RHDN remained little changed after Clingfilm wrapping of the model aorta in the first set of experiments, #1 vs. #1+Cf (Figure 7.31), but this was not the case on repeating this in the second set, #2 vs. #2+Cf (Figure 7.31), when RHDN was reduced. Further studies are needed to explain why

decreasing the compliance appeared to reduce RHDN; however, the interesting observation was that the application of the distal compliances clearly further reduced the RHDN (Figures 7.31 and 7.33). Thus, this model demonstrates that distal compliance affects the waveform occurring in the aorta. However, to address the RHDN in a peripheral artery would require that one of the conduit arteries of the model, appropriately one or both the subclavian arteries, be extended to make the brachial artery and further extended to model the radial artery; this would be appropriate as it is from the radial and even digital arteries where clinical studies assess the RHDN and apply other methods of pulse wave analysis.

PWV measured by the foot-to-foot method was determined along the length (ascending aorta to aorto-iliac bifurcation; 45.6cm) of the normal and Clingfilm wrapped model aorta. This determination showed that PWV was increased in the Clingfilm wrapped model aorta (Figure 7.35) – an expected result since the compliance of the model was reduced by wall stiffening. Ideally, measurements should be made local to where data is acquired, namely here at the UpSt and DnSt sites of measurement. Indeed, measurements for $C_{ft\text{-}ft}$ (Figure 7.34) were taken over a distance of 50mm and locally to the UpSt and DnSt sites of measurement. In the normal model aorta, $C_{ft\text{-}ft}$ at the UpSt site was 10.55m.s^{-1} for model #1 and 11.03m.s^{-1} for model #2 (Figure 7.34); these values at this position in the model are close to those measured by Segers *et al*. (1998) in their similar model at their 'location 4-5' (Figure 7 in Segers *et al*., 1998), also measured by foot-to-foot method. At the DnSt site of measurement, $C_{ft\text{-}ft}$ was found to be 21.6 m.s^{-1} for model #1 and 20.95 m.s^{-1} for model #2 (Figure 7.34). These values seemed high and it is surprising that PWV should increase this much between the UpSt and DnSt sites of measurement; it is possible that the measurements were affected by wave reflection off the aorto-iliac bifurcation. These UpSt and DnSt values for $C_{ft\text{-}ft}$ were not changed by Clingfilm wrapping of the model aorta (Figure 7.34); this is surprising since Clingfilm wrapping increased PWV measured over the length of the aorta. An explanation for the lack of effect of Clingfilm wrapping on $C_{ft\text{-}ft}$ at the UpSt and DnSt sites is that it was very difficult to maintain a tight wrapping of the Clingfilm at these sites. The reasons for this difficulty are that at the UpSt site the space between the celiac and superior mesenteric arteries is narrow and also this space accommodated the blood flow probe, thus the Clingfilm flared here and loosened; at the DnSt site, again the Clingfilm tended to loosen here. Thus, it is likely at these localities of the UpSt and DnSt sites that Clingfilm wrapping was ineffective at stiffening the aorta wall, so the local PWV, namely $C_{ft\text{-}ft}$, over 50mm remained unchanged. Wave speed, C, obtained by PU loop plots is an alternative measure of the local wave speed for the vessel (Khir *et al*., 2001; Khir and Parker, 2002; Khir *et al*., 2004; Khir and Parker 2005). Wave speeds were derived from two separate PU loop plots: C_{Tpu} was from the measured pulse pressure, and C_{Wpu} was from the

wave pressure which is obtained by subtraction of the reservoir (Windkessel) pressure from the total (or measured) pressure. Data for C_{Tpu} and C_{Wpu} are shown in Figure 7.34. Values of C_{Tpu} at the UpSt site were 20.45m.s^{-1} for model #1 and 18.15m.s^{-1} for model #2, and at the DnSt site 24.95m.s^{-1} for model #1 and 18.91m.s^{-1} for model #2; these values of C_{Tpu} at the UpSt and DnSt sites seem high in comparison to the $C_{ft\text{-}ft}$ values measured by Segers *et al*. (1998) at similar locations in their similar model aorta. C_{Tpu} was little affected by Clingfilm wrapping (Figure 7.34); the latter may have been ineffective at stiffening the aorta at the local sites of UpSt and DnSt measurements, for the reasons explained earlier in this paragraph. C_{Wpu} was the other PU loop derived wave speed (Figure 7.34). Values of C_{Wpu} at the UpSt site were 8.76m.s^{-1} for model #1 and 8.28m.s^{-1} for model #2, and at the DnSt site 13.54m.s^{-1} for model #1 and 9.70m.s^{-1} for model #2; these values are realistic for the UpSt and DnSt sites in the aorta though are lower in comparison with $C_{ft\text{-}ft}$ values as measured by Segers *et al*. (1998) in their similar model at equivalent locations. Clingfilm wrapping did not increase, if anything decreased, C_{Wpu} in model #1, but did have the expected effect of increasing C_{Wpu} in model #2. Application of distal compliances would not be expected to affect PWV or local wave speed at an upstream site, here the aorta; indeed, the distal compliances had no effect on PWV along the length of the aorta (Figure 7.35), or locally on $C_{ft\text{-}ft}$, (Figure 7.34) and had no consistent effect on C_{Tpu}, (Figure 7.34), but did appear to decrease C_{Wpu} which had been elevated by Clingfilm wrapping (Figure 7.34) – further experiments are needed to determine if this effect of distal compliances is real.

Although PWV along the length of the aorta (Figure 7.35) is not a local measurement, the values obtained, namely 12.85m.s^{-1} for model #1 and 11.63m.s^{-1} for model #2 are close to those obtained by Segers *et al*. (1998) for their measurement at 'location of 4-5'. Furthermore, PWV along the length of the aorta increased, as expected, after Clingfilm wrapping of the model aorta (Figure 7.35) to values of 15.22m.s^{-1} for #1+Cf and 15.06m.s^{-1} for #2+Cf. Given the discussion in the previous paragraph, Clingfilm wrapping might not have had the required effect of stiffening the aorta locally at the UpSt and DnSt sites. It was therefore decided that the PWV values for the length of the aorta, before and after Clingfilm wrapping, would be realistic values for wave intensity analysis (WIA).

Two separated WIA were carried out, one using wave pressure (Pw) and the other using total pressure (P_T).

Wave intensity plots from WIA using Pw are shown in Figures 7.36 and 7.37; for conciseness only the UpSt site plots are shown. The plots show the incident compression wave followed by an incident expansion wave with little reflection occurring; the incident compression wave resulted from the ejection phase while the expansion wave results from

cessation of ejection and valve closure. While Clingfilm wrapping increased compression and expansion wave energies, incident and reflected, it also changed the profile of the plots: i) for #1+Cf (Figure 7.36) the expansion wave became more of a 'spike' with an amplitude of some 4-5x that occurring before Clingfilm wrapping; ii) for #2+Cf (Figure 7.37) the amplitude of the compression wave increased some 10x, also the compression and expansion wave profile became very similar to that observed *in vivo*, furthermore the two waves became even more *in vivo*-like after application of the distal compliances which also quelled what little reflection existed after wrapping with Clingfilm (Figure 7.37). It would be useful to explore further this finding that Clingfilm wrapping causes *in vivo*-like profiles to develop for incident compression and expansion waves. Perhaps the Clingfilm coat wrapped about the model aorta has, in addition to its stiffening effect on the model aorta wall, a tethering effect that constrains the model from excessive movement and vibration which does tend to happen. The overall effects of Clingfilm wrapping on compression and expansion waves, incident or reflected, are difficult to explain. Values for WRI *in vivo* range some 2 - 10 fold greater than those observed for the model aorta (c.f. data with that in Chapters 4 and 5); thus, the low intensity of reflection in the model suggests that arterial bifurcations are well matched. It seems that Clingfilm wrapping of the model aorta does not have a remarkable effect on reflections within the model; indeed the effects are equivocal since Clingfilm wrapping either increased or decreased WRI for compression or expansion wave energies (Figures 7.39 and 7.41). With regard to the effects of distal compliances, these were quite varied making explanation of their effects difficult. A consistent effect of the distal compliances was to reduce WRI at the UpSt site while increasing WRI at the DnSt site; the WRI being for compression and expansion waves (Figures 7.39 and 7.41).

Wave intensity plots from WIA using P_T are shown in Figures 7.42 and 7.43; for conciseness only the UpSt site plots are shown. The wave intensity profiles were similar to those obtained using Pw for WIA; however, for WIA using P_T, compression wave intensity amplitudes (Figures 7.42 and 7.43) and intensity energies (Figures 7.44), for incident and reflected, were much greater than those observed from WIA using Pw; WRI for compression waves was also greater when P_T rather than Pw was used for WIA (Figure 7.45). Interestingly, incident and reflected expansion wave energies (Figure 7.46) and WRI for expansion waves (Figure 7.47) were little different between using Pw or P_T for WIA. Differences found for the compression wave intensities while no differences found for the expansion wave energies between using Pw or P_T for WIA suggests that the reservoir (Windkessel) component contributes to the compression wave energy but not to the expansion wave energy.

WIA was used for estimating distances to sites of reflection in the model aorta. In the case of WIA using Pw, reflected wave intensities were of small magnitude so careful consideration was required selecting the foot of the reflected compression wave for estimation of transit time hence distances to sites of reflection. Where reflected wave intensities were of small magnitude, care was taken to avoid reading artefact or general "noise" of the system as reflected wave intensity. This also applied to the model with distal compliances, where compression wave reflection as obtained from WIA using P_T was virtually non-existent thus making difficult the accurate measure of transit time and thus the distance to reflection site. The disparate values obtained might be indicative of incorrect choice of foot of a reflected intensity. Bifurcations are known to be sites of reflection. However, other than only one estimate, namely the distance 17cm (P_T: #2+Cf; UpSt) which was precise for the aorto-iliac bifurcation, no other distances precisely indicated sites of reflection at bifurcations; distances were either close to a bifurcation or between two bifurcations. An ambiguous distance, i.e. a distance to a site mid-way between two bifurcations, might indicate a mean of reflections from bifurcations and vessel tapering. Use of either Pw or P_T for WIA showed neither to be best for accurate measurement of distance to sites of reflection.

Objective Outcomes:

- *Objective*: To ascertain that decreased compliance of the model aorta increases wave speed and increases pressure pulse amplitude by increasing systolic pressure while decreasing diastolic pressure, and also increases reservoir (Windkessel) pressure increases.

  Outcome: PWV over the length of the model aorta was increased in the Clingfilm wrapped aorta model, i.e. a model of decreased aortic compliance. The more local measures of wave speed, at the UpSt and DnSt sites in the abdominal aorta section of the model, were not convincingly altered by Clingfilm wrapping but this is believed to be due to the Clingfilm becoming loosely wrapped at these sites. Pulse amplitude was increased in the Clingfilm wrapped model aorta, the amplitude being increased by increased systolic pressure and decreased diastolic pressure; furthermore, reservoir (Windkessel) pressure was found to increase after Clingfilm wrapping.

  Conclusion: Decreased compliance of the aorta model increases wave speed, but this was only conclusively found with PWV along the length of the model aorta. Pulse pressure and reservoir (Windkessel) pressure were also increased in the model aorta of decreased compliance.

- *Objective*: To ascertain that decreased compliance of the model aorta increases wave reflection in the model.

  Outcome: Wave reflection was not remarkable in the normal model aorta when Pw was used for WIA, though wave reflection energy was greater when P_T was used for WIA. However, there was no conclusive evidence from WRI values that wave reflections increased in the model after Clingfilm wrapping – data were equivocal.

The Hypotheses – supported or not supported:

- *Hypothesis*: Decreased compliance of the model aorta increases RHDN

  Findings: RHDN was not increased by Clingfilm wrapping, if anything, it was either unchanged or decreased.

  Support: The hypothesis that RHDN is increased in the model aorta of decreased compliance is not supported.

- *Hypothesis*: Application of distal compliances attenuates the effects of decreased compliance of the model aorta.

  Findings: Application of distal compliances attenuated the increased pulse pressure amplitude by decreasing the previously raised systolic pressure and increasing the previously reduced diastolic pressure. Furthermore, application of distal compliances decreased the previously increased reservoir (Windkessel) pressure. Although decreased compliance did not increase RHDN, the latter whatever its value after Clingfilm wrapping, was decreased by the application of distal compliances. Wave reflection was little affected by distal compliances as indicated by WRI when Pw was used for WIA, however distal compliances had marked effect in reducing wave reflection as indicated by WRI when P_T was used for WIA.

  Support: The data support the hypothesis that distal compliances attenuate the effects of decreased compliance of the model aorta.

Limitations of Experiment are discussed in Chapter 8.

CHAPTER 8

FINAL DISCUSSION:

LIMITATIONS OF EXPERIMENTS
COMMENTS:
RETROSPECTIVE & PROSPECTIVE

CONCLUSIONS

This chapter discusses the limitations of experiments, how the quality of data might have been affected by technical issues, and comments on ways in which these technical issues could be overcome. A number of conclusions are then drawn.

Waveform Analysis

For this thesis blood pressure and flow waveforms were studied in the abdominal aorta of rabbits (Chapters 4 & 5) and in the abdominal aorta section of a polyurethane model of a human aorta (Chapter 7). For studies of this kind the ascending aorta is often used. However, the aim of this thesis was to determine what relationship, if any, abdominal aortic blood pressure and flow wave phenomena might have with blood pressure and flow waveforms in distal arteries, here in the central ear, or auricular, artery of rabbits. Thus, as stated in Chapter 2, consideration must be given to the applicability and suitability of use of the calculation and Matlab algorithm used to analyse blood pressure waveforms in the abdominal aorta. The analysis involved deriving reservoir (Windkessel) pressure (Pwk or RP) from the measured (Total) pressure (P_T) then subtracting the former from the latter to obtain wave pressure (Pw). This analysis was proposed by Aguado-Sierra *et al*. (2008) who extended the concept put forward by Wang *et al*. (2003); the latter based their concept on the relationships of blood pressure and flow in the central, i.e. the ascending, aorta whereas Aguado-Sierra *et al*. (2008) extended the theory to measurements at an arbitrary location in (large) arteries, and in the aorta, at sites distal to the ascending aorta. Aguado-Sierra *et al*. (2008) based their proposal on two observations which are stated briefly in Chapter 2 but

were not tested in this thesis. However, on the strength of the proposals made by Aguado-Sierra *et al*. (2008) the calculation was applied, as a tool, for analysis of blood pressure waveforms in the abdominal aorta of rabbits and pressure waveforms in the abdominal aorta section of the polyurethane model of the human aorta. Thus, data has been obtained and accepted although potential errors might arise from use of the calculation and algorithm at the level of the abdominal aorta. Despite potential errors, in the case for the *in vivo* experiments with rabbits, wave pressure (Pw) was used for wave intensity analysis (WIA), while in the case for experiments with the model aorta, both Pw and measured (Total) pressure (P_T) were used for WIA. This is commented on below (see under *Aorta Model Circulation*).

Anaesthesia, Posture and Surgery

In vivo haemodynamic data were obtained from anaesthetised rabbits in a supine position; this set-up would likely affect blood flow and vascular status. There are many anaesthetic agents to choose from and these have their various effects on the cardiovascular system and its function; a barbiturate anaesthetic was used for these experiments, such anaesthetics are thought to enhance sympathetic tone (Page and McCubbin, 1965; Lokhandwala *et al*., 1973) and thus could have confounding effects on cardiovascular function making difficulties for interpreting data. Body core temperature is also affected owing to lack of muscular activity and anaesthetic effect, and the absence of limb vascular activity may affect venous return.

It is suggested that the pressure pulse waveform of the central ear artery might have been affected by the anaesthetic chosen, namely sodium pentobarbitone, since the waveform was very different to that observed by Nier and Weinberg (unpublished data) who applied a different anaesthetic regimen (Hypnorm and Hypnovel) and obtained pulse waveforms very similar to those they observed in unanaesthetised rabbits (Weinberg *et al*., 2001; Nier and Weinberg, 2007; Nier *et al*., 2008); however, in other experiments (general observation) the Hypnorm with Hypnovel regimen resulted in rabbits having low blood pressure, diastolic blood pressure of ~40mmHg (~5.33kPa). Avolio *et al*. (1976) used sodium pentobarbitone to anaesthetise rabbits of their experiments and recorded mean blood pressures of 60-124mmHg; Katsuda *et al*. (2004) for their experiments, anaesthetised rabbits using sodium pentobarbitone and recorded diastolic blood pressures of 90-100mmHg. We therefore expected that barbiturate anaesthesia would result in rabbits having a diastolic blood pressure of ~70mmHg (~9.33kPa), but this was often not observed. Instead, diastolic pressures were observed to range between 55-65 mmHg (7.33-8.67kPa). Furthermore, it was found that if blood pressures rose to desired levels it often was associated with

anaesthesia wearing off, thus anaesthetic top-up was obligatory. For future studies other general anaesthetic regimens should be explored for improved blood pressure maintenance.

Care was taken to minimise blood loss. Nevertheless, the lower than expected blood pressures in these experiments may have been caused by trauma due to the invasive surgical procedure affecting haemodynamic status, perhaps even reducing cardiac output, although this was not measured. Avolio *et al*. (1976) subjected rabbits to thoracotomy which might explain why some of their rabbits had low blood pressures; the only surgical procedure used by Katsuda *et al*. (2004) was cannulation of a carotid and a femoral artery, thus minimally invasive surgery resulting in good maintenance of arterial blood pressure. In the experiments of this thesis, laparotomy was used to gain access to the abdominal cavity. Laparotomy is a major procedure and in these experiments was extensive with displacement of intestinal viscera and attachment of blood flow probes to the aorta at two sites, though, after attachment of the blood flow probes the intestinal viscera were returned to the peritoneal cavity and the abdomen partially closed by clamps.

A way to avoid access by laparotomy and just have the dissection to a femoral artery would be to use a catheter that measures pressure and blood velocity together; such a catheter is the Volcano ComboWire. Measurement of arterial pressure with this system was not difficult; however great difficulty was experienced in achieving good velocity waveforms from which useable data could be obtained. Because of those difficulties, the Volcano ComboWire system was abandoned for the invasive procedure to use Transonic blood flow probes. The ComboWire system would be worth pursuing and perfecting the technique. However, the ComboWire has only one pressure sensor which negates measurement of PWV between two sensors at a known and set distance apart – this was the convenience of using the dual pressure sensing Millar catheter. Perhaps a bespoke ComboWire catheter could be made facilitating dual pressure measurement, although this would be expensive, or a second wire could be joined to the ComboWire catheter.

An ambitious approach to having the animal in a natural state for haemodynamic readings, avoiding anaesthesia and surgical trauma would be to use instrumented animals with implanted blood flow probes and an internal catheter system for monitoring blood pressure read by telemetry; thus surgery under general anaesthesia would apply for implanting the measuring devices but the experiments for haemodynamic data be applied when the animal had recovered from surgery and was unanaesthetised, some 14 days onwards post-operation. On the other hand, if the ComboWire system were to be used for blood pressure and velocity, rather than blood volume flow or PWV by a dual sensor catheter, in unanaesthetised rabbits then the aorta could be accessed by use of a carotid skin-loop

preparation; this is a published technique for measurement of blood pressure in dogs, cats and rabbits (Geddes, 1970; O'Brien *et al*., 1971; Hunt *et al*., 1997).

Measurement of Arterial Diameter

An apparatus that would have been useful but was not available is that for sonomicrometry. This would have allowed measurement of abdominal aortic diameter simultaneously with pressure measurement and blood flow, rather than performing those separate experiments with the Ultrasonix system (Chapter 4). Sonomicrometry used in this way would enable derivation of local aortic distensibility from the pressure-diameter plot (Bertram, 1977; Patel and Vaishnav, 1980); if a ComboWire velocity sensor was used then local wave speed could also be obtained from plots of lnDU-Loop method (Feng and Khir, 2010).

Applanation Tonometry

Although, in some experiments, good pulse waveforms were obtained from the rabbit central ear artery by applanation tonometry, many waveforms were of disappointing fidelity if not impossible to obtain. This technique needs much improvement so that reproducible and repeatable data can be obtained. In some experiments good waveforms were recorded at the start then for no obvious reason the waveforms deteriorated or even disappeared – since this occurred during a study, one did not wish to adjust the tonometer for fear of disturbing the entire experiment. The central ear artery, being peripheral and immediately sub-dermal, might be sensitive to external temperature or sensitive to body core temperature, thus if the animal is below its natural core temperature then the artery perhaps decreases its diameter; this may have happened on the occasions when poor or no pulse wave form could be recorded, despite care being taken to maintain the animal's body temperature. Raising room temperature might assist with this problem. Rabbits were on temperature controlled heating mats and wrapped in towels.

Waveform Types and the Fitting of Reservoir (Windkessel) Pressure Curves

Another aspect that requires improvement is understanding the origins of the two blood pressure waveform types, Type 1 and Type 2. The reason for these different waveforms was not clear; there did appear to be some relation to MAP, but not consistently. The physiological mechanism of autoregulation might have in part been responsible for the waveform shapes of Type 1 and Type 2. Autoregulation very likely was active to maintain constant blood flows through many parts of the circulation in those anaesthetised rabbits with low blood pressures – the cranial (brain), cardiac, renal and skeletal muscle circulations

are well known for their ability to autoregulate. Autoregulation maintains a constant blood flow through tissues by altering the bed vascular resistances despite, though within a range of, ongoing systemic blood pressure. This autoregulation of vascular resistances might impact on blood pressure waveforms. As has been pointed out (Chapter 4) the blood pressure waveform is important for algorithm fitting to obtain reservoir (Windkessel) pressure, wave pressure, estimate of P_∞ and calculated arterial compliance from the diastolic decay time constant, τ. Algorithm fitting appeared good with Type 1 pressure pulse waveforms but poor fitting with Type 2. In the case of the latter, derived data that appeared spurious were not used. Thus, further investigation is required into the application of the Windkessel Subtraction algorithm to pulse waves of the rabbit, certainly the Type 2 waveforms. The algorithm appears to work for dog and human ascending aortic blood pressure waveforms (Wang *et al*., 2003; Davies *et al*., 2007; Aguado-Sierra *et al*., 2008; Parker *et al*., 2011) but these have clear quasi-exponential decays, somewhat similar in form to the Type 1 waveforms observed in the rabbits. Indeed, Aguado-Sierra *et al*. (2008) do show an example of a waveform similar in shape to a Type 2 of rabbit (RHS of Fig.1 in Aguado-Sierra *et al*., 2008) – the diastolic decay of the reservoir pressure does not fit the diastolic decay of the measured waveform and the explanation for the disparity is the existence of reflected waves at that site of the aorta. However, Type 2 waveforms of the rabbit did not appear to be associated with any reflected wave intensity which would be expected to occur between 125-225ms of the waveform exemplified in Figure 4.24 – under L-NAME. Aguado-Sierra *et al*. (2008) and Parker *et al*. (2011) comment that the algorithm becomes less accurate when applied to measurements at sites much distal to the ascending aorta because of reflections, and furthermore the algorithm holds better at low heart rates – it seems that the point made about reflections is not obvious from WIA in rabbits in the studies of this thesis but the point made about heart rate might apply to anaesthetised rabbits, since heart rates were 240-300beats.min^{-1}.

Heart rate is important for the application of the algorithm since at high heart rates the algorithm does not satisfactorily identify exponential decays during short diastolic periods thus making estimates of parameter B and P_∞ unreliable (Parker *et al*., 2011). In the experiments of Chapter 4, the estimates for P_∞ are high as they are close to diastolic pressure (Figure 4.35) rather than what would be expected for mean circulatory filling pressure (6-10mmHg = 0.8-1.33kPa); though not plotted, the same applies to data in Chapter 5 (data in Table 5.1 for DBP and Table 5.3 for P_∞). However, it must also be considered that values obtained for P_∞ might be correct, certainly if P_∞ is *the*, if not closely

related to, critical closing pressure; control values for the latter in the hindlimb of anaesthetised dogs have been reported as ~40mmHg (5333Pa) - ~50mmHg (6667Pa) (Shrier *et al*., 1993) – such values are close to DBP values measured in some rabbits of experiments in this thesis – discussed in section 4.4 with Figure 4.35.

With further regard to waveform Types 1 and 2, another observation, though not quantified and not discussed in Chapters 4 and 5, was that of the pulse amplitudes of wave pressure, Pw, in relation to pulse amplitudes of the reservoir (Windkessel) pressure, P_{Wk} (or RP). Examples of these are:

- Pulse amplitude for Pw ≈ P_{Wk}: Figure 4.16 A
- Pulse amplitude for Pw < P_{Wk}: Figures 4.16 B; 4.17 C; 4.18 bottom panel; 5.1 A
- Pulse amplitude for Pw > P_{Wk}: Figures 4.16 C; 4.17 A&B; 4.18 top & middle panels; 5.1 B

Pulse amplitudes for Pw ≈ P_{Wk} and Pw < P_{Wk} appear to occur with curve fitting to Type 1 pressure waveforms, whereas pulse amplitudes for Pw > P_{Wk} appear to occur with curve fitting to Type 2 pressure waveforms. From a limited review of the literature, it appears that amplitudes that are *almost* equal, namely Pw ≈ P_{Wk} (Figure 1 in Wang *et al*., 2011) and amplitudes for Pw < P_{Wk} (Figure 1 in Wang *et al*., 2003; Figure 1-left in Aguado-Sierra *et al*., 2008; Figure 1 in Davies *et al*., 2010) occur in the aortic root or arch. In other studies, where Pw has been separated into its forward and backward components, summation of those components imply amplitudes for Pw ≈ P_{Wk} in the proximal aorta (Figure 1 in Davies *et al*., 2007; or Figure 2 in Davies *et al*., 2010) and in the distal thoracic aorta at the diaphragm (Figure 4 in Wang *et al*., 2011). For those cases, in the aorta from its root and into the thoracic aorta, the pressure waveforms tend to be Type 1-like and appear associated with amplitudes for Pw ≈ P_{Wk} and Pw < P_{Wk}. On the other hand, an amplitude for Pw > P_{Wk} has been shown in the abdominal aorta (Figure 2 in Aguado-Sierra *et al*., 2008) and this is from curve fitting to a Type 2-like waveform; though an exception to this appears in Figure 1-right in Aguado-Sierra *et al*. (2008) where fitting to a Type 2-like waveform in the thoracic aorta gave an amplitude for Pw just a little less than that of P_{Wk} i.e. Pw < P_{Wk}.

Thus, improved understanding of the causes of the two blood pressure waveform types, Type 1 and Type 2, would help reliable waveform analysis.

Measurement of PWV

Pulse wave velocity was an important measure in this thesis; it is a measure of regional wave speed in a vessel, here the abdominal aorta. Techniques for measurement of PWV are debated; several techniques are used and are outlined in Chapter 3. Katsuda *et al*. (2004) in experiments with anaesthetised rabbits measured local pulse wave velocities over the same segments of abdominal aorta as were measured in the experiments of this thesis (see Katsuda *et al*., 2004 - Fig. 1 & Fig.3, P3 – P6); they measured PWV by a foot-to-foot method with upstream and downstream pulses, marking the time at the first peak of the second derivative of the pulse as the foot since it coincided with the systolic rising point of the pressure wave. Their values of PWV along the abdominal aorta ranged between 5.8-7.2 $m.s^{-1}$ which are a little higher but close to the values for PWV found in this thesis; the likely reason their values were a little higher was their rabbits having higher blood pressures than those in this thesis. Thus, at the same regions of the abdominal aorta of rabbits, the foot-to-foot method of measurement used by Katsuda *et al*. (2004) resulted in values very similar to those obtained in this thesis using a different method of foot-to-foot measurement (Chapter 3). We conclude that the values of PWV ($C_{ft\text{-}ft}$) obtained in this thesis can be accepted as reliable.

Local wave speeds for the abdominal aorta were obtained by PU-loop plots (Chapter 2); these were plotted using measured abdominal aortic blood flow velocity, U, against abdominal aortic Pw or P_T. Theoretically, local wave speed using Pw or P_T and regional wave speed, namely PWV as $C_{ft\text{-}ft}$ over a short distance, should all have values close to each other in a reflection-free system in large arteries. Thus the null hypothesis proposed was that $C_{ft\text{-}ft} = C_{Tpu} = C_{Wpu}$. The null hypothesis was either not consistently found (Tables 4.14 & 4.15) or was consistently found (Table 5.8 & 5.9; Figure 5.18) in the *in vivo* experiments with rabbits and was not convincingly demonstrated in experiments with the Model Aorta (Figure 7.34); though in the latter there was some evidence of near agreement between $C_{ft\text{-}ft}$ and C_{Wpu} at the UpSt site of measurement and near agreement between $C_{ft\text{-}ft}$ and C_{Tpu} at the DnSt site. Values of C_{Tpu} and C_{Wpu} are dependent on the linearity in early systole of PU loops and the linearity is dependent on the accuracy of timing and “lining up” of the initiation of systole for U with Pw or P_T. PU loops with Pw are further dependent on the validity of Pw as obtained from reservoir (Windkessel) subtraction; the latter is discussed above under *Waveform Analysis* and below under *Aorta Model Circulation*.

Infusion of Drugs

The studies discussed in Chapter 4 used doses of Ach and L-NAME taken from Nier *et al*. (2008) and were intended not to have marked effects on the mean level of blood pressure but to have significant but submaximal effects on the pressure waveform; mean blood pressure affects the pressure waveform, and the experimental requirement was to investigate the direct effects of nitric oxide bioactivity on blood pressure and velocity waveforms. However, the doses of Ach and L-NAME used did affect blood pressure, markedly in some cases. Improvements for future experiments would be to conduct preliminary ones to establish dose-effect and then choose the doses with required effect; furthermore, protocols could be designed to included controls for effect of increasing or decreasing blood pressure on waveforms, by using a pressor agent such as phenylephrine (α_1-adrenoceptor agonist) or a vasodilator that does not work through nitric oxide, e.g. hydralazine.

Induction of AGEs

The experiments of Chapter 5, with fructose supplement to diet did not reveal any marked haemodynamic differences between fructose-treated and control rabbits. For future experiments, haemodynamic differences from controls might be achieved with a longer treatment schedule with fructose. Measurement by assay of AGEs in aortic and arterial walls would be a useful addition to experiments. An interesting experimental technique for studying the effects of AGEs is that of Vlassara *et al*. (1995) who used a protocol of 4months of daily *intravenous* administration of AGE-modified rabbit serum to rabbits; this is a direct way, rather than by fructose diet, of imposing AGE deposition into arterial structures.

In Chapter 5, haemodynamic differences were noted, especially regarding aortic wave reflections, between immature and mature rabbits; the former had markedly less reflections than the latter indicating that immature rabbits have an arterial system of well matched impedances for incident forward going waves traversing bifurcations and propagating along arteries of different wall composition and geometries. This is relevant to the research of Barnes and Weinberg (1998), Staughton *et al*. (2001) and Weinberg (2002, 2004) who observe changes in patterns of atherosclerotic lesion development between immature and mature rabbits. A long term study could be of following haemodynamic changes through the stages of rabbit life:

$$\text{Immature} \longrightarrow \text{mature} \longrightarrow \text{senescent}$$

Human ageing is associated often with isolated systolic hypertension (ISH). Animal models for this condition include those of inducing AGE formation - already discussed, and others such as a rat model of aortic stiffening by calcification (Niederhoffer *et al*., 1997; Atkinson, 1999; Kieffer *et al*., 2000; Marque *et a*l., 2001) and a mouse model (CF1-CRP mouse) that expresses elevated circulating levels of C-reactive protein associated with elevated systolic blood pressure (Vongpatanasin *et al*., 2007).

Aorta Model Circulation

Comment has been made above (see under *Waveform Analysis*) on the use of the calculation for subtraction of Pwk from P_T to obtain Pw and possible errors for use of this at the level of the abdominal aorta. However, in the case of experiments with the polyurethane model aorta, two wave intensity analyses (WIA) were carried out, one using P_W which was obtained by the calculation proposed by Aguado-Sierra *et al*. (2008), and the other using P_T so not requiring the calculation and acceptance of the two observations yet untested. Interestingly, WIA by either Pw or P_T did not result in any remarkable differences, other than with P_T when larger magnitudes than with Pw resulted for incident and reflected compression wave intensity and increased WRI for compression wave intensity (Chapter 7).

An attempt to simulate aortic stiffening with the model aorta is described in Chapter 7. The model aorta was constructed from a chosen polyurethane material (Chapter 6). Aortic stiffening was simulated by wrapping the aorta and iliac arteries in Clingfilm. This resulted in haemodynamic features, e.g. increased pressure pulse, resembling vascular ageing and ISH. However, local PWV values were not reliable and this was likely due to slippage and loss of grip of the Clingfilm wrap. For future experiments, a way of improved Clingfilm wrapping should be achieved or another method of stiffening could be tried – perhaps a close-fitting elasticated net material. It was interesting that Clingfilm wrapping in one of the two studies converted the pressure pulse waveform to one similar as observed *in vivo*. It would be useful for future simulations to establish how that was achieved and so reproduce for repeated experiments.

The pressure-volume and compliance curves of the model aorta (Figure 7.19 – normal aorta model) are not typical of a true aorta made up of elastin and collagen, along with other wall components, to form an elastic tube of heterogeneous composition and anisotropic elasticity. In the case of the true aorta, the pressure-volume curve gradually plateaus with little further change in volume for further increases in pressure, the compliance *decreases* as pressure increases. This was not the case with the polyurethane model aorta where there was no plateau in the pressure-volume curve and compliance *increased* with pressure.

Interestingly, Desai *et al*. (2011) have a polyurethane material that demonstrates pressure-compliance properties similar to porcine aorta, i.e. real aorta, where compliance decreases with increasing pressure; a future model aorta of this polyurethane might be useful to model aortic haemodynamics more realistically.

Measurements of Distances to Reflection Sites

Estimates, from WIA plots, of distances to reflection sites from sites of measurement in the abdominal aorta, *in vivo* (rabbits) or *in vitro* (model aorta), did not give clearly precise locations of reflection sites. This might be due to errors arising from the calculation used for subtraction of reservoir (Windkessel) pressure (see above under *Waveform Analysis*) but also, as pointed out in Chapter 2, errors might arise from incorrect reading of the WIA plot. Choice of the foot of incident compression energy and foot of reflected incident energy must be made with careful judgement to avoid what might be artefact (i.e. "noise" of the system) near to a foot and so must not be accepted as part of the compression wave intensity. Accurate estimates of sites of reflection might be achieved by use of a more sophisticated procedure than was used in this thesis. Such a procedure to adopt could be that of Wang *et al*. (2011) whereby several sites of pressure and flow measurement are made along the aorta; use of reservoir (Windkessel) pressure subtraction to obtain wave pressure, and use of WIA, allows resolution of measured pressure waveforms into their incident and reflected wave parts – the feet of the former and latter waves are plotted as time (ECG as a fiducial reference) vs. distance along the aorta, this plot is then used to estimate the location of reflection sites.

Conclusions

1. Haemodynamic changes in response to treatment with Ach and L-NAME were observed in rabbits; these changes were apparent as alterations in pressure pulse waveform; Ach increased whereas L-NAME decreased wave reflection. However, a mechanism was not found to explain the effects of Ach and L-NAME on RHDN in the central ear artery observed by Weinberg et al. (2001).
2. Fructose diet did not have any measurable effects on haemodynamics of immature or mature rabbits.
3. Immature rabbits exhibited less aortic wave reflection than did mature rabbits.
4. Experiments with anaesthetised rabbits could be improved using techniques with less surgical trauma and an anaesthetic regimen that enables good maintenance of

arterial blood pressure. An ambitious approach would be to use non-anaesthetised animals previously instrumented surgically under anaesthesia.

5. The algorithm for subtraction of reservoir pressure should be used with caution when applied to blood pressure waveforms of rabbits, especially when measurements are obtained at the level of the abdominal aorta where changes in waveform can occur during diastole. Furthermore, heart rate must be considered for performance of the algorithm.
6. The polyurethane model aorta has potential for simple modelling of haemodynamic function in health and hypertensive disease.

REFERENCES

Aguado-Sierra J, Alastruey-Arimon J, and Parker KH (2008). Separation of the Reservoir and Wave Pressure and Velocity from Measurements at an Arbitrary Location in Arteries. J. Eng. Med. (Proc. Inst. Mech. Eng., Part H), **222**: 403-416.

Akira K, Amano M, Okajima F, Hashimoto T, and Oikawa S. (2006). Inhibitory Effects of Amlodipine and Fluvastatin on the Deposition of Advanced Glycation End Products in Aortic Wall of Cholesterol and Fructose-Fed Rabbits. Biol. Pharm. Bull. **29**(1): 75-81.

Alam MG, and Barri YM. (2003). Systolic Blood Pressure is the Main Etiology for Poorly Controlled Hypertension. Am. J. Hypertens., **16**: 140-143.

Alastruey J (2006). Numerical modelling of pulse wave propagation in the cardiovascular system: development, validation and clinical applications. PhD thesis, Imperial College London, University of London.

Alastruey J, Parker KH, Peiró J, Sherwin SJ. (2009). Lumped Parameter Outflow Models for 1-D Blood Flow Simulations: Effect of Pulse Waves and Parameter Estimation. Commun. Comput. Phys., **4**(2): 317-336.

Alastruey J, Nagel SR, Nier BA, Hunt AAE, Weinberg PD, Peiro J. (2009). Modelling pulse wave propagation in the rabbit systemic circulation to assess the effects of altered nitric oxide synthesis. J. Biomech., **42**: 2116-2123.

Alastruey J, Parker KH, Peiró J, Sherwin SJ. (2009). Analysing the Pattern of Pulse Waves in Arterial Networks: A Time-Domain Study. J. Eng. Math., **64**: 331-351.

Arts T, Kruger RTI, van Gerven W, Lambregts JAC and Reneman RS. (1979). Propagation Velocity and Reflection of Pressure Waves in the Canine Coronary Artery. Am. J. Physiol., **237**(4) (Heart Circ. Physiol., **6**(4)): H469-H474.

Asif M, Egan J, Vasan S, Jyothirmayi GN, Masurekar M, Lopez S, Williams C, Torres RL, Wagle D, Ulrich P, Cerami A, Brines M. (2000). An Advanced Glycation Endproduct Cross-link Breaker can Reverse Age-related Increases in Myocardial Stiffness. Proc. Natl. Acad. Sci. USA., **97**(6): 2809-2813.

Asmar R, Benetos A, Topouchian J, Laurent P, Pannier B, Brisac A-M, Target R, Levy BI. (1995). Assessment of Arterial Distensibility by Automatic Pulse Wave Velocity Measurement: Validation and clinical Application Studies. Hypertension, **26**: 485-490.

Asmar R, Rudnichi A, Blacher J, London GM, and Safar M. (2001). Pulse Pressure and Aortic Pulse Wave are Markers of Cardiovascular Risk in Hypertensive Populations. Am. J. Hypertens., **14**: 91 – 97.

Atkinson J. (1999). Arterial Calcification. Mechanisms, consequences and animal models. Path Biol., **47**(7): 677-684.

Avolio AP, Chen S-G, Wang R-P, Zhang C-L, Li M-F, and O'Rourke MF (1983). Effects of aging on changing arterial compliance and left ventricular load in a northern Chineses urban community. Circ., **68** (1): 50-58.

Avolio AP, Deng Fa-Quan, Li Wei-Qiang, Luo Yao-Fei, Huang Zhen-Dong, Xing Lian-Fen, and O'Rourke, M.F. (1985). Effects of aging on arterial distensibility in populations with high and low prevalence of hypertension: comparison between urban and rural communities in China. Circ., **71** (2): 202-210.

Avolio AP, O'Rourke MF, Mang K, Bason PT, and Gow BS. (1976). A comparative study of pulsatile arterial hemodynamics in rabbits and guinea pigs. Am. J. Physiol., **230**(4): 868-875.

Babalis D, Levy B, Azancot I, Georgiopoulos G, Beaufils Ph and Slama R. (1982). Action de la nitroglycérine et de la N. éthoxycarbonyl-3-morpholinosydnonimine sur les parois de gros troncs artériels. Arch. Mal. Coeur, 75^{e} année, n^{o} 6: 677-686.

Bakris GL, Bank AJ, Kass DA, Neutel JM, Preston RA, and Oparil S. (2004). Advanced Glycation End-Product Cross-Link Breakers. Am. J. Hypertens., **17**: 23S-30S.

Baksi AJ, Treibel TA, Davies JE, Hadjiloizou N, Foale RA, Parker KH, Francis DP, Mayet J, Hughes AD. (2009). A Meta-Analysis of the Mechanism of Blood Pressure Change With Aging. J. Am. Coll. Cardiol., **54**(22): 2087-2092.

Barnard ACL, Hunt WA, Timlake WP, and Varley E. (1966a). A Theory of Fluid Flow in Compliant Tubes. Biophysical Journal, **6**: 717-724.

Barnard ACL, Hunt WA, Timlake WP, and Varley E. (1966b). Peaking of the Pressure Pulse in Fluid-Filled Tubes of Spatially Varying Compliance. Biophysical Journal, **6**: 735-746.

Barnes SE, and Weinberg PD. (1998). Contrasting Patterns of Spontaneous Aortic Disease in Young and Old Rabbits. Arterioscler. Thromb. Vasc. Biol., **18**: 300-308.

Baron AD. (1996). Insulin and the Vasculature – Old Actors, New Roles. J. Investig. Med., **44**(8): 406-412.

Baron AD. (1999). Vascular Reactivity. Am. J. Cardiol., **84**(1A): 25J-27J.

Baron AD. (2002). Insulin Resistance and Vascular Function. J. Diabetes Complications, **16**(1): 92-102.

Barva M, Kybic J, Mari J-M, and Cachard C. (2004). Radial Radon transform dedicated to micro-object localization from radio frequency ultrasound signal. Pages 1836–1839, in Proceedings of the IEEE Symposium on Ultrasonics, Ferroelectrics and Frequency Control (Editor Marjorie Passini Yuhas), IEEE, New York, USA, August 2004.

Bembridge J. (2007). Of Ranier Technologies Ltd.; personal communication.

Benetos A, Safar M, Rudnichi A, Smulyan H, Richard J-L, Ducimetière and Guize L (1997). Pulse Pressure. A Predictor of Long-term Cardiovascular Mortality in a French Male Population. Hypertension, **30**: 1410-1415

Bergel DH. (1960). The Visco-elastic Properties of the Arterial Wall. Ph.D. Thesis, University of London.

Bergel DH. (1961). The Static Elastic Properties of the Arterial Wall. J. Physiol., **156**: 445-457.

Bergel DH, and Schultz DL. (1972). Arterial Elasticity and Fluid Dynamics. Progress in Biophysics and Molecular Biology, **22**: 3-36.

Bertram CD. (1977). Ultrasonic Transit-time System for Arterial Diameter Measurement. Med. Biol. Eng. Comput., **15**: 489-499.

Bierhaus A, Hofmann MA, Ziegler R, Nawroth PP. (1998). AGEs and their interaction with AGE-receptors in vascular disease and diabetes mellitus. I. The AGE concept. Cardiovasc. Res., **37**: 586 – 600.

Blacher J, Asmar R, Djane S, London GM, Safar ME. (1999). Aortic Pulse wave Velocity as a Marker of Cardiovascular Risk in Hypertensive Patients. Hypertension, **33**: 1111-1117.

Bleasdale RA, Parker KH, and Jones CJH. (2003). Chasing the wave. Unfashionable but important new concepts in arterial wave travel. Am. J. Physiol. Heart Circ. Physiol., **284**: 1879-1885

Borhani NO, Applegate WB, Cutler JA, Davis BR, Furberg CD, Lakatos E, Page L, Perry HM, Smith WM, and Probstfield JL (1991) Part I: Rationale and Design. Systolic Hypertension in the Elderly Program (SHEP). Hypertension, **17** (3): II-2 – II-15.

Bortolotto LA, Hanon O, Franconi G, Boutouyrie P, Legrain S, and Girerd X. (1999). The Aging Process Modifies the Distensibility of Elastic but not Muscular Arteries. Hypertension, **34** [part 2]: 889-892.

Boutouyrie P, Laurent S, Benetos A, Girerd XJ, Hoeks APG, and Safar ME. (1992). Opposing effects of ageing on distal and proximal large arteries in hypertensives. J. Hypertens., **10** (suppl.6): S87 – S91.

Bramwell JC, and Hill AC. (1922). The Velocity of the Pulse Wave in Man. Proc. Roy. Soc., ser. B, 93: 298-306.

Brownlee M, Cerami A, and Vlassara H. (1988). Advanced Glycosylation End Products in Tissue and the Biochemical Basis of Diabetic Complications. NEJM., **318**(20):1315-1321.

Brownlee M, Vlassara H, Kooney A, Ulrich P, and Cerami A. (1986). Aminoguanidine Prevents Diabetes-induced Arterial Wall Protein Cross-linking. Science, **232**(4758): 1629-1632.

Brüel A, and Oxlund H. (1996). Changes in biomechanical properties, composition of collagen and elastin, and advanced glycation endproducts of the rat aorta in relation to age. Atherosclerosis, **127**: 155-165.

Bucala R, Tracey KJ, Cerami A. (1991). Advanced Glycosylation Products Quench Nitric Oxide and Mediate Defective Endothelial-dependent Vasodilatation in Experimental Diabetes. J.Clin. Invest., **87**:432-438.

Caro CG, Pedley TJ, Schroter RC, and Seed RC. (1978 1st Edn.; 2011 2nd Edn.). The Mechanics of the Circulation. 1st Edn. Oxford University Press; 2nd Edn. Cambridge University Press.

Celermajer DS. (1997). Endothelial Dysfunction: Does it Matter? Is it Reversible? J. Am. Coll. Cardiol., **30**: 325-333

Chang K-C, Liang J-T, Tseng C-D, Wu E-T, Hsu K-L, Wu M-S, Lin Y-T, and Tseng Y-Z. (2007). Aminoguanidine Prevents Fructose-Induced Deterioration in Left Ventricular-Arterial Coupling in Wistar Rats. Brit. J. Pharmacol., **151**: 341-346.

Chaudhry SI, Krumholz HM, and Foody JM (2004). Systolic Hypertension in Older Persons. JAMA, **292**: 1074 – 1080.

Choate, J. (1998). Does Nitric Oxide Modulate Cardiac Function? *The Bulletin*, The Journal of The British Society for Cardiovascular Research, **11**(1):4-8.

Chowienczyk PJ, Kelly RP, MacCallumH, Millasseau SC, Andersson TLG, Gosling RG, Ritter JM, and Änggård EE. (1999). Photoplethysmographic Assessment of Pulse Wave Reflection: Blunted Response to Endothelium-Dependent $Beta_2$-Adrenergic Vasodilation in Type II Diabetes Mellitus. J. Am. Coll. Cardiol., **34**(7): 2007-2014.

Cohn JN, Finkelstein S, McVeigh G, Morgan D, LeMay L, Robinson J, and Mock J. (1995). Noninvasive Pulse wave Analysis for the Early Detection of Vascular Disease. Hypertension, **26**:503-508.

Corman B, Duriez M, Poitevin P, Heudes D, Bruneval P, Tedgui A, and Levy BI. (1998). Aminoguanidine prevents age-related arterial stiffening and cardiac hypertrophy. Proc. Natl. Acad. Sci. USA., **95**: 1301-1306.

Cruickshank K, Riste L, Anderson SG, Wright JS, Dunn G, Gosling RG. (2002). Aortic Pulse-Wave Velocity and its Relation to Mortality in Diabetes and Glucose Intolerance. An Integrated Index of Vascular Function? Circulation, **106**:2085-2090.

Curtis SL, Zambanini A, Mayet J, Thom S A McG, Foale R, Parker KH, and Hughes AD. (2007). Reduced Systolic Wave Generation and Increased Peripheral Wave Reflection in Chronic Heart Failure. Am. J. Physiol. Heart Circ. Physiol., **293**: H557-H562.

Dai S, and McNeill JH. (1995). Fructose-Induced Hypertension in Rats is Concentration- and Duration- Dependent. J. Pharmacological and Toxicological Methods, **33**: 101-107.

Davies JE, Hadjiloizou N, Leibovich D, Malaweera A, Alastruey-Arimon J, Whinnett ZI, Manisty CH, Francis DP, Aguado-Sierra J, Foale RA, Malik IS, Parker KH, Mayet J, Hughes AD. (2007). Importance of the aortic reservoir in determining the shape of the arterial pressure waveform – The forgotten lessons of Frank. Artery Research, **1**: 40-45.

Davies JE, Baksi J, Francis DP, Hadjiloizou N, Whinnett ZI, Manistry CH, Aguado-Sierra J, Foale RA, Malik IS, Tyberg JV, Parker KH, Mayet J, and Hughes AD. (2010). The Arterial Reservoir Pressure Increases with Aging and it is the Major Determinant of the Aortic Augmentation Index. Am. J. Physiol. Heart Circ. Physiol., **298**: H580-H586.

Davies JE, Whinnett ZI, Francis DP, Manisty CH, Aguado-Sierra J, Willson K, Foale RA, Malik IS, Hughes AD, Parker KH and Mayet J. (2006). Evidence of a Dominant Backward-Propagating “Suction” wave Responsible for Diastolic Coronary Filling in Humans, Attenuated in Left Ventricular Hypertrophy. Circ., **113**, 1768-1778.

Davies JE, Whinnett ZI, Francis DP, Willson K, Foale RA, Malik IS, Hughes AD, Parker KH, and Mayet J. (2005). Use of Simultaneous Pressure and Velocity Measurements to

Estimate Arterial Wave Speed at a Single Site in Humans. Am. J. Physiol. Heart Circ. Physiol., **290**: H878-H885.

Davies MJ. (1996). Stability and Instability: The Two Faces of Coronary Atherosclerosis. Circulation, **94**(8): 2013-2020.

Dawber TR, Thomas HE, and McNamara PM. (1973). Characteristics of the Dicrotic Notch of the Arterial Pulse Wave in Coronary Heart Disease. Angiology, **24**: 244-255.

Desai M, Ahmed M, Darbyshire A, You Z, Hamilton G, and Seifalian AM. (2011). An Aortic Model for the Physiological Assessment of Endovascular Stent-Grafts. Ann. Vasc. Surg., In Press: 1-8.

Doggrell SA. (2001). ALT-711 Decreases Cardiovascular Stiffness and has Potential in Diabetes, Hypertension and Heart Failure. Exp. Opin. Invest. Drugs, **10**(5): 981-983.

Domanski M, Mitchell G, Pfeffer M, Neaton JD, Norman J, Svendsen K, Grimm R, Cohen J, and Stamler J. (2002). Pulse Pressure and Cardiovascular Disease-Related Mortality. Follow-up study of the Multiple Risk Factor Intervention Trial (MRFIT). JAMA, **287** (20): 2677 – 2683.

Domanski MJ, Davis BR, Pfeffer MA, Kastantin M, Mitchell GF. (1999). Isolated Systolic Hypertension. Prognostic information Provided by Pulse Pressure. Hypertension, **34**: 375-380.

Drexler H, and Hornig B. (1999). Endothelial Dysfunction in Human Disease. J. Mol. Cell. Cardiol., **31**: 51-60.

Drzewiecki GM, Melbin J, and Noordergraaf A. (1983). Arterial Tonometry: Review and Analysis. J. Biomechanics, **16**(2): 141-152.

Dujardin J-P L and Stone DN, (1981). Characteristic Impedance of the Proximal aorta determined in the time and frequency domain: a comparison. Med. & Biol. Eng. & Comput., **19**, 565-568.

Duncan T. (1978). Advanced Physics: Fields, Waves and Atoms. Publ. John Murray, London.

Endemann DH, and Schiffrin EL. (2004). Endothelial Dysfunction. J. Am. Soc. Nephrol., **15**: 1983-1992.

Falk E. (1992). Why Do Plaques Rupture? Circulation, 86(6Suppl): III30-III42.

Falk E, Shah PK, and Fuster V. (1995). Coronary Plaque Disruption. Circulation, **92**: 657-671.

Félétou M, and Vanhoutte PM. (1999). The Alternative: EDHF. J. Mol. Cell. Cardiol., **31**: 15-22.

Finkelstein SM, Cohn JN, Collins VR, Carlyle PF, Shelley WJ. (1985). Vascular Hemodynamic Impedance in Congestive Heart Failure. Am. J. Cardiol., **55**: 423-427.

Fitch RM, Vergona R, Sullivan ME, and Wang Y-X. (2001). Nitric Oxide Synthase Inhibition Increases Aortic Stiffness Measured by Pulse Wave Velocity in Rats. Cardiovasc. Res., **51**:351-358.

Fitchett DH, Simkus G, Genest J, Marpole D, and Beaudry P. (1988a). Effect of Nitroglycerin on Left Ventricular Hydraulic Load. Can. J. Cardiol., **4**(2): 72-75.

Fitchett DH, Simkus GJ, Beaudry JP, and Marpole DGF, (1988b). Reflected Pressure Waves in the Ascending Aorta: Effect of Glyceryl Trinitrate. Cardiovascular Research, **22**: 494-500.

Fleming I, and Busse R. (1999). NO: The Primary EDRF. J. Mol. Cell. Cardiol., **31**: 5-14

Forster BA, and Weinberg PD, (1997). Changes with age in the influence of endogenous nitric oxide on transport properties of the rabbit aortic wall near branches. Arterioscler. Thromb. Vasc. Biol., **17**: 1361-1368.

Franklin SS, Khan SA, Wong ND, Larson MG, and Levy D (1999). Is Pulse Pressure Useful in Predicting Risk for Coronary Heart Disease? : The Framingham Heart Study Circulation.; **100:**354-360

Fung YC, and Liu SQ. (1989). Change of Residual Stains in Arteries due to Hypertrophy Caused by Aortic Constriction. Circulation Research, **65**: 1340-1349.

Geddes LA. (1970). The Direct and Indirect Measurement of Blood Pressure. Year Book Medical Publishers, Inc.

Glass CK and Witztum JL. (2001). Atherosclerosis: The Road Ahead. Cell, **104**: 503-516.

Goldwyn RM, and Watt TB. (1967). Arterial Pulse Contour Analysis Via a Mathematical Model for the Clinical Quantification of Human Vascular Properties. IEEE Trans. BME 14(1):11-17.

Greenwald SE. (2007). Ageing of the Conduit Arteries. J. Pathol., **211**: 157-172.

Greenwald SE, Newman DL, and Bowden LR (1978). Comparison between theoretical and directly measured pulse propagation velocities in the aorta of the anaesthetised dog. Cardiovasc. Res., **12**: 407-414.

Gribbin B, Steptoe A, and Sleight P. (1976). Pulse Wave Velocity as a Measure of Blood Pressure Change. Psychophysiology, **13**(1): 86-90.

Guyton AC, and Greganti FP. (1956). A Physiological Reference Point for Measuring Circulatory Pressures in the Dog – Particularly Venous Pressure. Am. J. Physiol., **185**: 137-141.

Guyton AC, and Jones CE. (1973). Central Venous Pressure: Physiological Significance and Clinical Implications. American Heart Journal, **86**(4): 431-437.

Guyton AC, Polizo D, and Armstrong GG. (1954). Mean Circulatory Filling Pressure Measured Immediately After Cessation of Heart Pumping. Am. J. Physiol., **179**: 261-272.

Hallock P, and Benson IC. (1937). Studies on the Elastic Properties of Human Isolated Aorta. J. Clin. Invest., **16**: 595-602.

Hansson L. (1987). Isolated Systolic Hypertension. Current Opinion in Cardiology, **2** (suppl 1): S15 – S19.

Harada A, Okada T, Niki K, Chang D, Sugawara M. (2002). On-line non-invasive one-point measurements of pulse wave velocity. Heart Vessels, **17**: 61-68.

Harrison DG and Bates JN. (1993). The Nitrovasodilators: New Ideas about Old Drugs. Circulation, **87**: 1461-1467.

Hayashi K, Handa H, Nagaswa S, Okumura A, and Moritake K. (1980). Stiffness and Elastic Behaviour of Human Intracranial and Extracranial Arteries. J. Biomechanics, **13**: 175-184.

Hayashi K, Sato M, Handa H, and Moritake K. (1974). Biomechanical Study of the Constitutive Laws of Vascular Walls. Experimental Mechanics, **14**: 440-444.

Helgason S. (2007). The Radon Transform. Birkhauser, Boston.

Hu C-T, Chang K-C, Wu C-Y, and Chen HI. (1997). Acute Effects of Nitric Oxide Blockade with L-NAME on Arterial Haemodynamics in the Rat. Br. J. Pharmacol., **122**: 1237-1243.

Hughes AD, and Parker KH. (2009). Forward and Backward Waves in the Arterial System: Impedance or Wave Intensity Analysis? Med. Biol. Eng. Comput., **47**: 207-210.

Humphrey JD. (1995). Mechanics of the Arterial Wall: Review and Directions. Critical Reviews in Biomedical Engineering, **23**(1&2): 3-162 (see p27).

Hunt AAE, Hilditch A, and Drew GM. (1997). Effects of the Angiotensin AT1 Receptor Antagonist GR138950 on Haemodynamic Function in Dogs. J. Autonomic Pharmacol., **17**: 1-11.

Hunt AAE, Louttit JB, Maxwell MP, and White BP. (2001). An in vivo Comparison of Physical Properties of the Aortas of Hyperlipidaemic and Normal Rabbits using Intravascular Ultrasound (IVUS). 3rd European Meeting on Pulse Wave Analysis and Large Artery Function. Poster Abstract P.03. J. Human Hypertension, **15**: 820.

Huijberts MSP, Wolffenbuttel BHR, Struijker Boudier HAJ, Crijns FRL, Nieuwenhuijzen Kruseman AC, Poitevin P, and Lévy BI. (1993). Aminoguanidine Treatment Increases Elasticity and Decreases Fluid Filtration of Large Arteries from Diabetic Rats. J. Clin. Invest., **92**: 1407-1411.

Imhof PR, Ott B, Frankhauser P, Chu L-C, and Hodler J. (1980). Difference in Nitroglycerin Dose-Response in the Venous and Arterial Beds. Eur. J. Clin. Pharmacol., **18**: 455-460.

Izzo, JL. (2004). Arterial Stiffness and the Systolic Hypertension Syndrome. Curr. Opin. Cardiol., **19**: 341-352.

John S, and Schmieder R. (2000). Impaired Endothelial Function in Arterial Hypertension and Hypercholestrolemia: Potential Mechanisms and Differences. J. Hypertens., **18**:363-374

Jones CJH, Sugawara M, Kondoh Y, Uchida K, and Parker KH (2002). Compression and Expansion Wavefront travel in canine ascending aortic flow: wave intensity analysis. Heart Vessels, **16**: 91-98.

Kaplan NM (1992). Systolic Hypertension in the Elderly Program (SHEP) and Swedish Trial in Old Patients with Hypertension (STOP): The Promises and the Potential Problems. Am. J. Hypertens., **5**: 331 – 334.

Kass DA, Shapiro EP, Kawaguchi M, Capriotti AR, Scuteri A, deGroof RC, and Lakatta EG. (2001). Improved Arterial Compliance by a Novel Advanced Glycation End-Product Crosslink Breaker. Circulation, **104**: 1464-1470.

Katsuda S-I, Miyashita H, Hasegawa M, Machida N, Kusanagi M, Yamasaki M, Waki H, and Hazama A. (2004). Characteristic Change in Local Pulse Wave Velocity in Different Segments of the Atherosclerotic Aorta in KHC Rabbits. Am. J. Hypertens., **17**: 181-187.

Kawasaki T, Sasayama S, Yagi S-I, Asakawa T, and Hirai T. (1987). Non-Invasive Assessment of the Age Related Changes in Stiffness of Major Branches of the Human Arteries. Cardiovascular Research, **21**: 678-687.

Kelly R, Hayward C, Avolio A, and O'Rourke M. (1989). Noninvasive Determination of Age-Related Changes in the Human Arterial Pulse. Circulation, **80**: 1652-1659.

Kelly R, Hayward C, Ganis J, Daley J, Avolio A and O'Rourke M. (1989). Noninvasive Registration of the Arterial Pressure Pulse Waveform Using High-Fidelity Applanation Tonometry. J. Vasc. Med. Biol., 1(3): 142-149.

Khir AW, O'Brien AO, Gibbs JSR, and Parker KH (2001). Determination of wave speed and wave separation in the arteries. J. Biomechanics, **34** : 1145-1155.

Khir AW and Parker KH. (2002). Measurements of wave speed and reflected waves in elastic tubes and bifurcations. J. Biomechanics, **35**: 775-783.

Khir AW, and Parker KH. (2005). Wave intensity in the ascending aorta: effects of arterial occlusion. J. Biomechanics, **38**: 647-655.

Khir AW, Zambanini A, and Parker KH. (2004). Local and regional wave speed in the aorta: effects of arterial occlusion. Med. Eng. Phys., **26**: 23-29.

Kieffer P, Robert A, Capdeville-Atkinson C, Atkinson J, and Lartaud-Idjouadiene. (2000). Age-Related Arterial Calcification in Rats. Life Sciences, **66**(24): 2371-2381.

Klemsdal TO, Andersson TLG, Matz J, Ferns GAA, Gjesdal K, and Änggård EE. (1994). Vitamin E Restores Endothelium Dependent Vasodilation in Cholesterol Fed Rabbits: In Vivo Measurements by Photoplethysmography. Cardiovascular Research, **28**: 1397-1402.

Koh TW, Pepper JR, DeSouza AC, and Parker KH (1998). Analysis of wave reflections in the arterial system using wave intensity: a novel method for predicting the timing and amplitude of reflected waves. Heart Vessels, **13**: 103-113.

Kolyva C, Biglino G, Pepper JR, and Khir AW. (2010). A Mock Circulatory System With Physiological Distribution of Terminal Resistance and Compliance: Application for Testing the Intra-Aortic Balloon Pump. Artificial Organs. In Press.

Kontis S, and Gosling RG, (1989). On-line Doppler ultrasound measurement of aortic compliance and its repeatability in normal subjects. Clin. Phys. Physiol. Meas., **10** (2): 127-135.

Laogun AA and Gosling RG (1982). *In vivo* arterial compliance in man. Clin. Phys. Physiol. Meas., **3** (3): 201-212.

Laskey WK, Parker G, Ferrari V, Kussmaul WG, and Noordergraaf A. (1990). Estimation of Total Systemic Arterial Compliance in Humans. J. Appl. Physiol., **69**(1): 112-119.

Latham RD, Rubal BJ, Westerhof N, Sipkema P, and Walsh RA. (1987). Nonhuman Primate Model for Regional Wave Travel and Reflections along Aortas. Am. J. Physiol., **253** (Heart Circ. Physiol. **22**): H299-H306.

Latham RD, Westerhof N, Sipkema P, Rubal BJ, Reuderink P, and Murgo JP. (1985). Regional Wave Travel and Reflections along the Human Aorta: a Study with Six Simultaneous micromanometric Pressures. Circulation, **72**: 1257-1269.

Latson TW, Hunter WC, Katoh N, and Sagawa K. (1988). Effect of Nitroglycerin on Aortic Impedance, Diameter, and Pulse-Wave Velocity. Circulation Research, **62**: 884-890.

Laurent S, Boutouyerie P, Asmar R, Gautier I, Laloux I, Guize L, Ducimetiere P, Benetos, A. (2001). Aortic stiffness is an Important predictor of All-Cause and cardiovascular Mortality in Hypertensive Patients. Hypertension, **37**: 1236 – 1241

Lehmann ED, Hopkins KD, and Gosling RG (1993). Aortic Compliance Measurements using Doppler Ultrasound: *In Vivo* Biochemical Correlates. Ultrasound in Med. & Biol.**19** (9): 683-710.

Lehmann ED, Hopkins KD, Marsden RM, Brown I, Jones RL, Turay RC, Taylor MG, and Gosling RG. (1994). Aortic compliance measured by non-invasive Doppler ultrasound: application of a personal computer based Mk II system and its repeatability. Med. Eng. Phys., **16**: 213-221.

Lever AF (1987). Relationship between risk of stroke and systolic blood pressure in mild hypertension: Observations from the Medical Research Council Trial. Current Opinion in Cardiology, **2** (suppl 1): S6 – S14.

Li J K-J, (1986). Time Domain Resolution of Forward and Reflected Waves in the Aorta. IEEE Trans. Biomed. Eng., BME-**33** (8): 783-785.

Libby P. (2001). Current Concepts of the Pathogenesis of Acute Coronary Syndromes. Circulation, **104**: 365-372.

Libby P, Ridker PM, Maseri A. (2002). Inflammation and Atherosclerosis. Circulation, **105**: 1135-1143.

Lin Y-T, Tseng Y-Z, and Chang K-C. (2004). Aminoguanidine Prevents Fructose-Induced Arterial Stiffening in Wistar Rats: Aortic Impedance Analysis. Exp. Biol. Med., **229**: 1038-1045.

Liu Z, Brin KP, and Yin FCP. (1986). Estimation of Total Arterial Compliance: An Improved Method and Evaluation of Current Methods. Am. J. Physiol., **251** (Heart Circ. Physiol., **20**): H588-H600.

Lloyd-Jones DM, Evans JC, Larson MG, O'Donnell CJ, Roccella EJ, and Levy D. (2000). Differential Control of Systolic and Diastolic Blood Pressure: Factors Associated with Lack of Blood Pressure Control in the Community. Hypertension, **36**: 594-599.

Lokhandwala MF, Cavero I, Buckley JP, and Jandhyala BS. (1973). Influence of Pentobarbital Anesthesia on the Effects of Certain Autonomic Blocking Agents on Heart Rate. European J. Pharmacol., **24**: 274-277.

Love AEH. (1927). A Treatise on Mathematical Elasticity. 3rd ed., Cambridge University Press.

Lund F. (1986). Digital Pulse Plethysmography (DPG) in Studies of the Hemodynamic Response to Nitrates – A Survey of Recording Methods and Principles of Analysis. Acta. Pharmacol. Toxicol., **59** (Suppl. VI): 79-96.

Lusis AJ. (2000). Atherosclerosis. Nature, **407**: 233-241

MacDonald E, Lee WK, Hepburn S, Bell J, Scott PJW, and Dominiczak MH. (1992). Advanced Glycosylation End Products in the Mesenteric Artery. Clin. Chem., **38**(4): 530-533.

MacKay RS, Marg E, and Oechsli R. (1960). Automatic Tonometer with Exact Theory: Various Biological Applications. Science, **131**:1668-1669.

Maguire J, Wilkinson I, McEniery C and Davenport A. (2003). Vasoconstrictor responses to the elastin peptide VGVAPG in aging human arteries *in vitro*. Brit. J. Pharmacol., **138**(suppl 1): 164P

Malindzak GS, and Meredith JH. (1970). Comparative Study of Arterial Transmission Velocity. J. Biomechanics, **3**: 337-350.

Manning TS, Shykoff BE, and Izzo JL. (2002). Validity and Reliability of Diastolic Pulse Contour Analysis (Windkessel Model) in Humans. Hypertension, 39: 963-968.

Marque V, Van EssenH, Struijker-Boudier HAJ, Atkinson J, Lartaud-Idjouadiene I. (2001). Determination of Aortic Elastic Modulus by Pulse Wave Velocity and Wall Tracking in a Rat Model of Aortic Stiffness.. J. Vasc. Res., **38**: 546-550

Matthys KS, Alastruey J, Peiró J, Khir AW, Segers P, Verdonck PR, Parker KH, and Sherwin SJ (2007). Pulse wave propagation in a model human arterial network: Assessment of 1-D numerical simulations against in vitro measurements. J. Biomechanics, **40**(15): 3476-3486.

McDonald DA. (1960 1st Edn.; 1974 2nd Edn.). Blood Flow in Arteries. Pub.: Edward Arnold.

McDonald DA. (1968). Regional Pulse-wave Velocity in the Arterial Tree. J. Appl. Physiol., **24**(1): 73-78.

McKenzie AEE. (1965). A Second Course of Light. Cambridge University Press.

McVeigh GE, Burns DE, Finkelstein SM, McDonald KM, Mock JE, Feske W, Carlyle PF, Flack J, Grimm R, and Cohn J. (1991) Reduced Vascular Compliance as a Marker for Essential Hypertension. Am. J. Hypertens., **4**: 245-251.

Meaume S, Benetos A, Henry OF, Rudnichi A, and Safar ME (2001). Aortic Pulse Wave Velocity Predicts Cardiovascular Mortality in Subjects >70 Years of Age. Arterioscler. Thromb. Vasc. Biol., **21**: 2046-2050.

Mecham RP, Hinek A, Entwistle R, Wrenn DS, Griffin GL, and Senior RM. (1989). Elastin Binds to a Multifunctional 67-Kilodalton Peripheral Membrane Protein. Biochemistry, **28**: 3716-3722.

Merillon JP, Fontenier G, Lerallut JF, Jaffrin MY, Chastre J, Assayag P, Motte G, and Gourgon R. (1984). Aortic Input Impedance in Heart Failure: Comparison with Normal Subjects and its Changes During Vasodilator Therapy. Eur. Heart J. **5**: 447-455.

Mikulíková K, Eckhardt A, Kuneš J, Zicha J, and Mikšík I. (2008). Advanced Glycation End-Product Pentosidine Accumulates in Various Tissues of Rats with High Fructose Intake. Physiol. Res. **57**: 89-94.

Millasseau SC, Guigui FG, Kelly RP, Prasad K, Cockcroft JR, Ritter JM, Chowienczyk PJ. (2000). Noninvasive Assessment of the Digital Volume Pulse: Comparison with the Peripheral Pressure Pulse. Hypertension, **36**: 952-956.

Mills CJ. (1972). Measurement of Pulsatile Flow and Flow Velocity. Chapter 3. pp51-90. From: *Cardiovascular Fluid Dynamics*. Ed.: Bergel DH. Publ. Academic Press.

Milnor WR. (1982 1st Edn.; 1989 2nd Edn.). Hemodynamics. Pub.: Williams & Wilkins.

Mitchell GF. (2009). Arterial Stiffness and Wave Reflection: Biomarkers of Cardiovascular Risk. Artery Research, **3**: 56-64.

Mitchell GF, Parise H, Benjamin EJ, Larson MG, Keyes MJ, Vita JA, Vasan RS, and Levy D. (2004). Changes in Arterial Stiffness and Wave Reflection with Advancing Age in Healthy Men and Women. The Framingham Heart Study. Hypertension, **43**: 1239-1245.

Mitchell GF, Pfeffer JM, and Pfeffer MA (1997). The Heart and Conduit Vessels in Hypertension. Essential Hypertension, Part II. Medical Clinics of North America, 81 (6): 1247-1271.

Mitchell GF, Tardif J-C, Arnold JM, Marchiori G, O'Brien TX, Dunlap ME, Pfeffer MA. (2001). Pulsatile Hemodynamics in Congestive Heart Failure. Hypertension, **38**: 1433-1439.

Mitchell GF, Pfeffer MA, Finn PV, and Pfeffer JM. (1997). Comparison of Techniques for Measuring Pulse-Wave Velocity in the Rat. J. Appl. Physiol., **82**(1): 203-210.

Mombouli J-V, and Vanhoutte PM. (1999). Endothelial Dysfunction: From Physiology to Therapy. J. Mol. Cell. Cardiol., **31**: 61-74.

Morikawa Y. (1967). Characteristic Pulse Wave caused by Organic Nitrates. Nature, **213**: 841-842.

Murgo JP, Westerhof N, Giolma JP, and Altobelli SA. (1980). Aortic Input Impedance in Normal Man: Relationship to Pressure Wave Forms. Circulation, **62**(1): 105-116.

Murrell W. (1879). Nitro-glycerine as a Remedy for Angina Pectoris. Lancet, **80**: 113-115

Naghavi M, Libby P, Falk E., *et al*. (2003). From Vulnerable Plaque to Vulnerable Patient: A Call for New Definitions and Risk Assessment Strategies: Part I. Circulation, **108**: 1664-1672.

Naka Y, Yoshino G, Hirano T, Murata Y, Maeda E, Kazumi T, and Kasuga M. (1998). Triglyceride Metabolism in Heterozygote of Watanabe Heritable Hyperlipidemic Rabbit. Atherosclerosis, **136**: 325-332.

Nagle SR, (2007). Modelling the Effect of Drugs in the Pulse Wave of Rabbits. Dissertation for a Masters Degree, Department of Aeronautics, Imperial College London.

Nelson RR, Gobel FL, Jorgensen CR, Wang K, Wang Y, and Taylor HL. (1974). Hemodynamic Predictors of Myocardial Oxygen Consumption During Static and Dynamic Exercise. Circulation, **50**: 1179-1189.

Nichols WW and O'Rourke MF. (1990 3rd Ed.; 1998 4th Ed.; 2005 5th Ed.). McDonald's Blood Flow in Arteries. Theoretical, Experimental, and Clinical Principles. Pub.: Hodder Arnold (formerly Edward Arnold).

Niederhoffer N, Bobryshev YV, Lartaud-Idjouadiene I, Giummelly P, and Atkinson J. (1997). Aortic Calcification Produced by Vitamin D_3 plus Nicotine. J. Vasc. Res., **34**: 386-398.

Nier BA. (2007). Use of Pulse Wave Analysis for Assessing Nitric Oxide Bioactivity in vivo. Oral presentation to the Fourth Meeting of the Physiological Flow Network. Manchester University. April 2007.

Neir BA, Harrington LS, Carrier MJ, and Weinberg PD. (2008). Evidence for a Specific Influence of the Nitrergic Pathway on the Peripheral Pulse Waveform in Rabbits. Exp. Physiol. **93**: 503-512.

Nier BA and Weinberg PD. (2007). Development of a simple non-invasive technique for assessing vascular nitric oxide bioactivity *in vivo*. Poster Presentation at the Hounsfield Memorial Lecture. Imperial College London, 2007.

O'Brien DJ, Chapman WH, Rudd FV, and McRoberts JW. (1971). Carotid Artery Loop Method of Blood Pressure Measurement in the Dog. J. Appl. Physiol., **30**(1):161-163.

Oliver JJ, and Webb DJ. (2003). Noninvasive Assessment of Arterial Stiffness and Risk of Atherosclerotic Events. Arterioscler. Thromb. Vasc. Biol., **23**: 554-566.

O'Rourke MF, (1982). Arterial Function in Health and Disease. Pub.: Churchill Livinstone Medical Division of Longman Group Limited.

O'Rourke MF and Gallagher DE (1996). Pulse wave analysis. J. Hypertens., **14** (suppl 5): S147 – S157.

Page CM, Khir AW, Hughes AD, Chung R, and Henein MY. (2010). Normal Asynchrony of Left Ventricular Long and Short Axes: Their Relationship with Aortic Hemodynamics. Int. J. Cardiol., **142** (2): 166-171.

Page IH, and McCubbin JW. (1965). Autonomic Regulation of Arterial Pressure Responses. Arch. Int. Pharmacodyn., **157**(1): 152-165.

Parker KH. (2009a). A Brief History of Arterial Wave Mechanics. Med. Biol. Eng. Comput., **47**: 111-118.

Parker KH. (2009b). An Introduction to Wave Intensity Analysis. Med. Biol. Eng. Comput., **47**: 175-188.

Parker KH, Alastruey J, Aguado-Sierra J, Hughes AD, and Davies JE. (2011). An Algorithm for Calculating Reservoir Pressure from the Arterial Pressure Waveform (draft). Personal communication with Prof. K. Parker.

Parker KH and Jones CJH (1990). Forward and Backward Running Waves in the Arteries: Analysis Using the Method of Characteristics. J. Biomech. Eng., **112**: 322-326.

Parker KH, Jones CJH, Dawson JR, and Gibson DG (1988). What stops the flow of blood from the heart? Heart Vessels, **4**: 241-245.

Patel DJ, and Vaishnav RN. (1980). General Mechanical Properties of the Vascular Wall. Ch.4 in *Basic Hemodynamics And Its Role In Disease Processes*. Baltimore M.D. University Park.

Pepine CJ, Nichols WW, Curry RC, and Conti CR. (1979). Aortic Input Impedance During Nitroprusside Infusion: A Reconsideration of Afterload Reduction and Beneficial Action. J. Clin. Invest., **64**: 643-654

Pressman GL, and Newgard PM. (1963). A Transducer for the Continuous External Measurement of Arterial Blood Pressure. IEEE Trans. Biomed. Elect.; BME **10**:73-81

Pythoud F, Stergiopulos N, Meister J-J. (1996). Separation of Arterial Pressure Waves into their Forward and Backward Running Components. J. Biomech. Eng., **118**:295-301.

Raitakari OT, and Celermajer DS. (2000). Testing for Endothelial Dysfunction. Ann. Med., **32**:293-304.

Rang HP, Dale MM, Ritter JM, and Moore PK. (2003) **[a]** Cholinergic Transmission, Ch. 10; **[b]** Nitric Oxide, Ch. 14. In *Pharmacology*, 5th Edn., Publ. Churchill Livingstone

Reddy GK. (2004). AGE-related Cross-linking of Collagen is associated with Aortic Wall Matrix Stiffness in the Pathogenesis of Drug-induced diabetes in Rats. Microvascular Research, **68**: 132-142.

Resnick LM, Militianu D, Cunnings AJ, Pipe JG, Evelhoch JL, Soulen RL, and Lester MA. (2000). Pulse Waveform Analysis of Arterial Compliance: Relation to Other Techniques, Age, and Metabolic Variables. Am. J. Hypertens., **13**: 1243-1249.

Riemann GFB. (1859). Üeber die Fortzflanzung ebener Luftwellen von endlicher Schwingungsweite. Gesammelte mathematische Werke und wissenschaftlcher. Nachlass. Liepzig, Teubner BG (ed), pp 147-176 (originally published in Bande VIII, Abhandlungen der Königlechen Geselschaft der Wissenschaften zu Göttingen, pp 43-65).

Riemann GFB. (1860). Gesammelte mathematische Werke und wissenschaftlicher Nachlass. Liepzig BG Teubner (ed) 1876, pp 145-164. (Originally published as Üeber die Fortzflanzung ebener Luftwellen von endlicher Schwingungsweite. Technical report, Göttingen 8, 1860, 43).

Rietzschel E-R, Boeykens E, De Buyzere ML, Duprez DA, and Clement DL. (2001). A Comparison Between Systolic and Diastolic Pulse Contour Analysis in the Evaluation of Arterial Stiffness . Hypertension, **37**: e15-e22.

Roach MR, and Burton AC. (1957). The Reason for the Shape of the Distensibility Curves of Arteries. Can. J. Biochem. Physiol., **35**: 681-690.

Robert L (1996). Aging of the vascular wall and atherogenesis: role of the elastin-laminin receptor. Atherosclerosis, **123**: 169-179.

Robert L (1999). Aging of the vascular-wall and atherosclerosis. Experimental Gerontology, **34**: 491 – 501.

Ross R. (1993). The Pathogenesis of Atherosclerosis: A perspective for the 1990s. Nature, 362: 801-809

Ross R. (1999). Atherosclerosis – An Inflammatory Disease. New England Journal of Medicine, **340**(2): 115-126.

Rothe R. (1993). Mean Circulatory Filling Pressure: Its Meaning and Measurement. J. Appl. Physiol., **74**(2): 499-509.

Safar ME. (1993). Hemodynamic Changes in Elderly Hypertensive Patients. Am. J. Hypertens., **6**: 20S-23S.

Salvetti A, and Versari D. (2003). Control of Blood Pressure in the Community: An Unsolved Problem. Current Pharmaceutical Design, **9**: 2375-2384.

Sauer G, Wille H –H, Tebbe U, Neuhaus K –L, and Kreuzer H. (1981). Influence of Nitroglycerin on Aortic Compliance, Capacity of the Windkessel, and Peripheral Resistance. From: Nitrates III; Eds.: Lichtlen, Engel, Schrey, Swan. Pub.: Springer.

Schalkwijk CG, Stehouwer CDA, van Hinsbergh VMW. (2004). Fructose-Mediated Non-Enzymatic Glycation: Sweet Coupling or Bad Modification. Diabetes Metab. Res. Rev., **20**: 369-382.

Schmidt AM, Yan SD, Wautier J-L, and Stern D. (1999). Activation of Receptor for Advanced Glycation End Products: A Mechanism for Chronic Vascular Dysfunction in Diabetic Vasculopathy and Atherosclerosis. Circ. Res., **84**: 489-497.

Segers P, Dubois F, De Wachter D, Verdonk P. (1998). Role and Relevancy of a Cardiovascular Simulator. Cardiovascular Engineering, **3** (1): 48-56.

Segers P, Qasem A, De Backer T, Carlier S, Verdonck P, and Avolio A. (2001). Peripheral "Oscillatory" Compliance is Associated With Aortic Augmentation Index. Hypertension, **37**: 1434-1439.

Segers P, and Verdonck P (2000). Role of tapering in aortic wave reflection: hydraulic and mathematical model study. J. Biomechanics, **33**: 299-306.

Segers P, Verdonck P, Duprez D, De Buyzere M, and Verhoevan R. (1997). Evaluation of the Non-Invasive Determination of Arterial Compliance with the Goldwyn-Watt Model by a Transmission Line Model Study. Journal of Cardiovascular Diagnosis and Procedures, 14(1): 3-8

Sherwin SJ, Franke V, Peiró J, and Parker K. (2003). One-dimensional modelling of a vascular network in space-time variables. J. Engineering Mathematics, **47**: 217-250.

Shimokawa H. (1999). Primary Endothelial Dysfunction: Atherosclerosis. J. Mol. Cell. Cardiol., **31**: 23-37.

Shimokawa H, and Vanhoutte PM. (1997). 32. Endothelium and Vascular Injury in Hypertension and Atherosclerosis. Handbook of Hypertension, **17**: Pathophysiology of Hypertension, pp1007-1068.

Shrier IS, Hussain NA, and Magder S. (1993). Effect of Carotid Sinus Stimulation on Resistance and Critical Closing Pressure of the Canine Hindlimb. Am. J. Physiol. **264** (Heart Circ. Physiol. **33**): H1560-Hl566.

Simon A Ch, Levenson JA, Levy BY, Bouthier JE, Peronneau PP, and Safar ME. (1982). Effect of Nitroglycerin on Peripheral Large Arteries in Hypertension. Br. J. Clin. Pharmac., **14**: 241-246.

Sipkema P, Latham RD, Westerhof N, Rubal BJ, and Slife DM. (1990). Isolated Aorta Setup for Hemodynamic Studies. Annals of Biomedical Engineering, **18**: 491-503.

Skalak R. (1972). Synthesis of a Complete Circulation. In *Cardiovascular Fluid Dynamics*, Vol. 2, Ch.19 pp341-376; Ed. Bergel DH. Publ. Academic Press.

Sloop GD, Perret RS, Brahney JS, and Oalmann M. (1998). A Discription of Two Morphological Patterns of Aortic Fatty Streaks, and a Hypothesis of Their Pathogenesis. Atherosclerosis, **141**: 153-160

Spokas EG, Folco G, Quilley J, Chander P, and McGiff JC. (1983). Endothelial Mechanism in the Vascular Action of Hydralazine. Hypertension, **5**(Suppl I): I-107 – I-111.

Staughton TJ, Lever MJ, and Weinberg PD. (2001). Effect of altered flow on the pattern of permeability around rabbit aortic branches. Am. J. Physiol. Heart Circ. Physiol., **281**: H53-H59.

Stengele E, Winkler F, Trenk D, Jähnchen E, Petersen J, and Roskamm H. (1996). Digital Pulse Plethysmography as a Non-invasive Method for Predicting Drug-induced Changes in Left Ventricular Preload. Eur. J. Clin. Pharmacol., **50**: 279-282.

Stergiopulos N, Young DF, and Rogge TR. (1992). Computer simulation of arterial flow with applications to arterial and aortic stenoses. J. Biomechanics, **25** (12): 1477-1488.

Stergiopulos N, Meister J-J, and Westerhof N. (1995). Evaluation of Methods for Estimation of Total Arterial Compliance. Am. J. Physiol., **268** (Heart Circ. Physiol., **37**): H1540-H1548.

Stewart AD, Millasseau SC, Kearney MT, Ritter JM, and Chowienczyk PJ. (2003). Effects of Inhibition of Basal Nitric Oxide Synthesis on Carotid-Femoral Pulse Wave Velocity and Augmentation Index in Humans. Hypertension, **42**: 915-918.

Stitt AW, Bucala R, and Vlassara H. (1997). Atherogenesis and Advanced Glycation: Promotion, Progression, and Prevention. Ann. NY. Acad. Sci., 811: 115-127 & 127-129.

Strohm WD, Rahn R, Cordes H –J, Kurtz W, and Kober G. (1983). Diameters of Abdominal Veins and Arteries During Nitrate Therapy. Z. Kardiol., **72**(Suppl.3): 56-61.

Sugawara M, Niki K, Ohte N, Okada T, and Harada A. (2009). Clinical Usefulness of Wave Intensity Analysis. Med. Biol. Eng. Comput., **47**: 197-206.

Sundberg S, and Castrén M. (1986). Drug- and Temperature-induced Changes in Peripheral Circulation Measured by Laser-Doppler Flowmetry and Digital-Pulse Plethysmography. Scand. J. Clin. Lab. Invest., **46**: 359-365.

Susic D, Varagic J, Ahn J, and Frohlich ED. (2004). Crosslink Breakers: A New Approach to Cardiovascular Therapy. Curr. Opin. Cardiol., **19**: 336-340.

Susic D, Varagic J, Ahn J, and Frohlich ED. (2004a). Cardiovascular and Renal Effects of a Collagen Cross-link Breaker (ALT 711) in Adult and Aged Spontaneously Hypertensive Rats. Am. J. Hypertens., **17**: 328-333.

Susic D, Varagic J, Ahn J, Matavelli LC, and Frohlich ED. (2004b). Breaker of Glycated Collagen Cross-links, ALT-711, Improves Left Ventricular Function and Aortic Distensibilityin Elderly Spontaneously Hypertensive Rats. Am. J. Hypertens., **17**(5) part 2: 169A.

Tabas I. (1999). Nonoxidative Modifications of Lipoproteins in Atherogenesis. Annu. Rev. Nutr. **19**: 123-139.

Ting CT, Chang MS, Wang SP, Chiang BN, and Yin FCP. (1990). Regional Pulse Wave Velocities in Hypertensive and Normotensive Humans. Cardiovasc. Res., **24**: 865-872.

Tokita Y, Hirayama Y, Sekikawa A, Kotake H, Toyota T, Miyazawa T, Sawai T, Oikawa S. (2005). Fructose Ingestion Enhances Atherosclerosis and Deposition of Advanced Glycated End-products in Cholesterol-fed Rabbits. J. Atheroscler. Thromb., **12**: 260-267.

Tyberg JV, Davies JE, Wang Z, Whitelaw WA, Flewitt JA, Shrive NG, Francis DP, Hughes AD, Parker KH and Wang JJ. (2009). Wave Intensity Analysis and the Development of the Reservoir-wave Approach. Med. Biol. Eng. Comput., **47**: 221-232.

Ulrich P and Cerami A. (2001). Protein glycation, diabetes, and aging. Recent Progress in Hormone Research, **56**: 1-12.

Vaccarino V, Berger AK, Abramson J, Black HR, Setaro JF, Davey JA, and Krumholz HM (2001). Pulse Pressure and Risk of Cardiovascular Events in the Systolic Hypertension in the Elderly Program. Am. J. Cardiol., **88**: 980 – 986

Vaitkevicius PV, Lane M, Spurgeon H, Ingram DK, Roth GS, Egan JJ, Vasan S, Wagle DR, Ulrich P, Brines M, Wuerth JP, Cerami A, and Lakatta EG. (2001). A Cross-link Breaker has

Sustained Effects on Arterial and Ventricular Properties in Older Rhesus Monkeys. Proc. Natl. Acad. Sci. USA., **98**(3): 1171-1175

van der Heijden-Spek JJ, Staessen JA, Fagard RH, Hoeks AP, Struijker Boudier HA, and Van Bortel LM. (2000). Effect of Age on Brachial Artery Wall Properties Differs from the Aorta and is Gender Dependent: A Population Study. Hypertension, **35**: 637-642.

Vasan S, Zhang X, Zhang X, Kapurniotu A, Bernhagen J, Teichberg S, Basgen J, Wagle D, Shih D, Terlecky I, Bucala R, Cerami A, Egan J, and Ulrich P. (1996). An Agent Cleaving Glucose-derived Protein Crosslinks *in vitro* and *in vivo*. Nature, 382: 275-278.

Verwiebe FL, Van Hooft GE, and Suchy RR. (1962). Physics: A Basic Science. Publ. D. Van Nostrand Company Inc. USA.

Vlassara H. (2001). The AGE-receptor in the Pathogenesis of Diabetic Complications. Diabetes Metab. Res. Rev., **17**: 436-443.

Vlassara H, Fuh H, Donnelly T, and Cybulsky M. (1995). Advanced Glycation Endproducts Promote Adhesion Molecules (VCAM-1, ICAM-1) Expression and Atheroma in Normal Rabbits. Molec. Med., **1**: 447-456.

Vongpatanasin W, Thomas GD, Schwartz R, Cassis LA, Osborne-Lawrence S, Hahner L, Gibson LL, Black S, Samols D, and Shaul PW. (2007). C-Reactive Protein Causes Downregulation of Vascular Angiotensin Subtype 2 Receptors and Systolic Hypertension in Mice. Circ., **115**:1-9.

Waeber B (2003). Trials in Isolated Systolic Hypertension: An Update. Current Cardiology Reports. **5**: 427 – 434.

Wang J-J, Flewitt JA, Shrive NG, Parker KH, Tyberg JV (2006). Systemic venous circulation. Waves propagating on a windkessel: relation of arterial and venous windkessels to systemic vascular resistance. Am. J. Physiol., Heart Circ., Physiol., **290**: H154-H162.

Wang J-J, O'Brien AB, Shrive NG, Parker KH, Tyberg JV (2003). Time-domain representation of ventricular-arterial coupling as a windkessel and wave system. Am. J. Physiol., Heart Circ., Physiol., **284**: H1358-H1368.

Wang JJ. and Parker KH. (2004). Wave propagation in a model of the arterial circulation. J. Biomechanics, **37**: 457-470.

Wang JJ, Shrive NG, Parker KH, Hughes AD, and Tyberg JV. (2011). Wave Propagation and Reflection in the Canine Aorta: Analysis Using a Reservoir-Wave Approach. Canadian Journal of Cardiology **27**: 389.e1–389.e10 www.onlinecjc.ca

Watt TB, and Burrus CS. (1976). Arterial Pressure Contour Analysis for Estimating Human Vascular Properties. J. Appl. Physiol., 40(2): 171-176.

Weinberg PD. (2002). Disease patterns at arterial branches and their relation to flow. Biorheology, **39**: 533-537.

Weinberg PD. (2004). Rate-Limiting Steps in the Development of Atherosclerosis: The Response-to-Influx Theory. J. Vasc. Res., **41**: 1-17.

Weinberg PD, Habens F, Kengatharan, Barnes SE, Matz J, Änggård EE and Carrier MJ. (2001). Characteristics of the pulse waveform during altered nitric oxide synthesis in the rabbit. Br. J. Pharmacol., **133**: 361-370.

Westerbacka J, Wilkinson I, Cockcroft J, Utriainen T, Vehkavaara S, and Yki-Järvinen H. (1999). Diminished Wave Reflection in the Aorta: A Novel Physiological Action of Insulin on Large Blood Vessels. Hypertension, **33**: 1118-1122.

Westerhof N, Bosman F, De Vries CJ, Noordergraaf A. (1969). Analog studies of the human systemic arterial tree. J. Biomechanics, **2**: 121-143.

Westerhof N, Elzinga G, and Sipkema P. (1971). An Artificial Arterial System for Pumping Hearts. J. Appl. Physiol., **31**(5): 776-781.

Westling H, and Andersson H. (1986). Nitroglycerin and Arterial Compliance. Acta. Pharmacol. Toxicol., **59**(Suppl. VI): 97-102.

Westling H, Jansson L, Jonson B, and Nilsén R. (1984). Vasoactive Drugs and Elastic Properties of Human Arteries In Vivo, with Special Reference to the Action of Nitroglycerine. Eur. Heart J. **5**: 609-616

Widlanski ME, Gokce N, Keaney JF Jr, and Vita JA. (2003). The Clinical Implications of Endothelial Dysfunction.. J. Am. Coll. Cardiol., **42**(7): 1149-1160.

Wiggers CJ. (1944). Physiology in Health and Disease. 4th Edition, Publ. Henry Kimpton, London.

Wilkinson IB and Cockcroft JR (2000). Mind the Gap: Pulse Pressure, Cardiovascular Risk, and Isolated Systolic Hypertension. Am. J. Hypertens., **13**: 1315 – 1317.

Wilkinson IB, Franklin SS, and Cockcroft JR. (2004). Nitric Oxide and the Regulation of Large Artery Stiffness: From Physiology to Pharmacology. Hypertension, **44**: 112-116.

Wilkinson IB, Franklin SS, Hall IR, Tyrrell S and Cockcroft JR. (2001). Pressure Amplification Explains Why Pulse Pressure is Unrelated to Risk in Young Subjects. Hypertension, **38**: 1461-1466.

Wilkinson IB, Hupperetz PC, Van Thoor CJ, MacCalum H, Cockcroft JR, and Webb DJ. (1998). Acute Hyperglycaemia Reduces Central Arterial Pressure in Healthy Subjects. Br. J. Clin. Pharmacol., **46**: 289P.

Wilkinson IB, Qasem A, McEniery CM, Webb DJ, Avolio AP, and Cockcroft JR. (2002). Nitric Oxide Regulates Local Arterial Distensibility In Vivo. Circulation, **105**: 213-217.

Williams B, *et al*., of the CAFE Steering and Writing Committees. (2006). Differential Impact of Blood Pressure-Lowering Drugs on Central Aortic Pressure and Clinical Outcomes. Principle Results of the Conduit Artery Function Evaluation (CAFE) Study. Circulation, **113**: 1213-1225.

Wolffenbuttel BHR, Boulanger CM, Crijns FRL, Huijberts MSP, Poitevin P, Swennen GNM, Vasan S, Egan JJ, Ulrich P, Cerami A, Levy BI. (1998). Breakers of Advanced Glycation End Products Restore Large Artery Properties in Experimental Diabetes. Proc. Natl. Acad. Sci. USA., **95**: 4630-4634.

Yaginuma T, Avolio A, O'Rourke M, Nichols W, Morgan JJ, Roy P, Baron D, Branson J, and Feneley M. (1986). Effect of Glyceryl Trinitrate on Peripheral Arteries alters Left Ventricular Load in Man. Cardiovascular Research, **20**: 153-160.

Yaginuma T, Wakabayashi A, Shimono Y, Watanabe M, Murai K, and Sakai A. (1972). Effects of Aortic Distensibility on the Cardiac Force in Man. Jap. Circul. J., **36**: 1187-1203.

Zambanini A, Cunningham SL, Parker KH, Khir AW, Thom S A McG, and Hughes AD. (2005). Wave-energy patterns in carotid, brachial, and radial arteries: a non-invasive approach using wave-intensity analysis. Am. J. Physiol. Heart Circ. Physiol., **289**: 270-276.

APPENDIX

MATLAB ALGORITHMS

Reservoir (Windkessel) Pressure Calculation:

```
%% Pseg - segment pressure trace Reservoir (Windkessel)Pressure Calculation
% FOR A SINGLE ENSEMBLED BEAT
% KHP (29/01/09)
% input P - row vector of arterial pressures
P=data(:,2);   %pressure in pascal
p=P(1:1045);  %input manually
% N=---; Nd=---;
% Nt=length(p);
% find the first beat
% [pmin,nmin]=min(p(1:N));
nb=[1 1037]; % input manually

% plot(pr)
% hold on
% plot(nmin, pmin, 'rx')

%iterate to find all the beat starts
j=1;
% while (nb(j)+Nd+N<Nt & j<10)
%     [pmin,nmin]=min(p(nb(j)+Nd:nb(j)+Nd+N));
%     nb(j+1)=nb(j)+Nd+nmin;
%     j=j+1;
% end

%calculate reservoir pressures for each beat
J=length(nb);
len=min(diff(nb));
% pe=zeros(J-1,len);
% for j=1:J-1
    pe=data(1:1045,2); %input manually
    t=length(pe);
    [Pr,A,B,Pinf,Tn,Pn]=kreservoir_v10_simpsons(pe,t,0);
    Pra(j,:)=Pr(1:len);
% end

%plot result
% figure;
% plot(p),hold on,grid on
% for j=1:J-1
%     plot([nb(j):nb(j)+len-1],Pra(j,:),'r')
% end
%truncate the data to integral number of beats
q=p; qr=p;
for j=1:J-1
    qr(nb(j):nb(j)+len-1)=Pra(j,:);
end
q=q(nb(1):nb(J));
qr=qr(nb(1):nb(J));
qw=q-qr;
figure
```

```
plot(data(1:1037,1),q-min(q)); hold on %input manually
plot(data(1:1037,1),qr-min(q),'r') %input manually
plot(data(1:1037,1),qw,'g') %input manually
xlabel('Time (ms)');ylabel('Pressure, P2 (Pa)');
title('Plot of total pressure, windkessel and wave pressure for EXPT
DETAIL');
legend('total pressure, q','windkessel pressure, qr','wave pressure, qw');
```

kreservoir_v10_simpsons

```
%% kreservoir  -  calculate reservoir pressure from pressure waveform
%
%  Copyright 2008 Kim H Parker
%  This software is distributed under under the terms of the GNU General
Public License
%  This program is free software: you can redistribute it and/or modify
%  it under the terms of the GNU General Public License as published by
%  the Free Software Foundation, either version 3 of the License, or
%  (at your option) any later version.
%
%  This program is distributed in the hope that it will be useful,
%  but WITHOUT ANY WARRANTY; without even the implied warranty of
%  MERCHANTABILITY or FITNESS FOR A PARTICULAR PURPOSE.  See the
%  GNU General Public License for more details.
%
%  http://www.gnu.org/licenses/gpl.html
%
%  v.03 (06/03/08)
%  v.04 (27/03/08) eliminate anonymous functions for backward compatability
%  v.05 (11/04/08) separate pinf for systole and diastole
%  v.06 (26/04/08) clean up code for use on sphygmacor data sets
%  v.07 (30/07/08) optimise fit for the whole of diastole
%  v.07.1 (05/09/08) fit to model results during diastole rather than data
%  v.07.2 (01/10/08) fixed error in fitting routine
%  v.08 (02/11/09) use polynomial approximation for inverting R(B)
%  v.08 (03/11/09) if convergence fails set pr=min(p)
%  v.09 (18/11/09) use inflection point as marker of diastole
%  v.10 (21/01/10) redefine Pres using diastolic exponential decay
%  v.10 (10/02/10) use Simpson's rule to calculate integrals

function [Pr,A,B,Pinf,Tn,Pn]=kreservoir_v10_simpsons(P,Tb,Tn)

%   inputs  P    - pressure starting at diastolic pressure
%           Tb   - duration of beat
%           Tn   - time of start of diastole (if missing it is calculated
%                     found by the function; if ==0 it is done interactively
%   outputs Pr   - reservoir pressure waveform
%           A    - rate constant relating Pw to U
%           B    - rate constant = 1/tau
%           Pinf - pressure asymptote
%           Tn   - detected time of the dichrotic notch
%           Pn   - pressure at dichrotic notch
% uses functions: fsg521, kexpint, kexpmomrat, dias_int, dias_fit, beat_int
% assumes data are smooth enough to find derivative using 7-pt SG filter

plot_flag=0;        % set to 1 to plot the results
%plot_flag=1;        % set to 1 to plot the results

sP=size(P);
if (sP(1)>sP(2));
```

```
    P=P';
end
p=P;
Nb=length(P);
dt=Tb/(Nb-1);
t=(0:dt:Tb);

% determine Tn
if (nargin == 3)
    if (Tn~=0)              % Tn given as input
        tn=Tn;
%        nn=find(t == tn);
        [Tmin,nn]=min(abs(t-tn));
    else
        figure;             % determine Tn interactively
        plot(P);
        disp('click on start of diastole');
        inp=ginput(1);
        nn=round(inp(1,1));
        tn=t(nn);
    end
else
% determine Tn automatically
% find the minimum dp
    dp=fsg721(p);
    [dpmin,nn]=min(dp);
    tn=t(nn);
end

% calculate moments of pressure during diastole using model d=a*exp(-bt)+c
pd=p(nn:end);
td=t(nn:end)-tn;
Td=Tb-tn;
dt=td(2)-td(1);
N=length(pd)-1;
% calculation of E2/E1 using Simpson's rule
E0=(pd(1)+4*sum(pd(2:2:N))+2*sum(pd(3:2:N))+pd(N+1))*dt/(3*Td);
if (mod(N,2))
    E0=E0+(pd(N)+pd(N+1))*dt/(6*Td);
end
pde1=(pd-E0).*exp(td/Td);
E1=(pde1(1)+4*sum(pde1(2:2:N))+2*sum(pde1(3:2:N))+pde1(N+1))*dt/3;
if (mod(N,2))
    E1=E1+(pde1(N)+pde1(N+1))*dt/6;
end
pde2=(pd-E0).*exp(2*td/Td);
E2=(pde2(1)+4*sum(pde2(2:2:N))+2*sum(pde2(3:2:N))+pde2(N+1))*dt/3;
if (mod(N,2))
    E2=E2+(pde2(N)+pde2(N+1))*dt/6;
end
r=E2/E1;

% invert R(BTd)=r
global Rexp_inline
    Rexp_inline=r;

%options=optimset('Display','iter','TolX',1e-16);
options=optimset('TolX',1e-16);
y=fzero(@ratio21,1,options);
BTd=y;
```

```
% given b calculate a from E1
e1=exp(1);
if (BTd==1)
    denom= (3-e1-1/e1);
else
    denom=(1-e1*exp(-BTd))/(BTd-1) - (e1-1)*(1-exp(-BTd))/BTd;
end
a=E1(end)/(Td*denom);

% Given b & a calculate c from E0
c = E0 - ((a./BTd) *(1 - exp(-BTd)));

% calculate b in s
b=BTd/Td;
pinf=c;
prd=a*exp(-b*td)+c;

% new fitting algorithm (31/07/08)
%options=optimset('TolX',1e-6);
%afind = @ (aa) sum((p(nn:end) - dias_int(p,t,aa,b,pinf,nn)).^2);
%aa=fminsearch(afind,0,options);
%pr=beat_int(p,t,aa,b,pinf,nn);
% alternative that workds with earlier versions of Matlab
global p_inline
  p_inline=p;
global t_inline
  t_inline=t;
global b_inline
  b_inline=b;
global pinf_inline
  pinf_inline=pinf;
global nn_inline
  nn_inline=nn;
global prd_inline
  prd_inline=prd;

options=optimset('TolX',1e-6);
% following line can be used in versions that support explicit functions
%y=fminsearch(@dias_fit,[b],options);
[y,rhubarb,exitflag]=fminsearch(@dias_fit,b,options);
aa=y;
pr=beat_int(p,t,aa,b,pinf,nn);
if ~exitflag
    pr=min(p)*ones(1,length(p));
end

% plot fit
if (plot_flag)
    figure
    plot(t,p,'-'); hold on; grid on
    plot(t,pr,'r-');
    plot(t(nn:end),prd,'g-');
    xlabel('t (s)');
    ylabel('P (kPa)');
end
%find crossover point
Nd=length(pd);
np=[2:Nd Nd];
prend=pr(nn:end);
```

```
k=find((prend-prd).*(prend(np)-prd(np))<=0);
prr=pr;
prr(nn+k:end)=prd(k+1:end);

% if (plot_flag)
%     figure
%     plot(t,p,'-'); hold on; grid on
%     plot(t,prr,'r-');
%     xlabel('t (s)');
%     ylabel('P (kPa)');
% end
% if (plot_flag)
%     figure
%     plot(t,p,'.-'); hold on; grid on
%     plot(t,pr,'r.-');
%     plot(t(nn:end),prd,'g.-');
%     xlabel('t (s)');
%     ylabel('P (kPa)');
% end
% if (plot_flag)
%     figure
%     plot(t,p,'.-'); hold on; grid on
%     plot(t,pr,'r.-');
%     plot(t(nn:end),prd,'g.-');
%     plot(t,prr,'k.-');
%     xlabel('t (s)');
%     ylabel('P (kPa)');
% end


% return variables
Pr=prr;
A=aa;
B=b;
Pinf=pinf;
Tn=t(nn);
Pn=p(nn);
end

%% ratio21.m - calculate the ratio of exponential moments R(bTd)
% KHP (27/01/10)
% added y==0 condition (06/02/10)

function Rdiff=ratio21(y)
%   input   y - value of bTd
%   output  R - ratio of E2/E1

global Rexp_inline

if (y==1)
    R=((exp(1)-1)-(1-exp(-1))*(exp(2)-1)/2)/(1-(1-exp(-1))*(exp(1)-1));
elseif (y==2)
    R=(1-(1-exp(-2))*(exp(2)-1)/4)/(-(exp(-1)-1)-(1-exp(-2))*(exp(1)-1)/2);
elseif (y==0)
    R=1/(3-exp(1));
else
    R=((exp(2-y)-1)/(2-y)-(1-exp(-y))*(exp(2)-1)/(2*y))/((exp(1-y)-1)/(1-
y)-(1-exp(-y))*(exp(1)-1)/y);
end
Rdiff=R-Rexp_inline;
```

```
end


%% kexpint.m  -  calculate the exponential integral Z = I_0^t Y*exp(at)dt
%  KHP (27/02/08)
function Z=kexpint(Y,T,A)
%   inputs  Y(t) - row vector
%           T    - duration of Y
%           A    - exponential factor
%   Outputs Z    - row vector
N=length(Y)-1;
t=(0:N)*T/N;
dt=t(2)-t(1);
% calculate integral of y using trapezoidal rule
ye=Y.*exp(A*t);
Z=(cumtrapz(ye))*dt;

end

%% dias_int
%  khp (30/07/08)
% calculate the indefinite integral during whole beat, returning Pr_dias
% inputs    Ps   - row vector of pressure for whole beat
%           Ts   - row vector of times for whole beat
%           a    - fitting parameter
%           b    - reciprocal of the diastolic time constant tau
%           Pinf - asymptote of diastolic pressure
%           nn   - index of notch
% output    Prd  - Pr during diastole

function Prd = dias_int(Ps,Ts,a,b,Pinf,nn)

% modification to make fminsearch work in older versions of matlab
%function Pr = dias_int(a)
%global p_inline
%global t_inline
%global b_inline
%global Pinf_inline
%global nn_send_to_inline
%dt=t_inline(2)-t_inline(1);
%pse=cumtrapz(p_inline.*exp((a+b_inline)*ts_inline))*dt;
%prb=exp(-(a+b_inline)*t_inline).*(a*pse + p_inline(1) -
(b_inline*Pinf_inline/(a+b_inline))) + b_inline*Pinf_inline/(a+b_inline);
%Pr=prb(nn:end);
%end

% calculate the integral using the trapezoidal rule
dt=Ts(2)-Ts(1);
pse=cumtrapz(Ps.*exp((a+b)*Ts))*dt;
prb = exp(-(a+b)*Ts).*(a*pse + Ps(1) - (b*Pinf/(a+b))) + b*Pinf/(a+b);
Prd=prb(nn:end);
end

%% beat_int
%  khp (30/07/08)
% calculate the indefinite integral during whole beat
% inputs    Ps   - row vector of pressure for whole beat
%           Ts   - row vector of times for whole beat
%           a    - fitting parameter
%           b    - reciprocal of the diastolic time constant tau
```

```
%           Pinf - asymptote of diastolic pressure
%           nn   - index of notch

function Pr = beat_int(Ps,Ts,a,b,Pinf,rhubarb)
% calculate the integral using the trapezoidal rule
dt=Ts(2)-Ts(1);
pse=cumtrapz(Ps.*exp((a+b)*Ts))*dt;
prb = exp(-(a+b)*Ts).*(a*pse + Ps(1) - (b*Pinf/(a+b))) + b*Pinf/(a+b);
Pr=prb;
end

%% dias_fit
function afind = dias_fit(y)

global p_inline
global t_inline
global b_inline
global pinf_inline
global nn_inline
global prd_inline

aa=y;
%afind = sum((p_inline(nn_inline:end) -
dias_int(p_inline,t_inline,aa,b_inline,pinf_inline,nn_inline)).^2);
afind = sum((prd_inline -
dias_int(p_inline,t_inline,aa,b_inline,pinf_inline,nn_inline)).^2);
end

%% Savitsky-Golay smoothing filter function
% dx=fsg720(x)
%   7 point SavGol filter, 2nd order polynomial, 0th derivative
%   input   x
%   output  dx
%   corrected for time shift
% modified for linear interpolation at ends of data KHP (27/04/08)

function dx=fsg720(x)

% 2nd order polynomial
C=[-0.095238,0.142857,0.285714];

B=zeros(1,7);
for i=1:3;
    B(i)=C(i);
end
B(4)=0.333333;
for i=5:7
    B(i)=C(8-i);
end
A=[1,0];

s=size(x,2);
dx=filter(B,A,x);
% linear interpolation at ends
Dstart=(dx(7)-x(1))/3; Dend=(x(end)-dx(s))/3.;
dx=[x(1),x(1)+Dstart,x(1)+2*Dstart,dx(7:s),x(end)-2*Dend,x(end)-
Dend,x(end)];

end
```

```
%% Savitsky-Golay first derivative filter function
% dx=fsg721(x)
%   7 point SavGol filter, 2nd order polynomial, 1st derivative
%   input   x
%   output  dx
%   corrected for time shift

function dx=fsg721(x)

% 2nd order polynomial
C=[0.107143,0.071429,0.035714];

B=zeros(1,7);
for i=1:3;
    B(i)=C(i);
end
B(4)=0.0;
for i=5:7
    B(i)=-C(8-i);
end
A=[1,0];

s=size(x,2);
dx=filter(B,A,x);
dx=[dx(7),dx(7),dx(7),dx(7:s),dx(s),dx(s),dx(s)];

end

%% Savitsky-Golay first derivative filter function
% dx=fsg521(x)
%   5 point SavGol filter, 2nd order polynomial, 1st derivative
%   input   x
%   output  dx
%   corrected for time shift

function dx=fsg521(x)

C=[0.2,0.1];

B=zeros(1,5);
for i=1:2;
    B(i)=C(i);
end
B(3)=0.0;
for i=4:5;
    B(i)=-C(6-i);
end
A=[1,0];

s=size(x,2);
dx=filter(B,A,x);
dx=[dx(5)*ones(1,2),dx(5:s),dx(s)*ones(1,2)];

end
```

Wave Intensity Analysis:

```
% For WAVE INTENSITY ANALYSIS
t=data(:,1);   %Time (ms)
p=data(:,2);   %Pressure in pascal (Pa)
CF=1;      %Correction Factor (CF) for Diameter Changes: hi Ach CF=1.1185;
lo Ach CF=1.0817; lo L-NAME CF=0.9476; hi L-NAME CF=0.9250; none CF=1
u=CF*(data(:,3)); % Velocity (m/s)
dPo=diff(qw);      %calculates differences between adjacent elements of the
array
dUo=diff(u);      %qw is wave pressure; u is velocity.
                  %Their differences are assigned to variables dPo and dUo
respectively
dP=sgolayfilt(dPo,5,11);    %smoothing function for the waveform
dU=sgolayfilt(dUo,5,11);
x=1036;  % x is value for len which is obtained from the windkessel (i.e.
reservoir) subtraction algorithm
DU=dU(1:x);  %truncating the velocity data so that it matches the no of
data for wave pressure, namely the value of len

rho=1000; Cftft=xxx;   %REMEMBER: for WATER rho=1000; for BLOOD rho=1047;
put in Cftft values at xxx
fwd=(1/(4*rho*Cftft))*((dP+(rho*Cftft.*DU)).^2);      %wave separation; fwd
refers to forward travelling wave
bwd=-(1/(4*rho*Cftft))*((dP-(rho*Cftft.*DU)).^2);   %bwd refers to backward
travelling wave
I=dP.* DU;  %wave intensity
%T=1:1:274;
plot(data(1:x,1),I(1:x),'b-')
xlabel('Time (ms)')
ylabel('dqwdU (W/m^2)')
title('Graph of wave intensity against time for EXPT DETAIL','FontSize',12)
hold on
% figure

plot(data(1:x,1),fwd(1:x),'r-')  %plots the forward travelling wave
hold on
plot(data(1:x),bwd(1:x),'g-')  %plots the backward travelling wave
legend('dI','dI+','dI-')
% axis([0 610 -0.3 0.3])        %uncomment this code if the specification
                                % of axes needed. Alternative:use zoom
                                % function on graph

hold off
figure

% to plot the PU-loop
plot(u(1:length(qw)),qw(1:length(qw)))
axis([0 1.0 -200 1000])
xlabel('velocity,U (m/s)')
ylabel('P2 as qw (Pa)')
title('P(qw)U loop for EXPT DETAIL','FontSize',12)
grid off
```

Extra Data

```
%                          ExtraData
% Script file to derive extra data from Windkessel Subtractions and
% Wave Intensity Analyses
AA_EXPERIMENT='EXPT DETAIL'; % Reference to Experiment File No
SBP=max(data(1:end,2));        % gives value for Systolic Blood Pressure
(SBP)(Pa)
```

```
DBP=min(data(1:end,2));        % gives value for Diastolic Blood Pressure
(DBP)(Pa)
Pulse_Amp=SBP-DBP;               % gives value for pulse pressure amplitude
(Pulse)(Pa)
HDN=Pn-DBP;                   % gives value for ("height of") dicrotic notch
or inflection over DBP (Pa)
RHDN=HDN/Pulse_Amp;                  % gives value for Relative Height of
Dicrotic Notch (or inflection) to Pulse
tau=1/B;                      % gives value for tau (s); the time constant
(i.e. the RC) for the diastolic decay
Pulse_qr_Amp=max(qr)-min(qr);       % gives value for pulse amplitude of
Reservoir Pressure (qr)

% Areas under Curves (AUC)i.e. integrals
dt=0.001;      % this is the time increment in seconds - each increment is
1ms as data was acquired digitally at 1KHz

figure        % (Figure 1) To use for AUC of Reservoir Pressure curve
plot(qr(1:end,1)); xlabel('Time (ms)'); ylabel('qr (Pa)'); title('For AUC
of qr');
hqr=ginput(2);
hqrstart=round(hqr(1,1));
hqrstop=round(hqr(2,1));
qr_corr=qr-hqr(1,2);    % "correcting" qr to qr_corr to have Reservoir
Pressure curve less the diastolic pressure (the end diastolic pressure
before systole)
AUC_qr=trapz(qr_corr(hqrstart:hqrstop))*dt;   % gives value for AUC of the
Reservoir Pressure (qr) less diastolic pressure level
Pulse_qr_corr_Amp=max(qr_corr)-min(qr_corr);  % should be same as, or very
little different to, line 11 above

figure         % (Figure 2) To use for AUC of component waves of the Wave
Intensity curve
plot(fwd(1:end,1),'r');  hold  on;  plot(bwd(1:end,1),'k');  xlabel('Time
(ms)'); ylabel('fwd & bwd Wave Intensity (W/m^2)'); title('For AUCs of
component waves of Wave Inrensity curve');
AUC=ginput(10);

AUC_fwdstart=round(AUC(1,1));
AUC_fwdstop=round(AUC(10,1));
AUC_fwd=trapz(fwd(AUC_fwdstart:AUC_fwdstop))*dt;  % gives value for AUC of
entire forward-going Wave Intensity curve

AUC_bwdstart=round(AUC(2,1));
AUC_bwdstop=round(AUC(10,1));
AUC_bwd=trapz(bwd(AUC_bwdstart:AUC_bwdstop))*dt; % gives value for AUC of
entire backward-going Wave Intensity curve

Rcoef=AUC_bwd/AUC_fwd;    % gives value for Reflection Coefficient for
backward-(reflected):forward-(incident) going waves

AUC_Cfwdstart=round(AUC(1,1));
AUC_Cfwdstop=round(AUC(4,1));
AUC_Cfwd=trapz(fwd(AUC_Cfwdstart:AUC_Cfwdstop))*dt; % gives value for AUC
of forward-going compression wave of wave intensity curve
Amp_Cfwd=max(fwd(AUC_Cfwdstart:AUC_Cfwdstop))-
min(fwd(AUC_Cfwdstart:AUC_Cfwdstop));  % gives amplitude of forward-going
compression wave of wave intensity curve

AUC_Cbwdstart=round(AUC(3,1));
```

```
AUC_Cbwdstop=round(AUC(5,1));
AUC_Cbwd=trapz(bwd(AUC_Cbwdstart:AUC_Cbwdstop))*dt; % gives value for AUC
of backward-going compression wave of wave intensity curve
Amp_Cbwd=max(bwd(AUC_Cbwdstart:AUC_Cbwdstop))-
min(bwd(AUC_Cbwdstart:AUC_Cbwdstop));  % gives amplitude of backward-going
compression wave of wave intensity curve

RCcoef=AUC_Cbwd/AUC_Cfwd;   % gives value for Reflection Coefficient for
backward-(reflected):forward-(incident) going compression waves

AUC_Efwdstart=round(AUC(6,1));
AUC_Efwdstop=round(AUC(8,1));
AUC_Efwd=trapz(fwd(AUC_Efwdstart:AUC_Efwdstop))*dt;  % gives value for AUC
of forward-going expansion wave
Amp_Efwd=max(fwd(AUC_Efwdstart:AUC_Efwdstop))-
min(fwd(AUC_Efwdstart:AUC_Efwdstop));  % gives amplitude of forward-going
expansion wave of wave intensity curve

AUC_Ebwdstart=round(AUC(7,1));
AUC_Ebwdstop=round(AUC(9,1));
AUC_Ebwd=trapz(bwd(AUC_Ebwdstart:AUC_Ebwdstop))*dt;  % gives value for area
under curve of backward-going expansion wave
Amp_Ebwd=max(bwd(AUC_Ebwdstart:AUC_Ebwdstop))-
min(bwd(AUC_Ebwdstart:AUC_Ebwdstop));  % gives amplitude of backward-going
expansion wave of wave intensity curve

REcoef=AUC_Ebwd/AUC_Efwd; % gives value for Reflection Coefficient for
backward-(reflected):forward-(incident) going expansion waves

% Wave Transit Time (Wtt) & Wave Transit Distance (Wtd)
% Transit being overall to & from the site of reflection (Rsite)

% gives value for time of wave transit, i.e. wave transit time, in ms
%if httstart>httstop
    %Wtt=httstart-httstop;  % if 1st click is mistakenly applied at foot of
the reflected wave intensity then 2nd click at starting foot of incident
wave intensity
%elseif httstart<httstop
Wtt=AUC(3,1)-AUC(1,1);   % this is for the correct sequence of the two
clicks, i.e. vice versa of above comment
%end
Wtd=(Wtt*0.001)*Cftft; % gives value for distance of wave transit, i.e.
wave transit distance, in m
Rsite=Wtd/2;   % gives value for distance of reflection site from site of
recording of wave, in m

% Pressure:velocity loop plots to obtain wave speed

figure        % (Figure 3) Gives plot of qwU loop
plot(data(1:length(qw),3),qw(1:length(qw))); xlabel('U (m/s)'); ylabel('qw
(Pa)'); title('qwU loop');
hqwU=ginput(2);   % to select linear section in early systole of qwU loop
CqwUloop=((hqwU(2,2)-hqwU(1,2))/(hqwU(2,1)-hqwU(1,1)))/rho;   % gives wave
speed derived from qwU loop

figure        % (Figure 10) Gives plot of qU loop
plot(data(1:length(q),3),q(1:length(q)));   xlabel('U   (m/s)');   ylabel('q
(Pa)'); title('qU loop');
hqU=ginput(2);    % to select linear section in early systole of qU loop
```

```
CqUloop=((hqU(2,2)-hqU(1,2))/(hqU(2,1)-hqU(1,1)))/rho;   % gives wave speed
derived from qU loop

% To correct Tn, the time of the dicrotic notch (incisura)
% This is because of a modification that positions the initiation of the
pulse at 0 and the
% data starts at a -ve value of time (typically -19ms to -21ms) as a lead
into the pulse data - this
% modification was brought in after, and is separate from, the
kreservoir_v72 function

Tn_corr=Tn-(-1*data(1,1));
```